A STRATIGRAPHIC-STRUCTURAL INVESTIGATION OF AN AREA SOUTH OF POFADDER, NAMAQUA MOBILE BELT, SOUTH AFRICA.

Wayne Justin Nel

Submitted in fulfilment of the requirements for the degree of Magister Scientiae

In the

Faculty of Science

Geology Department

University of the Free State, Bloemfontein

Supervisor: Prof W.P. Colliston

December 2021

Declaration

I, Wayne Justin Nel, as a student at the University of the Free State, ID number 9004155048088, declare that this Magister Scientiae is my own work and that no script with the same content of this dissertation has been submitted for any degree or examination in any other university or tertiary institution. I also declare that all the sources I have used to cite or quote my work have been indicated and acknowledged by making use of complete references.

Wayne Justin Nel

10/12/2021
Date

Abstract

The area of the Namaqua Mobile Belt investigated is situated in the eastern part of the Aggeneys Terrane (2-1.06 Ga), south of Pofadder in the Northern Cape. The mapping campaign covered an area of 1,350 km², in the eastern Aggeneys Terrane which is juxtaposed against the Pofadder (2Ga) and Bladgrond Terranes. The terranes are separated by well-defined inter-terrane thrust boundaries, namely, the Groothoek Thrust that separates the Aggeneys and Pofadder Terranes in the north, and the Geelvloer Thrust separating the Bladgrond and Aggeneys Terranes in the south of the study area.

The study area is defined by kilometre scale sheet intrusives hosting 23 stacked sequences of sheath fold nappes characterised by double vergence geometries, representing four well defined structural domains; the Witkoppies, Samoep, Lekdam and Houmoed Structural Domains. Three of the four domains contain supracrustal sequences, that can be divided into prominent structural successions and sequences. One structural domain however, the Samoep Structural Domain, is defined by a well foliated medium quartz-feldspar gneiss and contains no isolated sheath fold structures. The structural domains are separated by intra-terrane thrust sheet boundaries that have been juxtaposed on top of one another. The stratigraphic sequences can be correlated with the upper succession of the Wortel Formation, defined in the west, together with a total new set of supracrustal rocks not yet identified in the Aggeneys Terrane.

The stacked sequences of isolated double vergent isoclinal fold structures can be classified as sheath folds using listed criteria. Three prominent planar fabrics were identified within the study area namely: S0, S1 and S2. The S2 fabric is however only identified in the hinges pf macroscopic sheath folds as a sillimanite grade axial planar fabric and forms the regional fabric, defining the XY plane of the regional strain ellipse. The S2 fabric is also identified on a mesoscopic scale, by F2 Model 1 and 2 flow perturbation folds, seen in the YZ and XZ planes of the regional foliation, all planar fabrics are co-planar. The macroscopic sheath folds mapped during this study contain co-linear L fabrics defined by stretching lineations, fold axes of various fold phases and the long axes of the sheath folds and represents the X-direction of the regional strain ellipse. The co-linear linear fabrics have a mean east-northeasterly trend and plunge indicating the southwesterly directed tectonic transport overthrust direction. The planar fabrics have a mean dip toward the north-northeast across the study area.

A progressive shear deformation model is proposed for the study area and is defined by six phases of deformation affecting all four structural domains, interpreted to take place under deep crustal conditions of upper amphibolite grade of metamorphism. The D1 phase is defined by the intrusion of kilometre scale sheet intrusives that define an S1 fabric, associated with

inter- and intra-terrane thrusting. The D2 phase is defined by the development of macroscopic F2 sheath folds that fold an S0-1 foliation and define an S2 regional axial planar foliation. The D2 phase is also defined by F2 Model 1 and Model 2 folds. The D3 phase is defined by macroscopic F3 folds that refold D2 sheath fold traces and define localised S3 foliations that are also co-planar with S2. The D4 phase is defined by macroscopic F4 open folds that define a characteristic Z asymmetry that refolds all earlier structures, including kilometre scale sheet intrusives. The study area itself can be defined as a macroscopic D4 antiformal-synformal structure. The D5 phase is defined by east-west shears that are associated with the reactivated movements of thrust boundaries, and movements associated with flexural slip on the limbs of major D2, D3 and D4 structures. The D5 phase also rotates linear and planar fabrics in the north-western sector of the study area on the limbs of the major D4 synformal structure. The D6 phase is associated with northwest-southeast oblique trending shears that effect the eastern sector of the study area and deforms all earlier D2-D5 structures. It is concluded that the structures identified across the eastern Aggeneys Terrane formed progressively during a single long-lived event, formed by a process of sub-simple/general shear conditions, under deep crustal conditions.

Table of Contents

Declaration I

Abstract II

Table of Contents IV

List of Figures VIII

List of Tables XXXI

List of Appendices XXXII

Chapter 1: Introduction

1.1 Introduction 1

1.2 Regional Perspective 2

1.3. Aim of Study 3

1.4 What was Achieved 3

1.5 Thesis Outline 5

Chapter 2: Stratigraphic Analysis

2.1 Tectonostratigraphy 8

2.1.1 Methodology 13

2.2 Structural Domains 16

2.3 Plutonic Rocks 19

2.4 Plutonic Rocks: The Aggeneys Terrane 21

2.4.1 The Vaalputs Suite 21

2.4.2. The Samoep Gneiss 23

2.4.3 The Lekdam Gneiss 25

2.4.4 The Achab Suite 27

2.4.5 The Namies Gneiss 30

2.5 Plutonic Rocks: The Pofadder Terrane 32

2.5.1 The Swartmodder Gneiss 32

2.6 Plutonic Rocks: The Bladgrond Terrane 34

2.6.1 The Van Tittensville Gneiss 34

2.7 Supracrustal Sequences 36

2.8. The Witkoppies Structural Domain 38

2.8.1 The Witkoppies Sequence 38

2.8.1.1 Inner Witkoppies Member 39

2.8.1.2 The Outer Witkoppies Member 42

2.9. The Lekdam Structural Domain 43

2.9.1 The Samoep Succession 44

2.9.1.1 The Gannapoort Berg Sequence 45

2.9.1.2 The Samoep se Berg Sequence 47

2.9.1.3 The Middle Samoep Sequence 49

2.9.1.4 The S-Berg Sequence 55

2.9.1.5 Correlation and Summary of the Samoep Succession 57

2.9.2 The Klein Pofadder Sequence 59

2.9.3 The Koppies Sequence 61

2.9.3.1 Inner Koppies Member 63

2.9.3.2 Outer Koppies Member 65

2.9.4 The T-Goob Succession 67

2.9.4.1 The Poort se Berg Sequence 68

2.9.4.1.1 Upper Poort se Berg Member 70

2.9.4.1.2 Lower Poort se Berg Member 70

2.9.4.2 T-Goob se Berg Sequence 71

2.9.4.3 The Outer Lekdam Sequence 74

2.9.4.4 Correlation and summary of the T-Goob Succession 76

2.9.5 Inner Lekdam Succession 78

2.9.5.1 The Skewe Berg Sequence 79

2.9.5.2 The Xenolith Sequence 81

2.9.5.3 The Draai-Berg Sequence 83

2.9.5.4 The Platberg Sequence 85

2.9.5.5 The Sy-Berg Sequence 86

2.9.5.6 Correlation of the Inner Lekdam Succession 87

2.10. The Houmoed Structural Domain 89

2.10.1 The De-Rust Succession 89

2.10.1.1 The Achab Sequence 89

2.10.1.2 The De Rust Sequence 93

2.10.1.3 The Dwarsberg Sequence 95

2.10.1.3.1 The Inner Dwarsberg Member 95

2.10.1.3.2 The Outer Dwarsberg Member 97

2.10.1.4 Correlation of the De-Rust Succession 100

2.11 The Inter-Terrane Thrust Contacts 102

2.11.1 The Pofadder Terrane Contact: The Hom Formation 102

2.11.2 The Bladgrond Terrane: The Van Tittensville Formation 104

Chapter 3: Deformation

3. Introduction 108

3.1 Methods of Structural Analysis 108

3.1.1 Theoretical Background: Mesoscopic Sheath Folds and Model 1-2 Flow Perturbation Folds 110

3.2 Summary of Regional Structures 117

3.2.1 Regional Fabric 119

3.3 Structural Framework 121

3.3.1 Summary 121

3.4 Regional Description of Structural Development 125

3.4.1 Long section and cross section description 125

3.4.2 Phases of Deformation 126

3.5 The Structural Analysis of Selected Structures 135

3.5.1 The Witkoppies 'Eye' Structure (Domain 1E) 135

3.5.2 The Gannapoort Berg 'Eye" Structure (Domain 3A) 141

Chapter 4: Discussion

4.1 Comparison and Correlation of Stratigraphy 150

4.1.1 Comparison of Stratigraphy 150

4.1.2 Correlation of Stratigraphy to the West 155

4.1.3 Summary 159

4.2 Sheath Fold Theory and Application 160

Chapter 5: T-Goob se Berg Sheath Fold

5.1 Introduction 178

5.2 Methods 182

5.3 Stratigraphy 184

5.3.1 The T-Goob Structure: Supracrustal Sequence 184

5.4 Structure 200

5.5 Discussion 216

5.5.1 Phases of Deformation 216

5.5.2 Summary and Classification of the T-Goob Sheath Fold 223

5.5.3 Sheath Fold Classification 225

5.5.4 Model 1 and Model 2 folds 228

5.5.5 Interpretation Compared to Previous Workers 230

5.6 Summary 236

Chapter 6: Summary and Conclusion

6.1 Summary and Conclusion 238

Chapter 7: Acknowledgements

7.1. Acknowledgements 242

Chapter 8: References

8.1 References..... 243

List of Figures

Figure 1.1: Google Earth image: Location of the study area in relation to the western Namaqua Natal Mobile Belt (NNMB), major towns and the boundary with the Kaapvaal Craton is also indicated toward the east (Google Earth,2018). 1

Figure 1.2: Figure A: Detailed map depicting the regional perspective of the Namaqua Mobile Belt and its proximity to the Kaapvaal craton (Colliston et al., 2015). Figure B: Detailed map showing the relevant tectonostratigraphic terranes and their terrane boundaries (inter-terrane thrust faults). The study area is also depicted with the arrows showing the prominent regional stretching lineation direction in each terrain (modified after Colliston and Schoch, 2013)..... 4

Figure 1.3: Mind map of the chapter layout within this thesis. 6

Figure 2.0: Mind map summary of the main aspects covered in Chapter 2. 7

Figure 2.1: Regional form line map, showing the western portion of the Aggeneys Terrane, together with the location of the study area in the east. The study area is depicted by the red polygon, representing the eastern portion of the Aggeneys Terrane. The purple dotted polygon and dark-blue polygons represents the Western Aggeneys Terrane, depicting the major sheath fold structures and thrust zones previously mapped by Colliston et al., (1986). Zone I(dark-blue polygon): Zone of lower strain associated with the western part of the Aggeneys Terrane, showing the Haramoep Mountains and structures located in the northwestern part of the Aggeneys Terrane. Zone II(purple dotted polygon):Zone of higher strain, representing fragmented stratigraphy in the form of macroscopic sheath folds, which include the Aggeneys Hills, Gamsberg, Swartberg, and Achab se Berg. The Groothoek and Geelvloer inter-terrane thrust zones can be seen separating the boundaries between the adjacent Bladgrond and Pofadder Terranes, located in the north and south. 9

Figure 2.2: Simplified stratigraphic profiles that represent the stratigraphic successions in the western Aggeneys Terrane defining the Bushmanland Group (Colliston et al., 1986; Praekelt and Schoch, 1997), and the stratigraphic successions found in the study area (eastern Aggeneys Terrane). The different formations in the west and their order of stacking are also presented; their attributes are described in Table 2.2. The stratigraphy in the study area is also presented, and interpreted to have the same characteristics as that of the lower Wortel Formation found in the west. The upper assemblages identified in the study area, represent new stratigraphy not previously identified in the west. 12

Figure 2.3: The structural relationship between diagnostic packages identified in the field and the defined stratigraphic polarity, which can be coincidental with the direction of younging. Figure A: Represents an isoclinal fold illustrating the structural effects on the stratigraphy in

the overturned limb. Figure B: The effects on the stratigraphy associated with thrust duplications/fold nappes. Figure C: The effects on the stratigraphy associated with the refolding of earlier sheath folds. Figure D: Depicts the erosion which occurs on the flanks and hinge zones of these highly folded structures. Diagram A & B modified after Colliston et al., 2012. 15

Figure 2.4: Diagram represents the retention of primary relationships in spite of metamorphism and the various upward coarsening and upward fining 2nd and 3rd order cycles (centimetre to metre scale) enabling the depositional orientation and younging direction (Praekelt and Schoch, 1997). The upper diagram represents quartzite-schist relationships prevalent in the rocks under discussion and were derived from the original precursor mudstone-sandstone relationships. The lower diagram illustrates the second and third order sedimentological cycles which can still be recognized in diagnostic stratigraphic packages and aid in the stratigraphic interpretation associated with metamorphic meta-sedimentary environments. 16

Figure 2.5: Simplified geological map showing the distribution and classification of the four main Structural Domains in the eastern part of the Aggeneys Terrane, defining large intra-terrane thrust sheets. Structural Domain 1 (purple) represents the Witkoppies thrust sheet with its associated sheath fold structures (1A-E). Structural Domain 2 (green) represents the Samoep thrust sheet. Structural Domain 3 (red) represents the Lekdam thrust sheet with its associated fold structures (3A-3M). Structural Domain 4 (orange) represents the Houmoed thrust sheet with its associated structures (4A-C) (Grt: Groothoek Thrust; Gvt: Geelvloer Thrust; LekT: Lekdam Thrust; SamT: Samoep Thrust, WitT: Witkoppies Thrust). 18

Figure 2.6: Distribution of all the plutonic units throughout the study area and their relationship to the major structural domains/intra-terrane thrust sheets. A: Depicts the distribution of the different plutonic rocks associated with each intrastratigraphic terrane. B: Depicts the association of the main plutonic units with the various intra-terrane thrust sheets and their sub-division into prominent structural domains. The associated inter- and intra-terrane thrusts are also represented (Grt: Groothoek Thrust; Gvt: Geelvloer Thrust; LekT: Lekdam Thrust; SamT: Samoep Thrust, WitT: Witkoppies Thrust). 20

Figure 2.7: Distribution of the Vaalputs Suite throughout the study area in purple. A: Shows the distribution of the Vaalputs Suite close to the Groothoek Thrust, where the Vaalputs gneiss becomes highly mylonitic and deformed due to later stages of deformation. B: Shows the Vaalputs Suite folding within the Houmoed Mountains. C: Location of a prominent branch point, where the Witkoppies thrust sheet (Structural Domain 1) cuts out against the Groothoek

Thrust (Grt: Groothoek Thrust; Gvt: Geelvloer Thrust; LekT: Lekdam Thrust; SamT: Samoep Thrust; WitT: Witkoppies Thrust). 21

Figure 2.8: Variation in K-feldspar Porphyroclasts associated with the Vaalputs Suite. The porphyroclasts vary between 1 and 4 centimetres from left to right within this outcrop, which is a definitive characteristic associated with the Vaalputs Suite. 22

Figure 2.9: Different xenoliths found within the Vaalputs Suite. A represents a xenolith of calc-silicates associated with meta-sedimentary units found at Nouzees, 148 exposed on the YZ foliation plane. B represents xenoliths of biotite gneiss associated with the Witkoppies Suite on the Farm Witkoppies, exposed on the YZ foliation plane. 23

Figure 2.10: Distribution of the Samoep Gneiss throughout the study area in green. A: Shows the Samoep Gneiss (Structural Domain 2) forming a branch point with the Groothoek Thrust. B: Represents the best exposure of the Samoep Gneiss adjacent to the Samoep se Berg structure. C: The zone where the Samoep Gneiss folds within the Gannapoort Berg sheath fold structure (Grt: Groothoek thrust; Gvt: Geelvloer thrust; Lek T: Lekdam thrust; SamT (Samoep thrust); WitT (Witkoppies thrust). 24

Figure 2.11: Image A: Outcrop of the Samoep Gneiss in which a prominent biotite foliation can be observed. Image B: Development of a prominent foliation, also defined by biotite, seen in the proximity of the Houmoed Mountains. Within both diagrams can the prominent biotite bands be observed on the YZ planes of the foliation. 24

Figure 2.12: Distribution of the Lekdam Gneiss in the study area in red. A: Zone showing the folding of the Lekdam gneiss (Structural Domain 3) with the associated metasedimentary units. B: Best exposure of the garnet-bearing variations of the Lekdam Gneiss within the Poort se Berg sheath fold structure. C: Another zone exposing the garnet variations of the Lekdam Gneiss (Grt: Groothoek Thrust; Gvt: Geelvloer Thrust; LekT: Lekdam Thrust; SamT: Samoep Thrust; WitT: Witkoppies Thrust). 25

Figure 2.13: Xenoliths in the Lekdam Gneiss. A: Depicts the Lekdam Gneiss intruding within a thick package of biotite gneiss at Samoep se Berg. B: Lekdam Gneiss containing xenoliths of biotite gneiss at Gannapoort Berg. Both locations in Image A and B can be viewed in the Samoep se Berg and Gannapoort Berg region in Figure 2.11 A. 26

Figure 2.14: Large garnet minerals (1-4 centimetres in diameter) with feldspar halos, found within the Lekdam Gneiss. 27

Figure 2.15: Distribution of the Achab Suite in the study area in orange. A: The best exposures are associated with the Achab Suite at the base of Skeur se Berg. B: Best exposures of the

Achab Suite on the farm De Rust. C: Best exposures of the Achab Suite on the inside of the De Rust structure (Grt: Groothoek Thrust; Gvt: Geelvloer Thrust; LekT: Lekdam Thrust; SamT: Samoep Thrust; WitT: Witkoppies Thrust). 28

Figure 2.16: Strain variations in the Achab Suite associated with the feldspar augen on the YZ foliation planes. A: Represents a flattening of K-feldspar augen to form leucobands. Prominent foliation of biotite is also observed concerning the adjacent leuco-bands. B: Shows the less strained variation of the feldspar augen. Prominent biotite foliations can be seen enveloping the feldspar augen on the XZ foliation planes. 29

Figure 2.17: Figure 2.17: Xenoliths found within the Achab Suite A: Represents a xenolith of biotite gneiss within the Achab Suite at Skeur se Berg. B: Xenolith of a coarser quartz-feldspar gneiss found within the Achab Suite at the base of the Achab structure. 30

Figure 2.18: Distribution of the Namies Gneiss throughout the study area in purple. A: The zone where the Namies Gneiss is best exposed at Achab se Berg. B: Another zone within the study area where the Namies Gneiss is best exposed around the De-Rust structure (Grt: Groothoek thrust; Gvt: Geelvloer thrust; LekT: Lekdam thrust; SamT: Samoep thrust; WitT: Witkoppies Thrust). 31

Figure 2.19: Lithological features associated with the Namies Gneiss. A: Prominent banding is seen within the Namies Gneiss on the YZ foliation plane. B: Prominent banding seen in the Namies Gneiss on the XZ foliation plane. The Namies gneiss has a homogenous character throughout the study area. No xenoliths were found associated with this gneiss. 31

Figure 2.20: Distribution of the Swartmodder Gneiss in the adjacent Pofadder Terrane in green. A: Best exposure of the Swartmodder gneiss south of the town of Pofadder. B: Continuation of the Swartmodder Gneiss adjacent to the Groothoek Thrust toward the east (Grt: Groothoek Thrust; Gvt: Geelvloer Thrust; LekT: Lekdam Thrust; SamT: Samoep Thrust and WitT: Witkoppies Thrust). 32

Figure 2.21: Xenolith of biotite gneiss associated with the Hom Formation within the Swartmodder Gneiss. 33

Figure 2.22: Outcrop characteristics seen within the Swartmodder Gneiss. A: Flattening of feldspar augen closer toward the Groothoek Thrust contact. B: Closer to the contact augen become smaller in size and start to form mylonitic bands. 34

Figure 2.23: Distribution of the Van Tittensville gneiss (in pink) within the confines of the study area (Grt: Groothoek Thrust; Gvt: Geelvloer Thrust; LekT: Lekdam Thrust; SamT: Samoep Thrus and WitT: Witkoppies Thrust). 35

Figure 2.24: Image A: Represents the unstrained appearance of the Van Tittensville Gneiss, with prominent feldspar augen Image B: Represents the more strained variation of the VanTittensville Gneiss, augen flattening and the development of a prominent biotite foiliation. 35

Figure 2.25: Distribution of all the supracrustal sequences in the eastern part of the Aggeneys Terrane. The supracrustal rocks have been divided into various tectonic successions, sequences, and formations with the various structural domains (Grt: Groothoek Thrust; Gvt: Groothoek Thrust; LekT: Lekdam Thrust; SamT: Samoep Thrust and WitT: Witkoppies Thrust). 37

Figure 2.26: Distribution of the Witkoppies Sequence throughout the study area in green (Grt: Groothoek Thrust; Gvt: Geelvloer Thrust; LekT: Lekdam Thrust; SamT: Samoep Thrust and WitT: Witkoppies Thrust). 38

Figure 2.27: Distribution of the Outer (B-B') and Inner Witkoppies Members (A-A') together with the distribution of the Vaalputs Suite. 39

Figure 2.28: Profile A-A' (Figure 2.27): Stratigraphic succession associated with the Inner Witkoppies Member. The offset profile shows the unfolded succession. Letters A to F represent locations and photographs (Appendix 2.1). 41

Figure 2.29: Profile B-B' (from Figure 2.27): Represents the stratigraphic succession of the Witkoppies Sequence in the Outer Member of the structure. Letters A to F represent locations and photographs (Appendix 2.2). 43

Figure 2.30: Distribution of the Samoep Succession throughout the study area. The structures associated with the Samoep Succession, namely: The S-berg, Middle Samoep, Samoep Se Berg, and Gannapoort Berg structures are identified on the map (Grt: Groothoek Thrust; Gvt: Geelvloer Thrust; Lek T: Lekdam Thrust; SamT: Samoep Thrust and WitT: Witkoppies Thrust). 44

Figure 2.31: Sequences and stratigraphic profiles associated with the Samoep Succession. The profiles associated with each sequence is represented in the figure above. The facing (younging) direction and defined polarity are represented for each sequence. 45

Figure 2.32: Profile A-A' (Figure 2.31) depicts the stratigraphy associated with the Gannapoort Berg Sequence. The profile represents the entire folded succession, with the separate profile representing the unfolded succession, which is best indicated by the northern limb. An isolated sheath-fold structure is often found in the center or top of the succession within the massive

biotite-sillimanite schist unit. The letters A to F represent locations and photographs (Appendix 2.3). 46

Figure 2.33: Simplified geological map showing Profile locations A, B, and C in Figure 2.30. A geometrically controlled long section from south west to north east parallel to the regional foliation is represented by Y-Y' (The section can be seen in Figure 2.35). The younging direction and regional dips throughout the structure are also presented. Profile A-A' (Figure 2.31) depicts the stratigraphy related to the Samoep se Berg Sequence. The extension represents the unfolded succession. The letters A to F represent locations and photographs (Appendix 2.4). 48

Figure 2.34: Simplified geological map showing Profile locations A, B, and C in Figure 2.30. A geometrically controlled long section from south west to north east parallel to the regional foliation is represented by Y-Y' (see Figure 2.35). The younging direction and regional dips throughout the structure are also presented. 50

Figure 2.35: Stratigraphic profiles of the Middle Samoep Sequence. Profiles A-A', B-B' and C-C' (from Figure 2.34) represents the entire succession. The lower most profile represents the unfolded sequence associated with the Samoep Sequence. The letters A to F represent locations and photographs (Appendix 2.5). 52

Figure 2.36: Geometrically controlled long section across the Middle Samoep sheath fold showing the complexities associated with this Sequence. The lower succession (biotite gneiss with interbands of feldspathic quartzite) can be seen folding entirely around the macroscopic sheath fold structure, with the middle and upper successions staggered above. The middle succession which resembles a flattened ellipsoidal fold structure can be seen overlying the lower succession toward the southeast. The upper succession is highly folded and is represented by an elliptical 'eye' structure in the center of the structure. 54

Figure 2.37: Profile A-A' (from Figure 2.31) represents the stratigraphic succession associated with the S-Berg Sequence. The offset profile represents the unfolded succession of the S-Berg Sequence. The letters A to F represent locations and photographs (Appendix 2.6). 56

Figure 2.38: Horizontally restored correlation between all the different sequences associated with the Samoep Succession. The profiles represent the Gannapoort Berg Sequence, Middle Samoep Sequence, Samoep se Berg Sequence and S- berg Sequence, showing the most prominent characteristics. 58

Figure 2.39: Distribution of the Klein Pofadder Sequence throughout the study area in orange (Grt: Groothoek Thrust; Gvt: Geelvloer Thrust; LekT: Lekdam Thrust; SamT: Samoep Thrust and WitT: Witkoppies Thrust). 59

Figure 2.40: Distribution of the Klein Pofadder Sequence, together with the location of profile A-A'. The defined polarity is also represented throughout the structure. 60

Figure 2.41: A-A' (from Figure 2.39) represents the stratigraphic succession associated with the Klein Pofadder Sequence. The entire folded sequence, with the smaller projected profile representing the unfolded sequence. The unfolded sequence shows the defined polarity for the Klein Pofadder Sequence. The letters A to C represent locations and photographs (Appendix 2.7). 61

Figure 2.42: Distribution of the Koppies Sequence in the study area (green) (Grt: Groothoek Thrust; Gvt: Geelvloer Thrust; LekT; Lekdam Thrust, SamT: Samoep Thrust and WitT: Witkoppies Thrust). 62

Figure 2.43: Distribution of profiles A and B, across the Inner Koppies Member (red) and the Outer Koppies Member (green-purple). 62

Figure 2.44: Profile A-A' (from Figure 2.43), represents the stratigraphic succession associated with the Inner Koppies Member. The folded and unfolded sequence is represented, with the unfolded sequence representing the defined polarity for this structure. The letters A to D represent locations and photographs (Appendix 2.8). 64

Figure 2.45: Profile B-B' (from Figure 2.43) representing the stratigraphic succession associated with the Outer Koppies Member. Both the folded and unfolded sequence is represented in the diagram. The unfolded sequence shows the defined polarity for this specific structure. The letters A to C represent locations and photographs (Appendix 2.9). 66

Figure 2.46: Distribution of the T-Goob Succession throughout the study area in purple (Grt: Groothoek Thrust; Gvt: Geelvloer Thrust; LekT: Lekdam Thrust; SamT: Samoep Thrust and WitT: Witkoppies Thrust). 67

Figure 2.47: Distribution of the three structures associated with the T-Goob Succession: The T-Goob se Berg Sequence (purple), Poort se Berg Sequence (red and blue), and the Outer Lekdam Sequence (orange). The relevant profiles for each structure that give the best stratigraphic representation for the Goob Succession is also indicated for each sequence. 68

Figure 2.48: Profile A-A' and B-B' (from Figure 2.47) which represents the Poort se Berg Sequence, which is divided into an upper and lower Poort se Berg Member. Profile A-A'

represents the folded sequence associated with the upper Poort se Berg Member, with the offset profile to the right representing the unfolded sequence. Profile B-B' depicts the stratigraphy associated with the lower Poort se Berg Member, with the offset profile toward the right representing the unfolded sequence. The letters A to G represent locations and photographs (Appendix 2.10). 69

Figure 2.49: Profile A-A' (from Figure 2.47) which best represents the T-Goob Sequence. Both the folded and unfolded sequence is represented. Within the folded sequence the northern limb and southern limb is represented. The small letters A to H represent photographs associated with the stratigraphy and can be found in Appendix 2.11. 73

Figure 2.50: Profile A-A' (from Figure 2.47) represents the stratigraphic succession associated with the Outer Lekdam Sequence. Both the folded sequence and unfolded sequence are represented. The small letters A to H represent photographs associated with the stratigraphy and can be found in Appendix 2.12. 75

Figure 2.51: Horizontally restored comparison diagram associated with the stratigraphic profiles of the Outer Lekdam and T-Goob se Berg Sequences and the Upper and Lower Poort se Berg Members, which define the T-Goob Succession. Within all sequences the volcanic/chemogenic unit is clearly visible with interbanded biotite gneiss, biotite-sillimanite schist and garnet meta-quartzite units. The most distinctive difference is that this volcanic/chemogenic unit is situated within the hinge zone of the T-Goob Sequence and on the limbs of the Outer Lekdam and Poort se Berg Sequences. 77

Figure 2.52: Distribution of the Inner Lekdam Succession. A: Regional map, showing the location of the Inner Lekdam Sequence B: Aerial photograph, outlining the structures and various profile locations associated with the Inner Lekdam Succession. The structures associated with the Inner Lekdam Succession are, the Skewe Berg Sequence (light green: A-A') Xenolith Sequence (red: B-B'), Draai-Berg Sequence (turquoise: C-C'), Platberg Sequence (blue: D-D'; E-E') and Sy-Berg Sequence (brown: F-F'). 78

Figure 2.53: Profile A-A' (from Figure 2.52B) represents the best exposure of the Skewe Berg Sequence. Profile A represents the entire succession, with the offset profile toward the right representing the unfolded part of the succession: The small letters A to D represent photographs associated with the stratigraphy and can be found in Appendix 2.13. 80

Figure 2.54: Profile B-B' associated with the Xenolith Sequence. The location can be found in Figure 2.52 B. The profile represents the folded and unfolded sequence, which depicts the defined polarity. The letters A to D represent locations and photographs (Appendix 2.14). 82

Figure 2.55: Profile C-C' (from Figure 2.52 B) represents the stratigraphy associated with the Draai-Berg Sequence. Profile C represents the entire succession, with the offset profile representing the unfolded succession. The letters A to D represent locations and photographs (Appendix 2.15). 84

Figure 2.56: Profiles D-D' and E-E' (Figure 2.52 B) represent the Platberg Sequence. The Letters A and B represent photographs and location (Appendix 2.16). 85

Figure 2.57: Profile F-F' (Figure 2.52 B) represents the stratigraphy associated with the Sy-Berg Sequence. Both the folded sequence and unfolded sequence are represented. The Letters A to C represent locations and photographs (Appendix 2.17). 87

Figure 2.58: Horizontally restored interpretation of stratigraphic profiles associated with the Skewe Berg, Xenolith, Draai Berg, Platberg, and Sy-Berg Sequences, which define the Inner Lekdam Succession. 88

Figure 2.59: The distribution of the De Rust Succession throughout the Houmoed Structural Domain (red) and is defined by the Achab, De Rust, and Dwarsberg Sequences. 89

Figure 2.60: Achab Sequence with profile A-A', which best represents the stratigraphy. The distribution and location of the Achab Sequence throughout the study area can be seen in Figure 2.58. 90

Figure 2.61: Profile A-A' (Figure 2.60) which best represents the stratigraphic succession associated with the Achab Sequence. The letters A to F represent locations and photographs (Appendix 2.18). 92

Figure 2.62: The distribution of the De Rust sequence throughout the study area, with the relevant stratigraphic Profile. 93

Figure 2.63: Profile A-A' (Figure 2.62) which represents the stratigraphic succession associated with the De Rust Sequence. The letters A to D represent locations and photographs (Appendix 2.19). 94

Figure 2.64: Distribution of the Inner (turquoise) and Outer Dwarberg Members (light green), which define the Dwarsberg Sequence. The locations where the profiles were constructed are also represented, for both the Inner and Outer Dwarsberg Members. 95

Figure 2.65: Profiles A-A' and B-B (from Figure 2.64) associated with the Inner Dwarsberg Member. The letters A to D represents locations and photographs (Appendix 2.20). Horizontally restored comparison of both unfolded sequences can be found at the base of the diagram in Figure C. 97

Figure 2.66: Profiles (from Figure 2.64) A-A', B-B', C-C', and D-D' related to the Outer Dwarsberg Member. Prominent duplication of quartzites, biotite-sillimanite schist and nodular sillimanite-quartz-feldspar gneisses is seen due to intra-stratigraphic thrusting (imbricates) seen on the rim of the structure. The letters A to D represent locations and photographs (Appendix 2.21). 99

Figure 2.67: Correlation diagram between the three sequences associated with the De Rust Succession when restored horizontally. The Achab Sequence and De Rust Sequence have similar attributes, and are both associated with the Namies Gneiss, while the Dwarsberg Sequence has similar charateristics, except for the thick packages of quartzite which form due to isoclinal folding and thrusting. 101

Figure 2.68: Distribution of the Hom Formation throughout the study area in green with the relevant stratigraphic profile locations (Grt: Grootheok Thrust; Gvt: Geelvloer Thrust; LekT: Lekdam Thrust; SamT: Samoep Thrust and WitT: Witkoppies Thrust). 102

Figure 2.69: Profiles (Figure 2.68) A-A' to D-D' associated with the Hom Formation. The letters A to D represent locations and photographs (Appendix 2.22). 103

Figure 2.70: Distribution of the Van Tittensville Formation throughout the study area in red, together with the relevant stratigraphic profiles A-A' to D-D' (Grt: Groothoek Thrust; Gvt: Geelvloer Thrust; LekT: Lekdam Thrust; SamT: Samoep Thrust and WitT: Witkoppies Thrust). 105

Figure 2.71: Profiles (Figure 2.70) A-A' to D-D' associated with the Van Tittensville Formation. The letters A to D represent locations and photographs (Appendix 2.23). 106

Figure 3.0: Mind map summary of the main aspects covered in Chapter 3. 107

Figure 3.1: Model for the development of model 1 and model 2 flow perturbation folds, found throughout the study area on macroscopic and mesoscopic scale. A: Model showing the development of model 1 and 2 folds, with model 1 folds forming on the YZ foliation planes and model 2 folds forming on the XZ foliation planes. The model 1 fold axes form sub-parallel to the flow direction, with the model 2 fold axes forming oblique to normal concerning the flow direction. B: Model showing model 1 folds forming on the YZ foliation planes (lateral ramps of thrusts) and model 2 folds on the XZ foliation planes (frontal ramps of thrusts). Model 1 folds form due to layer normal shear (black shear symbols) and model 2 folds due to layer parallel shearing (white shear symbols) (Modified after Alsop and Holdsworth, 2007). C: General shear model with associated flow cells and related layer parallel and layer normal shear processes (modified after Alsop and Holdsworth,1999).Plan view of a flow cell during non-coaxial flow. The ellipse represents a flow cell, with the open arrows representing constant flow velocities.

In areas A and B sinistral and dextral shear is caused by retardation in flow. The retardation inflow results in the small strain ellipsoids (on both sides represented by A and B) fall within the shortening sector forming S and Z folds, associated with model 1 folds seen in diagrams A and B, forming on the YZ foliation planes. The Z folds will have fold axes sub-parallel to the flow direction and have a clockwise sense of rotation to the flow direction, while an S fold will have an anti-clockwise sense of rotation to the flow direction. In area C layer-parallel shear will form folds at a high angle to the flow direction, verging in the direction of flow forming model 2 folds. Area D represents an area of stretching and elongation. Modified after Alsop and Holdsworth (2007). 111

Figure 3.2: Characteristics associated with model 1 folds on an outcrop scale. A: Photograph of a model 1 fold within a biotite gneiss, which illustrates the model 1 fold, folding with the YZ foliation plane, also folds an S0//S1 foliation, and defines an S2 axial planar foliation. Stereonet shows the fold axes trend toward the north-northeast, together with the S0//S1 having a coplanar relationship to S2. B: Model 1 Z fold within the Namies gneiss, and illustrates the coplanar relationship between S1 and S2. Stereonet shows the fold axes trending toward the northeast, with the S1 and S2 foliations being co-planar to one another. 112

Figure 3.3: Characteristics associated with model 2 folds on outcrop scale. A: Centimetre scale model 2 S fold within the X-Z foliation plane. The S0//S1 foliation has a coplanar relationship to S2. The stereonet also show the fold axes trending toward the east, as well as the S0//S1 and S2 planes having a coplanar relationship. B: Model 2 fold within the Achab Suite, folding within the X-Z foliation plane. The S1 foliation has a coplanar relationship to S2, with the fold axes trending toward the east-northeast. 113

Figure 3.4: Examples of mesoscopic sheath folds found in the study area. A: Mesoscopic elliptical sheath folds within the YZ foliation plane, found within the Lekdam Gneiss, folding an S1 foliation, and defining an S2 axial planar foliation. Fold axes trend toward the east, with the axial plane having a shallow dip also toward the east. B: Mesoscopic sheath fold structure found within the T-Goob Sequence, having double vergence geometries in the form of S and Z folds found on the associated limbs. The sheath fold is exposed on the YZ foliation plane and folds an S0//S1 foliation and defines an S2 axial planar foliation. The fold axes trend toward the east-northeast, east, and southeast, the axial plane has a shallow dip toward the east. The rotational effect of lineations toward the south-east is due to the later D4-D6 phases of deformation. C: Example of an ‘omega ‘ sheath fold with double vergence geometries (S and Z), found within the Vaalputs structure, which folds obliquely within both the YZ and XZ foliation planes, and is therefore oblique to both foliation planes. This sheath fold also folds an S0//S1 foliation and defines an axial planar foliation. Fold axes trend toward the west-

southwest and northwest, with axial planes dipping toward the southwest. The sheath fold has been rotated on a limb of a major isoclinal sheath fold structure (Vaalputs sheath fold; Domain 3B) by the later phases of deformation (D4-D6), and therefore has different geometry to the sheath folds in A and B. 116

Figure 3.5: Simplified map depicting all the structural domains and associated structures within the study area. The study area can be sub-divided into four main structural domains, with each domain being sub-divided into smaller sub-domains according to the isolated fold structures identified within each domain. Domain 1 represents the Witkoppies Structural Domain; Domain 2 the Samoep Domains, Domain 3 the Lekdam Domain, and Domain 4 the Houmoed Structural Domain. The structural domains are seperated by intra-terrane thrust contacts, namely; the Lekdam Thrust (LekT); Samoep Thrust (SamT); Witkoppies Thrust (WitT). The Groothoek Thrust (Grt) and Geelvloer Thrust (GvT) are found in the north and south of the study area. 120

Figure 3.6: Simplified diagram showing the correlation of regional phases of deformation within the eastern Aggeneys Terrane. S0=Relict bedding; S1 regional transposed foliation; S2-S4= mineral foliation/ axial traces of earlier folds; S5-6 shear fabric. 122

Figure 3.7: Contacts and foliations: A: Mesoscopic F2 folds found within the Achab Suite, the F2 folds fold feldspar bands within incompetent zones. B: Interpretation of diagram A, the S1 foliation is folded and boudinaged on the limbs of F2 rootless folds, defining a penetrative transposed S2 foliation. Both the S1 and S2 foliations are boudinaged and flattened. C: Lithological contact between a well bedded quartzite (competent unit) and the Achab Suite (incompetent unit), where the regional S2 foliation is sub-parallel to the regional compositional S0-1 banding. 127

Figure 3.8: A: Model 1 fold seen within a xenolith found within the Achab Suite. The penetrative S1 foliation is seen within the Xenolith and Achab Suites. B: Close up view of the model 1 fold found within the Xenolith Suite contained within the Achab Suite. C: Interpretation of the S1 foliation is only seen on the limbs of the F2 model 1 fold, with the development of a penetrative S2 axial planar cleavage within the hinge of the fold, resulting in the S1 and S2 foliation becoming coplanar to one another. 128

Figure 3.9: Western D2 fold hinge of the Samoep se Berg sheath fold (Appendix 3.4.2; Domain 3B; Zone C3). The western fold closure folds an S0//S1 foliation and develops a penetrative S2 axial planar foliation. 129

Figure 3.10: The intense folding of D3 folds, seen within the Upper Poort se Berg fold structure (Appendix 3.4.3; Domain 3G; Zone B3). The photo is taken looking toward the east. 132

Figure 3.11: Location of the Witkoppies 'Eye' Structure (purple) and the Houmoed Structure (blue) found on the lower limb of the macroscopic 'Eye' structure, described in the text. The Vaalputs Suite (pink) is also infolded within both structures. 136

Figure 3.12: Stereonets depicting the regional L1 stretching lineations found throughout the Witkoppies 'Eye' Structure, both in the western and eastern sectors of the structure (Appendix 3.5). A: The regional L1 stretching lineations in the far western sector of the Witkoppies 'Eye' Structure, associated with a major F2 fold hinge. The stretching lineations have a mean trend and plunge of 073-24 (n=147). B: The regional (L 1) stretching lineation in the far eastern sector of the Witkoppies 'Eye' Structure and Houmoed Structure, which have a mean trend and plunge of 040-30 (n=127). Both sets of lineations include both the supracrustal sequences and intrusive rocks. C: L1 lineation seen within the Vaalputs Suite within the western sector, which has a mean trend and plunge of 079-22 (n=48). D: The L1 lineations associated with the Vaalputs Suite within the eastern sector have a mean trend and plunge of 061-21 (n=26). 137

Figure 3.13: Fold geometry associated with prominent F2 and F3 fold structures found throughout the Witkoppies 'Eye" Structure (Appendix 3.5). A: Fold geometry associated with the far western closure. Pi pole represents the fold axis of the macroscopic F2 fold structure, which has a trend and plunge of 081-30, with the axial plane having a sub-vertical dip toward the northwest. The poles to the S0-1 foliation, define a mean pi-girdle; the L1 stretching lineation is also represented and lies oblique to the F2 fold hinge. B: Illustrates the poles to the S1 foliation associated with the Vaalputs Suite and has the same geometry as in Figure A. C: Fold geometry associated with the western fold closure of the inner 'eye' structure. The Pi pole represents the F2 fold axis which trends toward 087-39 in an easterly direction, with an axial plane having a sub-vertical attitude toward the north (poles n=10). The L1 lineation lies oblique to the F2 hinge. D: Fold geometry associated with the F3 fold closure found toward the east of the Witkoppies 'Eye' Structure. The Pi pole representing the F3 fold axis has a trend and plunge of 052-52. The axial plane has a sub-vertical dip toward the northeast (poles n=7). 138

Figure 3.14: Mesoscopic structures of the Witkoppies 'Eye' Structure. A: F2 model 2 sheath fold within a banded amphibolite sequence, that folds an S0//S1 foliation and defines an S2 axial planar foliation within the XZ and YZ traces of the foliation plane; with fold axes trending and plunging toward the south and axial planes dipping sub-vertically toward the south. B: F2 model 1 Z fold within the Achab Suite found on the northern limb of the Witkoppies 'Eye' Structure, folding an S1 foliation and defining an S2 axial planar foliation within the YZ plane; fold axes plunging steeply eastward, with axial planes dipping sub-vertically toward the

northeast. C: Model 2 Z fold within the Achab Suite found on the northern limb of the Witkoppies 'Eye' Structure which folds an S1 foliation and defines an S2 axial planar cleavage within the YZ plane of the foliation (S2). The fold plunges shallowly toward the northeast and the axial plane has a sub-vertical dip toward the southeast. 140

Figure 3.15: Mesoscopic structures of the Witkoppies 'Eye' Structure. A: Horizontal S-C cleavage in biotite gneiss which shows a sinistral sense of shear, with an S-C cleavage, with the S0//S1 foliation, rotated by the S2 regional foliation. The L1 intersection lineation plunges steeply toward toward the north. B: Vertical sigmoidal shear within the Achab Suite which illustrates a north-up and south-down sense of movement found on the northern limb of the Witkoppies 'Eye' Structure. 141

Figure 3.16: Location of the Gannapoort Berg 'Eye' Structure within the study area. 142

Figure 3.17: The regional lineation (L1) and foliation (S2) associated with the Gannapoort Berg 'Eye' Structure. A: The regional lineation (L1) has a mean trend and plunge of 053-31 (n=64). The lineations are associated with both the Lekdam Gneiss, Samoep Gneiss, and supracrustal rocks associated with the Gannapoort Berg Structure. B: The regional foliation (S2) has a mean dip direction and dip of 013-58 (n=124). The foliations are associated with both the Lekdam Gneiss, Samoep Gneiss, and supracrustal succession. C: The regional L1 lineation within the intrusives surrounding the Gannapoort Berg Structure. The lineations have a mean trend and plunge of 052-35 (n=29). D: Foliations associated with the intrusive rocks surrounding the Gannapoort Berg Structure. The regional S2 foliation has a mean dip direction and dip of 022-56 (n=51). 143

Figure 3.18: Stereonets depicting the fold geometry associated with the Gannapoort Berg 'Eye' Structure. A: Far western F2 fold closure associated with the lower isoclinal fold (Appendix 3.6, fold hinge A). The fold axis has a mean trend and plunge of 067-30 (poles n=8), with the axial plane dipping moderately in a northeasterly direction. The L1 lineation lies oblique to the F2 fold hinge. B: Fold hinge of the 'eye' structure in the far western F2 fold closure (Appendix 3.6; fold hinge B). The fold axis has a mean trend and plunge of 070-39 in an east-north-easterly direction (poles n=7), with the axial plane dipping moderately toward the north-northeast. C: Far eastern fold closure associated with the lower isoclinal fold (Appendix 3.6; fold hinge C). The fold axis has a mean trend and plunge of 067-39 (poles n=6), with the axial plane having a sub-vertical dip toward the north. D: Far western closure associated with the upper F2 isoclinal fold (Appendix 3.6; fold hinge D). The fold axis trends and plunges toward 078-38 (poles n=6), with the axial plane having a sub-vertical dip toward the north-northeast. E: Lower south eastern F2 fold closure associated with the upper isoclinal fold (Appendix 3.6; fold hinge E). The fold axis has a mean trend and plunge of 047-30 (poles

n=6), with the axial plane having a sub-vertical dip toward the north-northeast.F: F5 fold closure associated with the western fold closure of the upper isoclinal fold structure (Appendix 3.6; fold hinge F). The fold axis) has a mean trend and plunge of 081-45 (poles n=6), with the axial plane having a sub-vertical dip toward the north-northeast. 145

Figure 3.19: Stereonets depicting the fold geometry associated with the Gannapoort Berg 'Eye' Structure. A: The fold geometry associated with the far eastern F3 fold closure (Appendix 3.6, fold hinge G). The fold axis has trend and plunge in the direction of 079-45 (poles: n=10), with an axial plane having a sub-vertical dip toward the northeast. The regional L1 lineation has an oblique relationship to the axial plane of the structure. B: F5 oblique fold associated with the Gannapoort Berg Structure (Appendix 3.6; fold hinge H). The fold axis trends and plunges in the direction of 321-57 (poles: n=6), and has an axial plane that has a sub-vertical dip west-south-westerly direction. C: The fold geometry of the F4 open fold located on the lower isoclinal fold structure toward the northwest (Appendix 3.6, fold hinge I). The fold axis has a trend and plunge in the direction of 037-49 (poles n=6). The axial plane has a sub-vertical dip in a north-westerly direction, with the regional L1 lineation having an oblique relationship to the axial plane. 146

Figure 3.20: Mesoscopic structures associated with the Gannapoort Berg 'Eye' Structure. A: Model 2 Z fold within mylonitic quartzite, located on the northern limb of the lower isoclinal fold structure. Model 2 fold, folds an S0//S1 foliation and defines an S2 axial planar foliation; vergence is toward the southwest, coinciding with the movement associated with over thrusting. B: Model 1 Z fold within mylonitc quartzite, found on the northern limb of the lower isoclinal fold structure. Model 1 fold, folds an S0//S1 foliation and defines an S2 axial planar foliation. The fold axes trend in an east-north-easterly direction, with axial plane having a sub-vertical dip toward the northeast. C: Model 1 Z-fold within biotite gneiss, found on the northern limb of the lower isoclinal fold structure and folds an S0//S1 foliation and defines an S2 axial planar foliation. The fold axes trend toward the east, with the axial plane dipping toward the east-south-east in a sub-horizontal fashion (Apc = Axial planar cleavage; AP: Axial plane). 147

Figure 3.21: Mesoscopic structures associated with the Gannapoort Berg 'Eye' Structure. A: Mesoscopic S-C cleavage within mylonitic quartzite found on the southern limb of the upper isoclinal fold structure, having a sinistral sense of shear and rotating the S0-1 parallel to the regional S2 foliation, with S-C cleavage intersection lineation (L1) having a trend and plunge steeply toward the east-north-east. B: Vertical mesoscopic shear within mylonitic quartzite, showing a sigmoidal rotation with north-down and south-up sense of movement. 148

Figure 4.0: Mind map summary of the main aspects covered in Chapter 4. 149

Figure 4.1: Simplified section displaying the structural restoration of macroscopic sheath folds, oblique on the XZ foliation planes, together with representative stratigraphic profiles of each tectonic sequence. Figure A: Structurally restored map oblique to the XZ foliation plane, which removes the D4-D6 phases of deformation. The various domains with associated structures is also represented. The upright and overturned limbs are displayed for each structure. Figure B: The lateral distribution of stratigraphic profiles within Structural Domain 1 (1A-E); Structural Domain 2; Structural Domain 3 (3A-3N) and Structural Domain 4 (4A-C). Figure C: Shows the location across where the section was constructed. 152

Figure 4.2: Simplified stratigraphic comparison of the different tectonic sequences in the study area and the Wortel Formation in the Haramoep Mountains, found toward the west of the study area (modified after Praekelt, 1994.) For the stratigraphic sequences in the study area, the upright limbs of all the sheath fold structures were used to construct the main stratigraphic profile seen above. 158

Figure 4.3: Schematic diagram illustrating the development of D2 sheath folds, together with facing azimuths, to illustrate why the overturned limb is in the north and not the south. Figure A: A folded sequence in section verging toward the southwest, looking toward the west. The vergence direction is ideal, together with the upright limb being represented by the northern limb. The facing azimuths in the antiformal and synformal components are directed toward southwest. Figure B: The antiformal component being thrusted and weathered away, resulting in the synformal component remaining. Figure C: A synformal sheath fold, with the northern limb being the overturned limb. This is the case in most of the sheath fold throughout the study area. 164

Figure 4.4: A: Form line map of the Samoep se Berg sheath fold with associate stratigraphic younging direction. B: Shows the Samoep se bergs sheath fold not affected by the later phases of deformation, which gives it an omega shape both in the northern and southern limbs of the F2 sheath fold. 166

Figure 4.5: Stereonet of the Samoep se Berg sheath fold, showing the co-linear relationship between the F2 S and Z folds, and F2 sheath fold axes and associated L1 stretching lineation. All the fold axes and mean stretching lineation have a mean trend toward the northeast, coinciding the northeast-southwest tectonic transport direction. The mean axial plane associated with the structure together with the poles to the F2 axial planes is also defined, having a subvertical dip toward the north-northwest. 167

Figure 4.6: Stereonet showing the co-linear relationship between the F2 S and Z folds, F2 sheath folds, F3 folds and the regional stretching lineation. The F2, F3 and stretching lineation have a mean trend toward the northeast, coincinding with the northeast-southwest tectonic

transport direction. The mean F2 and F2 axial planes is also represented, having sub-vertical dips toward the north and northeast respectively. 168

Figure 4.7: Diagram illustrating the formation of the Gannapoort Sheath fold structure, and the effect of the D3 and D5 event on its formation. Figure A: The development of the Gannapoort Berg sheath fold (D2) and overlying Samoep Thrust sheet. Figure B: The effect of the D3 and D5 east-west shears on the Gannapoort Berg sheath fold. The tightening of hinge zones can be seen due to D5 east-west shearing, together with the infolding of the Samoep Thrust Sheet (Structural Domain 2). 168

Figure 4.8: Schematic 3-D illustration of the X, Y and Z axes of a sheath fold structure, together with the inter-limb angle and apical angle showing the curvilinear attributes of the fold hinge line. The outer most elliptical ratios (Ryz) and innermost (Ry'Z') ratios are illustrated, together with the thickness of individual layers measured along the y-a axis (ty) and z-axis (tz) to provide a ratio (Tyz) of layer thickening/thinning. B: Schematic diagram showing the the classification of sheath folds according to elliptical ratios (R'). Within type A, analogous-eye-folds are formed (R=1), Type B, bull's-eye-fold (R'>1) and Type C, cast-eye-fold (R'<1) (Modified after Alsop and Holdsworth, 2006). 170

Figure 4.9: The locations were the Z values associated with each structure were measured throughout the study area. The Y and Z values, together with the attributes associated with each structure is summarised in Table 4.4. The various codes (3A-J and 4C), correspond to the various domains defined in Chapter 2 and 3. 173

Figure 4.10: A: Logarithmic plots of y and z axes of sheath folds displaying a range of scales and environments in various parts of the world (Alsop et al., 2007). The log-log plots of the different sheath folds are compared to the sheath fold structures located within the study area. B: Plots of mean Ryz ratios against the values of eight orders of magnitude from outcrop scale to kilometre scale. The cat's-eye and bull's-eye folds are compared to that of the sheath fold structures located within the study area. Diagrams modified after (Alsop et al., 2007). 175

Figure 4.11: Flinn Plot showing 2D strain associated eight different sheath fold structures throughout the study area, together with the Gamsberg structure located within the eastern Aggeneys Terrane. The Y-values can be seen in Table 4.4. A mean Z-value of 650m, modelled for the Gamsberg structure was used for all the structures. Modified after Flinn (1962). .. 176

Figure 5.0: Mind map summary of the main aspects covered in Chapter 5. 177

Figure 5.1: Simplified geological map of the western and eastern Aggeneys Terranes. Modifed after Colliston et al., (2012). The lower norther strain domain is also shown in Zone (I) (blue polygon), together with the higher strain zone depicting the zones of fragmented

structures, shown in Zone (II)(purple dashed polygon). The T-Goob Structure is also shown just towards the west of the town of Pofadder. The different structural domains (thrust sheets) are also represented by the numbers 1 to 4. 180

Figure 5.2: Simplified diagram of the T-Goob Structure, showing the division of domains and sub-domains. 183

Figure 5.3: Simplified geological map of the T-Goob se Berg Structure, together with the profile locations A to H (Lekt: Lekdam Thrust; Grt: Groothoek Thrust). 187

Figure 5.4: Stratigraphic properties associated with the Northern Domain (Profiles A, B and C) of the T-Goob Structure. The folded and restored succession is illustrated for each sub-domain. Profile locations shown in Figure 5.3. 189

Figure 5.5: Stratigraphic properties associated with the Central Domain of the T-Goob Structure (Profiles D, E and F). The folded and restored successions are illustrated. The profile locations are shown in Figure 5.3. 192

Figure 5.6: The stratigraphic properties associated with the Southern Domain (Profiles G and H). The folded and restored successions are represented. The profile locations can be seen in Figure 5.3. 194

Figure 5.7: Stratigraphic interpretation of the D2 T-Goob Structure. The D3 and D4 phases of deformation have been removed. The profile locations can be seen in Figure 5.3. The small letters are the locations of photographs asspciated with the stratigraphy and intrusives throughout the study area, and can be seen in Figures 5.8 and 5.9. 196

Figure 5.8: Stratigraphic photographs associated with the T-Goob Structure, the locations of the photographs can be seen in Figure 5.7. A: Volcanic/chemogenic unit defined by banded quartzite, diopside and actinolite, found within the central hinge of the structure. B: Well foliated biotite gneiss associated with the central hinge zone of the structure. C: Biotite-sillimanite schist often found in the central hinge of the structure. D: Garnet meta-quartzite interbanded within the biotite-sillimanite schist unit, and found surrounding the central hinge of the structure. E: Contact between the nodular rhythmic sillimanite-quartz-feldspar gneiss and poorly bedded quartzite, defining a second order upward coarsening cycle, on the lower limb of the structure. F: Nodular rhythmic sillimanite-quartz-feldspar gneiss found on the limbs of the structure. Prominent ellipsoidal sillimanite nodules are associated with this unit. G: Well foliated medium quartz-feldspar gneiss found on the northern limb of the structure. H: Cross bedding within the volcanoclastic/chemogenic unit, displayed within a feldspathic quartzite unit. 197

Figure 5.9: Photographs associated with the Lekdam Gneiss and Achab Suite. I: Poorly foliated massive grey appearance synonymous with the Lekdam Gneiss. J: Reddish appearance of the Lekdam Gneiss, with garnet overgrowths associated with the Lekdam Gneiss, giving it a speckled appearance. K: Xenolith of biotite gneiss found within the biotite gneiss on the northern limb of the T-Goob Structure. L: Quartz-feldspar augen gneiss ± biotite associated with the Achab Suite. M: Flattened banded variation of the Achab Suite within high strain zones of the Achab Suite on the southern limb of the structure. N: Well foliated variation of the Achab Gneiss, alsp located within a high strain zone within the southern limb of the T-Goob Structure. O: Xenolith of biotite gneiss found within the Achab Suite on the southern limb of the T-Goob Structure. P: Sharp contact between the Lekdam Gneiss and Achab Suite on the southern limb of the T-Goob Structure within the Samoep Sub-domain. 199

Figure 5.10: Simplified formline map associated with the T-Goob Structure. The fold traces, domains, sub-domains and section locations (AA-II) are illustrated. The section details can be seen in Appendix 5.1 and Figure 5.18. 201

Figure 5.11: Structural formline associated with the Northern Domain of the T-Goob Structure. The fold axes, fold traces and stretching lineations are illustrated. Figure A: Blow-up diagram of the northern section of the T-Goob Sub-domain, showing the various imbricate structures found on the upper and lower limb of the structure. Figure B: Imbricate structures found on the upper northern limb associated with the Skeur se Berg Sub-domain. The locations of relevant photographs in Figure 5.12; 5.13 and 5.14 are also represented in the diagram. 206

Figure 5.12: Photographs depicting structural characteristics associated with the Eenriet Sub-domain. Figure A: Photograph of the northwestern Eenriet synformal fold closure, looking towards the east. Figure B: Mesoscopic F2 fold, folding within the XZ foliation plane, folding an S0//S1 foliation and defining an S2 axial planar cleavage. The fold axes trend towards the southeast, with the axial planes dipping moderately towards the northeast. Figure C: A F2 mesoscopic Z fold, folding within the YZ foliation planes. The F2 fold, folds a S0//S1 foliation and defines an S2 axial planar cleavage, with the fold axes trending toward the north-northeast and an axial plane dipping moderately towards the north. Figure D: Mesoscopic F2 S fold folding within the YZ foliation planes, folding an S1 foliation and defining an S2 axial planar foliation. The fold axes trend towards the northeast, with the axial plane having a sub-horizontal dip towards the northeast. 206

Figure 5.13: : Illustrates the structural and kinematic characteristics associated with the Central Domain of the T-Goob Structure. A and B: Diagrams showing the contact relationships associated with the structure looking towards the south; the various lithologies and thrust contacts are depicted on the limbs and central hinge zone of the structure C: A mesoscopic

model 2 F2 folds within the XZ plane of the foliation defining Z assymmetries looking toward the south. The F2 folds verge in the direction of overthrusting and fold an S0//S1 foliation, defining an S2 axial planar cleavage.The axial planes are parallel to the bedding and dip moderately towards the east, with the fold axis trending toward the southeast. Figure D: Defines a mesoscopic model 1 F2 fold in YZ plane of the foliation, forming an omega structure. The structure folds an S0//S1 foliation and defines an S2 axial planar foliation. The axial plane dips moderately toward the east-north-east, with the fold axis plunging steeply toward the east. E: Mesoscopic F2 sheath fold, located in XZ planes of the foliation. The structure folds an S0//S1 foliation and has a prominent S2 axial planar foliation. The axial plane dips moderately toward the east, with the fold axes trending toward the north and south-southeast. The fold axes show a curvilinear trend associated with the hinge zone as they rotate around the hinge zone. 210

Figure 5.14: Structural and kinematic characteristics associated with the Central Domain. A and B: The lithological contacts and intra-stratigraphic thrusting on the upper limb of the structure. The diagram is taken looking towards the east-southeast. C: Formline interpretation of Diagram B Imbricates on the northern limb, together with branch points, cutting out the different lithologies. D Mesoscopic F2 fold found within the XZ foliation plane. The structure folds an S0//S1 foliation and defines an S2 axial planar foliation, that has a co-planar relationship. The fold axes has a shallow plunge towards the northeast, with the axial plane having a shallow dip towards the east-southeast. E: Decametre scale F2 fold, that is folded within the YZ foliation plane. The structure folds an S0//S1 foliation and defines an S2 axial planar foliation. The fold axis has a shallow plunge toward the east-southeast, with the axial plane having a shallow dip in the same direction. F: Mesoscopic S-C cleavage, showing a sinistral sense of movement, deforming the S0//S1 and S2 foliations. The cleavage-bedding intersection (S1//S2), trends toward the northeast. 211

Figure 5.15: Formline map of the Southern Domain. The fold axes, fold traces and lineations are also illustrated. The sections drawn across the Southern Domain are indicated by the letters G to I. Figure A: A simplified diagram of imbricate structures located on the southern limb of the T-Goob structure. The location of relevant photographs taken within the Southern Domain is shown in Figure 5.16 A. 214

Figure 5.16: Photographs and diagrams associated with the structural and kinematic characteristics associated with the Ou-Samoep Sub-Domain. A: The Ou-Samoep fold closure looking towards the east, with the Achab Suite and supracrustal rocks folding around the hinge. B: Defines a mesoscopic Model 1 F2 fold within the YZ plane of the foliation. The F2 fold is associated with a xenolith located within the Achab Suite. The structure folds an S1

foliation and defines an S2 axial planar foliation. C: A F2 mesocopic fold within the YZ foliation planes and folds an S1 foliation and defines an S2 axial planar foliation. The fold axes trend towards the northeast and the axial plane dips moderately toward the northeast. D: Mesocopic F2 fold that folds within the XZ foliation plane, and folds an S1 foliation and defines an S2 axial planar cleavage. The hinge has a curvilinear characteristics as the fold axes rotate around the hinge and have shallow plunges towards the northeast and southwest. The axial plane dips moderately towards the north. Figure E: Defines dextral S-C clevages, whiich are parasitic to the larger F2 fold closure toward the west. The bedding cleavage intersection trends toward the southwest. 215

Figure 5.17: : Schematic model of the character of D2 imbricates associated with the supracrustal rocks on the limbs of the T-Goob Structure on the Y-Z plane of the foliation. A:A schematic restoration of the T-Goob structure during the D1 phase. Imbrication is clearly noted within the poorly bedded quartzite and nodular rhythmic gneiss units. The well foliated medium quartz-feldspar gneiss is also thrusted in above the upper most poorly bedded quartzite. The medium grained quartz-feldspar gneiss is interpreted to be a possible sheet of Lekdam Gneiss that has been deformed. What is also apparent is that the upper stratigraphic units are not duplicated. The relationship between the Lekdam Gneiss and Achab Suite is also well illustrated, with the central section being highly sheared by the D5 phase of deformation, shearing out the Lekdam Gneiss on the thrust contact. B: Schematic diagram of the D1 imbricates being folded by the D2 phase of deformation. The Lekdam Thrust is also folded by the D2 phase of deformation. 219

Figure 5.18: A series of restored exploded sections on the XZ plane of the regional foliation. The section locations can be seen in the location map on the diagram, and correspond to the section locations in Figure 5.10. A: Cross section associated with the Eenriet fold closure in the northwest of the structure. The Achab Suite can be seen folding around the fold closure, with the Groothoek Thrust found adjacent to the structure. B: Cross section on the XZ plane of the foliation at Annakoppies. The Achab Suite folds around the fold hinge and cuts out against the Groothoek Thrust. The sillimanite body is seen in the central hinge of the structure. C: Cross section across the T-Goob se Berg Sub-domain. The Lekdam Thrust is found on the southern limb of the structure. The Lekdam Gneiss is cut-off by the Achab Suite around the F2 fold hingeon the XZ plane of the regional foliation. A set of imbricate structures is found on the lower and upper limb of the structure. The D1 imbricates are interpreted to be folded by the D2 phase of deformation. D: The D2 fold closure found in the southeast of the structure. The D2 fold closure is completely enveloped by the Lekdam Gneiss, with the Lekdam Thrust found adjacent to the structure on the northern limb. 222

Figure 5.19: Schematic diagram illustrating a restored version of the T-Goob Structure with the removal of the D4 phases of deformation. The restoration is done on the YZ plane of the regional foliation. A: T-Goob Structure represents a sheath fold structure defining macroscopic S and Z structures, if the D4 phase is removed. The criteria needed to define sheath fold structures is defined by numbers 1-7, with the description, found adjacent to the diagram. B: A flow cell model associated with layer normal shearing and the clockwise and anticlockwise rotation of folds to form S and Z structures associated with the macroscopic 'omega' structure. Dextral shearing results in the development of S structures, with sinistral shearing forming Z structures. Localised reversals in fold obliquity are also illustrated, rotating fold hinges toward the horizontal (modified after Alsop and Holdsworth, 2007). C: Stereonets associated with the D2 fold closures drawn at both ends of the T-Goob sheath fold, and are co-linear to the tectonic transport direction. The geometry of these two closure give information regarding the nature and orientation of the regional strain ellipse. 227

Figure 5.20: Schematic illustration of model 1 and model 2 folds identified within the T-Goob structure. A: Schematic depiction of a model 1 fold formed through layer normal shearing. Model 1 folds, fold the layering, and fold within the YZ plane of the foliation. B: Schematic illustration of Model 2 folds which form due to layer-parallel shear. Model 2 folds, fold within the layering, and therefore folds within the XZ foliation planes. C: Depicts a schematic diagram of a Model 1 synclinal sheath fold that has been refolded by later phases of folding. The example is synonymous with the attributes associated with the T-Goob sheath fold, with the younging direction directed toward the inside of the structure, and facing azimuths that is directed toward the inside of the structure. 229

Figure 5.19: Comparitive diagram illustrating the mapping differences between this study and Watkeys (1986). Figure A: A simplified geological map of the T-Goob sub-domain mapped by the author. Section A-A' represents a section across the XZ foliation plane illustrating the Lekdam Thrust contact and folded imbricates seen within the T-Goob Sub-domain. Figure B: A simplified geological map of Watkeys (1986) of the T-Goob Sub-domain. Section A-A' represents a section across the XZ foliation plane illustrating the stratigraphy mapped by Watkeys (1986) and the melange zones (M1, M2 and M3) interpreted by Watkeys (1986). Modified after Watkeys (1986). 232

Figure 5.22: Photographic differences illustrate in section on XZ planes to the foliation at the Skeur se Berg looking toward the east (location can be seen in Figure 5.21; section B-B'), depicting the differences in mapping between the author and Watkeys (1986). A; Photo of a section across the structure, with an interpretation of the stratigraphic units as identified by

Watkeys (1986). B: Same photo of a section across the structure, with a different interpretation of the stratigraphic units as identified by the author across the structure. ... 233

Figure 5.23: Comparative diagram of the geology associated with the Northern Domain between the author and Pretorius (1986). A: The geological map modified after Pretorius (1986). The map is insufficiently compiled, with fragmented stratigraphic units. The sillimanite ore body associated with the core of the structure is missing at the large question mark sign. The variations in the Achab Suite is well represented in the southwestern portion of the structure. The northern Lekdam Gneiss in the north of the structure is not mapped at all. B: Represents a simplified geological map by the author of the Northern Domain, illustrating the relationship between the supracrustal and the intrusive rocks. 235

List of Tables

Table 2.1: Earlier and recent stratigraphic interpretations of the Bushmanland Group. Compiled previously by Tankard et al., (1982); Rozendaal (1982); Praekelt (1994); Maclaren (1988); McClung (2006). 10

Table 2.2: The different lithostratigraphic units of the Bushmanland Group. After Praekelt and Schoch, (1997); Colliston et al. (2012). 11

Table 3.1: Summary of the different phases of deformation (D1-D3), together with the attributes and map location of the different phases of deformation seen in Appendix 3.2-3.4. 123

Table 3.2: Summary of the different phases of deformation (D1-D3 phase), together with attributes and map location of the different phases of deformation seen in Appendix 3.5 and 3.6. 124

Table 4.1: Summary of the Lithological characteristics associated with each tectonic sequence within the eastern sector of the Aggeneys Terrane. For each associated sequence and succession certain lithological properties are depicted. The various sequences are also compared to the Wortel Formation supracrustal rocks toward the west. 153

Table 4.2: Summary of lithostratigraphic characteristics associated with each tectonic sequence associated with the eastern sector of the Aggeneys Terrane. For each associated sequence and succession certain lithological properties are depicted. The various sequences are also compared to the Wortel Formation supracrustal rocks toward the west. 154

Table 4.3: Table illustrating the sheath fold criteria, together with relevant examples from domains in the study area. 160

Table 4.4: The Ryz ratios, y and z values, together with the classification of the various sheath fold structures throughout the study area. The location of the Y and Z values can be seen in Figure 4.9, and are calculated using the nomenclature by Alsop and Holdsworth, 2006 in Figure 4.8. 174

Table 5.1: Attributes of domains and sub-domains within the T-Goob Structure. 185

Table 5.2: Attributes of domains and sub-domains of the T-Goob Structure. 186

Table 5.3: Summary of geometric data associated with the northern and central domains. The Annakoppies Sub-domain is the only sub-domain where no geometric data could be collected. 202

Table 5.4 Summary of the geometric data associated with the southern domains of the T-Goob Structure 203

Table 5.5: The general attributes and characteristics associated with the phases of deformation observed within the T-Goob Structure. 218

Table 5.6: Comparison table of the structural features of the T-Goob structure, and the sheath fold criteria, necessary for the T-Goob structure to be classified as a sheath fold. 224

Table 6.1: Correlation of age dates associated with the Pofadder and Aggeneys Terranes, and their association with the structural domains found within the eastern Aggeneys Terrane. 241

List of Appendices

(In Appendix booklet)

Appendix 1.1: Reference map showing previous research conducted regionally adjacent to the study area. 3

Appendix 2.1: Witkoppies Sequence: The Inner Witkoppies Member. Figure A: Actinolite lenses found at the base of the succession and gives a light greyish colour in the field. Figure B: Sillimanite nodules associated with the actinolite lenses .Figure C: Feldspar bands are often associated with the black-banded calc-silicate rocks found throughout the stratigraphic succession.Figure D: Banded variation associated with the calc-silicate rocks. Banded variations are often associated with feldspar leucosome melts, which are parallel to the foliation planes. Figure E: Light coloured calc-silicate rocks, crystals of magnetite are often

associated with these type of rocks. Figure F: Represents the massive amphibolite units found throughout the succession. 4

Appendix 2.2: Photographs of lithologies related to the Outer Witkoppies Member. Figure A: Shows the biotite gneiss unit which makes up the bulk of the Outer Sheath Member. Figure B: Quartz clasts (lapilli) are associated with volcanic bombs, and occur sporadically throughout the stratigraphic succession. Figure C: Poorly foliated light calc-silicate rock showing prominent growth of epidote minerals. Figure D: Prominent feldspar leucobands associated with light banded calc-silicate rock. Figure E: Feldspar bands associated with dark calc-silicate rocks found throughout the succession. Figure F: Coarse-grained feldspar leucosomes associated with metatexite melts which occur throughout the stratigraphic succession. 5

Appendix 2.3: Lithological features associated with the Gannapoort Berg Sequence. Figure A: Thick biotite gneiss unit found at the base of the Gannapoort Berg Member. Figure B: Sharp contacts associated with the upper quartzite, lower biotite-sillimanite schist, and biotite gneiss units in the northern limb of the structure. Figure C: Upper quartzite showing a prominent 2nd order upward coarsening cycle, indicating the younging direction. The quartzite also has a mylonitic texture due to late shearing. Figure D: Biotite-sillimanite schist with prominent sillimanite nodules found on top of the stratigraphic succession. Figure E: Amphibolite associated with the intercalated volcanic unit found within the upper biotite-sillimanite schist unit. Figure F: Intercalated units of calc-silicate rock associated with the volcanic unit found on top of the stratigraphic succession. 6

Appendix 2.4: Lithological features of the Samoep se Berg Sequence. Figure A: Thick unit of biotite gneiss found at the base. Figure B: Interbanded units of black calc-silicate rocks within the lower biotite gneiss unit. Figure C: Biotiet- sillimanite schist found close to the contact with the upper quartzite. Figure D: Dark-blue garnet quartzite unit found on the contact with the upper quartzite. Figure E: Upper poorly bedded quartzite, often associated with a 2nd order upward coarsening cycle. Figure F: Primary bedding in the form of cross-bedding associated with the upper quartzite. 7

Appendix 2.5: Lithological features of the Middle Samoep Sequence. Figure A: Feldspathic quartzite with inter-banded units of biotite gneiss. Figure B: Represents a 3rd order upward fining cycles associated with the feldspathic quartzite unit. Prominent laminations of biotite and feldspar define the 3rd order fining cycles. Figure C: Cross-bedding associated with the feldspathic quartzite unit and shows younging direction toward the top of the succession. Figure D: Illustrates biotite sillimanite schist with interbanded units of dark-blue garnet-bearing quartzite. Figure E: Garnet overgrowths on the dark-blue quartzite unit within the XY foliation plane, which are interpreted to be late to syntectonic growths. Figure F: Bedded quartzite

associated with the upper succession. At certain locations defines a prominent second-order upward coarsening cycle. 8

Appendix 2.6: Lithological features of the S-Berg Sequence. Figure A: Thick units of biotite gneiss found at the base of the succession. Figure B: Ferruginous magnetite quartzite units interlayered within the lower biotite gneiss unit. Figure C: Inter-banded calc-silicate units found within the biotite gneiss unit. Figure D: Biotite bands associated with the upper quartzite, further toward the east. Figure E: Poorly bedded quartzite displaying a prominent 2nd order upward coarsening cycle. Figure F: Biotite-sillimanite schist unit found at the top of the stratigraphic succession. 9

Appendix 2.7: Lithological features of the Klein Pofadder Sequence. Figure A: Thick biotite-sillimanite schist associated with the lower succession. Figure B: Massive poorly bedded quartzite defining a prominent second-order upward coarsening cycle. Figure C: Dark-blue poorly bedded quartzites associated with the upper succession. Figure D: Late to syntectonic garnets associated with the upper dark-blue quartzite unit. 10

Appendix 2.8: Lithological features of the Inner Koppies Member. Figure A: Biotite-sillimanite schist associated with the lower succession. Figure B: Interbande ferruginous garnet meta-quartzite found in the lower portion of the stratigraphic succession. Figure C: Poorly bedded upper quartzite found in the upper succession defining prominent second-order upward coarsening cycle. Figure D: Nodular sillimanite-quartz-feldspar rhythmic gneiss found in the upper part of the succession. Prominent nodules of sillimanite can be observed on the YZ foliation plane. 11

Appendix 2.9: Photos associated with the stratigraphy related to the Outer Koppies Member. Figure A: Intercalated units of ferruginous garnet quartzite associated within the biotite-sillimanite schist unit. Figure B: Dark-blue character often associated with the upper quartzite. Figure C: Nodular rhythmic gneiss associated with the top portion of the outer sheath member. 12

Appendix 2.10: Lithological features associated with the Poort se Berh Sequence (upper (Figures A-E) and lower Poort se Berg Member (Figures F-H)). Figure A: Massive biotite sillimanite schist unit, with intrusive units of Lekdam Gneiss found within. Figure B: Depicts the feldspathic quartzite unit associated with the volcanic/chemogenic unit found at the base of the Poort Member. Primary bedding in the form of flame structures, can be observed within the feldspathic quartzite. Figure C: The ferruginous garnet quartzite unit intercalated within the large biotite-sillimanite schist unit associated with upper Poort se Berg Member.Figure.D: Upper poorly bedded quartzite displaying a prominent second-order upward coarsening cycle. Figure E: Nodular rhythmic sillimanite- quartz-feldspar gneiss found toward the top of the

upper Poort se Berg Member. Prominent sillimanite nodules can be seen in the diagram. Figure F: Thick well laminated feldspathic quartzite unit associated with the lower Poort se Berg Member. Figure G: Centimetre to metre scale biotite gneiss found at the base of the lower Poort se Berg Member. Figure H: Nodular rhythmic sillimanite-quartz-feldspar gneiss showing prominent sillimanite nodules found in the upper section of the lower Poort se Berg Member. 13

Appendix 2.11: Lithological features of the T-Goob se Berg Sequence. Figure A: Contact between the upper quartzite and lower nodular sillimanite-quartz-feldspar rhythmic gneiss defining a second-order upward coarsening cycle. Figure B: Volcanic unit defined by blue-white quartzites with interlayered units of diopside, actinolite, and biotite gneiss. Figure C: Volcanic/chemogenic unit depicting interbanded quartzite and diopside units. Figure D: Interlayered sequences of actinolite associated with the central volcanic unit found within the biotite-sillimanite schist unit. Figure E: Biotite gneiss associated with the central portion of the stratigraphic succession. Figure F: Biotite gneiss with overgrowths of garnet seen on the XZ foliation plane. Figure G: Well laminated medium quartz-feldspar gneiss found on the top portion of the stratigraphic succession. Figure H: Nodular sillimanite-quartz-feldspar rhythmic gneiss associated with the upper succession of the T- Goob Sequence. 14

Appendix 2.12: Lithological features associated with the Outer Lekdam Sequence. Figure A: Feldspathic quartzite with interbanded units of biotite gneiss. Figure B: Feldspathic quartzite units intercalated within the biotite-sillimanite schist units. Figure C: Biotite-sillimanite schist associated with the lower succession of the Outer Lekdam Sequence. Figure D: Poorly to well-bedded upper quartzite displaying prominent biotite bands. Figure E: Well bedded character depicted within certain portions of the Outer Ledkam Sequence, displaying prominent second-order upward coarsening cycles. Figure F: Nodular sillimanite-quartz-feldspar rhythmic gneiss associated with the top part of the stratigraphic succession. Sillimanite nodules can be seen on the YZ and XY foliation planes. 15

Appendix 2.13: Lithological features of the Skewe Berg Sequence: Figure A: Garnet meta-quartzite units interbanded within the lower biotite-sillimanite schist unit. Figure. B: Biotite gneiss interbanded within the biotite-sillimanite schist unit. Figure C: Thick sequence of biotite-sillimanite schist associated with the middle and lower portion of the stratigraphic succession. Figure D: Nodular sillimanite-quartz-feldspar rhythmic gneiss associated with the upper portion of the stratigraphy, often associated with prominent sillimanite nodules. 16

Appendix 2.14: Lithostratigraphic features associated with the Xenolith Sequence. Figure A: Garnet bearing meta-quartzite; and showing chocolate tablet boudinage. Garnets are aligned parallel to the foliation planes. Figure B: Depicts the feldspathic quartzites associated with the

Xenolith Member. Figure C: Biotite-sillimanite schist unit associated with the upper stratigraphic succession. Figure D: Biotite-sillimanite schist unit. Small sillimanite nodules can be seen on the YZ foliation plane at centimetre scale. 17

Appendix 2.15: Lithostratigraphic features of the Draai-Berg Sequence. Figure A: Feldspathic quartzite unit found within the lower succession. Figure B: Garnet-bearing meta-quartzite units interbanded within the lower biotite-sillimanite schist unit. Figure C: Dark calc-silicate rocks with prominent feldspar bands found at the base of the succession. Figure D: Poorly bedded quartzite defining a second-order upward coarsening cycle, associated with the upper echelon of the sequence. 18

Appendix 2.16: Lithostratigraphic features associated with the Platberg Sequence: Figure A: Biotite sillimanite schist unit in contact with a poorly bedded quartzite, displaying a second-order upward coarsening cycle.Figure B: Prominent garnet-bearing quartzite unit (BIF), which folds around the Platberg structure and is found at the bottom of the stratigraphic succession. 18

Appendix 2.17: Photos of the stratigraphy related to the Sy-Berg Sequence. Figure A: Small feldspathic quartzite unit found at the base of the succession. Figure B: Poorly to well-bedded quartzite, showing a second-order upward fining cycle. Figure C: Dark-blue quartzite unit interlayered within the central biotite-sillimanite schist unit. 19

Appendix 2.18: Lithological features of the Achab Sequence. Figure A: Medium quartz-feldspar Namies Gneiss found at the base of the succession. Figure B: Massive units of biotite-sillimanite schist found at the base of the Achab Sequence just above the Namies Gneiss. Figure C: Interbanded units of amphibolite associated with the stratigraphic succession. Figure D; Interbanded units of calc-silicate rock which occur sporadically throughout. Figure E: Banded units of ferruginous garnet meta-quartzites, interbanded within the lower biotite-sillimanite schist units. Figure F: Massive poorly bedded quartzites which show second-order upward coarsening cycles. 20

Appendix 2.19: Lithostratigraphic features of the De Rust Sequence. Figure A: Nodular sillimanite-quartz-feldspar rhythmic gneiss, found at the base of the succession. Prominent sillimanite nodules can be viewed on the YZ foliation surface. Figure B: Thick unit of biotite-sillimanite schist unit, found toward the top of the succession. Figure C: Upper poorly bedded quartzite, showing a second-order upward coarsening cycle. Figure D: Well to poorly foliated medium quartz-feldspar Namies Gneiss found at the top of the stratigraphic succession. .. 21

Appendix 2.20: Lithostratigraphic features associated with the Inner Dwarsberg Member. Figure A: Biotite-sillimanite schist associated with the lower and upper portions of the Inner

Dwarsberg Member. Figure B: Black calc-silicate rock unit found at the base of the stratigraphic succession, found within the biotite-sillimanite schist unit. Figure C: Large amphibolite interbanded within the lower biotite-sillimanite schist unit. Figure D: Second-order upward coarsening cycle associated with the upper quartzite. 22

Appendix 2.21: Lithostratigraphic features associated with the Outer Dwarsberg Member: Figure A: Biotite-sillimanite schist unit associated with the Outer Dwarsberg Member. Figure B: Second-order upward coarsening cycle associated with the upper quartzite unit. 22

Appendix 2.22: Lithostratigraphic features associated with the Hom Formation. Figure A: Swartmodder Gneiss which intrudes within the entire succession. Figure B: Leucobands associated with a higher strain variation of the Swartmodder Gneiss. Figure C: Leucocratic finely laminated felsic gneiss found throughout the succession. Figure D: Poryphyritic volcanic bombs, showing a porphyritic appearance of mafic and feldspar clasts. Figure E: Volcanoclastic bombs, which at certain locations have leucocratic appearance due to an increase in feldspar clasts. Figure F: Quartz eyes found in the interbanded amphibolite units. The quartz eyes are often associated with most of the hornblende gneisses, biotite gneiss, and calc-silicate rocks. 23

Appendix 2.23: Lithostratigraphic features associated with the Van Tittensville Formation. Figure A: Lower biotite gneiss unit found at the base of the succession. Figure B: Calc-silicate units interbanded within the Van Tittensville Formation, often associated with the lower biotite gneiss unit. Figure C: Biotite-muscovite-sillimanite schist associated with the upper part of the stratigraphic succession. Figure D: Prominent magnetite bands associated with the upper quartzite, displaying a third-order upward fining cycle. 24

Appendiix 2.24: Geologiical map of an area south of Pofadder. 25

Appendix 3.1: Detailed structural formline map across the study area. The location map of the different domains can be viewed to the left of the diagram. 26

Appendix 3.1 A: Lineation pattern across all domains. 27

Appendix 3.1 B: Detailed structural formline map of the far western fold closure associated with the major D4 synformal structure. A: Location of the detailed map within the study area (in purple). 28

Appendix 3.1 C: Detailed structural formline map of the central section of the major D4 synformal structure. A: Location of the detailed map within the study area (in purple). 29

Appendix 3.1 D: Detailed structural formline map of the northeastern limb of the major D4 synformal structure. A: Location of the detailed map within the study area (in purple). 30

Appendix 3.1 E: Detailed structural formline map of the southeastern limb of the major D4 synformal structure. A: Location of the detailed map within the study area (in purple). 31

Appendix 3.2: Geometric properties associated with eight prominent structural domians, together with a description of the general characteristics associated with each structure. The geometric properties have the same general characteristics as all 22 structures encountered within the study area. A: Diagram showing a fold illustrating the rotation foliations from north to south around the D4 hinges.This rotational effect can be seen in Domains 1 E, 3D, 3I and 3J; and is represented by the inverted stereonets. B: Regional location map, showing the distribution of all structures across the domains and sub-domains. 32

Appendix 3.3.1: Structural long section across the study area. Section was constructed using a combination of the Busk Method (Busk, 1929) and the projection technique by Stockwell (1960). Figure A: Composite long section across the study area drawn perpendicular to the transport direction. D2 and D3 fold structures, are located on both the northwestern and southeastern limbs of a major synformal D4 structure. Intra-terrane thrust contacts are also seen folding around the D4 hinge in the center of the structure. Figure B: Simplified geological map, showing the positions (A-C) where the long section was constructed. Figure C and D: Stereonets showing the average trend of the regional L1 stretching lineation, with average trends toward the north-east with mean plunge of 30°..... 33

Appendix 3.3.2: Structural cross section across the study area. Section was constructed using a combination of the Busk Method (Busk, 1929) and the projection technique of Stockwell (1960). Figure A: Composite cross section drawn oblique to the tectonic transport direction. Shows the folding of D2 structures by D4 phase of folding and the location of D3 and D2 structures on the southeastern limb of the major D4 structure. The tightening of D2, D3 and D4 hinges can be seen on the southeastern limb, caused by the D5 east-west shear effects. Towards the far east, the fold traces are drawn parallel due to the D6 phase of deformation (D2-D3). Thrust contacts can also be seen folding around the D4 hinges. Figure B: Shows a simplified geological map, which shows the positions (A-F) where the sections were constructed. Figure C: Stereonet diagram depicting the average regional stretching lineation trend (L1). The L1 lineations have an average plunge of 30° in a northeasterly direction. 34

Appendix 3.4.1: Simplified structural form line map depicting the best locations associated with the D1 phase of deformation throughout the study area. The red star symbols (★) represent locations where the D1 fabric (S1) can be seen. The purple star symbol (★) shows the location where the D1 phase of intra-stratigraphic thrusting can be seen, where imbrication and cut-out structures can be seen duplicating the S1//S0 fabric. 35

Appendix 3.4.2: Simplified structural form line map depicting the F2 fold traces throughout the study area. The star symbols (★) represent locations where the D2 phase (macroscopic F2 folds closures) is visible on macroscopic scale. 36

Appendix 3.4.3: Simplified structural formline map depicting the F3 fold traces throughout the study area. The pentagon symbols (⬟) represent locations where the D3 phase (F3 fold closures) is visible on macroscopic scale. 37

Appendix 3.4.4: Simplified structural form line map depicting the F4 fold traces throughout the study area. The pentagon symbols (⬟) represent locations where the D4 phase (F4 fold closures) are visible on macroscopic scale. 38

Appendix 3.4.5: Simplified structural formline map depicting the D5 and D6 phase of deformation throughout the study area. The D5 east-west shear zones are located on intra-terrane thrust contacts and on the limbs of D2, D3 and D4 structures. The D6 NW-SE shear zones are found in the far eastern sector of the study area. The F5 oblique open folds are also seen across the study area. 39

Appendix 3.5: Structural formline map of the Witkoppies 'Eye' Structure. Figure A: Simplified locality map of the structure within the study area. The map is divided into a western and eastern sector representing a lower strain zone and the latter a higher strain zone. The various fold phases with their respective fold traces, branch points, foliations and lineations are represented. 40

Appendix 3.6: Structural formline map associated with the Gannapoort Berg "Eye' structure that is defined by two isoclinal fold structures refolding adjacent to one another. Figure A: Locality map of the Gannapoort Berg 'Eye' Structure within the study area. Figure B: Simplified geological map showing the major lithologies and intrusives associated with the Gannapoort Berg Structure. It can be noted how the two isoclinal fold structures are refolded adjacent to one another. Figure C: Simplified formline map depicting the location of the mesoscopic Model 1 folds. 41

Appendix 4.1: The comparison between the Samoep Succession and the Wortel Formation supracrustal succession toward the west. Figure A: Shows the similarities and dissimilarities between the Samoep Succession and Wortel Formation in the Haramoep Mountains. Figure B: The location of the Stratigraphic profiles associated with the Samoep Succession and Wortel Formation toward the west. Figure C: An enlarged location diagram depicting the profile positions of the Samoep Succession. The Wortel Formation profiles were modified after Praekelt (1994). For the construction of all stratigraphic profiles, the upright limbs of structures are used for interpretation. 42

Appendix 4.2: The comparison between the Koppies Sequence, Klein Pofadder Sequence and the Wortel Formation supracrustal succession toward the west. Figure A: The similarities and dissimilarities associated with the Koppies-Klein Pofadder Sequences and the Wortel Formation in the west. Figure B: The location of the stratigraphic profiles associated with the Koppies, Klein Pofadder Sequence and the Wortel Formation rocks in the Haramoep Mountains. Figure C: Offset diagrams showing the profile locations of the Koppies and Klein Pofadder Sequences. The stratigraphic profiles of the Wortel Formation towards the west is modified after Praekelt (1994). For the construction of all stratigraphic profiles, the upright limbs of structures are used in the interpretation. 43

Appendix 4.3: The comparison between the T-Goob Succession and the Wortel Formation rocks found toward the west. Figure A: The similarities and dissimilarities in stratigraphy between the T-Goob Succession and Wortel Formation. Figure B: The location of the stratigraphic profiles of the Wortel Formation found in the Haramoep Mountains. Figure C: An offset diagram showing the location of the stratigraphic profiles associated with T-Goob Succession. The Wortel Formation profiles are modified after Praekelt (1994). For the construction of all stratigraphic profiles, the upright limbs of structures are used in the interpretation. 44

Appendix 4.4: The comparison between the Inner Lekdam Sequence and the Wortel Formation supracrustal succession toward the west. Figure A: The similarities and dissimilarities in stratigraphy between the Inner Lekdam Succession and Wortel Formation. Figure B: The location of the stratigraphic profiles associated with the Wortel Formation in the west. Figure C: An offset diagram showing the location of the Inner Lekdam Succession throughout the study area. For the construction of all stratigraphic profiles, the upright limbs of structures are used in the interpretation. 45

Appendix 4.5: The comparison between the De Rust Succession and the Wortel Formation toward the west. Figure A: The similarities and dissimilarities in the stratigraphy between the De-Rust Succession and Wortel Formation in the west. Figure B: The location of the stratigraphic profiles associated with the Wortel Formation in the west. Figure C: An offset diagram showing the location of the stratigraphic profiles associated with the De Rust Succession. Stratigraphic profiles associated with the Wortel Formation toward the west is modified after Praekelt (1994). For the construction of all stratigraphic profiles the upright limbs of structures are used in the interpretation. 46

Appendix 4.6: Examples of two prominent sheath fold structures within the study area, namely; the Samoep se Berg Sheath Fold (A) and Dwarsberg Sheath Fold (B). For each structure a set of criteria (1-10) is applied, proving that the structures are indeed sheath fold

structures as discussed in chapter 4.2. Figure A: The Samoep se Berg Sheath fold in its deformed state and in its undeformed state where the later phases of deformation is removed. Stereonet depicting the F2 folds and regional stretching lineations is also shown. Figure B: The Dwarsberg Sheath fold in its deformed state and undeformed state, where the D3 phase of folding is removed, the geometric properties in the form of F2-F3 fold axes and regional L1 stretching lineation is also presented. 47

Appendix 5.1: Sections (AA-ii) constructed parallel and oblique to the regional stretching lineation, together with the 2D cutaway diagrams, that show the structural and stratigraphic variation across the T-Goob Sheath fold. Figure A: Location map of the section locations. Figure B: Stereonet showing the restored lineation trend across the study area. 48

CHAPTER 1

Introduction

1.1 Introduction

The study area is located in the Northern Cape Province (Republic of South Africa) near the town of Pofadder, with the mining town of Aggeneys found further toward the west (Figure1.1). The town of Pofadder is situated in the northern portion of the study area which encompasses an area of 1,350 km², and is 45 km long and 30 km wide. The geographic location of the study area extends from west (29˚09'01''S; 19˚12'54''E) to east (29˚17'0, 5'' S; 19˚39'05''E) and from north (29˚06'39''S; 19˚23'35''E) to south (29˚21'26''E; 19˚29'49''E). Regionally the study area is characterised by an inselberg-type landscape, pink and grey gneisses, and supracrustal lithologies such as meta-quartzites,banded iron formations (BIFS), amphibolites, rhythmic quartz-feldspar gneisses, and schistose units. The Cu-Pb-Zn massive sulphide deposits of Aggeneys and Gamsberg occurr to the west of the study area, and are interpreted to be hosted within mega-scale sheath folds (Colliston and Schoch, 2002; Colliston et al., 2012).

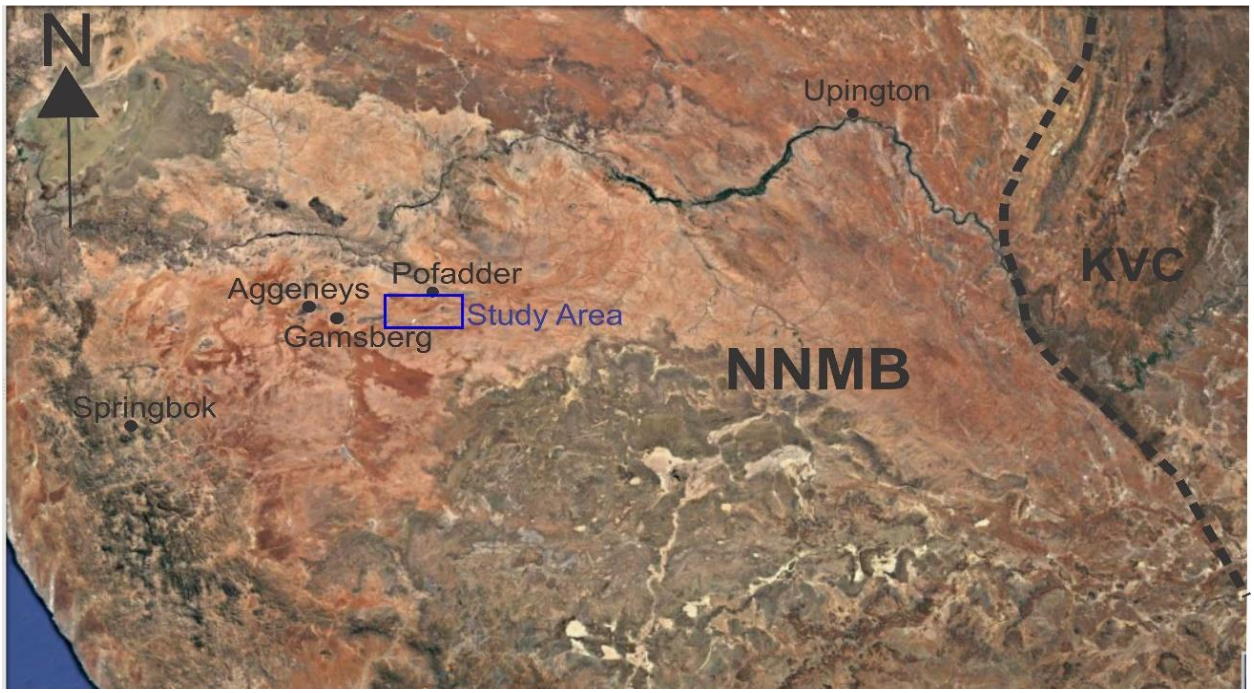

Figure 1.1: Google Earth image: Location of the study area in relation to the western Namaqua Natal Mobile Belt (NNMB), major towns and the boundary with the Kaapvaal Craton is also indicated toward the east (Google Earth,2018).

The study was conducted over a five year period, with two years full time and three years part time. For the first part of the study satellite SPOT images were used, which proved to be inadequate for mapping due to very low resolutions, later high resolution satellite images were obtained from the department of Rural Development, which were used to remap large fold traces in the study area. The study area with its inselbergs rock sub-outcrops and complex fold structures, required a lot of legwork and dedication to map the 1,350km² area and to unravel its structural history.Project dynamics:

- Total days in the field: 317
- Average distance walked in a day: ±12 kilometres
- Area mapped: 1,350km²
- Twenty three separate inselberg structures were mapped, together with surrounding intrusives. The data presented in this study is less than half due to time constraints and complexities to vast for a M.Sc thesis. Each structure was traversed twice, with some highly folded structures being traversed up to five times to understand the structural and stratigraphic complexities.
- Total distance covered: >3000km.

1.2 Regional Perspective

The Namaqua Natal Metamorphic Complex in South Africa is a region subjected to various grades of metamorphism and is characterised by folded thrust belts and distinct tectonostratigraphic terranes (Figure 1.2 A and B). It has undergone a sub-horizontal ductile shear deformation at mid-crustal conditions (Colliston et al., 1991; Colliston and Schoch, 2000). The region has been subjected to the 1.2-1.0 Ga Namaqua (Grenvillian) Orogeny (Barton, 1983; Reid and Barton, 1983; Thomas et al., 1994; McCourt et al., 2006), which formed subsequent to the Eburnian 2.0 Ga Orange River Orogeny (Blignault et al., 1983; Reid and Barton, 1983).The style of deformation seen regionally is associated with a prominent S-L tectonite fabric. The co-planar S fabric strikes mostly east-west and dips gently northerly, while the prominent L fabric is defined by prominent regional mineral stretching lineation which plunges obliquely toward the northeast, down-dip with respect to the regional S-fabric. This fabric defines the south-westerly directed tectonic transport direction (Colliston and Schoch, 2013; Strydom and Visser, 1986; van Aswegen et al., 1986).

Histrorically and traditionally the Namaqua Mobile Belt has been subdivided into an eastern Namaqua Province, known as the Gordonia Sub-province (Maclaren, 1988; Joubert, 1986) and a western Namaqua Province, traditionally known as the Bushmanland Sub-province (Hartnady et al., 1985; Stowe et al., 1984). Through decades of regional stratigraphic and structural studies, these Sub-provinces have been sub-divided into a set of well-defined tectonostratigraphic ‘suspect terranes’ (Figure 1.2 A) as defined by the guidelines of Coney et al. (1980). These various terranes have been defined and summarised in Thomas et al. (1994); Cornell et al. (2006); Colliston and Schoch (2013). The study area is situated in the Aggeneys Terrane, which is separated from the Pofadder and Bladgrond Terranes by the Groothoek thrust in the north and to the south by the Geelvloer thrust as tectonic boundaries (Figure 1.2 B). The various terranes are interpreted to be a set of major thrust sheets with the exposed sections being interpreted to be lateral ramps, which were juxtaposed during the

Namaqua Orogeny (Colliston and Schoch, 2013). Associated with the juxtaposition of these large thrust sheets is the syntectonic intrusion of large volumes of sheeted silicic granitoids, which intrude pre-tectonic supracrustal sequences comprising of metasedimentary and volcanic lithological sequences (Colliston and Schoch, 2006). The peak metamorphism conditions equilibrated for the Aggeneys Terrane (Bushmanland Sub-province) are represented at 650°± 20°C and 5 ±1 kilobar (Diener, 2014), with other authors obtaining similar results (Pretorius, 1986 and van Zyl, 1986). A summary of previous work conducted within and adjacent to the study area is documented in Appendix 1.1.

1.3. Aim of Study

The aim of the field mapping done in the study area:

- To map the extension of the Aggeneys Terrane toward the east.
- To interpret the deformation locally and to provide a proper tectonic and structural framework, which incorporates the mesoscopic structures together with macroscopic structures.
- To provide a detailed stratigraphic complilation for the eastern section of the Aggeneys Terrane.

1.4 What was Achieved

Previously the study area has been poorly mapped and interpreted, this is especially evident in the 1: 250000 Pofadder map (Agenbacht and Praekelt, 2007). The stratigraphy is not well represented, with certain mountain ranges not visible on the map, together with a poor extrapolation of stratigraphy in the western Aggeneys Terrane toward the east. Therefore, the following was achieved during this study:

- The stratigraphy from the western sector of the Aggeneys Terrane was successfully extrapolated toward the east.
- New stratigraphic successions were defined, which have not been previously identified.
- New intra-terrane thrust sheets were identified, hosting kilometre scale sheath folds, which have been severly deformed.
- A structural framework was established for the eastern Aggeneys Terrane.
- The Identification of isoclinal sheath folds, and sheath folds with double vergence geometries in the eastern Aggeneys Terrane, both on macroscopic and mesoscopic scale.

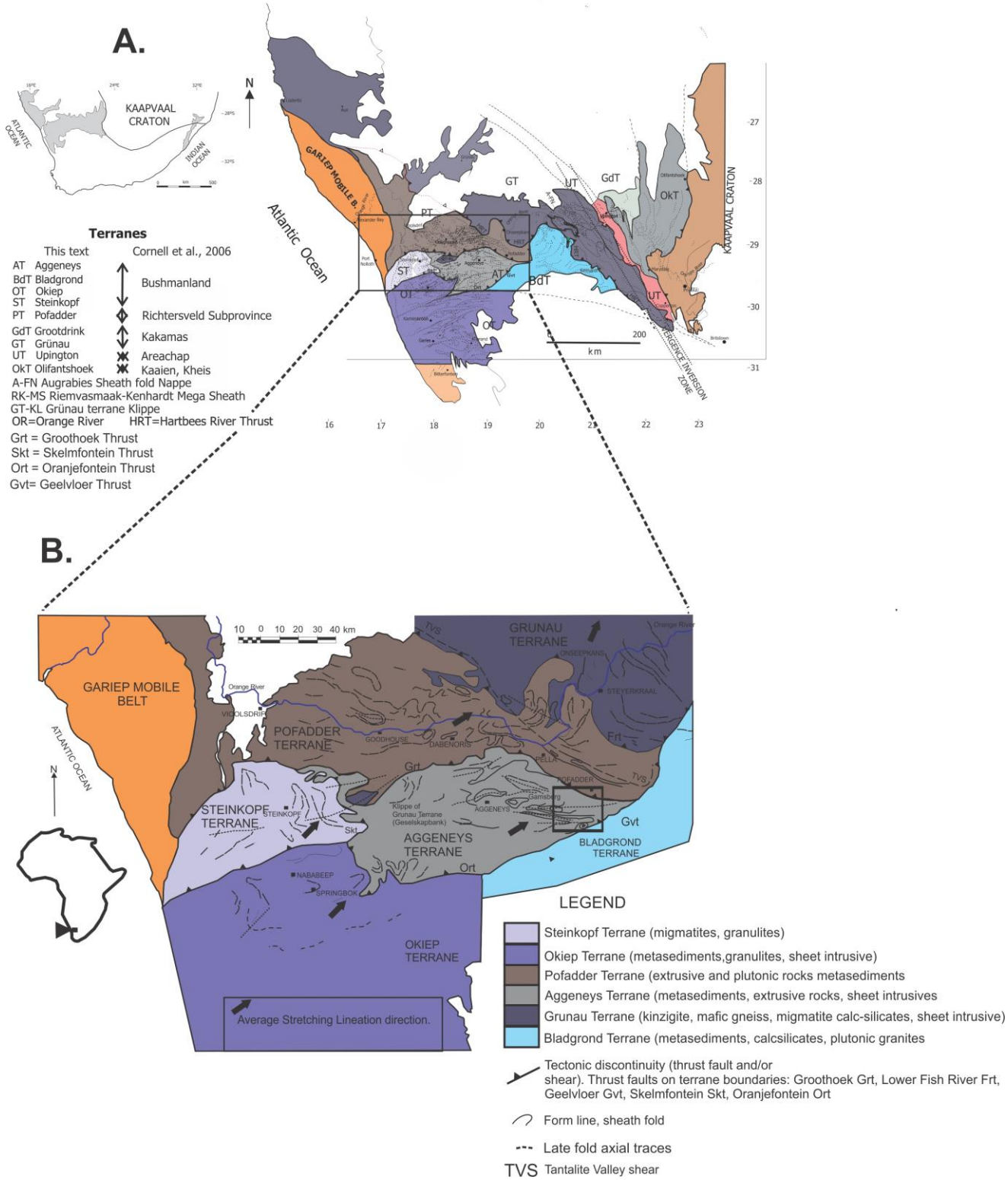

Figure 1.2. Figure A: Detailed map depicting the regional perspective of the Namaqua Mobile Belt and its proximity to the Kaapvaal craton (Colliston et al., 2015). Figure B: Detailed map showing the relevant tectonostratigraphic terranes and their terrane boundaries (inter-terrane thrust faults). The study area is also depicted with the arrows showing the prominent regional stretching lineation direction in each terrain (modified after Colliston and Schoch, 2013).

1.5 Thesis Outline

The thesis is comprised out of 6 chapters, and is summarised in the flow diagram in Figure 1.3. Before each chapter a flow diagram or mindmap summary is given, highlighting the main characteristics associated with each chapter. A separate appendix booklet containing a number of maps and diagrams is also provided for this thesis. The thesis outline is as follows:

- Chapter 1: Introduction
- Chapter 2: Stratigraphic Development
- Chapter 3: Deformation
- Chapter 4: Discussion
- Chapter 5: T-Goob se Berg Sheath Fold
- Chapter 6: Summary and conclusions

Figure 1.3: Mind map of the chapter layout within this thesis

CHAPTER 2

Stratigraphic Development

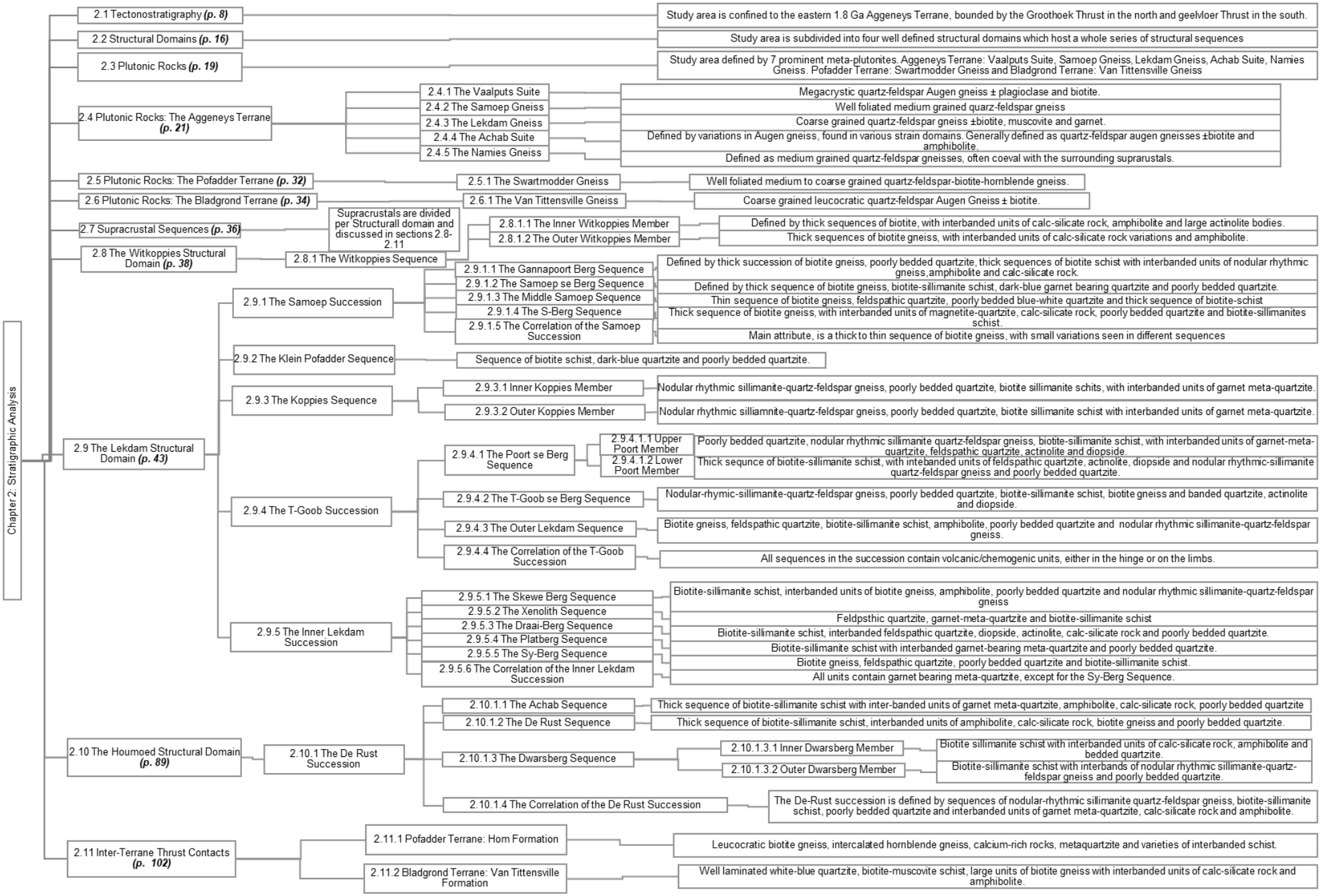

Figure 2.0: Mind map summary of the main aspects covered in Chapter 2.

2.1 Tectonostratigraphy

The study area is confined to the eastern segment of the 1.8 Ga Aggeneys Terrane (Figure 2.1), which is bounded by the Groothoek Thrust in the north and Geelvloer Thrust in the south (previously mapped as the Putsberg shear zone by Maclaren, 1988); the bounding thrusts separate the Aggeneys Terrane from 2 Ga Pofadder Terrane in the north and Bladgrond Terrane in the south. Toward the west, the Aggeneys Terrane is bounded by the Skelmfontein and Oranjefontein Thrust Zones (Colliston et al., 1991). The three terranes are defined as tectonostratigraphic terranes based on the guidelines of Coney et al., (1980), which state terranes are defined by coherent stratigraphic sequences which cannot be traced across terrane boundaries represented by major inter-terrane thrust zones.

The Aggeneys Terrane can be sub-divided into two easterly trending strain domains (Colliston et al., 1991; Colliston et al., 2012); namely a northern lower strain domain (Figure 2.1; Zone I) in which there is a continuity of structures and stratigraphy; and a southern high strain domain (Figure 2.1; Zone II), which represents discrete individual structures of which the stratigraphy is fragmented and displaced due to thrusting and is only preserved in mega-sheath-fold nappes (Colliston et al., 2012). These complex structures are separated by intrusive mega-sheets of syntectonic granite, which mostly have sub-horizontal attitudes and are associated with the Little Namaqualand Suite and Spektakel Suites, which were emplaced during the 1.02 Ga Namaqua Orogeny (Colliston and Schoch, 2002).

The regional stratigraphy has been defined and redefined by various authors for the Aggeneys Terrane and is summarised in Table 2.1, where a simplistic stratigraphy has been provided, with various authors providing different views based on individual interpretations in different areas. For this study, the stratigraphic successions provided by Praekelt and Schoch (1997) and Colliston et al. (1989) toward the west of the study area was used, because distinctive stratigraphic packages were defined by detailed regional sequence mapping, which provided a better structural control for the establishment of a stratigraphic framework for the western Aggeneys Terrane (Colliston et al., 2012).

Within the study area, the stratigraphy is also structurally controlled, and is located in a zone of high strain, with fragmented stratigraphy, within kilometre scale sheath fold nappes, enveloped by various intrusive sheets. Based on this, the study area is divided into four well defined intra-terrane thrust sheets that can be classified as structural domains (Figure 2.1). Each structural domain (thrust sheet), is sub-divided according to the emplacement of kilometre scale intrusive sheets of granitoids, that are separated from one another by intra-terrane thrusts.

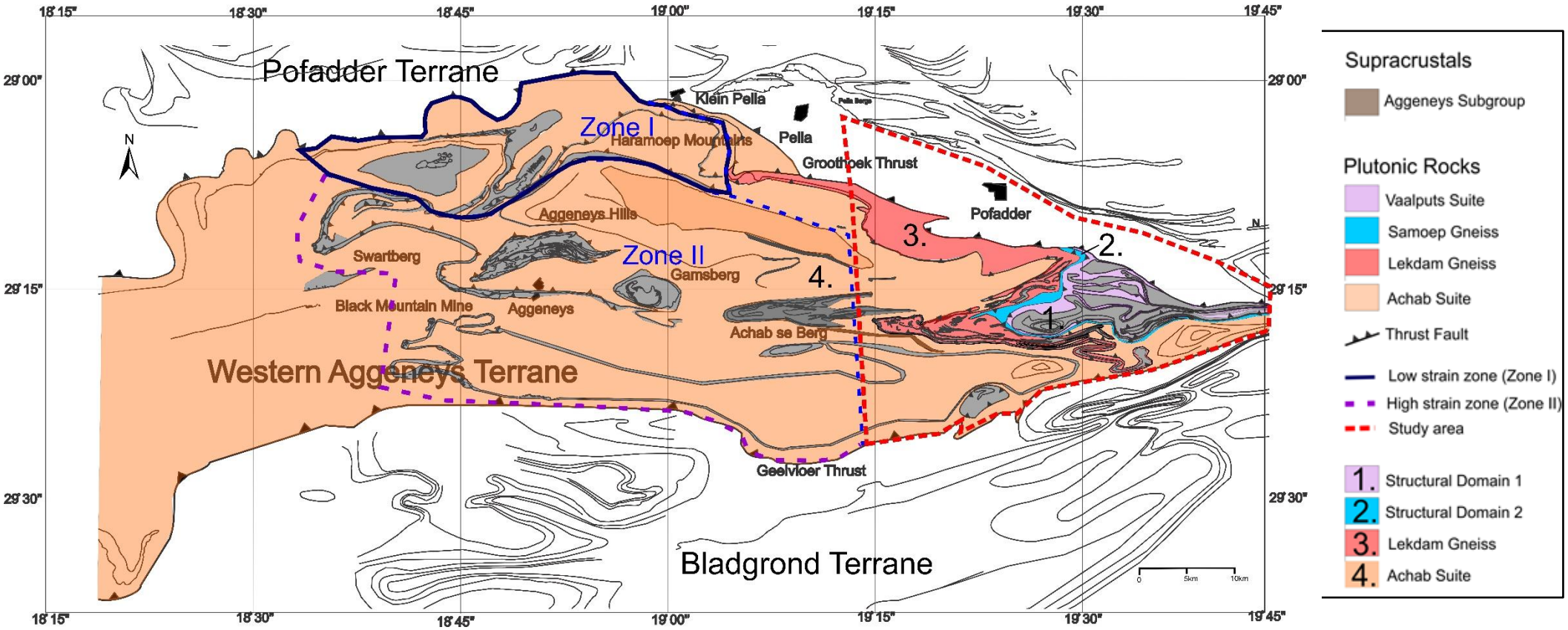

Figure 2. 1: Regional form line map, showing the western portion of the Aggeneys Terrane, together with the location of the study area in the east. The study area is depicted by the red polygon, representing the eastern portion of the Aggeneys Terrane. The purple dotted polygon and dark-blue polygons represents the Western Aggeneys Terrane, depicting the major sheath fold structures and thrust zones previously mapped by Colliston et al., (1986). Zone I(dark-blue polygon): Zone of lower strain associated with the western part of the Aggeneys Terrane, showing the Haramoep Mountains and structures located in the northwestern part of the Aggeneys Terrane. Zone II(purple dotted polygon):Zone of higher strain, representing fragmented stratigraphy in the form of macroscopic sheath folds, which include the Aggeneys Hills, Gamsberg, Swartberg, and Achab se Berg. The Groothoek and Geelvloer inter-terrane thrust zones can be seen separating the boundaries between the adjacent Bladgrond and Pofadder Terranes, located in the north and south.

Table 2. 1: Earlier and recent stratigraphic interpretations of the Bushmanland Group. Compiled previously by Tankard et al., (1982); Rozendaal (1982*); Praekelt (1994); Maclaren (1988); McClung (2006).*

Joubert (1973a,b and 1974 regional	Moore (1977) Namiesberg	Lipson (1978) Aggeneys	Rozendaal (1978) Gamsberg	Rozendaal (1982) Regional	McClung (2006) Regional	Maclaren (1988)	Paizes (1975)
				Felsic granitoid (± calcite sillimanite, quartzite, mafic rocks; nouzees melanocratic gneiss	Quartz-sericite schists conglomerates, amphibolites & leucocratic gneiss		
Granitoids (with or without dark minerals) "grey gneiss"		Granitoid "grey gneiss" (melanocratic)	Nouzees formation: Amphibolite				Vaalkop Formation: Calc-silicate rocks, cherty quartzite
Pella formation: Semi-pelitic schist		Spring schist and quartzite formation quartz-feldspar-biotite schist & meta-quartzite	Nouzees formation: Quartz-feldspar gneiss (meta-conglomerate and cross-bedding) (± semi-pelitic rocks)	Nouzees Formation: Quartz-muscovite schist (conglomerate and quartzite bands)			Geelvloer Formation: Biotite gneiss, dolomitic marble, amphibolite
Iron Formarion		Iron formation, calc-silicate and marble. (Sphalerite, galena chalcopyrite, magnetite, hematite, pyrite and pyrrhotite-bearing	Gamsformation: Sphalerite, galena, chalcopyrite, magnetite, hematite, pyrite & pyrrhotite-bearing rocks, iron formation (± pelitic- schist and gneiss and calc-silicates)	Gamsformation: Iron formation and massive sulphides	Quartz-sillimanite biotite-iron-sulphide graphite schist garnet quartzite,diopside, amphibolite, quartz-sillimanite, biotite-sulphide graphite schist quartz-magnetite rock, massive sulphide and garnet quartzite	Glassy Quartzite, quartz-feldspathic gneiss, iron formation, Calc-silicate gneiss and biotite schist, muscovite schist	Geelvloer Formation: Biotite gneiss, dolomitic marble, amphibolite
		Fly schist formation pelitic schist and gneiss (including conglomerate)			Clean darkish quartzite quartz-muscovite-biotite-sillimanite-garnet-magnetite schist	Calc-silicate gneiss, marble, pyroxenite and calc-silicate conglomerate	Houmoed Formation: Grey glassy quartzite, pink gneiss, biotite gneiss, amphibolite, biotite-sillimanite schits and blue streaky meta-quartzite
Pella Formation: Meta-quartzite (± semi-pelitic schist)	Meta-quartzite(Magnetite hematite, pyrite and pyrrhotite-bearing rocks) (± iron formation)	White meta-quartzite formation: Meta-quartzite	Pella formation: Meta-quartzite (Including conglomerate), (± pelitic to semi-pelitic rocks)	Zuurwater formation meta-quartzite (including conglomerate) (± pelitic and semi-pelitic rocks	Clean white quartzite		Pella Formation:White quartzite, aluminous schist, & feldspathic pink gneiss
Namies formation: Pelitic schist and gneiss (± semi-pelitic,mafic schist, gneiss and meta-quartzite)	Sillimanite-bearing schists, gneisses and massive sillimanite bodies	Al bearing schist formation: Sillimanite-bearing mica-schist, gneiss and massive sillimanite bodies with meta-quartzite lenses	Namies formation: Sillimanite-bearing mica-schist, gneisses and massive-sillimanite bodies (± meta-quartzite)	Sillimanite bearing mica-schist and gneiss with massive sillimanite bodies and meta-quartzite lenses	Quartz-biotite-sillimanite-spessaritine-almandine garnet, muscovite, cordierite magnetite schist		Namies formation:White quartzite, siliceous pink gneiss with quartzite interlayers
Haramoep Formation: Quartz-feldspar gneiss, "pink gneiss" (partly intrusive)	Quartz-feldpsar gneiss, "pink gneiss"(± amphibolite, actinolite schist and calc-silicate at the base)	Pink gneiss formation: Quartz-feldspar gneiss (including minor schist and gneiss)	Haramoep formation: Quartz-feldspar gneiss "pink gneiss" (including augen and partly intrusive rocks			Quartz-feldspar gneiss, megacrystic leucgneiss, leucogneiss	
Aroams formation: Augen gneiss intrusive	Augen gneiss (intrusive)						
	Leucocratic granitoids						
	Layered biotite gneiss						

The lower part of the stratigraphy within the study area can be correlated to the lower Wortel Formation of the Bushmanland Group (Figure 2.2), which is characterised by thick sequences of quartzite, biotite-sillimanite schist with intercalated units of garnet quartzite and lenses of amphibolite and calcium-rich rock (Praekelt and Schoch, 1997). However, the upper assemblages in the study area represents new stratigraphy not previously identified, and differ from the Wortel Formation rocks in the west (Figure 2.2).

Table 2. 2: The different lithostratigraphic units of the Bushmanland Group. After Praekelt and Schoch, (1997); Colliston et al. (2012).

Regional Stratigraphy	
Formation	Litho-stratigraphic unit
Koeris Formation	A lower to middle sequence of conglomerate, amphibolite and quartz-muscovite-feldspar schist and upper sequence of layered meta-quartzite and schist
Gams Formation	Upper Member: Quartz-muscovite schist with ferriferous magniferous rocks and massive sulphides Lower Member: Quartz-muscovite-biotite-sillimanite schist, thick bedded quartzites and diamactite
Hotson Formation	Interbedded rhythmic units (consisting of gneiss, quartzite and biotite-sillimanite schist), laminated quartzite, quartz-feldspar gneiss, thinly to mediumly bedded quartzite
T'hammaberg Formation	Muscovite-sillimanite schist, thin to thick bedded blue-grey to white quartzites and quartz-feldspar-biotite-gneiss
Skelmpoort Formation	Layered metaquartzite, quartzite-muscovite-biotite schist and quartz-graphite-fuchsite rock
Wortel Formation	Biotite-muscovite-sillimanite schist interbanded with amphibolite, calcareous rocks, massive aluminous rocks and ferriferous rocks
Witputs Formation	Layered sequence of medium to thick bedded meta-quartzite with thin quartz-biotite-sillimanite-schist (± garnet)

Due to the complex nature of the stratigraphy and structures under discussion, the recognition and mapping out of lithostratigraphic sequences is critical. In order to unravel the structural history, and define the stratigraphy of these sheath fold nappe structures, a systematic approach is therefore required. The method entails the mapping out of fold closures and thrust sequences to reconstruct a stratigraphy for each and every sheath fold nappe identified within the study area. The details of this approach are described in Chapter 2.1.1.

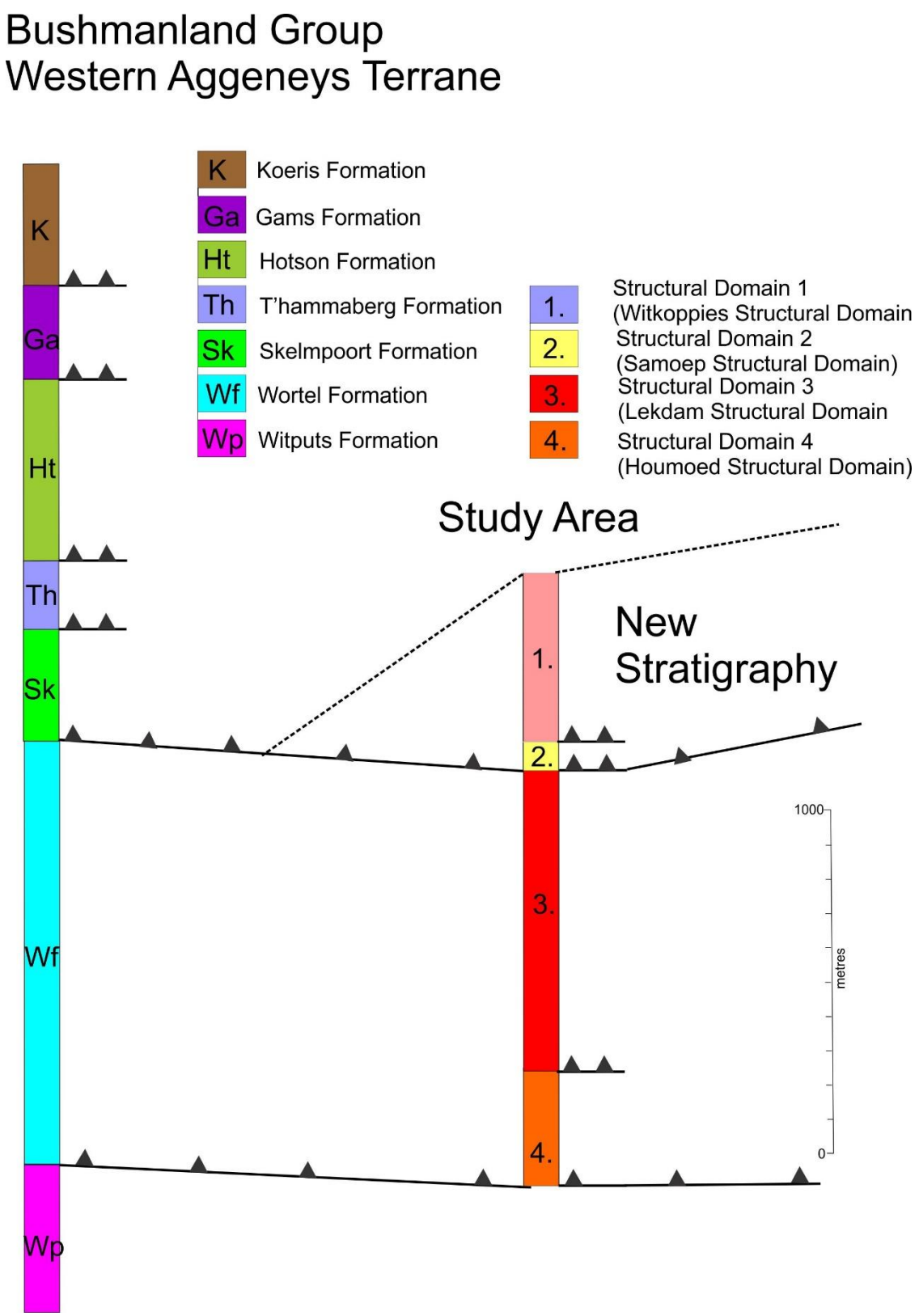

Figure 2. 2: Simplified stratigraphic profiles that represent the stratigraphic successions in the western Aggeneys Terrane defining the Bushmanland Group (Colliston et al., 1986; Praekelt and Schoch, 1997), and the stratigraphic successions found in the study area (eastern Aggeneys Terrane). The different formations in the west and their order of stacking are also presented; their attributes are described in Table 2.2. The stratigraphy in the study area is also presented, and interpreted to have the same characteristics as that of the lower Wortel Formation found in the west. The upper assemblages identified in the study area, represent new stratigraphy not previously identified in the west.

2.1.1 Methodology

Within highly deformed areas such as the Namaqua Metamorphic Mobile Belt, there is often a juxtaposition of supracrustal sequences and syntectonic intrusives, together with complications associated with isoclinal folding and thrusting. It can become a daunting task to unravel the pre-tectonic history of supracrustal sequences and intrusive units. Lithological and traverse mapping alone is not sufficient enough to interpret the geological history often associated with metamorphic belts. Therefore, a systematic approach is required when conducting a structural and tectonic study within metamorphic environments. The approach or method required is termed 'sequence mapping' (Colliston et al., 2012) which entails mapping the lateral delineation of stratigraphic packages on a hectometre to decametre scale (Figure 2.3).This method was applied during the mapping of structures in the eastern Aggeneys Terrane.

For each structure or supracrustal sequence key lithological units are identified in zones of lower strain, within the hinges of earlier macroscopic folds and duplicated or thrusted sequences (Figure 2.3 A and B). Within isoclinal folds, mapping out the fold axial trace and identifying key lithostratigraphic units within the hinge zone and limbs (units which fold around the hinge zone), the defined polarity (Colliston et al., 2012) for a specific structure or package can be determined, this in turn helps to define the upright and overturned limb of the structure being investigated (Figure 2.3 A). This method can also be used to identify structural duplications in the form of imbricate structures often occurring in the hinge, limbs of isoclinal folds, and on a regional scale associated with nappes and fold nappes (Figure 2.3 B). Defined polarity associated with sequence mapping is particularly useful if no primary sedimentary structures such as cross-beds have been identified, which determine the 'younging' direction. And if cross-bedding or primary structures have been identified, the defined polarity can be confirmed as also showing the younging direction. From this the upright limb of a structure can be identified, e.g. of this can be seen in Chapter 4.1.

However, this sector of the Aggeneys Terrane has undergone polydeformation, and highly folded isoclinal folds (D2) are refolded by later D3 isoclinal fold structures. Stratigraphic units thin dramatically, and several duplications occur due to isoclinal folding. It can therefore become a daunting task to consistently follow the stratigraphic units along strike, using the defined polarity established within the hinge zone and limbs of the fold structure (Figure 2.3 C). The stratigraphic column X in Figure 2.3 C illustrates the structural complications. A disciplined approach is required to document and interpret the mapped structure correctly; this entails mapping the fold axial trace of the 1st identified fold hinge along strike. Further complications may occur due to erosion in which certain segments of the related structure are poorly exposed and not discernible (Figure 2.3 D). It is therefore imperative that lithological

sequences identified in hinges of early isoclines together with the defined polarity is determined when mapping highly folded isoclinal structures. Another complication associated with mapping high-grade metamorphic rocks is the identification of precursor rocks (mudstone-schist, and sandstone-quartzite, etc.) and relict or primary bedding or primary structures, such as cross-bedding (Figure 2.4). The above-mentioned features are needed to construct a pre-metamorphic depositional environment. The 2nd and 3rd order cyles can be used to show the younging direction (stratigraphic polarity) and are always upward fining, except for delta front type environments. This approach is useful in areas where primary structures are lacking (Praekelt and Schoch., 1997). The collective interpretation and synthesis of diagnostic packages in terms of energy (high energy-sandstones (quartzites), low energy-mudstones (schist)), and enables the interpretation of facies and depositional environments (Colliston et al., 2012). Complications of syntectonic sheet granitoids, can also further complicate matters, as they can inter-finger or intrude within the supracrustal successions, specifically within the less competent units.

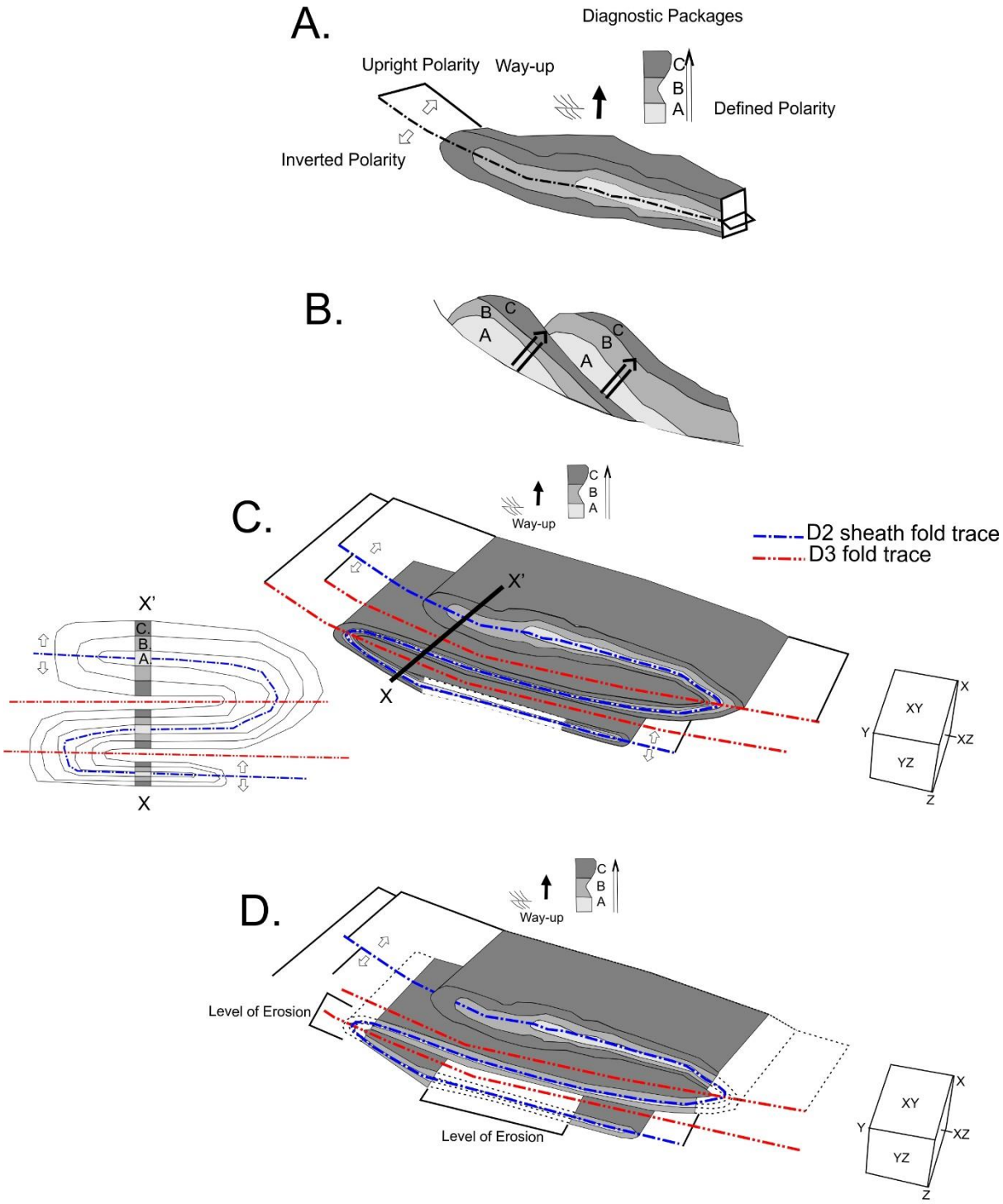

Figure 2. 3: The structural relationship between diagnostic packages identified in the field and the defined stratigraphic polarity, which can be coincidental with the direction of younging. Figure A: Represents an isoclinal fold illustrating the structural effects on the stratigraphy in the overturned limb. Figure B: The effects on the stratigraphy associated with thrust duplications/fold nappes. Figure C: The effects on the stratigraphy associated with the refolding of earlier sheath folds. Figure D: Depicts the erosion which occurs on the flanks and hinge zones of these highly folded structures. Diagram A & B modified after Colliston et al., 2012.

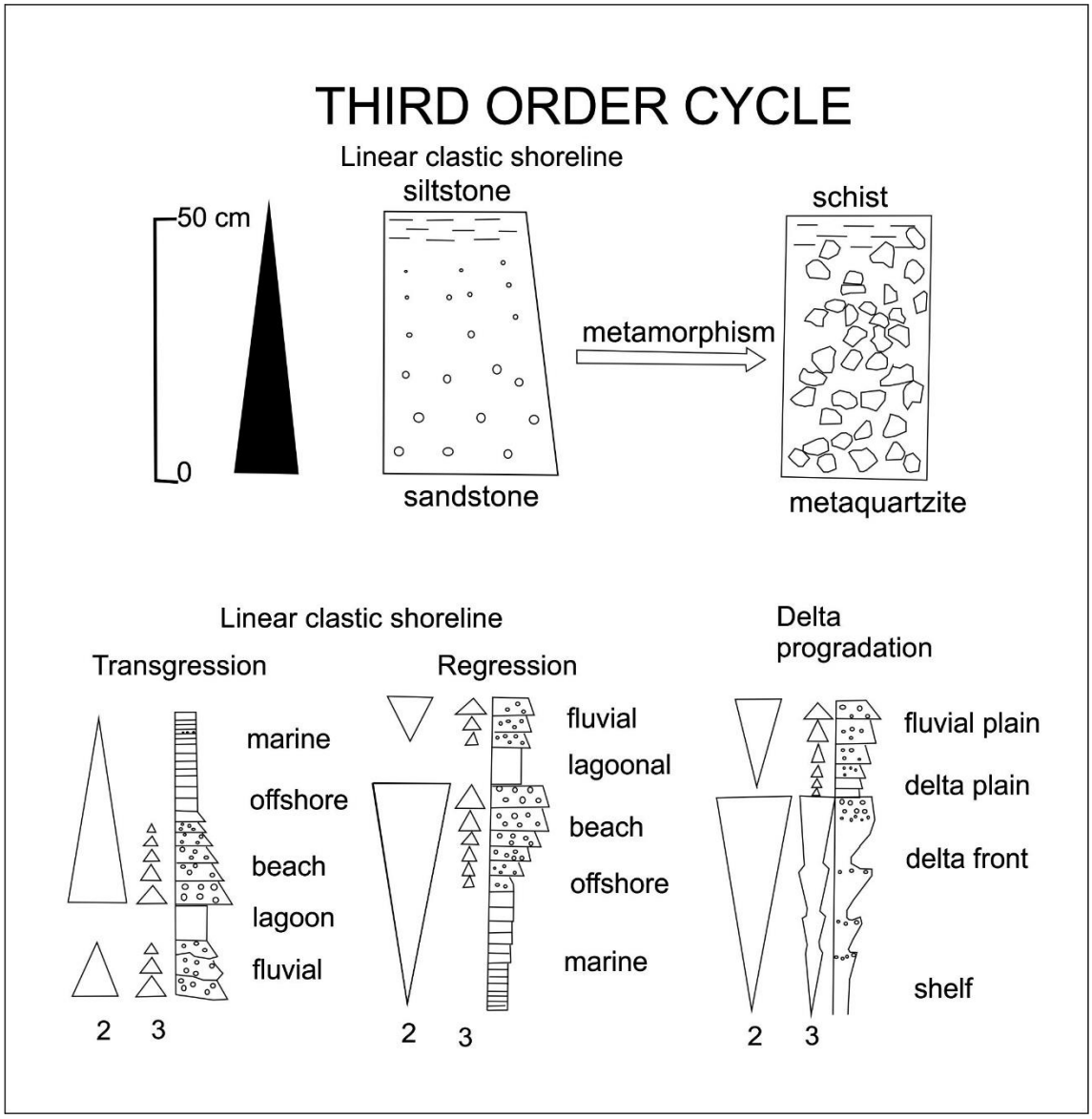

Figure 2. 4: Diagram represents the retention of primary relationships in spite of metamorphism and the various upward coarsening and upward fining 2nd and 3rd order cycles (centimetre to metre scale) enabling the depositional orientation and younging direction (Praekelt and Schoch, 1997). The upper diagram represents quartzite-schist relationships prevalent in the rocks under discussion and were derived from the original precursor mudstone-sandstone relationships. The lower diagram illustrates the second and third order sedimentological cycles which can still be recognized in diagnostic stratigraphic packages and aid in the stratigraphic interpretation associated with metamorphic meta-sedimentary environments.

2.2 Structural Domains

The eastern Aggeneys Terrane can be subdivided into four prominent structural domains that represent intra-terrane thrust sheets as indicated in Figures 2.1 and Figure 2.5. The structural domain classification is based on the distribution of sheath fold nappes within the thrust sheets/structural domains and the various plutonic rocks that surrounded them. The distribution of sheath fold nappe structures are structurally controlled, and have their own stratigraphic assemblages. The order of stacking of these different intra-terrane thrust sheets/structural domains and stratigraphic assemblages is based upon the southwesterly

tectonic overthrust direction for the terranes (Colliston et al., 1991 and references therein). Each sheath fold nappe structure is defined by a stratigraphic sequence that is grouped into successions based on lithological similarities (Figure 2.5). The structural domains are grouped and defined as follows:

- Structural Domain 1 (Witkoppies Structural Domain): The Witkoppies Structural Domain is defined by five stratigraphic sequences (Figure 2.5), which have supracrustal sequences that have a meta-volcanic nature, different from the stratigraphic Wortel Formation rocks identified in the west (Figure 2.2). The Vaalputs Suite (comprising of variations in plagioclase-quartz feldspar gneisses) envelops the sheath fold nappe structures in the Witkoppies Domain.
- Structural Domain 2 (Samoep Structural Domain): Is defined by the well foliated medium grained quartz-feldspar that extends for kilometres across the study area. This domain hosts no supracrustal sequences.
- Structural Domain 3 (Lekdam Structural Domain): Defined by 15 stratigraphic sequences that are enveloped within by the coarse grained quartz-feldspar Lekdam Gneiss. The stratigraphic sequences associated with the Lekdam Structural Domain, have assemblages similar to that of the Wortel Formation
- Structural Domain 4 (Houmoed Structural Domain): Defined by 3 stratigraphic sequences enveloped within the Achab Suite, that comprises of large variations of quartz-feldspar augen gneiss.

Out of the four structural domains, only structural domain 1, 3 and 4 contain sheath fold nappe structures, while structural domain 2 contains none. The stratigraphic sequences and plutonic rocks related to all four structural domains (Figure 2.2), together with the stratigraphy of various isolated structures toward the south and east will be discussed in the ensuing chapters; descriptions related to the plutonic rocks occurring in each structural domain as well as adjacent inter-terrane thrust contacts will be discussed in sections 2.3 to 2.6. A short discussion on the various supracrustals within the structural domains and adjacent structures is given in sections 2.7 to 2.11.

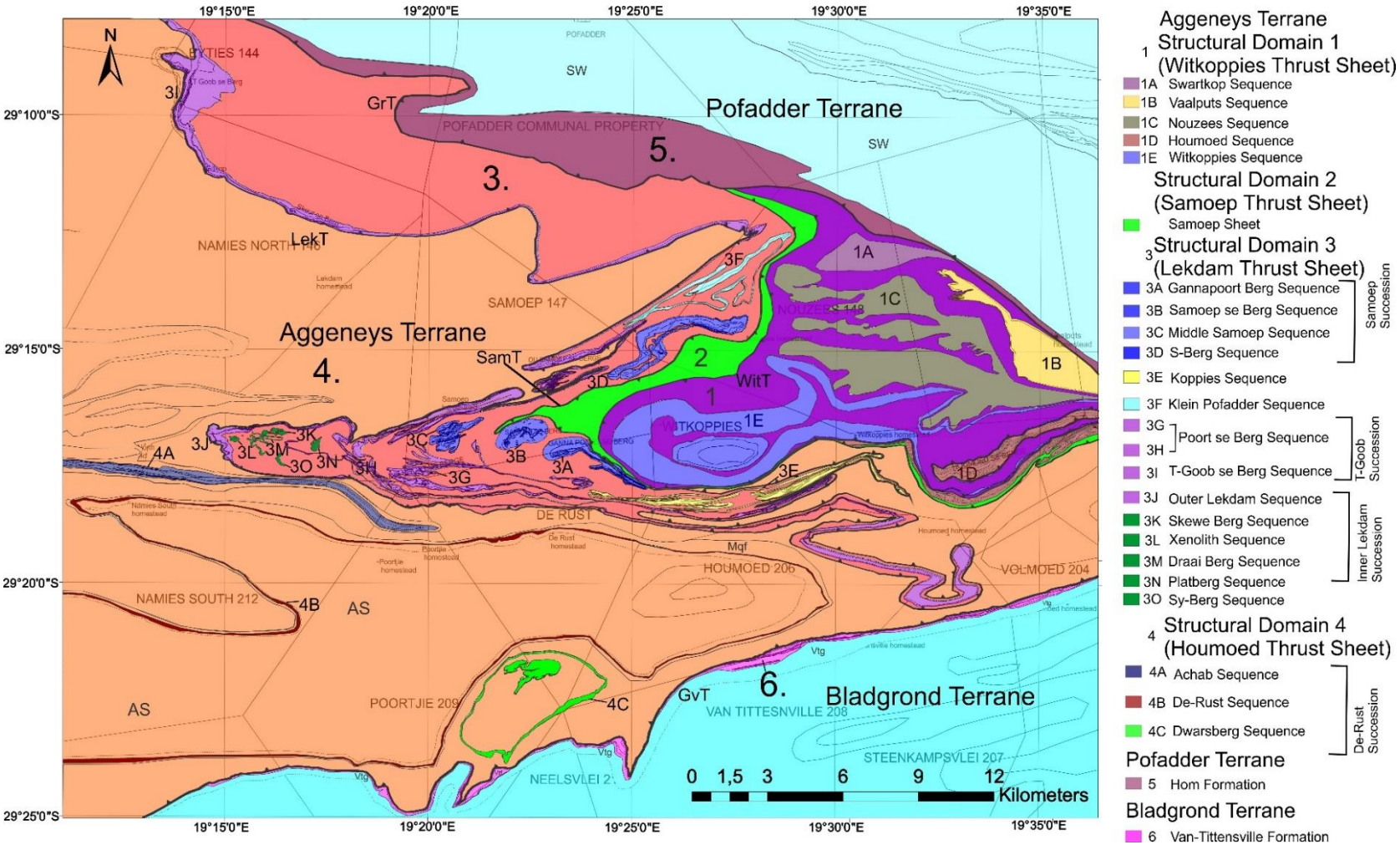

Figure 2.5: Simplified geological map showing the distribution and classification of the four main Structural Domains in the eastern part of the Aggeneys Terrane, defining large intra-terrane thrust sheets. Structural Domain 1 (purple) represents the Witkoppies thrust sheet with its associated sheath fold structures (1A-E). Structural Domain 2 (green) represents the Samoep thrust sheet. Structural Domain 3 (red) represents the Lekdam thrust sheet with its associated fold structures (3A-3M). Structural Domain 4 (orange) represents the Houmoed thrust sheet with its associated structures (4A-C) (Grt: Groothoek Thrust; Gvt: Geelvloer Thrust; LekT: Lekdam Thrust; SamT: Samoep Thrust, WitT: Witkoppies Thrust).

2.3 Plutonic Rocks

During the regional mapping, seven prominent meta-plutonites were identified regionally throughout the study area (Figure 2.6 A). Five major gneissic meta-plutonites were identified within the Aggeneys Terrane, namely the Vaalputs Suite (hosts large variations), Samoep Gneiss, Lekdam Gneiss, Achab Suite (hosts large variations), and Namies Gneiss. Another two prominent gneisses were identified on the inter-terrane thrust contacts, namely the Swartmodder Gneiss was identified within the Pofadder Terrane, and the Van-Tittensville Gneiss identified for the Bladgrond Terrane. Mapping of these gneisses showed that they were in strike continuity to the Groothoek Thrust and Geelvloer Thrust contacts, and are located adjacent to both inter-terrane thrust boundaries (Figure 2.6 A). The relevant field characteristics associated with each gneiss will be discussed in detail in the section below.

Within the Aggeneys Terrane, the various plutonites define distinct structural domains. The Vaalputs Suite defines the base of Structural Domain 1, the Samoep Gneiss defines Structural Domain 2, the Lekdam Gneiss Structural Domain 3, and the Achab Suite defines Structural Domain 4. All four structural domains are separated by three distinct intra-terrane thrust contacts, namely, the Lekdam, Samoep and Witkoppies Thrusts (Figure 2.6 B). The Groothoek Thrust and Geelvloer inter-terrane thrust contacts are found in the north and south of the study area, adjacent to the four distinct structural domains (Figure 2.6 B).

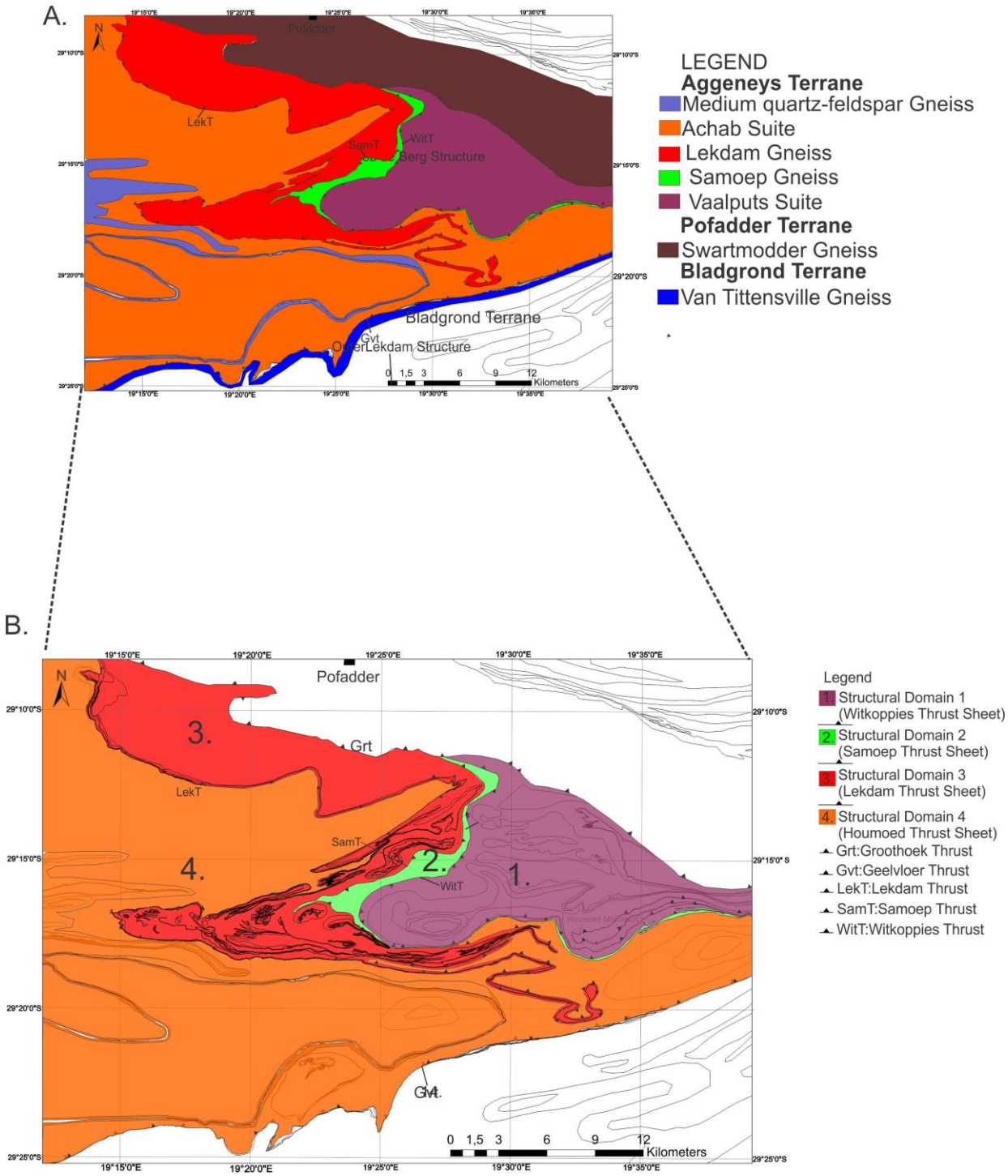

Figure 2.6: Distribution of all the plutonic units throughout the study area and their relationship to the major structural domains/intra-terrane thrust sheets. A: Depicts the distribution of the different plutonic rocks associated with each intrastratigraphic terrane. B: Depicts the association of the main plutonic units with the various intra-terrane thrust sheets and their sub-division into prominent structural domains. The associated inter- and intra-terrane thrusts are also represented (Grt: Groothoek Thrust; Gvt: Geelvloer Thrust; LekT: Lekdam Thrust; SamT: Samoep Thrust, WitT: Witkoppies Thrust).

2.4 Plutonic Rocks: The Aggeneys Terrane

2.4.1 The Vaalputs Suite

The distribution of the Vaalputs Suite is controlled by the geometry of Structural Domain 1 (Witkoppies Structural Domain; Figure 2.7). Maclaren (1988) mapped this intrusive unit as the megacrystic quartz-feldspar gneiss, recording variations in K-feldspar augen sizes. Varying percentages of quartz (30%), K-feldspar (40%), plagioclase (20), and biotite (10%) were identified for this specific rock type (Maclaren, 1988). The author has defined this intrusive unit as a “suite” rather than a single granitic gneiss. This is due to the large textural variations seen across Structural Domain 1. The Vaalputs Suite, although not defined geochemically, has banded, coarse grained and porphyritic textural variations, with different augen sizes seen throughout Structural Domain 1, representing different granitic gneiss variations which form part of the Vaalputs Suite, similar to the variations of grey and pink gneisses seen in the Gladkop Suite toward the far west of the study area (van Aswegen, 1983). The Vaalputs Suite is therefore broadly defined as quartz-K-feldspar-plagioclase gneisses with banded, coarse and porphyritic variations seen across Structural Domain 1. Foliation, predominantly of biotite, often inter-leaved between the various augen, which consists of K-feldspar.

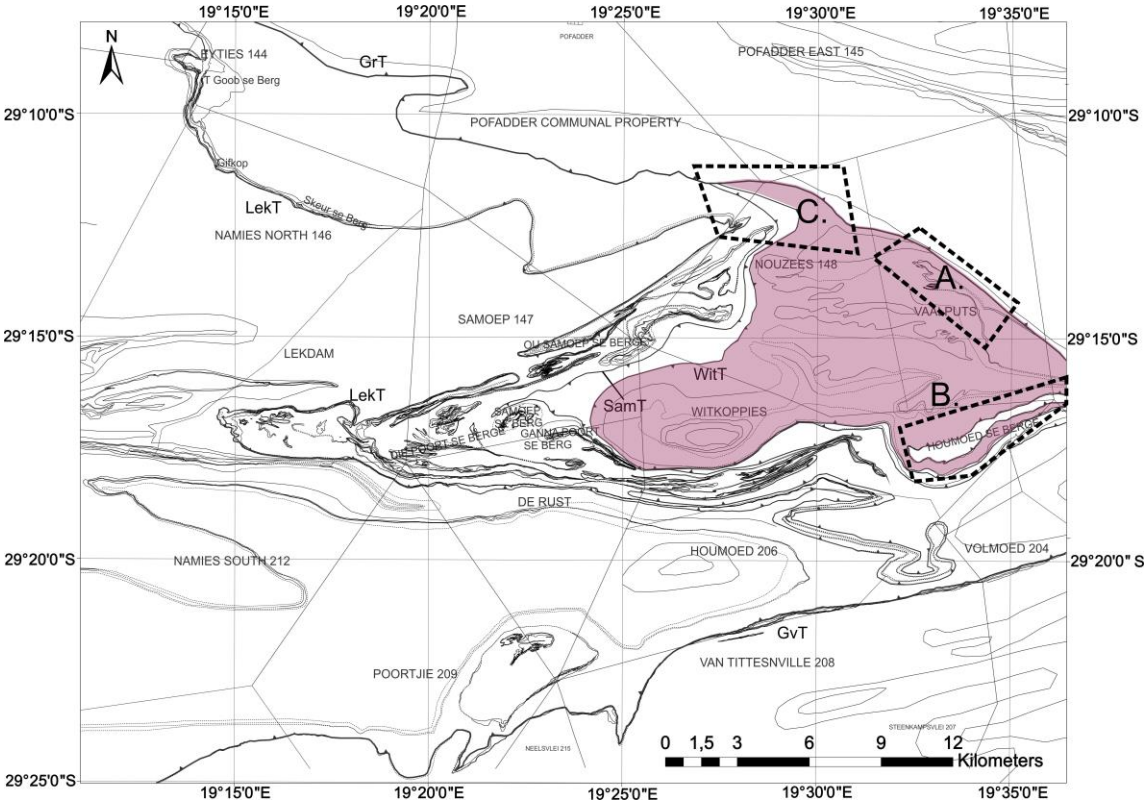

Figure 2.7: Distribution of the Vaalputs Suite throughout the study area in purple. A: Shows the distribution of the Vaalputs Suite close to the Groothoek Thrust, where the Vaalputs gneiss becomes highly mylonitic and deformed due to later stages of deformation. B: Shows the Vaalputs Suite folding within the Houmoed Mountains. C: Location of a prominent branch point, where the Witkoppies thrust sheet (Structural Domain 1) cuts out against the Groothoek Thrust (Grt: Groothoek Thrust; Gvt: Geelvloer Thrust; LekT: Lekdam Thrust; SamT: Samoep Thrust; WitT: Witkoppies Thrust).

The Vaalputs Suite is often recognized by its distinctive ‘porphyroblastic-megacrystic’ appearance and variation of K-feldspar augen (Figure 2.8). Augen sizes vary from between 1-15 centimetres at certain locations. The Vaalputs Suite can be prominently observed on the farms Vaalputs, Nouzees 148, and Witkoppies .On the farm Vaalputs, closer to the Groothoek Thrust the Vaalputs Suite becomes highly mylonitic due to later D6 shearing effects and is very difficult to recognize in the field at certain locations (Figure 2.7 A). Mylonite bands of between 5 to 15 centimetres can be observed at certain locations. The Vaalputs Suite can be easily confused with the adjacent Swartmodder Gneiss due to both plutonites having augen. However, the Swartmodder Gneiss has an abundance of amphibole whereas the Vaalputs Suite variations do not, and contain more plagioclase than the Swartmodder Gneiss.

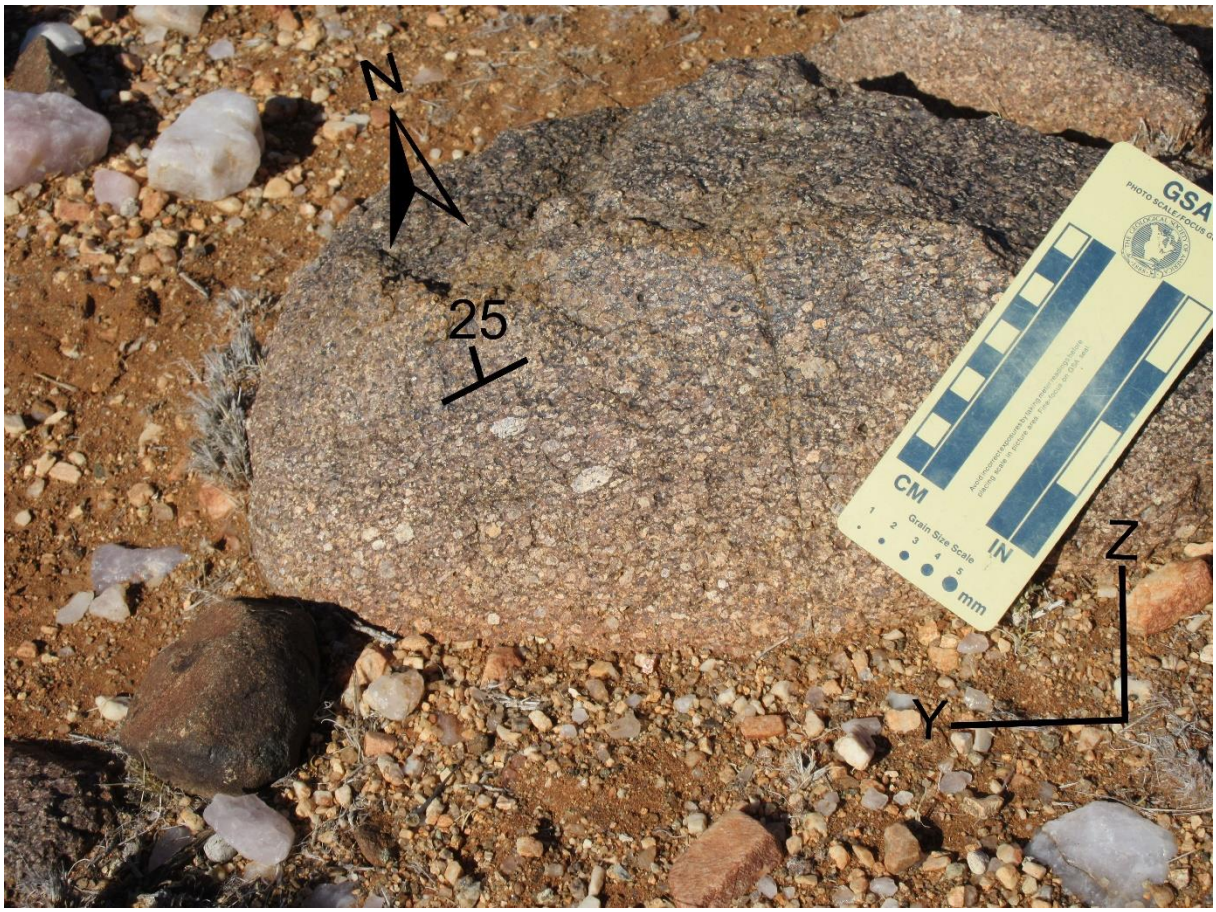

Figure 2.8: Variation in K-feldspar Porphyroclasts associated with the Vaalputs Suite. The porphyroclasts vary between 1 and 4 centimetres from left to right within this outcrop, which is a definitive characteristic associated with the Vaalputs Suite.

The Vaalputs Suite also carries xenoliths of calc-silicates, biotite gneiss and amphibolites associated with the Witkoppies Sequence, as well as the various metavolcanic/metasedimentary units it encloses toward the east (Figure 2.9 A and B). A wide variety of xenoliths were also encountered by Maclaren (1988). The Vaalputs Suite folds with the Witkoppies Sequence within the Houmoed Mountains and extends further toward the east,

where it extends subparallel to the Groothoek Thrust (Figure 2.7 B). The contact between the Vaalputs Suite and Samoep Gneiss is sharp and defines the intra-terrane Witkoppies Thrust which forms a branch point on the farm Nouzees against the Groothoek Thrust in the north (Figure 2.7 C). The textural variation in K-feldspar and plagioclase augens is a dominant characteristic associated with the Vaalputs Suite, with large variable percentages of biotite (5-15%) and plagioclase minerals (5-10%).

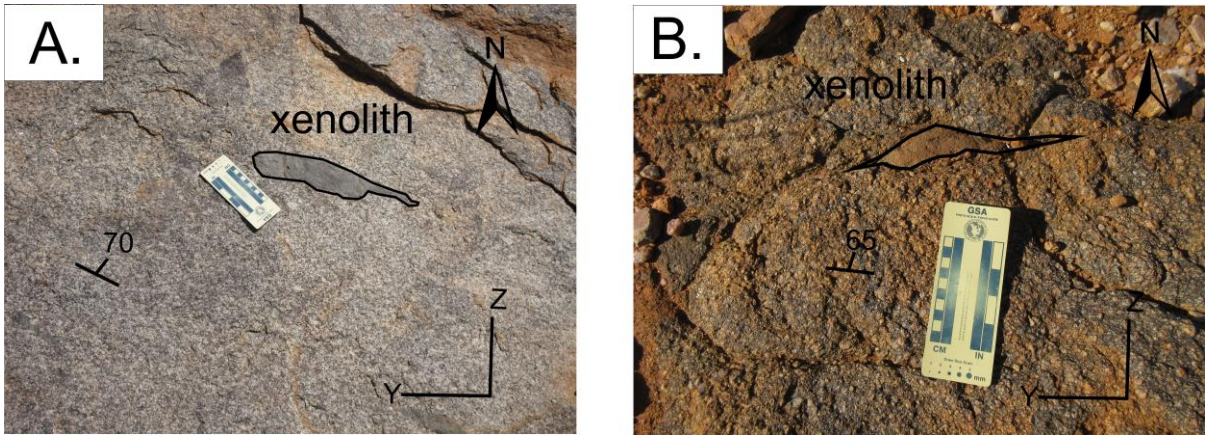

Figure 2.9: Different xenoliths found within the Vaalputs Suite. A represents a xenolith of calc-silicates associated with meta-sedimentary units found at Nouzees, exposed on the YZ foliation plane. B represents xenoliths of biotite gneiss associated with the Witkoppies Suite on the Farm Witkoppies, exposed on the YZ foliation plane.

2.4.2. The Samoep Gneiss

The Samoep Gneiss extends from the Houmoed Mountains in the south to Nouzees 148 in the north where it cuts out and forms a branch point against the Groothoek Thrust (Figure 2.10 A); it represents Structural Domain 2. The best exposures of this gneiss can be seen on the farm Samoep where large bodies of this medium to fine grained quartz-K-feldspar gneiss can be seen adjacent to the Samoep se Berg fold (Figure 2.10 B). This granitic gneiss has a prominent reddish-pink appearance in the field and gives a red-brownish appearance when weathered. The Samoep Gneiss folds within the Gannapoort-Berg fold structure (Figure 2.10 C) and around the Houmoed Mountains, and is wedged in between the Witkoppies Structural Domain, Lekdam Structural Domain, and Houmoed Structural Domain toward the east.

Texturally the Samoep Gneiss is a homogeneous medium to fine grained, poorly to well banded quartz-feldspar gneiss ±biotite and plagioclase. Nowhere within the study area were any xenoliths found in this gneiss. The homogeneous character of the Samoep Gneiss is evident throughout, with prominent foliation bands of biotite (Figure 2.11 A), close to the Witkoppies thrust contact. This prominent regional foliation can also be seen in the proximity of the Houmoed Mountains (Figure 2.11 B) and certain outcrops close to the contacts with the Samoep and Witkoppies thrusts.

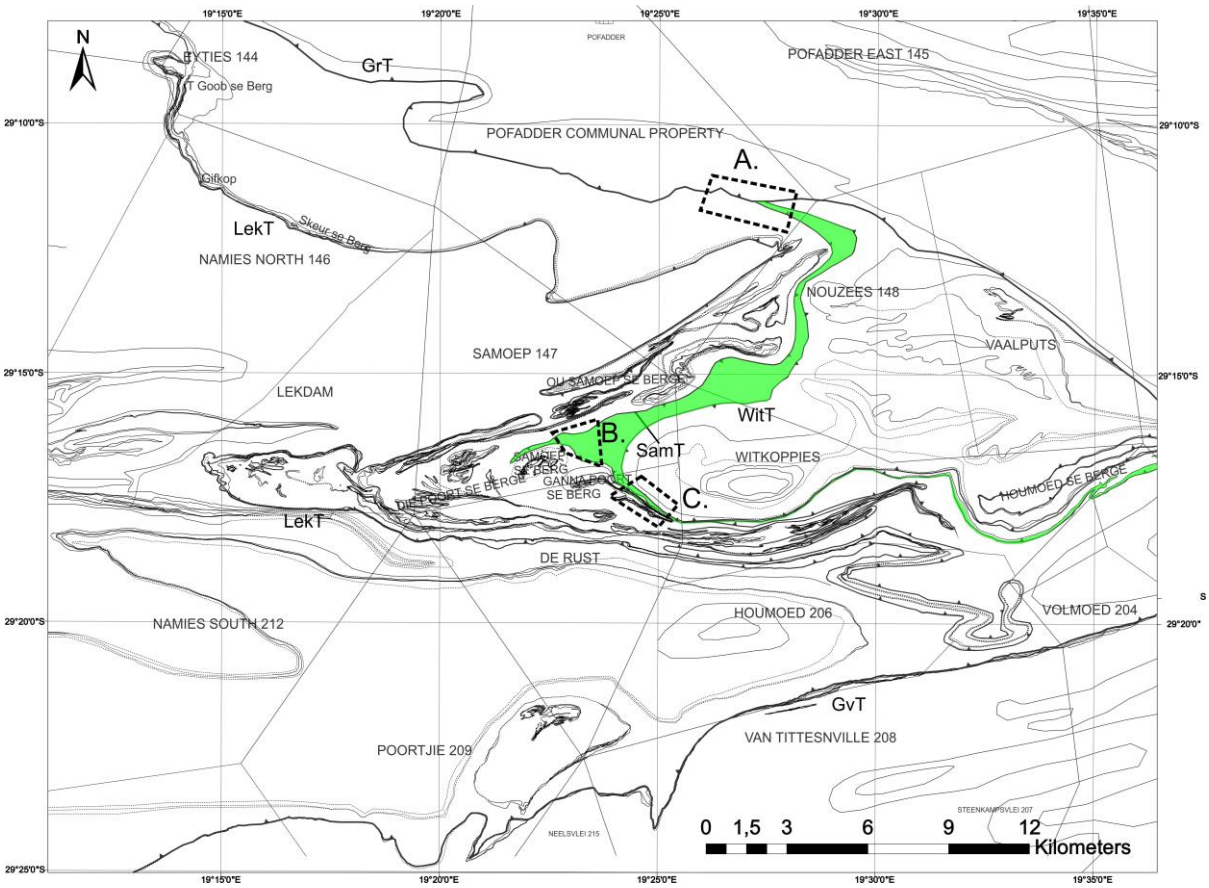

Figure 2.10: Distribution of the Samoep Gneiss throughout the study area in green. A: Shows the Samoep Gneiss (Structural Domain 2) forming a branch point with the Groothoek Thrust. B: Represents the best exposure of the Samoep Gneiss adjacent to the Samoep se Berg structure. C: The zone where the Samoep Gneiss folds within the Gannapoort Berg sheath fold structure (Grt: Groothoek thrust; Gvt: Geelvloer thrust; Lek T: Lekdam thrust; SamT (Samoep thrust); WitT (Witkoppies thrust).

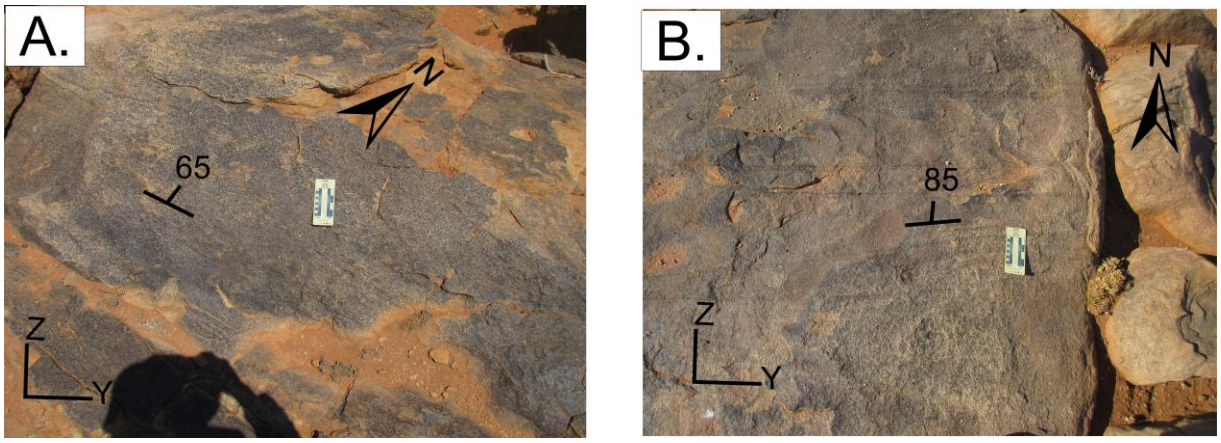

Figure 2.11: Image A: Outcrop of the Samoep Gneiss in which a prominent biotite foliation can be observed. Image B: Development of a prominent foliation, also defined by biotite, seen in the proximity of the Houmoed Mountains. Within both diagrams can the prominent biotite bands be observed on the YZ planes of the foliation.

2.4.3 The Lekdam Gneiss

The distribution and extension of the Lekdam Gneiss are controlled by the shape of Structural Domain 3 (Figure 2.12). Interbanded within the thrust sheet is series of meta-sediments that can be correlated to the Wortel Formation (Praekelt and Schoch, 1997) in the west. The Lekdam Gneiss is host to all the structures within Structural Domain 3 and folds with all the structures contained within. This gneiss also intrudes all the metasedimentary units it surrounds and contains xenoliths of almost all the supracrustal rocks related to the Lekdam Thrust Sheet (Figure 2.13 A and B). The regional distribution of xenoliths within the Lekdam Gneiss varies from centimetre to decametre scale and is defined by quartzite, biotite-sillimanite schist, and biotite gneiss. The most prominent exposure of xenoliths can be seen in Figure 2.12 A in the Samoep se Berg and Gannapoort Berg region.

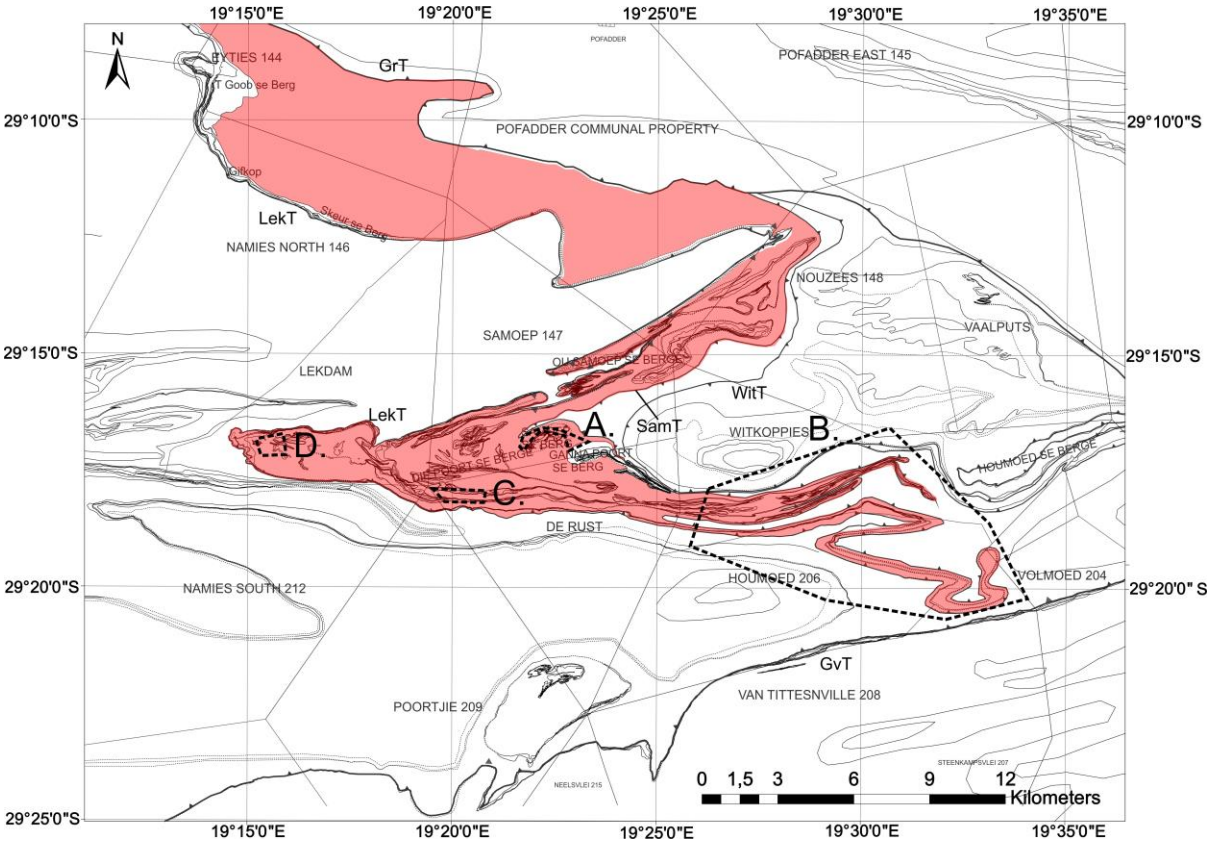

Figure 2.12: Distribution of the Lekdam Gneiss in the study area in red. A: Zone showing the folding of the Lekdam gneiss (Structural Domain 3) with the associated metasedimentary units. B: Best exposure of the garnet-bearing variations of the Lekdam Gneiss within the Poort se Berg sheath fold structure. C: Another zone exposing the garnet variations of the Lekdam Gneiss (Grt: Groothoek Thrust; Gvt: Geelvloer Thrust; LekT: Lekdam Thrust; SamT: Samoep Thrust; WitT: Witkoppies Thrust).

The Lekdam Gneiss has a sharp contact with the Achab Suite, specifically in the south of the structure where the Lekdam Gneiss is present in the lower extension of the T Goob se Berg sheath fold. Toward the southwest and southeastern sections of Structural Domain 3, the Lekdam Gneiss can be seen folded together with the supracrustal rocks and cuts out against the medium-quartz-feldspar Samoep Gneiss in the south (Figure 2.12 B). Toward the

northeast, outside the study area, it is deduced that the Lekdam Gneiss folds and branches out against the Groothoek Inter-Terrane Thrust. The Lekdam Gneiss often sits on the footwall side of the Groothoek Thrust, with the Hom meta-volcanic's and Swartmodder Gneiss sitting in the hanging wall, defining an inter-terrane thrust contact to the northeast and west outside of the study area.

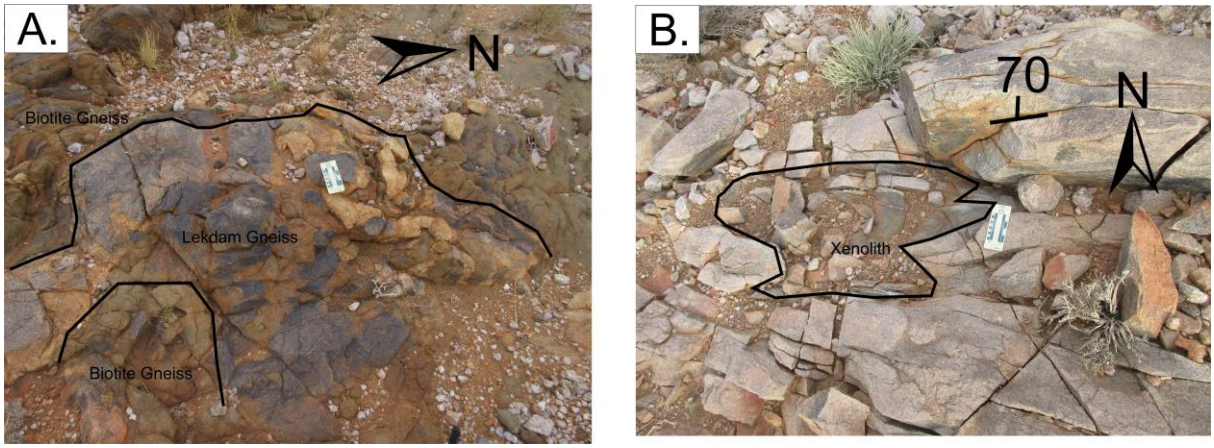

Figure 2.13: Xenoliths in the Lekdam Gneiss. A: Depicts the Lekdam Gneiss intruding within a thick package of biotite gneiss at Samoep se Berg. B: Lekdam Gneiss containing xenoliths of biotite gneiss at Gannapoort Berg. Both locations in Image A and B can be viewed in the Samoep se Berg and Gannapoort Berg region in Figure 2.11 A.

In outcrop, the Lekdam Gneiss has a greyish appearance that weathers to reddish-brown and has a poorly developed foliation, comprising of biotite and muscovite. It is defined as a medium to coarse-grained quartz-feldspar gneiss ± amphibole, ± garnet, muscovite and biotite. The most distinguishing characteristic of this gneiss is the sporadic occurrence of garnet (Figure 2.14), which can be seen at various localities throughout the Lekdam Thrust Sheet. The most prominent outcrops occur in the centre of the Poort se Berg structure (Figure 2.12 C) and the thick succession of garnet-bearing gneiss on the inner portion of the Lekdam thrust sheet on the inside of the farm Lekdam (Figure 2.12 D). The garnet porphyroclasts vary in size from between 1 centimetre up to 4 centimetres in certain localities. The garnets postdate the regional fabric associated with the Lekdam gneiss. The garnet crystals can be seen growing over the regional foliation in the Lekdam Gneiss and are interpreted as late syntectonic to post-tectonic growths.

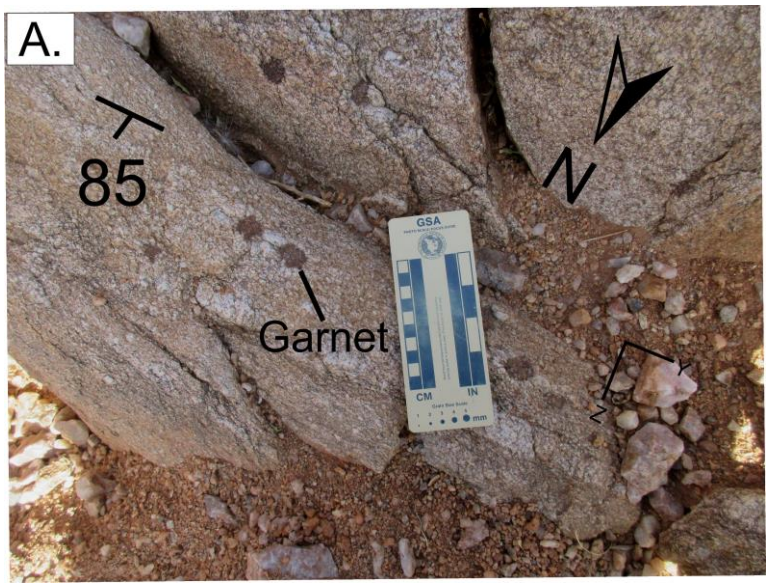

Figure 2.14: Large garnet minerals (1-4 centimetres in diameter) with feldspar halos, found within the Lekdam Gneiss.

2.4.4 The Achab Suite

The Achab Suite, formally known as the Achab Gneiss, covers the largest portion of the study area and extends from west to east across the entire study area (Figure 2.15). It represents Structural Domain 4 (The Houmoed Thrust Sheet). The Achab Suite areas have been given "suite" status by the author due to its large compositional variation across the study area, similar to variations seen in the Vaalputs Suite (p.21), Gladkop Suite (van Aswegen, 1983) and the Vioolsdrif Suite (Colliston and Schoch, 2006). The Achab Suite has been mapped in detail by Pretorius (1986). However, he named the variations within the Achab Suite as separate granite gneisses e.g. The Achab Gneiss, Springputs Gneiss, and the Koupsleegte Gneiss, owing to their leucocratic variations and different percentages of biotite. They can be grouped as a suite due to their field relationships, as they all have feldspar augens with percentage variations in biotite within zones of lower strain, and also have a prominent foliation or banding in zones of high strain, and intrusive relationships with the associated supracrustals (Pretorius, 1986). A section of the Achab Suite was mapped by Watkeys (1986) who interpreted it to represent the basement to the upper supracrustal successions, due to its wide distribution, and was interpreted to intrude a "pre-Bushmanland" sequence. This, however, was disputed by Colliston et al. (2012) as xenoliths associated with the Wortel Formation have been found within the Achab Suite in the Aggeneys Hills and Gamsberg area.

The portion of the Achab Suite mapped by Pretorius (1986) was interpreted to constitute quartz, plagioclase, and K-feldspar, with accessory biotite and amphibole, with grain sizes varying from coarse to medium. Minerals like cordierite, spheen, zircon, allanite, apatite and rutile have also been identified within variations of the Achab Suite. In the study area, the

Achab Suite has a heterogeneous character, due to variations in strain across the study area. This is observed as a change in shape of The K-feldspar augen, from 1-8 cm, and to highly flattened augen forming prominent leucobands (Figure 2.16 A and B). Together with these leucobands prominent foliation bands of biotite are often observed (Figure 2.16A). Good examples of this are seen specifically in the T Goob and Skeur se Berg areas. The biotite foliation often wraps around the K-feldspar porphyroblasts, good examples occur on the farm Namies South 212 or within the central portion of the De Rust structure (Fig 2.15 A, B, and C).

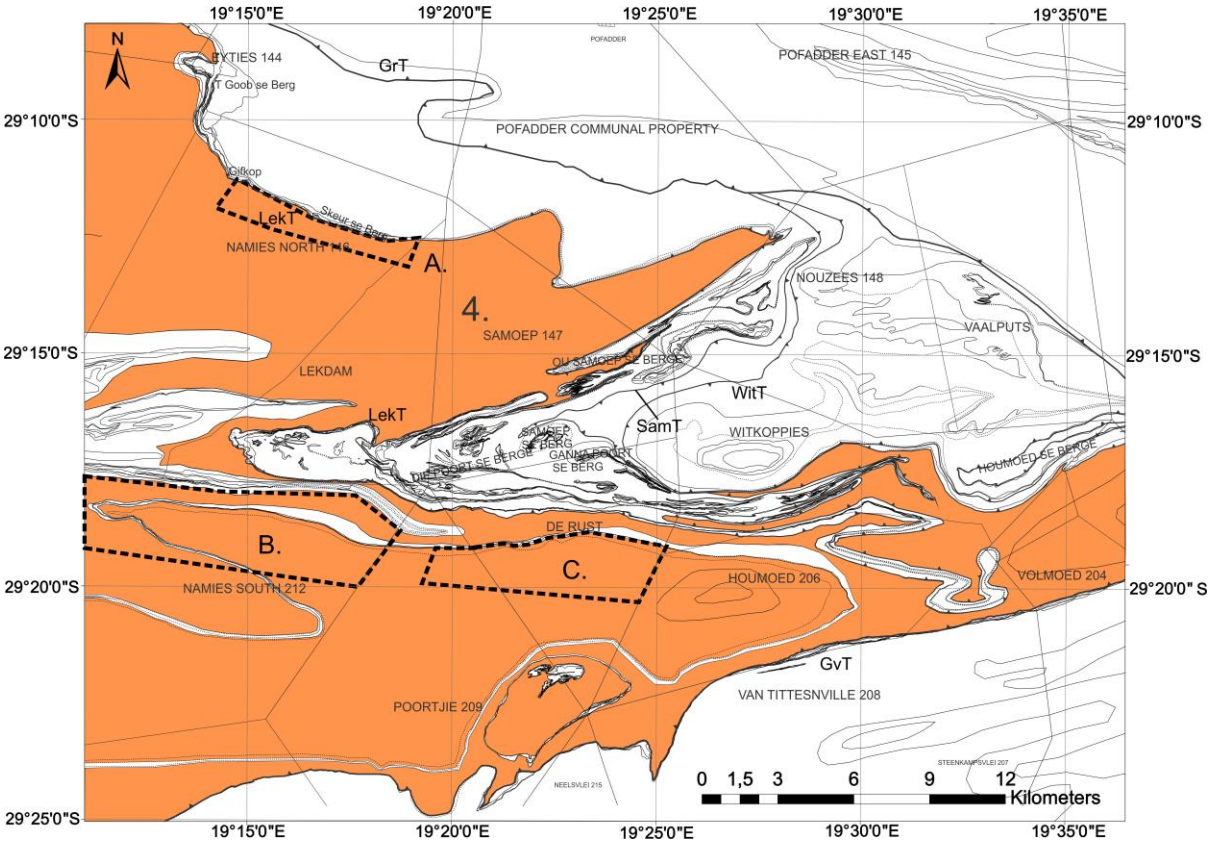

Figure 2.15: Distribution of the Achab Suite in the study area in orange. A: The best exposures are associated with the Achab Suite at the base of Skeur se Berg. B: Best exposures of the Achab Suite on the farm De Rust. C: Best exposures of the Achab Suite on the inside of the De Rust structure (Grt: Groothoek Thrust; Gvt: Geelvloer Thrust; LekT: Lekdam Thrust; SamT: Samoep Thrust; WitT: Witkoppies Thrust).

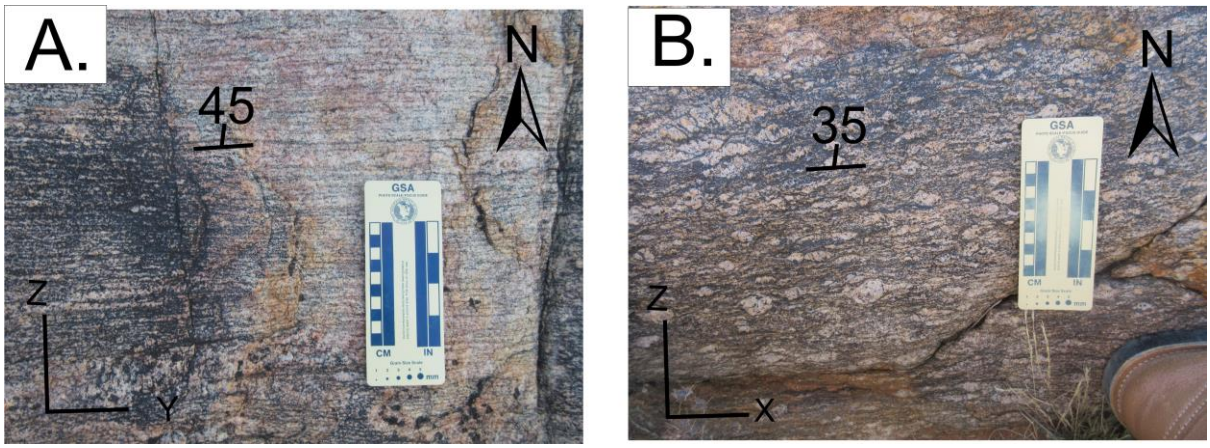

Figure 2.16: Strain variations in the Achab Suite associated with the feldspar augen on the YZ foliation planes. A: Represents a flattening of K-feldspar augen to form leucobands. Prominent foliation of biotite is also observed concerning the adjacent leuco-bands. B: Shows the less strained variation of the feldspar augen. Prominent biotite foliations can be seen enveloping the feldspar augen on the XZ foliation planes.

Irrespective of the heterogeneity of the Achab Suite, it is often identified in the field by an increase in biotite minerals and identification of large K-feldspar augens. More than often a prominent biotite foliation develops and is well represented in higher strain zones. A sharp contact is seen between the Achab Suite and the Lekdam Gneiss, specifically around the Outer Lekdam fold structure and certain portions of the Poort se Berg structure. The Achab Suite also has a migmatitic texture at certain locations, with the development of small metatexite melts associated, with melanosomes and plagioclase-quartz-rich leucosomes are observed (Sawyer, 2008). Concerning the Achab structure toward the west, the Achab Suite oftens has a sharp contact with the medium well-foliated medium quartz-feldspar Namies Gneiss, which envelopes most of the Wortel Formation supracrustal rocks west and south within the Houmoed Structural Domain. The Achab Suite and Samoep Gneiss extend toward the east on the southern side of the Houmoed Mountains, which is outside of the study area. Xenoliths of biotite gneiss, amphibolites and various quartzites can be observed throughout the entire study area. Best examples are seen at Skeur se Berg in the north, at the southern base of Achab se Berg, and in the central portion of the De Rust structure (Figure 2.17 A and B).

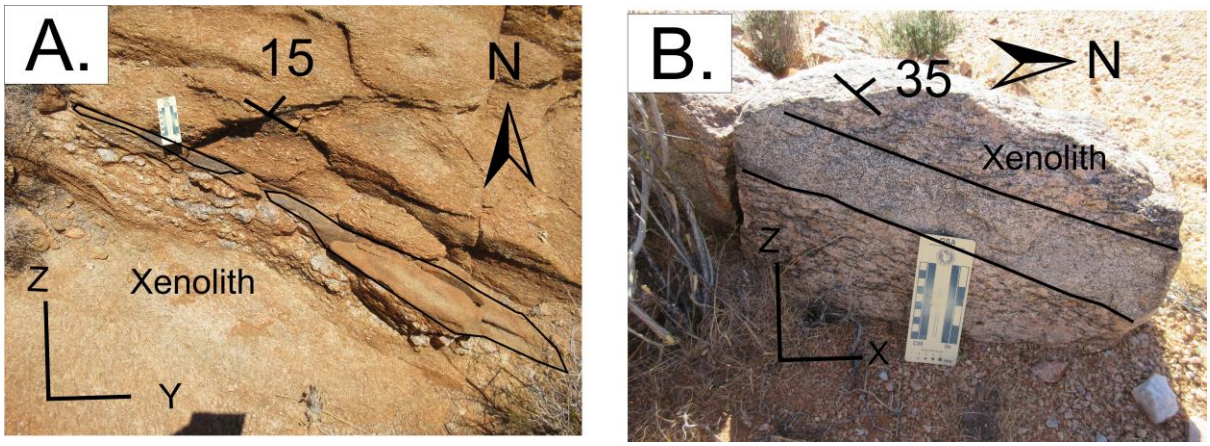

Figure 2.17: Xenoliths found within the Achab Suite A: Represents a xenolith of biotite gneiss within the Achab Suite at Skeur se Berg. B: Xenolith of a coarser quartz-feldspar gneiss found within the Achab Suite at the base of the Achab structure.

2.4.5 The Namies Gneiss

The Namies Gneiss is found within Structural Domain 4 and often folds with the associated supracrustal sequences (Figure 2.18). The Namies Gneiss has a sharp contact associated with the various supracrustal sequences and, as with the Samoep Gneiss, have a very prominent well-laminated foliation, often comprised of biotite at certain localities. In the study area, these gneisses are associated with the supracrustal sequences associated with the De-Rust structure and Achab se Berg structure (Figure 2.18). These prominent foliations are associated with high strain zones commonly close to contacts. Best examples are seen at the base and on the inside of Achab se Berg, and the outer rim associated with the De-Rust structure (Figure 2.18 A and B).

The Namies Gneiss is similar to the Samoep Gneiss and is often spatially associated with supracrustal sequences within the Houmoed Thrust Sheet. The Namies Gneiss often folded with most of the supracrustal sequences, and no xenoliths were observed in the mapped outcrop of the gneiss. The Namies Gneiss often displays a prominent banding and at stages has a homogenous character (Figure 2.19 A and B). Moore (1977) and Watkeys et al. (1988) often refer to these gneisses as leucogneisses, and are interpreted to have a rhyolitic character (Moore, 1977). At Achab se Berg and the De-Rust structure they often have a sharp contact with the lower more prominent Achab Suite. According to Colliston et al. (1986), these leucogneisses may be coeval to the lower Wortel Formation, associated with the basal succession of the Bushmanland Group.

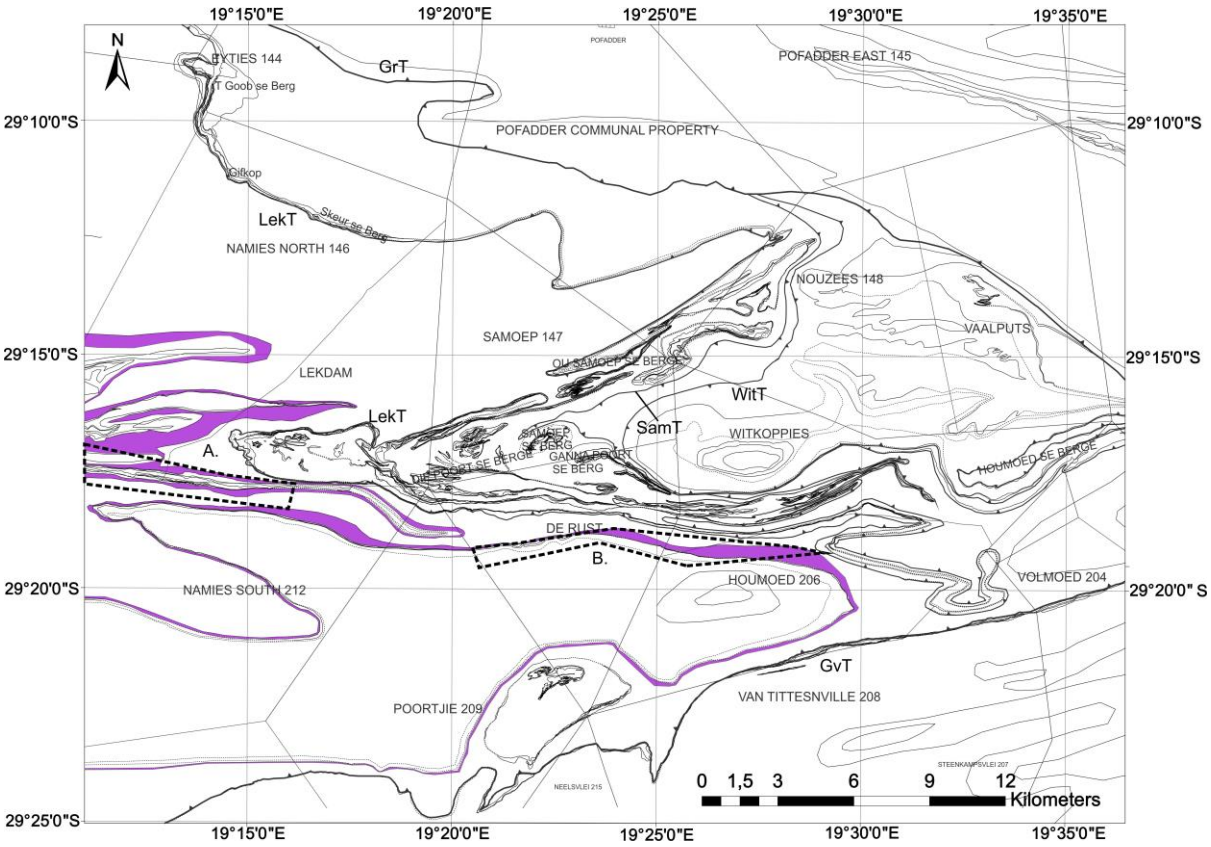

Figure 2.18: Distribution of the Namies Gneiss throughout the study area in purple. A: The zone where the Namies Gneiss is best exposed at Achab se Berg. B: Another zone within the study area where the Namies Gneiss is best exposed around the De-Rust structure (Grt: Groothoek thrust; Gvt: Geelvloer thrust; LekT: Lekdam thrust; SamT: Samoep thrust; WitT: Witkoppies Thrust).

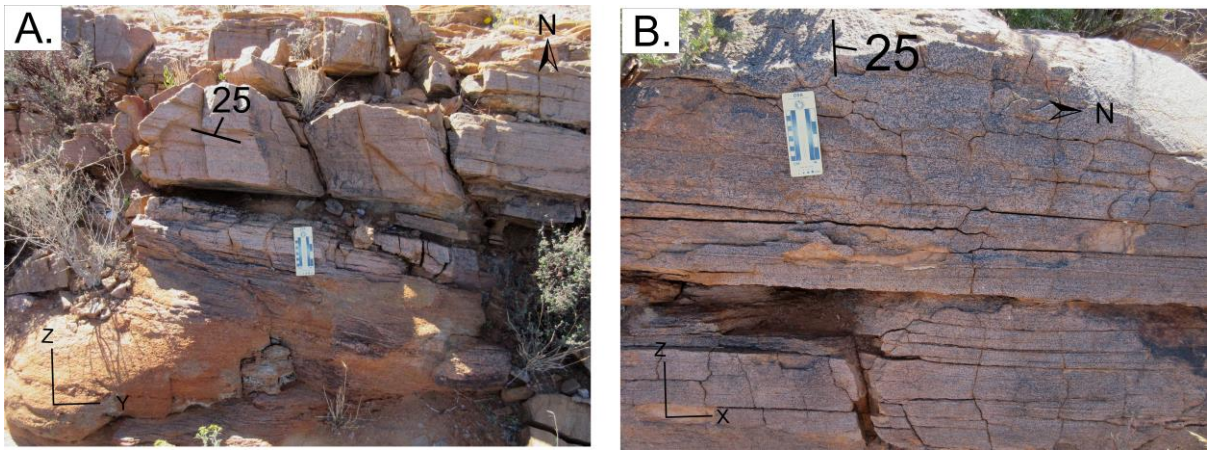

Figure 2.19: Lithological features associated with the Namies Gneiss. A: Prominent banding is seen within the Namies Gneiss on the YZ foliation plane. B: Prominent banding seen in the Namies Gneiss on the XZ foliation plane. The Namies gneiss has a homogenous character throughout the study area. No xenoliths were found associated with this gneiss.

2.5 Plutonic Rocks: The Pofadder Terrane

2.5.1 The Swartmodder Gneiss

The Swartmodder Gneiss previously mapped by Pretorius (1986) as the Pella Augen Gneiss is defined as a well-foliated medium to coarse-grained quartz-feldspar-biotite-hornblende augen gneiss. The Swartmodder Gneiss is confined within the Pofadder Terrane and it lies adjacent to the Hom Formation (Colliston et al., 1991), which defines the Groothoek Thrust contact with the Aggeneys Terrane (Figure 2.20). In the study area, the Swartmodder Gneiss, together with the Hom Formation, can be traced along strike from west to east and consequently also following the Groothoek Thrust between the Pofadder and Aggeneys Terranes. The best exposures within the study area can be seen just south of the town of Pofadder (Figure 2.20 A). Various xenoliths of the Hom Formation, Tsams Formation, and varieties of the Kabis Gneiss have been recorded in the Swartmodder Gneiss (Colliston and Schoch, 2006). In the study area, mostly xenoliths of biotite gneiss related to the Hom Formation were observed (Figure 2.21). The Swartmodder Gneiss extends up to the Pella and Matheus Gat Mountains and extends laterally outside the study area toward the east along the Groothoek Thrust contact (Figure 2.20 B).

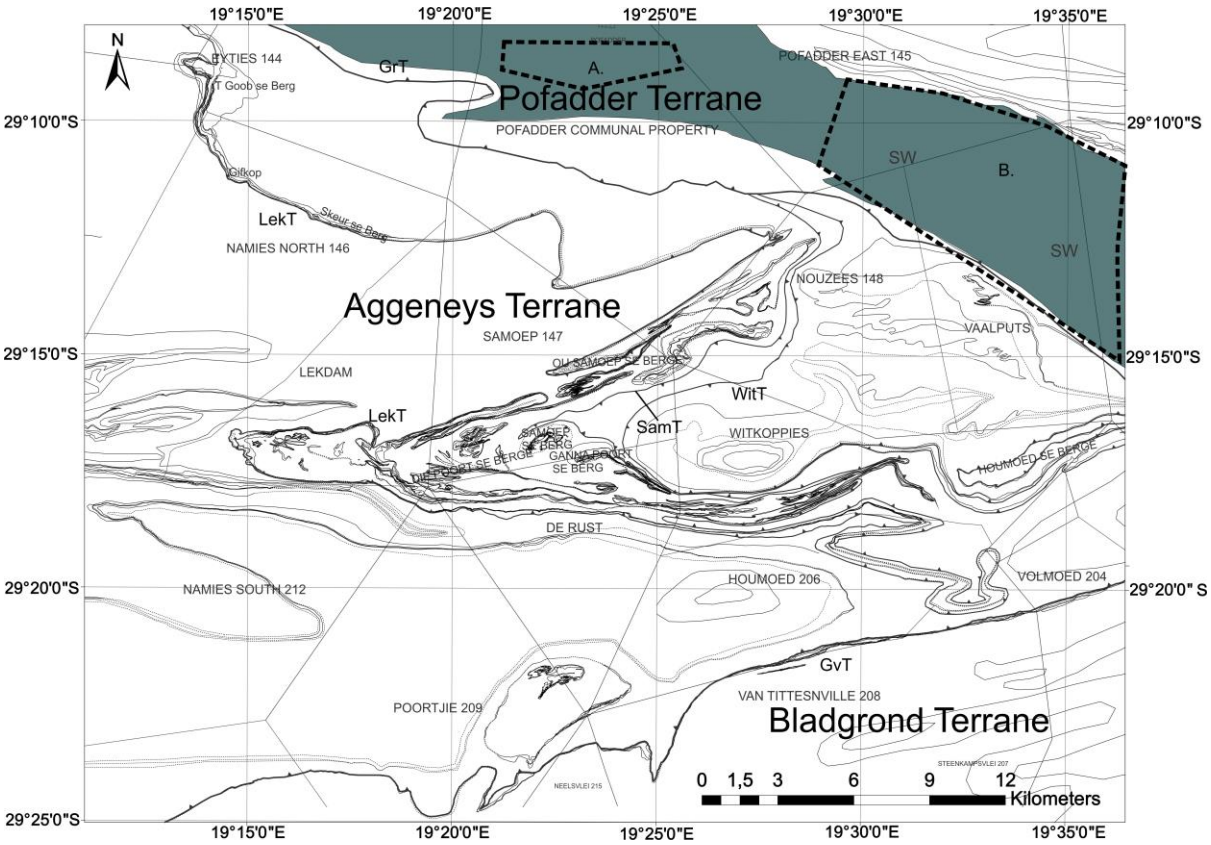

Figure 2.20: Distribution of the Swartmodder Gneiss in the adjacent Pofadder Terrane in green. A: Best exposure of the Swartmodder gneiss south of the town of Pofadder. B: Continuation of the Swartmodder Gneiss adjacent to the Groothoek Thrust toward the east (Grt: Groothoek Thrust; Gvt: Geelvloer Thrust; LekT: Lekdam Thrust; SamT: Samoep Thrust and WitT: Witkoppies Thrust).

Figure 2.21: Xenolith of biotite gneiss associated with the Hom Formation within the Swartmodder Gneiss.

The Swartmodder Gneiss weathers to a grey-brownish colour, and augens vary in size from 3 to 7 millimetres. Closer toward the Groothoek Thrust contact, and further on towards the southeast, the Swartmodder Gneiss exhibits a prominent mesoscopic banding or foliation, often represented by biotite. Augens flatten (Figure 2.22 A) closer to the contact and foliations rotate toward the vertical due to regional east-west shearing deformation. Augen also flatten, and undergo grain size reduction and start to develop a mylonitic foliation at certain localities (Figure 2.22 B). Most of the outcrops close to the Groothoek Thrust have been affected by later shear deformation (D5-D6) parallel to the early foliation. Similar observations were made by Colliston (1990) and Colliston and Schoch, (2006) further toward the west. The Swartmodder Gneiss continues along the Groothoek Thrust further toward the east (Figure 2.20 B), till it terminates as a cut off against the Groothoek Thrust, or as a fold closure (this remains to be determined by more extensive mapping outside of the study area toward the east).

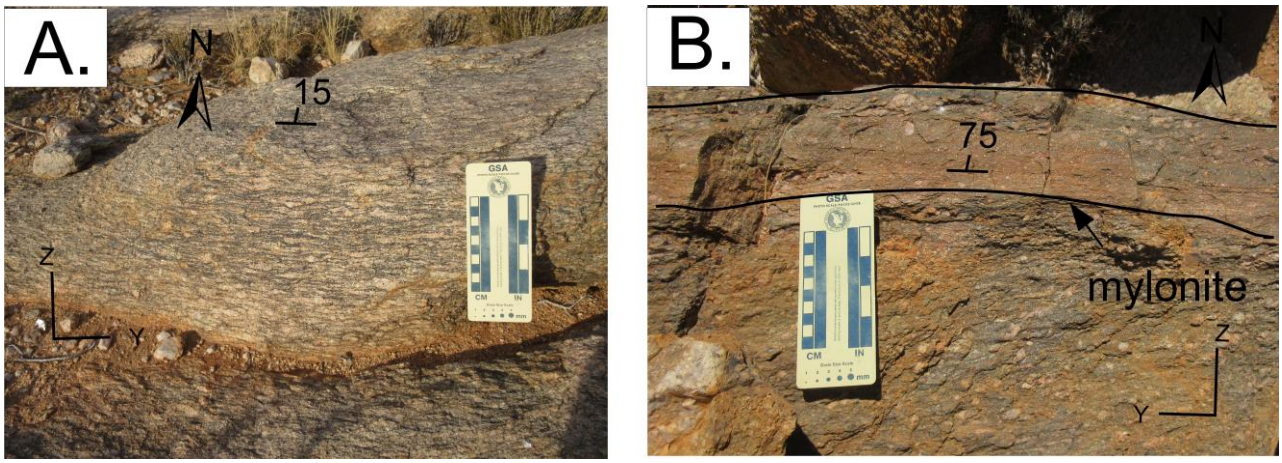

Figure 2.22: Outcrop characteristics seen within the Swartmodder Gneiss. A: Flattening of feldspar augen closer toward the Groothoek Thrust contact. B: Closer to the contact augen become smaller in size and start to form mylonitic bands.

2.6 Plutonic Rocks: The Bladgrond Terrane

2.6.1 The Van Tittensville Gneiss

The Van Tittensville Gneiss is confined to the Bladgrond Terrane and is situated at the base of the Van Tittenville Formation above which the Geelvloer Thrust contact is found (Figure 2.23.) The name is derived from the farm Van Tittensville 208 where some of the best exposures of this gneiss can be seen. The Van Tittensville Gneiss is found along strike on the Geelvloer Thrust contact and can be followed consistently for over 45 kilometers, and often has a sharp contact with the overlying supracrustal rock. This gneiss has been previously mapped by Joubert (1971) and Albat (1984) as a quartz-feldspar pink gneiss, leptynite and leptite. Agenbacht (2007) refers to it as the Lekkerdrink Gneiss. However, this gneiss has been broadly classified by the above mentioned authors and its textural variations and structural emplacement have not been considered. It is defined by the author as a quartz-feldspar--biotite augen gneiss (Figure 2.24 A), a prominent foliation defined by biotite wraps around K-feldspar augen. At localities, toward the east on the farms Van Tittensville 208 and Volmoed 204, the augen flatten, resulting in the development of a prominent biotite foliation, due to later D5 east-west shear deformation effects (Figure 2.24 B). Due to the extreme flattening at certain locations, the Van Tittensville gneiss shows a porphyritic to coarse appearance, and where the east-west shear effects are prominently seen, mylonites bands are prominently visible. Compared to the other augen gneisses identified throughout the study area, the Van Tittensville Gneiss has a more leucocratic appearance and has an absence of amphibole minerals.

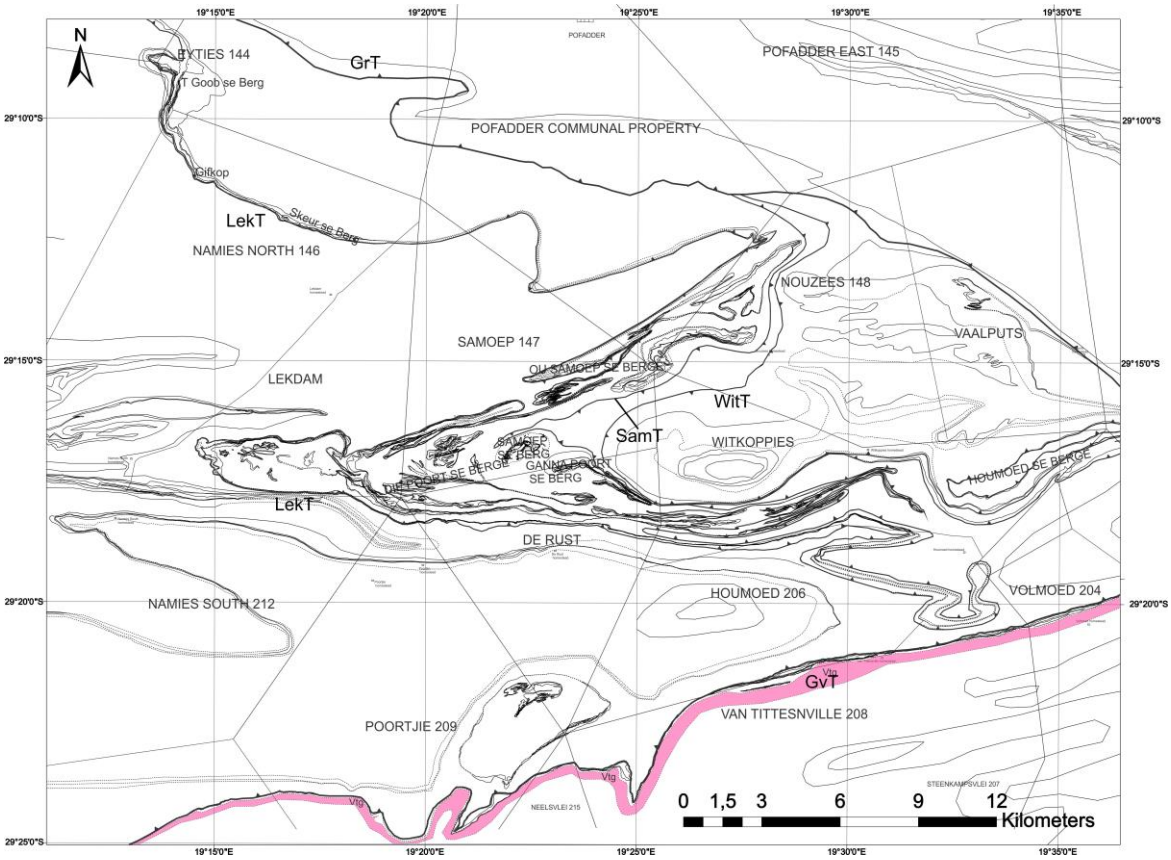

Figure 2.23: Distribution of the Van Tittensville gneiss (in pink) within the confines of the study area (Grt: Groothoek Thrust; Gvt: Geelvloer Thrust; LekT: Lekdam Thrust; SamT: Samoep Thrus and WitT: Witkoppies Thrust).

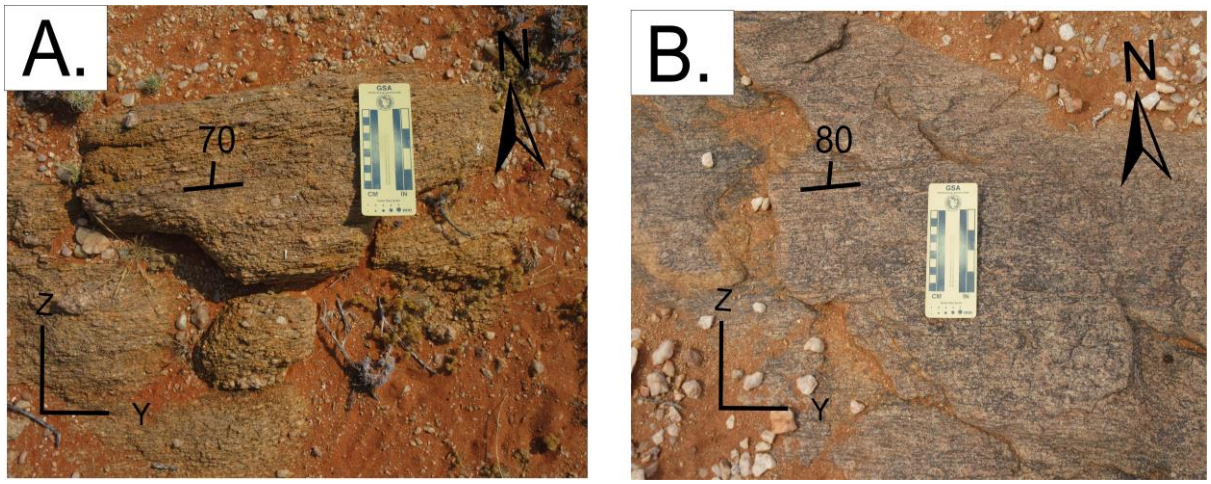

Figure 2.24: Image A: Represents the unstrained appearance of the Van Tittensville Gneiss, with prominent feldspar augen Image B: Represents the more strained variation of the VanTittensville Gneiss, augen flattening and the development of a prominent biotite foiliation.

2.7 Supracrustal Sequences

For this section, all the structural domains within the Aggeneys Terrane will be discussed in detail, together with the Hom Formation and Van Tittensville Formations, which are associated with the adjacent Pofadder and Bladgrond Terranes, and are structurally separated from the Aggeneys Terrane by the Groothoek and Geelvloer thrusts respectively (inter-terrane boundaries) (Figure 2.25). It is only within Structural Domain 1 (Witkoppies Structural Domain), that all the stratigraphic sequences will not be discussed and only the Witkoppies Sequence will be discussed. The other sequences such as the Houmoed, Nouzees, Vaalputs, and Swartkop Sequences will not be discussed in detail, as they fall outside the scope of this study (Figure 2.25).

A series of seventeen sequences will also be discussed in this section, fourteen of which are interbanded within the Lekdam Structural Domain, and three sequences interbanded within the Houmoed Structural Domain. The fourteen sequences within the Lekdam Structural Domain can be grouped into four main stratigraphic successions, which contain sequences having similar lithological characteristics (Figure 2.25). In the following Chapters, 2.8 to 2.11. The most emphasis will be placed on the Lekdam and Houmoed Structural Domains, due to their prominent Wortel Formation attributes (Figure 2.2).

For each structural sequence, the associated supracrustal rocks will be viewed in the form of a stratigraphic profiles constructed in key locations where the lithologies are well preserved. The stratigraphic profiles for each sequence will show the defined polarity (showing the diagnostic features for each sequence in the form of structurally controlled stratigraphic sequence defined by sequence mapping), key lithologies, and photographic descriptions found in Appendix 2.1-2.23. The different sequences will be described starting with the Witkoppies Structural Domain in the northeast, moving toward the Houmoed Structural Domain in the southwest. The order of description is based on the interpretation that the different structural/stratigraphic sequences were stacked on top of one another due to northeast to southwest overthrusting (Colliston et al., 1991), from the oldest to the youngest sequence. Therefore the Witkoppies Sequence (Figure 2.25 (1E)) will be described first, ending with the Dwarsberg Sequence in the Houmoed Structural Domain (Figure 2.25 (4C)). The final geological map is presented in Appendix 2.24.

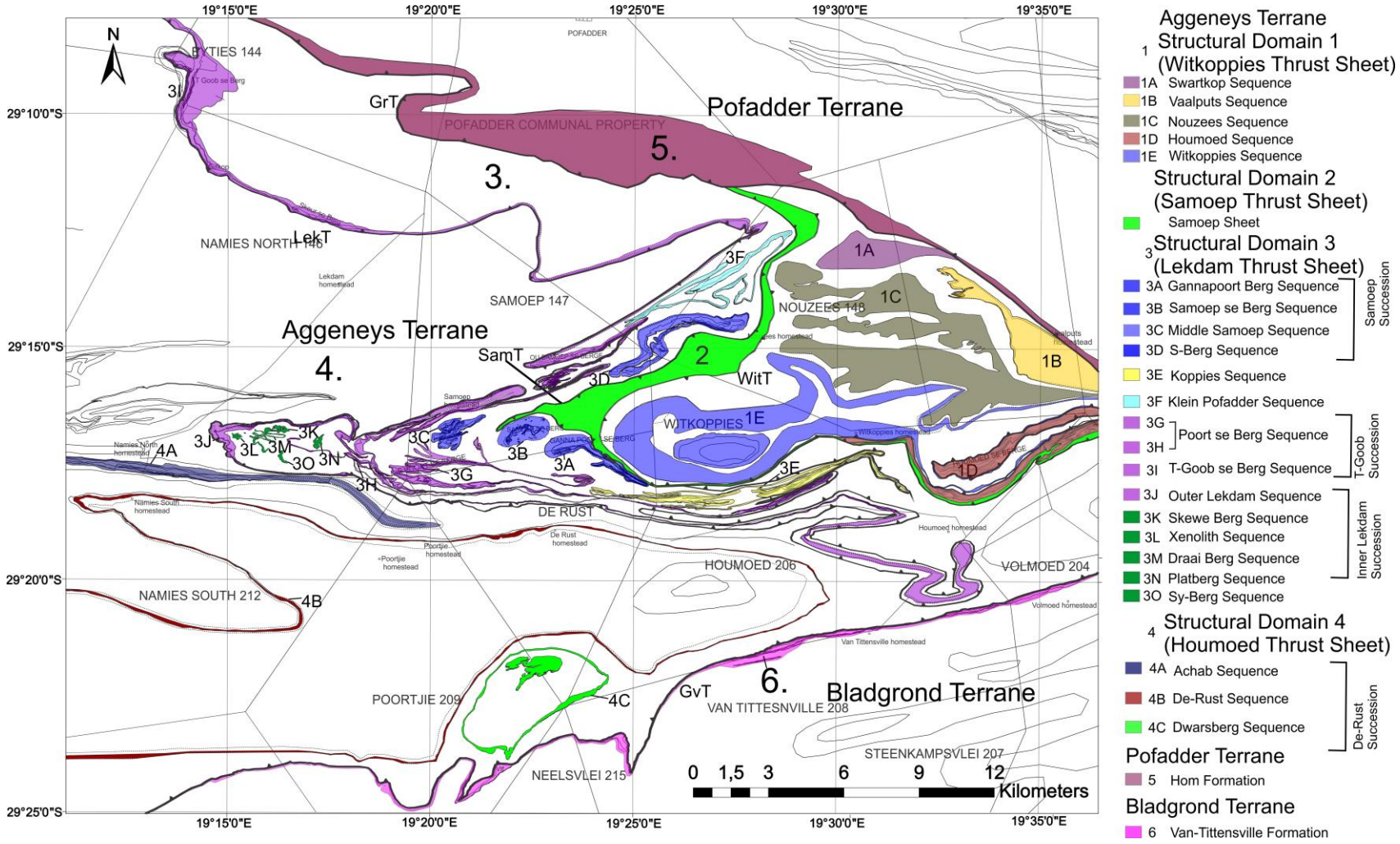

Figure 2.25: Distribution of all the supracrustal sequences in the eastern part of the Aggeneys Terrane. The supracrustal rocks have been divided into various tectonic successions, sequences, and formations with the various structural domains (Grt: Groothoek Thrust; Gvt: Groothoek Thrust; LekT: Lekdam Thrust; SamT: Samoep Thrust and WitT: Witkoppies Thrust).

2.8. The Witkoppies Structural Domain

2.8.1 The Witkoppies Sequence

The Witkoppies Sequence is confined to the Witkoppies Structural Domain (Structural Domain 1), with the Samoep Structural Domain (Structural Domain 2) and Lekdam Structural Domain (Structural Domain 3) located in the footwall of the sequence. It forms the central portion of the study area and defines a macro sheath fold with double vergence geometries (Figure 2.26 and Appendix 3.5). On the southeastern edge, the structural domain continues eastward running sub-parallel to the Groothoek Thrust. The Witkoppies Sequence is defined by thick units of medium to coarse biotite gneiss, calc-silicate rock variations, and amphibolite. The Vaalputs Suite intrudes throughout the entire succession (Chapter 2.4; Figure 2.7), both in the inner and outer segments of the succession. Due to the layered nature of the Witkoppies Sequence, it has been divided into two members, namely; the Outer Witkoppies Member and Inner Witkoppies Member, defining the inner and outer portion of the megascopic elliptical 'eye' fold structure (Figure 2.26).

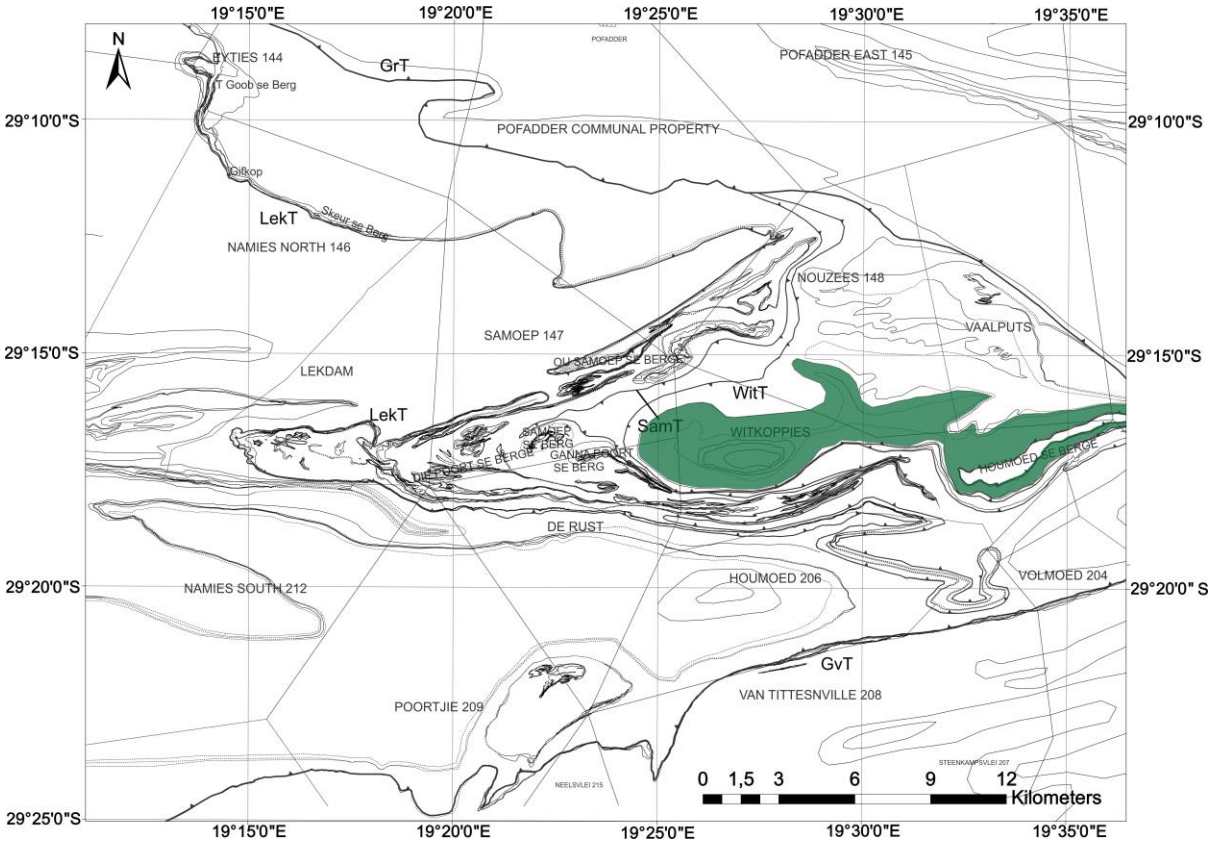

Figure 2.26: Distribution of the Witkoppies Sequence throughout the study area in green (Grt: Groothoek Thrust; Gvt: Geelvloer Thrust; LekT: Lekdam Thrust; SamT: Samoep Thrust and WitT: Witkoppies Thrust).

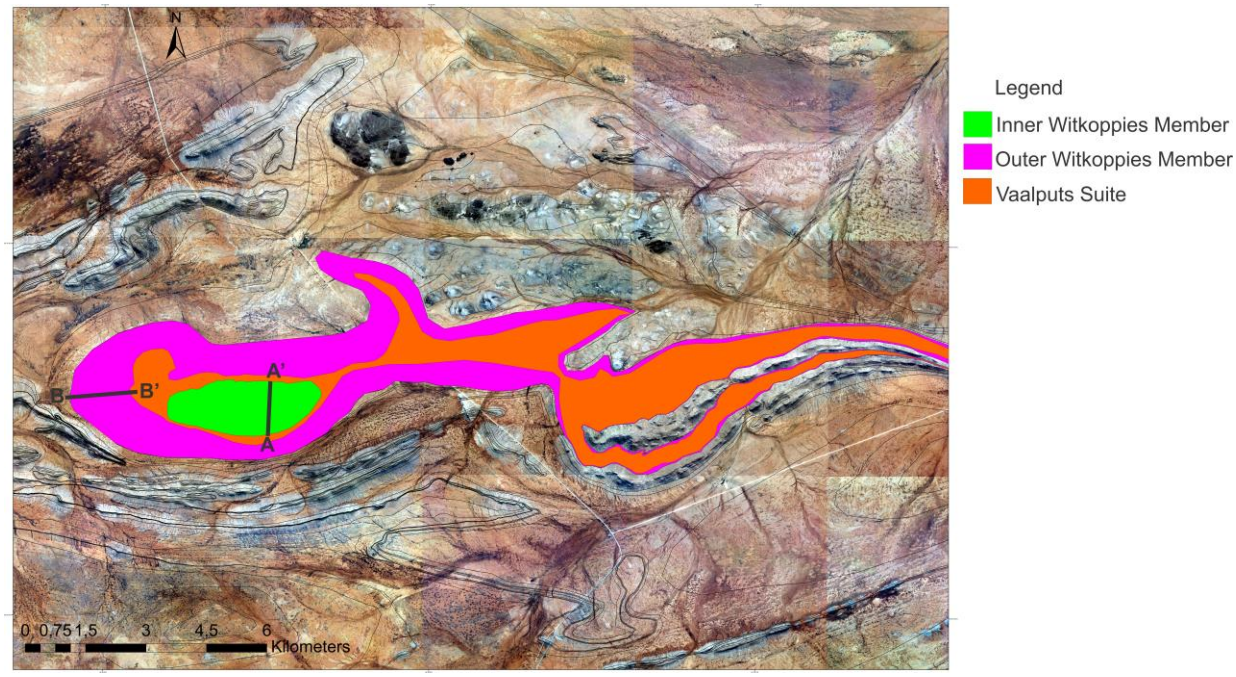

Figure 2.27: Distribution of the Outer (B-B') and Inner Witkoppies Members (A-A') together with the distribution of the Vaalputs Suite.

2.8.1.1 Inner Witkoppies Member

The more complete exposure of the Inner Witkoppies Member is found in the central portion of the structure and shown in profile A-A' (Figure 2.27). The Inner Witkoppies Member, as is the Outer Witkoppies Member, is surrounded by the Vaalputs Suite. The Inner Witkoppies Member extends for more than 580 meters, is poorly exposed in the north, but well exposed in the south. The Inner Witkoppies Member is dominated by thick portions of biotite gneiss, calc-silicate units, amphibolite, and actinolite bodies, which is intruded by the Vaalputs Suite. The basal portion of the succession is defined by a thick sequence of massive actinolite (Appendix 2.1 A and B), which has a grey-black appearance in the field. The actinolite body acts as a marker, along the edge of the Inner Sheath Member. Small sillimanite nodules occur within these actinolite bodies (Appendix 2.1 B).

Overlying the actinolite bodies higher up in the succession, black-banded calc-silicate rocks are found with interlayered light banded calc-silicate rocks. These banded variations appear migmatitic and are interlayered as zones of metatexite melts which are defined as segments of a rock that has undergone 1-20% melting, in which the paleosome (unmelted rock) is still visible (Sawyer, 2008). Feldspar leucobands, together with centimetre scale metatexite melts, are associated with both black calc-silicate rocks (Appendix 2.1 C) and light banded calc-silicate rocks. A higher frequency of leucobands associated with metatexite melts is observed in certain areas (Appendix 2.1 D). Further up in the succession fragments of massive, poorly bedded white calc-silicate rocks were found with interbanded sequences of biotite gneiss.

These white calc-silicate rocks often contain magnetite, garnet, and diopside minerals when not banded (Appendix 2.1 E). Toward the top of the succession the sporadic appearance of white massive calc-silcates is found, together with metre to centimetre scale amphibolite bodies (Appendix 2.1 F), which represents the top portion (central hinge of the structure) of the stratigraphic succession (Figure 2.28). Both in the north and south as you move out of the succession the augen-bearing Vaalputs Suite is found and contains xenoliths of calc-silcate rocks and biotite gneiss units associated with the Witkoppies Sequence. Throughout Profile A-A' it can be noted that stratigraphic sequences duplicate; this duplication is because the Inner Witkoppies Member defines an elliptical 'eye' structure. Therefore stratigraphic sequences duplicate due to macro-scale folding (Figure 2.28). The defined polarity associated with the Witkoppies Member is defined by large actinolite bodies at the base of the succession, overlain by black and white variations of calc-silicate rock, large sequences of biotite gneiss and centimetre to metre scale amphibolites, which represent the top of the stratigraphic sequence (Figure 2.28).

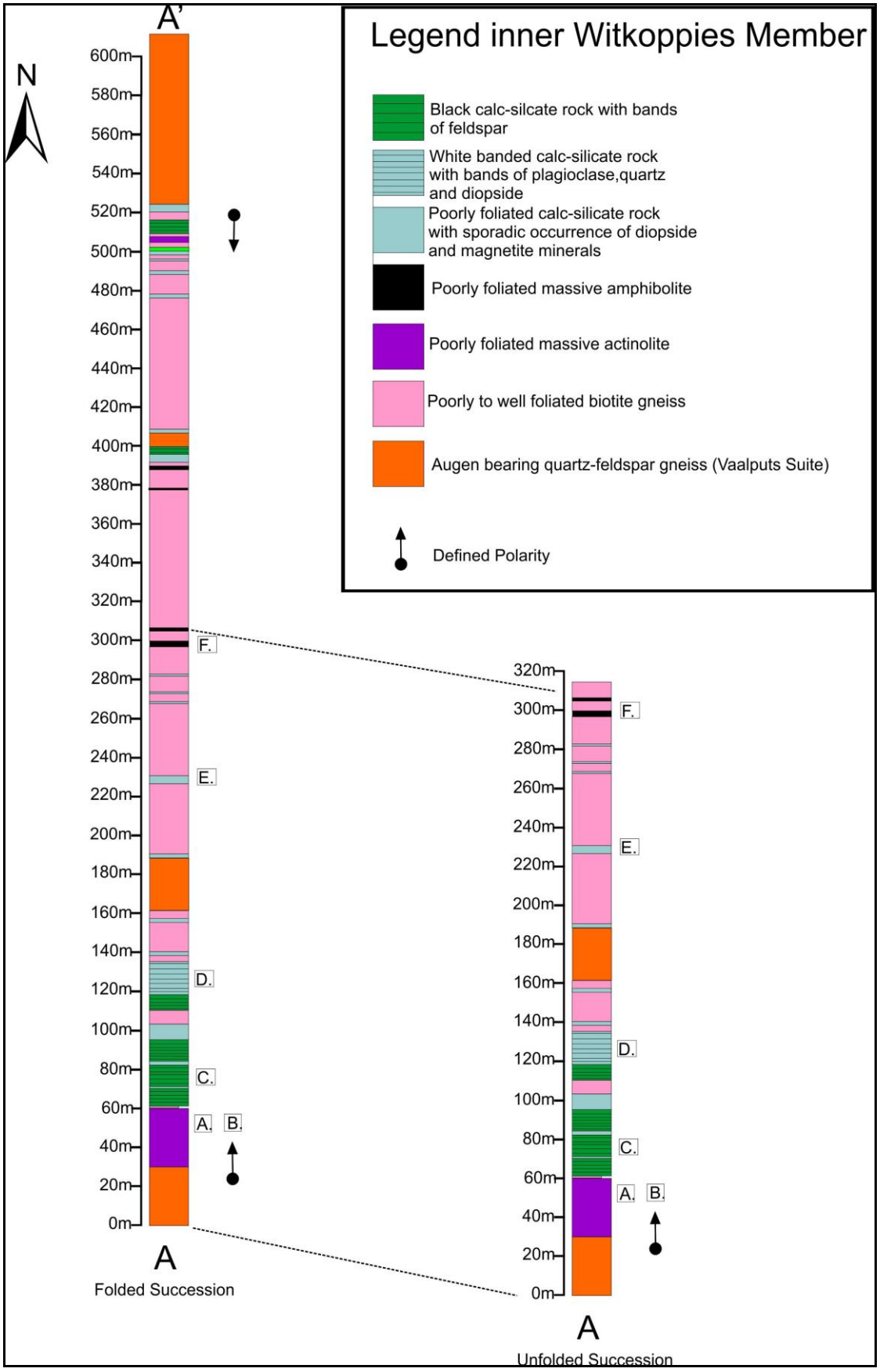

Figure 2.28: Profile A-A' (Figure 2.27): Stratigraphic succession associated with the Inner Witkoppies Member. The offset profile shows the unfolded succession. Letters A to F represent locations and photographs (Appendix 2.1).

2.8.1.2 The Outer Witkoppies Member

The Outer Witkoppies Member is very similar to the rocks associated with the Inner Witkoppies Member. The Outer Witkoppies Member constitutes thick portions of medium quartz-feldspar biotite gneiss (Appendix 2.2 A), black and white calc-silicate rocks, and amphibolite. The Vaalputs Suite separates the Inner and Outer Witkoppies Members. The best exposure of the Outer Witkoppies Member is seen in the far western portion of the structure and can be seen toward the northwest and west of the structure (profile B-B'; Figure 2.27 and Figure 2.29).The base of the succession is defined by the Vaalputs Suite, which also intrudes throughout the stratigraphic succession. A sharp contact is found with the Vaalputs Suite and the upper quartz-feldspar biotite gneiss.

Xenoliths of the biotite gneiss are also found within the Vaalpits Suite, as with the Inner Sheath Member. Small intercalated units of amphibolite, black-banded calc-silicate rocks (bands defined by feldspar), and white banded calc-silicate rocks (bands associated with biotite and amphibolite). Small lapilli clasts (quartz eyes) varying in diametres from 1 to 5 centimetres, are often associated with black banded calc-silicate and biotite gneiss rocks (Appendix 2.2 B). Another thick succession of biotite gneiss is found up to 60m thick, in which the foliation planes are well exposed. Overlying the biotite gneiss units, is a thick to thin succession of dark and light banded calc-silicate rocks, with banded units of amphibolite and biotite gneiss, which vary in thickness from between 0,3 to 4 metres occurs.

The calc-silicate rocks associated with the outer Witkoppies Member have 3 variations. The first is a massive, poorly bedded variation, with the sporadic occurrence of diopside and magnetite on the foliation planes, together with the occurrence of prominent epidote minerals, which give a greenish speckled appearance (Appendix 2.2 C). The second is defined by prominently laminated bands defined by biotite, amphibolite, and feldspar. This variation is associated with both the dark and white variations in calc-silicate rock (Appendix 2.2 D and E). The third variation is defined by leuco-bands/leucosomes of metatexite melts, which occur throughout the succession (Appendix 2.2 F). The metatexite bands are subparallel to the foliation bands and seem to post-date the foliation. A higher percentage of melt is associated with diatexites, which represent a rock with more than 20% melted material (Sawyer, 2008), also seen throughout on centimetre scale. The melts identified in the Outer Witkoppies Member post-date the regional S0//S1 foliation, but could also be late to syntectonic to the regional foliation.

The succession has intercalated units of amphibolite, biotite gneiss, light and dark calc-silicate rocks have a thickness of ±120 metres. The intercalated units vary in texture and composition,

with biotite gneiss being inter-banded throughout. Toward the top of the succession prominent amphibolitic units are found with distinctive bands of plagioclase, biotite, and amphibolite. Above the biotite gneiss, exposures are found of a coarse-quartz-feldspar variation of the Vaalputs Suite is found, with a thickness of 20 meters. The major difference between the Outer and Inner Witkoppies Member is the presence of large bodies of actinolite associated with the Inner Witkoppies Member.

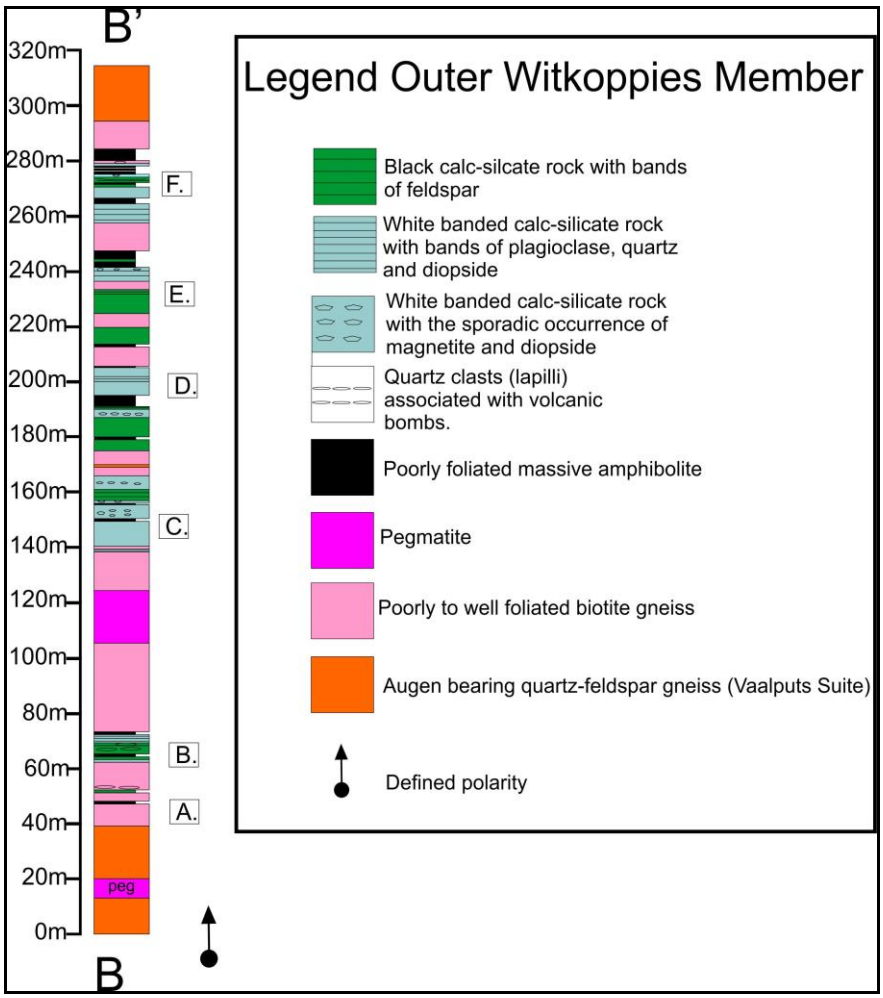

Figure 2.29: Profile B-B' (from Figure 2.27): Represents the stratigraphic succession of the Witkoppies Sequence in the Outer Member of the structure. Letters A to F represent locations and photographs (Appendix 2.2).

2.9. The Lekdam Structural Domain

The Lekdam Structural Domain (Structural Domain 3) is defined by fourteen sequences and three major stratigraphic successions which are listed in Figure 2.25. Each sequence defines a set of isolated sheath folds. The different sequences will be described in the following section 2.9.1-2.9.5 from east to west across the entire structural domain. The different members associated with each sequence will also be discussed.

2.9.1 The Samoep Succession

The Samoep Succession occurs in four isolated isoclinal fold structures that are stacked within the Lekdam Structural Domain. These fold structures have similar stratigraphic characteristics, and upon restoration, lie adjacent and stacked above one another. The Samoep Succession is defined by the Gannapoort Berg Sequence (Domain 3A), Samoep se Berg Sequences (Domain 3B), Middle Samoep Sequence (Domain 3C), and the S-Berg Sequence (Domain 3D) from east to west, as seen in Figure 2.30.

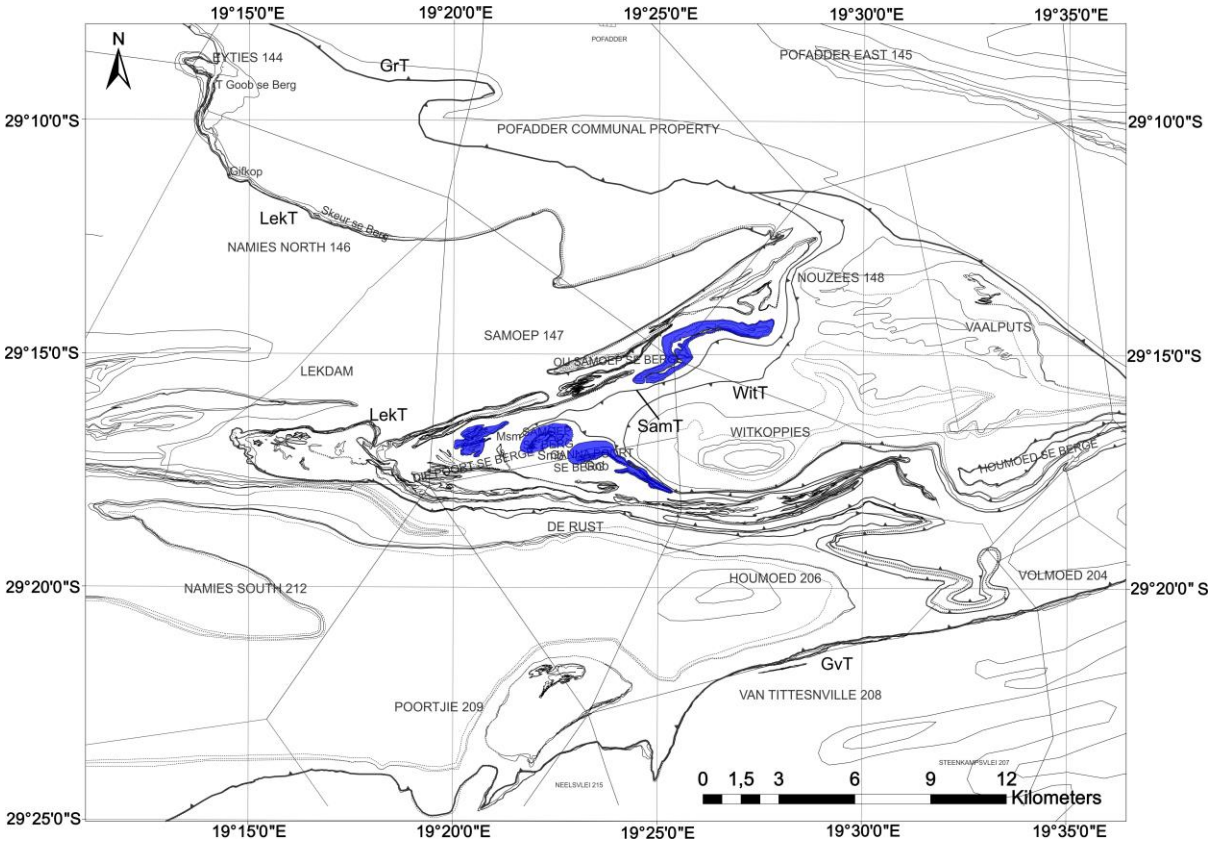

Figure 2.30: Distribution of the Samoep Succession throughout the study area. The structures associated with the Samoep Succession, namely: The S-berg, Middle Samoep, Samoep Se Berg, and Gannapoort Berg structures are identified on the map (Grt: Groothoek Thrust; Gvt: Geelvloer Thrust; Lek T: Lekdam Thrust; SamT: Samoep Thrust and WitT: Witkoppies Thrust).

The Samoep Succession generally constitutes thick to thin units of biotite gneiss with intercalated bands of feldspathic quartzite, magnetite-quartzite, thin to thick sequences of biotite-sillimanite schist, with inter-banded dark-blue garnet-bearing quartzites, dark and light banded calc-silicate rocks, and poorly to well-bedded white-blue quartzites. Although these are the general characteristics of the succession, there are small noticeable differences associated with each sequence; the only lithology in common being a thick to thin succession of biotite gneiss that is seen throughout all four sequences. The exposures measured for the stratigraphic profiles are shown in Figure 2.31.

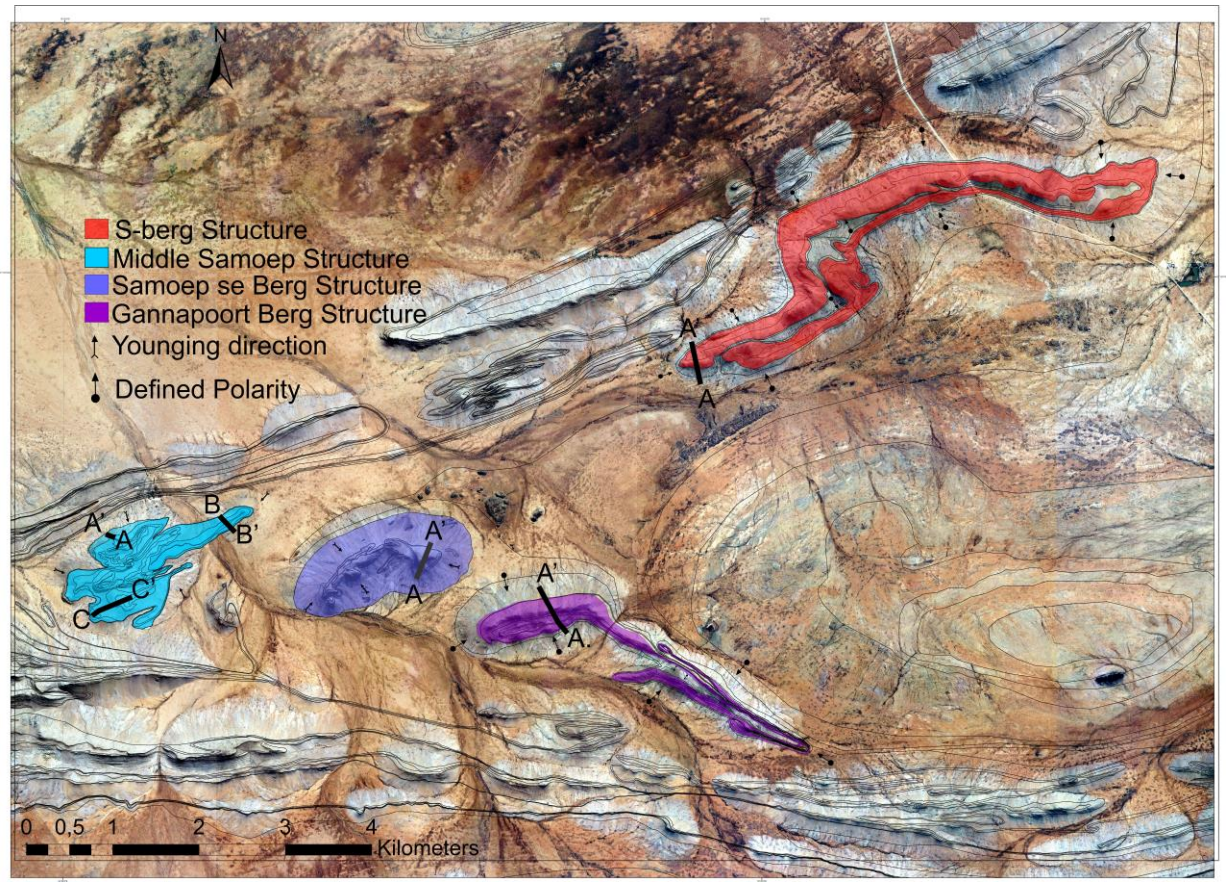

Figure 2.31: Sequences and stratigraphic profiles associated with the Samoep Succession. The profiles associated with each sequence is represented in the figure above. The facing (younging) direction and defined polarity are represented for each sequence.

2.9.1.1 The Gannapoort Berg Sequence

The Gannapoort Berg Sequence is associated with two refolded isoclinal fold structures lying adjacent to one another, and the stratigraphy hosted by both is similar. The Gannapoort Berg Sequence is best represented toward the west through the hinge zone of the D2 isoclinal fold. Profile A-A' best represents the stratigraphy of this portion of the Gannapoort Berg Sequence (Figure 2.31). The sequence is comprised of a thick succession of biotite gneiss, poorly bedded quartzite, dark-blue quartzite, biotite-sillimanite schist, amphibolite, and calc-silicate rock (Figure 2.32).

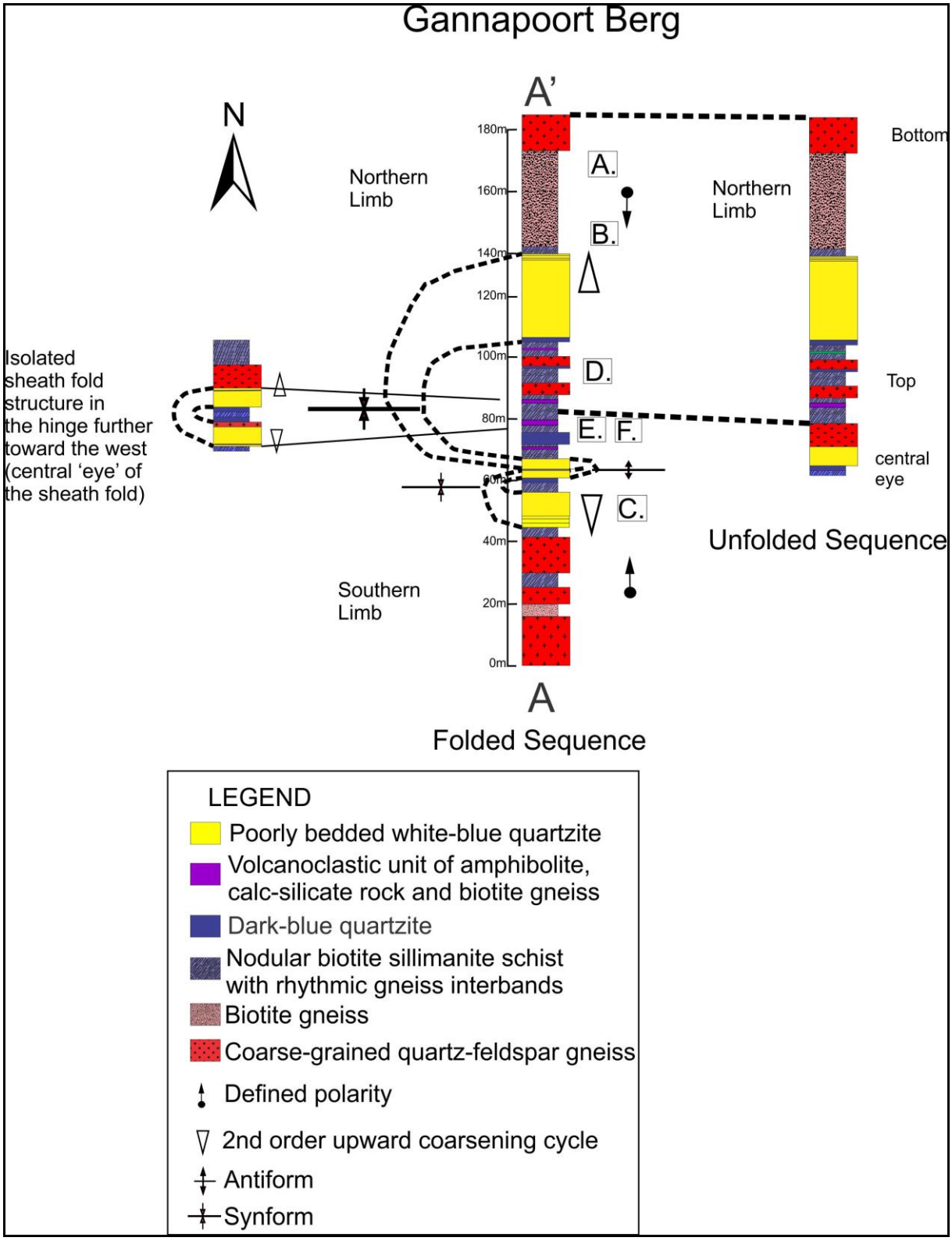

Figure 2.32: Profile A-A' (Figure 2.31) depicts the stratigraphy associated with the Gannapoort Berg Sequence. The profile represents the entire folded succession, with the separate profile representing the unfolded succession, which is best indicated by the northern limb. An isolated sheath-fold structure is often found in the center or top of the succession within the massive biotite-sillimanite schist unit. The letters A to F represent locations and photographs (Appendix 2.3).

The basal section of the stratigraphy is defined by a thick sequence of biotite gneiss (Appendix 2.3 A), which has a sharp contact with the overlying biotite-sillimanite schist unit (Appendix 2.3 B), which is best exposed on the northern part of the mountain, representing the northern limb of the isoclinal fold structure. Above the biotite-sillimanite schist, a sharp contact is found with a poorly bedded quartzite, displaying a prominent second-order upward coarsening cycle (Appendix 2.3 C). Overlying the thick succession of massive, poorly bedded quartzite, a thick succession of nodular biotite-sillimanite schist is found. The sillimanite nodules range in length between 2 and 15 millimeters (Appendix 2.3 D).

The upper, massive poorly bedded quartzite varies in thickness from 20 metres down to 2 metres from west to east. Within the biotite-sillimanite schist unit, intercalated volcanoclastic units of amphibolite, calc-silicate rock, and biotite gneiss are found (Appendix 2.3 E and F). Within the biotite sillimanite schist-volcanoclastic unit, a poorly bedded quartzite unit is found toward the west, also capped by biotite-sillimanite schist, interbanded with centimetre-metre scale dark-blue quartzite. This separate unit represents a macroscopic elliptical structure located in the hinge of the western fold closure and represents a central ‘eye’ of the Gannapoort Berg fold structure (Figure 2.32).

The stratigraphy toward the east is similar, the only difference is that the stratigraphic units are highly thinned, mylonitic, and boudend, due to differences in strain attributed, to later deformation effects. The defined polarity within this structure is represented by the coarse-grained Lekdam Gneiss at the base, overlain by a thick succession of biotite gneiss, biotite-sillimanite schist, and massive poorly bedded quartzite, displaying a second-order upward coarsening cycle. Above the massive, poorly bedded quartzite, nodular biotite-sillimanite schist is found with intercalated volcanoclastic units, overlain by a poorly bedded.

2.9.1.2 The Samoep se Berg Sequence

The Samoep se Berg Sequence is defined by a thick sequence of biotite gneiss with interlayered lenticular units of calc-silicate rocks at the base, and with thick poorly bedded quartzite and biotite schist at the top of the sequence, as seen in Profile A-A’ (Figure 2.31 and 2.33). The Samoep se Berg Sequence represents a D2 macroscopic fold structure, displaying double vergence geometries, situated in the centre of the Lekdam Structural Domain, and is also surrounded by the coarse-grained quartz-feldspar Lekdam Gneiss.

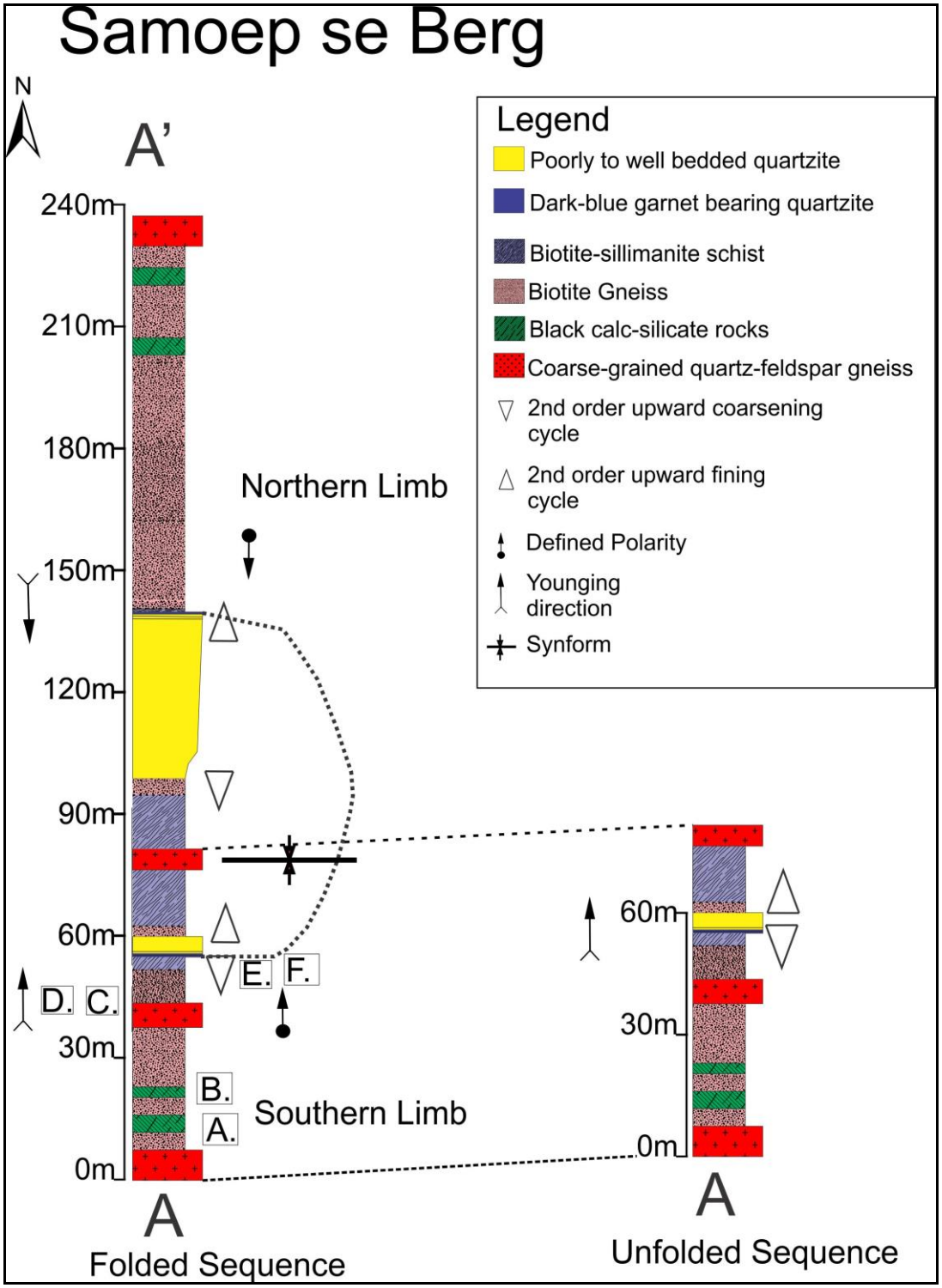

Figure 2.33: Profile A-A' (Figure 2.31) depicts the stratigraphy related to the Samoep se Berg Sequence. The extension represents the unfolded succession. The letters A to F represent locations and photographs (Appendix 2.4).

The basal sequence is characterised by a thick succession of biotite gneiss, which surrounds the entire structure (Appendix 2.4 A). The thick succession of biotite gneiss has a lit-par-lit contact relationship at the base with the Lekdam Gneiss, xenoliths of biotite gneiss are also found within the Lekdam gneiss. Interbanded units of calc-silicate rock, with marble bands,

are found within the biotite gneiss (Appendix 2.4 B). The calc-silicate rock units vary in thickness from a few centimetres (30-50 centimetres) to 5-8 metres.

Above the biotite gneiss unit, units of biotite-sillimanite schist, which range from a few centimetres to a few metres are found (Appendix 2.4 C). A garnet-bearing dark blue quartzite overlies the biotite schist unit and occurs sporadically throughout (Appendix 2.4 D). The garnet-bearing dark blue quartzite is found close to the contact of the upper, poorly to well-bedded white-blue quartzite, in which a prominent second-order upward coarsening cycle is defined (Appendix 2.4 E). Within the upper quartzite the original S0 bedding was identified in the form of cross-bedding, which indicated the younging (facing) direction toward the top of the succession, showing younging toward the central hinge of the structure, with the northern limb being overturned (Appendix 2.4 F).

Biotite-sillimanite schist together with biotite gneiss is found above the well to poorly bedded quartzite, encapsulates the upper extent of the succession. The biotite-sillimanite schist and biotite gneiss units have a gradational contact to one another and define the inner hinge zone of the fold structure, with the core of the fold structure represented by the biotite-sillimanite schist unit. Lenticular units of Lekdam Gneiss are also seen intruding the upper central portion of the sequence, with a certain portion of the hinge zone being fully intruded by the Lekdam Gneiss.

The defined polarity of the Samoep se Berg Sequence is defined by the coarse-grained Lekdam Gneiss at the base, overlain by a thick succession of biotite gneiss and a thin succession of biotite-sillimanite schist. Overlying these units are a dark-blue garnet-bearing quartzite, poorly bedded quartzite, defining a prominent second-order upward coarsening cycle, overlain by biotite gneiss and biotite-sillimanite schist units, also defining a second-order upward fining cycle. The defined polarity and younging (facing direction) are coincidental with one another (Figure 2.33).

2.9.1.3 The Middle Samoep Sequence

The Middle Samoep fold forms a flat hill just toward the west of the Samoep se Berg structure, and hosts the Middle Samoep Sequence; it is also situated in the center of the Lekdam Structural Domain (Figure 2.31). The structure represents a highly folded structure with double vergence geometries (S and Z structures), together with elliptical fold structures. The structure is defined by a biotite gneiss unit with interbedded feldspathic quartzite, poorly bedded light-blue quartzites, biotite-sillimanite schist, with interbedded dark-blue quartzite with garnet overgrowths, and a poorly bedded quartzite unit. Profiles A-A’, B-B’, and C-C’ are taken where the stratigraphy succession of the Middle Samoep Sequence is well exposed (Figure 2.34 and Figure 2.35).

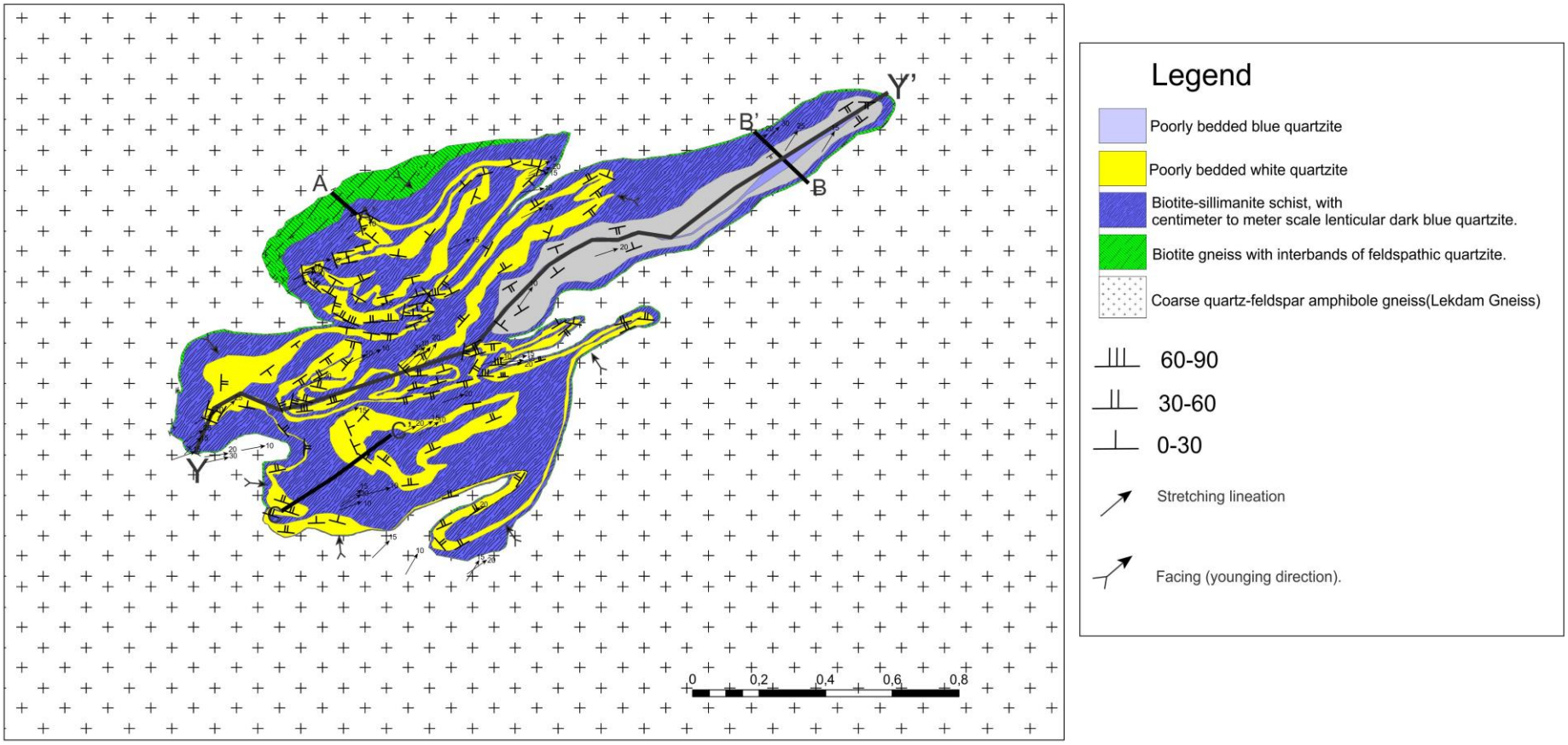

Figure 2.34: Simplified geological map showing Profile locations A, B, and C in Figure 2.30. A geometrically controlled long section from south west to north east parallel to the regional foliation is represented by Y-Y' (see Figure 2.35). The younging direction and regional dips throughout the structure are also presented.

The lower succession has a sharp contact with the underlying Lekdam Gneiss and is separated by a 1-2 metre biotite gneiss unit which represents the first unit in the succession and is prominently presented in Profile A. The biotite gneiss unit is interbanded with a thick succession of feldspathic quartzites (Appendix 2.5 A). The feldspathic quartzite unit consists of various laminites of tourmaline and biotite, which display small third-order upward fining cycles, and have small interbands of biotite gneiss (Appendix 2.5 B). Pegmatite veins and small-scale metatexite melts are also seen on the 'YZ' foliation planes and postdates the regional foliation. The total thickness varies from 7 to 8 metres in the north, but is poorly represented in the rest of the structure, with a total thickness of between 1 metre and 50 centimetres in the south. The basal portion (Profile A-A') is also significant in the fact that it carries a primary structure represented by cross-bedding (S0) which defines the younging direction (structural facing), which indicates younging toward the top of the stratigraphic succession (Appendix 2.5 C).

Above the formerly mentioned units a very thick succession of biotite-sillimanite schist is found, with interstitial units of dark-blue garnet-bearing quartzites (Appendix 2.5 D and E). The dark blue quartzites occur sporadically within the biotite schist unit as large lenticular bodies, between 5 to 10 metres, or as small interbands of between 5 and 15 centimetres. There is also a sporadic occurrence of post-growth garnets within the blue quartzite and biotite sillimanite schist units throughout the structure (Appendix 2.5 E). Above the lower succession another staggered unit of light poorly bedded quartzite is found, represented in Profile B-B'. The poorly bedded character and light blue colour, and the fact that it is a separate ellipsoidal fold unit makes it different from the lower and upper portions of the of the succession (Figure 2.33 and 2.34). Above the light blue quartzite, a small biotite-sillimanite schist unit is found defining the hinge zone of the isolated ellipsoidal fold structure. The Lekdam Gneiss is also found intruding in and around the structure (Figure 2.36). Another staggered sequence is found, which represents the upper portion of the Middle Samoep Sequence, and is represented by profile C-C' (Figure 2.34 and Figure 2.35).

The upper succession is defined by a poorly bedded quartzite, displaying a prominent second-order upward coarsening cycle (Appendix 2.5 F), overlain by a thick biotite-sillimanite schist unit with interbands of dark-blue quartzite. Another poorly bedded quartzite overlies the former and defines the limbs of another isolated ellipsoidal fold structure (Profile C-C'). Another prominent biotite-sillimanite schist unit is found above the upper quartzite, defining the central hinge zone of the elliptical fold structure.

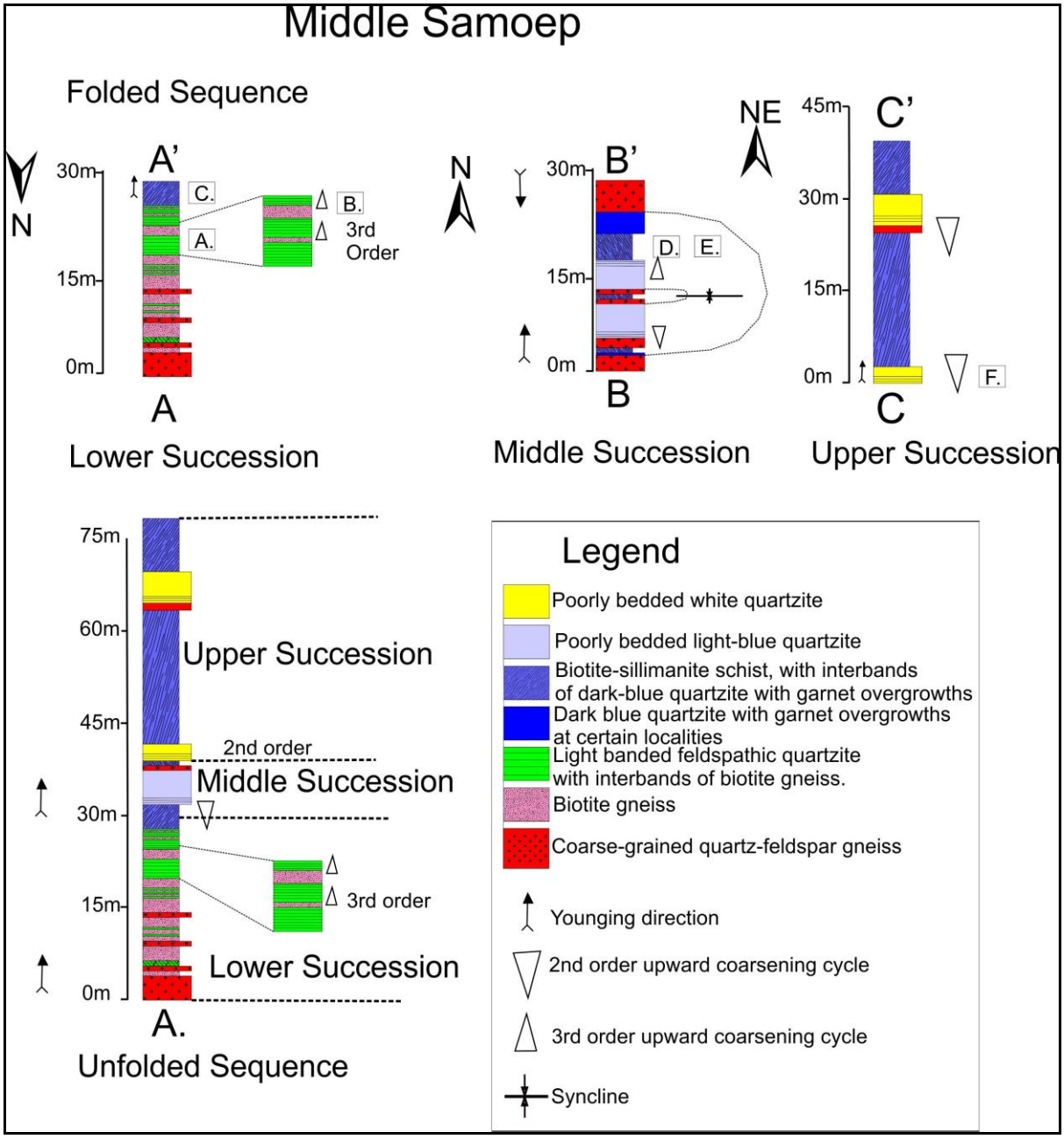

Figure 2.35: Stratigraphic profiles of the Middle Samoep Sequence. Profiles A-A', B-B' and C-C' (from Figure 2.34) represents the entire succession. The lower most profile represents the unfolded sequence associated with the Samoep Sequence. The letters A to F represent locations and photographs (Appendix 2.5).

The full succession defines a heavily folded D2 fold structure with double vergence geometries, with the lower succession folding around the entire structure as seen in section in Figure 2.36. Above the lower succession, the middle succession is found also seen in Figure 2.36 and defines an isolated ellipsoidal fold structure composed of poorly bedded light-blue quartzites. The upper succession also defines two elliptical fold structures, of the two structures the lower structure is heavily folded, with the upper or central fold structure representing the core or central 'eye' of the Middle Samoep Structure (Figure 2.36).

The defined polarity of this sequence is defined by Lekdam Gneiss at the base, in contact with a biotite gneiss with interbanded feldspathic quartzites, overlain by a biotite-sillimanite schist with interbands of dark-blue garnet-bearing quartzites (lower succession). A poorly bedded-light blue quartzite with overlying biotite-sillimanite schist is then found (middle succession). Overlying these units is a poorly bedded quartzite in contact with a thick sequence of biotite-sillimanite schist, overlain by a poorly bedded quartzite, above which a biotite sillimanite schist unit is found (upper succession) (Figure 2.35 and 2.36). Concerning the defined polarity in this instance, it is the same as the younging direction for the Middle Samoep Sequence.

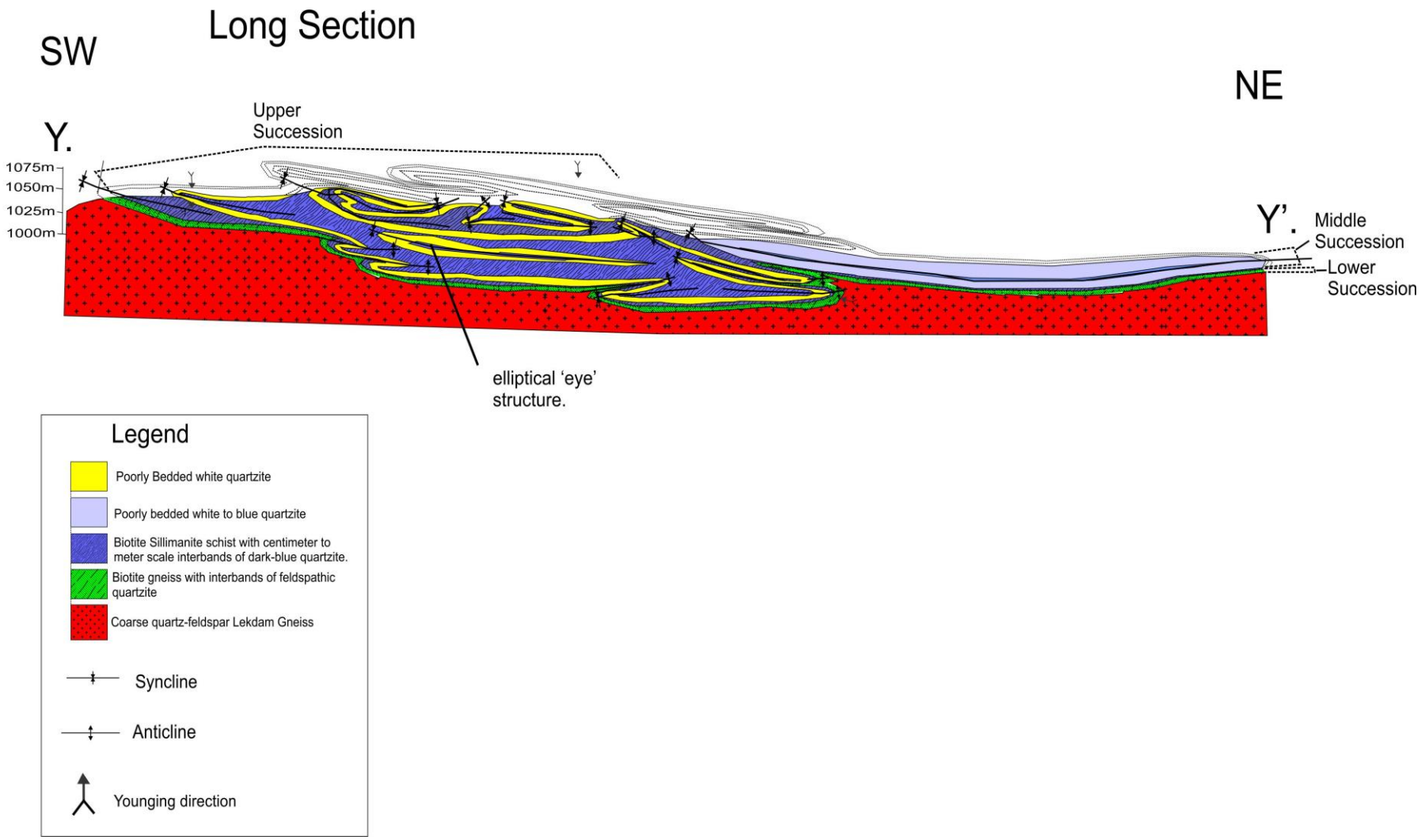

Figure 2.36: Geometrically controlled long section across the Middle Samoep sheath fold showing the complexities associated with this Sequence. The lower succession (biotite gneiss with interbands of feldspathic quartzite) can be seen folding entirely around the macroscopic sheath fold structure, with the middle and upper successions staggered above. The middle succession which resembles a flattened ellipsoidal fold structure can be seen overlying the lower succession toward the southeast. The upper succession is highly folded and is represented by an elliptical 'eye' structure in the center of the structure.

2.9.1.4 The S-Berg Sequence

The S-Berg Sequence is represented as an isoclinal fold structure and is confined to the northern section of the Lekdam Structural Domain, and is found adjacent to the Klein Pofadder fold structure and the extension of the T-Goob-se Berg structure in the north (Figure 2.31). S-Berg Sequence is mapped as an isolated refolded isoclinal fold structure and is also surrounded by the Lekdam Gneiss. The S-Berg Sequence is well represented particularly on the far western extremity on the northern fold closure of the structure represented by Profile A-A' (Figure 2.31 and Figure 2.37). The S-Berg Sequence is defined by a thick succession of biotite gneiss with intercalated units of magnetite quartzite and light banded feldspathic calc-silicate rock, poorly to well-bedded white-blue quartzite and biotite-sillimanite schist with intercalated meter to centimetre dark-blue quartzites.

The lower portion of the succession is defined by a thick basal sequence of biotite gneiss, which varies in thickness from about 21 to 1 metres across at certain locations (Appendix 2.6 A). The Lekdam Gneiss is found just below the biotite gneiss and has a lit-par lit relationship similar to the one observed at the base of the Samoep se Berg and Gannapoort Berg Sequences. Toward the top of the biotite gneiss, lenticular units of blue to black magnetite quartzite are found (Appendix 2.6 B). These lenticular units vary in thickness from 5 metres to up to 50 centimetres in length (Appendix 2.6 C). Small intercalated units of light banded calc-silicate rock occur together with the magnetite quartzites within the thick biotite gneiss unit. Above the thick biotite gneiss unit, a poorly to well-bedded quartzite is found, which occasionally displays prominent biotite bands (Appendix 2.6 D). The white quartzite has a dark-bluish colour at certain locations and also varies in thickness throughout from 10-5 meters up to 20-25 metres along strike.

Prominent second-order upward coarsening cycles are associated with the upper quartzite (Appendix 2.6 E). Above the poorly bedded quartzite a thick sequence of biotite- sillimanite schist found with the sporadic occurrence of sillimanite nodules (Appendix 2.6 F), a prominent second-order upward fining cycle is also defined in the upper succession. Centimetre to metre-scale dark-blue quartzites are interbanded within the upper biotite-sillimanite schist unit. The upper biotite-sillimanite schist unit is located in the core or hinge zone of the S-Berg structure and is best viewed in the northern hinge toward the west of the structure.

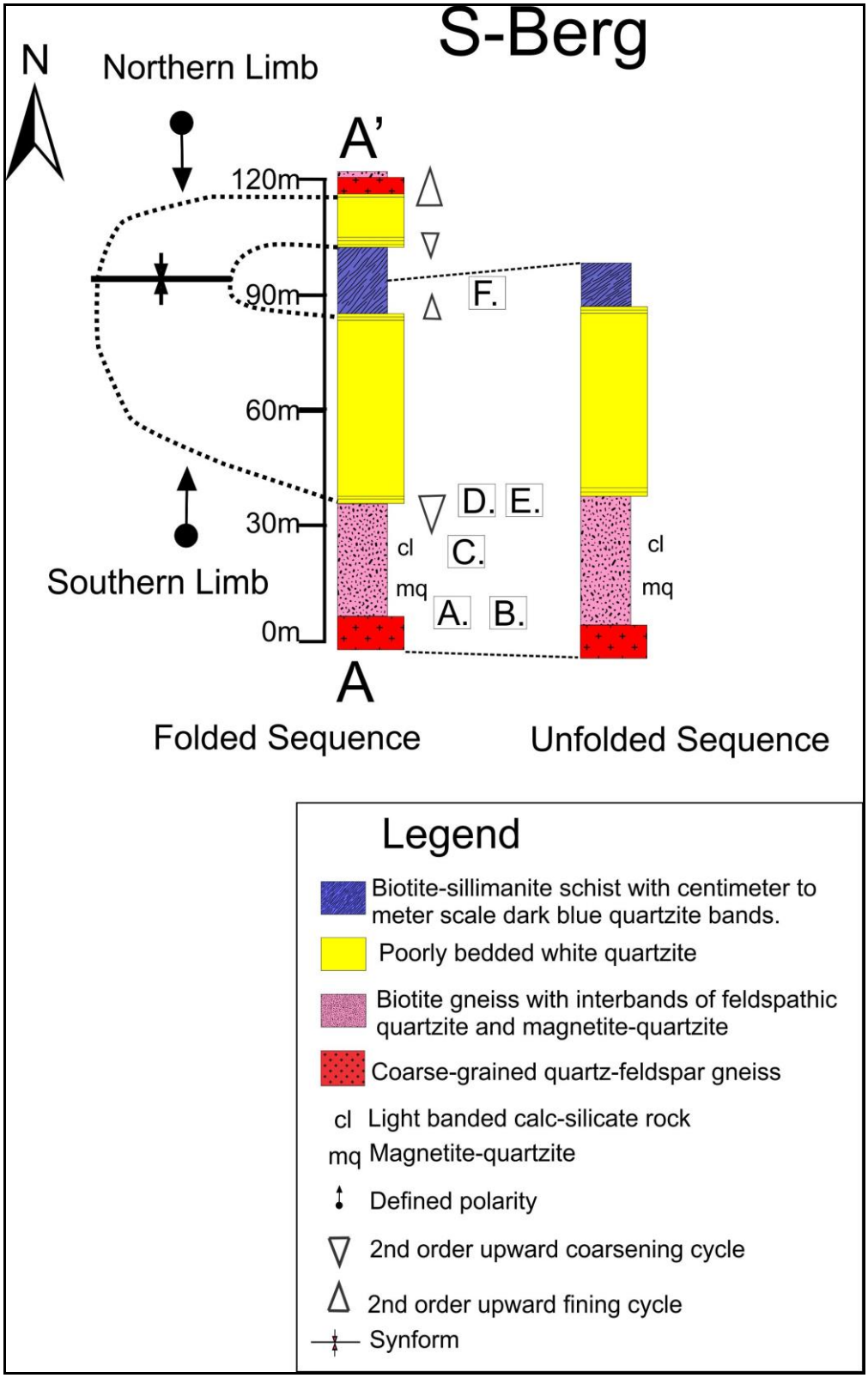

Figure 2.37: Profile A-A' (from Figure 2.31) represents the stratigraphic succession associated with the S-Berg Sequence. The offset profile represents the unfolded succession of the S-Berg Sequence. The letters A to F represent locations and photographs (Appendix 2.6).

2.9.1.5 Correlation and Summary of the Samoep Succession

In Figure 2.38 a horizontal restored correlation of all the sequences associated with the Samoep Succession is presented. All four sequences have thick to thin successions of biotite gneiss at the base, with minor differences in overlying lithologies with each sequence. The Gannapoort Berg Sequence is found in the east, followed by the Samoep se Berg, Middle Samoep, and S-Berg sequences to the west, upon doing a structural restoration. The coarse-grained quartz-feldspar Lekdam Gneiss is located at the base of each member having a lit-par-lit relationship with the overlying lithologies.

The main lithology which defines the Samoep Succession is a thick to thin successions of biotite gneiss that is situated at the base of every sequence. Only the Middle Samoep Sequence has intercalated units of feldspathic quartzite within the biotite gneiss. The feldspathic quartzite unit within the Middle Samoep Sequence defines the only third-order upward fining cycle found throughout the Samoep Sequence. Out of the four structures, three have gradational contacts of biotite gneiss in contact with a biotite-sillimanite schist unit in moving toward the upper poorly bedded quartzite unit, with the S-Berg Sequence being the exception. Concerning the upper lithologies, all four structures have prominent successions of biotite-sillimanite schist and thick to thin poorly bedded quartzite. The upper poorly bedded quartzites define second-order upward coarsening cycles. The upper quartzite thickness varies for each structure, which is dependent on variations in strain and competency difference. Second-order upward fining cycles were also identified in the upper sections of the Samoep se Berg and S-Berg Sequences.

Only the Gannapoort Berg Sequence contains slithers of volcanoclastic units of amphibolite and calc-silicate rocks within the upper biotite-sillimanite schist unit. In all four structures, the stratigraphic polarity and younging direction coincide with one another (Figure 2.38). Throughout the Samoep Succession, only the Middle Samoep Sequence has staggered upper sequences of light blue and poorly bedded white quartzites defining separate ‘eye’ fold structures.

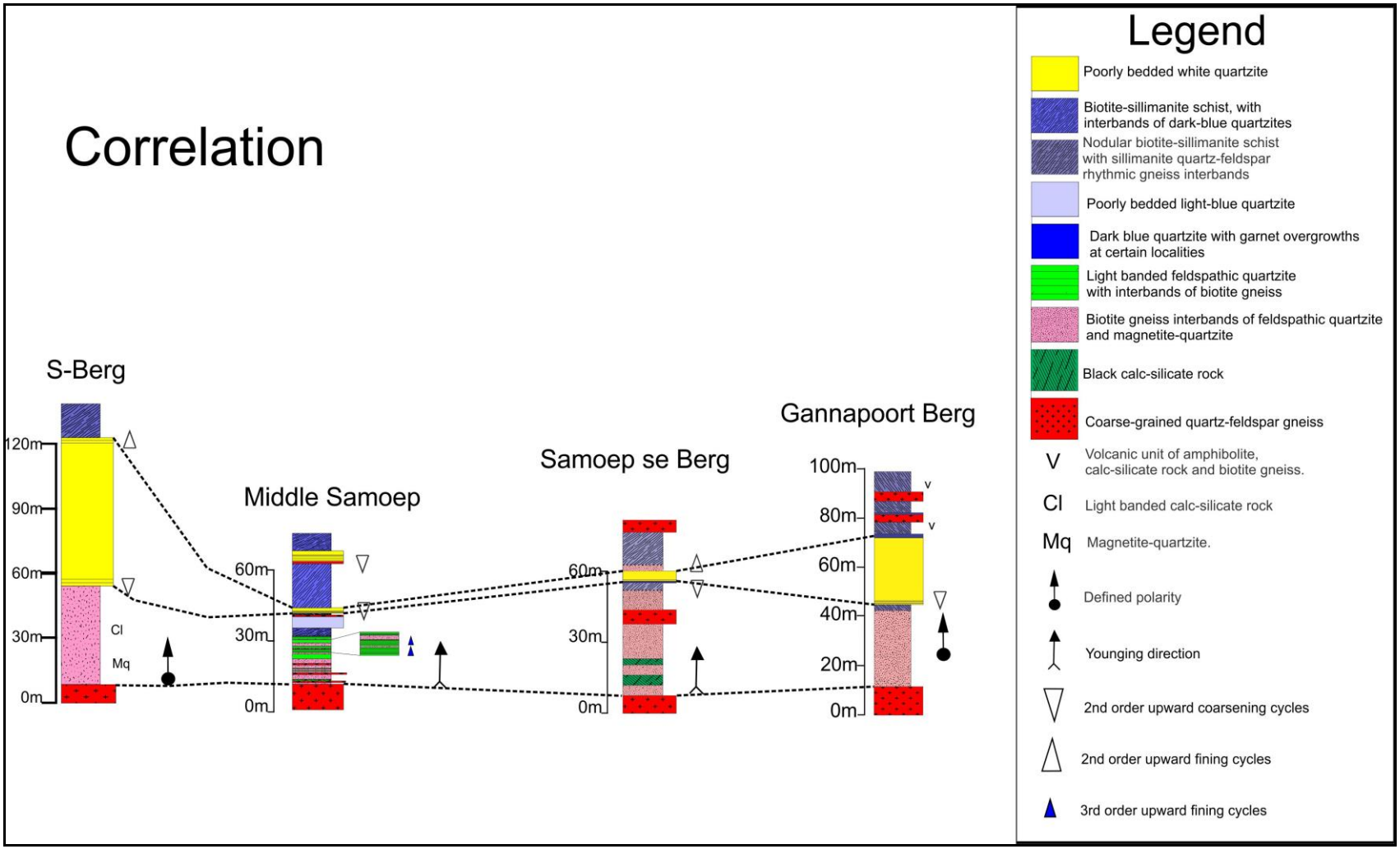

Figure 2.38: Horizontally restored correlation between all the different sequences associated with the Samoep Succession. The profiles represent the Gannapoort Berg Sequence, Middle Samoep Sequence, Samoep se Berg Sequence and S- berg Sequence, showing the most prominent characteristics.

2.9.2 The Klein Pofadder Sequence

The Klein Pofadder Sequence is confined to an isolated isoclinal refolded structure, just adjacent to the T-Goob se Berg structure (Figure 2.39). The Klein Pofadder Sequence is defined by dark-blue garnet-bearing quartzite, thick massive poorly bedded quartzite, and biotite sillimanite schist. The structure is also surrounded by the Lekdam Gneiss, which intrudes various units throughout the sequence. Compared to the other sequences, the Klein Pofadder Sequence is rather simplistic, and no volcanic units or ferruginous meta-quartzites (BIFs) were identified along strike. Profile A-A' best represents the stratigraphic sequence (Figure 2.40 and 2.41).

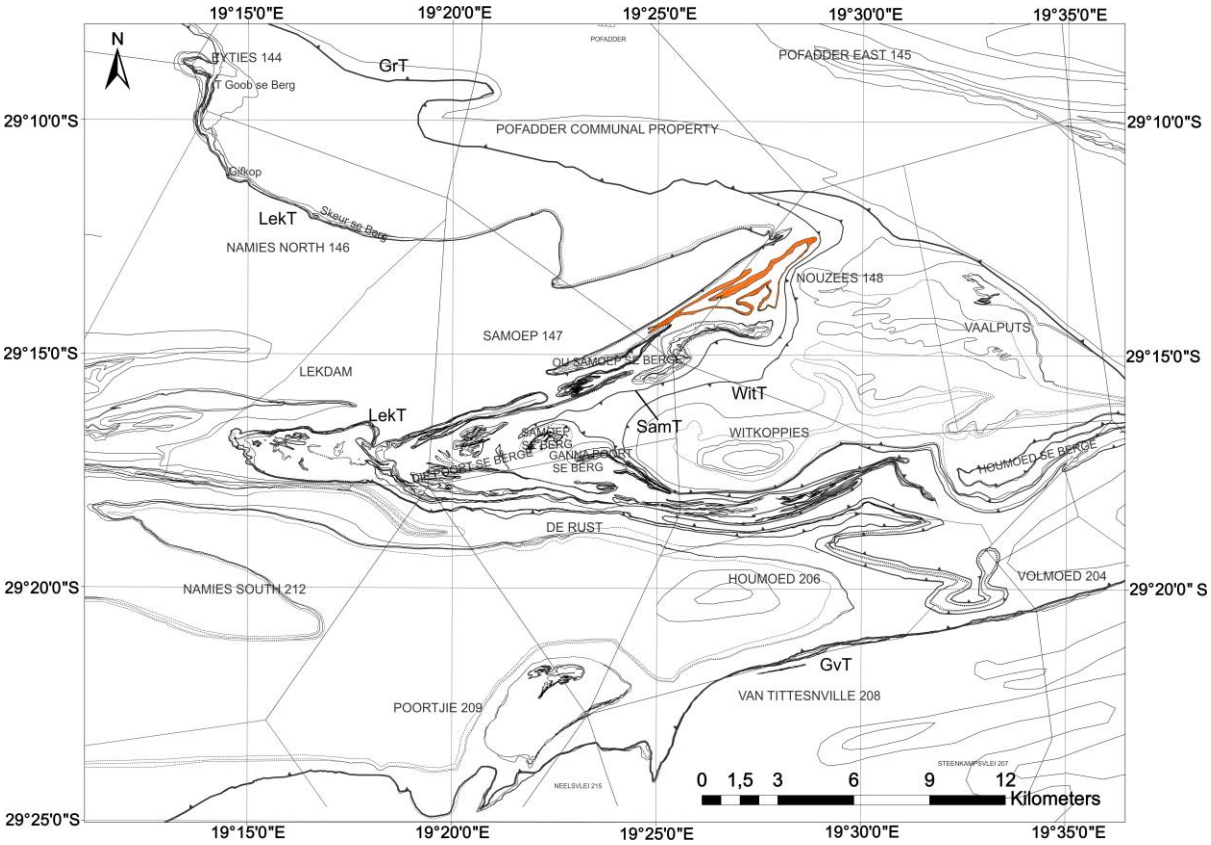

Figure 2.39: Distribution of the Klein Pofadder Sequence throughout the study area in orange (Grt: Groothoek Thrust; Gvt: Geelvloer Thrust; LekT: Lekdam Thrust; SamT: Samoep Thrust and WitT: Witkoppies Thrust).

The lower succession of the Klein Pofadder Sequence is defined by a thick succession of biotite-sillimanite schist, having a dark-grey appearance, and occurs at the base of the succession (Appendix 2.7 A). The thickness of the biotite-sillimanite schist varies along strike due to the intrusion of the Lekdam Gneiss within the sequence. Garnet overgrowths are found within the Lekdam Gneiss surrounding the Klein Pofadder structure. As you move more toward the west the biotite-sillimanite schist component increases and the interlayered Lekdam Gneiss decreases. However, the exposure of the lower biotite-sillimanite schist is often poor and not well represented and can only be seen at certain localities.

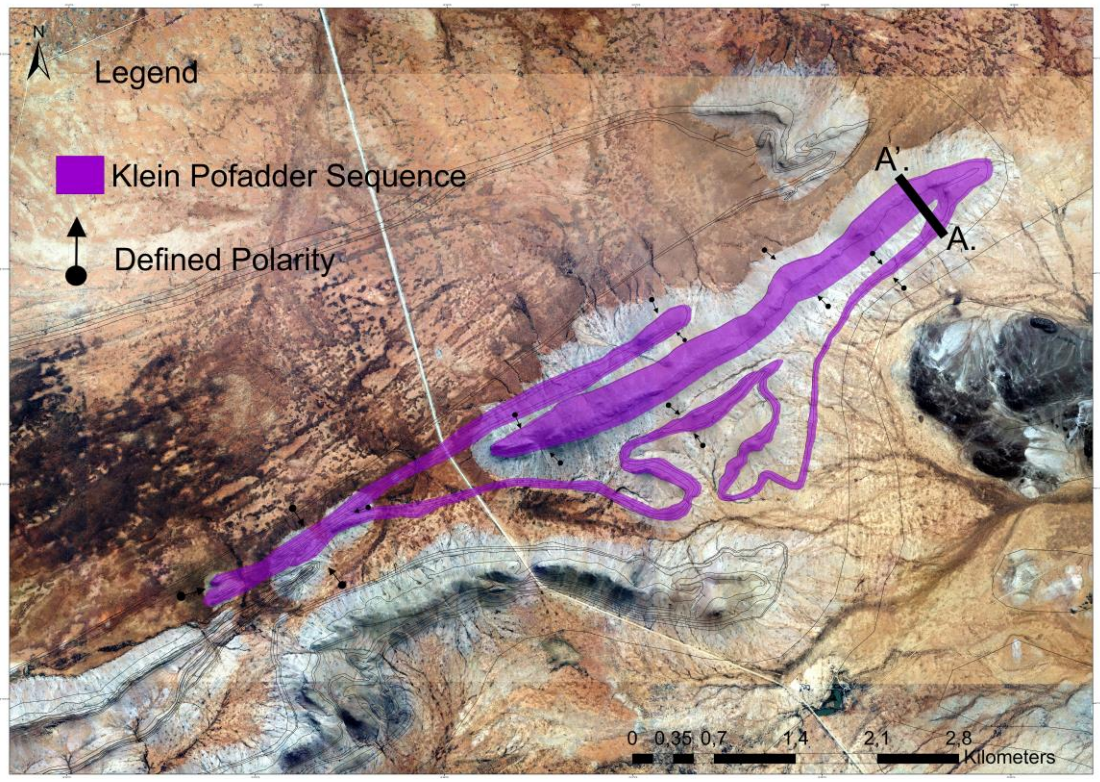

Figure 2.40: Distribution of the Klein Pofadder Sequence, together with the location of profile A-A'. The defined polarity is also represented throughout the structure.

Above the biotite-sillimanite schist unit, a poorly bedded dark-blue quartzite is found. Garnet overgrowths at stages are found within the dark blue quartzite, but occur sporadically throughout (Appendix 2.7 D). The dark blue quartzite units occur on a meter to centimetre-scale and have a greyish appearance (Appendix 2.7 C). Above the dark blue quartzite, a poorly to well-bedded white quartzite is found which defines a second-order upward coarsening cycle (Appendix 2.7 B). The upper white quartzite is a very thick unit and at stages displays prominent biotite bands. Along strike, a biotite-sillimanite schist unit is interbedded within, which defines the uppermost unit and defines the central hinge zone of the structure. The succession of interbedded biotite-sillimanite schist thickens dramatically as you move toward the east. The defined polarity associated with this structure is defined by biotite-sillimanite schist, dark-blue quartzite with garnet overgrowths in contact with a poorly bedded massive white quartzite, displaying a prominent second-order upward coarsening cycle, above which a small unit of biotite-sillimanite schist is found (Figure 2.41).

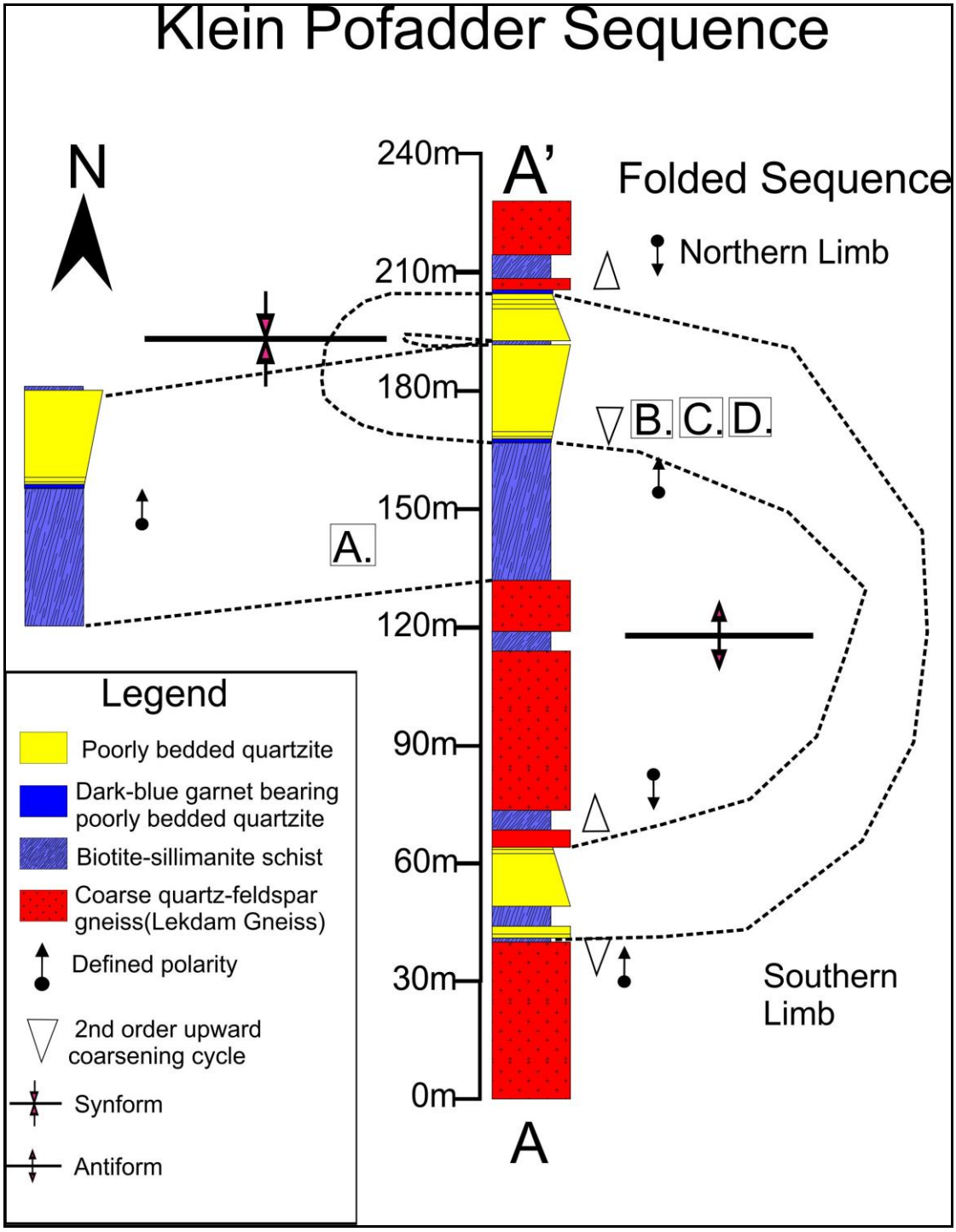

Figure 2.41: A-A' (from Figure 2.39) represents the stratigraphic succession associated with the Klein Pofadder Sequence. The entire folded sequence, with the smaller projected profile representing the unfolded sequence. The unfolded sequence shows the defined polarity for the Klein Pofadder Sequence. The letters A to C represent locations and photographs (Appendix 2.7).

2.9.3 The Koppies Sequence

The Koppies Sequence is located in the southern part of the Lekdam Structural Domain. The Koppies Sequence is hosted by a highly refolded-flattened isoclinal fold structure with double vergence geometries and is also enclosed within the Lekdam Gneiss (Figure 2.42). To the north, the Witkoppies Sequence is found and toward the south, a part of the Lekdam Outer

structure is found. The Koppies structure extends for a total distance of 12 kilometers along strike from east to west. The Koppies Sequence is defined by biotite-sillimanite schist, poorly to well-bedded massive white-blue quartzite and thick units of nodular rhythmic sillimanite-quartz-feldspar gneiss. For ease of description, the Koppies Sequence has been divided into an Inner Koppies and Outer Koppies Member represented in Figure 2.43.

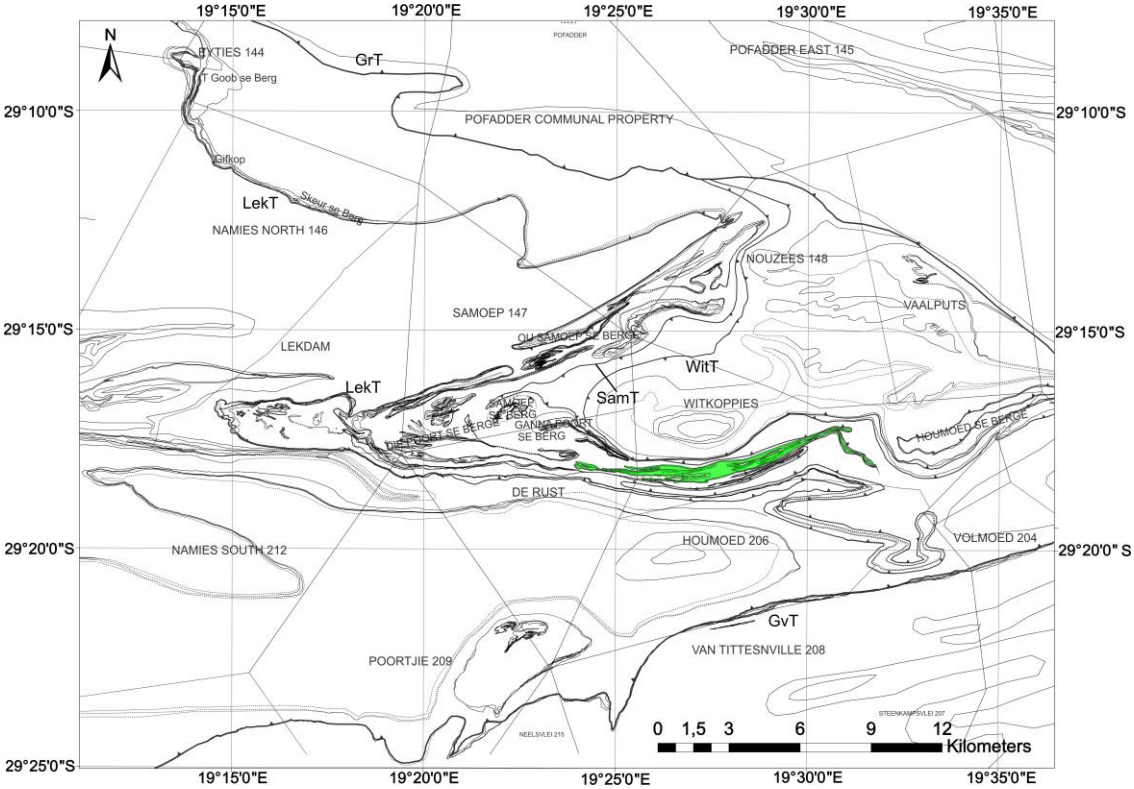

Figure 2.42: Distribution of the Koppies Sequence in the study area (green) (Grt: Groothoek Thrust; Gvt: Geelvloer Thrust; LekT; Lekdam Thrust, SamT: Samoep Thrust and WitT: Witkoppies Thrust).

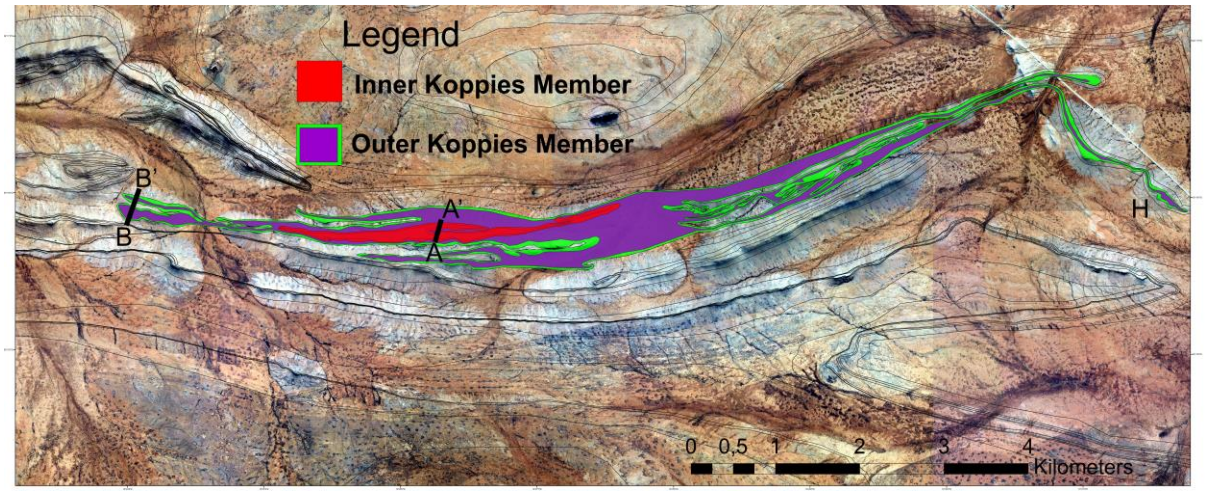

Figure 2.43: Distribution of profiles A and B, across the Inner Koppies Member (red) and the Outer Koppies Member (green-purple).

2.9.3.1 Inner Koppies Member

The Inner Koppies Member is defined as the central zone of the Koppies structure and is shown in Profile A-A' in Figure 2.44, which represents the best-exposed portion of the stratigraphic succession. The Inner Koppies Member is surrounded by the coarse-grained-quartz-feldspar Lekdam Gneiss. The basal part of the inner sheath member is defined by biotite-sillimanite schist with intercalated units of ferruginous garnet meta-quartzite and underlain by a poorly bedded white-blue quartzite (Appendix 2.8 A). The intercalated ferruginous garnet meta-quartzites are mostly represented on a centimetre scale (Appendix 2.8 B). The garnet-bearing ferruginous quartzite acts as a marker for the upper portion of the Inner Koppies Member and can be found folding around the central hinge zone of the structure, together with the thick to thin sequence of biotite-sillimanite schist.

Prominent second-order upward coarsening cycles were identified on the contact with the biotite-sillimanite schist and upper quartzite (Appendix 2.8 C). Above the poorly bedded quartzite, a thick sequence of nodular sillimanite-quartz-feldspar gneiss is found with interbanded units of biotite-sillimanite schist (Appendix 2.8 D). The defined polarity of the Inner Koppies Member is defined by thin to thick succession of biotite-sillimanite schist with intercalated units of garnet meta-quartzite, in contact with a poorly to well-bedded white-blue quartzite, displaying a prominent second-order upward coarsening cycle, overlain by a nodular sillimanite quartz-feldspar gneiss, with interbanded units of biotite-sillimanite schist. Due to the severely folded nature of this particular structure, great resourcefulness is required when mapping out the full sequence (Figure 2.44).

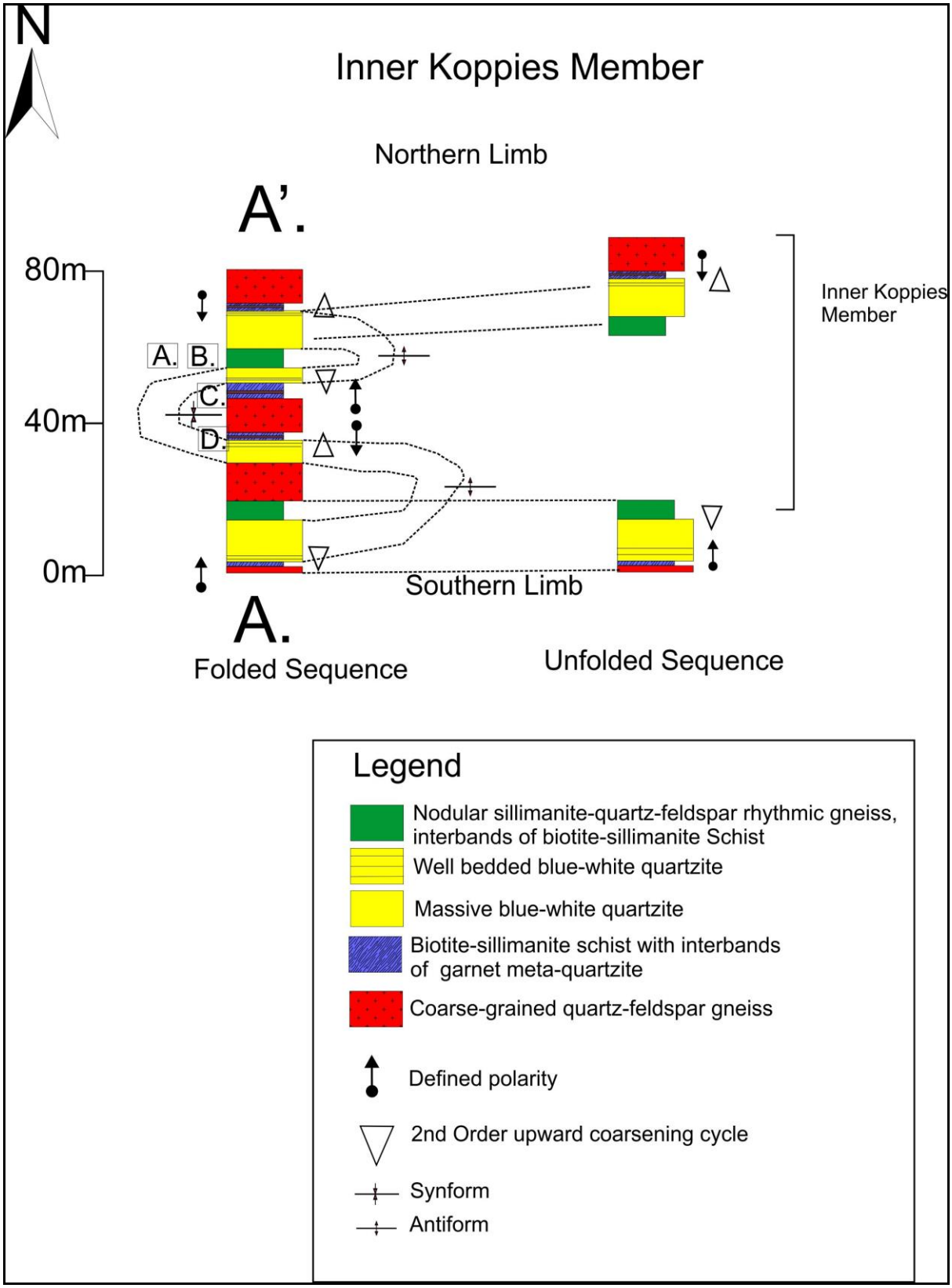

Figure 2.44: Profile A-A' (from Figure 2.43), represents the stratigraphic succession associated with the Inner Koppies Member. The folded and unfolded sequence is represented, with the unfolded sequence representing the defined polarity for this structure. The letters A to D represent locations and photographs (Appendix 2.8).

2.9.3.2 Outer Koppies Member

In terms of the stratigraphy, it is very similar to that of the Inner Koppies Member and is shown in Profile B-B' (Figure 2.43 and 2.45). The Outer Koppies Member is surrounded by the Lekdam Gneiss that intrudes the central portion of the refolded fold structure. Due to the highly folded nature of this structure, and the fact that the metasediments are folded together with the Lekdam Gneiss, it can be an arduous task to determine which units are contained within the central and outer portions of the structure. The lower portion of the Outer Koppies Member is defined by a thick to thin biotite-sillimanite schist with, interbands of garnet-bearing ferruginous quartzite (Appendix 2.9 A). Above this unit, a thick sequence of poorly bedded blue-white quartzite is found (Appendix 2.9 B). This specific quartzite is folded heavily in an isoclinal fashion; extends for kilometres along strike; defines a prominent second-order upward coarsening cycle and thickens and thins along strike, which is more than often controlled by the amplitude of isoclinal folds and competency differences.

Overlying the poorly bedded quartzite unit, a thick to thin sequence of nodular-sillimanite quartz-feldspar gneiss with interbands of biotite-sillimanite schist is found (Appendix 2.9 C). Prominent nodules of sillimanite can be viewed throughout the succession. In the upper portion of the stratigraphy associated with the Outer Koppies Member, the Lekdam Gneiss occupies large areas within the entire fold structure and contains xenoliths of the associated supracrustal succession. The defined polarity of this particular structure is defined by a biotite-sillimanite schist unit, with interbands of garnet meta-quartzites, in contact with a poorly bedded white-blue quartzite defining a second-order upward coarsening cycle, followed by a thick to thin succession of nodular sillimanite-quartz-feldspar rhythmic gneiss, with interbands of biotite-sillimanite schist (Figure 2.45).

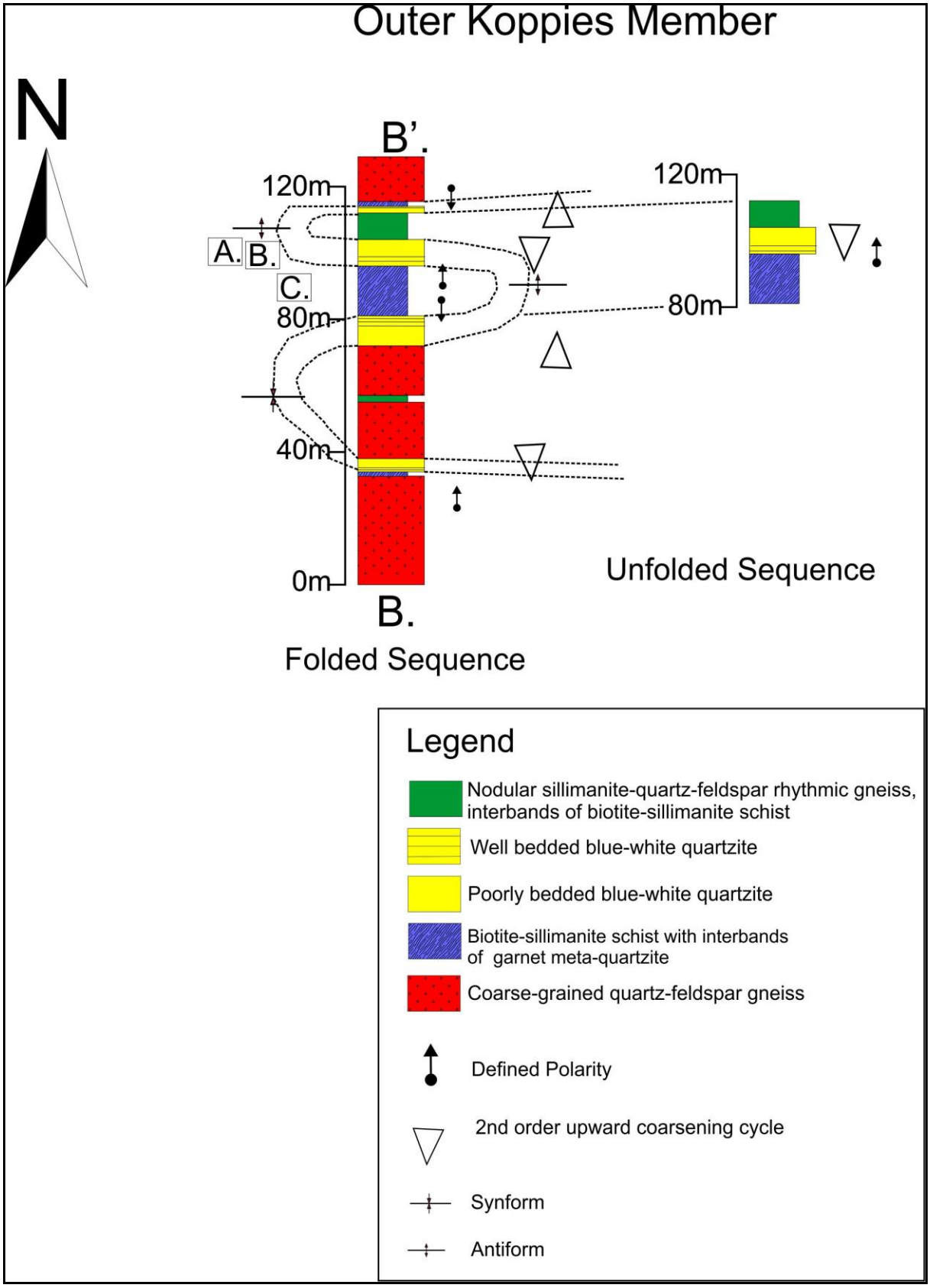

Figure 2.45: Profile B-B' (from Figure 2.43) representing the stratigraphic succession associated with the Outer Koppies Member. Both the folded and unfolded sequence is represented in the diagram. The unfolded sequence shows the defined polarity for this specific structure. The letters A to C represent locations and photographs (Appendix 2.9).

2.9.4 The T-Goob Succession

The T-Goob Succession is found within the Lekdam Structural Domain (Structural Domain 3) and encompasses the three largest and most refolded isoclinal structures throughout the study area. The succession is named after the T-Goob se Berg structure where the stratigraphic succession is best exposed. The T-Goob Succession is defined by thick to thin successions of biotite-sillimanite schist, biotite gneiss, ferruginous garnet-bearing quartzites, thin to thick sequences of nodular sillimanite-quartz-feldspar rhythmic gneiss, thick successions of poorly bedded quartzite, and volcanoclastic/chemogenic units of feldspathic quartzite, diopside, actinolite, and biotite gneiss. The volcanoclastic/chemogenic unit is the most noticeable stratigraphic marker associated with the succession. The T-Goob Succession is defined by three prominent sequences namely: the T-Goob se Berg Sequence, Poort se Berg Sequence and Outer Lekdam Sequence (Figure 2.46). In each structure, the stratigraphic succession varies distinctively along strike, with only key stratigraphic markers being noticeable due to complications associated with intense isoclinal folding, boudinage, variations in strain (strain partitioning), and duplications associated with thrusting. The Outer Lekdam Sequence is interpreted to be the oldest, followed by the T-Goob se Berg and Poort se Berg Sequences (Chapter 4.1). The best exposures associated with the T-Goob Succession are represented in Figure 2.47.

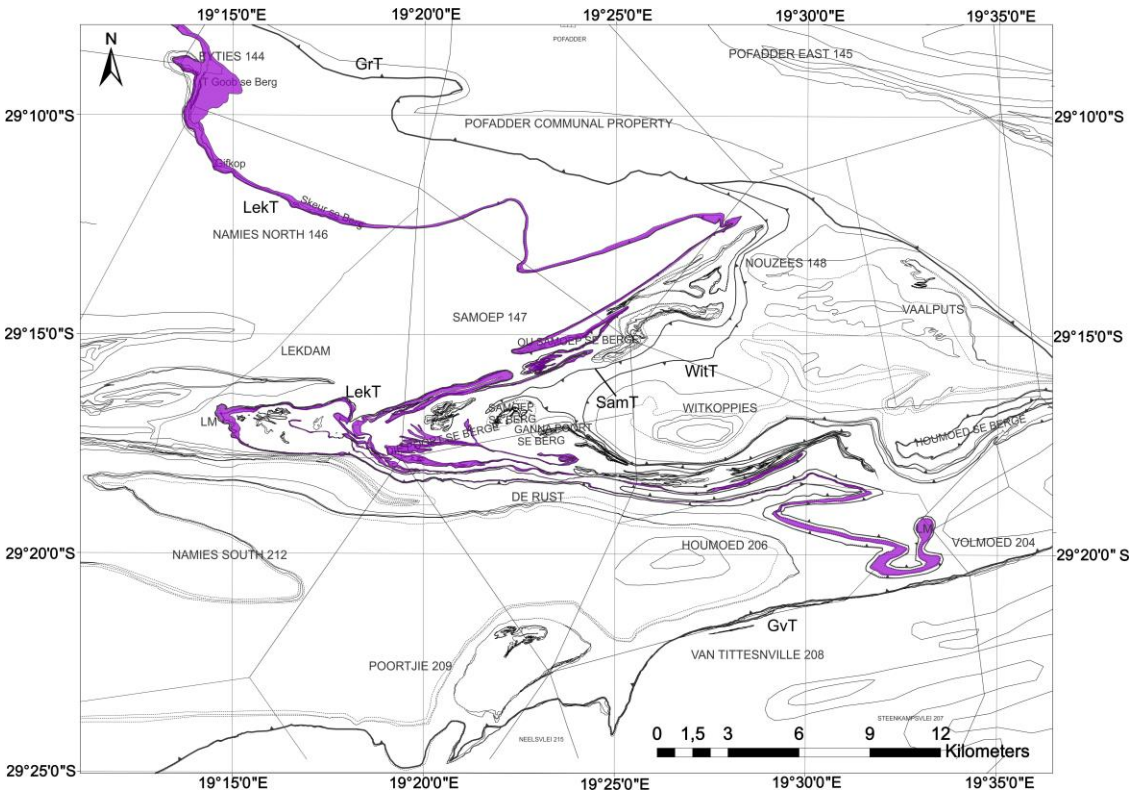

Figure 2.46: Distribution of the T-Goob Succession throughout the study area in purple (Grt: Groothoek Thrust; Gvt: Geelvloer Thrust; LekT: Lekdam Thrust; SamT: Samoep Thrust and WitT: Witkoppies Thrust).

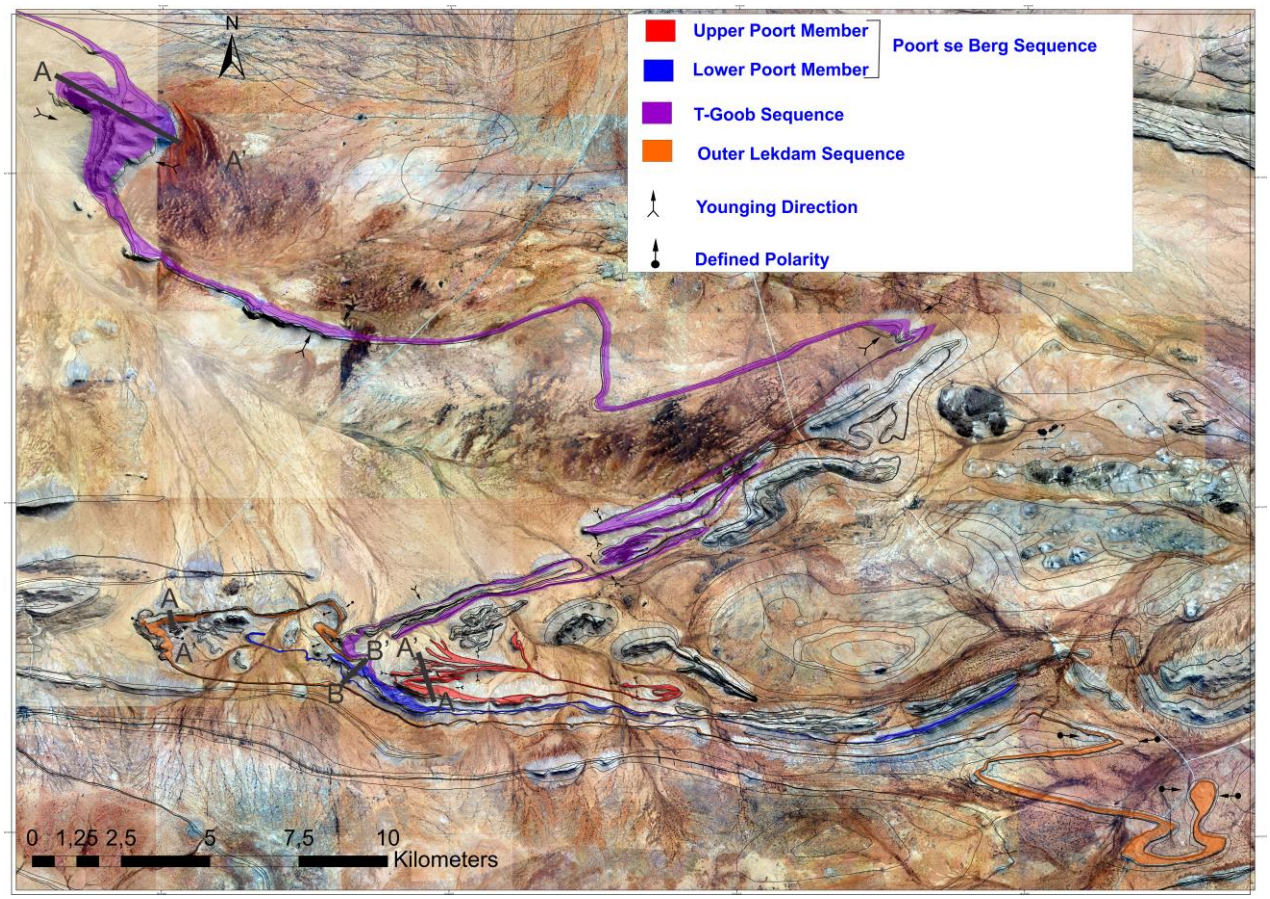

Figure 2.47: Distribution of the three structures associated with the T-Goob Succession: The T-Goob se Berg Sequence (purple), Poort se Berg Sequence (red and blue), and the Outer Lekdam Sequence (orange). The relevant profiles for each structure that give the best stratigraphic representation for the Goob Succession is also indicated for each sequence.

2.9.4.1 The Poort se Berg Sequence

The Poort se Berg Sequence defines two highly folded isoclinal folds and extends along strike from east to west. The Poort Sequence is divided into an upper and lower Poort Member, which have very similar attributes to one another. The Poort se Berg Sequence is represented by thick to thin sequences of biotite-sillimanite schist, garnet-bearing meta-quartzite, volcanoclastic/chemogenic sequences, thick poorly bedded white-blue quartzite, and nodular sillimanite-quartz-feldspar gneisses. The Lekdam Gneiss is also associated with both the upper and lower Poort Members which surrounds both structures. The best example of the stratigraphy associated with the Poort-se-Berg Members can be seen in profiles A-A' and B-B' (Figure 2.47 and Figure 2.48). Thick stratigraphic sequences thin out as you move toward the east due to shearing and isoclinal folding.

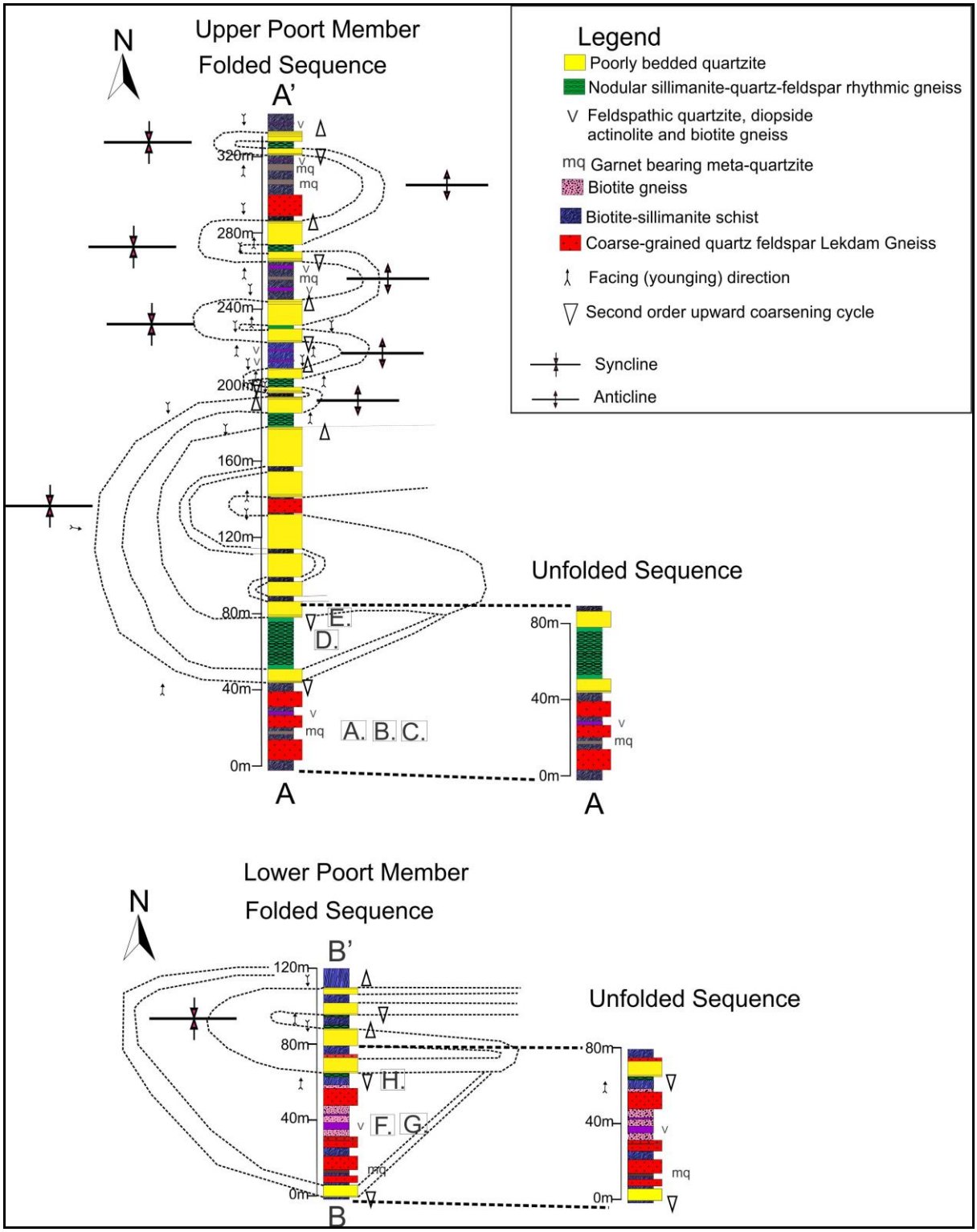

Figure 2.48: Profile A-A' and B-B' (from Figure 2.47) which represents the Poort se Berg Sequence, which is divided into an upper and lower Poort se Berg Member. Profile A-A' represents the folded sequence associated with the upper Poort se Berg Member, with the offset profile to the right representing the unfolded sequence. Profile B-B' depicts the stratigraphy associated with the lower Poort se Berg Member, with the offset profile toward the right representing the unfolded sequence. The letters A to G represent locations and photographs (Appendix 2.10).

2.9.4.1.1 Upper Poort se Berg Member

The base of the stratigraphic succession is defined by a thick succession of biotite-sillimanite schist (Appendix 2.10 A), with interbanded units of garnet-bearing meta-quartzite and volcanic/chemogenic units. The chemogenic/volcanoclastic unit is defined by slivers of biotite gneiss, calc-silicate rock, feldspathic quartzite (Appendix 2.10 B), with banded units of diopside, and actinolite.The volcanic/chemogenic unit often varies in thickness between 1 and 5 metres respectively. Primary bedding in the form of flame structures can also be observed in certain localities associated with the volcanic unit, showing stratigraphic younging toward the top of the succession (Appendix 2.10 B). This specific volcanic sequence often acts as a prominent marker unit right across the structure. Prominent successions of garnet quartzites (banded variations also found) occur as lenticular units above and below the volcanoclastic sequence within the biotite-sillimanite schist unit (Appendix 2.10 C). The upper portion of the upper Poort se Berg Member is affected by thrusting and kilometre scale boudinage effects. Due to this effect, a poorly bedded white-blue quartzite occurs just above the biotite-sillimanite schist unit, and is only seen in certain portions of the Poort se Berg structure and defines prominent second-order upward coarsening cycle (Appendix 2.10 D). This specific quartzite is folded heavily with the volcanic sequence and garnet quartzites in the northern portion of the structure and is best represented by Profile A-A' (Figure 2.48).

Overlying the thick poorly bedded quartzite, a succession of nodular sillimanite-quartz-feldspar rhythmic gneiss is found with slivers of biotite-sillimanite schist. Prominent sillimanite nodules with diameters ranging between 2 to 7 centimeters in certain locations is associated with the upper nodular rhythmic gneiss (Appendix 2.10 E). Nodular rhythmic sillimanite-quartz-feldspar gneiss is also seen folding around the entire succession and has a sharp contact with an overlying poorly bedded quartzite, also displaying prominent second-order upward coarsening cycles. A prominent biotite-sillimanite schist unit overlies the lower poorly bedded quartzite and defines the central hinge zone of the Poort se Berg structure, and is only fully visible within lower strain zones across the structure.

2.9.4.1.2 Lower Poort se Berg Member

The lower Poort se Berg Member is also defined by an isolated isoclinal fold structure and is best represented by Profile B-B' (Figure 2.47 and 2.48). The Lekdam Gneiss is found at the base of the succession and has a sharp contact with a biotite-sillimanite schist unit in contact with a poorly bedded quartzite, defining a second-order upward coarsening cyle. The quartzite-biotite-sillimanite schist unit defines a duplicated unit that branches out toward the east and is strongly boudinaged toward the west of the structure, where it folds back toward the east. Above the poorly bedded quartzite, a thick sequence of biotite sillimanite schist is

found with interbanded units of biotite gneiss, garnet bearing meta-quartzite, a volcanoclastic/chemogenic unit of feldspathic quartzite (Appendix 2.10 F), biotite gneiss (Appendix 2.10 G) actinolite, and diopside. Centimetre to metre scale units of rhythmic nodular sillimanite-quartz-feldspar gneiss (Appendix 2.10 H) is also found interbanded within. A gradational contact is found with another poorly bedded quartzite toward the top of the succession that also defines a second-order upward coarsening cycle. Overlying the poorly bedded quartzite is a biotite-sillimanite schist unit, capped by another poorly bedded quartzite. The biotite sillimanite schist unit represents the central fold hinge of the isoclinal fold structure.

2.9.4.2 T-Goob se Berg Sequence

The T-Goob se Berg Sequence is regionally one of the most complex structures and extends along strike for a distance of about 121 kilometres when the individual stratigraphic units are traced out. The Groothoek Thrust Zone runs sub-parallel to the structure, with the southern side of the structure underlain by the Achab Suite, where the northern side of the structure is overlain by the Lekdam Gneiss, with the structure being situated on the contact between the Houmoed and Lekdam Structural Domain (thrust sheets). The best exposure of the entire succession can be seen in the thickest portion within the study area associated with profile A-A' in Figure 2.47 and Figure 2.49. Complications associated with this portion of the T-Goob Sequence occur along strike and will be discussed in Chapter 5. The T-Goob Sequence was previously mapped by Pretorius (1986) and Watkeys (1986). Pretorius mapped the T-Goob Sequence in a fair amount of detail toward the northwest of the study area in the Annakoppies and Eenriet vicinity and on T-Goob se Berg itself, where thicker successions occur. Watkeys (1986) also mapped the T-Goob Sequence at T-Goob se Berg, simplifying the stratigraphic sequence, specifically concerning the volcanoclastic succession and intrusives surrounding the T-Goob se Berg structure.

The southern base of the T-Goob Sequence is defined by the augen bearing component of the Achab Suite, which also folds symmetrically with the above metasedimentary units along strike. Three variations of the Achab Suite are found. The variations that are found are due to strain variations associated with the Achab Suite as you move closer to the upper supracrustal succession. Above the Achab Suite, a small rhythmic nodular sillimanite-quartz-feldspar gneiss is found, with small interbands of biotite-sillimanite schist. Overlying the nodular sillimanite-quartz-feldspar rhythmic gneiss a poorly bedded quartzite is found, displaying a prominent second-order upward coarsening cycle and this represents the southern lower limb of the T-Goob se Berg sheath fold structure (Appendix 2.11 A). Above the poorly bedded quartzite, the middle portion of the stratigraphic succession is defined and represents the hinge zone of the structure. The middle portion is defined by a thick sequence of biotite-sillimanite schist with lenticular units of volcanoclastic/chemogenic sediments defined by

amphibolite, banded white-blue quartzite with interbands of actinolite, diopside, and large to thin lenses of biotite gneiss (Appendix 2.11 B, C, and D). The middle portion was mapped as a massive biotite schist unit with interlayered amphibolite by both Pretorius (1986) and Watkeys (1986). However, the author has re-interpreted the middle portion of the stratigraphy and differs vastly from previous interpretations.

The base of the middle portion is defined by a thick unit of biotite-sillimanite schist, which grades into biotite gneiss (Appendix 2.11 E), and which at certain localities has garnet overgrowths, which vary in size from 1 to 10 centimetres in width (Appendix 2.11 F). The biotite gneiss encapsulates the volcanoclastic unit and has an intriguing relationship with the biotite-sillimanite schist, these two units often inter-finger with one another along strike and often have gradational contacts throughout the central portion of the succession. The volcanoclastic/chemogenic unit in its entirety is thickest at T-Goob se Berg, with a total thickness of 20m. However, along strike this unit thins out dramatically on a decameter to centimeter scale.

Above the volcanoclastic/chemogenic unit, a sharp contact is found with a thick well foliated medium-quartz feldspar gneiss (Appendix 2.11 G). The well-foliated medium quartz-feldspar gneiss extends for a distance of 10 kilometers from T-Goob se Berg, to where it branches out toward the east. Above the medium quartz-feldspar gneiss a sharp contact is found with a nodular sillimanite-quartz-feldspar rhythmic gneiss, with interbands of biotite-sillimanite schist; prominent sillimanite nodules can often be viewed on outcrop scale (Appendix 2.11 H). The sillimanite nodules vary between 2 and 8 centimetres in diameter. Overlying this unit, a poorly bedded quartzite is found, which is interpreted to be the northern limb associated with the T-Goob se Berg sheath fold structure. Duplications, are found due to thrusting of the nodular sillimanite-quartz-feldspar rhythmic gneiss unit and poorly bedded quartzite is found toward the upper portion of the northern limb. Prominent second-order upward coarsening and fining cycles can be seen within the upper poorly bedded quartzite (Figure 2.49). Overlying the upper quartzite is the coarse-quartz-feldspar Lekdam Gneiss, which overlies the meta-sedimentary succession in the north.

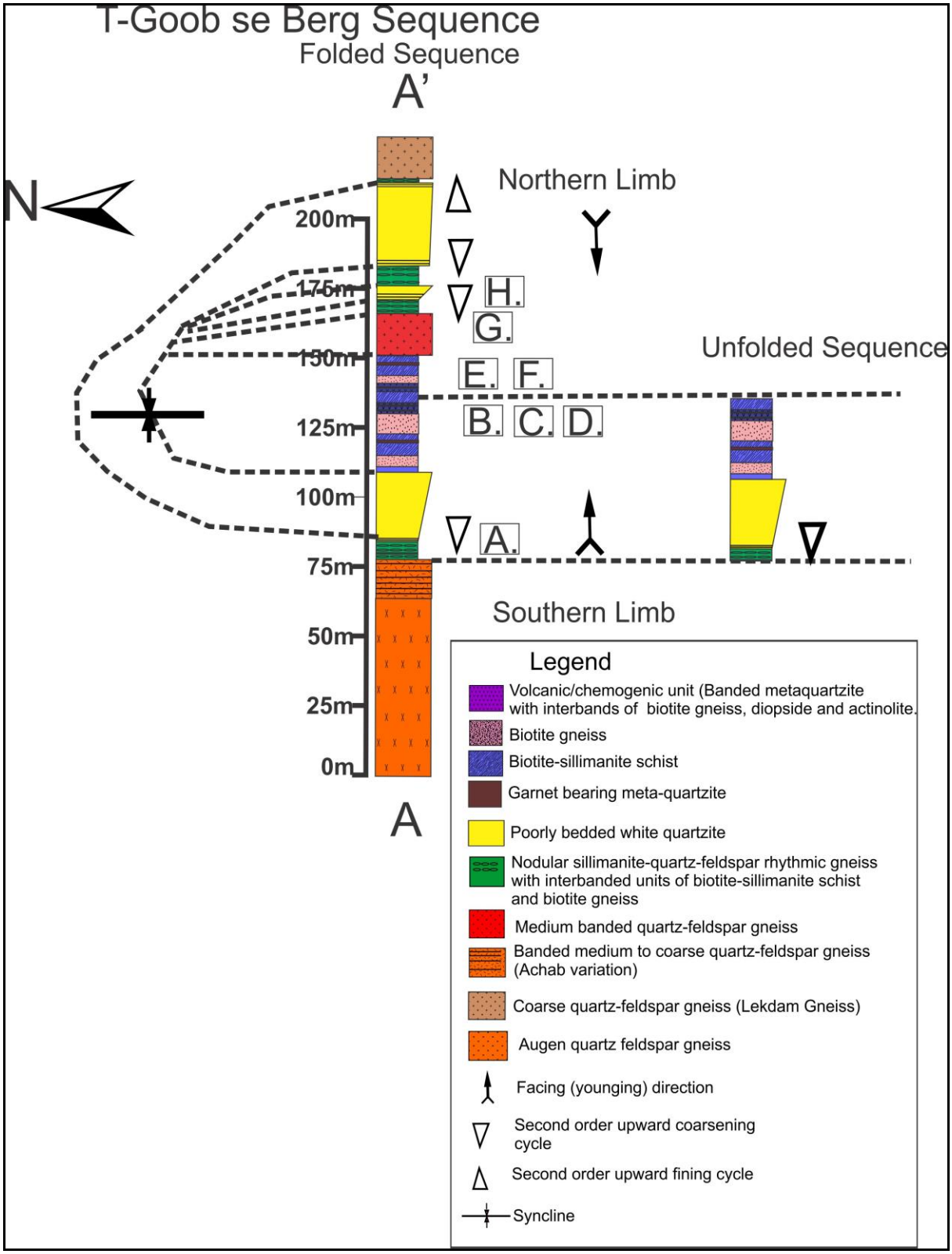

Figure 2.49: Profile A-A' (from Figure 2.47) which best represents the T-Goob Sequence. Both the folded and unfolded sequence is represented. Within the folded sequence the northern limb and southern limb is represented. The small letters A to H represent photographs associated with the stratigraphy and can be found in Appendix 2.11.

2.9.4.3 The Outer Lekdam Sequence

The Outer Lekdam Sequence is defined by a highly flattened isolated refolded isoclinal structure that extends along strike for a distance of ±52 kilometres. The Outer Lekdam Sequence, as with the T-Goob Sequence, is also situated on the contact between the Houmoed and Lekdam Thrust Sheets. The best exposure of the Outer Lekdam Sequence can be found in Profile A-A' in Figure 2.47 and Figure 2.50. The basal portion of the Outer Lekdam Sequence is defined by the Achab Suite, which is seen in the north and south of the structure. Above the Achab Suite a sharp contact is found with the above Lekdam Gneiss. Overlying the Lekdam Gneiss a thin sequence of biotite gneiss is found with inter-bands of feldspathic quartzite and biotite gneiss (Appendix 2.12 A and B). Above the feldspathic quartzite unit, a thick succession of biotite-sillimanite schist is found (Appendix 2.12 C), with interbands of nodular sillimanite-quartz-feldspar rhythmic gneiss and ferruginous garnet meta-quartzites. The biotite-sillimanite schist unit various in thickness from 30 metres to 1 metre along strike, with the best exposures seen in the north of the structure.

Above the biotite sillimanite schist unit a poorly bedded thick white quartzite is found, with prominent bands of biotite (Appendix 2.12 D). Along strike, as you move toward the east this specific quartzite becomes mylonitic due to east-west shearing. Prominent second-order upward coarsening cycles are seen concerning the upper quartzite. Duplications are also seen due to parasitic folding along strike (Appendix 2.12 E). Above the quartzite, a nodular rhythmic gneiss (Appendix 2.12 F), and interbands of biotite sillimanite schist are found representing the hinge zone of the D2 isoclinal fold structure. The defined polarity associated with this sequence is defined by the Lekdam Gneiss at the base of the succession, overlain by feldspathic quartzite, with interbands of biotite gneiss, overlain by a thick sequence of biotite-sillimanite schist, in contact with a poorly bedded quartzite displaying a second-order upward coarsening cycle. The upper succession is defined by nodular sillimanite-quartz-feldspar gneiss, with interbands of biotite-sillimanite schist, which defines the hinge zone of the Outer Lekdam Structure.

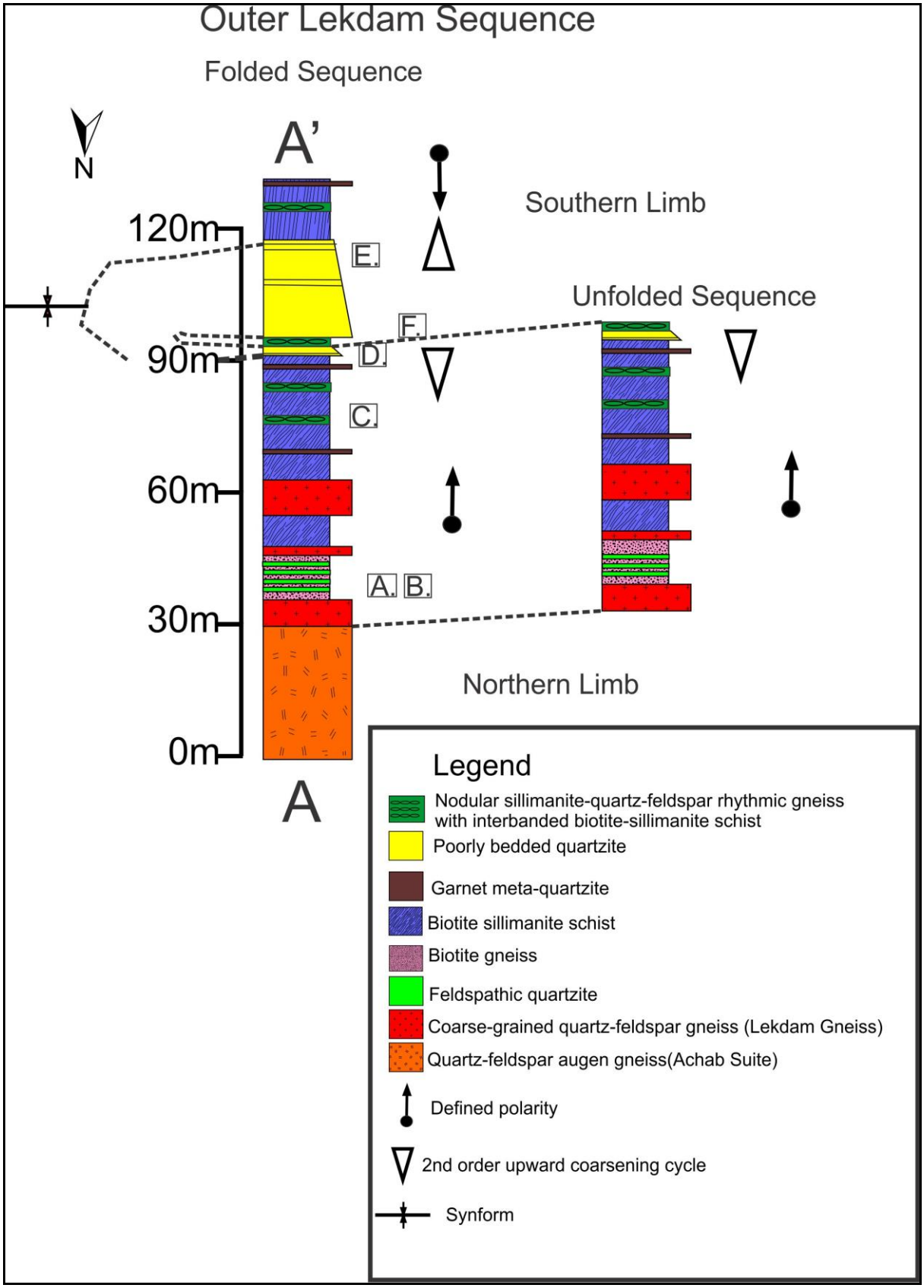

Figure 2.50: Profile A-A' (from Figure 2.47) represents the stratigraphic succession associated with the Outer Lekdam Sequence. Both the folded sequence and unfolded sequence are represented. The small letters A to H represent photographs associated with the stratigraphy and can be found in Appendix 2.12.

2.9.4.4 Correlation and summary of the T-Goob Succession

When all three sequences which constitute the T- Goob Succession are horizontally restored, the characteristics are well displayed (Figure 2.51). All three structures have the same attributes, with one or two lithological differences owed to structural complications, such as isoclinal folding, strain partitioning and thrusting. All three structures essentially contain metre to centimeter scale volcanoclastic/chemogenic units of feldspathic quartzite, diopside, actinolite and biotite gneiss. All the volcanoclastic/chemogenic units are surrounded by a thick sequence of biotite-sillimanite schist, with interlayered biotite gneiss having a gradational contact with the enveloping biotite sillimanite schist units. The volcanoclastic/chemogenic unit associated with the T-Goob se Berg Sequence is the best exposed when compared to the Lekdam and Poort se Berg Sequences, and has a more chemogenic nature. The vast difference between the three structures is that the volcanoclastic sequence/chemogenic is contained within the hinge zone of the T-Goob se Berg Sequence, whereas the volcanoclastic/chemogenic unit in the Poort se Berg and Outer Lekdam Sequences is confined to the limbs of the large isoclinal fold structures (Figure 2.51). The volcanoclastic/chemogenic unit associated with the Outer Lekdam Sequence has a higher feldspathic quartzite component when compared to the other two sequences.

All three sequences have a prominent poorly bedded thick to thin quartzite, displaying a prominent upward coarsening cycle. These poorly bedded quartzites define the upright and over-turned limbs associated isoclinal fold structures related to the T-Goob Succession. Another lithological unit associated with the T-Goob Succession is the presence of thick to thin sequences of nodular rhythmic sillimanite-quartz-feldspar gneisses, mostly found toward the top of the succession, with the exception being the T-Goob se Berg Sequence, where the nodular rhythmic gneiss is found at the base. Throughout the study area the slivers of biotite-sillimanite schist is often interbanded within the thick nodular sillimanite-quartz-feldspar rhythmic gneisses. The younging direction and defined polarity for all three members coincide with one another (Figure 2.51).

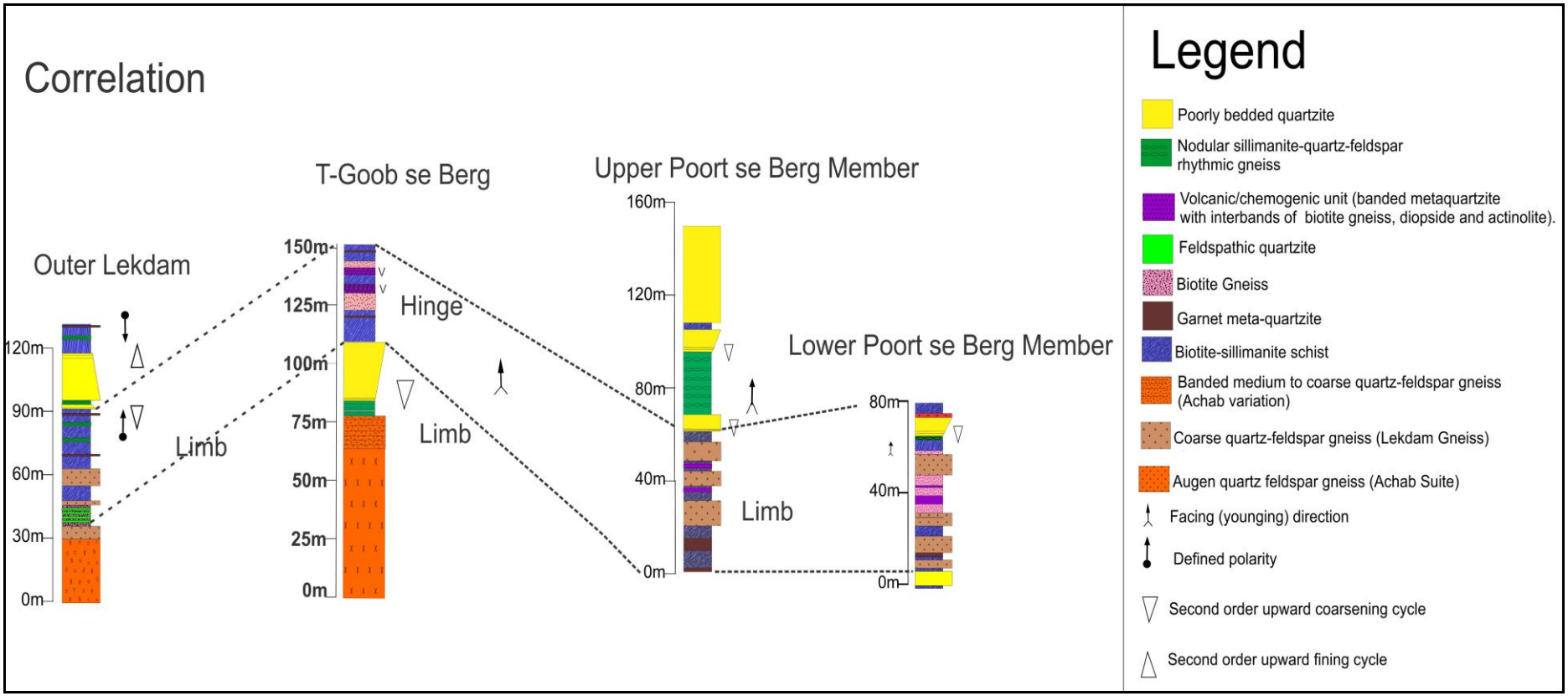

Figure 2.51: Horizontally restored comparison diagram associated with the stratigraphic profiles of the Outer Lekdam and T-Goob se Berg Sequences and the Upper and Lower Poort se Berg Members, which define the T-Goob Succession. Within all sequences the volcanic/chemogenic unit is clearly visible with interbanded biotite gneiss, biotite-sillimanite schist and garnet meta-quartzite units. The most distinctive difference is that this volcanic/chemogenic unit is situated within the hinge zone of the T-Goob Sequence and on the limbs of the Outer Lekdam and Poort se Berg Sequences.

2.9.5 Inner Lekdam Succession

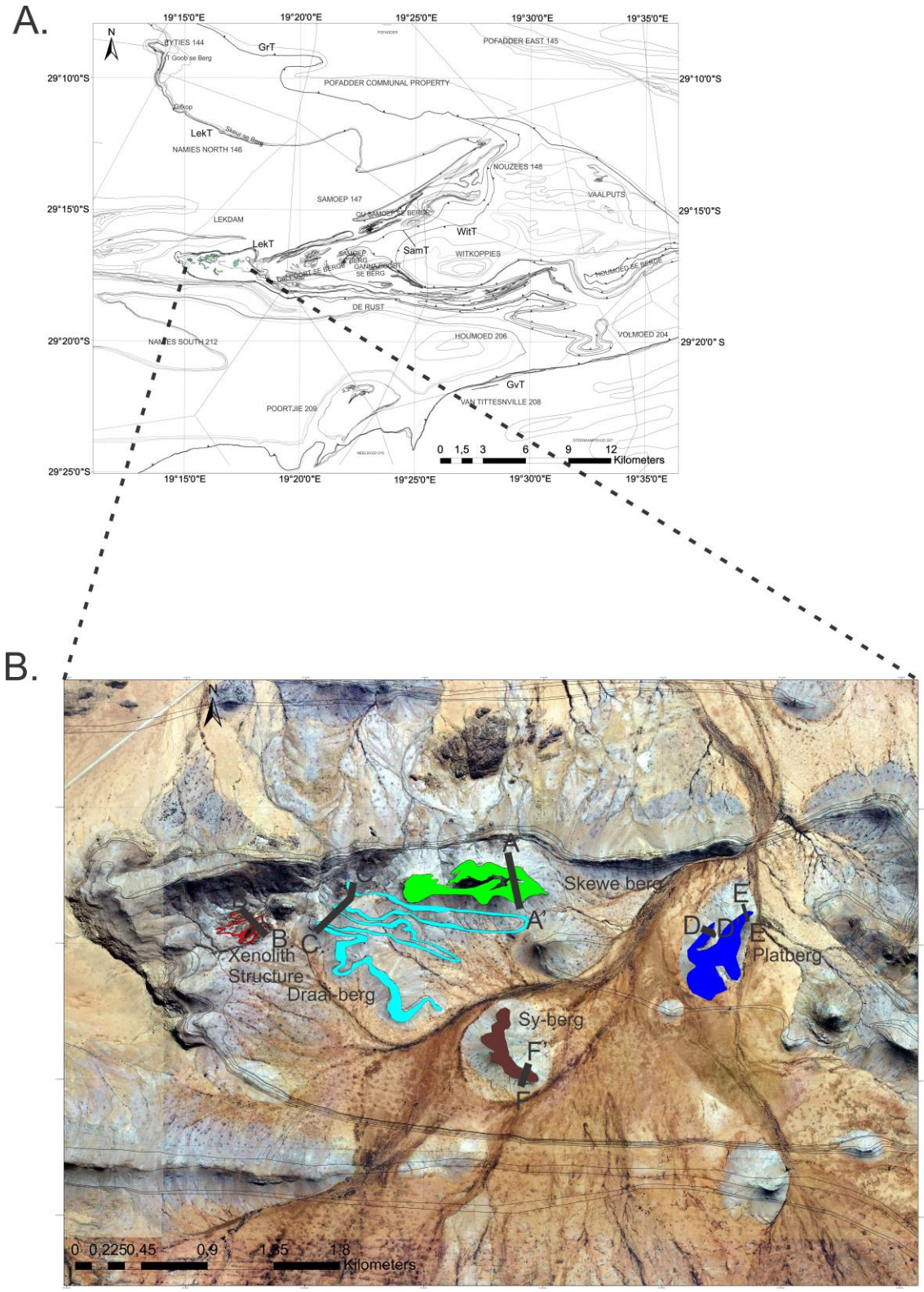

Figure 2.52: Distribution of the Inner Lekdam Succession. A: Regional map, showing the location of the Inner Lekdam Sequence B: Aerial photograph, outlining the structures and various profile locations associated with the Inner Lekdam Succession. The structures associated with the Inner Lekdam Succession are, the Skewe Berg Sequence (light green: A-A') Xenolith Sequence (red: B-B'), Draai-Berg Sequence (turquoise: C-C'), Platberg Sequence (blue: D-D'; E-E') and Sy-Berg Sequence (brown: F-F').

The Inner Lekdam Succession is defined by five prominent sequences found in the far west of the study area (Figure 2.52 A and B). All five sequences are encapsulated by the coarse-quartz-feldspar Lekdam Gneiss. Five of the four sequences are defined as isolated isoclinal fold structures having their own stratigraphic successions, with one structure being interpreted as a folded xenolith within the Lekdam Gneiss. The stratigraphic succession is defined by thin to thick successions of biotite-sillimanite schist with intercalated units of garnet-bearing ferrigunous BIFs, feldspathic quartzites, nodular sillimanite-quartz-feldspar rhythmic gneiss, calc-silicate rock, and biotite gneiss. The succession is dominated by the presence of garnet-bearing ferruginous meta-quartzites, which define the succession. The Inner Lekdam Succession is defined by the Skewe Berg Sequence, Xenolith Sequence Draai-Berg Sequence, Platberg Sequence, and Sy-Berg Sequence (Figure 2.52 B).

2.9.5.1 The Skewe Berg Sequence

The Skewe Berg Sequence is defined by an isolated hill just to the south of the Outer Lekdam Sequence within the Lekdam Gneiss. The Skewe Berg Sequence represents an isolated refolded isoclinal fold structure having its own stratigraphy (Profile AA; Figure 2.53). The base of the Skewe Berg Sequence is defined by a thick succession of biotite-sillimanite schist, with lenticular units of garnet quartzite, biotite gneiss, amphibolite and thick to poorly bedded quartzite. The best exposure of the Skewe Sequence is found in profile A (Figures 2.51 B and 2.52). At the base of the succession, thick units of Lekdam Gneiss are found, above which a thick sequence of biotite-sillimanite schist is found (Appendix 2.13 A). The biotite-sillimanite schist drastically thins out around the over-turned limb toward the south of the mountain. Toward the top of the sequence, a prominent layer of biotite gneiss is found (Appendix 2.13 B), which disappears and folds out towards the south of the structure. Prominent lenticular units of garnet quartzite and amphibolite are found throughout the succession (Appendix 2.13 C). These units occur sporadically around the Skewe Berg structure. Toward the top of the succession, a poorly bedded thick white quartzite is found, above which a nodular rhythmic sillimanite-quartz-feldspar gneiss unit is found.

The sillimanite nodules are a prominent feature and vary between 2 and 4 centimeters along strike (Appendix 2.13 D), with slivers of interbanded biotite-sillimanite schist. These units define the central hinge of the Skewe Berg structure. The upper quartzite defines a second-order upward coarsening cycle. The defined polarity is identified by a thick succession of biotite–sillimanite schist with interbanded units of biotite gneiss and garnet-bearing meta-quartzite in contact with a poorly bedded quartzite, defining a prominent second-order upward coarsening cycle, capped by a prominent sequence of nodular rhythmic sillimanite-quartz-feldspar gneiss with interbanded units of biotite-sillimanite schist.

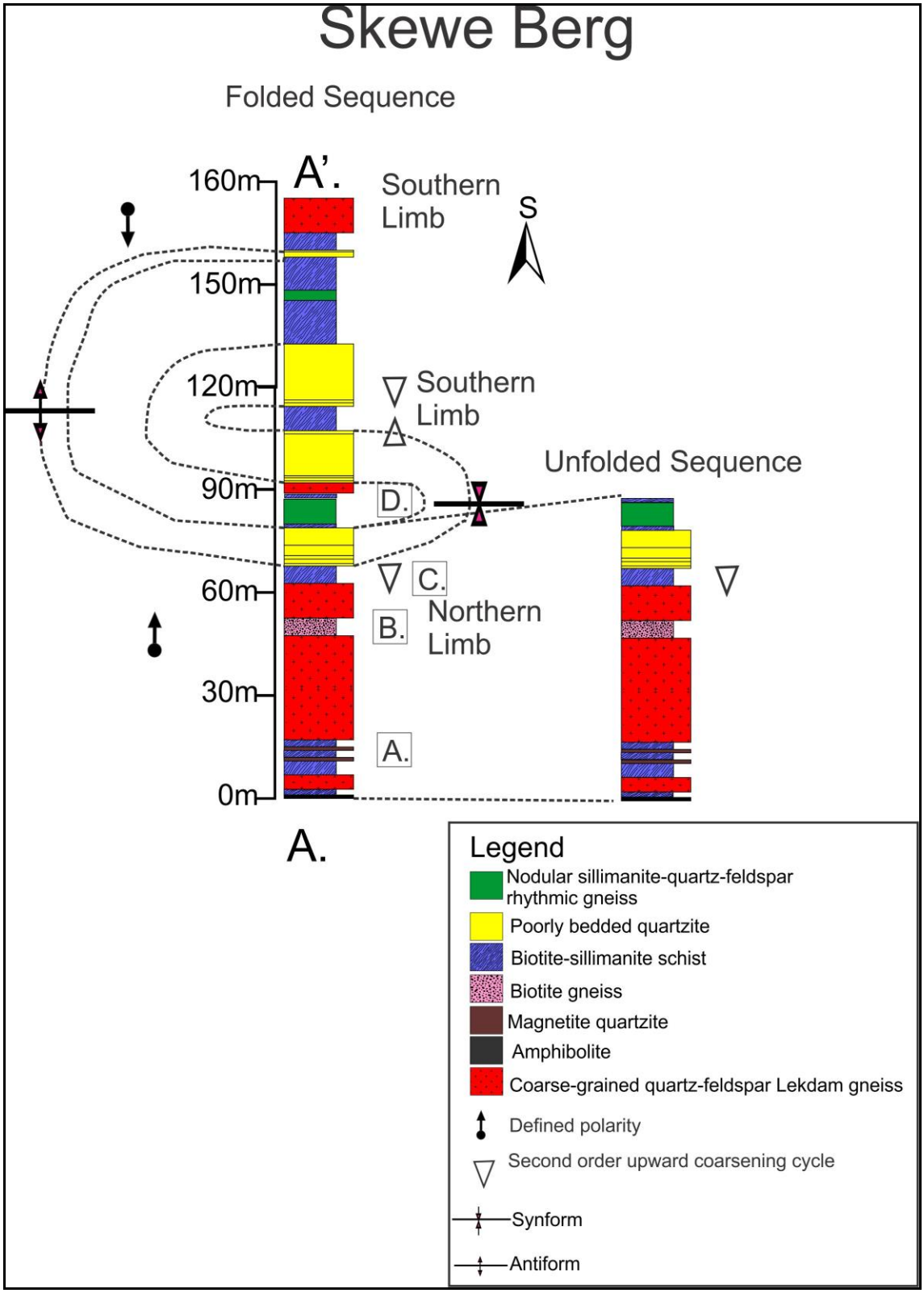

Figure 2.53: Profile A-A' (from Figure 2.52B) represents the best exposure of the Skewe Berg Sequence. Profile A represents the entire succession, with the offset profile toward the right representing the unfolded part of the succession: The small letters A to D represent photographs associated with the stratigraphy and can be found in Appendix 2.13.

2.9.5.2 The Xenolith Sequence

The Xenolith Sequence is located adjacent to the Outer Lekdam Sequence (T-Goob Succession) toward the west of the structure, with the Skewe Berg and Draai-Berg Sequences situated just toward the east of the structure (Figure 2.52 B). The name is derived from the fact that this sequence resembles a meta-sedimentary assemblage folding within the coarse-grained quartz feldspar Lekdam Gneiss, and is interpreted to be a folded xenolith. The entire sequence is folded in an isoclinal fashion. Profile B-B' in Figure 2.52 B best represents the stratigraphic succession related to the Xenolith Sequence. The base of the stratigraphic succession is defined by banded feldspathic quartzite, overlain by biotite-sillimanite schist, with interbanded units of ferruginous garnet meta-quartzite (Appendix 2.14 A and B). The garnet metaquartzites and feldspathic quartzites are surrounded by a sequence of biotite-sillimanite schist (Appendix 2.14 C). Small sillimanite nodules are often seen within the biotite-sillimanite schist and have diameters of between 2 and 4 centimeters (Appendix 2.14 D). The coarse-grained quartz-feldspar Lekdam Gneiss also intrudes throughout the Xenolith Sequence. Garnet overgrowths on the Lekdam Gneiss are very clearly represented in this location and are interpreted to be late to syntectonic, with respect to the regional foliation. The defined polarity is defined by feldspathic quartzite, overlain by the ferruginous garnet meta-quartzite and biotite-sillimanite schist units (Figure 2.54).

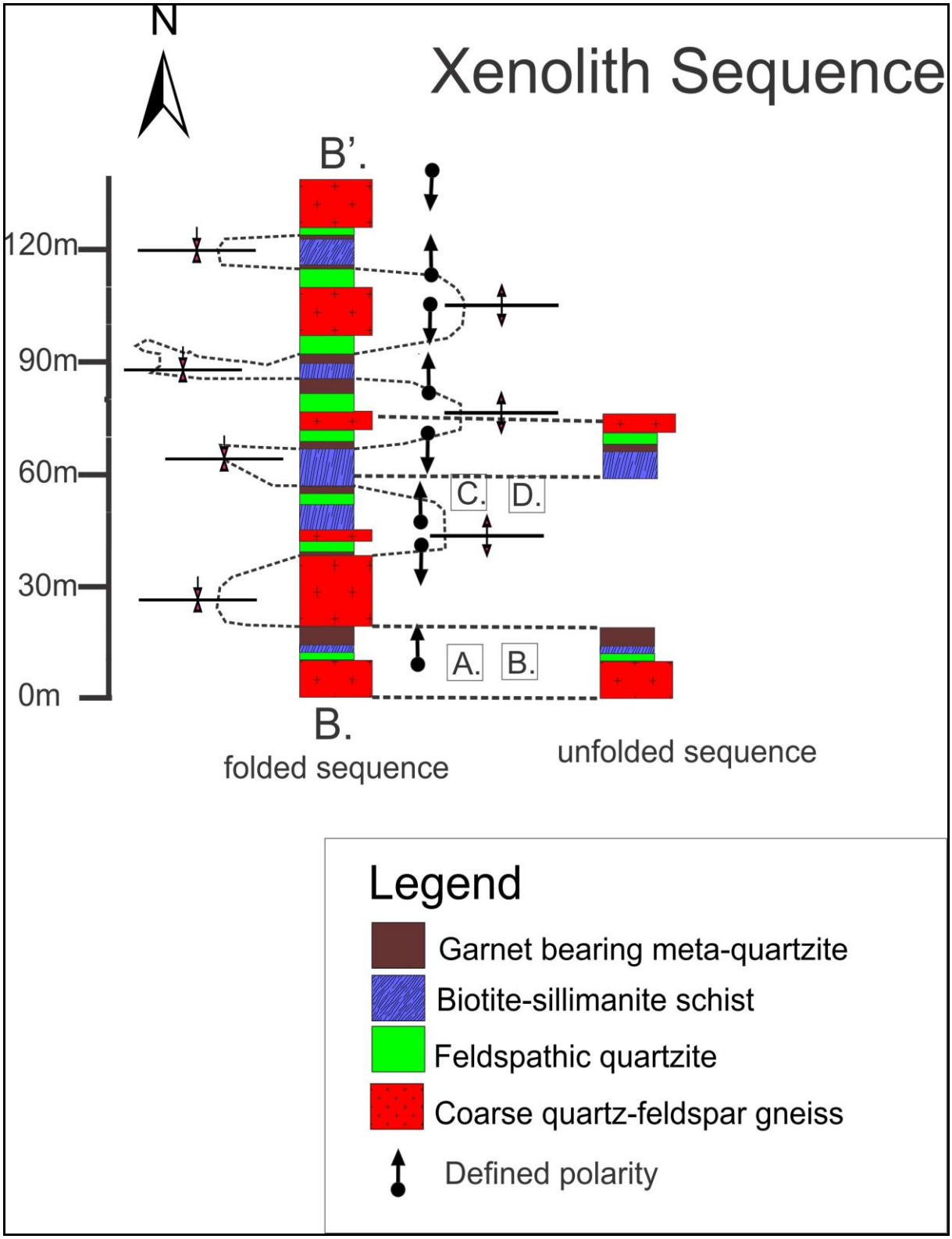

Figure 2.54: Profile B-B' associated with the Xenolith Sequence. The location can be found in Figure 2.52 B. The profile represents the folded and unfolded sequence, which depicts the defined polarity. The letters A to D represent locations and photographs (Appendix 2.14).

2.9.5.3 The Draai-Berg Sequence

The Draai-Berg Sequence represents a highly folded isoclinal structure. Poor exposures of the Draai-Berg Sequence are found toward the south, especially concerning the less competent units (Profile C-C'; Figure 2.52 B). Within this structure, the Draai-Berg Sequence is best exposed toward the north-west where the hinge zone of the structure is exposed, represented by profile C-C' in Figure 2.55. The base of the succession is defined by thin successions of biotite-sillimanite schist with intercalated units of feldspathic quartzite found on centimetre scale (Appendix 2.15 A). Within the biotite-sillimanite schist unit centimetre to metre scale of lenticular units of garnet metaquartzites and black calc-silicate rocks are also found (Appendix 2.15 B and C). The dark calc-silicate units have feldspar bands and occur sporadically together with the garnet-bearing meta-quartzites. Above these units a thick poorly bedded quartzite is found (Appendix 2.15 D), overlain by a poorly defined biotite-sillimanite schist unit defining the hinge of the structure. The defined polarity is represented by biotite-sillimanite schist, with interbanded units of feldspathic quartzite, garnet-bearing meta-quartzite, and dark calc-silicate rock, in contact with a poorly bedded quartzite, defining a second-order upward coarsening cycle, with the uppermost unit being defined by a meter scale biotite-sillimanite schist.

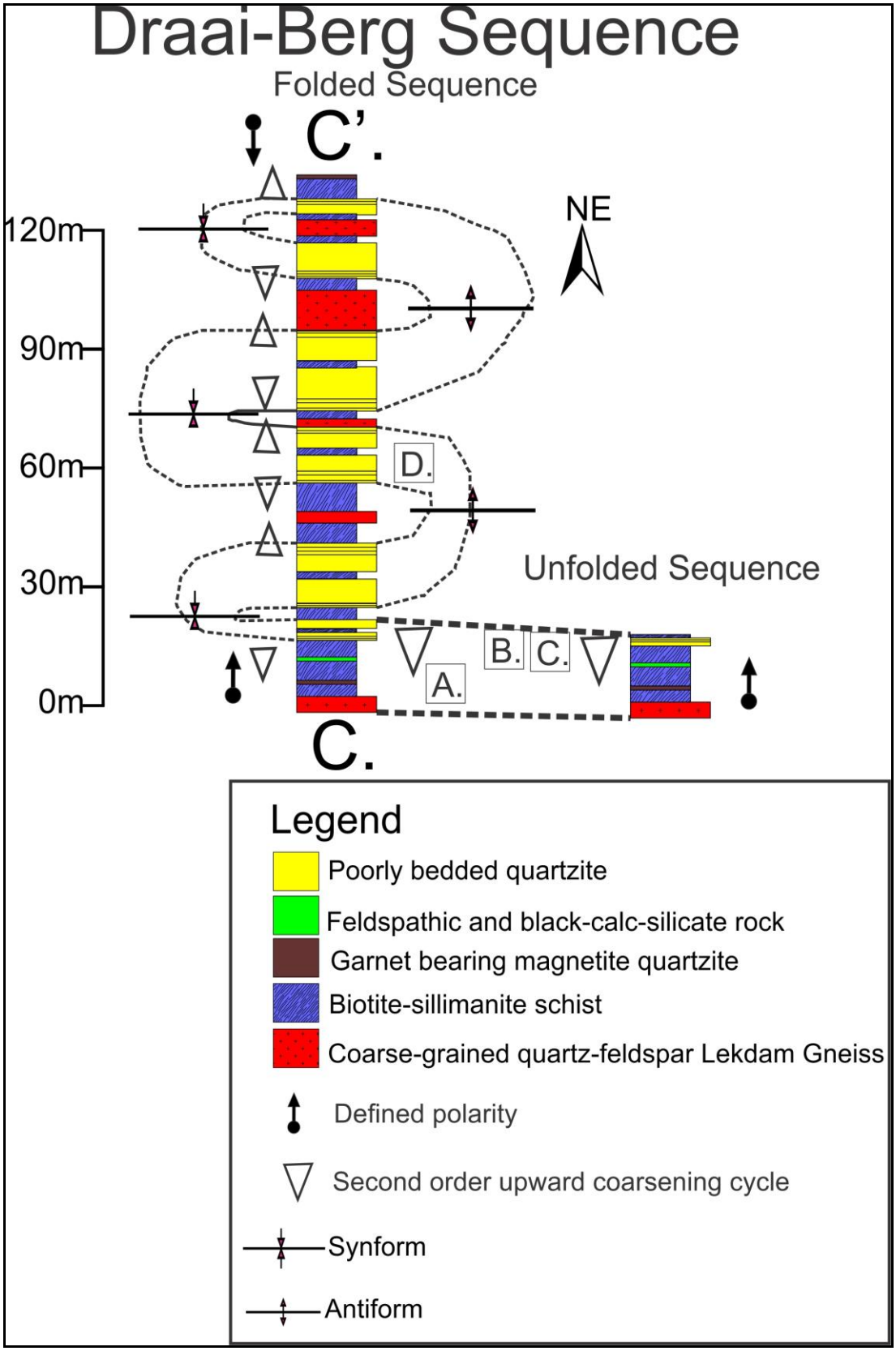

Figure 2.55: Profile C-C' (from Figure 2.52 B) represents the stratigraphy associated with the Draai-Berg Sequence. Profile C represents the entire succession, with the offset profile representing the unfolded succession. The letters A to D represent locations and photographs (Appendix 2.15).

2.9.5.4 The Platberg Sequence

The Platberg Sequence is relatively poorly exposed, except for the north and northwestern sectors of the structure, represented by profiles D and E in Figures 2.52 B and Figure 2.56. The lower portion of Platberg Sequence is defined by a thick to thin sequence of biotite-sillimanite schist, which is overlain by a thick poorly bedded quartzite, which defines a second-order upward coarsening cycle (Appendix 2.16 A). The biotite-sillimanite schist unit folds around the upper quartzite and contains intercalated units of ferruginous garnet-bearing meta-quartzites (BIFs), which act as a marker folding around the structure (Appendix 2.16 B). The entire structure is surrounded by the coarse-grained quartz-feldspar Lekdam Gneiss, which has a lit-par-lit contact with the upper stratigraphic succession. The defined polarity is represented by the biotite-sillimanite schist, with interbanded units of garnet meta-quartzite, overlain by a poorly bedded quartzite unit, defining a second-order upward coarsening cycle. The Platberg Sequence represents an isolated Ramsay type 2 interference structure and is located just to the south of the Outer Lekdam isoclinal fold structure.

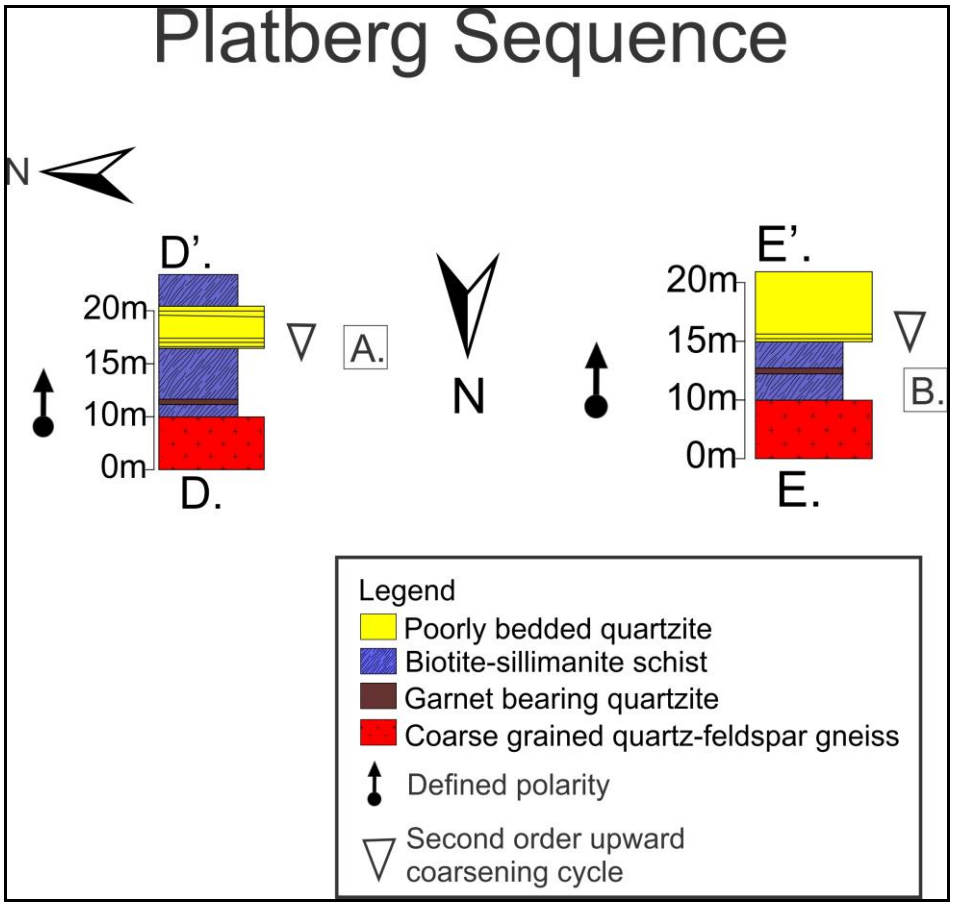

Figure 2.56: Profiles D-D' and E-E' (Figure 2.52 B) represent the Platberg Sequence. The Letters A and B represent photographs and location (Appendix 2.16).

2.9.5.5 The Sy-Berg Sequence

The Sy-Berg Sequence is confined to a ridge just to the south of the Draai-Berg structure and represents the southernmost isoclinal fold structure (Figure 2.52 B). The Sy-Berg Sequence is also surrounded by the coarse-grained quartz-feldspar Lekdam Gneiss and represents a flattened ellipsoidal fold structure. Throughout the stratigraphic succession, the associated lithological units are relatively poorly exposed, with only the more competent quartzitic units being exposed, and less incompetent units like biotite-sillimanite schist and feldspathic quartzites units being rarely seen, and occurring sporadically throughout at the base of the stratigraphic succession. The stratigraphy associated with the Sy-Berg Sequence is best represented by Profile F (Figure 2.52 B and Figure 2.57)

Small lenticular units of feldspathic quartzites are found with slivers of biotite gneiss (Appendix 2.17 A), above which a thin succession of biotite-sillimanite schist is found. The lower succession is heavily intruded by the Lekdam Gneiss, which encompasses the succession. The top of the succession is defined by a thick to thin to poorly bedded quartzite, defining a prominent second-order upward fining cycle, often observed on the contact with the biotite-sillimanite schist and the quartzite (Appendix 2.17 B). Above the poorly bedded quartzite, a poorly exposed thick to thin unit of biotite-sillimanite schist is found, defining the hinge zone of the structure. Within the biotite-sillimanite schist lenticular units of dark-blue quartzite are found (Appendix 2.17 C). The defined polarity is distinguished by the biotite gneiss-feldspathic quartzite unit in contact with the biotite-sillimanite schist unit, in contact with a poorly bedded quartzite, defining a second-order upward fining cycle, overlain by biotite-sillimanite schist interbanded with dark-blue quartzite units.

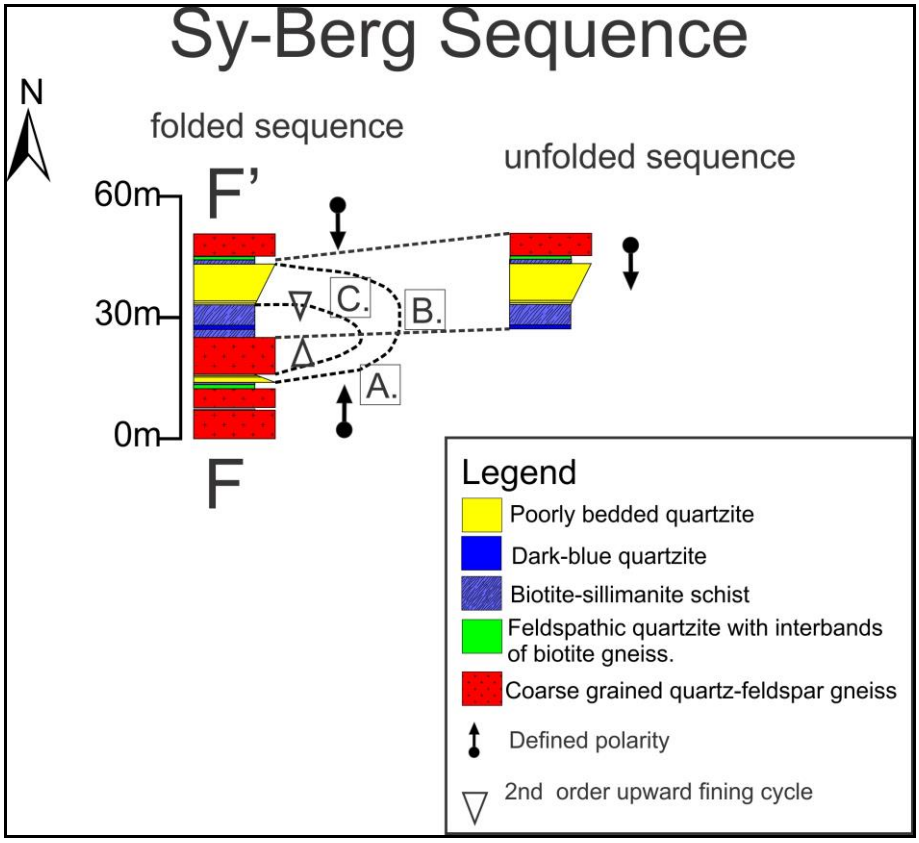

Figure 2.57: Profile F-F' (Figure 2.52 B) represents the stratigraphy associated with the Sy-Berg Sequence. Both the folded sequence and unfolded sequence are represented. The Letters A to C represent locations and photographs (Appendix 2.17).

2.9.5.6 Correlation of the Inner Lekdam Succession

All five sequences exhibit the same characteristics, with thick to thin successions of biotite-sillimanite schist, with intercalated units of feldspathic quartzite, calc-silicate rock, biotite gneiss, and amphibolite (Figure 2.58). The Skewe Berg Sequence has the thickest biotite-sillimanite schist unit, with the other sequences having thinner less prominent units of biotite-sillimanite schist. One of the most noticeable lithological units is the garnet-bearing magnetite quartzite unit, which is associated with the Inner Lekdam Succession and is found in all the sequences except for the Sy-berg Sequence. The other noticeable difference is that the thick to thin biotite–sillimanite schist unit defines the hinge zone of the Sy-berg Sequence, while the biotite sillimanite schist unit is found on the limbs of the other structures. All the structures have been intruded by the Lekdam Gneiss and envelopes all the sequences associated with the Inner Lekdam Succession. Only the Skewe Berg Sequence contains nodular rhythmic gneiss, found in the upper part of the stratigraphic succession. All the mentioned sequences have second-order upward coarsening cycles associated with the upper poorly bedded quartzite unit, with the only exception being the S-Berg Sequence, which defines a second-order upward fining cycle.

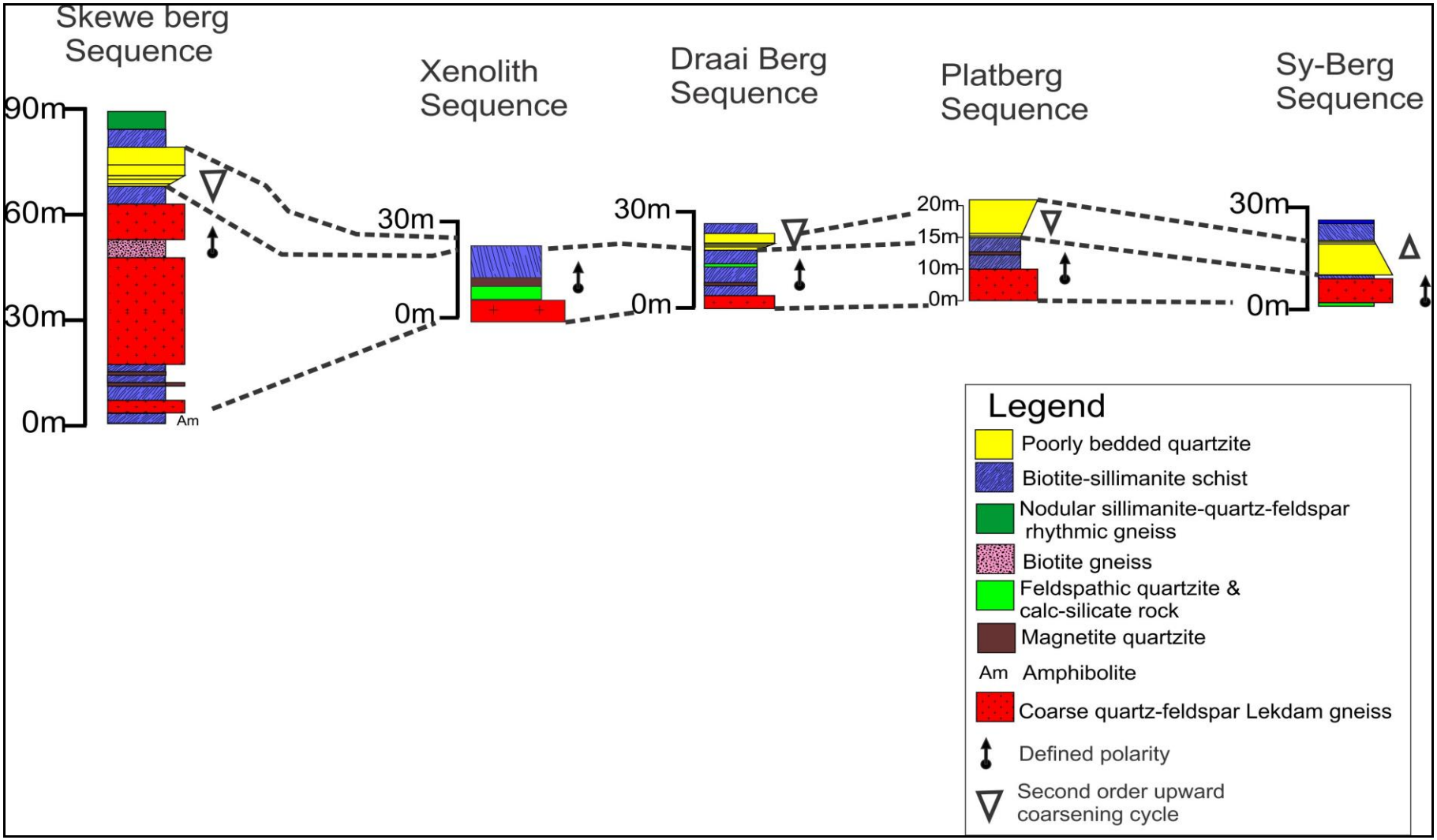

Figure 2.58: Horizontally restored interpretation of stratigraphic profiles associated with the Skewe Berg, Xenolith, Draai Berg, Platberg, and Sy-Berg Sequences, which define the Inner Lekdam Succession.

2.10. The Houmoed Structural Domain

2.10.1 The De-Rust Succession

The De Rust Succession is associated with the Houmoed Structural Domain and includes the Achab, De Rust, and Dwarsberg Sequences (Figure 2.59). The succession has thick to thin sequences of biotite-sillimanite schist, with interbanded units of amphibolite, calc-silicate rock and slithers of biotite gneiss, with thick poorly to well-bedded white quartzite displaying second-order upward coarsening cycles. The succession is associated with kilometre scale sheath folds, and refolded isoclinal sheath folds with double vergence geometries.

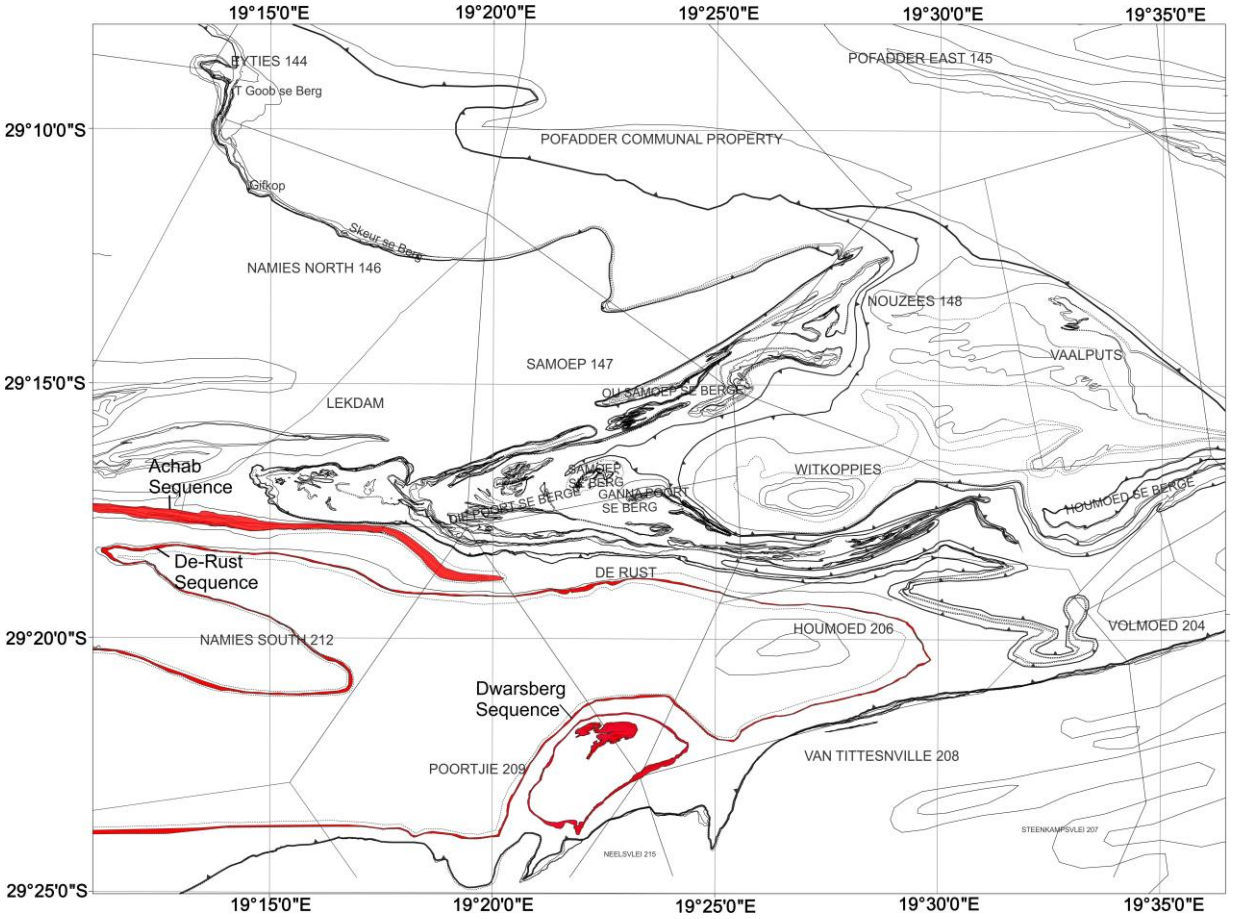

Figure 2.59: The distribution of the De Rust Succession throughout the Houmoed Structural Domain (red) and is defined by the Achab, De Rust, and Dwarsberg Sequences.

2.10.1.1 The Achab Sequence

The Achab Sequence is located just toward the north of the De Rust structure (Figure 2.59). The Achab Sequence is interpreted to be a separate isoclinal fold structure, not related to the main structure toward the northwest, although the stratigraphy is the same (Figure 2.60). The Achab Sequence resembles a stratigraphy typical of that related to the Wortel Formation (Praekelt and Schoch, 1997). Part of the Achab Sequence has been mapped by Moore (1977)

specifically the entire Achab se Berg structure, while geochemical interpretations were conducted by Wilner et al. (1990), looking at the chemistry of the calc-silicate, garnet meta-quartzite, and amphibolite rocks as indicators for stratiform ore deposits (peraluminous rocks), interpreting them to originate as aluminous clays and hydroxides near hydrothermal vents during an intermediate stage of rifting. The sequence has thick successions of biotite sillimanite schist, with interbands of garnet-bearing meta-quartzite, calc-silicate rock, and amphibolite. The stratigraphic succession is also defined by large poorly bedded quartzites, and small lenses of sillimanite (Moore, 1977; Willner et al., 1990), typically associated with the Wortel Formation toward the west. Surrounding the succession is a prominent medium-grained-quartz feldspar Namies Gneiss, which is folded around this particular sequence toward the north (Appendix 2.18 A). Profile A-A', best represents the stratigraphic succession of the Achab sequence, which extends through the hinge zone of the macroscopic isoclinal fold structure (Figure 2.60 and Figure 2.61).

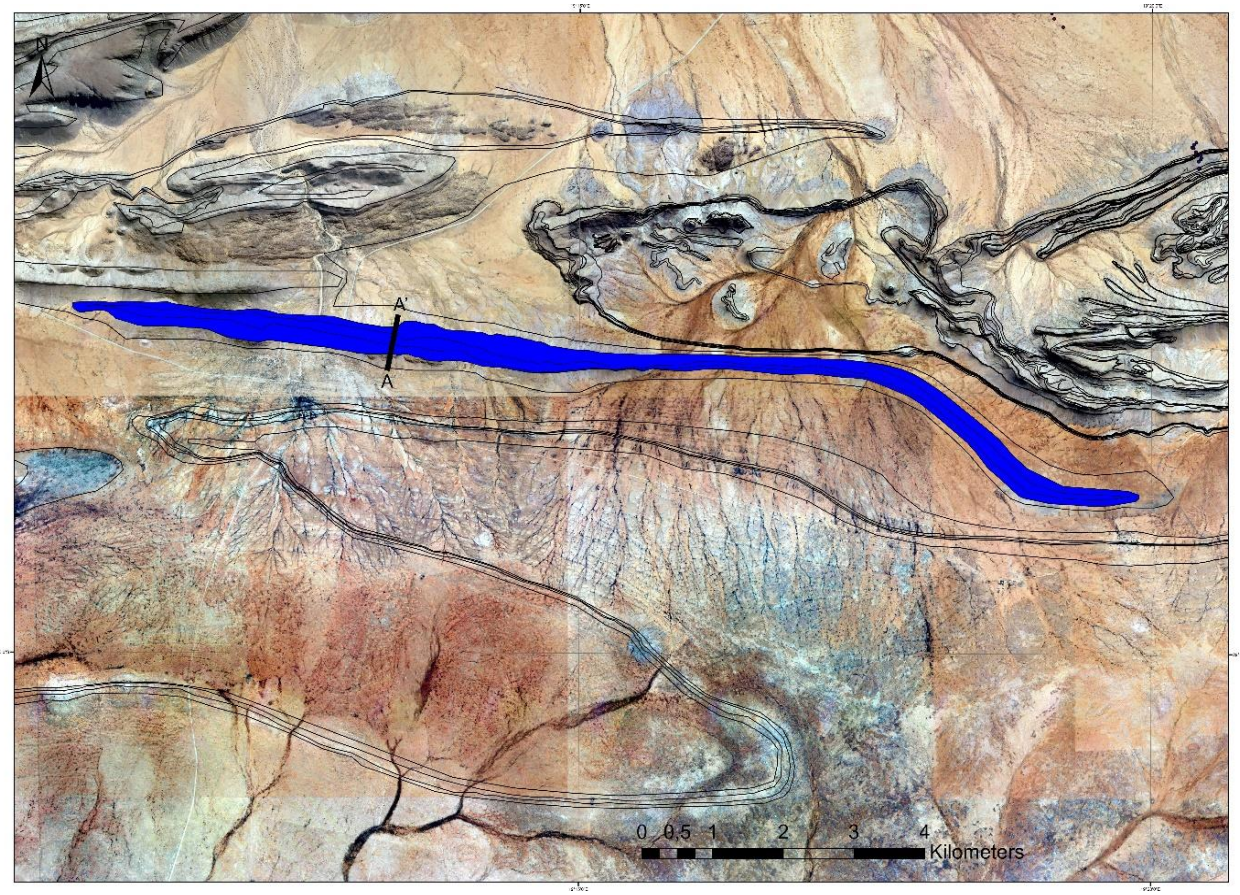

Figure 2.60: Achab Sequence with profile A-A', which best represents the stratigraphy. The distribution and location of the Achab Sequence throughout the study area can be seen in Figure 2.58.

The base of the Achab Sequence is defined by the well-foliated medium-grained-quartz feldspar Namies Gneiss. No xenoliths of intrusives features were identified in this specific unit. Above the medium-grained-quartz-feldspar gneiss is a sharp contact with the above biotite-

sillimanite schist unit (Appendix 2.18 B). The biotite-sillimanite schist unit thickens significantly toward the west and thins out toward the east. Interbanded units of metre-scale amphibolites, calc-silicates, and ferruginous garnet meta-quartzites occur sporadically within (Appendix 2.18 C, D, and E). Within this section of the Achab Sequence, no sillimanite lenses were identified within the succession. However, sillimanite lenses have been identified further toward the west (Moore, 1977; Wilner et al., 1990).

Overlying the biotite-sillimanite schist, a gradational contact is found with the overlying quartzite, defining a second upward coarsening cycle (Appendix 2.18 E). Overlying the quartzite, a thick to thin succession of biotite-sillimanite schist is found, forming the hinge of the isoclinal fold structure. Along strike the quartzite and biotite sillimanite schist unit duplicates, and cut out on the various limbs of the structure due to thrusting or imbrication on the limb of the Achab structure. The best examples can be seen in the middle and toward the west of the structure. The defined polarity associated with this structure is defined by the lower medium quartz-feldspar Namies Gneiss, thick biotite-sillimanite schist, and overlying poorly bedded quartzite, displaying a second-order upward coarsening cycle, overlain by another biotite-sillimanite schist unit, representing the top part of the stratigraphic succession (Figure 2.61).

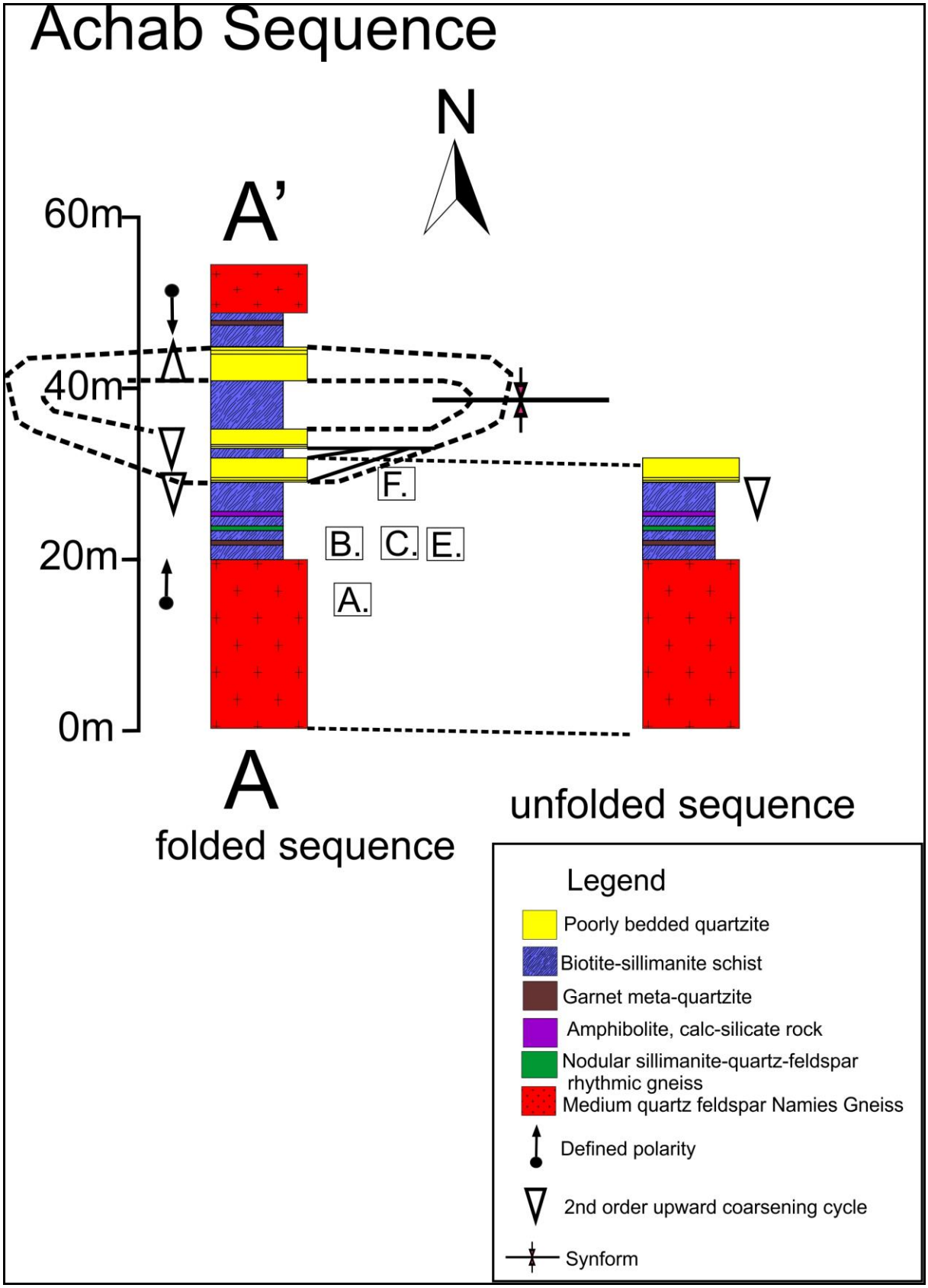

Figure 2.61: Profile A-A' (Figure 2.60) which best represents the stratigraphic succession associated with the Achab Sequence. The letters A to F represent locations and photographs (Appendix 2.18).

2.10.1.2 The De Rust Sequence

The De Rust Sequence is located in the southern portion of the study area, below it, the Dwarsberg refolded isoclinal fold structure is found and to the north, the outer Lekdam structure is located (Figure 2.59). The De Rust Sequence is enclosed within the Achab Suite and has the medium-quartz-feldspar Namies Gneiss on the outside of the structure, representing the upper part of the sequence. The De Rust Sequence closes off in the east and extends further on toward the west, where it is interpreted by the author to close off forming a macroscopic elliptical double vergence fold structure. The stratigraphy is best represented by profile A-A' in Figure 2.62 on the central portion of the northern limb.

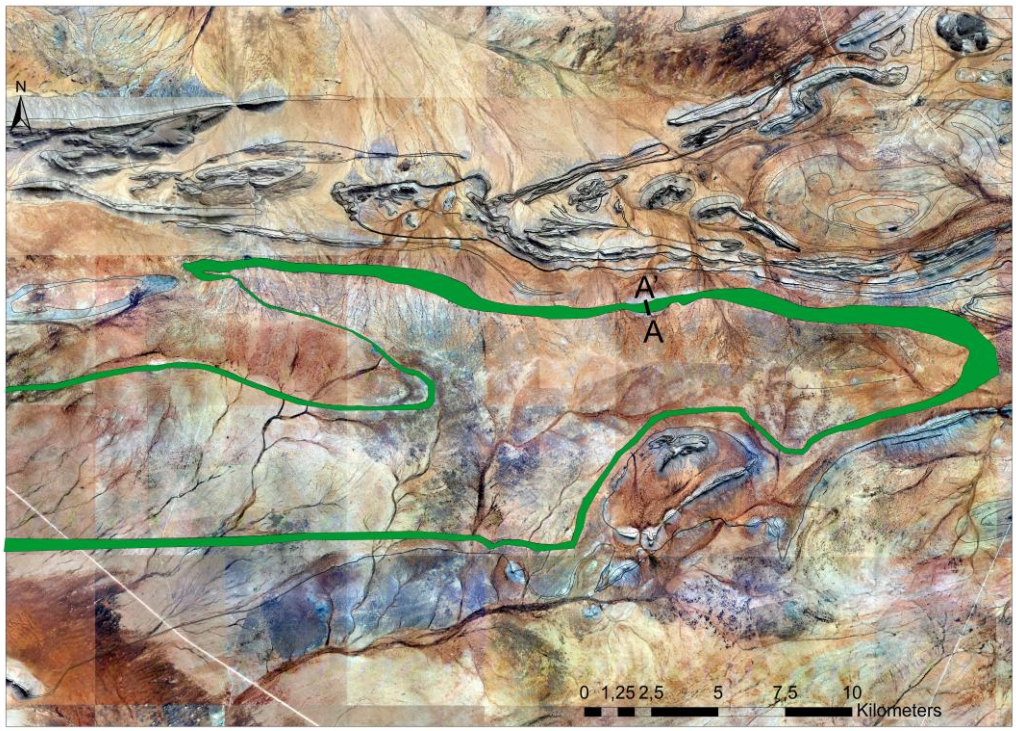

Figure 2.62: The distribution of the De Rust sequence throughout the study area, with the relevant stratigraphic Profile.

The base of the De Rust Sequence is defined by the Achab Suite, in which large K-feldspar augen are clearly defined. Clear regional foliation of biotite is also seen concerning the variation of Achab Suite. As you move upwards in the stratigraphy, augens flatten and have a coarse to porphyritic appearance, and closer toward the metasedimentary succession a well-banded variation is found. The Achab Suite is overlain by thick successions of nodular rhythmic sillimanite-quartz-feldspar gneiss is found (Figure 2.63), which has a sharp contact.

The nodular rhythmic sillimanite-quartz-feldspar gneiss gives of a grey to reddish appearance and is often well foliated (Appendix 2.19 A). Overlying the nodular rhythmic sillimanite-quartz-feldspar gneiss, a thick unit of biotite sillimanite schist is found (Appendix 2.19 B). Small lenticular volcanic units of amphibolite, calc-silicate rocks, and biotite gneiss are interbanded

within the latter. Above the biotite-sillimanite schist, a poorly bedded thick white quartzite is found, displaying a prominent second-order upward coarsening cycle (Appendix 2.19 C). Overlying the quartzite the well-foliated medium grained quartz-feldspar Namies Gneiss, with prominent foliation bands of biotite is found. The medium grained quartz-feldspar Namies Gneiss displays a reddish appearance and has a consistent homogeneous appearance (Appendix 2.19 D). The defined polarity associated with the De Rust Sequence is defined by nodular sillimanite-quartz-feldspar gneiss, overlain by thick to thin biotite-sillimanite schist with interbanded volcanoclastic sequences in contact with a poorly bedded quartzite, showing a second-order upward coarsening cycle, capped by the prominent medium quartz feldspar Namies Gneiss (Figure 2.62).

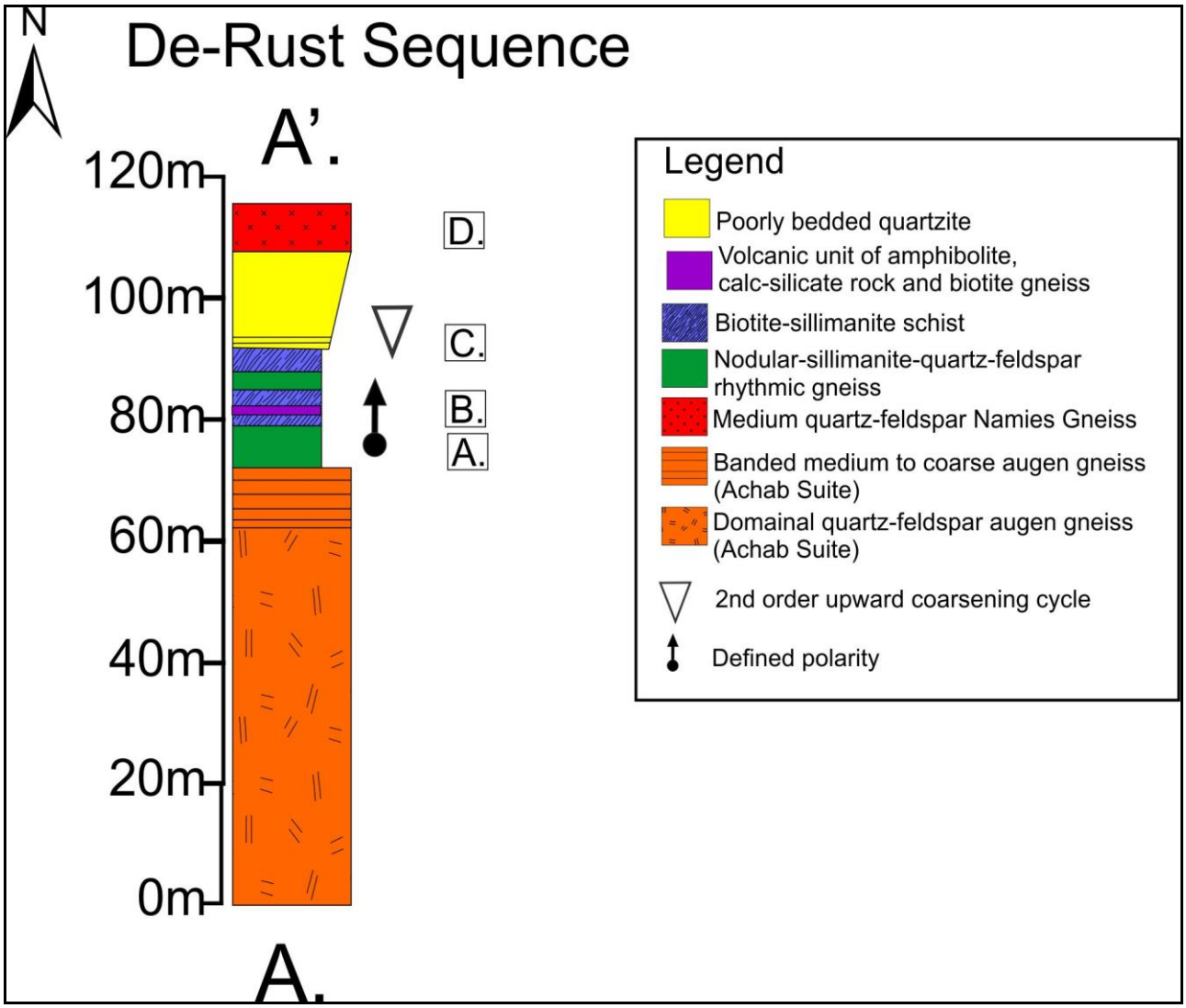

Figure 2.63: Profile A-A' (Figure 2.62) which represents the stratigraphic succession associated with the De Rust Sequence. The letters A to D represent locations and photographs (Appendix 2.19).

2.10.1.3 The Dwarsberg Sequence

The Dwarsberg Sequence is represented by an isolated refolded isoclinal structure in the south of the study area, relatively close to the Geelvloer thrust contact (Figure 2.59). The Dwarsberg Sequence is composed of biotite-sillimanite schist, thick, poorly to well-bedded quartzites, amphibolites, and calc-silicate rocksThe Dwarsberg Sequence can be subdivided into an Inner Dwarsberg and Outer Dwarsberg Member. The Inner Dwarsberg Member resembles a refolded isoclinal fold structure, while the Outer Dwarsberg Member is associated with the outer elliptical fold structure, which envelopes the Inner Dwarsberg Member. Various profiles associated with each member is represented in Figure 2.64, showing the best exposures associated with the Dwarsberg Sequence. On the inside portion of the structure, the Lekdam Gneiss is found, while the outer rim of the structure is surrounded by the Achab Suite.

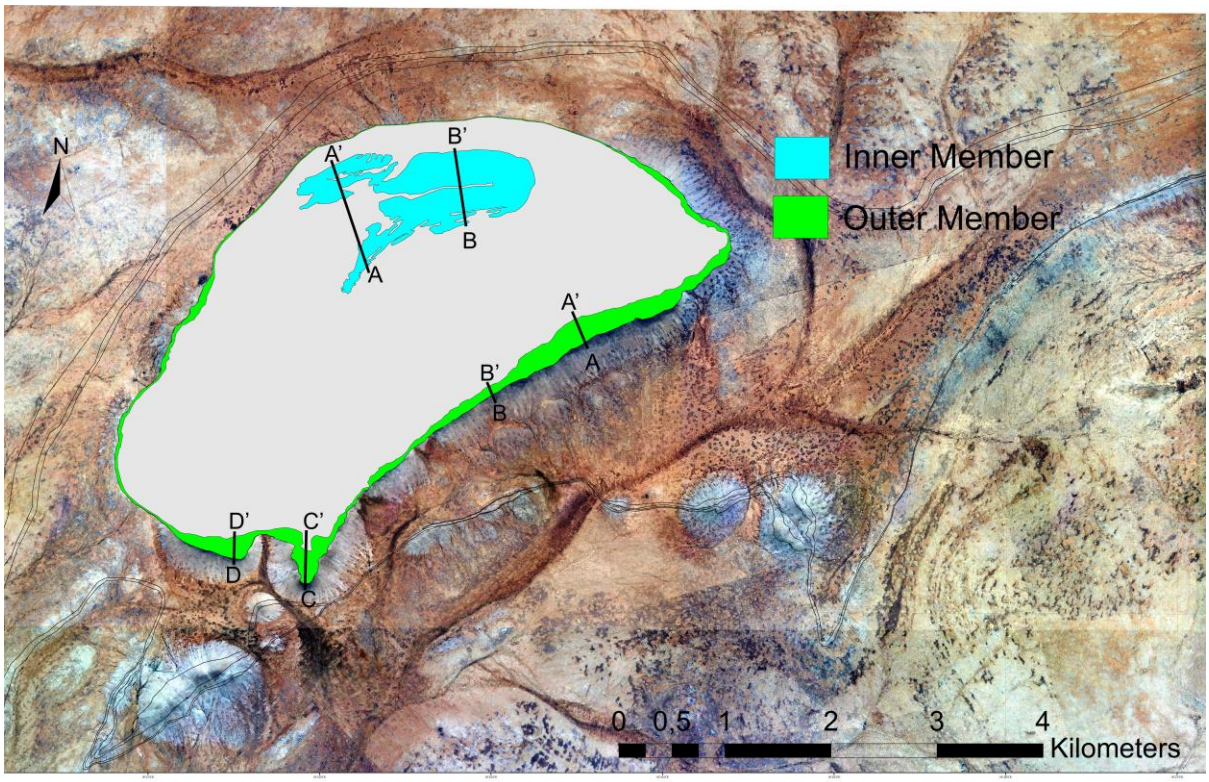

Figure 2.64: Distribution of the Inner (turquoise) and Outer Dwarberg Members (light green), which define the Dwarsberg Sequence. The locations where the profiles were constructed are also represented, for both the Inner and Outer Dwarsberg Members.

2.10.1.3.1 The Inner Dwarsberg Member

The Inner Dwarsberg Member is best represented by profiles A and B (Figure 2.64 and 2.65 A & B). At the base the coarse-grained quartz-feldspar Lekdam Gneiss is found, xenoliths of the above supracrustal rock are found around the structure, specifically the contact with the above supracrustal succession. Above the Lekdam Gneiss, a sharp contact is found with the surrounding biotite-sillimanite schist (Appendix 2.20 A), although poorly exposed, it surrounds

the entire inner sheath fold structure. The lower schist unit contains lenticular units of interbanded biotite gneiss, amphibolite, and calc-silicate rocks, which define a small volcanic unit (Appendix 2.20 B and C). This volcanic unit acts as a marker and folds along strike around the entire Inner Member. Decametre and centimetre variations are found throughout. The best exposures are seen in the northern limb of the inner isoclinal double vergence fold structure.

Above the biotite-sillimanite schist unit, a sharp contact is found with the overlying quartzite, which is well to poorly bedded and varies in thickness throughout, due to the refolding that takes place along strike. The thicknesses vary between 60 metres and 1 metre along strike. Associated with the upper quartzite, a distinct second-order upward coarsening cycle is found, specifically on the lower contact with the biotite-sillimanite schist unit (Appendix 2.20 D). The most upper unit has a thick succession of biotite sillimanite schist, with small lenticulars units of amphibolite, calc-silicate rocks, and small laths of biotite gneiss, capped by another poorly bedded quartzite. Second order upward fining and coarsening cycles are found in both upper and lower quartzites (Figure 2.65 A and B). The upper biotite-sillimanite schist unit represents the central hinge of the Dwarsberg fold structure and varies in thickness along strike. The upper quartzite also defines a second-order upward coarsening cycle, which varies dramatically in thickness, due to the intense isoclinal folding associated with this unit (Figure 2.65 A, B and C).

The upper and lower units are similar in character, the only difference is that better exposures are found in the latter than the former. The Inner Dwarsberg Sequence is also intruded by the Lekdam Gneiss, especially within the hinge zones of the major folds (Figure 2.64). The defined polarity (Figure 2.65 C) is therefore represented by biotite-sillimanite schist at the base, with interbands of amphibolite and calc-silicate rock, overlain by poorly bedded quartzite defining second order upward coarsening and fining cycles. Above the poorly bedded quartzite another unit of biotite-sillimanite schist is found, with interbanded units of amphibolite/calc-silicate rock, which define the central hinge of the structure. Overlying this unit another thick quartzite units found, defining a second order upward coarsening cycle, and represents the top part of the succession.

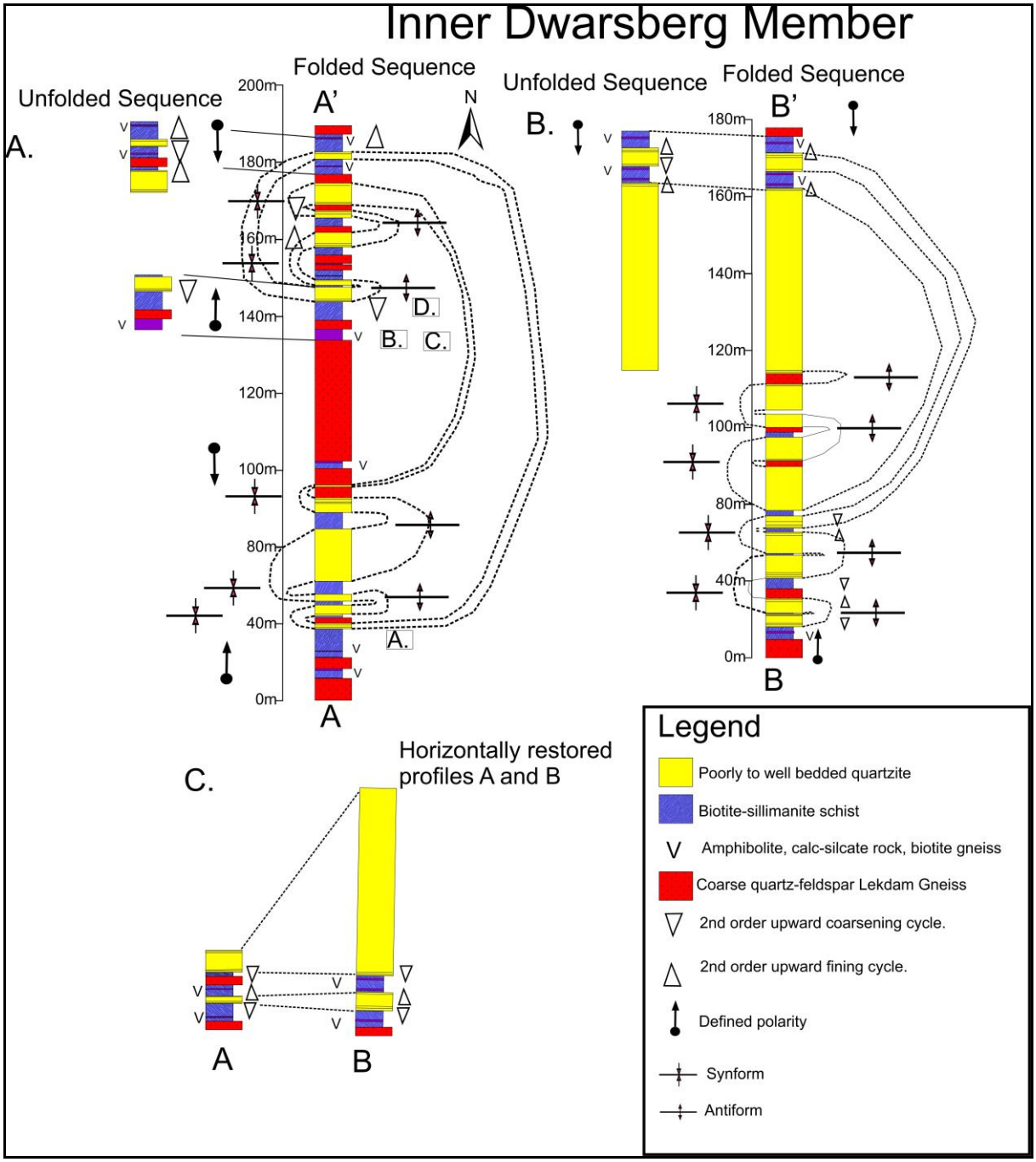

Figure 2.65: Profiles A-A' and B-B (from Figure 2.64) associated with the Inner Dwarsberg Member. The letters A to D represents locations and photographs (Appendix 2.20). Horizontally restored comparison of both unfolded sequences can be found at the base of the diagram in Figure C.

2.10.1.3.2 The Outer Dwarsberg Member

The Outer Dwarsberg Member is defined by a series of structurally duplicated layers of well-bedded quartzites and interlayered sequences of biotite-sillimanite schist units. Several imbricate structures result in duplications and cut-outs of lithological units (Figure 2.64). The best exposure of the Outer Member can be seen in the far south of the structure in the outer rim toward the Geelvloer Thrust contact and is best represented by profiles A, B, C, and D in Figures 2.64 and Figure 2.66. Toward the north and north east, the Outer Member is poorly

exposed and at stages not visible due to alluvium cover, and only remnants are found on the surface. At the base of the succession thin lenticular units of biotite-sillimanite schist are found (Appendix 2.21 A). Thick quartzite and rhythmic layered quartzites are found above the biotite-sillimanite schist units, displaying prominent second-order upward coarsening cycles (Appendix 2.21 B). Interbands of biotite-sillimanite schist are found at the base right across the entire succession. Small remnants of nodular rhythmic sillimanite-quartz-feldspar gneiss are inter-layered within the biotite-sillimanite schist units. Due to the stacking of imbricates the upper quartzite duplicates and thickens along strike at certain locations. The upper quartzite units also branch out against adjacent stratigraphic units (Figure 2.66). The duplications and branch points are best exposed on the southern limb of the major elliptical ring structure. The Lekdam Gneiss often intrudes into less competent biotite-sillimanite schist units throughout the area.

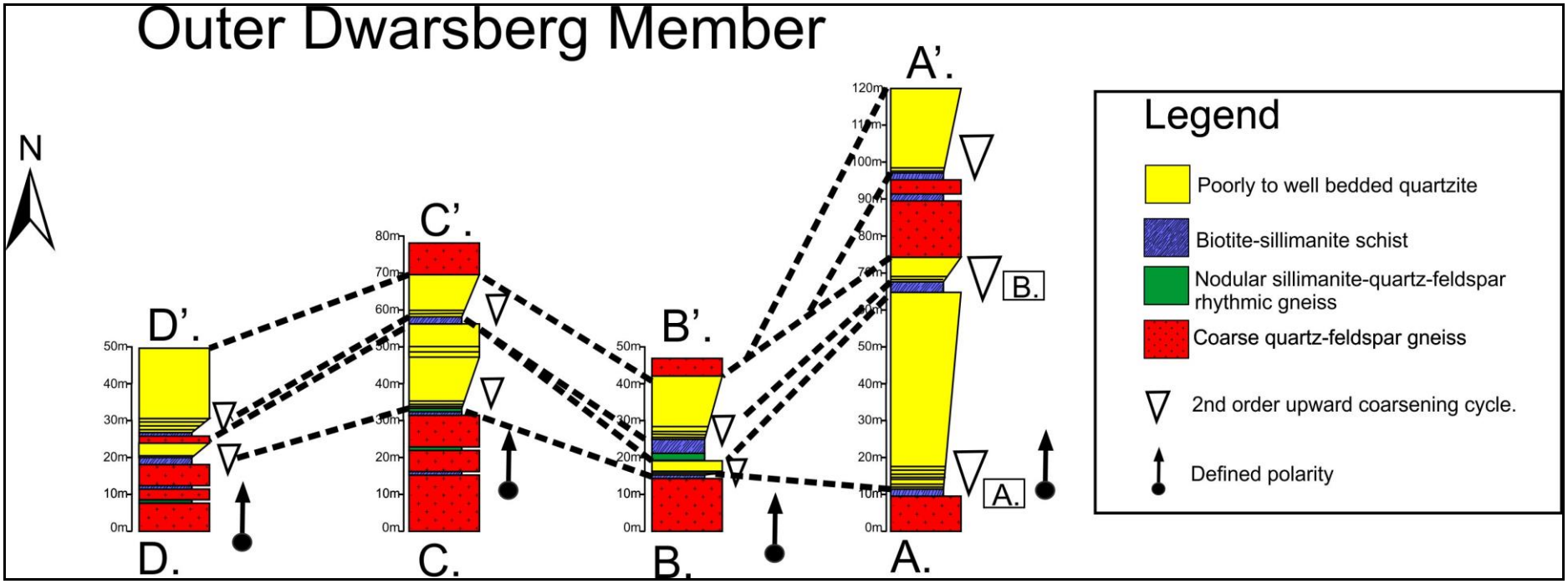

Figure 2.66: Profiles (from Figure 2.64) A-A', B-B', C-C', and D-D' related to the Outer Dwarsberg Member. Prominent duplication of quartzites, biotite-sillimanite schist and nodular sillimanite-quartz-feldspar gneisses is seen due to intra-stratigraphic thrusting (imbricates) seen on the rim of the structure. The letters A to D represent locations and photographs (Appendix 2.21).

2.10.1.4 Correlation of the De-Rust Succession

The De Rust Succession is defined by the Achab, De Rust, and Dwarsberg Sequences and has similar lithological characteristics to one another when restored horizontally (Figure 2.66). The Achab Sequence contains thick to thin sequences of biotite-sillimanite schist, with interbanded units of garnet meta-quartzite (BIF units), amphibolite, calc-silicate rock and biotite gneiss, and also contains thick, poorly bedded quartzites associated with the Wortel Formation (Praekelt and Schoch, 1997). The Dwarsberg Sequence contains the thickest assemblage of quartzite, but has smaller assemblages of biotite-sillimanite schist, while the De Rust and Achab Sequences do not have a thick succession of poorly bedded quartzite.The thick packages of quartzite in the Dwarsberg Sequence are visible due to the intense isoclinal folding and intra-stratigraphic thrusting seen in the structure. The Dwarsberg Sequence is the only sequence that does not contain any garnet meta-quartzite units, present in both the Achab and De Rust Sequences. The medium-well foliated Namies Gneiss is associated with both the De Rust and Achab Sequences and folds in conjunction with the supracrustal units, while it is absent within the Dwarsberg Sequence. All three sequences display prominent second-order upward coarsening cycles (Figure 2.67), which coincide with the defined polarity, with the upright limbs being represented in the south and the northern limbs being overturned. .

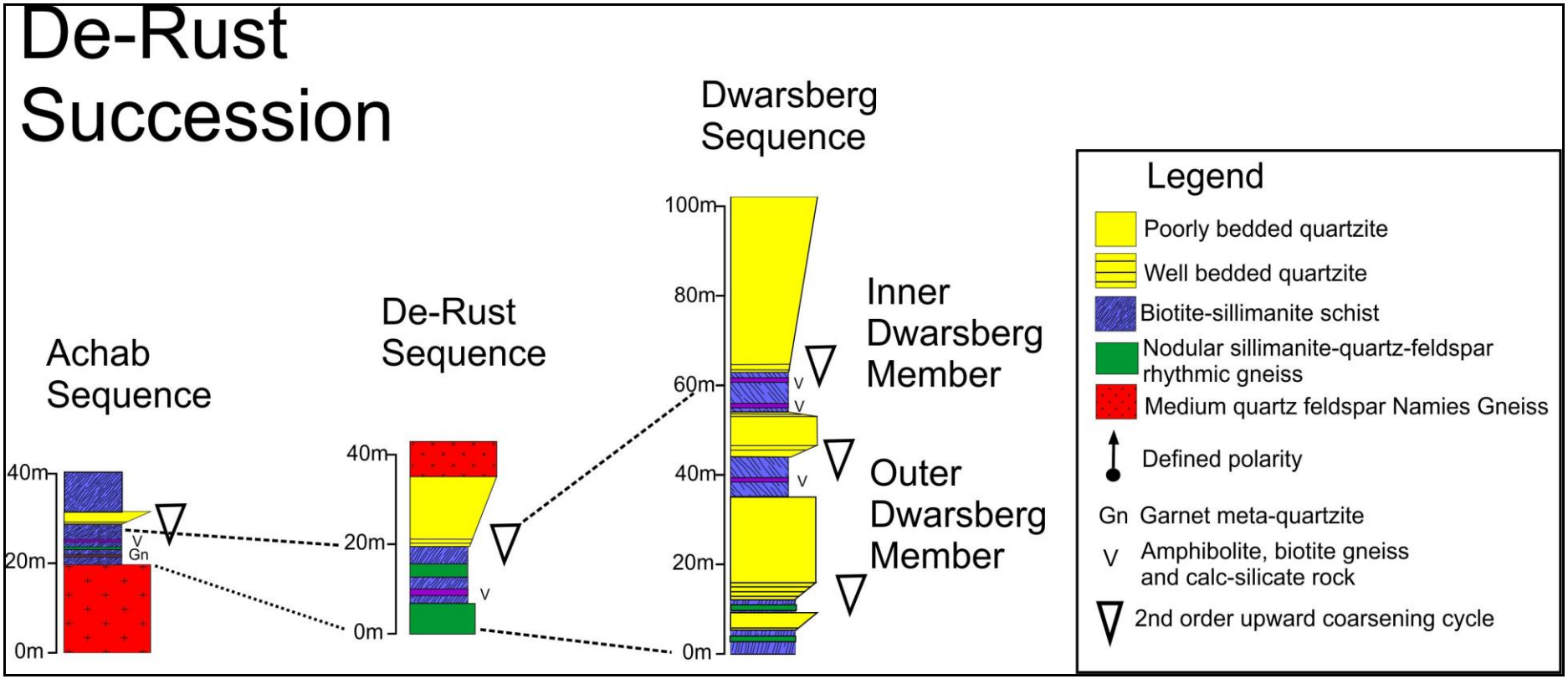

Figure 2.67: Correlation diagram between the three sequences associated with the De Rust Succession when restored horizontally. The Achab Sequence and De Rust Sequence have similar attributes, and are both associated with the Namies Gneiss, while the Dwarsberg Sequence has similar charateristics, except for the thick packages of quartzite which form due to isoclinal folding and thrusting.

2.11 The Inter-Terrane Thrust Contacts

2.11.1 The Pofadder Terrane Contact: The Hom Formation

The Hom Formation extends along strike in the study area on the Groothoek Thrust contact (Figure 2.68). The Hom Formation found in the Pofadder Terrane, which forms part of the Haib Subgroup, has been previously mapped by Blignault (1980), Pretorius (1986), and Colliston (1990) toward the west of the study area, where larger and more prominent exposures are seen. The Hom Formation is defined by leucocratic biotite gneiss, intercalated hornblende gneiss, calcium-rich rocks (calc-silicate rocks), meta-quartzite, and varieties of inter-banded sequences of schist (Colliston, 1990).

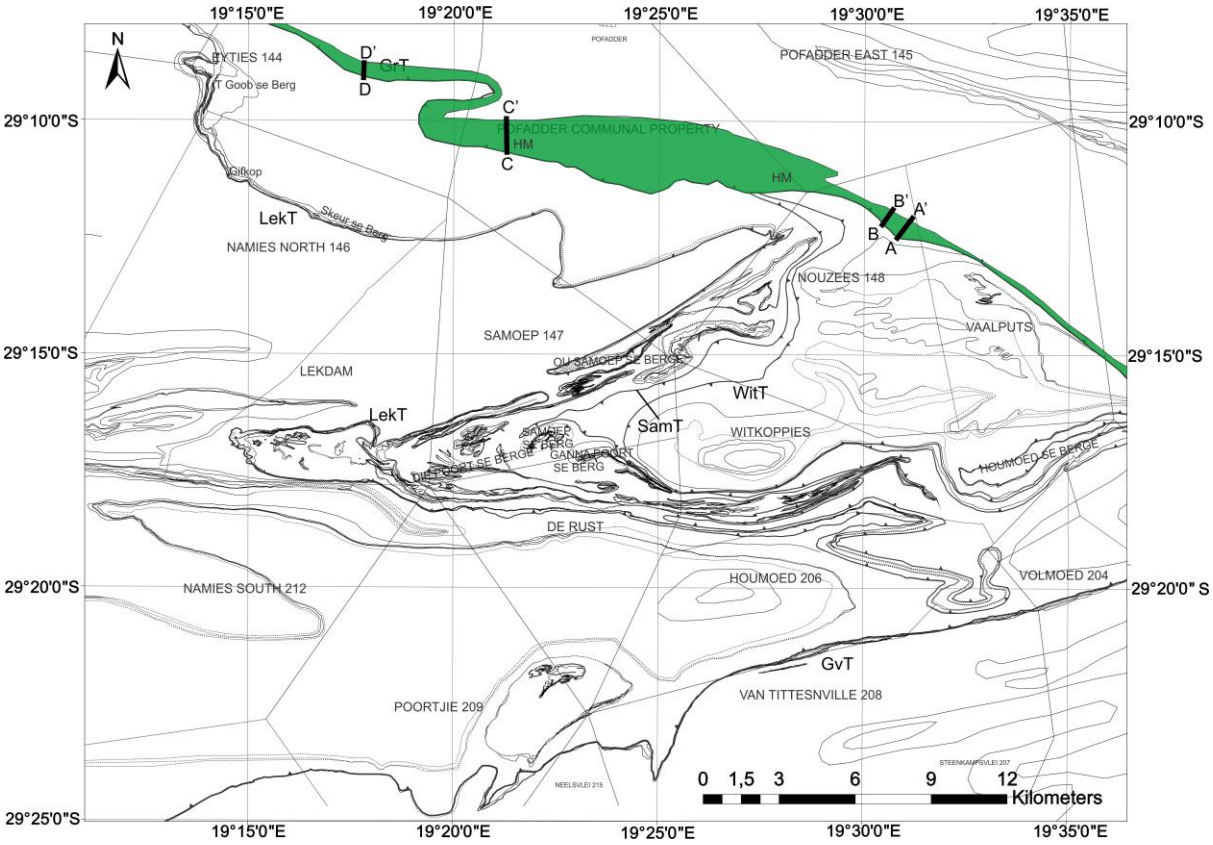

Figure 2.68: Distribution of the Hom Formation throughout the study area in green with the relevant stratigraphic profile locations (Grt: Grootheok Thrust; Gvt: Geelvloer Thrust; LekT: Lekdam Thrust; SamT: Samoep Thrust and WitT: Witkoppies Thrust).

The Hom Formation is more than often associated with the overlying Swartmodder Gneiss, which intrudes the succession regularly throughout the study area (Appendix 2.22 A). Variations in strain give the Swartmodder Gneiss different appearances, which result in a total banded variation with the flattening of feldspar augens (Appendix 2.22 B). The Hom Formation is poorly exposed within the study area and is only visible at certain locations where prominent outcrops are exposed (Figure 2.68 and 2.69). Profiles A, B, C, and D represent the localities where the Hom Formation is best exposed within the study area. The Hom Formation thins

out and becomes more mylonitic and deformed as you move eastwards in the study area, it is highly deformed due to the later phases of deformation (D5-D6).

Within the study area the Hom formation is defined by thin to massive laminated felsic gneiss (Appendix 2.22 C), and thin to thick sequences of biotite gneiss. Hornblende bands and volcanic bombs interlayered within the former and latter, often give the lithological units a porphyritic appearance at stages (Appendix 2.22 D). Small banded felsic and mafic calc-silicate rocks are also interbanded within, often having well laminated leuco- and felsic bands. Small lapilli (Appendix 2.22 E) and porphyritic volcanoclastic 'bombs' are visible in certain locations within the biotite gneiss, amphibole, calc-silicates, and felsic gneiss units.

The volcanic bombs often have a leucocratic appearance, defined by large K-feldspar and plagioclase clasts (Appendix 2.22 F). However, the quartz eyes (lapilli) and volcanic bombs occur sporadically throughout and only at certain locations toward the east of the study area, adjacent to the Groothoek Thrust contact. There is an increase in interbanded units of medium banded leucocratic feldspar gneiss as you move toward the east, and a decrease in amphibole is also observed. No real interbands of schist and metaquartzite were observed in this portion of the Hom Formation, and it is much smaller in thickness when compared to outcrops toward the west, adjacent to the study area.

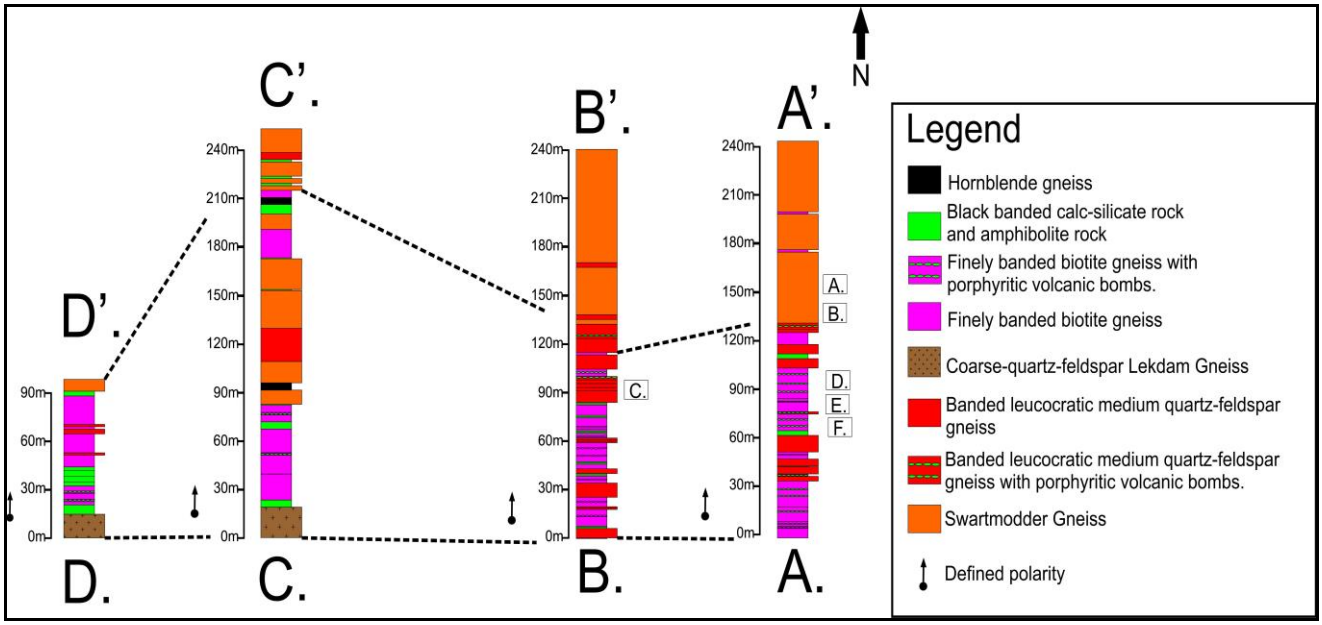

Figure 2.69: Profiles (Figure 2.68) A-A' to D-D' associated with the Hom Formation. The letters A to D represent locations and photographs (Appendix 2.22).

2.11.2 The Bladgrond Terrane: The Van Tittensville Formation

The upper contact of the Van Tittensville Formation with the Aggeneys supracrustal rocks defines the Geelvloer Thrust, separating the Aggeneys and Bladgond Terranes. The Van Tittensville Formation has been included by Paizes (1975) into his Kenhardt Group, consisting of the Geelvloer and Vaalkop Formations. Agenbacht (1992) includes these rocks into his Kraandraai Formationm, as sequences of migmatised, epidotised, quartzitic, and finely layered calc-silicate gneisses, amphibolite, and minor biotite schist/gneiss. However, the Kraandraai Formation of Agenbacht (1992) encapsulates all the rocks from the contact toward the south of the study area, while the Van Tittensville Formation as defined by the author is only related to the Geelvloer thrust contact (Figure 2.69). Profiles A, B, C, and D represent the best localities to view the Van Tittensville Formation (Figure 2.70 and 2.71).

The base of the Van Tittensville Formation is defined by the Van-Tittensville coarse quartz-feldspar leucocratic augen gneiss, which at stages is migmatitic, defining metatexite melts of schlieren and schollen structures. Slivers of an undifferentiated coarse-grained-quartz-feldspar gneiss is often found interlayered within the meta-sedimentary units. The coarse-grained-quartz-feldspar gneiss has at stages a porphyritic appearance. Above the coarse-grained-quartz-feldspar augen gneiss, a sharp contact is found with a thick succession of biotite gneiss (Appendix 2.23 A), with slivers of amphibolite, dark-blue quartzites, and calc-silicate rock (Appendix 2.23 B). Variations in thickness associated with the biotite gneiss also occur along strike (Figure 2.71).

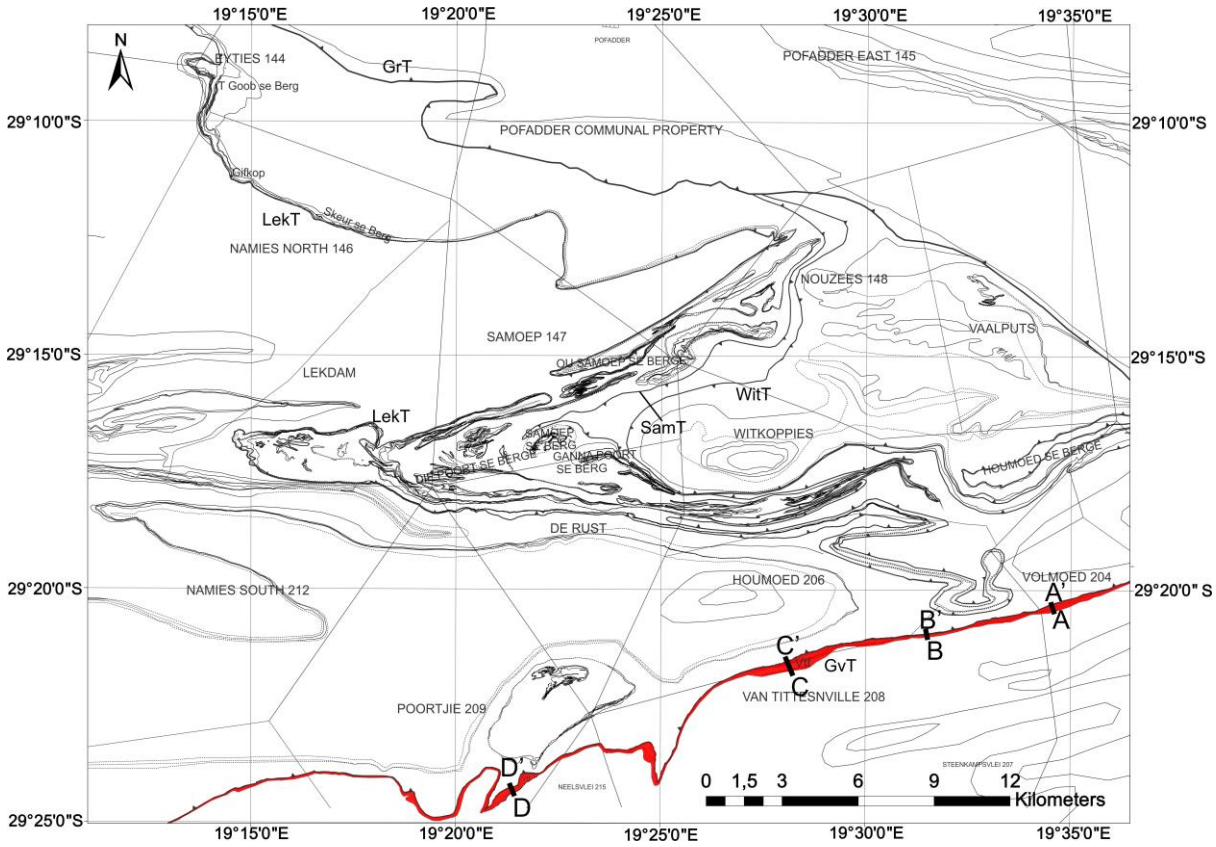

Figure 2.70: Distribution of the Van Tittensville Formation throughout the study area in red, together with the relevant stratigraphic profiles A-A' to D-D' (Grt: Groothoek Thrust; Gvt: Geelvloer Thrust; LekT: Lekdam Thrust; SamT: Samoep Thrust and WitT: Witkoppies Thrust).

Above the biotite gneiss a thick succession of well to poorly bedded quartzites occurs with interlayered sequences of biotite-muscovite-sillimanite schist (Appendix 2.23 C). The quartzite and schist units duplicate along strike due to imbrication associated with thrusting. Third-order upward fining sequences were observed within the quartzites, which are found on centimetre to metre scale (Appendix 2.23 D). The quartzites also vary in thickness along strike from two metres up to 20 metres at some locations. Relatively good exposures are seen toward the west of the study area. However, outcrops become less defined as you move toward the east of the study area. The entire stratigraphic succession is overlain by the Achab Suite, a sharp contact was found, which defines the Geelvloer Thrust contact at this locality.

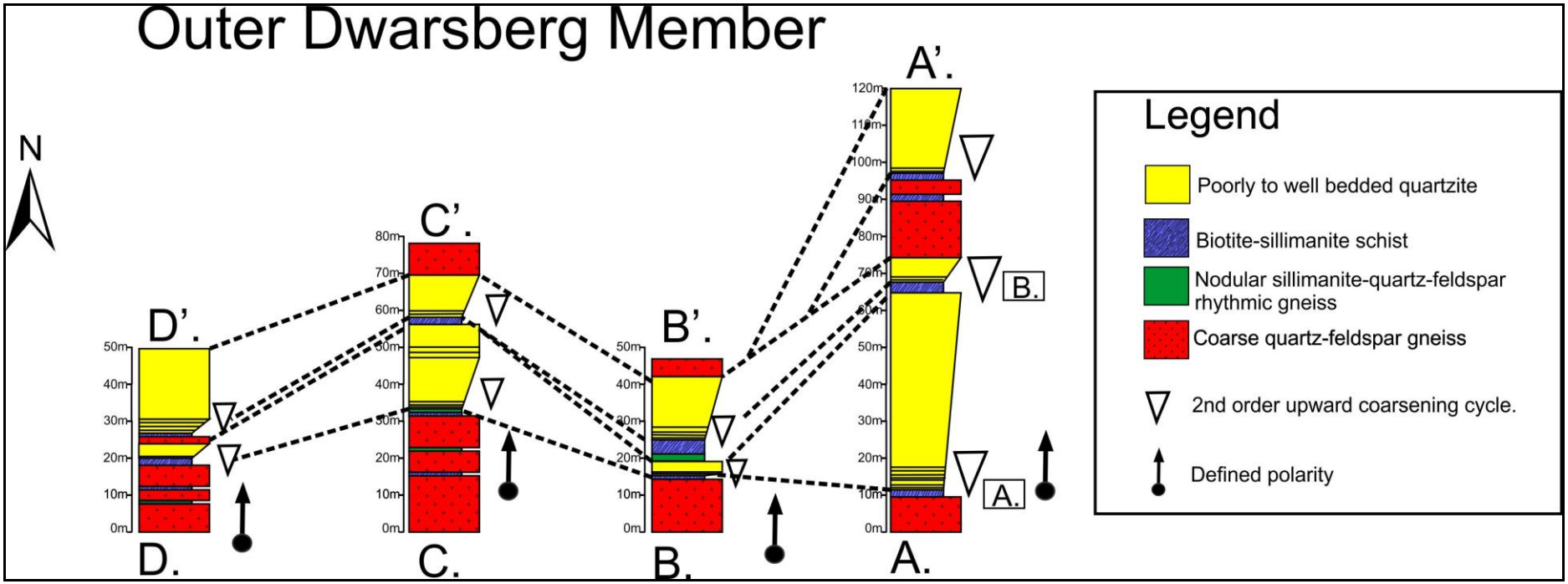

Figure 2.71: Profiles (Figure 2.70) A-A' to D-D' associated with the Van Tittensville Formation. The letters A to D represent locations and photographs (Appendix 2.23).

CHAPTER 3

Deformation

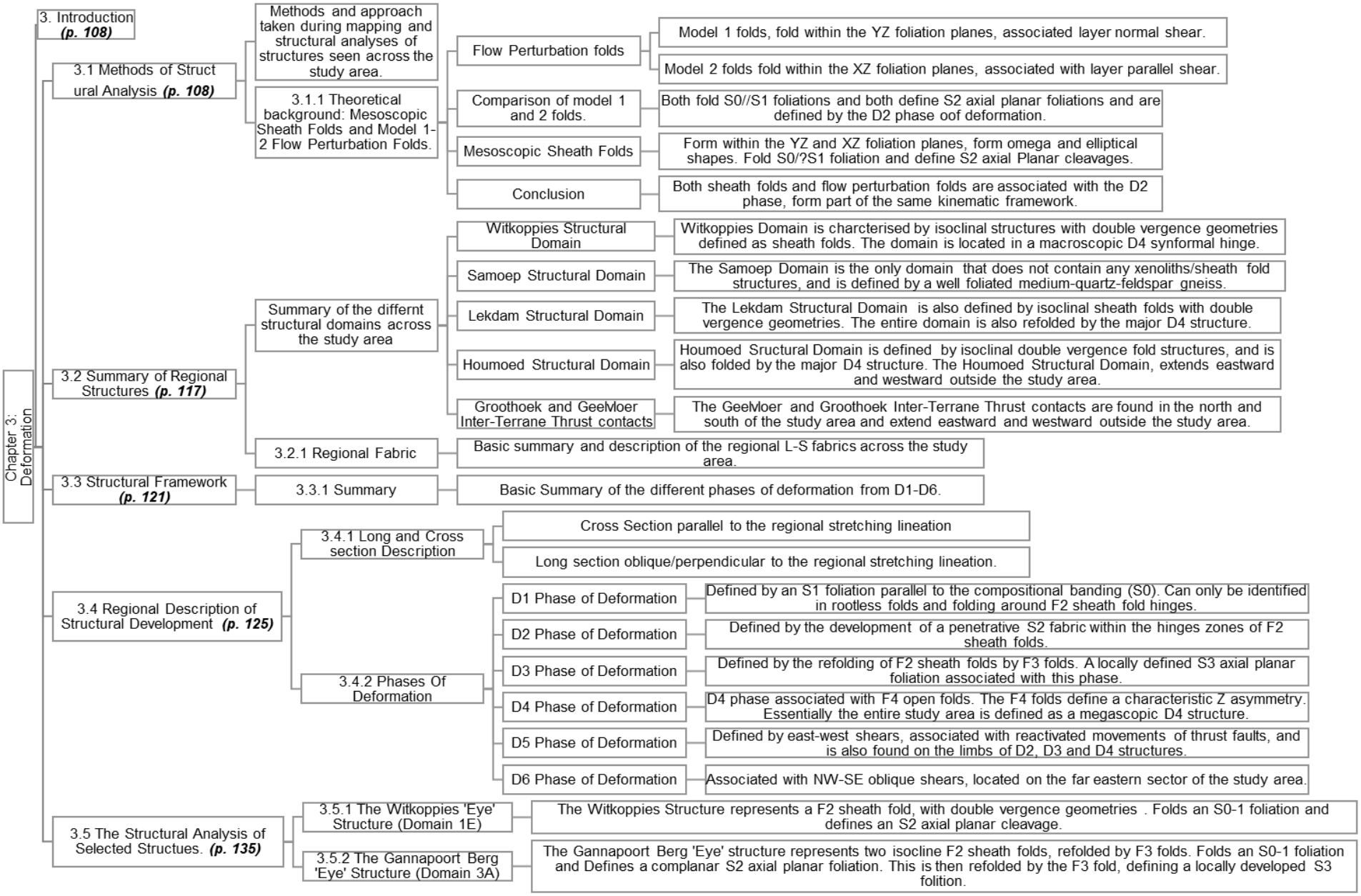

Figure 3.0: Mind map summary of the main aspects covered in Chapter 3.

3. Introduction

Due to the complexities associated with the study area, it was necessary to describe and summarise various complications and aspects in this chapter first, to make sense of the chaotic nature of the structures encountered (Appendix 3.1), after which the structural details are discussed and summarised later in this chapter. This chapter is therefore, sub-divided into five segments namely: 3.1-3.5. The chapters are sub-divided as follows:

- Chapter 3.1: Description of methods and approach to studying the various structures encountered within the study area.
- Chapter 3.1.1: Theoretical background necessary to understand certain structures encountered in the study area are described.
- Chapter 3.2: A regional summary is provided of the different structural domains encountered in the study area.
- Chapter 3.2.1: Summary of the regional L-S fabrics identified throughout the study area across all structural domains.
- Chapter 3.3: Structural framework is provided, summarising each phase of deformation, to create an understanding of the fabrics and attributes associated with each phase of deformation.
- Chapter 3.4: The regional structural development of the study area described in Chapter 3.4.1 and 3.4.2.
- Chapter: 3.4.1: Detailed cross and long section descriptions are given to define the regional characteristics seen in section across the study area.
- .Chapter 3.4.2: Detailed description of the different phases of deformation (D1-D6) and their locations seen within the study area are described.
- Chapter 3.5: Detailed structural analysis of two selected structures namely: the Witkoppies structure and Gannapoort Berg structure, are described in detail in Chapter 3.5.1-3.5.2.

3.1 Methods of Structural Analysis

The structural analysis was largely based on field mapping, stratigraphic and structural studies; not on metamorphic or geochronology studies. Regional metamorphic studies conducted by Diener et al. (2014); Pretorius (1986) and van Zyl (1986), who determined a regional metamorphic grade of upper amphibolite facies for the rocks, was taken into consideration for this study. Geochronology studies, however, have not been done within the eastern part of the study area to provide verification on the dates and ages of associated supracrustal rock and intrusives. In the study area the Achab Suite with ages of 1.3-1.7 Ga (Watkeys, 1986) has been dated, together with the Nouzees mafic intrusives, with a mean age

of 1.1 Ga (Joubert, 1986). The structural analysis undertaken during this study was based on standard procedures applied to highly folded and deformed areas (Hobbs et al., 1976). The study area was sub-divided into various domains and sub-domains based on fold style and stratigraphic interpretations as seen in Figure 3.5. The correlation of these domains was done both between and outward for each structural domain. The same penetrative foliation was seen throughout, together with the bedding, which was seen to be parallel with one another throughout the various domains and sub-domains (S0//S1). For each domain and sub-domain, the mapping of the various lithological units and macroscopic fold structures was done using high-resolution aerial photographs. Scales of between 1:2,000 to 1:20,000 were used and supplied by the Department of Rural Development.

The technique of sequence mapping (Chapter 2) (Colliston et al., 2012) was applied during the macroscopic interpretation of major structures, in which diagnostic lithostratigraphic units were mapped out on various scales and used to interpret and characterise major macroscopic fold structures (mapping out the axial trace of isoclinal folds and identifying duplications in the form of imbricate structures (Chapter 2.1.1; Figure 2.3). Overprinting relationships in terms of fabrics (S and L structures) and styles of folding were considered for each macroscopic structure. For the mesoscopic structures their style of folding, overprinting relationships, and their sense of asymmetry concerning the larger structures, as well as the fabrics they deform were considered. For each structural domain the measurement of geometric data for both mesoscopic and macroscopic structures in terms of foliations (S structures), lineations (L1 structures), fold axes and axial planes were documented. For the geometric analysis both the S and L structures were plotted on lower hemisphere equal area stereonets. All values for the S structures (planar structures) are annotated in terms of the direction of dip and dip (000-00) and L structures (linear structures) are presented in terms of trend and plunge (000-00). Stereonet software 9.6.10 (Allmendiger, et al., 2013) was utilized for the manipulation and illustration of geometric data.

Another important aspect that was considered during this study was to understand the 2D and 3D nature of the associated structures. Sections were constructed parallel/oblique to the stretching direction (long sections) and perpendicular to the stretching direction (cross-sections). The methods that were used involve the dip angles of the strata (Busk Method from Busk, 1929) and the down-plunge projection method (Stockwell, 1960), in which structures are projected on another plane perpendicular to the plunge of the fold axes or regional stretching lineation. For each structural domain and sub-domain observations on both macroscopic and mesoscopic scale were considered. For each domain, a criterion was established to denote the different phases of folding (macroscopic and mesoscopic) and their associated planar and linear structures. The terminology used for polyphase terranes is:

- Phases of Deformation: D1; D2; D3 etc...
- Fold Phases: F1; F2; F3 etc...
- Lineations (mineral + stretching): L1; L2; L3 etc...
- Axial Planar Foliation: S1; S2; S3 etc…
- Note: Bedding is determined to be S0

For each domain and sub-domain, the various methods and applications discussed were applied in this study, and carefully scrutinised. Great care however, was taken in correlating the different phases of deformation, as in highly deformed areas of amphibolite grade and higher, it is often a daunting task to distinguish different phases of deformation, with certain areas being more deformed than others during a single long-lived progressive ductile shear event. Correlation of outcrops and different structural domains was carefully interpreted due to the fact that structures may change their character when subjected to spatial changes associated with strain, fluid composition, thermal rate and finite conditions. (Fossen et al., 2019).

3.1.1 Theoretical Background: Mesoscopic Sheath Folds and Model 1-2 Flow Perturbation Folds

Within zones of high strain, different patterns of folds emerge, with variable orientations and geometries that develop on a regional scale. Two types of folds form in such zones of high strain, namely; folds which form due to large variations in flow, which generate folds with variable fold shapes and orientations, these folds are known as flow perturbation folds (Alsop and Holdsworth, 2002). The second type of folds, generate folds with extreme curvilinear hinges that rotate toward the transport direction, these folds are known as sheath folds (Cobbold and Quinquis, 1980; Ramsay, 1980). Both types of folds are prevalent throughout the study area on mesoscopic and macroscopic scale.

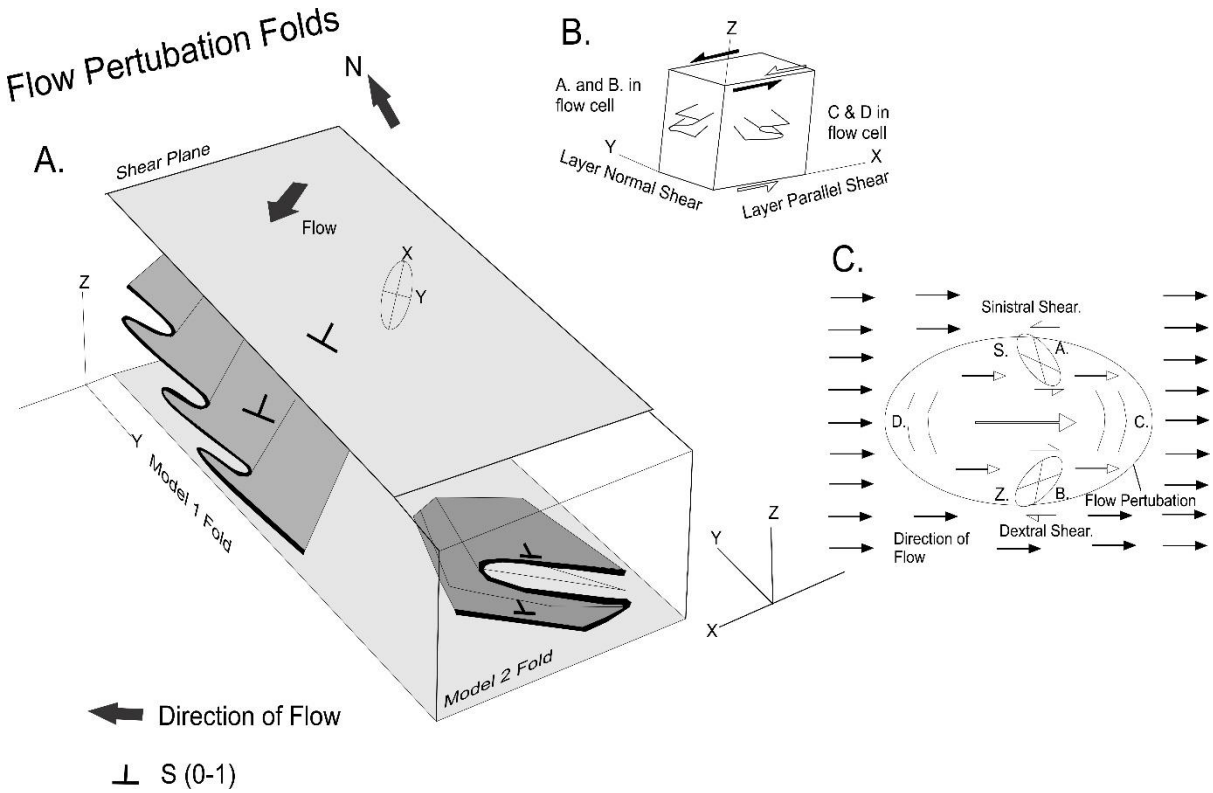

Figure 3.1: Model for the development of model 1 and model 2 flow perturbation folds, found throughout the study area on macroscopic and mesoscopic scale. A: Model showing the development of model 1 and 2 folds, with model 1 folds forming on the YZ foliation planes and model 2 folds forming on the XZ foliation planes. The model 1 fold axes form sub-parallel to the flow direction, with the model 2 fold axes forming oblique to normal concerning the flow direction. B: Model showing model 1 folds forming on the YZ foliation planes (lateral ramps of thrusts) and model 2 folds on the XZ foliation planes (frontal ramps of thrusts). Model 1 folds form due to layer normal shear (black shear symbols) and model 2 folds due to layer parallel shearing (white shear symbols) (Modified after Alsop and Holdsworth, 2007). C: General shear model with associated flow cells and related layer parallel and layer normal shear processes (modified after Alsop and Holdsworth,1999).Plan view of a flow cell during non-coaxial flow. The ellipse represents a flow cell, with the open arrows representing constant flow velocities. In areas A and B sinistral and dextral shear is caused by retardation in flow. The retardation inflow results in the small strain ellipsoids (on both sides represented by A and B) fall within the shortening sector forming S and Z folds, associated with model 1 folds seen in diagrams A and B, forming on the YZ foliation planes. The Z folds will have fold axes sub-parallel to the flow direction and have a clockwise sense of rotation to the flow direction, while an S fold will have an anti-clockwise sense of rotation to the flow direction. In area C layer-parallel shear will form folds at a high angle to the flow direction, verging in the direction of flow forming model 2 folds. Area D represents an area of stretching and elongation. Modified after Alsop and Holdsworth (2007).

Flow Perturbation folds

Folds generated by variation in flow patterns during progressive ductile shear deformation in zones of high strain, are known as flow perturbation folds and may define a large variation in arcuate fold patterns about the transport direction (Alsop and Holdsworth, 2002). These types of folds have been identified within the Caledonian Moine Nappe (Alsop and Holdsworth, 2007) and most recently within the Namaqua Mobile Belt within the Grunau Terrane (Mathee, 2017). Two types of flow folds were identified within the study area, namely; model 1 folds and model 2 folds (Figure 3.1 A).

Gradient velocities normal to the direction of flow will generate a differential layer-normal shearing (Figure 3.1 B and C), with fold hinges that form oblique or sub-parallel to the transport

direction (Alsop and Holdsworth, 2002), forming model 1 folds. Model 1 folds occur on mesoscopic scale both within intrusive and supracrustal successions, as seen in Figure 3.2 A and B. In both examples the fold axes plunge moderately and trend in a north-easterly to north-northeasterly direction. Throughout the study area the mesoscopic model 1 folds have a mean trend toward the northeast (Appendix 3.7).

- Model 1 folds form on the YZ foliation planes and are formed on lateral ramps
- Folds form within the layering.
- Forms S and Z asymmetries.
- Fold axes are co-linear to the regional (L1) lineation.
- Folds an S0//S1 foliation and defines an S2 axial planar foliation.
- The axial planes (S2) are co-planar to S0//S1 foliations.
- Related to the D2 phase of deformation.
- Seen folding within intrusive and supracrustal successions.

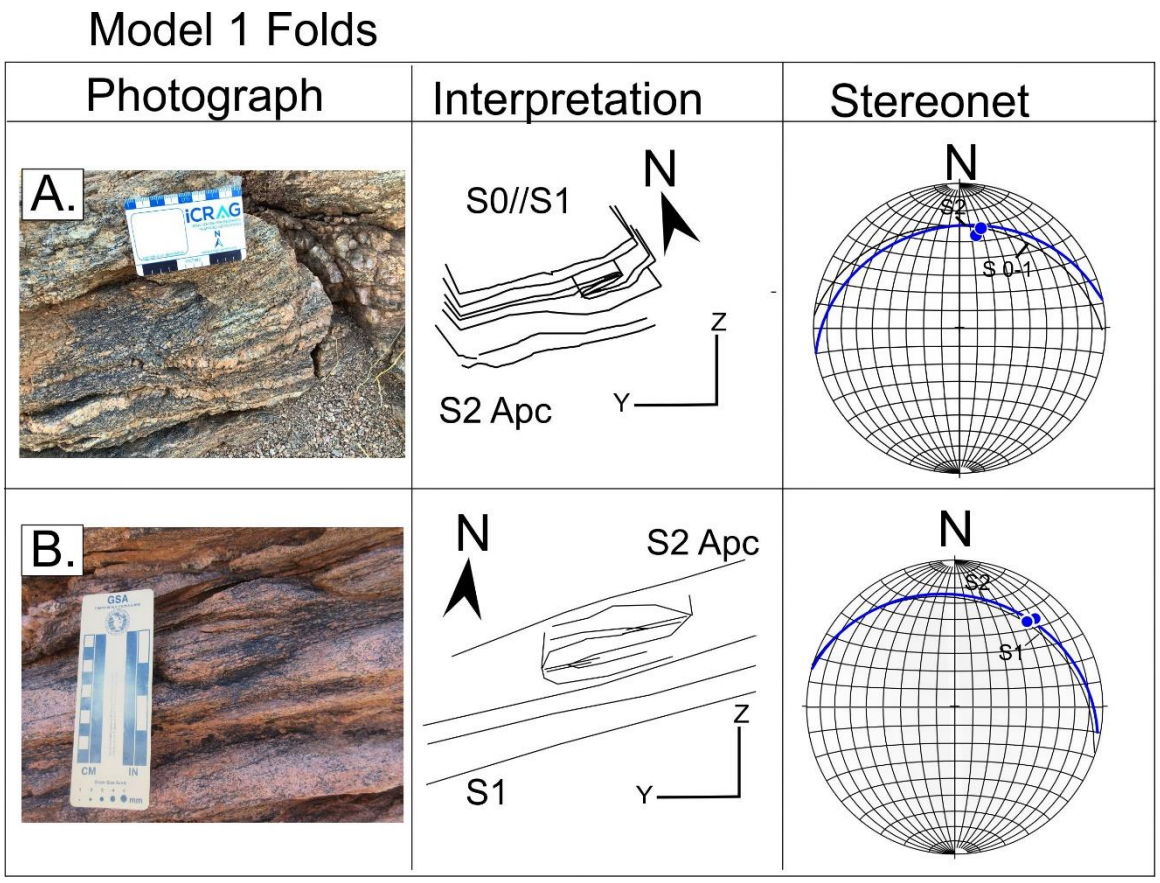

Figure 3.2: Characteristics associated with model 1 folds on an outcrop scale. A: Photograph of a model 1 fold within a biotite gneiss, which illustrates the model 1 fold, folding with the YZ foliation plane, also folds an S0//S1 foliation, and defines an S2 axial planar foliation. Stereonet shows the fold axes trend toward the north-northeast, together with the S0//S1 having a coplanar relationship to S2. B: Model 1 Z fold within the Namies gneiss, and illustrates the coplanar relationship between S1 and S2. Stereonet shows the fold axes trending toward the northeast, with the S1 and S2 foliations being co-planar to one another.

Gradient velocities parallel to the direction of flow, generate a layer parallel shear (Figure 3.3 C), with fold hinges generated at high angles to the flow direction (Alsop and Holdsworth, 2002), forming model 2 folds (Figure 3.1 A and B). Model 2 folds occur both within the intrusives and supracrustal sequences as seen in Figure 3.3 A and B. Fold axes have moderate to shallow plunges and trend in a easterly to north-easterly direction.

- Model 2 folds form on the XZ foliation plane and are formed on frontal ramps.
- Folds form oblique to the layering.
- Forms S and Z asymmetries, with S being the dominant asymmetry.
- Fold axes are normal or oblique to the regional (L1) lineation.
- Folds an S0//S1 foliation and defines an S2 axial planar foliation.
- The axial planes (S2) are coplanar to the S0//S1 foliations.
- Is related to the D2 phase of deformation.
- Is seen folding within both supracrustal and intrusive units.

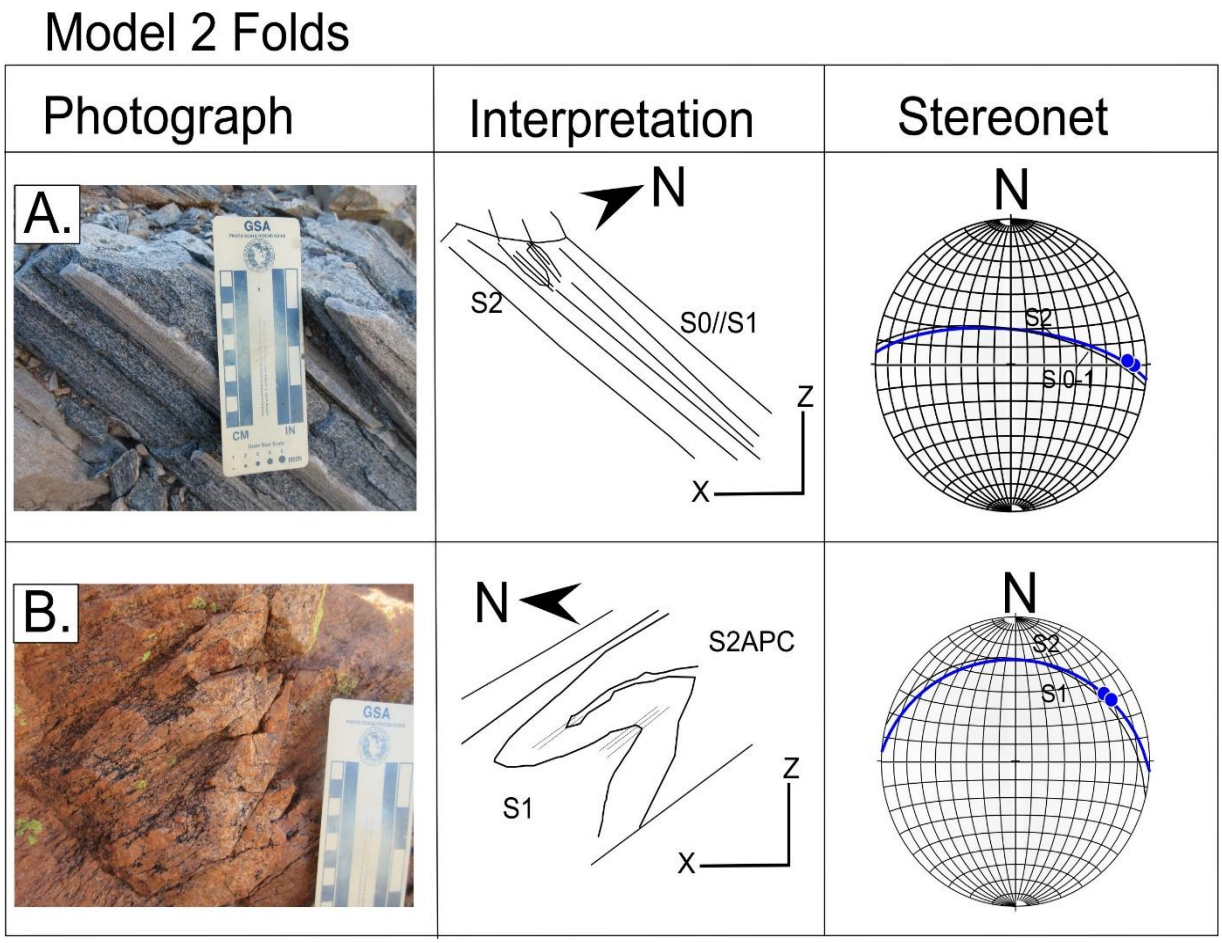

Figure 3.3: Characteristics associated with model 2 folds on outcrop scale. A: Centimetre scale model 2 S fold within the X-Z foliation plane. The S0//S1 foliation has a coplanar relationship to S2. The stereonet also show the fold axes trending toward the east, as well as the S0//S1 and S2 planes having a coplanar relationship. B: Model 2 fold within the Achab Suite, folding within the X-Z foliation plane. The S1 foliation has a coplanar relationship to S2, with the fold axes trending toward the east-northeast.

Comparison of model 1 and model 2 folds

The main difference between the model 1 and model 2 folds is that the model 1 folds form within the YZ foliation plane and the model 2 folds form within the XZ foliation planes (Figure 3.3 A and B). The fold axes associated with the model 1 folds are co-linear with the regional lineation and the model 2 folds form oblique or normal to the regional stretching lineation. The fold axes of model 1 and 2 folds form oblique to one another and form an acute angle to the model 1 folds and stretching lineations. The model 1 and 2 folds have a co-planar relationship with the regional bedding and foliation, with both model 1 and 2 folds folding S0//S1 and defining S2 axial planar foliations, resulting in the co-planar relationship between S0//S1//S2. Also the model 1 and model 2 folds do not deform or fold each other, they are therefore deduced to be of the same age. The fold axes of model 1 and model 2 folds, regionally trend toward the northeast and east-northeast, there are however exceptions where the fold axes and axial planes together with the regional fabric and stretching lineation are rotated toward the southeast and east-southeast. This rotational effect is due to the later phases of deformation (D5). A summary of the model 1 and 2 geometry is illustrated in Appendix 3.2.

Mesoscopic Sheath Folds

Fold structures that show hinge-line curvatures of greater than 90˚, showing curvilinear hinge geometries represent sheath fold structures (Cobbold and Quinquis, 1980; Ramsay, 1980). They have also been classified as isoclinal tubular folds of apical angles of <20˚ (Skjernaa, 1989), and also defined by double vergence geometries (omega structures with S and Z asymmetries), showing reversals in asymmetry across major fold axial traces (Alsop and Holdsworth, 2002). Sheath folds also form elliptical ‘eye’ structures, which often represent the ‘core’ of the sheath fold. These inner elliptical ‘eye’ folds, long and short axes often lie parallel to the y and z short axes, with the central hinge line extending toward the X direction within the XY foliation plane, which is interpreted to be parallel to tectonic transport direction (Alsop and Holdsworth, 2006; Alsop et al., 2007).

Within the study area various elliptical ‘eye’ structures, which close off on both sides have been identified on mesoscopic scale within the Structural Domains 1 to 4. Sheath folds have also been identified on macroscopic scale, their characteristics and details will be discussed in Chapter 4.2. Various styles of sheath folds were identified on a mesoscopic scale, with elliptical ‘eye’ structures being visible (Figure 3.4 A), together with sheath folds showing double vergence geometries and sheath folds with highly curvilinear hinges (Figure 3.4 B). Sheath folds were also identified within the YZ foliation plane (model1), folding within the layering, as well as on the XZ foliation plane (model 2) oblique to the layering (Figure 3.4 C). All three sets of mesoscopic sheath folds fold an S0//S1 foliation and define a penetrative S2 axial planar

foliation, also resulting in the co-planar relationship between S0//S1 and S2. The long axes of the sheath folds identified often trend toward the northeast, east-northeast and east (Figure 3.4 A and B). The fold axes also often rotate around the curvilinear hinge lines toward the southeast in certain mesoscopic sheath folds (Figure 3.4 B). The mesoscopic sheath folds are also rotated by the later phases of deformation (D4-D6) and also trend toward northwest, west and south-west-south where rotated within the study area. The long axes of the mesoscopic sheath folds throughout the study area often have a general trend toward the northeast, and east-northeast and correspond to the regional tectonic transport direction (Colliston et al., 1991) where not rotated by the later phases of deformation.

Conclusion

Both flow perturbation and sheath fold structures result in variable fold styles, orientations, and geometries, and in this case, may be part of the same kinematic framework and can be related to the same phase of deformation, namely; the D2 phase of deformation. Both sets of structures have co-planar relationships regarding their fabrics (S0//S1//S2) and have fold axes which are co-linear to the regional L1 stretching lineation. The flow perturbation folds may themselves be modified and accentuated during progressive deformation, forming sheath fold structures with parabolic hinge-line geometries.

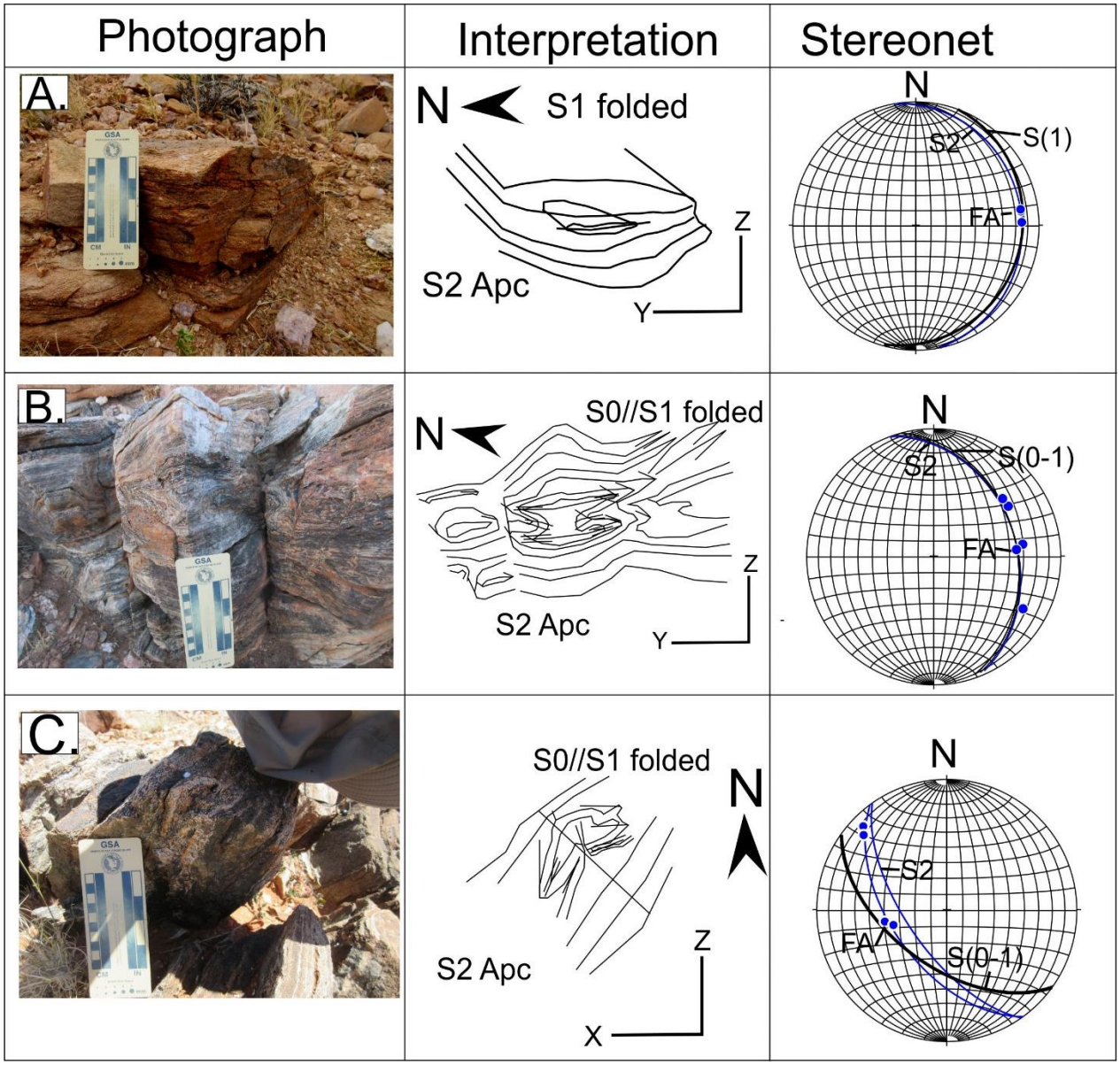

Figure 3.4: Examples of mesoscopic sheath folds found in the study area. A: Mesoscopic elliptical sheath folds within the YZ foliation plane, found within the Lekdam Gneiss, folding an S1 foliation, and defining an S2 axial planar foliation. Fold axes trend toward the east, with the axial plane having a shallow dip also toward the east. B: Mesoscopic sheath fold structure found within the T-Goob Sequence, having double vergence geometries in the form of S and Z folds found on the associated limbs. The sheath fold is exposed on the YZ foliation plane and folds an S0//S1 foliation and defines an S2 axial planar foliation. The fold axes trend toward the east-northeast, east, and southeast, the axial plane has a shallow dip toward the east. The rotational effect of lineations toward the south-east is due to the later D4-D6 phases of deformation. C: Example of an 'omega ' sheath fold with double vergence geometries (S and Z), found within the Vaalputs structure, which folds obliquely within both the YZ and XZ foliation planes, and is therefore oblique to both foliation planes. This sheath fold also folds an S0//S1 foliation and defines an axial planar foliation. Fold axes trend toward the west-southwest and northwest, with axial planes dipping toward the southwest. The sheath fold has been rotated on a limb of a major isoclinal sheath fold structure (Vaalputs sheath fold; Domain 3B) by the later phases of deformation (D4-D6), and therefore has different geometry to the sheath folds in A and B.

3.2 Summary of Regional Structures

During the investigation of the eastern part of the Aggeneys Terrane, it became apparent that the area can be subdivided into a set of structural domains based on the structures and stratigraphic units identified during large-scale regional mapping. The study area can be sub-divided into four main structural domains (Figure 3.5), namely the Witkoppies Structural Domain (Domain 1), Samoep Structural Domain (Domain 2), Lekdam Structural Domain (Domain 3), and Houmoed Structural Domain (Domain 4). The subdomain division is based on the juxtaposition of four prominent intra-terrane thrust sheets, with the inter-terrane Groothoek Thrust (contact between the Aggeneys and Pofadder Terranes) situated in the hanging wall and the Geelvloer Thrust (contact between the Aggeneys and Bladgrond Terranes) located in the footwall (Figure 3.5).

Witkoppies Structural Domain

The Witkoppies Structural Domain (Figure 3.5; Structural Domain 1) extends eastward outside the study area and branches out on the footwall of the Groothoek Thrust contact, and is defined by the Vaalputs Suite. The Witkoppies Structural Domain is characterised by isoclinal structures with double vergence geometries (Chapter 4.2) and fold structures with macroscopic elliptical ‘eye’ structures. The Witkoppies Structural Domain is located in a macroscopic D4 (Figure 3.5) synformal hinge, which is well exposed in the west and extends toward the east outside the study area. A prominent penetrative foliation is found throughout the domain and is consistently visible throughout. The penetrative foliation has a sub-vertical attitude on the limbs of the major structures and flattens out within the hinges, where not strongly affected by shearing.

Samoep Structural Domain

The Samoep Structural Domain (Figure 3.5; Structural Domain 2) cuts out against the footwall of the Groothoek Thrust in the northwest of the study area and extends toward the east, outside of the study area. The Samoep Structural Domain is the only domain that does not contain any isolated fold structures and is defined by a well-foliated medium quartz-feldspar gneiss (Samoep Gneiss), which does not contain any xenoliths. The Samoep Structural Domain is folded by the macroscopic D4 fold and lies within the hinge. The southern limb also tightens and is isoclinally folded toward the southeast of the structure (Figure 3.5; Structural Domain 2). The regional penetrative foliation is consistently visible throughout the structural domain. The orientation of the foliation changes from sub-vertical on the limbs of the major D4 hinge and flattens in the far western fold hinge.

Lekdam Structural Domain

The Lekdam Structural Domain (Figure 3.5; Structural Domain 3), extends in a northwest direction out of the study area where it is interpreted to branch out against the hanging wall of the Groethoek Thrust contact (Figure 3.5). The Lekdam Structural Domain also extends toward the south where it branches out against the footwall of the Samoep Structural Domain in the southeast. The Lekdam Structural Domain can be sub-divided into a series of sub-domains which represent fold structures with double vergence geometries and isoclinally refolded structures which are separated from one another (Figure 3.5). The Lekdam Structural Domain is defined by the Lekdam Gneiss with all the isoclinal structures/sub-domains situated within. The Lekdam Structural Domain is folded by a macroscopic D4 fold, with the southern limb being severely shortened, resulting in it being heavily folded in an isoclinal fashion. Penetrative foliation is also constantly visible throughout the study area, with sub-vertical orientations on the limbs of major fold structures and on thrust boundaries, with sub-horizontal attitudes within the hinge zones of the respective structures.

Houmoed Structural Domain

The Houmoed Structural Domain (Figure 3.5; Structural Domain 4) covers the largest part of the study area and extends outside the study area both toward the west and the east (Figure 3.5; Structural Domain 4). The Houmoed Structural Domain also hosts fold structures with double vergence geometries, together with isoclinally refolded structures and macroscopic elliptical ‘eye’ structures, which close off on both sides. The isoclinal fold structures and elliptical structures are all surrounded by the Achab Suite. The Houmoed Structural Domain is also folded by the major D4 fold structure, with a sharp contact in the footwall with the Geelvloer Thrust in the south. The contact with the hanging wall Groothoek Thrust is seen toward the northwest outside of the study area. The contact with Structural Domain 3 is located on the limb of a major isoclinal fold structure in the northwest of the study area. The Houmoed Structural Domain also extends toward the east outside the study area, and cuts out toward the southeast of the study area against the footwall of Structural Domain 2.

All the Structural Domains discussed are defined by macroscopic intrusive sheets (intra-terrane thrust sheets) which host a series of fold structures with double vergence isoclinal structures and elliptical fold structures. All four Structural Domains contain the same penetrative regional foliation, which is consistently visible in outcrops throughout. The Groothhoek Thrust contact (Figure 3.5) is visible in the north and northeastern part of the study area and extends along strike from northwest to southeast across the study area (Figure 3.5). The Groothoek Thrust contact extends outside the study area both toward the west and east of the study area (Colliston et al., 2012). The Witkoppies and Samoep Structural Domains

branch out against the Groothoek Thrust in the northwest, with the Lekdam and Houmoed Structural Domains, also interpreted to branch out against the Groothoek Thrust contact outside of the study area. The contact with the Bladgrond Terrane/Geelvloer Thrust contact (Figure 3.5) is situated in the southern part of the study area and represents the footwall thrust contact with the Aggeneys Terrane (Figure 3.5). The Geelvloer Thrust contact extends eastward past the study area into an area mapped by Maclaren (1988) and also westwards (unmapped currently).

3.2.1 Regional Fabric

Regionally the study area is defined by a well-defined penetrative S2 regional fabric. The S2 fabric is exposed within all four structural domains defined in the study area. The S1 penetrative foliation also produced during upper amphibolite grade conditions (van Zyl, 1986), and associated with intrusion of granitic thrust sheets, is often sub-parallel to the compositional banding seen within the associated supracrustals (S0). The S0//S1 foliation can only be identified by folding around the hinges of macroscopic F2 sheath folds (Chapter 4.2). Almost all the F2 sheath folds identified within the study area, define prominent S2 axial planar foliations that becomes the regional penetrative S2 foliation seen regionally across the study area, both within the intrusives and supracrustal sequences. The S2 foliation is therefore co-planar to the S0//S1 foliations, and can easily be misinterpreted, if the hinge zones of the macroscopic structures aren't investigated sufficiently.

The regional S2 foliation is defined by biotite, muscovite, amphibole and diopside within the supracrustal rocks encountered throughout all four structural domains. Within the feldspar augen gneisses the foliation is associated with biotite, amphibole, interleaved beween feldspar and plagioclase augen, and within the medium and coarse grained gneisses the foliation is defined by muscovite and biotite. The regional S2 foliation as a mean dip toward the north, north-northeast and northeast (Appendix 3.2) in both the supracrustal rocks and intrusives. The regional foliation is rotated toward the south and southeast by the later phases of deformation (D4), the rotation only occurs on the northern limb of the major D4 structure, examples can be seen in Appendix 3.2.The linear structures seen throughout the study area are all co-linear and consist of mineral lineations, such as stretching lineations, fold axes and long axes of sheath folds, as has been documented for the Western Aggeneys Terrane (Strydom and Visser, 1986; Colliston et al., 1991). The XY-planes of the finite strain ellipsoid are defined by the regional S2 foliation planes, with the development of an L1 lineation within the XY plane of the regional strain ellipse.

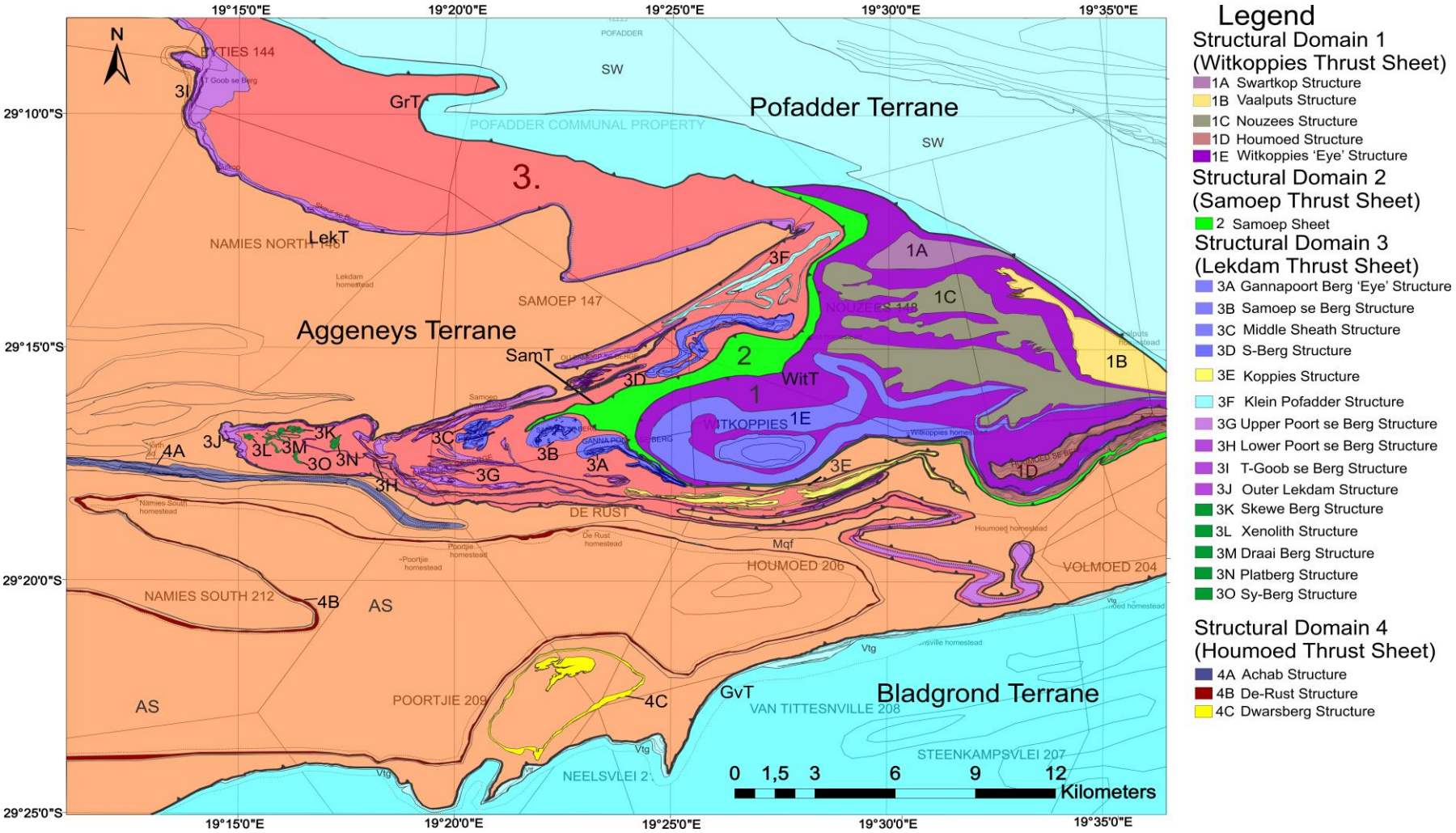

Figure 3.5: Simplified map depicting all the structural domains and associated structures within the study area. The study area can be sub-divided into four main structural domains, with each domain being sub-divided into smaller sub-domains according to the isolated fold structures identified within each domain. Domain 1 represents the Witkoppies Structural Domain; Domain 2 the Samoep Domains, Domain 3 the Lekdam Domain, and Domain 4 the Houmoed Structural Domain. The structural domains are seperated by intra-terrane thrust contacts, namely; the Lekdam Thrust (LekT); Samoep Thrust (SamT); Witkoppies Thrust (WitT). The Groothoek Thrust (Grt) and Geelvloer Thrust (GvT) are found in the north and south of the study area.

Therefore, the L1 lineation is considered to represent the X direction of the regional strain ellipse, with the X-direction being co-linear to the southwestern directed tectonic transport direction (Colliston et al., 1991; Colliston, 1990). The L1 stretching is found within both intrusive and supracrustal rocks across the study area. The L1 lineations are defined by biotite, amphibole, stretched augen (feldspar and plagioclase) and K-feldspar aggregates within the intrusives. Within the supracrustal rocks the L1 lineation consists of biotite, sillimanite, amphibole, diopside, feldspar and actinolite. The L1 stretching lineations have a mean trend toward the northeast and north-northeast, both in the supracrustals and intrusives (Appendix 3.2), and this corresponds to the southwestern directed transport direction (Colliston et al., 1991; Colliston and Schoch, 2013). The L1 regional stretching lineation is however, also rotated toward the south-east-south and southeast on the northern limb of the major D4 structure (Appendix 3.1 A & 3.2). Throughout the study area the L1 regional lineations are colinear to the F2, F3 and F4 fold axes, and is representative of the X direction of the regional strain ellipse (Colliston and Schoch, 2013), and is seen throughout all four structural domains within the eastern Aggeneys Terrane (Appendix 3.2).

3.3 Structural Framework

For the ease of description, a brief summary and description is provided in Chapter 3.3.1 regarding the structural framework in the study area. Each phase of deformation is briefly summarised and described in Figure 3.6 and Table 3.1 and 3.2. This is done in order to provide background information on the regional structural framework, to better illustrate the structural complications associated with the study area as depicted in Appendix 3.1 and in the proceeding Chapters 3.4 and 3.5.

3.3.1 Summary

Structural and stratigraphic studies conducted in the western Aggeneys Terrane (Colliston et al., 1991), proved that the Namaqua Orogeny is defined by a single long-lived progressive shear deformation event, under deep crustal conditions, with no evidence seen to support multiple orogenic episodes, the same is true for the eastern Aggeneys Terrane. For the eastern Aggeneys Terrane six phases of deformation were identified to form progressively and is summarised in Figure 3.6, with details of fabrics, attributes and locations within the study area summarised in Table 3.1 and 3.2.

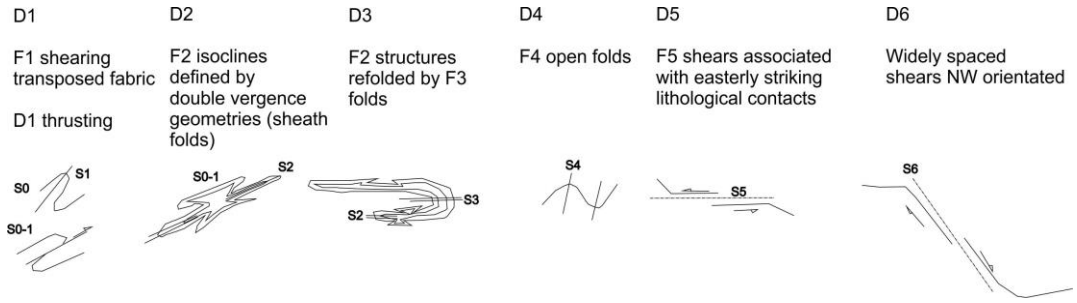

Figure 3.6: Simplified diagram showing the correlation of regional phases of deformation within the eastern Aggeneys Terrane. S0=Relict bedding; S1 regional transposed foliation; S2-S4= mineral foliation/ axial traces of earlier folds; S5-6 shear fabric.

- The D1 phase is defined by a penetrative S1 foliation of upper amphibolite grade (van Zyl, 1986) seen throughout the study area and is sub-parallel to the compositional banding (S0).The S1 foliation is associated with the intrusion of massive granite sheets, that define kilometre scale intra-terrane thrust sheets (Figure 3.6; Table 3.1). The D1 phase is only visible folding around the hinges of macroscopic F2 sheath folds. An L1 stretching lineation also lies within the XY foliation plane and represents the long axes of the regional strain ellipse that is sub-parallel to the regional southwest direction of overthrusting (Colliston et al., 1991).
- D2 phase is defined by double vergence isoclinal fold structures, which are classified as sheath folds (Chapter 4.2). The F2 sheath folds fold an S0-1 fabric and develop a prominent S2 axial planar foliation (Figure 3.6; Table 3.1). The S2 foliation therefore defines the regional S2 foliation within the XY plane of the regional finite strain ellipse, defined across all structural domains and associated with all the sheath fold structures identified in the study area.
- The D3 phase is recognised by the refolding of double vergence sheath folds on a kilometre scale, with a locally developed S3 axial planar foliation, with the S2 regional foliation folding around the F3 hinges (Figure 3.6; Table 3.1). The D3 phase is recognised on the northern and southern limb of the major synformal D4 structure.
- The D4 phase is manifested by a kilometre scale D4 Z fold, which folds all four structural domains (Figure 3.6; Table 3.2). The antiformal component is located in the northwestern sector of the study area, with the large synformal hinge found in the central western sector of the study area (Appendix 3.1). The D4 phase of folding folds both the D2 and D3 sheath folds throughout the study area.
- The D5 phase is associated with reactivated movements within D1 intra-terrane and inter-terrane thrust boundaries (Figure 3.6; Table 3.2), together with the reactivated movements found on the limbs of major D2, D3 and D4 fold structures across all domains.

Table 3.1: Summary of the different phases of deformation (D1-D3), together with the attributes and map location of the different phases of deformation seen in Appendix 3.2-3.4

Phase of Deformation	S and L Structures	Attributes	Folds	Map Ref	Example: Domain
D1 Phase	Penetrative S1 fabric-formed at upper amphibolite grade conditions. The S1 fabrics is parallel to the regional S0 banding. Ubiquitous linear L1 structure is associated with the D1 phase and is defined by acicular minerals (sillimanite, feldspar aggregates & amphibole) and long axes of clasts.	No identifiable macroscopic F1 structures. S1 fabric associated with the emplacement of intrusive sheets, due to D1 intra-terrane thrusting. D1 intra-stratigraphic thrusting.	Mesoscopic intrafolial folds seen in both xenoliths, supracrustal and intrusive rocks. S1 foliations are seen folding the limbs of the F2 intrafolial model 1 and 2 folds.	Zone B3, C3 and C4 in Appendix 3.2.	Domain 3G: On the limb of the major F2 structure. Domain 4C: Limb on the major F2 structure
D2 Phase	Penetrative S2 foliation also formed at upper amphibolite grade conditions. The S2 foliations is parallel to the regional S0-1 foliation. S2 foliation is identified in F2 fold hinges as an axial planar foliation.	Formation F2 model 1 and 2 mesoscopic flow pertubation folds associated with a progressive ductile shear model. Formation of F2 macroscopic sheath folds with double vergence geometries. The mesocopic F2 folds and macroscopic F2 fold structures have a co-linear relationship to the regional L 1 stretching lineation and correspond to the north east to south west tectonic transport direction.	Mesoscopic model 1 and 2 folds which fold both within the YZ and XZ foliation planes. Both fold an S0//S1 foliation and define an S2 axial planar foliation. Mesoscopic folds, fold both the intrusive (S1//S2) and supracrustal (S0//S1//S2) rocks. Formation of F2 fold structures with double vergence geometries. All the macroscopic F2 fold structures fold an S0//S1 foliation and define an S2 axial planar foliation, which becomes the regional S2 foliation. F2 fold structures fold both intrusive rocks and supracrustals.	Zones D2,D3, C3.C4 and E2. Appendix 3.3	Domain 1A Domain 1B Domain 1C Domain 1E Domain 3A Domain 3B Domain 3C Domain 3E Domain 3G Domain 3H Domain 3I Domain 3J Domain 3K Domain 3M Domain 3N Domain 3O Domain 3 Domain 4A Domain 4B
D3 Phase	Penetrative S3 axial planar foliation also formed at upper amphibolite grade. Only develops locally and not seen everywhere. The locally developed S3 foliation is co-planar with respect to the S0;S1 and S2 foliations.	Defined by another phase of folding (F3), which refolds earlier F2 fold structures. Refolds all earlier foliations (S0//S1//S2) and defines an S3 axial planar foliation at certain locations, which is co-planar to all earlier foliations The F3 fold axes are co-linear with respect to the L1 stretching lineations and F2 mesoscopic and macroscopic fold axes.	Formation of refolded F3 Ramsay type 3/isoclinal fold structures, and refolds all F2 fold structures (S0//S1//S2). The F3fold structures at certain locations define an S3 axial planar foliation and folds both the intrusive rocks and supracrustals.	Zone: B3, C3, D2, D3 and E3. Appendix 3.4	Domain 3A Domain 3D Domain 3F Domain 3G Domain 3H Domain 3I Domain 3K Domain 3M Domain 3O Domain 4C

Table 3.2: Summary of the different phases of deformation (D1-D3 phase), together with attributes and map location of the different phases of deformation seen in Appendix 3.5 and 3.6.

Phase of Deformation	S and L Structures	Attributes	Folds	Map Ref	Example: Domain
D4 Phase	Results in the refolding of S0//S1//S2//S3, no locally developed S4 foliation were identified.	Formation of F4 open folds which form due to sinistral wrench shear. The F4 folds refold earlier F2 and F3 structures and kilometer scale intra-terrane thrust sheets. The F4 fold axes have a co-linear relationship to the L1, F2 and F3 structures where not affected by later phases of deformation. The entire western part of the study area is defined as a megascopic F4 structure.	All four major thrust sheets (Witkoppies, Samoep, Lekdam and Houmoed Thrust sheets) folded by the D4 phase and represents a major F4 fold, which has a Z asymmetry. The D4 folds refold earlier D2 and D3 structures on the NW and SE limbs of the major D4 structure.	Zone A3,B2, C2, C3, D2 and E3. Appendix 3.5	Domain 2: Folding of the Structural Domain 2. Domain 3J: Folding of the Outer Lekdam Structure and Lekdam Thrust by the major f4 fold. Domain 3 I: folding of the T-Goob structure by F4 folds, which form characteristic Z folds
D5 Phase	Deforms all earlier foliations and is defined by a conspicuous mylonitic foliation.	Defined by prominent east-west shear zones, which is associated with reactivated movements on the intra-terrane thrust contacts and on the limbs of major F2, F3 and F4 structures. The late easterly trending shear zones also tighten up later F2, F3 and F4 fold structures to form isoclinal fold structures. This is well illustrated on the southern limb of the major F4 fold.	Formation of F5 oblique folds which result in the buckling of major F2 and F3 fold structures and form as a result of the D5 east-west shear zones.	Zone A3, C3,D3 and E4. Appendix 3.6	Limb of Domain 3H: Reactivated movements of the Lekdam Thrust. Domain 6: Reactivated movements of the Geelvloer Thrust. Domain 4A and B: Major reactivated movements on the Achab and De Rust Structures. D5 structures occur throughout all domains, on the limbs of all major F2, F3 and F4 structures.
D6 Phase	Deforms all earlier foliations as well as mylonitic foliation into the associated shear planes.	Defined by NW-SE subvertical shear zones, which deforms all earlier structures.	Tightens and flattens D2 and D3 hinges in the far eastern sector of the study area.	Zone: D2, E2 and F3. Appendix 3.6	Domain 5: reactivated movements on the Groothoek Thrust Domain1 D: D6 effects transposed on the Houmoed Mountains (Domain 1D) and the limb of the Witkoppies sheath fold(Domain1E).

- The D6 phase affects earlier D2, D3 and D4 fold structures (Figure 3.6; Table 3.2), and the deformation results from south-east striking Tanatalite Valley Shear Zone Deformation (Colliston, 1990); it has the effect of tightening up/flattening all structures toward the far east of the study area, close to the Groothoek Thrust Fault (Appendix 3.1).

3.4 Regional Description of Structural Development

Within the eastern part of the Aggeneys Terrane, there are a total of 23 isolated sheath fold structures (Chapter 4.2) with double vergence geometries and elliptical sheath folds, being refolded by the later D3-D4 phases of deformation. For the ease of description only certain aspects and details will be discussed in this chapter to illustrate the various complexities associated with the eastern Aggeneys Terrane. Chapter 3.4 is sub-divided as follows: In chapter 3.4.1 cross-sections perpendicular (Appendix 3.3.1) and parallel to the regional stretching lineation (Appendix 3.3.2) will be described in detail. The various phases of deformation will be described in detail in chapter 3.4.2, with each phase being summarised using selected examples from key locations. The following appendices accompany this section.

- Appendix 3.1 represents a detailed 1:40,000 structural formline map, together with a grid system that aids in the description and location of certain structures.
- Appendix 3.1 A: Represents the L1 lineation trends and plunges across the study area; Appendix 3.1 B-E represent detailed maps of allocated zones within the study area, and show details related to the macroscopic D4 stucture that defines the study area.
- Appendix 3.2: The geometric properties of 8 selected structures is used as examples across the study area. The geometry represents characteristics seen regionally across all the structures encountered in the study area.
- Appendix 3.3: Shows details of a cross section and long section constructed across the study area, discussed in chapter 3.4.1.
- Appendices 3.4.1-3.4.5 represent 1:40,000 maps illustrating the different phases of deformation that are discussed in chapter 3.4.2. A grid system is also used to identify and find key locations within the study area.

3.4.1 Long section and cross section description

Section Perpendicular to the regional stretching lineation (Appendix 3.3.1)

The long section in Appendix 3.3.1 is a section drawn perpendicular to the regional stretching lineation, and most of the fold hinges were projected using the down plunge projection method (Stockwell, 1960). The regional stretching lineation on both the northern and southern sections

of the section have average plunges of 30˚ and were projected accordingly (Appendix 3.3.1 C and D). The section is represented by lines A-B-C, that cut across the macroscopic D4 synformal structure (Appendix 3.3.1 A and B). All four structural domains are represented in section, with structural Domain 2, 3 and 4 being folded by the D4 phase of folding around the inner Witkoppies D2 fold hinge located in structural Domain 1 (Appendix 3.3.1 B). The northern and southern limbs of the synformal structure are well represented, with prominent D2 and D3 structures located on both limbs and interpreted to be folded by the D4 phase of deformation. Intra-terrane thrust faults like the Lekdam, Samoep and Witkoppies Thrusts are also folded by the D4 phase of folding (Appendix 3.3.1 B). What is also clear is that the regional foliation planes, as well as the D2 and D3 sheath fold structures are rotated toward the south on the northern limb, and rotate back toward the north on the southern limb around the major D4 hinge.

Section Oblique to the regional stretching lineation (Appendix 3.3.2)

Appendix 3.3.2 represents a cross section oblique to the regional stretching lineation, and is represented by section line A-B-C-D-E-F, and cuts across all four structural domains. The sections were constructed using a combination of the Busk Method (Busk, 1929) and the down plunge projection method (Stockwell, 1960). The average stretching lineation used for the projection has an average plunge of 28˚ on the southern limb of the major D4 structure. The section was constructed parallel to the major D4 axial trace, thus the D4 effect is removed in the synformal component of the section. The D2 and refolded D3 sheath fold structures are located on the southern limb of the structure, and have been highly attenuated and flattened by the D5 phase of deformation. Major intra-terrane thrust boundaries like the Lekdam, Samoep and Witkoppies Thrusts are also heavily attenuated and flattened by the D5 east-west shears. The D5 shearing effects can also be seen by a change in thickness in the Samoep Thrust sheet (Structural Domain 2) and the Witkoppies Structure, where the lithological units flatten and attenuate on the southern limb toward the east (Appendix 3.3.2 A). The D4 hinges on the southern limb are also attenuated and heavily folded by the D5 east-west shears. Toward the far east of the section close to the Groothoek Thrust, the F2 and F3 fold traces are drawn parallel to one another by the reactivated movements associated with the D6 phase of deformation.

3.4.2 Phases of Deformation

The D1 Phase of Deformation

The D1 phase of deformation is defined by an S1 penetrative foliation of amphibolite grade (van Zyl, 1986). The S1 fabric is associated with the emplacement of intrusive sheets during D1 intra-terrane thrusting and can be seen within all four structural domains. The S1 foliation

is sub-parallel to the S0 compositional banding, and is often only identified on a mesoscopic scale in mesoscopic F2 folds (Figure 3.7 and 3.8) within more incompetent bands. The S0-1 foliation is isoclinally folded and defines an S2 transposed fabric in the hinges of rootless F2 mesoscopic model 1-2 folds. In the Achab Suite (Figure 3.7 A and B) this is also clearly seen in high strain zones, where the S1 foliation is isoclinally folded and dismembered, together with transposed F2 hinges (S2), so that the S1 and S2 fabrics are discontinuous, becoming scattered with isolated isoclinal hinges recognised as thick feldspar boudins unconnected to each other, with F2 fold axial surfaces (S2) being parallel to the S1. The S2 regional fabric is well represented in certain locations, both in the supracrustal and intrusive rocks (Figure 3.7 C), and only seen within incompetent layers, if the correct observations are made, such as in Figures 3.7 and 3.8. If not, errors can be made regionally regarding the S1 and S2 foliations.

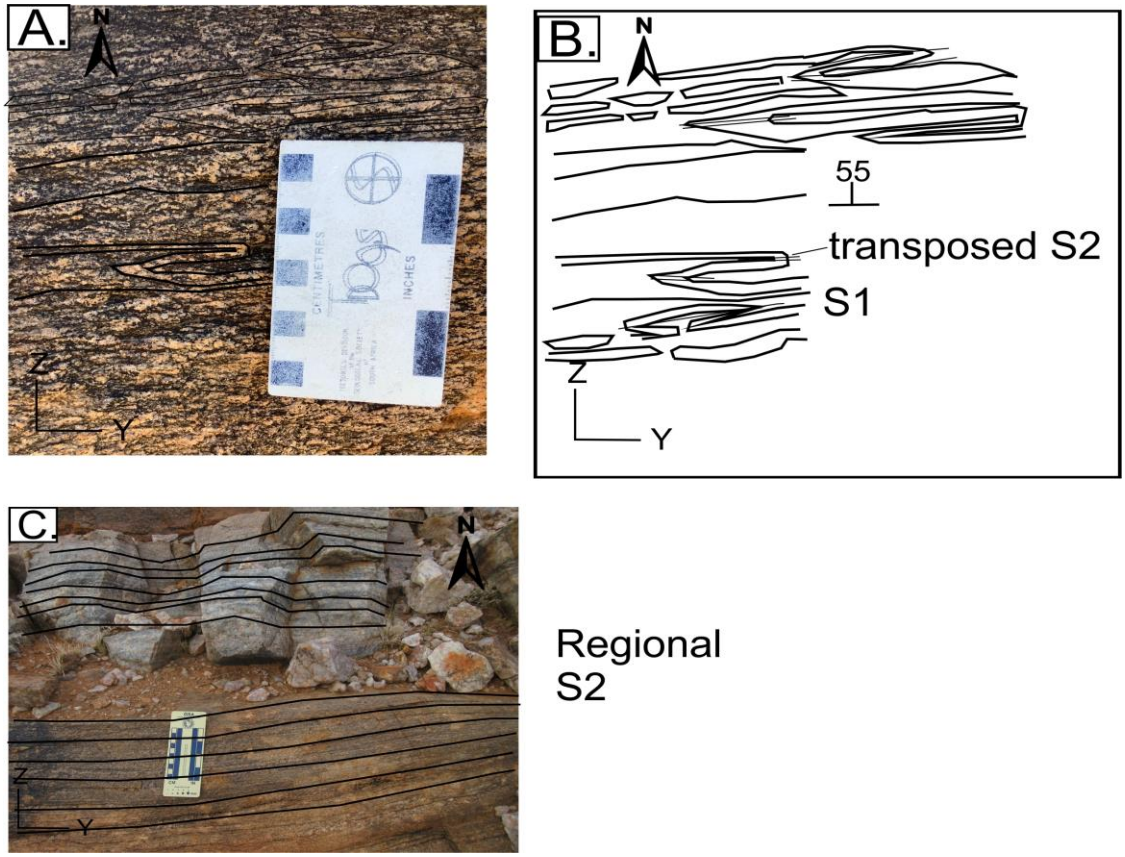

Figure 3.7: Contacts and foliations: A: Mesoscopic F2 folds found within the Achab Suite, the F2 folds fold feldspar bands within incompetent zones. B: Interpretation of diagram A, the S1 foliation is folded and boudinaged on the limbs of F2 rootless folds, defining a penetrative transposed S2 foliation. Both the S1 and S2 foliations are boudinaged and flattened. C: Lithological contact between a well bedded quartzite (competent unit) and the Achab Suite (incompetent unit), where the regional S2 foliation is sub-parallel to the regional compositional S0-1 banding.

The D1 phase is therefore recognised, within model 1-2 folds, that fold the compositional banding (S0) and S1 on the limbs and form a transposed S2 fabric, that is seen in both supracrustal (Chapter 3.1.1) and intrusive rocks (Appendix 3.4.1; Domain 3I; Zone C3 and Figure 3.7 B and C). Another example can be viewed in Figure 3.8 A, B and C where the S1

fabric can be seen folding in an incompetent transposed xenolith layer around a model 1 F2 fold, defining a penetrative S2 axial planar cleavage, that becomes the regional S2 penetrative foliation (Appendix 3.4.1; Domain 3I; Zone C3).

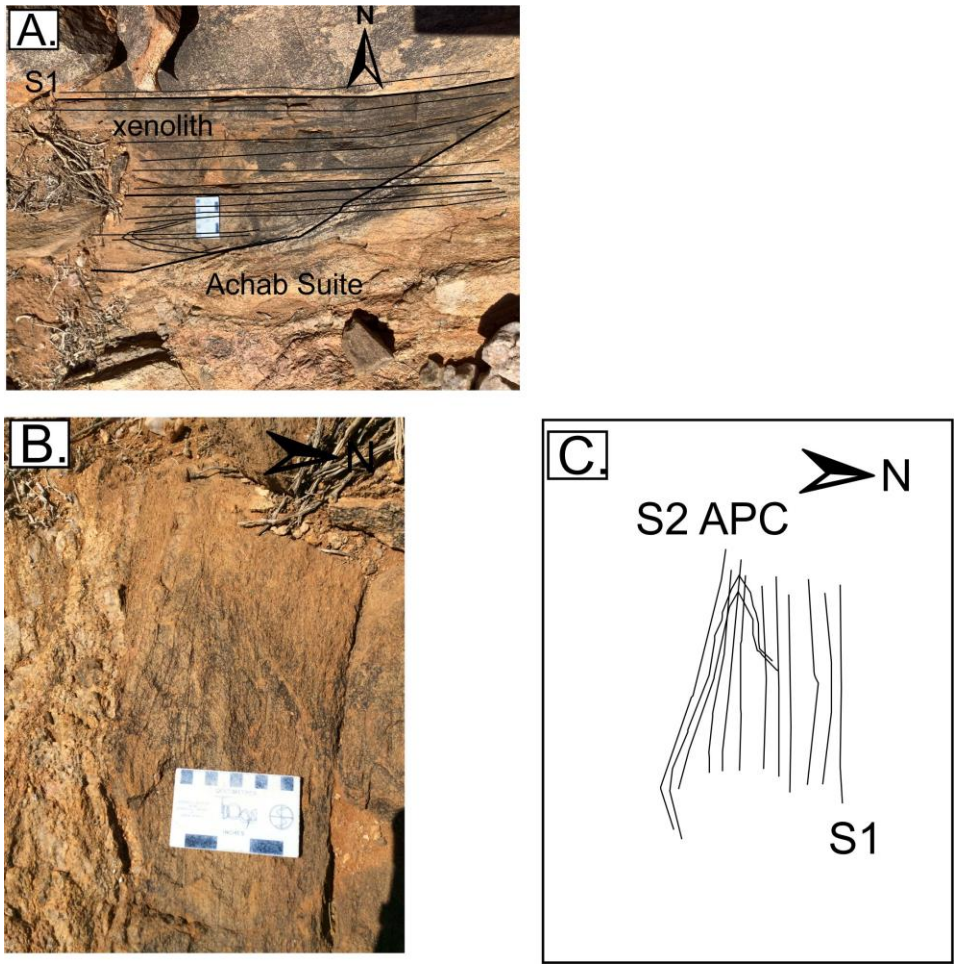

Figure 3.8: A: Model 1 fold seen within a xenolith found within the Achab Suite. The penetrative S1 foliation is seen within the Xenolith and Achab Suites. B: Close up view of the model 1 fold found within the Xenolith Suite contained within the Achab Suite. C: Interpretation of the S1 foliation is only seen on the limbs of the F2 model 1 fold, with the development of a penetrative S2 axial planar cleavage within the hinge of the fold, resulting in the S1 and S2 foliation becoming coplanar to one another.

The S1 foliation can also be seen duplicating and cutting out on the limbs of sheath folds, and close to intra- and inter-terrane thrust boundaries. Intra stratigraphic thrusting sequences were identified by the asymmetric stacking of certain stratigraphic units (1-2-1-2 or 1-2-3-1-2-3), forming imbricate structures (McClay, 1991) and cut-out structures on the limbs of sheath folds, and in intra-terrane thrust boundaries (Chapter 2; Figure 2.3). Similar structures have been identified within the Haramoep Mountains (Praekelt, 1994); Aggeneys Hills (Colliston and Schoch, 2002), and the Pella sheath fold (Colliston, 1990; Colliston and Schoch, 2000). Intra-stratigraphic thrusting was identified within the T-Goob se Berg structure (Appendix 3.4.1; Zone A1), Dwarsberg Structure (Appendix 3.2, Zone C4) and on the Geelvloer Thrust contact (Appendix 3.4.1; Zone E4). However, intra-stratigraphic thrusting is not as pervasive

when compared to the western portion of the Aggeneys Terrane, this could be attributed to higher zones of strain. The early S0//S1 fabric has a strongly developed L1 stretching lineation, which is oblique with respect to the regional fabric, and has a distinct northeasterly trend and plunge, coinciding with the regional tectonic transport direction (Colliston et al., 1991).

D2 Phase of Deformation

The D2 phase of deformation is attributed to the formation of F2 fold structures on both mesoscopic and macroscopic scale. A penetrative S2 foliation is formed and interpreted to form at upper amphibolite grade conditions, similar to S1 (van Zyl, 1986). The co-planar S0, S1 foliation is folded around the F2 hinges, with the S2 foliation forming as an axial planar foliation within, and is defined as the regional foliation developed across the entire study area. The most prominent examples can be seen in the hinge zones of the Gannapoort Berg structure (Appendix 3.4.2; Domain 3A; Zone C3); Samoep se Berg structure (Appendix 3.3; Domain 3B; Zone C3); S-Berg structure (Appendix 3.3; Domain 3D; Zone 3D) and the Klein Pofadder structure (Appendix 3.4.2; Domain 3F; Zone C3). The best example can be seen on the western hinge of the Samoep se Berg structure (Figure 3.9) On mesoscopic scale the S2 foliation can be identified in both the XZ and YZ foliation planes of the model 1 and model 2 folds, which fold S0-1 and defines a penetratively developed S2 axial planar foliations, resulting in the S2 foliation being co-planar to the S0//S1 fabrics (Chapter 3.1.1).

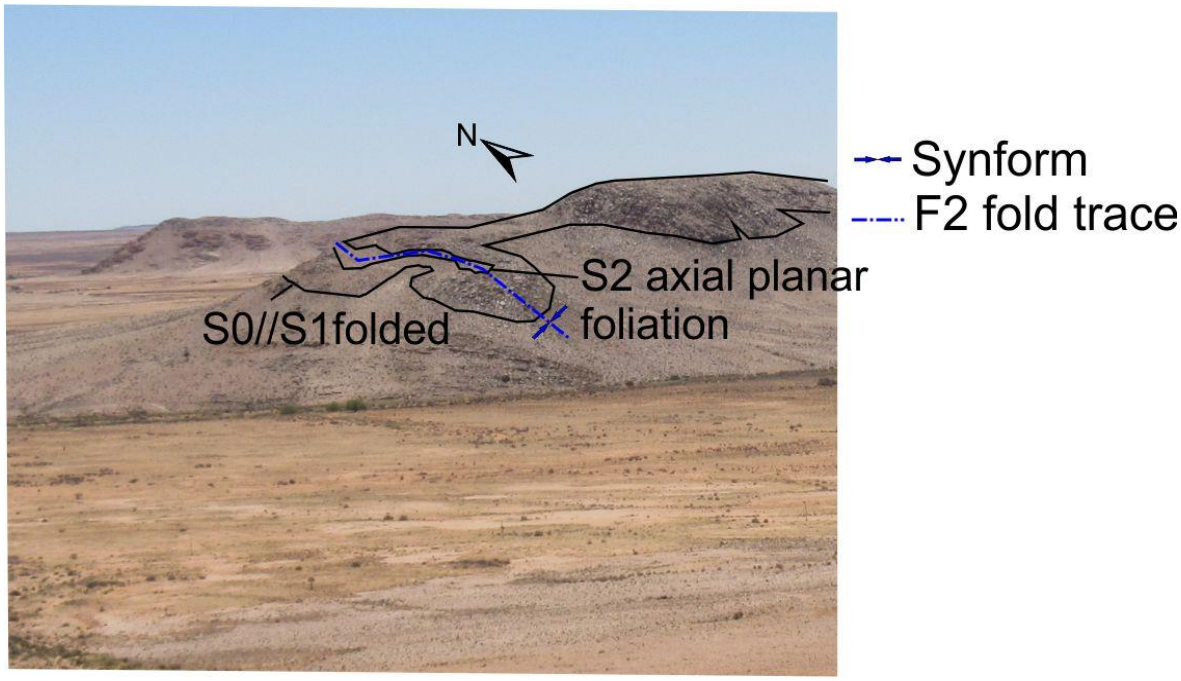

Figure 3.9: Western D2 fold hinge of the Samoep se Berg sheath fold (Appendix 3.4.2; Domain 3B; Zone C3). The western fold closure folds an S0//S1 foliation and develops a penetrative S2 axial planar foliation.

The fold axes associated with D2 phase of deformation have a general trend toward the northeast and east-northeast and is co-linear to the regional L1 stretching lineation (Appendix

3.2). Good examples can be seen in the F2 fold axes of the Gannapoort Berg structure, Samoep se Berg structure, T-Goob se Berg structure, Outer Lekdam structure and the Dwarsberg structure, which have moderately plunging fold axes (between 25˚ and 40˚) and northeast to east-northeast ternding fold axes (Appendix 3.2). The F2 axial planes (S2) are also co-planar to the S0//S1 foliations and have a mean dip and dip direction toward the north and northeast (Appendix 3.2).The axial planes of the Gannapoort Berg (Domain 3A), T-Goob se Berg (Domain 3I), Outer Lekdam (Domain 3J) and Dwarsberg structures (Domain 4C) have moderately north to northeast dipping axial planes, which are parallel to the S0//S1 foliations (Appendix 3.2).

However, there are exceptions to the shallow northeast dips of strata. A case point is the Witkoppies (Domain 1E) and Samoep se Berg (Domain 3B) structures having steeply inclined axial planes (Appendix 3.2). Other complications are also seen, especially with the D2 fold structures located on the northwestern limb of the major D4 structure, that have fold axes, axial planes and foliation planes that have been rotated toward the east-southeast and southeast (Appendix 3.2). The S-Berg structure (Domain 3D) is a good example, with a fold axes plunging moderately in an east-southeasterly direction, with an axial plane dipping moderately in a southeasterly direction (Appendix 3.2). The L1 stretching lineation's have also been rotated toward the southeast and east-south-east and have a co-linear relationship with rotated F2 fold axes (Appendix 3.2; Domain 3D). The rotated axial planes also have a co-planar relationship with regard to the rotated regional foliation planes. The mesoscopic model 1 and model 2 folds also have fold axes which trend toward the north-east and east-north-east where it was not rotated and also have a co-linear relationship with regard to the L1 regional stretching lineation (Appendix 3.2). Good examples can be seen within the Gannapoort Berg, Samoep se Berg and Dwarsberg structures, where no rotational effects are seen with regard to the mesoscopic model 1 and 2 folds (Appendix 3.4.2, Domain 3A, 3B and 4C). There are, however examples of mesoscopic model 1 and 2 folds that have been rotated toward the southeast and east-southeast. This can be seen within the Witkoppies, S-Berg and T-Goob se Berg structures (Appendix 3.4.2; Domain 1E, 3D and 3I). The rotation of the regional L1 llineations can also be viewed in Appendix 3.1 A.

The D2 fold structures are all observed to be synformal fold structures, with most of the upright limbs being represented by the southern limbs and overturned limbs representing the northern limbs (Appendix 3.4.2). The defined polarity for most of the D2 fold structures show 'younging' toward the inside fold hinges of most of the structures, with confirmed 'younging' directions in four structures (Appendix 3.4.2; Domain 3B, 3C; 3G, 3I), showing younging toward the cores of the D2 structures confirming the stratigraphic polarity. The fold facing of various structures, show fold facing directed towards the northeast and southwest respectively (Appendix 3.4.2;

Domains 3B; 3D and 3G), with certain structures which show facing toward the northwest (Appendix 3.4.2; Domain 3I).

D3 Phase of Deformation

The D3 phase of deformation is exemplified by the refolding of earlier F2 fold structures by F3 isoclinal folding, forming Ramsay type 2, type 3 interference folds (Ramsay, 1967) or refolded sheath fold structures (Ghosh and Segupta, 1999) (Appendix 3.4.3). The D3 fold structures fold an S0//S1//S2 foliation and define a locally developed S3 foliation, not seen everywhere. The S3 foliation also has a co-planar relationship with regard to the S0//S1//S2 foliations. The D3 fold structures refold foliations associated with both the intrusive units and supracrustal successions in the D2 fold structures. Within the study area the S3 foliation is most visible within the Skewe Berg fold structure (Appendix 3.4.3; Domain 3K; Zone B3), Dwarsberg fold structure (Appendix 3.4.3; Domain 4C; Zone C4) and Klein Pofadder structure (Appendix 3.4; Domain 3F; Zone D2). Another good example can be seen within the Upper Poort se Berg fold structure (Appendix 3.4.3; Domain 3G; Zone B3) where the F3 traces can be seen folding dramatically (Figure 3.10). The F3 fold axes trend toward the northeast and east-northeast, and have a colinear relationship to the F2 fold axes and regional L1 mineral stretching lineations (Appendix 3.2). The D3 hinges of the Witkoppies (Domain 1E), Gannapoort Berg (Domain 3A) and Dwarsberg (Domain 4c) structures are good examples, as their fold axes plunge moderately in a northeasterly and east-northeasterly direction. The F3 axial planes of the Witkoppies (Domain 1E), Gannapoort Berg (Domain 3A) and Dwarsberg (Domain 4C) fold structures dip toward the north, north-east and north-north-east and are co-planar relationship to the regional S2 regional foliation (Appendix 3.2). The D3 structures are also rotated on the northern limb of the major D4 structure, which rotates F3 fold axes, F3 axial planes together with D2 structures and L1 stretching lineations. The D3 hinges of the S-Berg (Domain 3D) and T-Goob structures (Domain 3I) are good examples; with the F3 fold axes plunging moderately and trending toward the east-southeast, and F3 axial planes inclined moderately toward the south-east (Appendix 3.2). Where rotated; the F3 fold axes are colinear to the rotated L1 stretching lineations and F3 axial planes are coplanar to the regionally rotated S2 fabric (Appendix 3.2; Domain 3D and 3I).

F2 Fold Trace
F3 Fold Trace
Synform
Antiform

Figure 3.10: The intense folding of D3 folds, seen within the Upper Poort se Berg fold structure (Appendix 3.4.3; Domain 3G; Zone B3). The photo is taken looking toward the east.

The D4 Phase of Deformation

The D4 phase of deformation resulted in the formation of F4 post accretionary open folds, and associated with wrench shearing (Colliston and Schoch, 2013). Essentially, the entire study area can be defined as a macroscopic D4 synformal structure, which folds Structural Domains 2, 3 and 4, forming a kilometre scale Z fold structure (Appendix 3.4.4). The D4 phase also folds earlier D2 and D3 sheath fold structures, often located on the northwestern and southeastern limbs of the major D4 structure as seen in section (Appendix 3.4.4). The best location to see the F4 fold hinges is on the Lekdam intra-terrane thrust contact found between Structural Domain 4 and Structural Domain 3, as well as on the Samoep Thrust contact between Structural Domain 2 and Structural Domain 1 (Appendix 3.4.4). The far eastern antiformal fold closure (Appendix 3.4.4; Domain 2; Zone D2) and far western synformal closure (Appendix 3.4.4; Domain 3J; Zone A3) are good examples of the F4 folds seen regionally. Other good examples are also seen more toward the southeast, on the lower limb of the Outer Lekdam sheath fold (F2 sheath fold structure) that has also been folded by the F4 folds (Appendix 3.4.4; Domain 3J; Zone 3E), forming a characteristic Z asymmetry (Colliston and Schoch, 2013). This is also well exemplified in Appendix 3.9, where the F2 trace of the Outer Lekdam sheath fold is folded by the F4 folds. The F4 fold axes regionally are moderately plunging (20˚- 40˚) and trend toward the northeast and east-northeast, and have a co-linear relationship to the F2, F3 fold axes and L1 stretching lineation (Appendix 3.7).This co-linear relationship can be noted within the T-Goob se Berg fold structure (Domain 3I) and Outer Lekdam structure (Domain 3J).

The axial plane orientations vary, with the F4 T-Goob hinges having steeply inclined axial planes dipping toward the north-west (Appendix 3.2,Domain 3I), while the F4 Outer Lekdam axial planes dip moderately toward the north (Appendix 3.2; Domain 3J). However, there are zones within the same D4 structures where S and L tectonites rotate together with fold axes and axial planes of fold structures, rotate around the D4 hinges and are interpreted to be rotated by the reactivated movements of D5 shear zone phase. The zones where F4 fold axes are rotated together with the L1 lineations have a mean trend toward the east and east-southeast with moderate to shallow trending plunges, and also have a co-linear relationship to the F2, and F3 fold axes that have also been rotated by the D5 phase around the D4 hinges (Appendix 3.2; Domains 3I and 3J). The F4 axial planes are parallel to the S2 regional foliation and S2 is also rotated by the D5 phase, then so will the S4 also be rotated (Appendix 3.2; Domains 3I and 3J).

D5 Phase of Deformation

East-west trending sub-vertical shears are superimposed on earlier D1-D4 structures, and represents the D5 phase of deformation regionally. The D5 shears are also superimposed on north dipping and south-dipping layering and are co-planar to the regional S2 foliation. Throughout the study area a dominant sinistral sense of shear was observed, with a vertical north up-south down and south down-north up vertical sense of shear identified throughout the study area (Appendix 3.4.5). The easterly trending shears develop on zones of weakness and are preferentially located on the flanks of major D2, D3 and D4 structures, as well as on intra- and inter-terrane thrust contacts (Appendix 3.4.5; Zone D3 and E4). The easterly trending shears result in the rotation of foliation planes toward the sub-vertical, also result in the tightening of D2, D3 and D4 hinges. This is evident especially on the southern flank of the major D4 structure (Appendix 3.4.5; Zone D3 and E3). Boudinage structures seen in the hinge zones and flanks of D2 and D3 structures are also evident throughout the study area. In section, parallel to the regional foliation, this is also evident as D3, D2 and D4 structures are dramatically flattened and sheared (Appendix 3.3.2)

The most prominent effects of the east-west shears are seen on both the northern and southern flanks of the D4 structure (Appendix 3.4.5; Domain 3I, Zone C3). The intense shearing of the Gannapoort Berg structure on the Witkoppies Thrust contact is also a good example of the easterly trending shear effects, as the hinge zone is flattened and tightly attenuated (Appendix 3.4.5, Domain 3A; Zone C3 and D3). Another effect seen due to easterly trending shears is the formation of F5 oblique open folds (Appendix 3.4.5), which partially buckle D2 and D3 structures. These F5 open folds can be seen in the Samoep se Berg structure (Domain 3B), S-Berg structure (Domain 3D) and the Dwarsberg structure (Domain 4C).

D6 Phase of Deformation

The D6 phase of deformation is defined by the NW-SE trending shears associated with the Tantalite Valley deformation effects (Colliston, 1990). The D6 effects can clearly be seen in the far eastern extremities of the study area, parallel to the Groothoek Thrust contact (Appendix 3.4.5; Domain 5; Zones; D2, E2 and F3), and in the far eastern portion of the Houmoed structure (Appendix 3.4.5; Domain 1D; Zone F3). An oblique shear is associated with the D6 Tantalite Valley Shear deformation, a vertical component with a south down-north up, and a horizontal component of dextral movement is associated with the D6 phase. Similar results were obtained by Colliston (1990) in the Pofadder Terrane. Centimetre to metre scale mylonite bands are observed, with undeformed lithological units forming laterally continuous entities, together with associated mylonite bands. The intense flattening and shearing of

structures due to the D6 phase of deformation can also clearly be seen in section (Appendix 3.3.2) on the far eastern sector of the study area, on the southern limb of the major D4 structure, where the D2 and D3 structures and their fold traces are flattened and drawn parallel to one another.

3.5 The Structural Analysis of Selected Structures

The details associated with two prominent structures, namely; The Witkoppies 'Eye' and Gannapoort Berg 'Eye' Structures will be discussed in detail in Chapters 3.5.1 and 3.5.2. The structural details are provided in Appendix 3.5 and 3.6. The geometric properties, macroscopic and mesoscopic details will be discussed regarding each structure. The Witkoppies Structure resembles a macroscopic F2 fold structure with double vergence geometries, while the Gannapoort Berg structure is defined by two F2 isoclinal fold structures refolded by F3 folds. Both structures have attributes similar to the surrounding structures seen throughout the study area.

3.5.1 The Witkoppies 'Eye' Structure (Domain 1E)

The Witkoppies 'Eye' Structure is associated with the Witkoppies Sequence, which forms a macroscopic 'eye' fold structure with elliptical rings in the central core of the structure (Appendix 3.5 A; Figure 3.11). The structure can be divided into a western sector and eastern sector (Appendix 3.5), with the eastern sector representing a zone of higher strain, as all the fold traces are drawn parallel to one another. The elliptical 'eye' fold is associated with the core of the far western fold closure and has an upright synformal character. In the central portion of the structure on the northern limb, a set of double vergence fold structures are found displaying both S and Z asymmetries forming an omega structure. The southern limb refolds an inter-sheeted unit (Houmoed Structure: Domain 1 D), together with the Witkoppies Sequence and Vaalputs Suite (Appendix 3.5 A; Figure 3.11), forming a macroscopic S structure, which extends further toward the east outside the study area, and extends parallel to the Groothoek Inter-Terrane Thrust. The Witkoppies Sequence is defined by a thick sequence of biotite gneiss with intercalated variations of calc-silicate rock and actinolite, with the defined polarity showing toward the inside of the structure (Appendix 3.5).

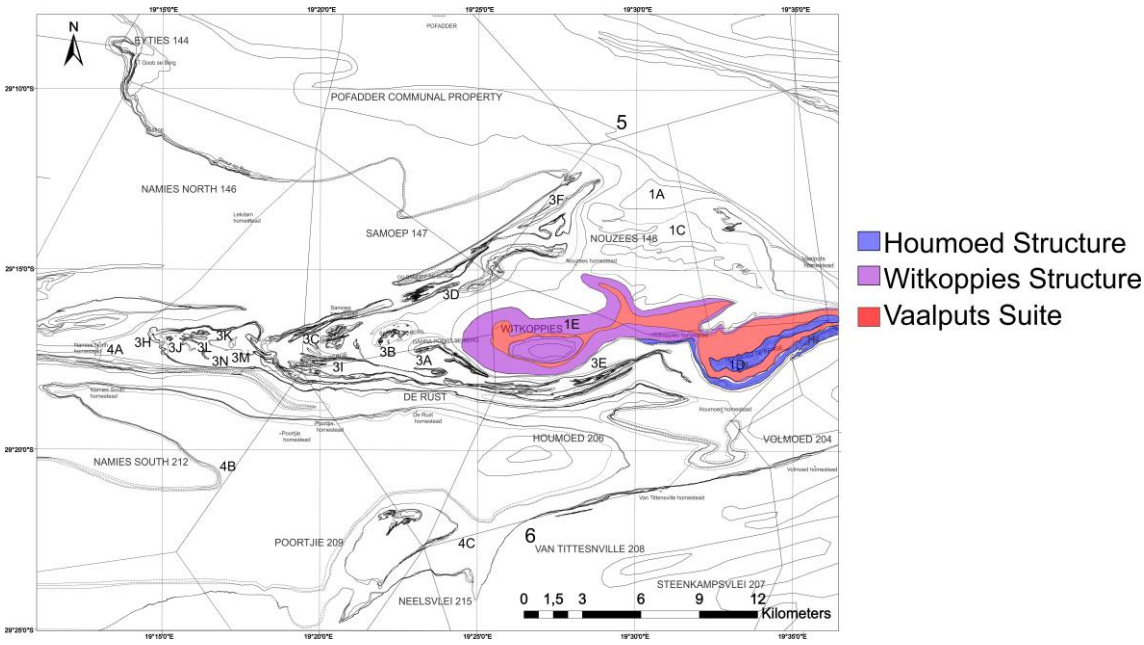

Figure 3.11: Location of the Witkoppies 'Eye' Structure (purple) and the Houmoed Structure (blue) found on the lower limb of the macroscopic 'Eye' structure, described in the text. The Vaalputs Suite (pink) is also infolded within both structures.

The major F2 fold trace lies within the YZ plane of the structure and folds an S0//S1 foliation in the far western hinge that has a poorly defined S2 axial planar foliation (Appendix 3.5; fold hinge A). The Witkoppies Structure is defined as a macroscopic F2 fold and a central elliptical 'eye' fold, with double vergence geometries (Appendix 3.5). The F2 axial trace extends for a distance of 24 kilometres within the study area and extends further eastwards outside the study area. A prominent branch point can be seen on the central portion of the southern limb representing the start of the inter-sheeted unit defined by the Houmoed Structure (Appendix 3.5). The F2 Houmoed Structure is bound by the Witkoppies and Samoep Thrusts; it's an F2 axial trace that extends eastwards. The Houmoed F2 fold is refolded by another phase of folding (F3), folds the F2 fold trace (Appendix 3.5; fold hinge C). The F3 fold trace also extends toward the east of the study area and is subparallel to the F2 fold trace. Later F4 open folds also form on the lower limb of the Witkoppies Structure and represent the antiformal component of the large synformal D4 structure which folds around the Witkoppies 'Eye' Structure. The D5 phase of deformation is defined by macroscopic east-west shears, found on the limbs of the macroscopic 'eye' fold, as well as on the intra-terrane thrust contacts (Witkoppies and Samoep Thrust contacts) found on the southern limb of the Witkoppies Structure. The D6 NW-SE shearing also affects the far eastern sector, namely the Houmoed Structure and the Groothoek Thrust (Appendix 3.4).

Within the Witkoppies Structural Domain, the stretching lineations (L1) in the western sector (around the F2 fold hinge) have a mean trend and plunge in the direction of 073-24, with some lineations rotating toward the southeast (Figure 3.12 A), specifically on the northern limb of the structure. The regional lineations (L1) in the eastern sector of the Witkoppies 'Eye' Structure have a mean trend and plunge of 040-30 (Figure 3.12 B). The L1 lineation in the western sector, associated with the Vaalputs Suite also has a mean trend and plunge of 079-22 (Figure 3.12 C). Within the eastern sector the L1 lineation within the Vaalputs Suite has a mean trend and plunge of 061-21 (Figure 31.2D). In the far western part of the Witkoppies Structure, the foliations dip both toward the south and the north and define a prominent F2 fold closure (Appendix 3.10; fold hinge A), which has a fold axis that trends and plunges toward 081-30 (Figure 3.13 A). The axial plane has an upright orientation and dips steeply toward the northwest. The poles to the foliations within the Vaalputs Suite (S1 Fabric), has more or less the same geometry around the western F2 fold closure (Fig 3.13 B).

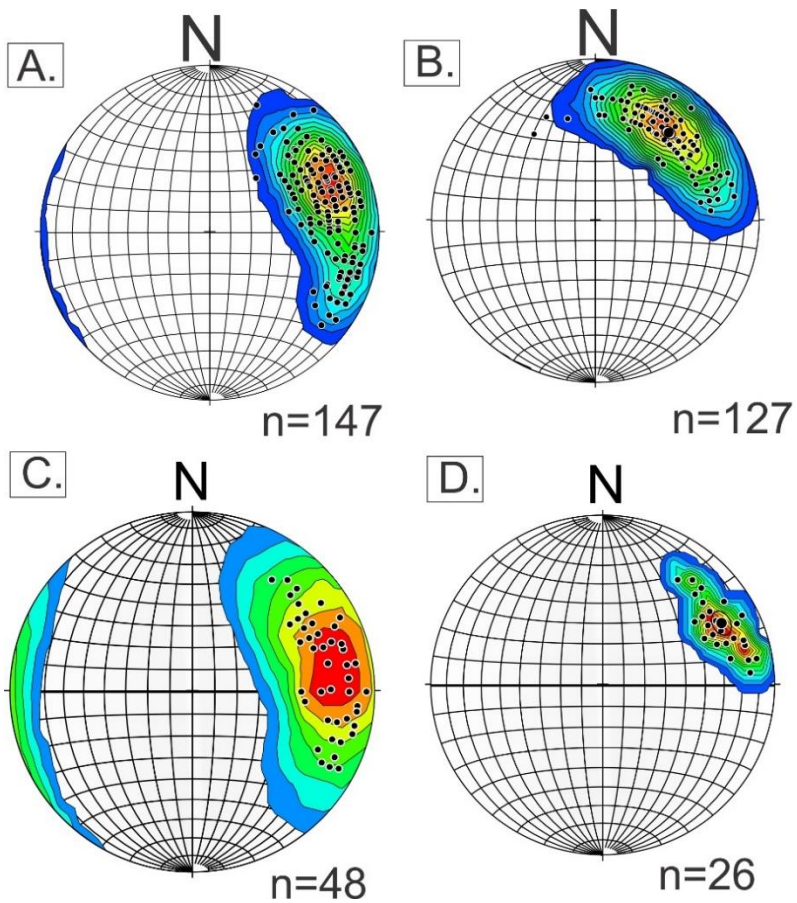

Figure 3.12: Stereonets depicting the regional L1 stretching lineations found throughout the Witkoppies 'Eye' Structure, both in the western and eastern sectors of the structure (Appendix 3.5). A: The regional L1 stretching lineations in the far western sector of the Witkoppies 'Eye' Structure, associated with a major F2 fold hinge. The stretching lineations have a mean trend and plunge of 073-24 (n=147). B: The regional (L 1) stretching lineation in the far eastern sector of the Witkoppies 'Eye' Structure and Houmoed Structure, which have a mean trend and plunge of 040-30 (n=127). Both sets of lineations include both the supracrustal sequences and intrusive rocks. C: L1 lineation seen within the Vaalputs Suite within the western sector, which has a mean trend and plunge of 079-22 (n=48). D: The L1 lineations associated with the Vaalputs Suite within the eastern sector have a mean trend and plunge of 061-21 (n=26).

The fold axes associated with western F2 fold closure and associated with the inner 'eye' structure (Appendix 3.5; fold hinge B) trend and plunge in the direction of 087-30 and has an upright axial plane that dips steeply toward the north (Figure 3.13 C). Toward the far east within the Houmoed Structure, the F3 fold closure (Appendix 3.5; fold hinge C) trends toward 052-52, with the axial plane having a sub-vertical dip toward the northeast (Figure 3.13 D). The regional stretching lineation is oblique to all 3 fold hinges (Figure 3.13 A, C and D). All three fold axes trend toward the north-east-north and east, and have sub-vertical to vertical axial planes dipping toward the north, north-west, and north-east (Figure 3.8 A, C, and D). All three folds can be defined as moderately plunging upright to steeply inclined fold structures according to the classification of Fleuty (1964).

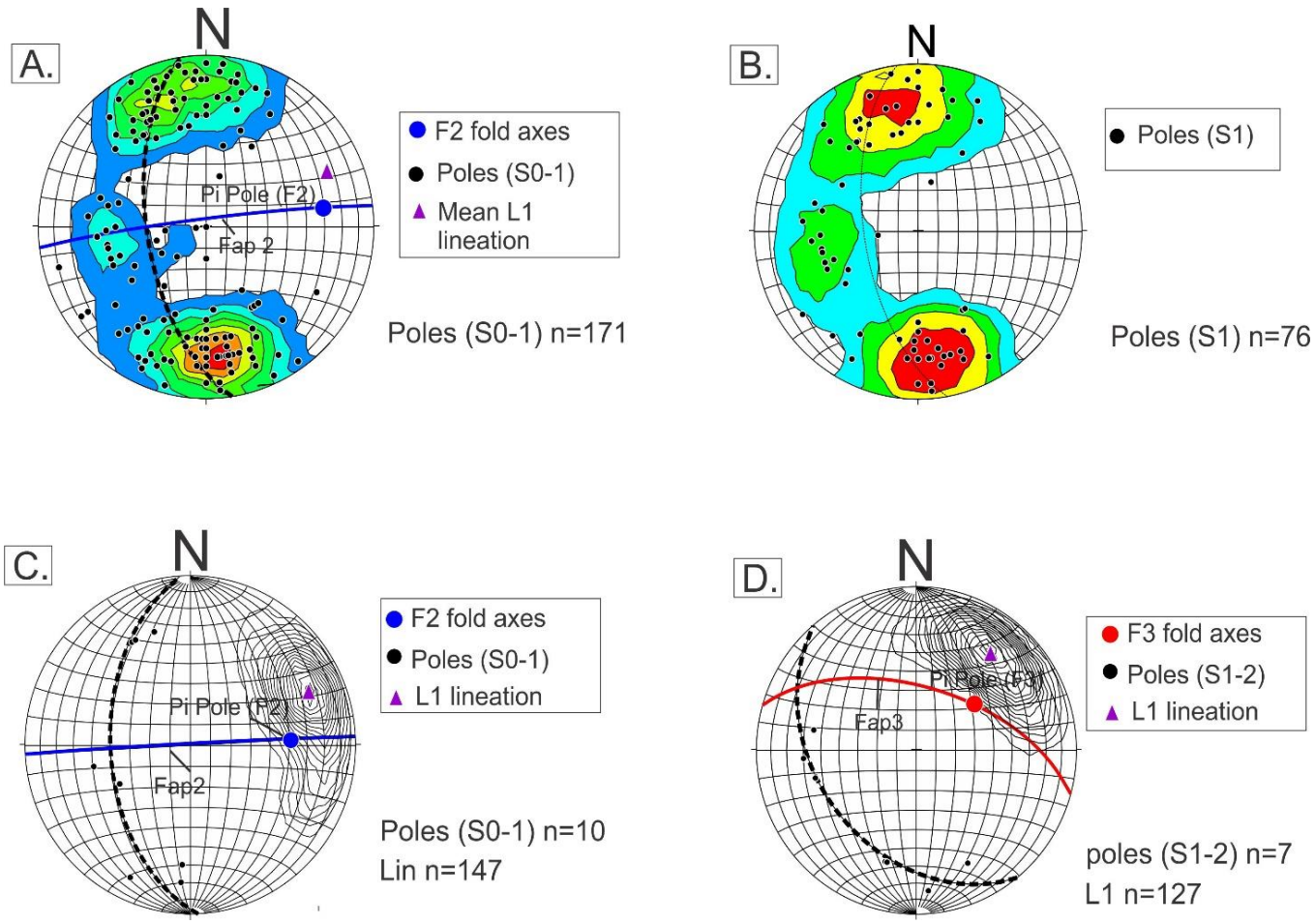

Figure 3.13: Fold geometry associated with prominent F2 and F3 fold structures found throughout the Witkoppies 'Eye" Structure (Appendix 3.5). A: Fold geometry associated with the far western closure. Pi pole represents the fold axis of the macroscopic F2 fold structure, which has a trend and plunge of 081-30, with the axial plane having a sub-vertical dip toward the northwest. The poles to the S0-1 foliation, define a mean pi-girdle; the L1 stretching lineation is also represented and lies oblique to the F2 fold hinge. B: Illustrates the poles to the S1 foliation associated with the Vaalputs Suite and has the same geometry as in Figure A. C: Fold geometry associated with the western fold closure of the inner 'eye' structure. The Pi pole represents the F2 fold axis which trends toward 087-39 in an easterly direction, with an axial plane having a sub-vertical attitude toward the north (poles n=10). The L1 lineation lies oblique to the F2 hinge. D: Fold geometry associated with the F3 fold closure found toward the east of the Witkoppies 'Eye' Structure. The Pi pole representing the F3 fold axis has a trend and plunge of 052-52. The axial plane has a sub-vertical dip toward the northeast (poles n=7).

Mesoscopic Structures

Within the F2 Witkoppies ‘Eye’ Structure mesoscopic F2 model 1 and model 2 folds are found together with mesoscopic elliptical sheath fold structures (Figure 3.14 A). Both the mesoscopic model 1, model 2, and mesoscopic sheath folds fold an S0//S1 foliation and define an S2 axial planar foliation and are associated with the D2 phase of deformation. The model 1 folds form both S and Z asymmetries and are parasitic to the larger macroscopic F2 and F3 fold closures (Appendix 3.5) and also define ‘omega’ S and Z structures with respect to the larger F2 fold closures. The mesoscopic model 1 folds also have fold axes that trend toward the east-northeast with axial planes (S2) sub-parallel to the co-planar S1 foliation (Figure 3.14 B). The mesoscopic model 2 folds at certain locations have curvilinear hinges and also form mesoscopic S and Z ‘omega’ structures (Figure 3.14 C). The model 2 axial planes (S2) are co-planar to the regional S1 foliation (Figure 3.14 C). Mesoscopic S-C cleavage is also found throughout the Witkoppies ‘Eye’ Structure, with a dominant sinistral sense of shear found throughout the structure (Figure 3.15 A). The intersection lineations (L1) of the S-C cleavages (S0-1 and S2) trends and plunges steeply toward the north (L1 intersection lineation) (Figure 3.15 A). Vertical shears also associated with reactivated movements on thrust contacts and on the limbs of the Witkoppies Structure related to the D5 phase (east-west shear zones) show a north up and south down sense of movement, with vertical shears showing sigmoidal rotations (Figure 3.15 B).

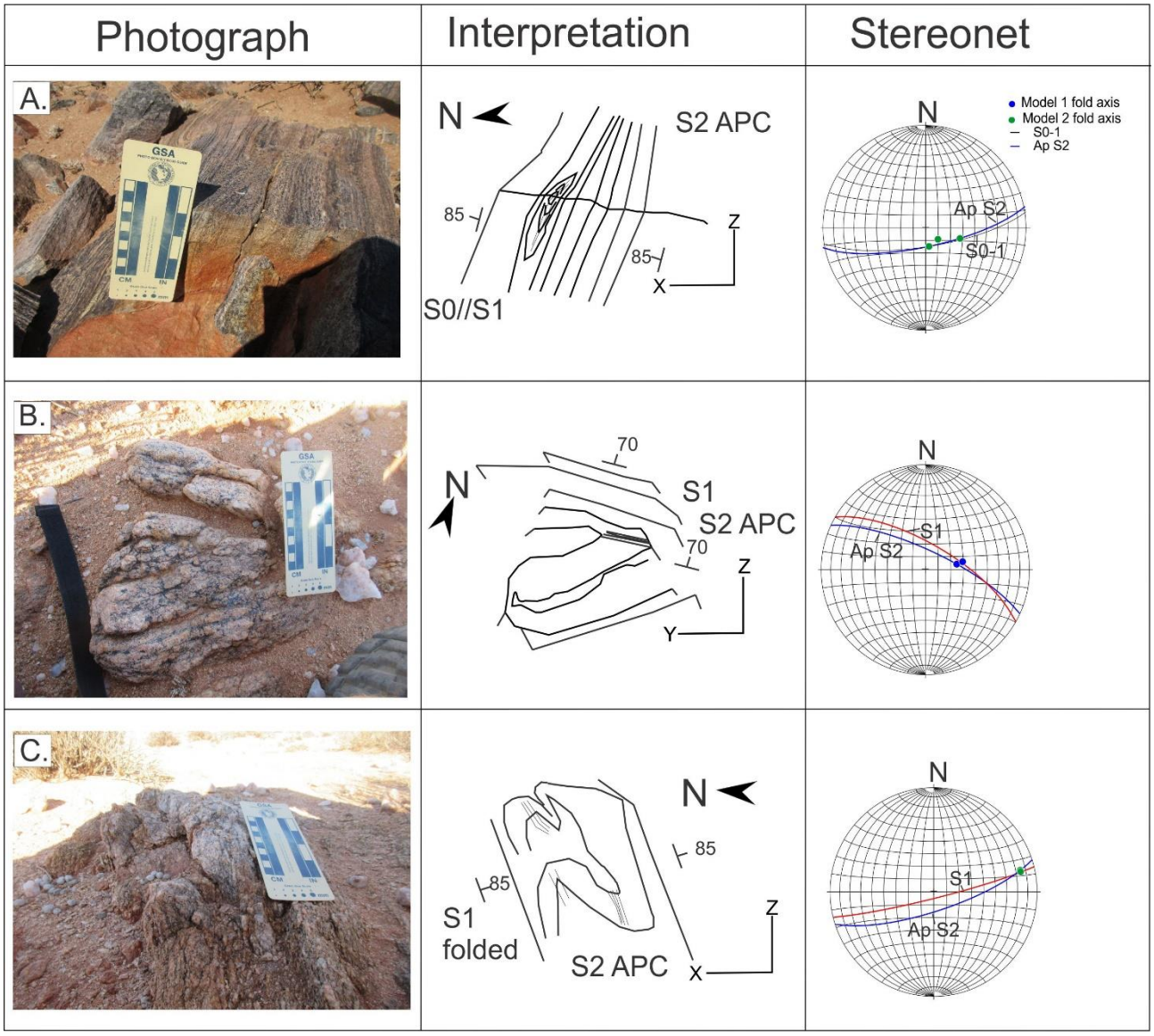

Figure 3.14: Mesoscopic structures of the Witkoppies 'Eye' Structure. A: F2 model 2 sheath fold within a banded amphibolite sequence, that folds an S0//S1 foliation and defines an S2 axial planar foliation within the XZ and YZ traces of the foliation plane; with fold axes trending and plunging toward the south and axial planes dipping sub-vertically toward the south. B: F2 model 1 Z fold within the Achab Suite found on the northern limb of the Witkoppies 'Eye' Structure, folding an S1 foliation and defining an S2 axial planar foliation within the YZ plane; fold axes plunging steeply eastward, with axial planes dipping sub-vertically toward the northeast. C: Model 2 Z fold within the Achab Suite found on the northern limb of the Witkoppies 'Eye' Structure which folds an S1 foliation and defines an S2 axial planar cleavage within the YZ plane of the foliation (S2). The fold plunges shallowly toward the northeast and the axial plane has a sub-vertical dip toward the southeast.

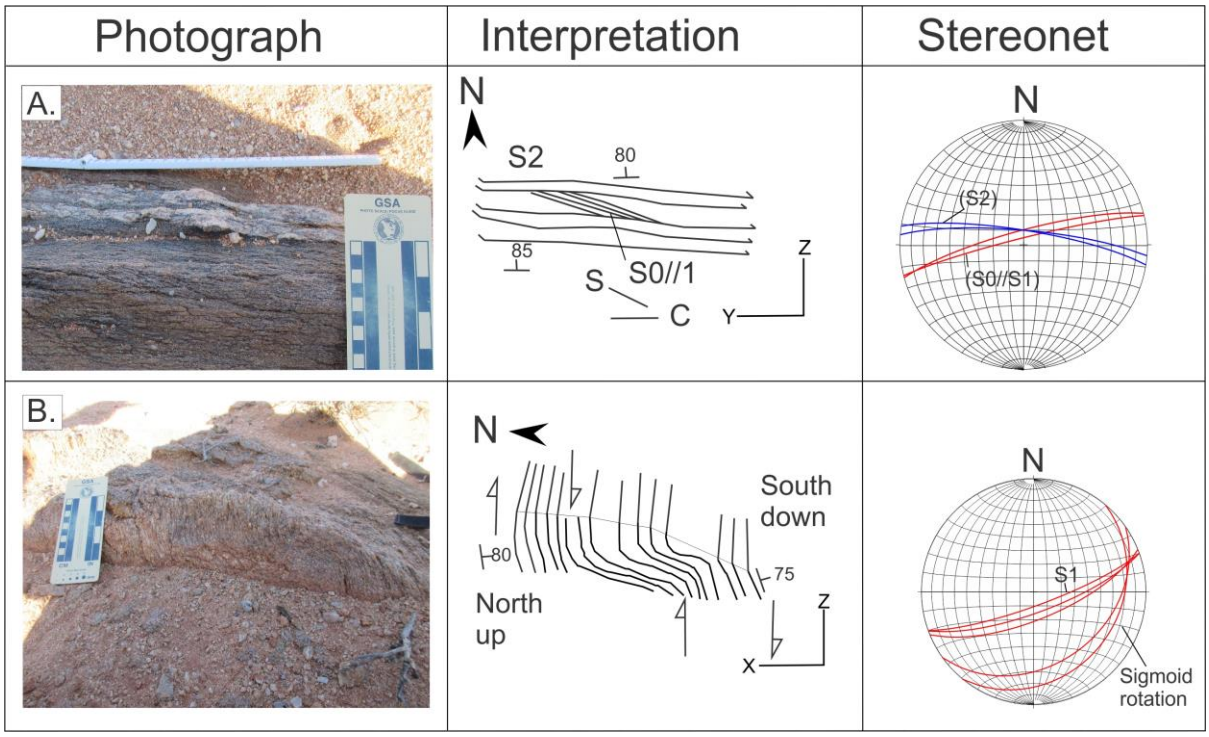

Figure 3.15: Mesoscopic structures of the Witkoppies 'Eye' Structure. A: Horizontal S-C cleavage in biotite gneiss which shows a sinistral sense of shear, with an S-C cleavage, with the S0//S1 foliation, rotated by the S2 regional foliation. The L1 intersection lineation plunges steeply toward toward the north. B: Vertical sigmoidal shear within the Achab Suite which illustrates a north-up and south-down sense of movement found on the northern limb of the Witkoppies 'Eye' Structure.

3.5.2 The Gannapoort Berg 'Eye" Structure (Domain 3A)

The Gannapoort Berg 'Eye' Structure is situated in the central part of the study area and is located within the Lekdam Structural Domain (Appendix 3.6 A.; Figure 3.16). The Gannapoort Berg contains two elliptical 'eye' fold structures refolded isoclinally (Appendix 3.6 B). The structure is well represented toward the west and is severely thinned out toward the east. The Lekdam Gneiss envelops the entire structure and branches out in the northwestern part of the structure and also forms a major Z fold with the Lekdam Gneiss folding within the two refolded isoclinal fold structures (Appendix 3.6 B). The Samoep Gneiss (representing Structural Domain 2) is folded between the two isoclinal fold structures toward the northeast of the structure (Appendix 3.6 B). The Gannapoort Berg structure is defined by the Gannapoort Berg Sequence, consisting of a thick succession of biotite gneiss, biotite sillimanite schist, poorly bedded quartzite overlain by biotite sillimanite schist interbanded with quartzite, dark-blue quartzite, and amphibolite. The defined polarity has a direction toward the inside of the structure as seen in Chapter 2.9.1.1.

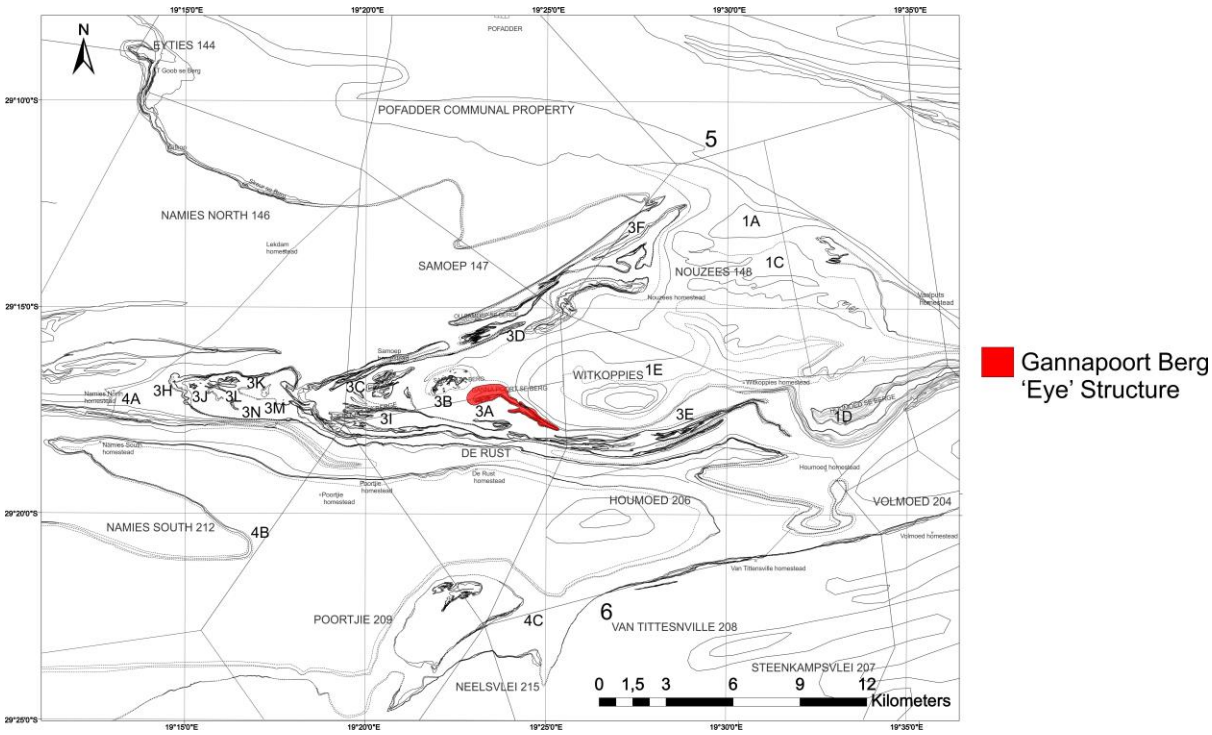

Figure 3.16: Location of the Gannapoort Berg 'Eye' Structure within the study area.

The Gannapoort Berg 'Eye' structure can be sub-divided into an upper synformal and lower synformal isoclinal fold structure. The lower isoclinal fold structure contains a prominent 'eye' structure in its core toward the far west of the structure. Both isoclinal fold structures fold bedding and co-planar S1 foliation on the limbs and define S2 penetrative axial planar foliations in both the far western hinges of the upper and lower isoclinal fold structures (Appendix 3.6, fold hinges A, B, and D). These structures are thus defined as F2 elliptical isoclinal fold structures. Both F2 fold traces are refolded by a later phase of folding, namely the F3 isoclinal fold phase, and refolds an S0//S1//S2 fabrics and defines a locally developed S3 foliation, which transposes all earlier structures (Appendix 3.6, fold hinge G). Later D4 and D5 effects are noticeable, especially in the central sector of both isoclinal fold structures. The entire structure buckles due to the later D4 and D5 effects (Appendix 3.6, fold hinges F, H, and I). An F4 fold is seen 'bending' the lower F2 isoclinal fold structure toward the west (Appendix 3.6, fold hinge I), while toward the east it is also buckled on the lower limb. However, the buckle toward the east is not an F4 fold, but rather an F5 (Appendix 3.6, fold hinge H), due to the later sinistral shear effects transposed over the structure. The upper F2 isoclinal fold hinge is also tightly folded by an F5 fold (Appendix 3.6, fold hinge F) due to east-west shearing effects on the structure. The Samoep Gneiss is also folded due to later D5 east-west shearing (Appendix 3.6 B), and shears out along strike, together with other stratigraphic units due to flexural slip. The D5 effects are also seen on the limbs of the F2 and F3 structures, especially toward the east of the structure; this results in the thinning of limbs, tightening of fold hinges, and the development of boudinage structures on macroscopic scale. The L1 stretching

lineations have a mean trend and plunge of 053-31 (Figure 3.17 A). The regional foliation has a mean dip and dip direction of 013-58 (Figure 3.17 B). The L1 lineations within the intrusives surrounding the Gannapoort Berg Structure have a mean trend and plunge of 052-35 (Figure 3.17 C). The regional foliations within the intrusives surrounding the Gannapoort Berg Structure have a mean dip and dip direction of 022-56 (Figure 3.17 D). The geometrical analysis of foliations and lineations within the supracrustal and intrusive rocks are co-linear and co-planar respectively.

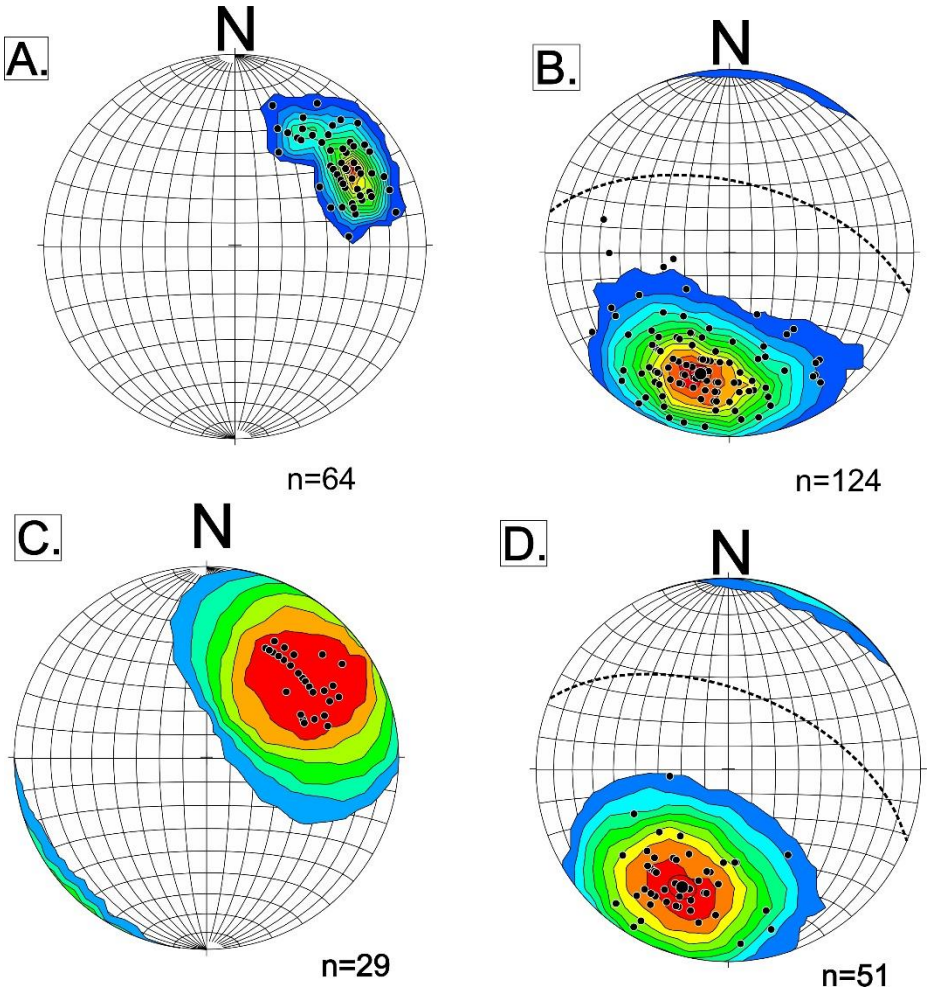

Figure 3.17: The regional lineation (L1) and foliation (S2) associated with the Gannapoort Berg 'Eye' Structure. A: The regional lineation (L1) has a mean trend and plunge of 053-31 (n=64).The lineations are associated with both the Lekdam Gneiss, Samoep Gneiss, and supracrustal rocks associated with the Gannapoort Berg Structure. B: The regional foliation (S2) has a mean dip direction and dip of 013-58 (n=124). The foliations are associated with both the Lekdam Gneiss, Samoep Gneiss, and supracrustal succession. C: The regional L1 lineation within the intrusives surrounding the Gannapoort Berg Structure. The lineations have a mean trend and plunge of 052-35 (n=29). D: Foliations associated with the intrusive rocks surrounding the Gannapoort Berg Structure. The regional S2 foliation has a mean dip direction and dip of 022-56 (n=51).

The fold axes associated with various phases of deformation (D2-D5) all have co-linear fold axes that trend toward the northeast and east-northeast and are also co-linear to the regional stretching lineation (L1). There are, however, two F4 and F5 open folds that differ in their fold geometry due to them being 'open' folds and have not been folded isoclinally. The far western

and southeastern F2 fold axes and fold axes associated with the ‘eye’ of the lower isoclinal fold structure, have trends and plunges of 067-30, 070-39, and 067-39 (Appendix 3.6, fold hinges A, B, and C), with axial planes having sub-vertical dips toward north and north-east (Figure 3.18 A, B, and C). The western and southeastern F2 fold closures associated with the upper isoclinal fold structure (Appendix 3.6; fold hinges D and E) have fold axes that trend and plunge in a direction of 078-38 and 047-30. The axial planes have sub-vertical dips toward the north-north-east (Figure 3.18 C and D). All five F2 fold structures have co-linear and co-planar relationships with their fold axes and axial planes respectively. The F5 fold identified within the western fold closure (Appendix 3.6; fold hinge F) has fold axes which trend and plunge in the direction of 081-45, with an axial plane having a sub-vertical dip toward the north-north-east (Figure 3.18 F). The F5 fold axial plane and fold axis are coplanar and colinear to the F2 geometry.

The main F3 fold hinge toward the far east (Appendix 3.6; fold hinge G) has a trend and plunge of 079-45, with an axial plane having a sub-vertical dip toward the northeast (Figure 3.19 A). The F3 fold axial plane and fold axis have a co-linear and co-planar relationship to the main F2 fold closures. The F5 open fold identified on the lower limb of the lower isoclinal fold structure (Appendix 3.6; fold hinge H) has a fold axes which trends and plunges in the direction of 321-57 with an axial plane having a sub-vertical dip toward the west-southwest (Figure 3.19 B). The main F4 open fold identified lower isoclinal fold structure (Appendix 3.6; fold hinge H) trends and plunges in the direction of 037-49 in a northeasterly direction with an axial plane dipping sub-vertically toward the northwest (Figure 3.19 C).

Most of the F2 and F3 fold structures have moderately plunging fold axes and moderately inclined axial planes, while the F4 open fold and F5 oblique open fold have steeply inclined axial planes and moderately plunging fold axes (Fleuty, 1964). The F5 fold on the upper isoclinal fold, which is rotated and tightened in an isoclinal fashion, also has moderately plunging fold axis and a moderately inclined axial plane. The axial planes and fold axes of the F2, F3 and F5 folds are co-planar and co-linear respectively. Their fold axes are also collinear to the regional stretching lineation (L1).

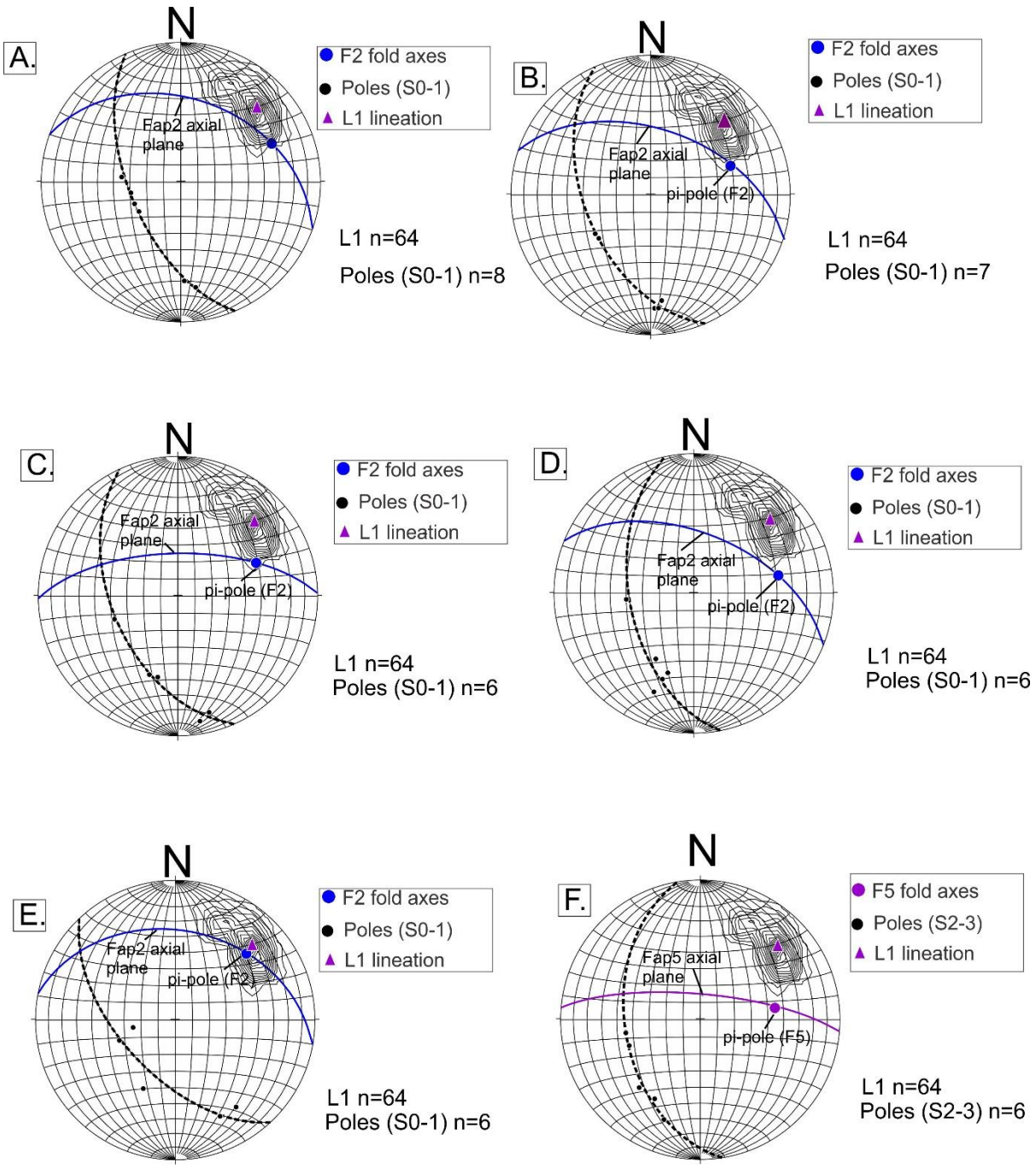

Figure 3.18: Stereonets depicting the fold geometry associated with the Gannapoort Berg 'Eye' Structure. A: Far western F2 fold closure associated with the lower isoclinal fold (Appendix 3.6, fold hinge A). The fold axis has a mean trend and plunge of 067-30 (poles n=8), with the axial plane dipping moderately in a northeasterly direction. The L1 lineation lies oblique to the F2 fold hinge. B: Fold hinge of the 'eye' structure in the far western F2 fold closure (Appendix 3.6; fold hinge B). The fold axis has a mean trend and plunge of 070-39 in an east-north-easterly direction (poles n=7), with the axial plane dipping moderately toward the north-northeast. C: Far eastern fold closure associated with the lower isoclinal fold (Appendix 3.6; fold hinge C). The fold axis has a mean trend and plunge of 067-39 (poles n=6), with the axial plane having a sub-vertical dip toward the north. D: Far western closure associated with the upper F2 isoclinal fold (Appendix 3.6; fold hinge D). The fold axis trends and plunges toward 078-38 (poles n=6), with the axial plane having a sub-vertical dip toward the north-northeast. E: Lower south eastern F2 fold closure associated with the upper isoclinal fold (Appendix 3.6; fold hinge E). The fold axis has a mean trend and plunge of 047-30 (poles n=6), with the axial plane having a sub-vertical dip toward the north-northeast.F: F5 fold closure associated with the western fold closure of the upper isoclinal fold structure (Appendix 3.6; fold hinge F). The fold axis) has a mean trend and plunge of 081-45 (poles n=6), with the axial plane having a sub-vertical dip toward the north-northeast.

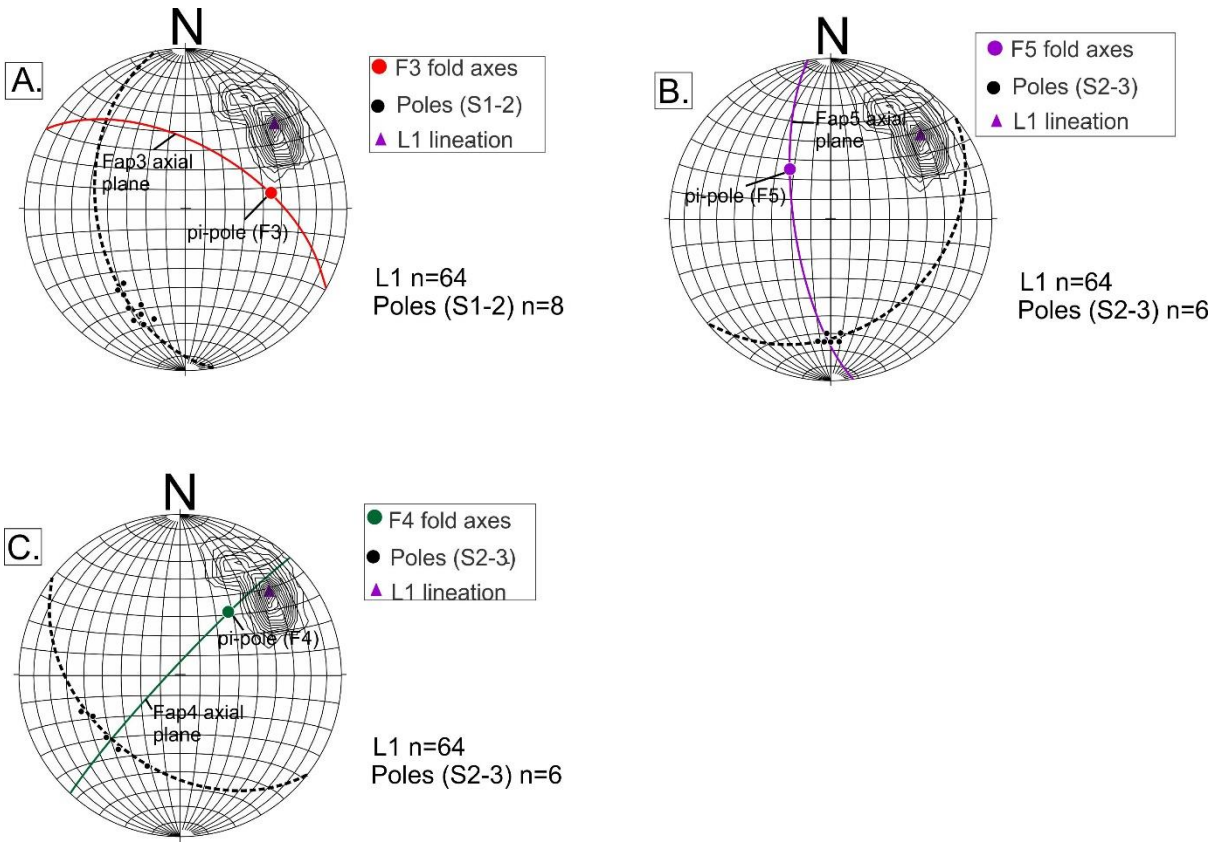

Figure 3.19: Stereonets depicting the fold geometry associated with the Gannapoort Berg 'Eye' Structure. A: The fold geometry associated with the far eastern F3 fold closure (Appendix 3.6, fold hinge G). The fold axis has trend and plunge in the direction of 079-45 (poles: n=10), with an axial plane having a sub-vertical dip toward the northeast. The regional L1 lineation has an oblique relationship to the axial plane of the structure. B: F5 oblique fold associated with the Gannapoort Berg Structure (Appendix 3.6; fold hinge H). The fold axis trends and plunges in the direction of 321-57 (poles: n=6), and has an axial plane that has a sub-vertical dip west-south-westerly direction. C: The fold geometry of the F4 open fold located on the lower isoclinal fold structure toward the northwest (Appendix 3.6, fold hinge I). The fold axis has a trend and plunge in the direction of 037-49 (poles n=6). The axial plane has a sub-vertical dip in a north-westerly direction, with the regional L1 lineation having an oblique relationship to the axial plane.

Mesoscopic Structures

Within the Gannapoort Berg "Eye' Structure both model 1 and model 2 recumbent isoclinal fold structures are found. The model 1 and 2 folds are related to the D2 phase of deformation and have both 'S' and 'Z' asymmetries. Both the model 1 and 2 folds fold S0//S1 foliation and define S2 axial planar foliations (Figure 3.13 A, B, and C). The model 2 folds identified form within the XZ foliation plane perpendicular to the YZ foliation plane containing the compositional layering (S0) and regional co-planar foliation (S1), and often verge toward the south, showing the direction of over thrusting (Figure 3.20 A). The model 1 folds are folded within compositional banding (S0) and regional co-planar foliation (S1) that is contained within the XY plane of the regional strain ellipse and have fold axes trending in an east-northeasterly and easterly direction (Figure 3. 20 B and C). The model 1 folds have 'S' and 'Z' folds which are parasitic to the macroscopic F2 isoclinal folds found on both the upper and lower isoclinal structures and vary between centimetre-scale and metre scale (Appendix 3.11 C). The model

1 folds also have opposite vergence asymmetries, most prominently seen in the far western lower isoclinal fold structure (Appendix 3.11 C). The model 1 and 2 folds have fold axes that are co-linear to the regional stretching lineations. Horizontal S-C cleavages are also identified throughout, showing a sinistral sense of movement; representing reactivated movements associated with D5 east-west shears. The S-C cleavage intersections (L1 intersection lineation) have a steep plunge steeply in an east-north-easterly direction (Figure 3.21 A). Mesoscopic vertical shears were commonly identified throughout the structure, showing a sigmoidal rotation of a mylonitic S0//S1 fabric, defining a north-down and south-up sense of shear associated with the D5 phase of deformation (Figure 3.21 B).

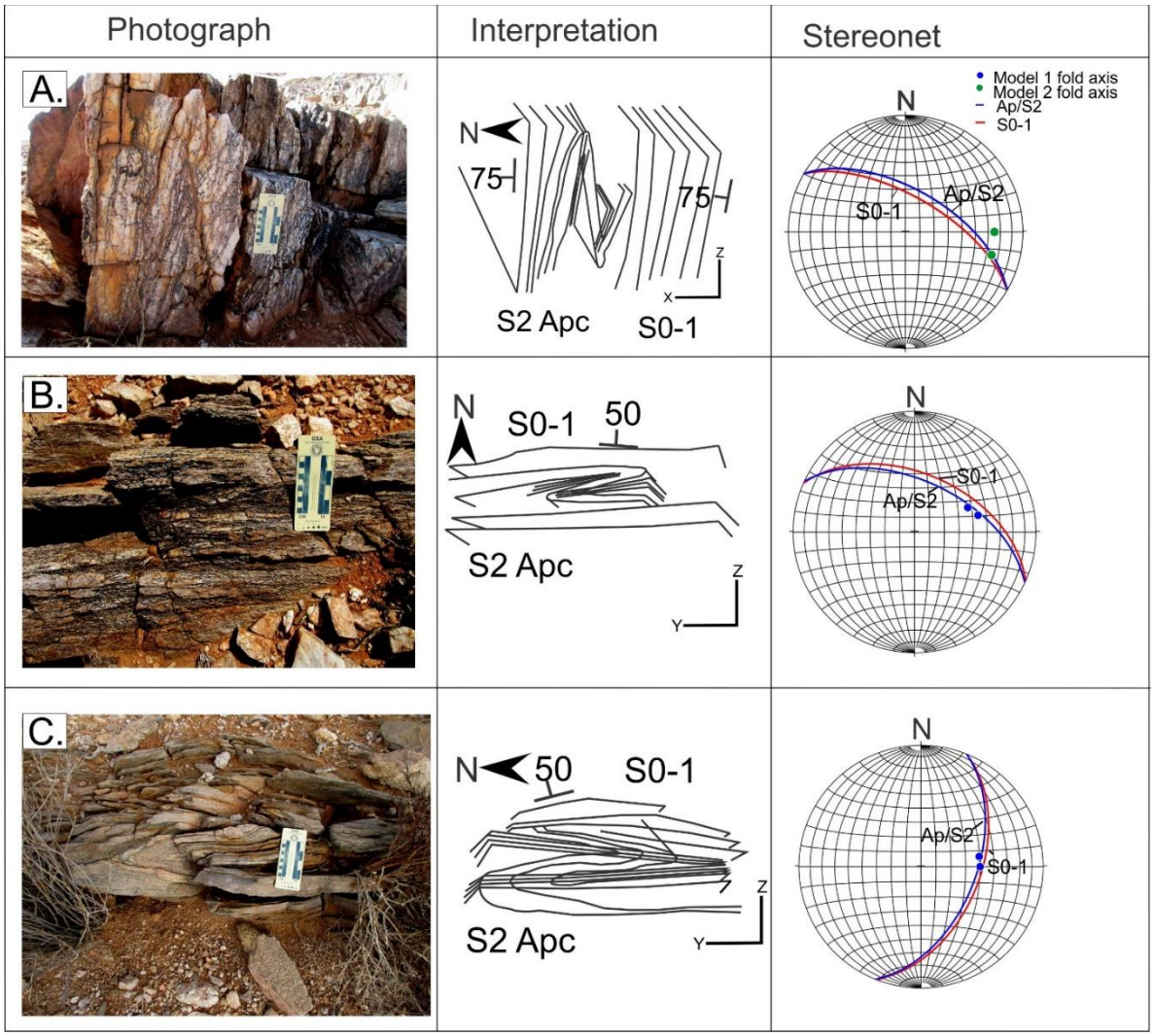

Figure 3.20: Mesoscopic structures associated with the Gannapoort Berg 'Eye' Structure. A: Model 2 Z fold within mylonitic quartzite, located on the northern limb of the lower isoclinal fold structure. Model 2 fold, folds an S0//S1 foliation and defines an S2 axial planar foliation; vergence is toward the southwest, coinciding with the movement associated with over thrusting. B: Model 1 Z fold within mylonitc quartzite, found on the northern limb of the lower isoclinal fold structure. Model 1 fold, folds an S0//S1 foliation and defines an S2 axial planar foliation. The fold axes trend in an east-north-easterly direction, with axial plane having a sub-vertical dip toward the northeast. C: Model 1 Z-fold within biotite gneiss, found on the northern limb of the lower isoclinal fold structure and folds an S0//S1 foliation and defines an S2 axial planar foliation. The fold axes trend toward the east, with the axial plane dipping toward the east-south-east in a sub-horizontal fashion (Apc = Axial planar cleavage; AP: Axial plane).

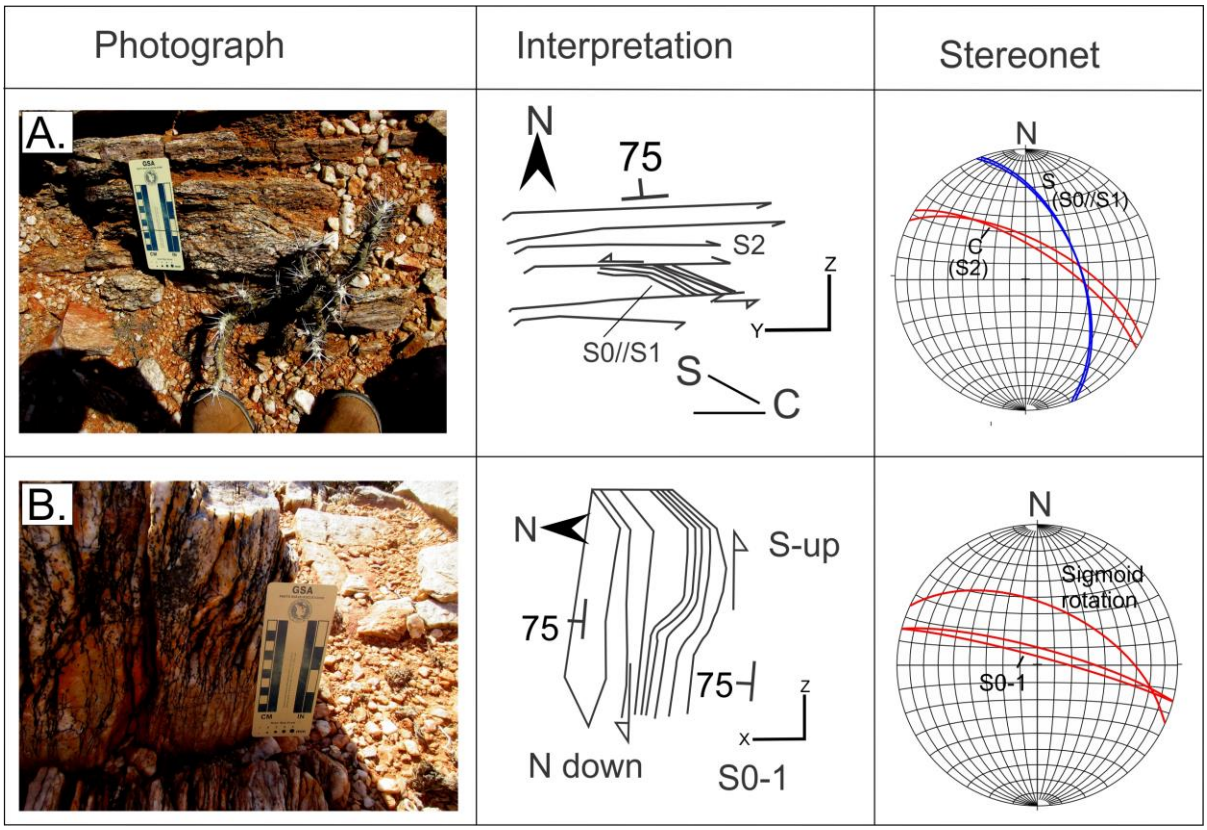

Figure 3.21: Mesoscopic structures associated with the Gannapoort Berg 'Eye' Structure. A: Mesoscopic S-C cleavage within mylonitic quartzite found on the southern limb of the upper isoclinal fold structure, having a sinistral sense of shear and rotating the S0-1 parallel to the regional S2 foliation, with S-C cleavage intersection lineation (L1) having a trend and plunge steeply toward the east-north-east. B: Vertical mesoscopic shear within mylonitic quartzite, showing a sigmoidal rotation with north-down and south-up sense of movement.

CHAPTER 4

Discussion

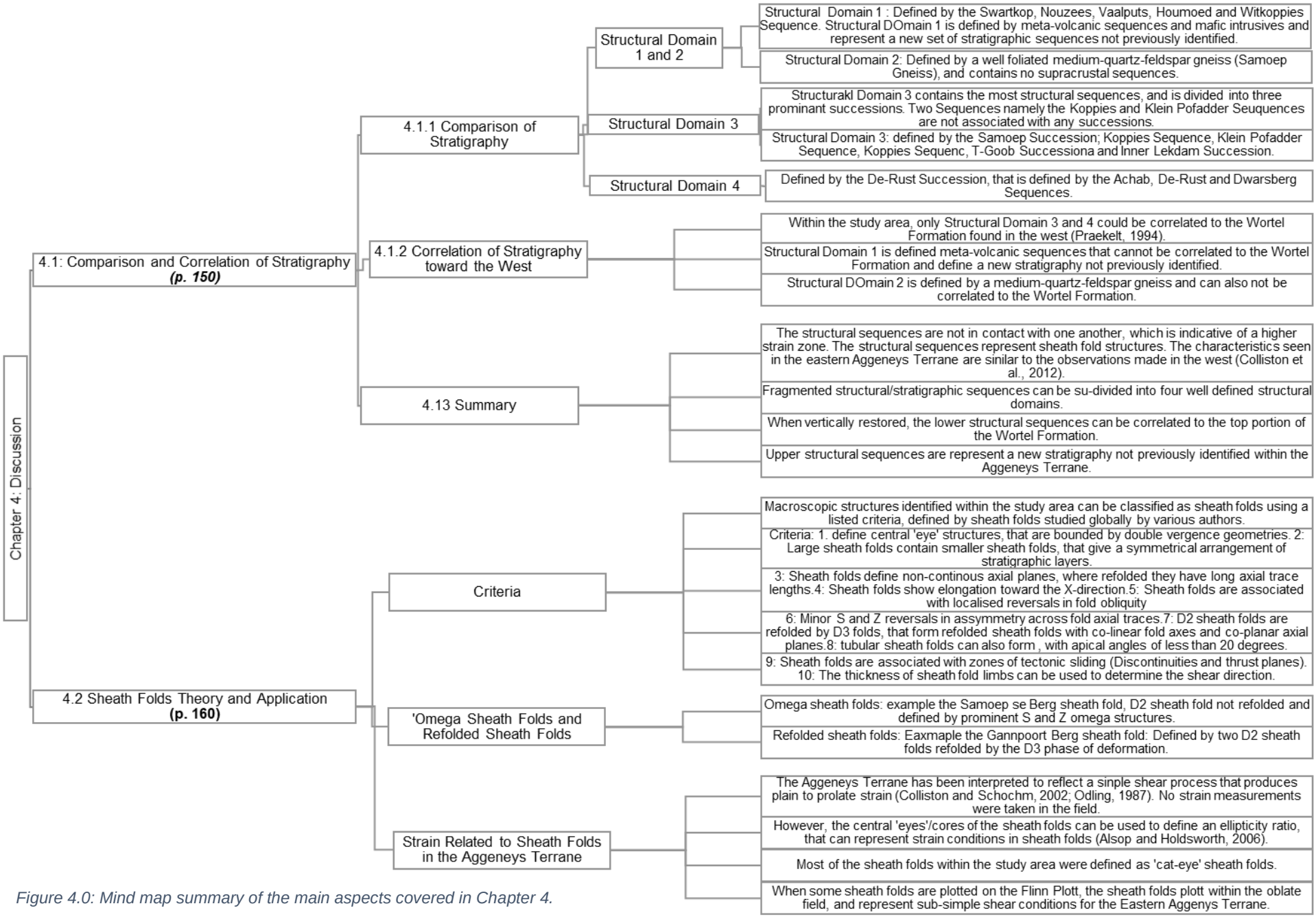

Figure 4.0: Mind map summary of the main aspects covered in Chapter 4.

4.1 Comparison and Correlation of Stratigraphy

4.1.1 Comparison of Stratigraphy

The eastern part of the Aggeneys Terrane is defined by a total of twenty-three tectonic sequences, which resembles fragmented stratigraphy in the form of isolated elliptical double verged fold structures, and refolded isoclinal fold structures (Figure 4.1), which are interpreted as sheath folds (Chapter 4.2). The different structural sequences are located within four well-defined structural domains (Figure 4.1 A), which represent kilometre scale intra-terrane thrust sheets. Structural Domain 1 (Witkoppies Structural Domain) contains five tectonic sequences (Figure 4.1 A: 1A-E), Structural Domain 2 contains none, as it is defined by a well foliated medium quartz-feldspar gneiss (Samoep Gneiss), Domain 3 (Lekdam Structural Domain), contains fourteen tectonic sequences (Figure 4.1 A: 3A-N) and the Structural Domain 4 (Houmoed Structural Domain) contains three tectonic sequences (Figure 4.1 A: 4A-C). The different sequences occur laterally across the study area and have been structurally stacked on top of one another during D1 thrusting phase of deformation (Figure 4.1 B). The different tectonic sequences and their various attributes have been summarised in Tables 4.1 and 4.2.

Structural Domain 1and 2

The Witkoppies Sequence is the only sequence within this domain that has been described in detail, as the other sequences such as the Swartkop, Nouzees, Vaalputs, and Houmoed Sequences lie outside the scope of this study. They, however, represent a new series of stratigraphic sequences not previously identified within the Aggeneys Terrane toward the west and are defined by meta-volcanic supracrustal sequences and mafic intrusive rocks. The Witkoppies Sequence is defined by thick successions of biotite gneiss, with interbands of amphibolite and large variations of calc-silicate rock. The Witkoppies Sequence differs from the sequences seen in Structural Domain 3 and 4 (Table 4.1). Structural Domain 2 is defined by a well foliated medium-quartz-feldspar Samoep Gneiss and contains no meta-sedimentary units. The Samoep Gneiss is intersheeted between Structural Domain 1, 3 and 4, and defines a sharp contact between all domains.

Structural Domain 3

Structural Domain 3 contains the most tectonic sequences within the study area and can be further subdivided into three prominent successions. Each succession is defined by a series of sequences that have major lithological similarities and can be correlated to one another. The Samoep, T-Goop and Inner Lekdam Successions (Table 4.1) have been defined in Structural Domain 3, but exclude the Koppies and Klein Pofadder Sequences, which do not correlate with any of the above mentioned successions. The Samoep Succession (Table 4.1)

is defined by thick sequences of biotite gneiss, with interbanded units of feldspathic quartzite, dark-blue quartzite, magnetite quartzite, amphibolite, calc-silicate rock and thick successions of poorly bedded quartzite. The Koppies and Klein Pofadder Sequences are not correlated to a succession, as they have no key lithological units which can be grouped to define a succession. The Koppies Sequence is defined by thick to thin sequences of biotite-sillimanite schist with interbanded units of garnet meta-quartzite (BIFs), poorly bedded dark-blue quartzites, and thick successions of nodular rhythmic sillimanite-quartz-feldspar gneiss. The Klein Pofadder Sequence is defined by thick to thin succession of biotite-sillimanite schist, dark-blue garnet-bearing quartzite, and poorly bedded quartzite. The T-Goob Succession is defined by nodular rhythmic sillimanite-quartz-feldspar gneiss, biotite-sillimanite schist, poorly bedded quartzite, and interbanded units of garnet meta-quartzite (BIFs), biotite gneiss, actinolite anddiopside units. The T-Goob Succession also contains a sillimanite ore body seen within the T-Goob structure at Annakoppies (Pretorius, 1986; Frik and Coetzee, 1974). Below the T-Goob Succession, the Inner Lekdam Succession is found which has similar characteristics with the difference being that the lithological units are not as thick as the T-Goob Succession and is dominated by the presence of garnet meta-quartzite rock.

The Inner Lekdam Succession is defined by thin to thick successions of poorly bedded quartzite, biotite sillimanite schist, interbanded units of feldspathic quartzite, diopside, actinolite, calc-silicate rock, and abundant units of garnet meta-quartzite (BIF). Within Structural Domain 3 the Samoep Succession is the only succession that contains large lithological units of biotite gneiss, but does not contain any large units of diopside and actinolite units, nor does the succession contain any garnet-bearing meta-quartzites (BIFs). The T-Goob Succession is synonymous with large units of feldspathic quartzite, actinolite and diopside units, which is not seen in any other successions and contains sillimanite ore bodies toward the west outside the study area (Pretorius, 1986). The Koppies Sequence is the only sequence that contains large successions of nodular rhythmic quartz-feldspar gneiss.

Structural Domain 4

Only three sequences are found within Structural Domain 4 and is grouped within the De Rust Succession. The succession is defined by poorly bedded quartzites, thick successions of biotite-sillimanite schist and interbanded units of calc-silicate rock, amphibolite, and garnet-bearing meta-quarztite (BIF). The medium-grained Namies Gneiss is seen within certain sequences across the succession and is coeval with the associated supracrustal rocks. Further toward the west sillimanite lenses have been identified within the De Rust succession (Wilner et al., 1990; Moore, 1977). The De Rust succession exemplifies supracrustals typically associated with the Wortel Formation (Praekelt and Schoch, 1997).

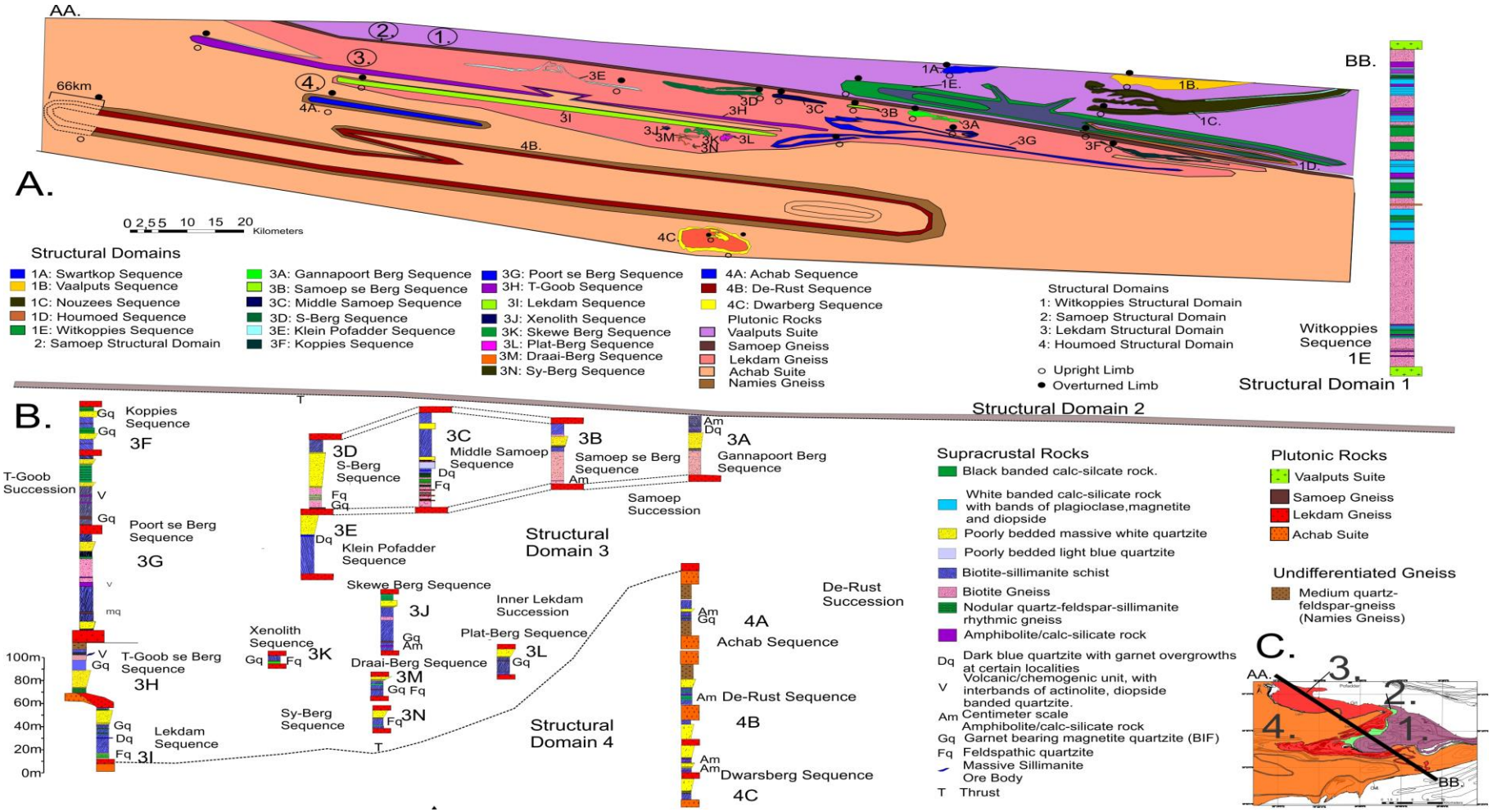

Figure 4.1: Simplified section displaying the structural restoration of macroscopic sheath folds, oblique on the XZ foliation planes, together with representative stratigraphic profiles of each tectonic sequence. Figure A: Structurally restored map oblique to the XZ foliation plane, which removes the D4-D6 phases of deformation. The various domains with associated structures is also represented.The upright and overturned limbs are displayed for each structure. Figure B: The lateral distribution of stratigraphic profiles within Structural Domain 1 (1A-E); Structural Domain 2; Structural Domain 3 (3A-3N) and Structural Domain 4 (4A-C). Figure C: Shows the location across where the section was constructed.

Table 4.1: Summary of the Lithological characteristics associated with each tectonic sequence within the eastern sector of the Aggeneys Terrane. For each associated sequence and succession certain lithological properties are depicted. The various sequences are also compared to the Wortel Formation supracrustal rocks toward the west.

Domain	Stratigraphic Succession	Sequence	Lithology	Diagnostic Lithology	Lithology not identified	Lithological similarities to the west	Lithological differences to the west
Structural Domain 1		Witkoppies Sequence	Thick succession of biotite gneiss with interbands of amphibolite, light banded magnetite-diopside bearing calc-silicate rocks and dark-banded quartz-feldspar calc silicate rocks.	Biotite gneiss with interbanded successions of dark-black and light calc-silicate lithologies.	Thick successions of poorly bedded massive quartzite, Nodular rhythmic quartz-feldspar-sillimanite gneiss, garnet bearing meta-quartzite, calc-silicate rock, amphibolite, biotite gneiss, feldspathic quartzite, diopside and actinolite.	None.	No sequences of massive poorly bedded quartzite, biotite-sillimanite schist, & sillimanite ore bodies. Has a larger mafic and meta-volcanic nature than the Wortel sediments found throughout the Aggeneys Terrane.
Structural Domain 3	Samoep Succession	Gannapoort Berg Sequence Samoep se Berg Sequence Middle Samoep Sequence S-Berg Sequence	Biotite gneiss with interbands of feldpsathic quartzite, magnetite-quartzite.Thick-thin poorly bedded white-blue quartzite, biotite-sillimanite schist with interbands of garnet bearing dark-blue quartzite, amphibolite and calc-silicate rock.	Thick to thin successions of biotite gneiss with interbands of feldspathic quartzite, and magnetite quartzite.	Nodular rhythmic quartz-feldspar-sillimanite gneiss and garnet bearing meta-quartzite.	Poorly bedded quartzite, biotite sillimanite schist, dark-blue quartzite, amphibolite and calc-silicate rock.	Thick successions of biotite gneiss, feldspathic quartzite, meta-quartzite (without garnet),large sequences of biotite-sillimanite schist and absence of sillimanite lenses.
		Klein Pofadder Sequence	Thick to thin poorly bedded quartzite, dark-blue garnet bearing quartzite, thick to thin sequences of biotite-sillimanite schist.	Dark-blue garnet bearing quartzite, thick to thin sequences of biotite-sillimanite schist and thick poorly to well bedded quartzite.	Nodular rhythmic quartz-feldspar-sillimanite gneiss, garnet bearing meta-quartzite, calc-silicate rock, amphibolite, biotite gneiss, feldspathic quartzite, diopside and actinolite.	Poorly bedded quartzite, biotite-sillimanite schist, and dark-blue quartzite.	Thick successions of biotite-sillimanite schist, amphibolite, calc-silicate rocks and sillimanite lenses.
		Koppies Sequence	Thick to thin poorly bedded white-blue quartzite, biotite-sillimanite schist with interbands of ferruginous garnet quartzite & thick to thin successions of nodular quartz-feldspar-sillimanite rhythmic gneiss.	Nodular rhythmic quartz-feldspar-sillimanite gneiss and garnet meta-quartzite. .	Feldspathic quartzite, calc-silicate rock, amphibolite, biotite gneiss, diopside and actinolite.	Poorly bedded quartzite, biotite-sillimanite schist, and dark-blue quartzite, garnet bearing meta-quartzite.	Large successions of nodular sillimanite-quartz-feldspar gneiss, large unit of biotite-sillimanite schist and sillimanite lenses.
	T-Goob Succession	Poort se Berg Sequence T-Goob se Berg Sequence Lekdam Sequence	Nodular quartz-feldspar-sillimanite rhythmic gneiss, Poorly bedded quartzite, biotite-sillimanite schist, garnet bearing meta-quartzite biotite gneiss with interbands of actinolite, diopside, feldspathic quartzite and sillimanite ore body.	Biotite gneiss with interbands feldspathic quartzite, actinolite, and diopside.	All Features identified.	Poorly bedded quartzite, biotite-sillimanite schist, garnet bearing meta-quartzite, medium-quartz-feldspar gneiss. .	Large successions of nodular sillimanite-quartz-feldspar gneiss, large biotite -sillimanite schist units and sillimanite lenses and interbanded units of feldspathic quartzite, actinolite and diopside.

Table 4.2: Summary of lithostratigraphic characteristics associated with each tectonic sequence associated with the eastern sector of the Aggeneys Terrane. For each associated sequence and succession certain lithological properties are depicted. The various sequences are also compared to the Wortel Formation supracrustal rocks toward the west.

Domain	Stratigraphic Succession	Sequence	Lithology	Diagnostic Lithology	Lithology not identified	Lithological similarities to the west	Lithological differences to the west
Structural Domain 3	Inner Lekdam Succession	Xenolith Sequence Skewe Berg Sequence Platberg Sequence Draai Berg Sequence Sy-Berg Sequence	Poorly bedded quartzite, biotite-sillimanite schist with interbands of feldspathic quartzite, nodular quartz-feldspar-sillimanite gneiss, calc-silicate rock, amphibolite and garnet bearing meta-quartzite.	Feldspathic quartzite, calc-silicate rock, amphiboliet and garnet bearing meta-quartzite.	All Features identified.	Poorly bedded quartzite, biotite-sillimanite schist, garnet bearing meta-quartzite, amphibolite, calc-silicate rock. .	Nodular rhythmic sillimanite-quartz-feldspar-gneiss. No sillimanite lenses. .
Structural Domain 4	De Rust Succession	Achab Sequence De-Rust Sequence Dwarsberg Sequence	Thick poorly bedded quartzite, thick sequence of biotite-sillimanite schist with interbanded units of garnet bearing meta-quartzite, amphibolite, calc-silicate rock and medium quartz-feldspar rock	Thick succession of biotite-sillimanite schist with interbanded units of garnet meta-quartzite, amphibolite, calc-silicate rock and medium-quartz-feldspar gneiss.	Biotite gneiss, feldspathic quartzite, actinolite and diopside units.	Poorly bedded quartzite, biotite-sillimanite schist, garnet meta-quartzite, amphibolite and calc-silicate rock. .	No sillimanite lenses. .

.

4.1.2 Correlation of Stratigraphy to the West

Within the study area, Structural Domain 3 and 4 contain supracrustal rocks that have similar attributes to the Wortel Formaion (Praekelt and Schoch, 1997), while the supracrustal rocks within the Structural Domain 1 are different and have a more meta-volcanic nature, while Structural Domain 2 is represented by a medium-quartz-feldspar gneiss sheet that does not contain any supracrustal sequences. The comparison to the Wortel Formation supracrustal rocks is done through selected stratigraphic profiles constructed in the Haramoep Mountains toward the west by Praekelt (1994). The profiles are representative of a lower strain zone (Colliston et al., 2012) where the Wortel Formation is found, and are associated with the eastern limb of the Haramoep Antiform (Appendix 4.1-4.6).

Structural Domain 3

The Samoep Succession when compared to the Wortel Formation rocks in the Haramoep Antiform (Appendix 4.1), differ in a sense that the Samoep Succession is synonymous with large thick units of biotite gneiss, which is not seen in the Wortel Formation. Large sequences of biotite-sillimanite schist is also not seen within the Samoep Succession, together with sillimanite lenses located above and below the Wortel stratigraphy (Appendix 4.1). Both successions have ferruginous meta-quartzites. However, the magnetite quartzites within the Samoep Succession (seen within the S-Berg Sequence), do not contain any garnets when compared to the Wortel Formation. Both the Wortel Formation and Samoep Succession define second order upward coarsening and fining cycles, the only difference is that the Samoep Succession also defines 3rd order fining cycles, not seen in the Wortel Formation. The Koppies Sequence, although not grouped in a succession, differs from the Wortel Formation in the west, by the abundance of nodular rhythmic sillimanite-quartz-feldspar gneiss associated with the succession (Appendix 4.2). Both the Koppies Sequence and Wortel Formation supracrustal rocks have garnet-bearing meta-quartzite units (BIF). Both successions have poorly bedded quartzites with second-order upward coarsening cycles. However, the Koppies Sequence contains no sillimanite lenses or large units of biotite-sillimanite schist.

The Klein Pofadder Sequence, as with the Koppies Sequence, is also not grouped to a specific succession and when compared to the Wortel Formation in the west, has similar attributes, with the main difference being the absence of garnet-bearing meta-quartzite (BIF), amphibolites, calc-silicate rocks and sillimanite lenses (Appendix 4.2). The Klein Pofadder sequence also defines second-order upward coarsening cycles, similar to the second-order cycles identified in the west. The T-Goob Succession has many similarities to the Wortel Formation in the west (Appendix 4.3). However, the succession has large sequences of nodular rhythmic sillimanite-quartz-feldspar gneiss, which is not seen toward the west. The T-

Goob succession also has large units of feldspathic quartzite, actinolite, and diopside not identified toward the west, only centimetre scale units have been identified (Praekelt, 1994; Wilner et al., 1990). Both the Wortel Formation toward the west and the T-Goob Succession contain sillimanite lenses, which is seen within the T-Goob Structure toward Annakoppies (Pretorius, 1986). However, no sillimanite lenses were identified toward the east. Garnet meta-quartzite units are found within both supracrustal sequences. However, the Wortel Formation in the west has vast amounts of amphibolite and calc-silicate rocks, which is not as abundant in the T-Goob Succession. Both sequences have second-order upward coarsening cycles and poorly bedded quartzites. The Wortel Formation in the west also defines a large second-order upward fining cycle (Praekelt, 1994), not seen in the T-Goob Succession. The Inner Lekdam Succession when compared to the Wortel Formation is devoid of large biotite-sillimanite schist units, sillimanite lenses and thick units of poorly bedded quartzite (Appendix 4.4). The Inner Lekdam Sequence also contains calc-silicate and amphibole rocks, which are also found in the Wortel Formation rocks toward the west. Both stratigraphic sequences have poorly bedded quartzites defining second-order upward coarsening cycles (Appendix 4.4).

Structural Domain 4

The De Rust Succession within Structural Domain 4 defines sequences very similar to the supracrustal rocks found towards the west (Appendix 4.5). Both the De Rust Succession and Wortel Formation sequences toward the west have small interbanded units of amphibolite, calc-silicate rock, and garnet-bearing meta-quartzite. Both sequences also have sillimanite lenses, with lenses identified in the De Rust Succession (Achab Sequence) toward the west (Moore, 1977; Wilner et al., 1990). Both sequences also have thick to thin sequences of interbanded medium quartz-feldspar gneisses (Namies Gneiss), which is coeval with both supracrustal sequences. Second-order upward coarsening cycles are also identified in both successions, often associated with the upper quartzite and schist units (Appendix 4.5).

Main Comparison

When all the tectonic sequences are compared with the Wortel Formation toward the west (Figure 4.2), using the upright limbs of all the sheath fold structures, it is clear that the De Rust Succession, Inner Lekdam Succession, T-Goob Succession, and both the Koppies and Klein Pofadder Sequences can be correlated with the upper part of the Wortel Formation, on the basis of the presence of calc-silicate rock, amphibolite, quartzite-diopside-actinolite rock and garnet meta-quartzite. The lower part of the Wortel Stratigraphy only has thick successions of biotite-sillimanite schist with sillimanite lenses at the base, which is not present toward the east. However, sillimanite lenses have been identified on the upper section of the Wortel Formation, which is also true for the T-Goob Sequence, which is one of the few tectonic

sequences in the study area which contain sillimanite lenses. What is also apparent is that the Samoep Succession and Witkoppies Sequence differ from the Wortel supracrustal rocks, with the Samoep Succession having thick successions of biotite gneiss, not seen in the Wortel Formation, while the Witkoppies Sequence also has thick successions of biotite with large variations of calc-silicate rocks, not typical of the Wortel Formation (Figure 4.2). Biotite-sillimanite schist represents 79% of the total stratigraphy of the Haramoep Mountains in the west, while it makes up 39% of the stratigraphy in the study area (Figure 4.2). The thick white poorly bedded quartzites synonymous with the Wortel Formation represents 18% of the stratigraphy in the west, while these quartzite units in the study area represent 21% of the total stratigraphy. The biotite gneiss component within the upper part of the stratigraphy in the study area is representative of 24% of the total stratigraphy, which is far more than the minor amounts of biotite gneiss recorded in the Wortel Formation (Colliston et al., 1989). The medium graned quartz-feldspar Namies gneiss, which is interbanded within both stratigraphic successions, represents 7% of the stratigraphy in the study area and 11% of the Wortel Formation in the west. The nodular sillimanite-quartz-feldspar gneiss has been identified by Moore (1977) and Paizes (1975) and has received scant attention, especially regarding its relationship with the Namies Gneiss and Wortel Formation in the west. This unit represents 4% of the total stratigraphy in the study area, when compared to minor lenses recorded in the western part of the Wortel Formation (Moore, 1977). When the garnet meta- quartzite units, amphibolites, chemogenic/volcanoclastic units are considered for both stratigraphic successions, 6% is defined for the Wortel Formation in the west and 12% is defined for the stratigraphy in the study area. Another factor to consider is that of strain, as the Wortel Formation rocks in the Haramoep Mountains represent the flank of a large antiformal structure in a low strain zone, whereas the stratigraphy in the study represents staggered sequences of sheath fold structures in a very high strain zone.

Figure 4.2

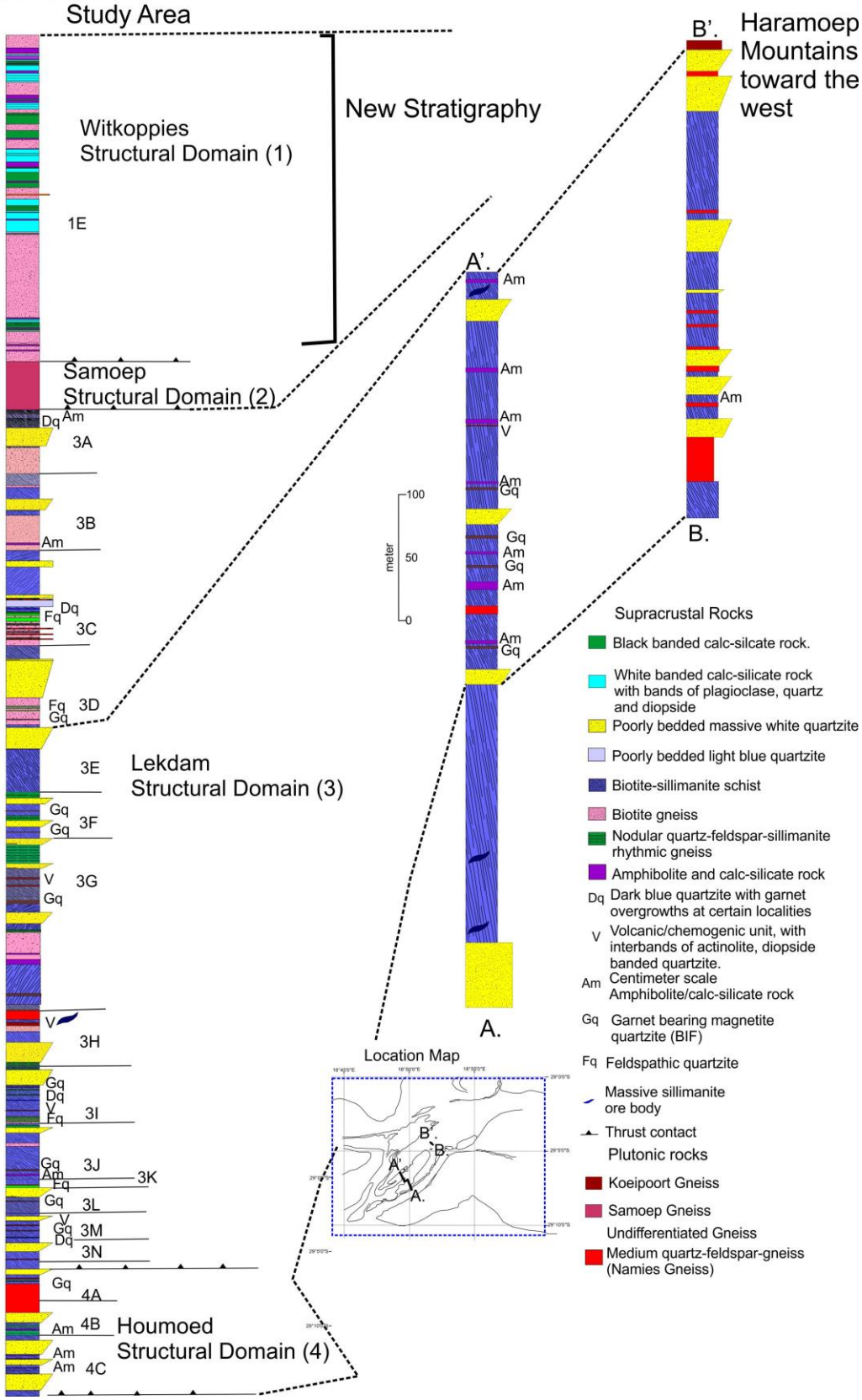

Figure 4.2: Simplified stratigraphic comparison of the different tectonic sequences in the study area and the Wortel Formation in the Haramoep Mountains, found toward the west of the study area (modified after Praekelt, 1994.) For the stratigraphic sequences in the study area, the upright limbs of all the sheath fold structures were used to construct the main stratigraphic profile seen above.

4.1.3 Summary

- The stratigraphic successions and style of deformation differ from west to east across the Aggeneys Terrane. One notable characteristic is the fragmented stratigraphy found in the eastern Aggeneys Terrane in the form of double vergence isoclinal structures, elliptical ring structures, which represent macroscopic sheath folds (Chapter 4.2). Nowhere in the study area are the stratigraphic sequences in contact with one another, which is representative of a higher strain zone, similar to what is seen in the Aggeneys and Gamsberg structures toward the west (Colliston et al., 2012).
- The fragmented stratigraphic sequences can be divided into four well-defined structural domains, Structural Domain 1 (Witkoppies Structural Domain), Structural Domain 2 (Samoep Structural Domain), Structural Domain 3 (Lekdam Structural Domain), and Structural Domain 4 (Houmoed Structural Domain) which represent kilometre scale intra-terrane thrust sheets.
- When vertically restored the lower tectonic sequences associated with Structural Domain 3 and 4 can be correlated to the top portion of the Wortel Formation related to the Haramoep Mountains (Praekelt, 1994) and therefore represent a new facies of the Wortel Formation.
- The upper tectonic sequences associated with the upper part of Structural Domain 3 (Samoep Succession) and Structural Domain 1 (Witkoppies Sequence) represent new stratigraphy not previously identified within the Aggeneys Terrane and differ from traditional Wortel Formation supracrustal rocks found in the west.

4.2 Sheath Fold Theory and Application

Sheath folds are defined as folds displaying curvilinear fold hinges which rotate towards parallelism with the X-direction or tectonic transport direction (Cobbold and Quinquis, 1980; Alsop and Holdsworth, 2007). Sheath folds occur in a wide range of environments, they occur in high strain zones associated with orogenic belts (Quinquis et al., 1978, Henderson 1981; Colliston and Schoch 2000, Alsop and Holdsworth, 2007); salt diapirs (Talbot, 1979; Velaj et al., 1999), soft sedimentary deformation structures (Roberts, 1989) and sub-glacial sediments (Huddelston, 1992). According to Ramsay and Huber (1987) sheath folds are classified as folds with hinge variations of larger than 90˚, whilst Skjernaa (1989) further sub-divides sheath folds into tubular folds with apical angles ≤20˚ and 'tongue' folds with apical angles of between 90 and 20˚. Within the Namaqua Mobile Belt, large macroscopic sheath folds have been recognised and documented with the 2Ga Pofadder Terrane, such as the Pella sheath fold structure and Dabenoris sheath fold structure (Blignault et al., 1983; Colliston, 1990). The 1.6 Ma Aggeneys Terrane hosts the Gamsberg sheath fold structure and Aggeneys Hills which represent a series of sheath fold nappes (Colliston and Schoch, 2000; Colliston and Schoch, 2002). More recently within the Grunau Terrane, the Riemvasmaak-Kenhardt Mega Sheath Fold structure (RK-MS) was identified and mapped in detail by Mathee (2017).

Criteria

The macroscopic structures identified in the study area are interpreted as sheath folds according to a certain criteria. The criteria can be used to typically classify the various sheath fold structures throughout the study area. The criteria is summarised in Table 4.3 below, together with the associated sheath fold structures. The criteria was successfully applied by Mathee, (2017) for the classification of the RK-MS sheath fold structure; also Alsop and Holdsworth, (2004b) in identifying sheath folds in the Melness-Sleteil area, as did various authors who have studied macroscopic sheath folds globally. Likewise, in this study area, the criteria has been applicable and leading to the recognition of the exceptional D2 and D3 sheath folds found in the various domains.

Table 4.3: Table illustrating the sheath fold criteria, together with relevant examples from domains in the study area.

Sheath Fold Criteria	Examples within the study area
1. Fold hinges with intensely curvilinear hinge lines often define the central core or 'eye' of the sheath fold (Alsop and Holdsworth, 2004b) and are often	Domain 1E: Witkoppies sheath fold, which has a well-defined central 'eye' structure, surrounded by double vergence asymmetries (S and Z) on the extremities of the fold in the YZ-plane.

bounded by double vergence asymmetries (Alsop and Holdsworth, 2004a)	
2. Large scale sheath fold structures contain smaller sheath fold structures within (Alsop, 1994; Alsop et al., 2007). Lithological layers also give symmetrical arrangement, found on the inside of sheath fold structure (various lithological layers folding).	A good example is domain 1E and domain 3C associated with the Middle Samoep and Witkoppies sheath fold structures.
3. Sheath folds have non-continuous axial plane. Where refolded they have long axial lengths (Fowler and Kalioubi, 2002).	Can be related to all F2 sheath fold structures within the study area.
4. Sheath folds often show elongation toward the X direction (tectonic transport direction) with their fold axes parallel to the regional L1 stretching lineations. The direction of shear is often constant, with fold hinges rotating toward the X (or transport) direction (Cobbold and Quinquis 1980; Fowler and Kalioubi, 2002).	This is the case as most of the F2 and F3 sheath fold axes are sub-parallel to the regional L1 stretching lineations (where not rotated by later phases of deformation), defining the tectonic transport direction from NE to SW.
5. Sheath folds are associated with localised reversals in fold obliquity, with minor fold hinges rotating toward the X-direction (Alsop and Holdsworth, 1999)	Good examples can be seen within the Samoep se Berg sheath fold (Domain 3B), The Middle Samoep sheath fold (Domain 3C), and Koppies sheath fold (Domain 3E).
6. Minor S and Z folds have reversals in asymmetry across the strike after crossing major axial planes of culmination and depression zones (Alsop and Holdsworth, 2004b)	Minor S and Z folds have reversals across all sheath fold structures associated with the entire study area.

7. Early D2 sheath fold structures are refolded by later D3 structures to form non-planar refolded sheath fold structures, typically found in zones of high strain (Ghosh and Segupta, 1999). The D2 and D3 sheath fold axes are co-linear to one another.	Refolded sheath fold structures are typically found associated with the Gannapoort Berg sheath fold structure (Domain 3A), S-Berg sheath fold structure (Domain 3D), Skeweberg (Domain 3K), Draaiberg (Domain 3L) and Dwarsberg Sheath Fold structures (Domain 4C).
8. Tubular type sheath folds can also be found, resulting in the refolding of the D2 hinges by later D3 and D4 folds, resulting in sheath folds with apical angles of < 20˚ (Skjernaa, 1989).	The most prominent examples are the T-Goob se Berg Sheath Fold (Domain 3G), the Outer Lekdam Sheath Fold (Domain 3H) and Poort se Berg Sheath Fold (Domain 3I).
9. Tectonic discontinuities and displacements due to thrusting that occurs in zones of high strain are often associated with sheath folds (Alsop, 1994; Alsop and Holdsworth, 1999).	All the sheath fold structures within the study area have been emplaced by the early D1 phase of intra-terrane thrusting, some of the kilometre scale sheath folds such as the Outer Lekdam and T-Goob se Berg sheath folds, and have been emplaced close to intra-terrane thrust boundaries between the Lekdam Thrust Sheet (Domain 3) and Houmoed Thrust Sheet (Domain 4). The Dwarsberg Sheath Fold Structures has also been cut off and emplaced within the Houmoed Thrust Sheet (Domain 4), as the inner sheath fold is surrounded by the Lekdam Gneiss, that was cut off from the Lekdam Thrust Sheet (Domain 3).
10. The thickness of sheath fold limbs can be used to determine the sense of shear and the direction in which the sheath fold closes (Fossen and Rykkelid, 1990).	Only the Witkoppies Sheath Fold (Domain 1E) can be used as an example, the other sheath fold structures are too affected by the later phases of deformation (boudinage and shear effects) for this method to be applied.

When the criteria is applied to the Samoep se Berg Sheath Fold structure (Domain 3B) and Dwarsberg Sheath Fold (Domain 4C), both types of sheath fold structures can be classified according to the criteria mentioned above (Appendix 4.6). The criteria is applied as follows:

- Both the Samoep se Berg and Dwarsberg sheath folds have structures that resemble double vergence asymmetries reflect ‘omega’ structures (1).
- Both structures have a symmetrical arrangement of stratigraphic units which define the hinge zones and limbs of these specific structures (2).
- Both the Samoep se Berg and Dwarsberg sheath folds have non-continuous hinge zones and axial planes due to their isolated nature (3)
- Both sheath folds have fold hinges that rotate toward the X direction, parallel to the tectonic transport direction (4).
- Both Samoep se Berg and Dwarsberg structures have axial planes, which have a reversal in obliquity with an increase in shear strain, due to rotation of fold axes toward the tectonic transport direction (5).
- Both sheath folds also have minor folds (S and Z structures), which have reversals in asymmetries across major fold axial traces (6).
- Both structures have the same characteristics as all the major sheath fold structures identified throughout the study area.

Throughout the eastern part of the Aggeneys Terrane, most of the D2 structures were identified as synformal sheath fold structures, with the direction of younging interpreted to be toward the axial plane. The fold facing, which is defined as the direction perpendicular to the fold axis and within the axial plane toward the direction of younging (Shackleton, 1958), associated with most of the structures, showed younging toward the inside of structures. The fold facing directions also vary from northeast to south-west, with facings directions, pointing towards one another. The variation in facing directions have also been noted within the western Aggeneys Terrane (Colliston et al., 1991) in most of the sheath fold structures. Most of the cross-beds and primary features showed younging toward the inside of the structures. Where the younging direction wasn't apparent, the defined polarity (using second order and third order cycles) also showed younging toward the inside of most of the structures. With the younging direction being directed toward the inside of most of the structures, the interpretation can be made, that most of the northern limbs represent the overturned limbs and southern limbs the upright limbs. However, this is problematic when one considers the vergence directions associated with the northeast to southwest direction of over thrusting (Figure 4.3), which shows the northern limb being upright and southern limb being the overturned limb. There is an explanation for this, as seen in Figure 4.3, where the antiformal hinge component

associated with the overturned flank is weathered away. This will result in sheath fold structures being synformal throughout the study area, with the antiforms being absent. Nowhere within the study area, are any antiformal sheath folds present, or any remnants of an antiformal sheath fold seen. Similar observations were made within the western Aggeneys Terrane, with most of the sheath fold structures being encountered having synformal components like the Quarry sheath fold structure (Colliston and Schoch, 2002), as well as the Gamsberg sheath fold (Colliston et al., 1986). Other examples include the Dabenoris sheath fold (Blignault et al., 1983) and the Pella Sheath Fold (Colliston, 1990).

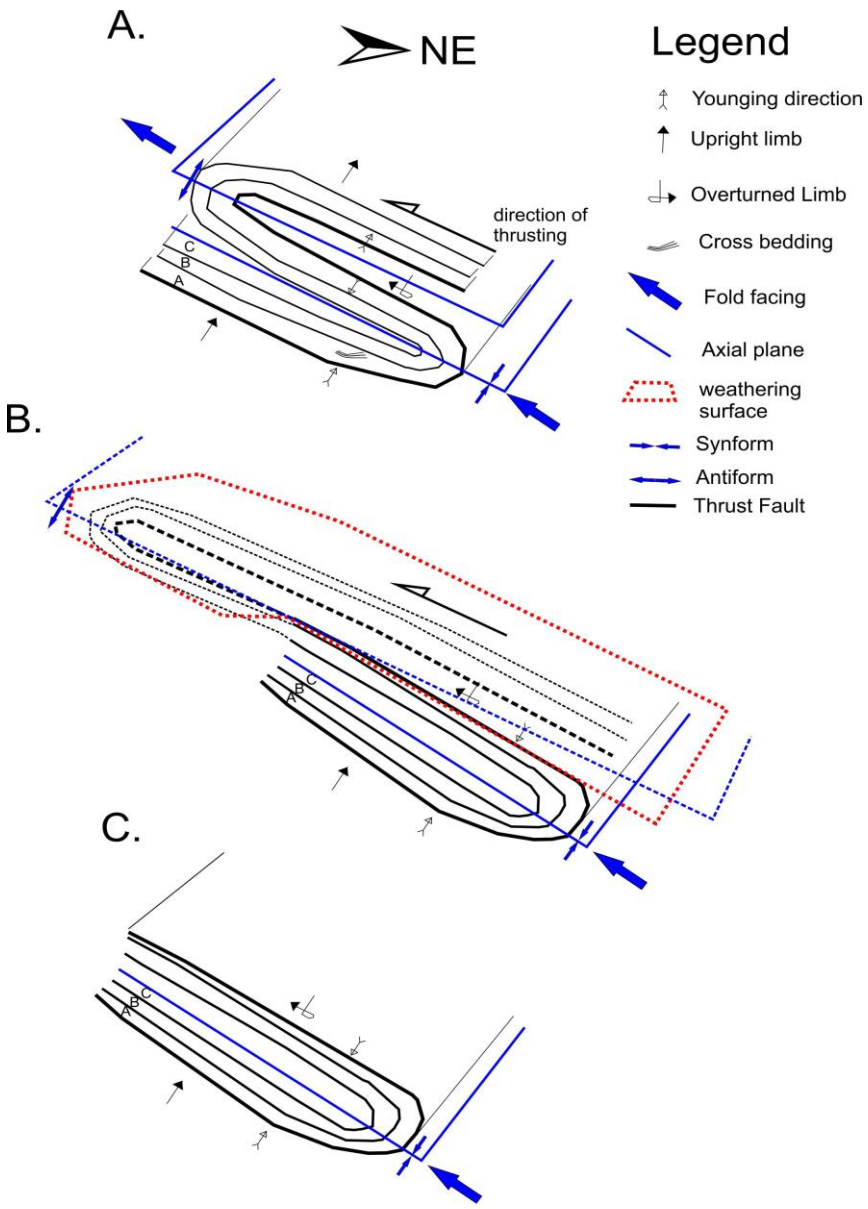

Figure 4.3: Schematic diagram illustrating the development of D2 sheath folds, together with facing azimuths, to illustrate why the overturned limb is in the north and not the south. Figure A: A folded sequence in section verging toward the southwest, looking toward the west. The vergence direction is ideal, together with the upright limb being represented by the northern limb. The facing azimuths in the antiformal and synformal components are directed toward southwest. Figure B: The antiformal component being thrusted and weathered away, resulting in the synformal component remaining. Figure C: A synformal sheath fold, with the northern limb being the overturned limb. This is the case in most of the sheath fold throughout the study area.

'Omega' Sheath Folds and Refolded Sheath Folds

Within the study area, two main types of sheath folds were identified: 'Omega' type sheath folds with double vergence geometries (D2 sheath fold structures), and refolded sheath fold structures (D2 refolded by D3 and D4). Examples of 'Omega' sheath folds showing double vergence geometries are the Samoep se Berg (Domain 3B) and Witkoppies Sheath Fold structure (Domain 1E), while the refolded sheath fold structures are defined by the S-Berg (Domain 3D), Dwarsberg (Domain 4C), and Gannapoort Berg Sheath Fold structures (Domain 3A). The buckled and flattened 'Omega' sheath folds although they been affected by the D4-D5 events, have not been refolded by the D3 and D4 phase of deformation, but rather attenuated, and sheared, with the F5 oblique folds forming due to D5 east-west shears, and D3 folds being absent due to competency differences and strain partitioning. The best example of an 'Omega' sheath fold is the D2 Samoep se Berg sheath fold (Figure 4.3).

The limbs deform an S0//S1 foliation, with an axial planar S2 foliation being identified in the hinge zone of the sheath fold structure. The limbs form both S & Z asymmetries reflecting an opposite sense of vergence, which is a common trend in sheath fold structures (Alsop and Holdsworth, 2002; Alsop and Holdsworth, 2004b). The Z asymmetries are associated with clockwise rotation and S asymmetries anticlockwise rotation (Alsop and Holdsworth, 2004b). If the later D5 buckle effect due to shearing is removed from the D2 Samoep se Berg Sheath Fold, the clear reversals in S and Z asymmetries can be observed. The Samoeps se Berg sheath fold is one of the few sheath fold structures that are not refolded by the D3 and D4 phases of deformation and are well preserved. The Samoep se Berg sheath fold, is however flattened, sheared, and buckled by the later D5 east-west shearing effects superimposed on the limbs of the structure. Cross bedding was identified within the Samoep se Berg sheath fold, showing younging direction toward the inside of the structure (facing directions interpreted to be toward the axial plane), defining a downward facing synformal sheath fold structure. The upright limb is represented by the southern limb, with the northern limb representing the overturned limb.

According to Alsop and Holdsworth, (1999) minor reversals in fold obliquity occur due to fold hinges rotating toward the X direction, resulting in the systematic reduction in the angle of fold obliquity to the axial plane and the shear plane (Alsop and Holdsworth, 2002; Alsop and Holdsworth, 2004a). This will result in the axial planes being co-planar to the regional S1//S2 foliation (Figure 4.4). The associated D2 S and Z folds and D2 sheath fold axes will also be co-linear to the L1 stretching lineations, and their relative angles toward one another will decrease as the fold hinges rotate toward the transport direction (Alsop and Holdsworth, 2004a; Alsop and Holdsworth, 1999). The angle between the D2 fold axes and stretching

lineations is 21,3˚, with the angle between the D3 hinges and stretching lineations being 25˚ (Figure 4.5). The mean axial plane associated with the D2 sheath fold has a low angle of 8,7˚ with the regional S1//S2 foliation. The data exemplifies that the D2 fold hinges have rotated more towards the transport direction, and their sense of obliquity has decreased concerning the regional foliation (Figure 4.5) . Also, the fold hinges rotate toward the transport direction X direction, which is typical of sheath folds with reverse asymmetries in high strain zones (Alsop and Holdsworth, 2004a). Other examples within the Namaqua Mobile Belt where fold hinges rotate towards the transport or X direction are shown by Mathee (2017) and Colliston and Schoch (2000).

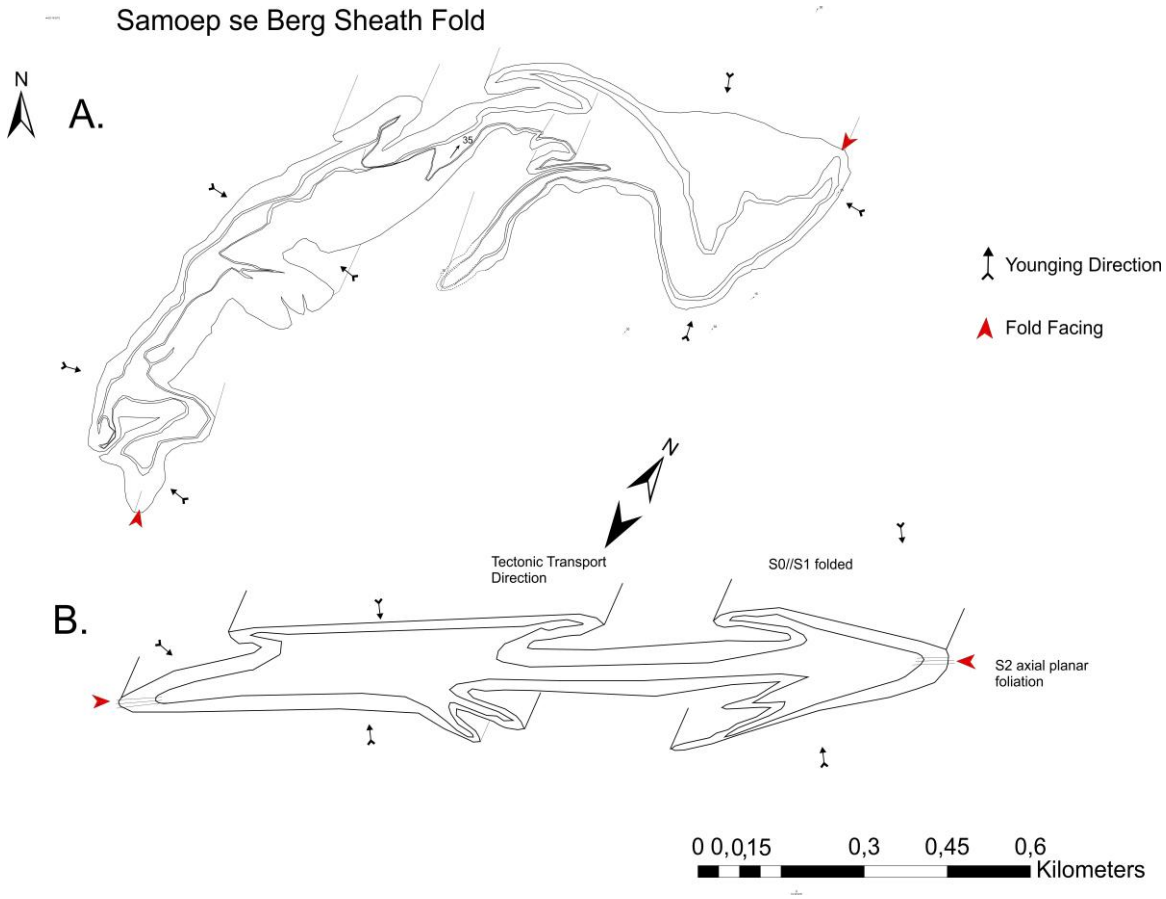

Figure 4.4: A: Form line map of the Samoep se Berg sheath fold with associate stratigraphic younging direction. B: Shows the Samoep se bergs sheath fold not affected by the later phases of deformation, which gives it an omega shape both in the northern and southern limbs of the F2 sheath fold.

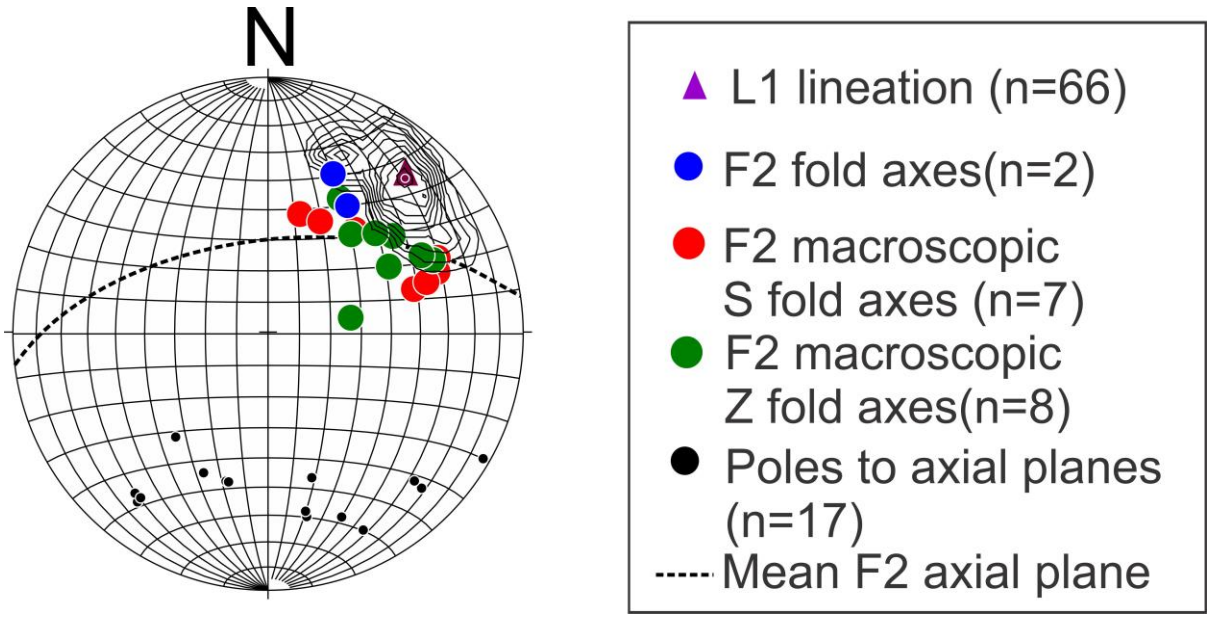

Figure 4.5: Stereonet of the Samoep se Berg sheath fold, showing the co-linear relationship between the F2 S and Z folds, and F2 sheath fold axes and associated L1 stretching lineation. All the fold axes and mean stretching lineation have a mean trend toward the northeast, coinciding the northeast-southwest tectonic transport direction. The mean axial plane associated with the structure together with the poles to the F2 axial planes is also defined, having a subvertical dip toward the north-northwest.

The second type of sheath folds are termed refolded sheath folds and have been refolded by the D3 phase of deformation. These kinds of sheath folds have been previously identified by Ghosh and Segupta (1999) within the Phulad shear zone in India on a centimetre scale, with the original sheath fold, being refolded by a later fold event, resulting in a refolded tubular type sheath fold (Ghosh and Segupta, 1999). Similar tubular type sheath folds have also been identified by Skjernaa (1989), within the Grapesvare area in Sweden associated with the Caledonian Seve Nappe on a centimetre scale. However, in the study area, these structures are identified on a kilometre scale, making them unique. The best example of a refolded sheath fold structure is the D3 Gannapoort Berg refolded sheath fold structure, which represents two refolded isoclinal sheath fold structures (D2 structures), one more flattened and sheared than the other, that is refolded by the F3 fold phase. The structure itself is located on the intra-terrane thrust boundary (Samoep Thrust) which is ideal for its formation due to movements and reactivated movements along the thrust boundary contact by later phases of deformation. The Gannapoort Berg structure has an elliptical shape, with the various fold axes associated with the D2 and D3 fold phases being co-linear, and their axial planes being co-planar (Figure 4.6), and forms part of a progressive ductile shear process (Colliston et al., 1991). The fold axes are co-linear to the regional L1 stretching lineation and have an angle of 11˚ to one another. The foliation plane S1//S2 is co-planar to the D2 and D3 axial planes and makes an angle of 9,6˚ (Figure 4.6).

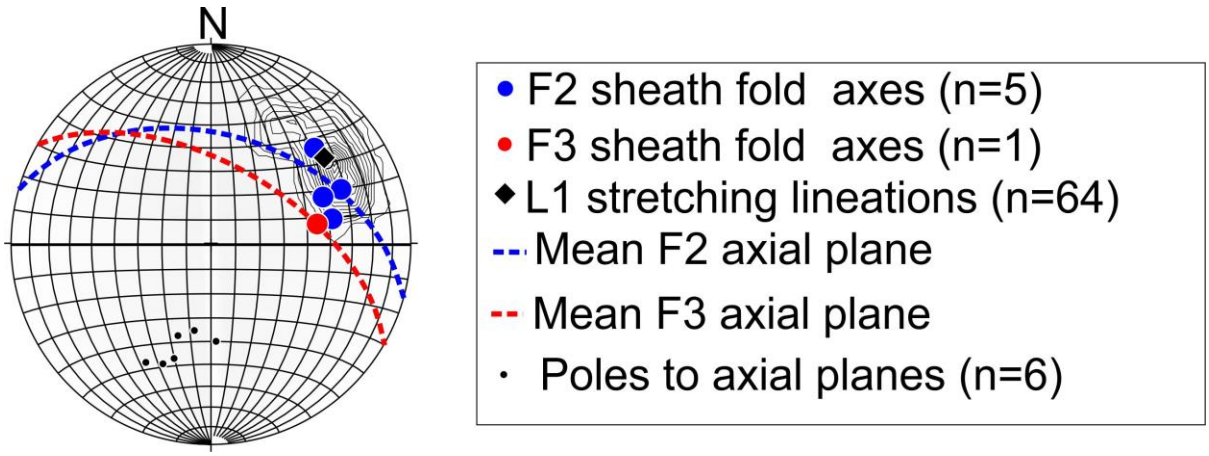

Figure 4.6: Stereonet showing the co-linear relationship between the F2 S and Z folds, F2 sheath folds, F3 folds and the regional stretching lineation. The F2, F3 and stretching lineation have a mean trend toward the northeast, coinciding with the northeast-southwest tectonic transport direction. The mean F2 and F2 axial planes is also represented, having sub-vertical dips toward the north and northeast respectively.

The Gannapoort Berg structure (Appendix 3.6) is a perfect example of a sheath fold, severely affected by the later phase of deformation especially the D5 east-west shears seen regionally throughout the Namaqua Mobile Belt (Colliston and Schoch, 2013). The D2 sheath fold has been refolded by the D3 phase and highly flattened by the D5 east-west shearing event during a progressive ductile shear process (Figure 4.7). Originally the two D2 sheath fold structures must have been adjacent to the Samoep Thrust-boundary, with the X direction of the sheath folds being parallel to the tectonic transport direction (Figure 4.7A). The sheath folds were most likely folded by the D3 phase of folding and then sheared by the D5 east-west shears, resulting in the refolding and flattening of the Gannapoort Berg Sheath Folds (Figure 4.7 B). There are also examples of D2 macroscopic sheath folds, which are folded by the D4 fold phase and not the D3 phase. This is exemplified in the T-Goob se Berg Structure (Domain 3I; Figure 3.5) and Outer Lekdam fold structure (Domain 3J; Figure 3.5), which also fold intra-terrane thrust sheet boundaries.

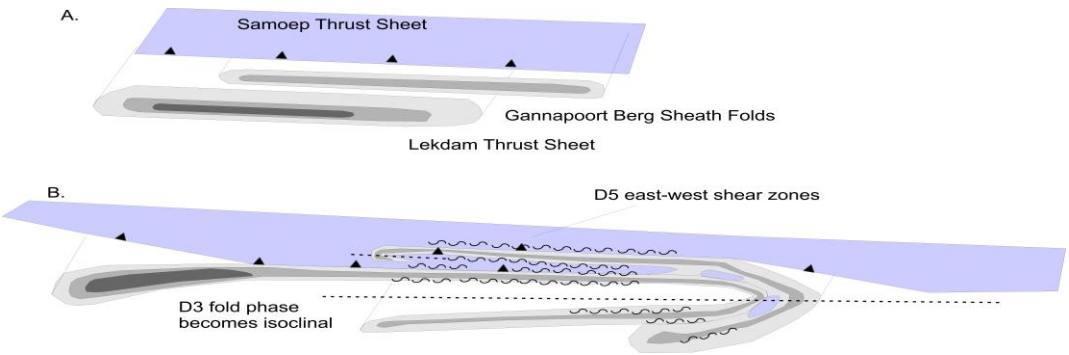

Figure 4.7: Diagram illustrating the formation of the Gannapoort Sheath fold structure, and the effect of the D3 and D5 event on its formation. Figure A: The development of the Gannapoort Berg sheath fold (D2) and overlying Samoep Thrust sheet. Figure B: The effect of the D3 and D5 east-west shears on the Gannapoort Berg sheath fold. The tightening of hinge zones can be seen due to D5 east-west shearing, together with the infolding of the Samoep Thrust Sheet (Structural Domain 2).

Strain Related to Sheath Folds in the Aggeneys Terrane

Within the western Namaqua Mobile Belt, the dominant type of strain identified at deeper crustal levels within the Pofadder, Steinkopf and Okiep Terranes is plain strain with minor deviations from prolate to oblate during the initial and later stages of deformation (Colliston and Schoch, 2013, van der Merwe, 1986). However, it is possible for strain variations to occur within a single terrane. A good example is the Pofadder Terrane where lateral variations in strain occur from west to east over a distance of 100 kilometres (y=0 to y>15) from the Richtersveld Domain toward the east of Pella, close to the Pella Sheath Fold (Colliston and Schoch, 2006). This change in strain also reflects changes in metamorphic conditions from greenschist facies to upper amphibolite facies, with the higher metamorphic grade also being synonymous with the development of kilometre scale sheath folds, such as the Pella and Dabenoris Sheath Folds within the Pofadder Terrane (Colliston, 1990; Colliston and Schoch, 2000). Within the Aggeneys Terrane, the large variation in strain is partitioned in a northerly lower strain zone and a southerly higher strain zone defined by fragmented stratigraphy and sheath folds (Colliston et al., 2012).

The Aggeneys Terrane has been interpreted to reflect a progressive simple shear process that produces plane to prolate strain (Colliston and Schoch, 2002; Odling 1987). Although no strain analysis was conducted in the eastern portion of the Aggeneys Terrane, it is possible to get an estimation on the type of strain by measuring the nested elliptical ‘eye folds’ or central core of sheath folds on the y-z foliation planes, giving a ‘bulk strain’ estimate on the conditions associated with sheath fold formation (Alsop and Holdsworth, 2006). The central core or ‘eye’ folds (y-z section) are considered to be representative of two-dimensional cross-sections cutting across the length of the X-direction. These ‘eye’ folds are defined by different layers which can be used to define aspect ratios defining the ellipticity of the sheath fold structures (Alsop and Holdsworth, 2006; Williams and Zwart, 1977). It is interpreted that the x, y, and z axes of the sheath folds are considered to be parallel to the finite strain ellipsoid (Alsop and Holdsworth, 2006; Alsop et al., 2007 and Minigh, 1979) Therefore a Cartesian reference system is used (Figure 4.8 A) to measure the elliptical ratios (Ryz) of ‘eye’ folds which are normal to the long axis (X-axis) of the sheath fold. The length of the y-axis is controlled by the degree of hinge line curvature reflected by the angle of the apical angle, with the shorter z-axis defining the interlimb angle. The layer thickness of individual layers is also measured (Tyz ratios=tz/ty) to reflect the thinning and thickening of limbs to the hinge of any measured sheath fold. Concerning the sheath folds, both the outer and inner elliptical ‘eye’ structures are measured giving an R’ ratio (Ryz/Ry’z’) from which three major categories are defined (Figure 4.8 B). Namely: Type A: analogous-eye- folds, Type B: bulls-eye-folds and Type C: cats-eye-folds (Alsop and Holdsworth 2006).

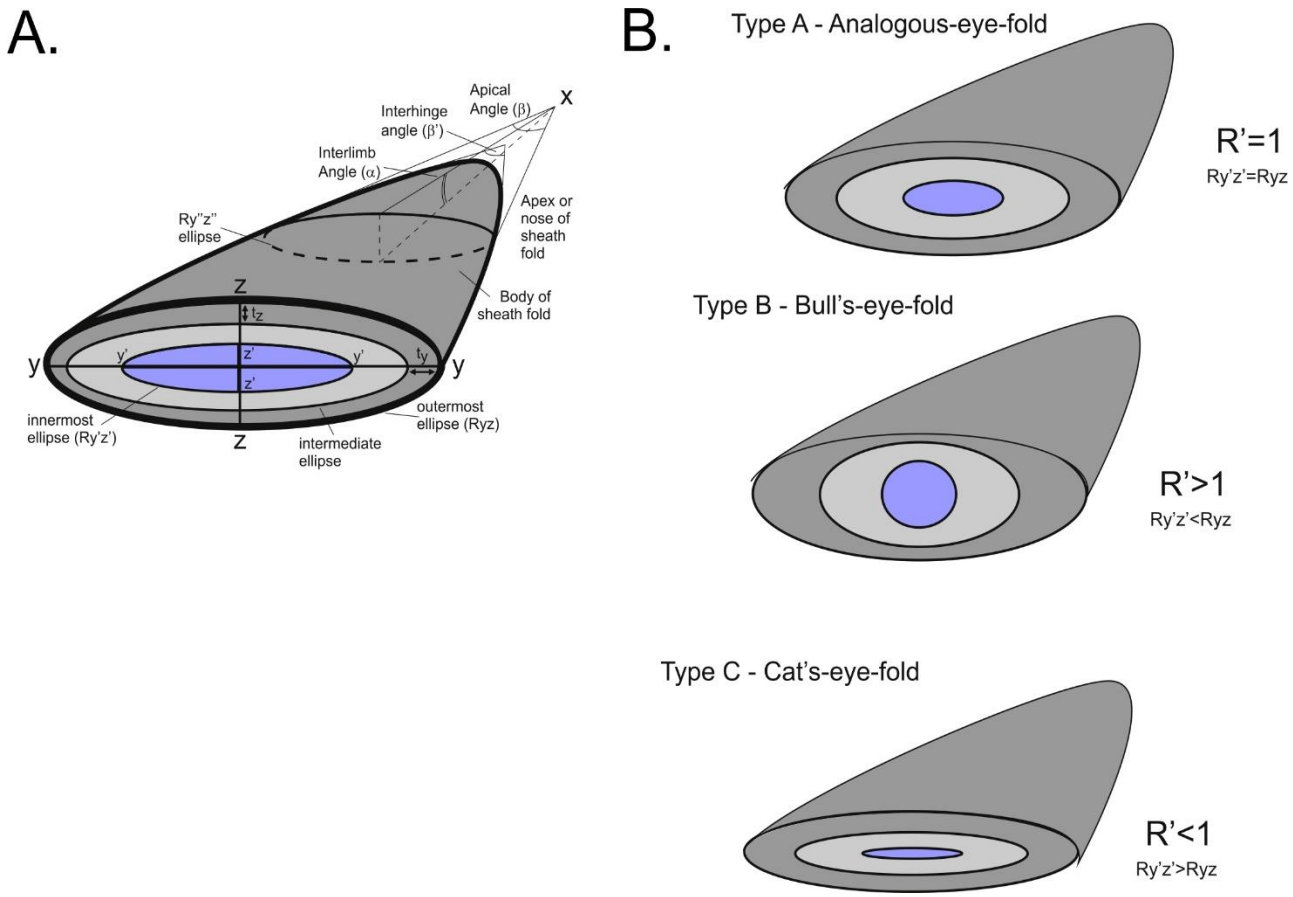

Figure 4.8: Figure A: Schematic 3-D illustration of the X, Y and Z axes of a sheath fold structure, together with the inter-limb angle and apical angle showing the curvilinear attributes of the fold hinge line. The outer most elliptical ratios (Ryz) and innermost (Ry'Z') ratios are illustrated, together with the thickness of individual layers measured along the y-a axis (ty) and z-axis (tz) to provide a ratio (Tyz) of layer thickening/thinning. Figure B: Schematic diagram showing the the classification of sheath folds according to elliptical ratios (R'). Within type A, analogous-eye-folds are formed (R=1), Type B, bull's-eye-fold (R'>1) and Type C, cast-eye-fold (R'<1) (Modified after Alsop and Holdsworth, 2006).

Type A: analogous folds (Figure 4.8 B) are defined by sheath folds where the elipticity of the inner 'eye' structure is equivalent to that of the outer 'eye' structure.Type B: bull's-eye-folds (Figure 4.8 B) are defined by sheath folds where the ellipticity of the inner 'eye' structures is less than that of the outer 'eye' structure. The last type of sheath fold to be encountered are Type C: cat's-eye=fold (Figure 4.8 B) which are defined by the ellipticity of the innermost 'eye' fold is larger than that of the outermost 'eye' structure (Alsop and Holdsworth, 2006).Although this classification is useful, there are constraints to this classification, as it is only useful with pristine examples, where the inner elliptical 'eyes' are preserved, and no accommodation is made for structures where the inner elliptical eyes are strongly deformed and refolded,not preserving the inner elliptical structures. Another disadvantage is that the X direction is not taken into consideration, to provide a k-value to define the shape of the strain ellipsoid. It is often a difficult task to get the precise depth or length of the X-axis, specifically in kilometre scale sheath folds. With regard to the study area, only two sheath fold structures, namely the Witkoppies sheath fold structure and the Gannapoort Berg sheath fold structure contain inner

elliptical ‘eye’ structures, while the rest of the other structures have inner ellipsoidal structures which are flattened, boudined and refolded. The Tyz ratios (Figure 4.7A) can also not be used, due to the effects of D4-D6 transposition of various sheath fold structures, which results in shortening and extension of stratigraphy on the limbs and hinge zones of the various structures.In the study area the Ryz ratios of certain sheath folds (8 in total) were measured (Figure 4.9) and summarised in Table 4.4. Most of the sheath folds were defined as Type C’ cat’s-eye sheath folds’, while two structures were classified as Type B ‘bull’s eye sheath folds’ (Table 4.4). What is quite striking is the high Ryz ratios encountered throughout the study area due to the large y values, associated with the kilometre refolded structures like the T-Goob se Berg (Domain 3I), Outer Lekdam (Domain 3J) and S-Berg sheath fold structures (Domain 3D). The Y and Z axes of the various sheath folds in the study area were plotted against one another in Figure 4.10, comparing them to sheath folds identified by Alsop et al., (2007) in different environments.

The data is presented on log-log graphs, being presented across eight values of magnitude. Based on replots in Figure 4.10 A, most of the sheath folds plot below the general population due to their large Y axes values. Also, the sheath folds used by Alsop et al., (2007) have Y axis values that don’t extend more than a kilometre, and have not been extended or folded like the sheath folds in the current study area, with the largest Y axis value exceeding 121 kilometres. The order of magnitude is also plotted against the Ryz values in Figure 4.10 B, which also show a large variation in Ryz values, with most ratios plotting level with that of the cat’s-eye-folds, except for the Gannapoort Berg (Domain 3A), S-Berg (Domain 3D), Outer Lekdam (Domain 3J) and Goob se Berg sheath folds (Domain 3I). The Ryz values were also calculated together with the Rxy ratios on a Flinn Diagram (Flinn, 1962) (Figure 4.11). An Z value maxima of 650 metres was used as a general mean for all the sheath folds in the study area, modelled after the Gamsberg Sheath Fold structure towards the west of the study area (Colliston et al., 1986). The X value can be calculated using the plunge of the long axes of the sheath folds, from which RXY and RYZ ratios can be used to represent the shape of the strain ellipse in 2D in Figure 4.11. It is interesting to note that the sheath folds fall in the oblate field ($k<1$) of the Flinn diagram, giving rise to general shear conditions, and not only simple shear conditions, as suggested by Colliston and Schoch (2002). The sheath fold structures, with very large Y-values (exceeding 50km) also form outliers with respect to the general population within Figure 4.11. This is evident in the study area, as all the sheath fold structures are refolded and flattened in zones of high strain.

Throughout the study area the regional strain ellipse is defined by the regional S2 foliation contained within the XY plane of the regional strain ellipse ,that dips shallowly north-north easterly, with the extension direction (X-direction) given by the orientation of the extension

lineations (L1), which trends north-northeasterly, sub-parallel to the tectonic transport direction. Throughout the study area (Colliston et al., 1991), a co-planar relationship is found regarding the various fabrics (S0, S1, S2) and a colinear relationship with regard to the regional L1 stretching lineations, D2, D3 and D4 fold axes, that reflects conditions associated with sub-simple shear (oblate component; Figure 4.11) where the regional foliations rotate into parallelism with the shear plane and the linear structures rotating toward the X-direction (Ramsay, 1980; Colliston et al., 1991). Another complication is seen during the D4 phase, with the superimposition of sinistral wrench shear on the earlier D1-D3 structures, forming folds with characteristic Z assymetries, changing the nature and orientation of the regional strain ellipse (Colliston and Schoch, 2013).

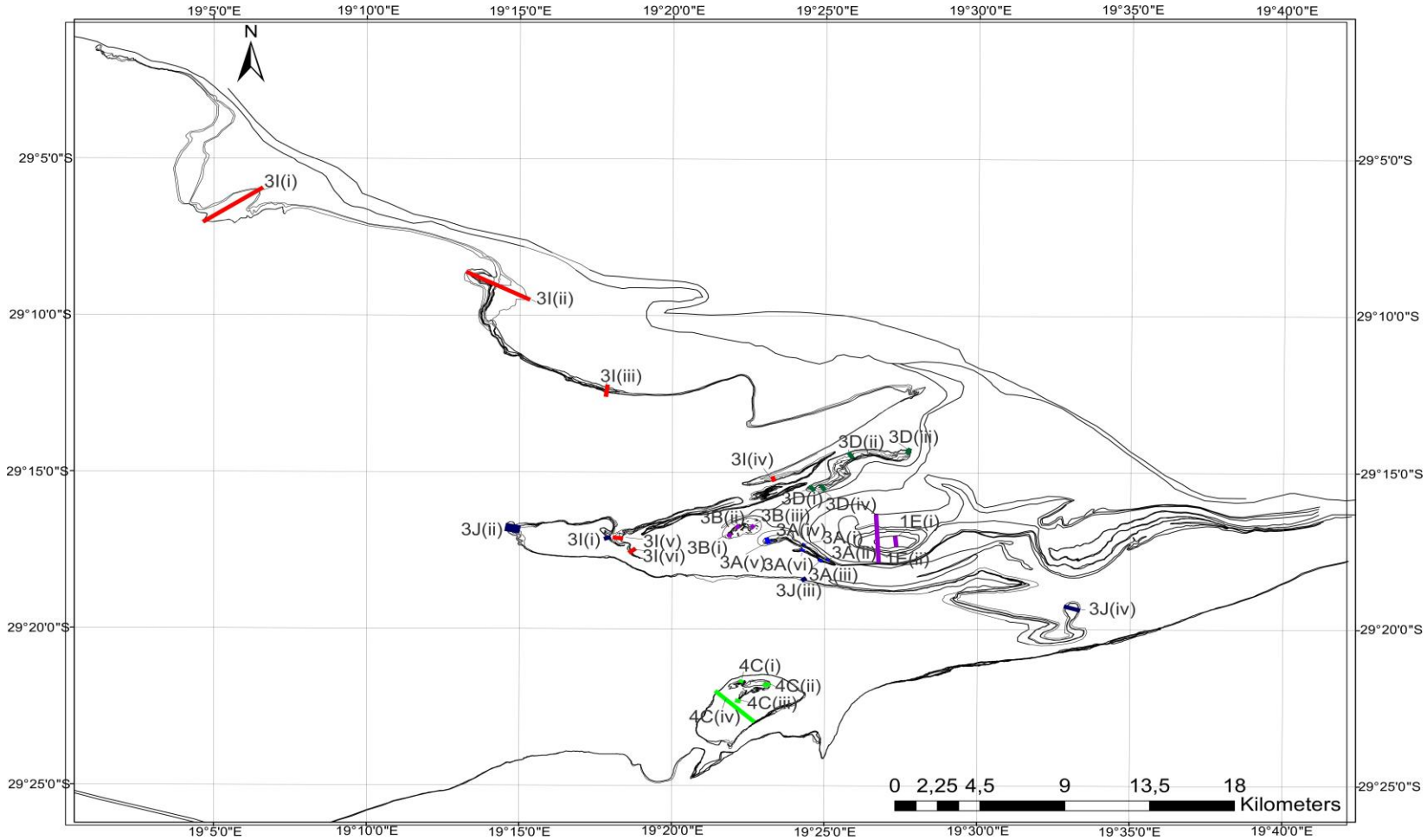

Figure 4.9: The locations were the Z values associated with each structure were measured throughout the study area. The Y and Z values, together with the attributes associated with each structure is summarised in Table 4.4. The various codes (3A-J and 4C), correspond to the various domains defined in Chapter 2 and 3.

Table 4.4: The Ryz ratios, y and z values, together with the classification of the various sheath fold structures throughout the study area. The location of the Y and Z values can be seen in Figure 4.9, and are calculated using the nomenclature by Alsop and Holdsworth, 2006 in Figure 4.8.

Domain	Ratio Ryz	Y and Z	Classification
Domain: 1E Witkoppies Sheath Fold	1E(i)= 2.59 1E(ii)= 5.58	1E (i) Y= 2.2km 1E(i) Z = 0.662km 1E(ii) Y= 24 km 1E(ii) Z= 3.02km	Bull's eye sheath fold
Domain: 3A Gannapoort Berg Sheath Fold Upper Sheath Fold Lower Sheath Fold	3A(i): 147,53 3A(ii): 74,10 3A(iii): 34,52 3A(iv): 4,45 3A(v): 15,22 3A(vi): 41,65	3A(i,ii,iii) Y= 3.29km 3A(i)Z= 0.0223km 3A(ii)Z= 0.0444km 3A(iii)Z= 0.0953km 3A(iv)Y= 0.5607km 3A(iv)Z= 0.1249km 3A(v,vi)Y= 6.75km 3A(v)Z= 0.4435km 3A(vi)Z= 0.1621km	Cat's-eye sheath fold Bull's eye sheath fold
Domain 3B: Samoep Se Berg Sheath Fold	3B(i): 24,23 3B(ii): 10,93 3B(iii): 12,88	3B (i,ii,iii) Y= 2.10km 3B(i) Z= 0.0866km 3B(ii) Z= 0.192km 3B(iii) Z= 0.163 km	Cat's-eye sheath fold
Domain 3D: S-Berg Sheath Fold	3D(i): 33,124 3D(ii): 32,38 3D(iii): 36,82 3Di(iv): 36,16	3D(i,ii,iii, iv)Y= 13.316km 3D(i)Z= 0.402km 3D(ii)Z= 0.4119km 3D(iii)Z= 0.3617km 3D(iv)Z= 0.3687km	Cat's-eye sheath fold
Domain 3I: T-Goob se-Berg Sheath Fold	3I(i): 201 3I(ii): 200 3I(iii): 201,66 3I(iv): 711,764 3I(v): 379 3I(vi): 744,61	3I(i,ii,iii,iv, v, vi) Y= 121km 3I(i) Z= 3.38km (0.60) 3I(ii)Z= 0.60km 3I(iii)Z= 0.170km 3I(iv)Z= 0.2556km 3I(v)Z= 0.3986km 3I(vi)= 0.1625km	Cat's-eye sheath fold
Domain 3J: Outer Lekdam Sheath Fold	3J(i): 443,51 3J(ii): 87,42 3J(iii): 320,63 3J(iv): 62,87	3J(i,ii,iii,iv)Y= 53km 3J(i)Z= 0.1195km 3J(ii)Z= 0.6062km 3J(iii)Z= 0.1653km 3J(iv)Z= 0.8430km	Cat's-eye sheath fold
Domain 4C: Dwarsberg Sheath Fold Inner Sheath Fold Outer Sheath Fold	4C(i): 40,99 4C(ii): 12,97 4C(iii): 55,21 4C(iv): 2,21	4C(i,ii,iii)Y= 5.35km 4C(i)Z= 0.1305km 4C(ii)Z= 0.4122km 4C(iii)Z= 0.0969km 4C(iv)Y= 6.04km 4C(iv)Z= 2.742km	Cat's-eye sheath fold

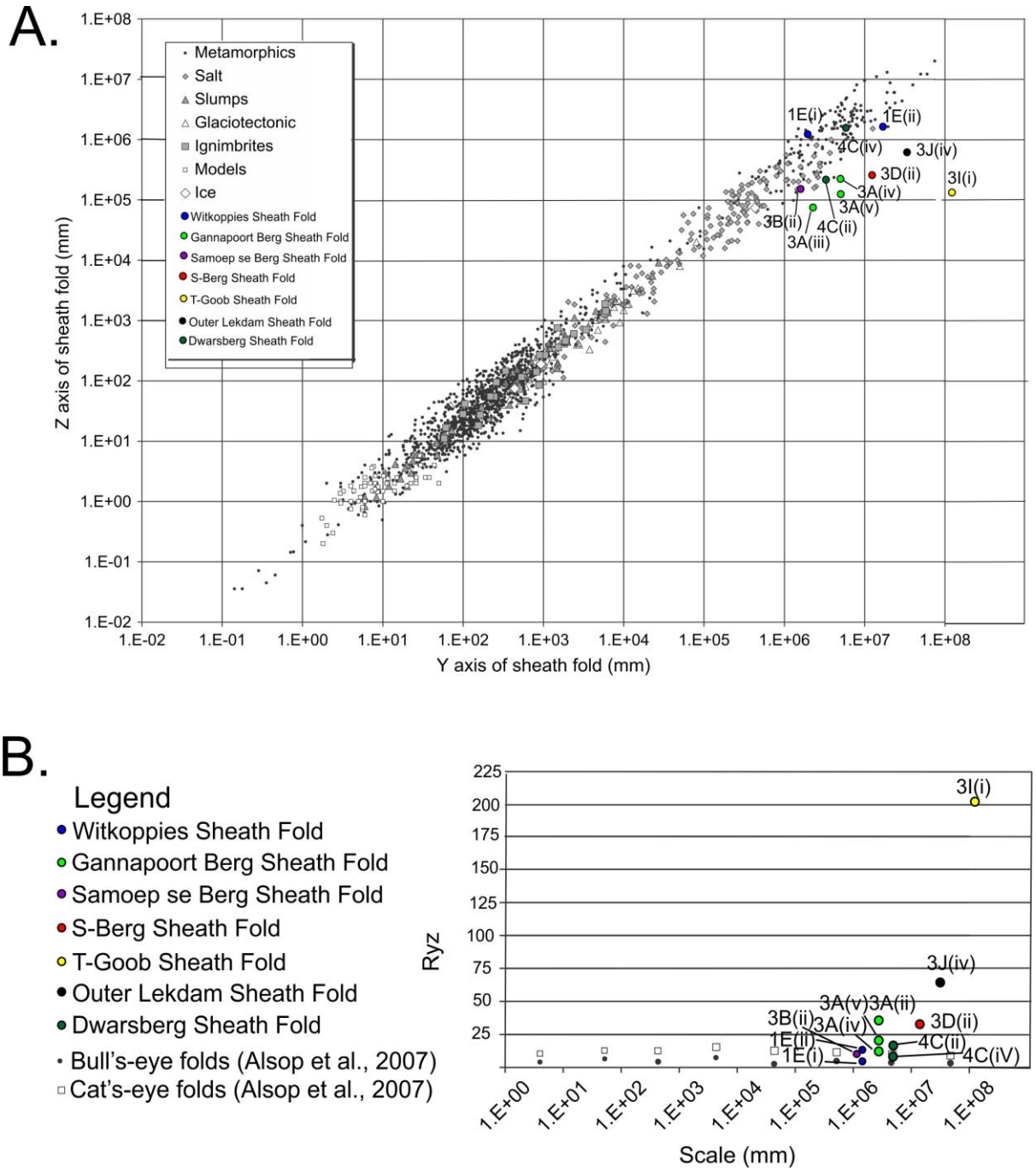

Figure 4.10: Figure A: Logarithmic plots of y and z axes of sheath folds displaying a range of scales and environments in various parts of the world (Alsop et al., 2007). The log-log plots of the different sheath folds are compared to the sheath fold structures located within the study area. Figure B: Plots of mean Ryz ratios against the values of eight orders of magnitude from outcrop scale to kilometre scale. The cat's-eye and bull's-eye folds are compared to that of the sheath fold structures located within the study area. Diagrams modified after (Alsop et al., 2007).

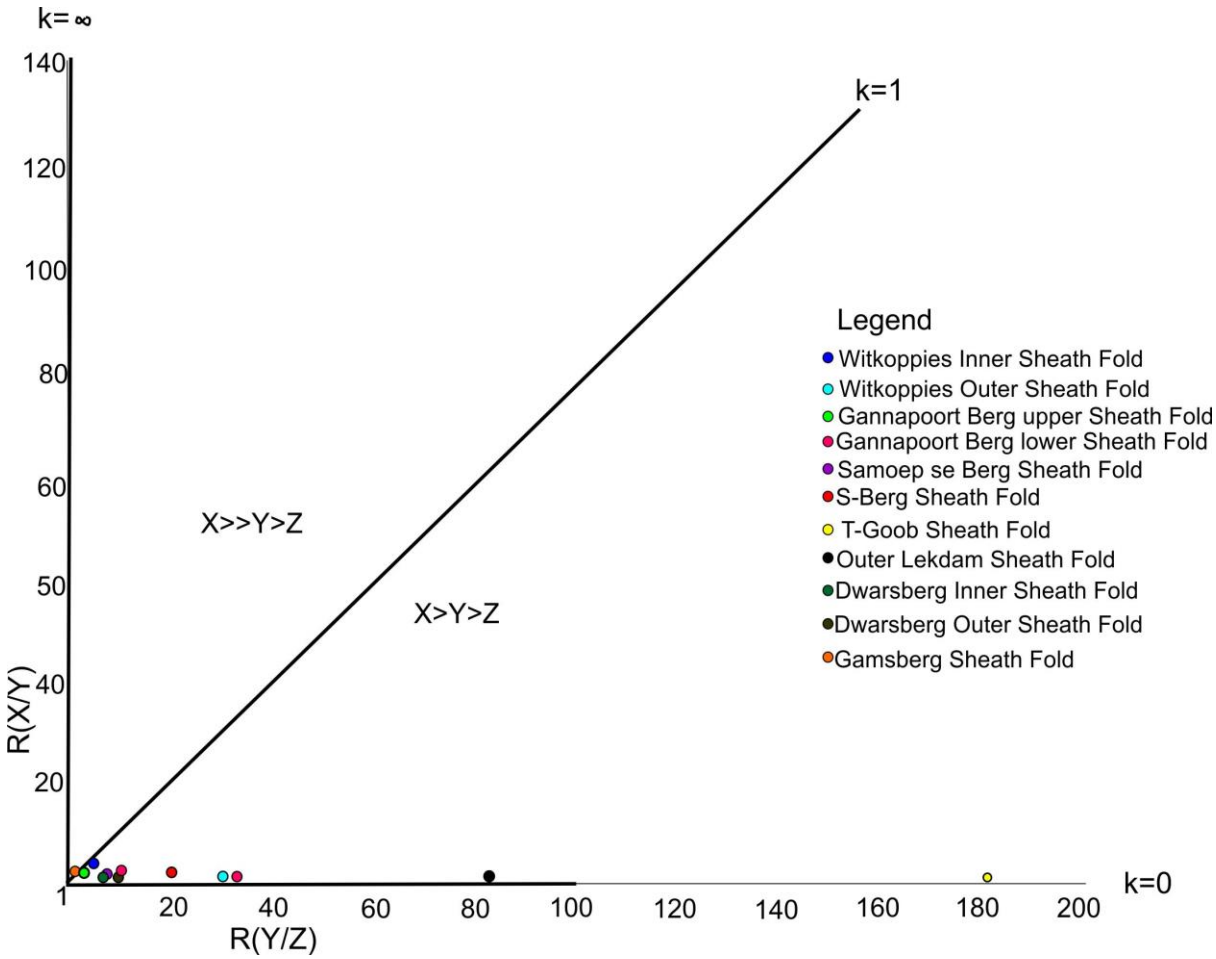

Figure 4.11: Flinn Plot showing 2D strain associated eight different sheath fold structures throughout the study area, together with the Gamsberg structure located within the eastern Aggeneys Terrane. The Y-values can be seen in Table 4.4. A mean Z-value of 650m, modelled for the Gamsberg structure was used for all the structures. Modified after Flinn (1962).

CHAPTER 5

T-Goob se Berg Sheath Fold

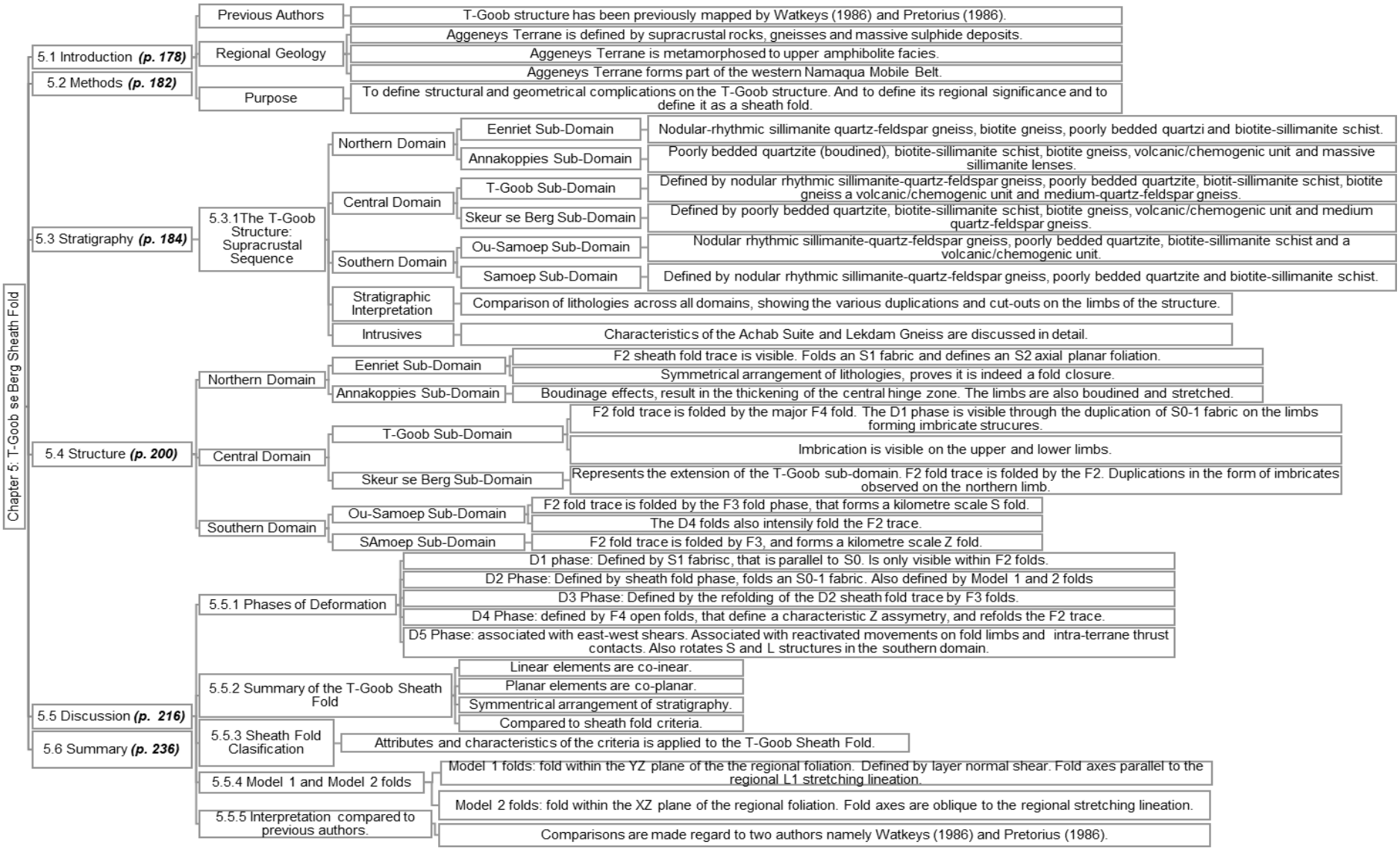

Figure 5.0: Mind map summary of the main aspects covered in Chapter 5.

5.1 Introduction

The T-Goob Structure is located close to the northeastern rim of the Aggeneys Terrane, adjacent to the Pofadder Terrane, and the west of the town of Pofadder in the Northern Cape, South Africa. The T-Goob structure extends along strike for a distance of 121 km, and represents one of the most intricately folded structures found in the Aggeneys Terrane (Figure 5.1).

The Aggeneys Terrane is subdivided from north to south and east to west into four well defined structural domains. Each domain is defined by different syntectonic intrusive granitic sheets (Figure 5.1), and hosts a series of isolated isoclinal structures with double vergence geometries and elliptical ring structures associated with supracrustal sequences. These isolated isoclinal fold structures are defined as sheath folds (Colliston and Schoch, 2002; Colliston and Schoch, 2013). Each structural domain is therefore defined by an intrusive granitic gneiss which surrounds and separates all the isolated sheath fold structures (Chapter 2). Not all the structural domains host sheath folds E.g. Structural Domain 2, that is defined by a well foliated medium quartz-feldspar gneiss (Samoep Gneiss).The structural domains are defined as:

- The Witkoppies Structural Domain (Structural Domain 1), defined by the Witkoppies Suite; that envelops sheath fold structures contained by meta-volcanic and meta-sedimentary successions.
- The Samoep Structural Domain (Structural Domain 2), defined by the Samoep Gneiss and represents a granitic sheet that contains no supracrustal sheath fold units.
- The Lekdam Structural Domain (Structural Domain 3), defined by the Lekdam Gneiss, that surrounds sheath folds containing various meta-sedimentary successions.
- Houmoed Structural Domain (Structural Domain 4) is defined by sheath folds enveloped by the Achab Suite. The augen gneisses which define the Achab Suite also surround supracrustal sequences and massive sulphide ore bodies (Colliston et al., 2012).

The Houmoed Structural Domain, extrapolated toward the western Aggeneys Terrane, was interpreted by Watkeys (1986) to be underlain by the Achab Gneiss. The author has considered the Achab Gneiss to rather be classified as a suite, due to the variations of augen gneiss within the western Aggeneys Terrane (Pretorius, 1986). The T-Goob Structure is located within the Lekdam Structural Domain, and adjacent to the contact with the Houmoed Structural Domain (Figure 5.1).The age dates for the supracrustal rock within the Aggeneys Terrane vary from 1.6 Ga for the Koeris Formation (Reid et al., 1987a) and 2Ga for the Wortel Formation (Colliston et al., 2012) for the Aggeneys Subgroup. The ages given for most of the

supracrustal rocks still remain contentious, as the age dates reflect the time of metamorphism, rather than the age of deposition (Colliston et al., 2012). Age dates for intrusives within the Aggeneys Terrane (1.2Ga), can be correlated with the Little Namaqualand Suite, which reflects a major magmatic event during the Namaqua Orogeny (Colliston et al., 2012; Colliston and Schoch, 2006; Reid 1987). Ages between 1.7-1.3 Ga have been given for the Achab Suite (Watkeys, 1986).

Previous Authors

The T-Goob Structure has previously been mapped by Watkeys (1986) and Pretorius (1986). Pretorius (1986) mapped the northwestern part of the T-Goob Structure, and never correlated the different stratigraphic segments of the T-Goob structure with one another, even though there were similarities. The central sillimanite ore body was also not mapped, together with the intrusive units surrounding the northern limb of the T-Goob structure. The structure was also interpreted to represent a thrust sequence, which branches out towards the northwest. Watkeys (1986) mapped the central part of the T-Goob Structure, and interpreted the T-Goob Structure to represent a thrust zone that separates the supracrustal rocks from the lower Achab Suite, which was interpreted to be basement, and that the Achab Suite intruded a pre-Bushmanland Sequence. However, the stratigraphy was mis-interpreted, specifically on the limbs of the T-Goob structure and also didn't recognise the central hinge zone of the structure. The intrusive units, especially toward the north, was also not considered by Watkeys (1986). The interpretations were also made on assumptions, and not on field mapping, as Watkeys (1986) only mapped 12 km (9%) of the T-Goob Structure, while Pretoruis (1986), mapped 35 km (28%), as compared to the author, who has mapped more than 91km (80%) of the structure, with interpretations made on the northeastern portion of the structure.

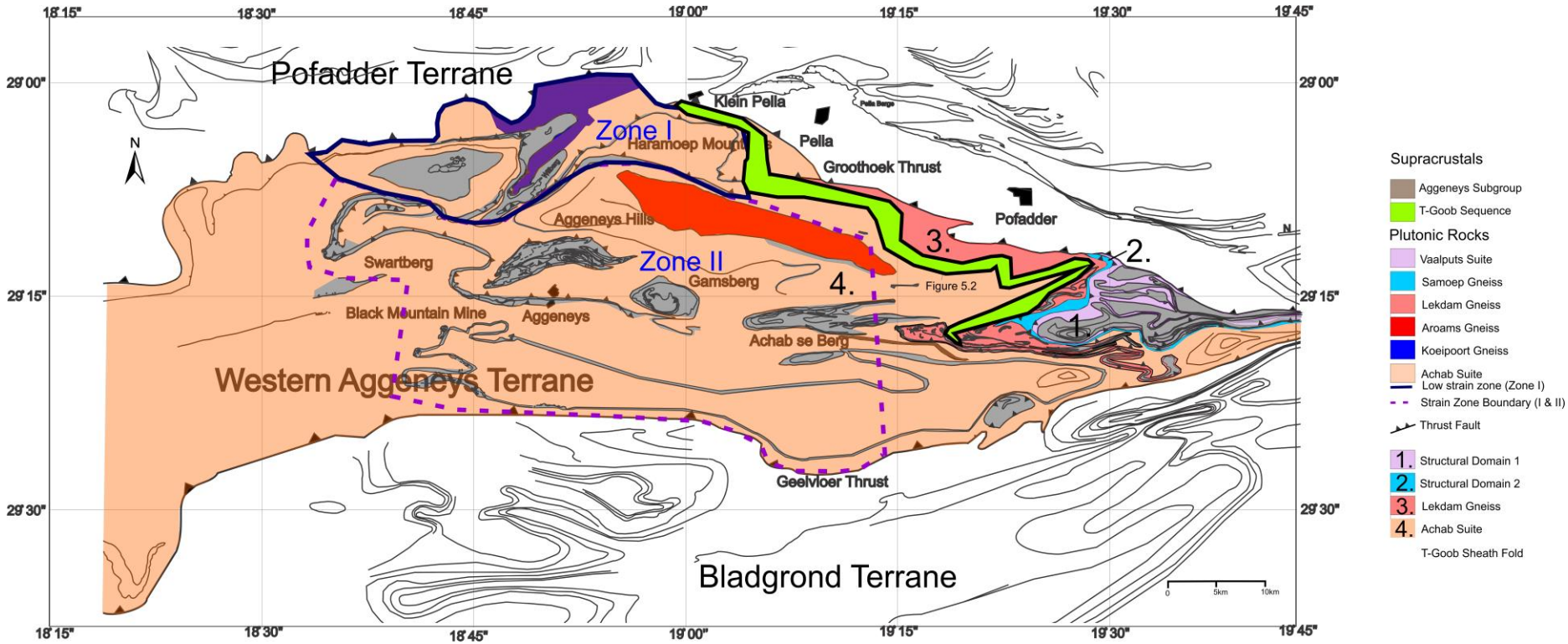

Figure 5.1: Simplified geological map of the western and eastern Aggeneys Terranes. Modifed after Colliston et al., (2012). The lower norther strain domain is also shown in Zone (I) (blue polygon), together with the higher strain zone depicting the zones of fragmented structures, shown in Zone (II)(purple dashed polygon). The T-Goob Structure is also shown just towards the west of the town of Pofadder. The different structural domains (thrust sheets) are also represented by the numbers 1 to 4.

Regional Geology

The Aggeneys Terrane is comprised of gneisses, supracrustal rocks and massive sulphide deposits that have been intensely deformed and metamorphosed to upper amphibolite grade facies (van Zyl, 1986; Pretorius, 1986). The Aggeneys Terrane forms part of the Namaqua Metamorphic Complex and amalgamated during the 1.1-1.2 Ma Namaqua Orogeny (Colliston and Schoch, 2013; Hartnady et al., 1985), which is regarded as a single long-lived compressional deformation event, in which the principal process was progressive ductile shear (Colliston et al., 1991). The Aggeneys Terrane also forms part of one of many tectonostratigraphic terranes defined through the guidelines of Coney et al. (1980), which constitute the western part of the Namaqua Mobile Belt (Colliston and Schoch, 2002; Colliston and Schoch, 2013). Deformation of the terranes took place at middle to lower crust conditions, with the development of a pervasive tectonic fabric found throughout the Aggeneys Terrane; it comprises of a sub-horizontal foliation and northeasterly plunging stretching lineation, that is sub-parallel to the southwestern directed tectonic transport direction (Colliston and Schoch, 2000; Colliston and Schoch, 2002).

The regional foliation is co-planar to the regional banding of supracrustal rocks and is defined by the axial planes of various phases of isoclinal folds, sheath folds, thrusts and mineral foliations. The northeasterly plunging co-linear fabric consists of stretching lineations and fold axes of various phases of folding (Colliston et al., 1991). Within the Aggenys Terrane there is large variation in strain dividing the Aggeneys Terrane in a northerly lower strain domain and a southern zone of higher strain (Figure 5.1), defined by fragmented stratigraphy and sheath fold structures containing massive sulphide deposits (Colliston et al., 2012). This study shows the extension of the high strain zone eastward, characterised by fragmented stratigraphy and sheath folds (Figure 5.1).

Purpose

This chapter is based on new lithological and structural field mapping done on the T-Goob Structure in the eastern sector of the Aggeneys Terrane. The identification of the earliest fold closures were used to establish a stratigraphic framework during regional mapping, as it was used to determine the structural geology from geometrically controlled sections. The data is then integrated with structural field data to place constraints on a sheath fold model for the macroscopic T-Goob Structure and its significance to regional deformation and kinematics. The results illustrate a ductile deformation process of sub-horizontal thrusting associated with penetrative amphibolite grade fabrics (van Zyl, 1986), macroscopic sheath folds and granitoid sheet intrusions.

5.2 Methods

The T-Goob se Berg Structure, was mapped on a scale of 1:20,000, using high resolution air photos supplied by the department of Rural Development. However, in certain domains 1:2,000 and 1:5,000 scale air photographs were used to interpret complexities. Throughout the structure GPS coordinates were also taken for locations/lithologies or structures, which convey important structural and stratigraphic characteristics. The complexity seen within the T-Goob se Berg Structure, makes traditional traverse mapping alone insufficient to unravel the geological complexities seen. Therefore, the method of sequence mapping was used (Colliston et al., 2012) for the interpretation of this structure. During mapping ,diagnostic lithostratigraphic packages are identified and mapped along strike, following the trace of the earliest identifiable fold closure as summarised in Chapter 2.2; Figure 2.3.

The T-Goob Structure will be described from northwest to southeast. For the ease of description the T-Goob structure has been divided into domains and sub-domains moving from northwest to southwest. The structure is divided into a northern, central and southern domain. Each domain is subdivided into various sub-domains (Figure 5.2). The domain subdivision is based on changes of strain, which increase from northwest to southeast. The southern domain, is the zone of highest strain throughout the structure, due to exceptional isoclinal folding and thinning of lithological units. The thickness of stratigraphic units thin out towards the south where not duplicated or cut-out by intra-stratigraphic thrusting. The thickness of the hinge zone of the T-Goob Structure also decreases toward the south east of the structure.

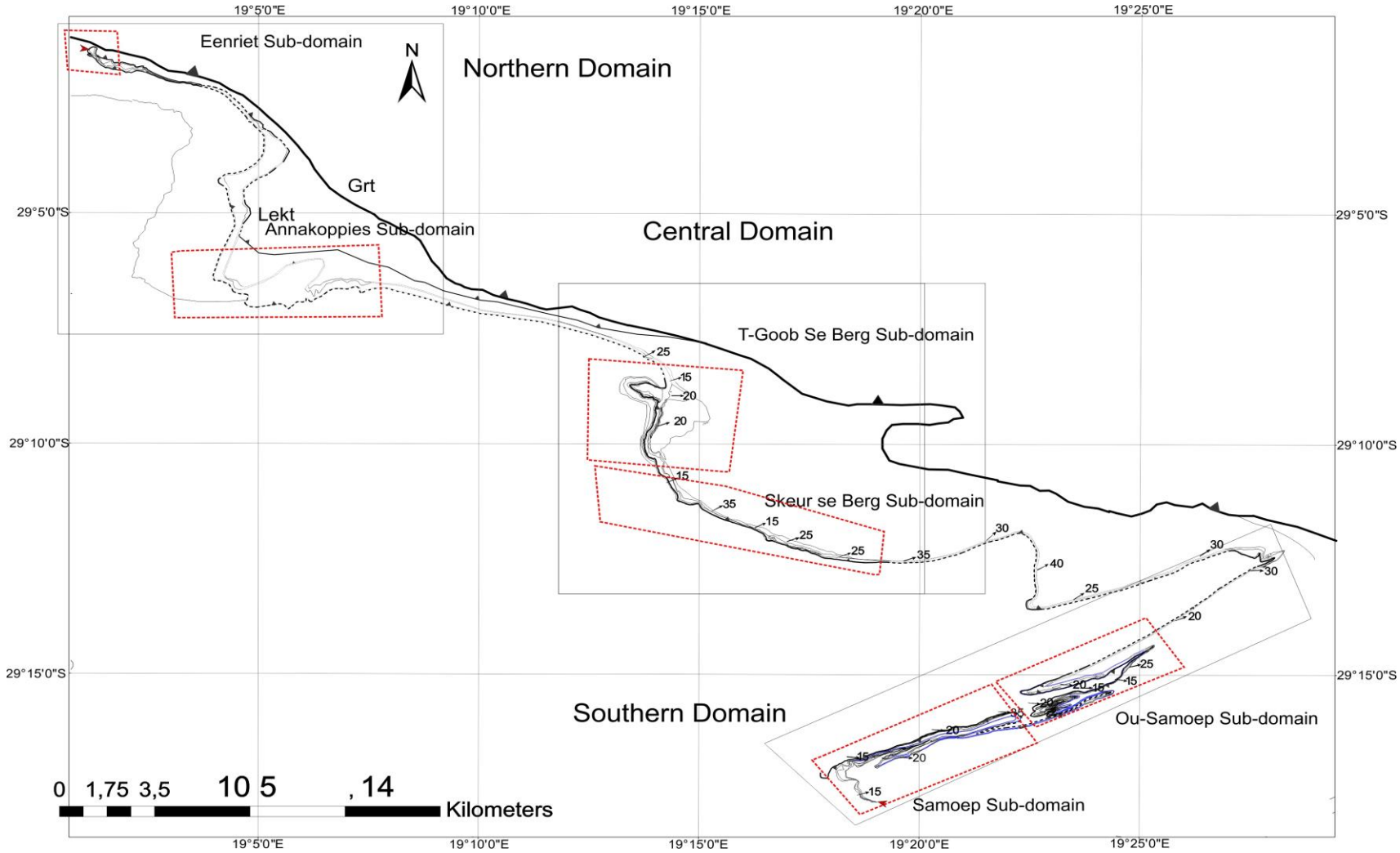

Figure 5.2: Simplified diagram of the T-Goob Structure, showing the division of domains and sub-domains.

5.3 Stratigraphy

5.3.1 The T-Goob Structure: Supracrustal Sequence

The stratigraphic sequence associated with the T-Goob Structure will be discussed per domain and sub-domain as shown in Figure 5.2, and from northwest to southeast across the structure. The lithological characteristics associated with each domain and sub-domain is summarised in Table 5.1. The profile locations associated with the T-Goob Structure can be seen in Figure 5.3, for each domain and sub-domain. A high degree of confidence is associated with the central and southern domains, as all lithologies and intrusives were mapped in detail. However, within the northern domain, a lower degree of confidence is expressed for the Eenriet and Annakoppies Sub-domains. For the Eenriet Sub-domain, only a small part of the hinge zone was mapped to confirm the symmetry of the northwestern fold closure. The rest of the interpretations for the Eenriet and Annakoppies Sub-domains was based on mapping done by Pretorius (1986) and Frik and Coetzee (1974).

Northern Domain

Eenriet Sub-domain

The Eenriet sub-domain is represented by profile A-A', as seen in Figure 5.3. Profile A-A' shows the lithologies seen in the far northwestern fold closure of the structure. The entire sequence is enveloped by the Achab Suite, which is defined by quartz-feldspar augen gneisses ± biotite, together with banded and medium grained variations, which define a well-developed biotite foliation (S1). The regional foliation is co-planar to the banding (S0) within the supracrustal rocks. The mineral assemblages and fabric attributes of the intrusive and supracrustal rocks, together with different rock units is summarised in Table 5.1. The base of the succession is defined by a nodular rhythmic sillimanite-quartz-feldspar gneiss, with interbands of biotite-sillimanite schist that has a sharp contact with the lower Achab Suite. Overlying this unit is a thick succession of biotite gneiss, which is in contact with a poorly bedded quartzite that defines a second order upward coarsening cycle. Lithologies defined by biotite-sillimanite schist and biotite gneiss overly this unit and represents the central hinge of the structure (Figure 5.4; Profile A-A').The nodular rhythmic sillimanite-quartz-feldspar unit, biotite gneiss and poorly bedded quartzite represent the lower southern limb of the fold structure. Most of the units are folded on the northern limb, except for the biotite gneiss unit, which cuts out against the poorly bedded quartzite (Figure 5.4; Profile A-A'). When the structure is 'unfolded' or restored, the defined polarity constitutes the nodular rhythmic sillimanite-quartz-feldspar gneiss at the base, overlain by a biotite gneiss unit and poorly bedded quartzite, with a second order upward coarsening cycle. Overlying the quartzite is the biotite-sillimanite schist unit and biotite gneiss unit that define the upper units.

Table 5.1: Attributes of domains and sub-domains within the T-Goob Structure.

Domain	Rock Type	Mineral Assemblage	Fabrics	Comments
Northern Domain Eenriet Sub-domain (Profile A)	Biotite gneiss, nodular rhythmic sillimanite-quartz-feldspar gneiss, poorly bedded quartzite and biotite-sillimanite schist. Achab Suite: quartz-feldspar augen gneiss ± biotite. Banded variation: Well foliated quartz-feldspar gneis ± biotite.	Supracrustals: Qtz, biotite, sillimanite, feldspar. Intrusive: Biotite, plagioclase, k-feldspar,amphibole.	Foliation: biotite, feldspar, amphibole. Lineation: biotite, feldspar, sillimanite & amphibole.	Eenriet Sub-domain: stratigraphy defines the NW fold closure. Supracrustal rocks are surrounded by the Achab Suite.
Northern Domain Annakoppies Sub-domain (Profile B & C)	Biotite-sillimanite schist, biotite gneiss, volcanoclastic/chemogenic unit comprised of diopside, actinolite and banded quartzite & massive sillimanite. Achab Suite: quartz-feldspar augen gneiss ± biotite. Lekdam Gneiss: Coarse grained quartz-feldspar gneiss ± biotite and muscovite.	Supracrustal rocks: Quartz, biotite, K-feldspar,sillimanite, diopside, actinolite. Intrusive: Biotite, muscovite, k-feldspar, plagioclase, amphibole, garnet.	Foliation: biotite, feldspar, amphibole. Lineation: biotite, feldspar , sillimanite & amphibole.	Annakoppies Sub-domain:The central core of the structure is exposed in the form of a sillimanite ore body. The stratigraphy is boudined resulting in the thickening of lithologies. Supracrustal rocks are surrounded by the Achab Suite and Lekdam Gneiss.
Central Domain T-Goob se Berg Sub-domain (Profile D & E)	Nodular rhythmic sillimanite-quartz-feldspar gneiss, poorly bedded quartzite, biotite-sillimanite schist, biotite gneiss, actinolite, diopside and well foliated medium grained quartz-feldspar gneiss. Achab Suite: quartz-feldspar augen gneiss ± biotite. Banded Variation: Well foliated quartz-feldspar gneiss ± biotite. Lekdam Gneiss: Coarse grained quartz-feldspar gneiss ± biotite and muscovite	Supracrustals: Qtz, biotite, K-feldspar,sillimanite, diopside, actinolite,garnet Intrusive: Biotite, muscovite, k-feldspar, plagioclase amphibole, garnet.	Foliation: biotite, feldspar, diopside, actinolite. Lineation: biotite, feldspar sillimanite, actinolite & diopside.	Goob se Berg Sub-domain: The central hinge of the structure is moderately exposed, with duplications located on the northern and southern limbs of the structure. A prominent well foliated medium-quartz-feldspar gneiss is sandwiched in between lithologies on the northern limb. Supracrustal rocks are surrounded by the Achab Suite and Lekdam Gneiss.

Table 5.2: Attributes of domains and sub-domains of the T-Goob Structure.

Domain	Rock Type	Mineral Assemblage	Fabrics	Comments
Central Domain Skeur se Berg Sub-domain (Profile D & E)	Nodular rhythmic sillimanite-quartz-feldspar gneiss, poorly bedded quartzite, biotite-sillimanite schist, biotite gneiss, actinolite, diopside and well foliated medium grained quartz-feldspar gneiss. Achab Suite: quartz-feldspar augen gneiss ± biotite. Banded Variation: Well foliated quartz-feldspar gneiss ± biotite. Lekdam Gneiss: Coarse grained quartz-feldspar gneiss ± biotite and muscovite.	Supracrustal rocks: Quartz, biotite, K-feldspar, sillimanite, diopside, actinolite, garnet. Intrusive: Biotite, muscovite, k-feldspar, plagioclase amphibole, garnet.	Foliation: biotite, feldspar, diopside, actinolite. Lineation: biotite, feldspar, sillimanite, actinolite & diopside.	Skeur se Berg Sub-Domain: The central hinge of the structure is thinned out when compared to the Goob se Berg Sub-domain. Duplications and cut-outs are seen on the northern limb. Supracrustal rocks are surrounded by the Achab Suite and Lekdam Gneiss..
Southern Domain Ou-Samoep Sub-domain (Profile G)	Nodular rhythmic sillimanite-quartz-feldspar gneiss, biotite gneiss, poorly bedded quartzite, biotite-sillimanite schist, actinolite and diopside. Achab Suite: quartz-feldspar Augen gneiss ± biotite. Banded Variation: Well foliated quartz-feldspar Gneiss± biotite. Lekdam Gneiss: Coarse grained quartz-feldspar gneiss ± biotite and muscovite	Supracrustal rocks: Quartz, biotite, K-feldspar,sillimanite, diopside, actinolite, garnet. Intrusive: Biotite, muscovite, K-feldspar, plagioclase amphibole, garnet.	Foliation: biotite, feldspar, diopside, actinolite. Lineation: biotite, feldspar, sillimanite, actinolite & diopside.	Samoep Sub-domain:Certain lithologies associated with the central hinge zone are missing. The symmetry associated with the stratigraphy represents the limbs and central hinge zone of the southeastern fold closure. Supracrustals are surrounded by the Achab Suite and Lekdam Gneiss..
Southern Domain Samoep Sub-domain (Profile H)	Nodular rhythmic sillimanite-quartz-feldspar gneiss, biotite gneiss, poorly bedded quartzite, biotite-sillimanite schist. actinolite and diopside. Lekdam Gneiss: Coarse grained quartz-feldspar gneiss ± biotite and muscovite.	Supracrustals: Qtz, biotite, K-feldspar,sillimanite. Intrusive: Biotite, muscovite, K-feldspar, plagioclase, garnet.	Foliation: biotite, feldspar. Lineation: biotite, feldspar, sillimanite, actinolite & diopside.	Samoep Sub-domain: Certain lithologies associated with the central hinge zone are missing. The symmetry associated with the stratigraphy represents the limbs and central hinge zone of the southeastern fold closure. Supracrustal rocks are surrounded by the Lekdam Gneiss.

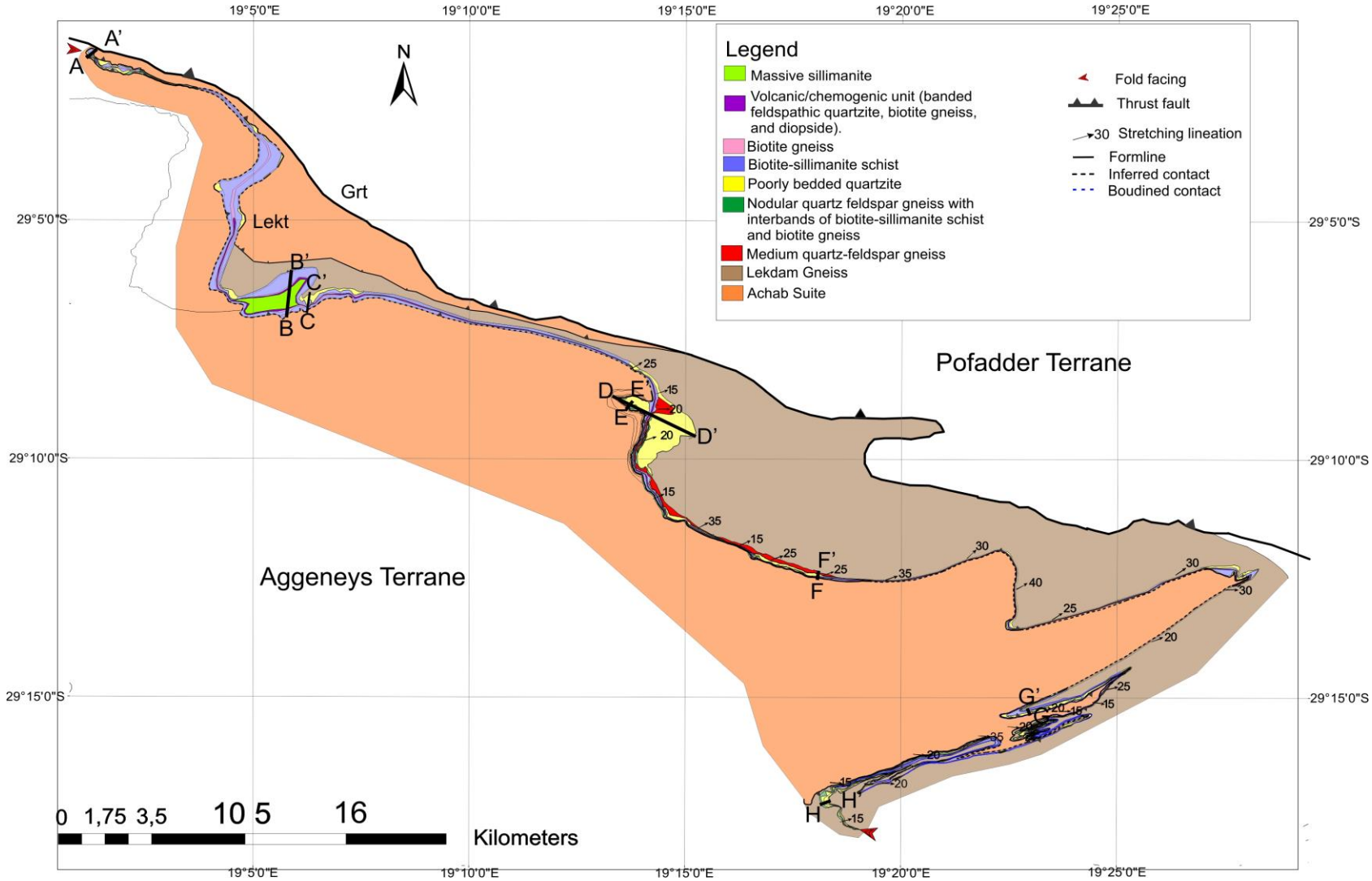

Figure 5.3: Simplified geological map of the T-Goob se Berg Structure, together with the profile locations A to H (Lekt: Lekdam Thrust; Grt: Groothoek Thrust).

Annakoppies Sub-domain

Profiles B-B' and C-C' represent the stratigraphic succession associated with the Annakoppies Sub-domain (Figure 5.3). The profiles are across the central hinge zone/core of the T-Goob Structure, which is defined by a sillimanite body (Frick and Coetzee, 1974; Pretorius, 1986). Both the Achab Suite and the coarse grained Lekdam Gneiss underly and overly the T-Goob Structure. In profile B-B', the Achab Suite has a sharp contact with the overlying supracrustal rocks. Overlying the Achab Suite is a biotite-sillimanite schist, and together with a biotite gneiss unit, is folded on the limb of the structure (Figure 5.4). Overlying the biotite gneiss unit, a volcanoclastic/chemogenic unit is found, defined by diopside and actinolite, together with a thick sequence of massive sillimanite, which defines the central hinge of the structure. The central hinge of the structure at Annakoppies is boudinaged, resulting in the thickening of the central sillimanite ore body. The limb of the structure is defined by biotite-sillimanite schist, together with biotite gneiss, and is found on both the upper and lower limbs of the structure. The defined polarity in Profile B-B' is represented by biotite-sillimanite schist, biotite gneiss and sillimanite ore body, which represents the hinge of the structure (Figure 5.4; Profile B-B').

Profile C-C' is found adjacent to Profile B-B', and is located along a thinned out section of the hinge zone in the core of the T-Goob Structure. The Achab Suite is also found at the base of the structure, which has a sharp contact with an overlying biotite-sillimanite schist unit. Overlying the biotite-sillimanite schist, a biotite gneiss is found together with the volcanoclastic/chemogenic unit. The units on the southern limb also fold around toward the northern limb. However, a complication is found with the presence of a thick poorly bedded quartzite found on the northern limb that is not seen on the southern limb of the structure. The defined polarity is the same as with profile B-B', except for the fact that the central sillimanite ore-body is not present in the central hinge of the structure at profile C-C'. When compared to the Eenriet Sub-domain, the Annakoppies Sub-domain contains a massive sillimanite body, not seen at Eenriet. The nodular rhythmic sillimanite-quartz-feldspar gneiss and poorly bedded quartzites are not seen on the southern limb and on certain sections of the northern limb in the Annakoppies sub-domain.

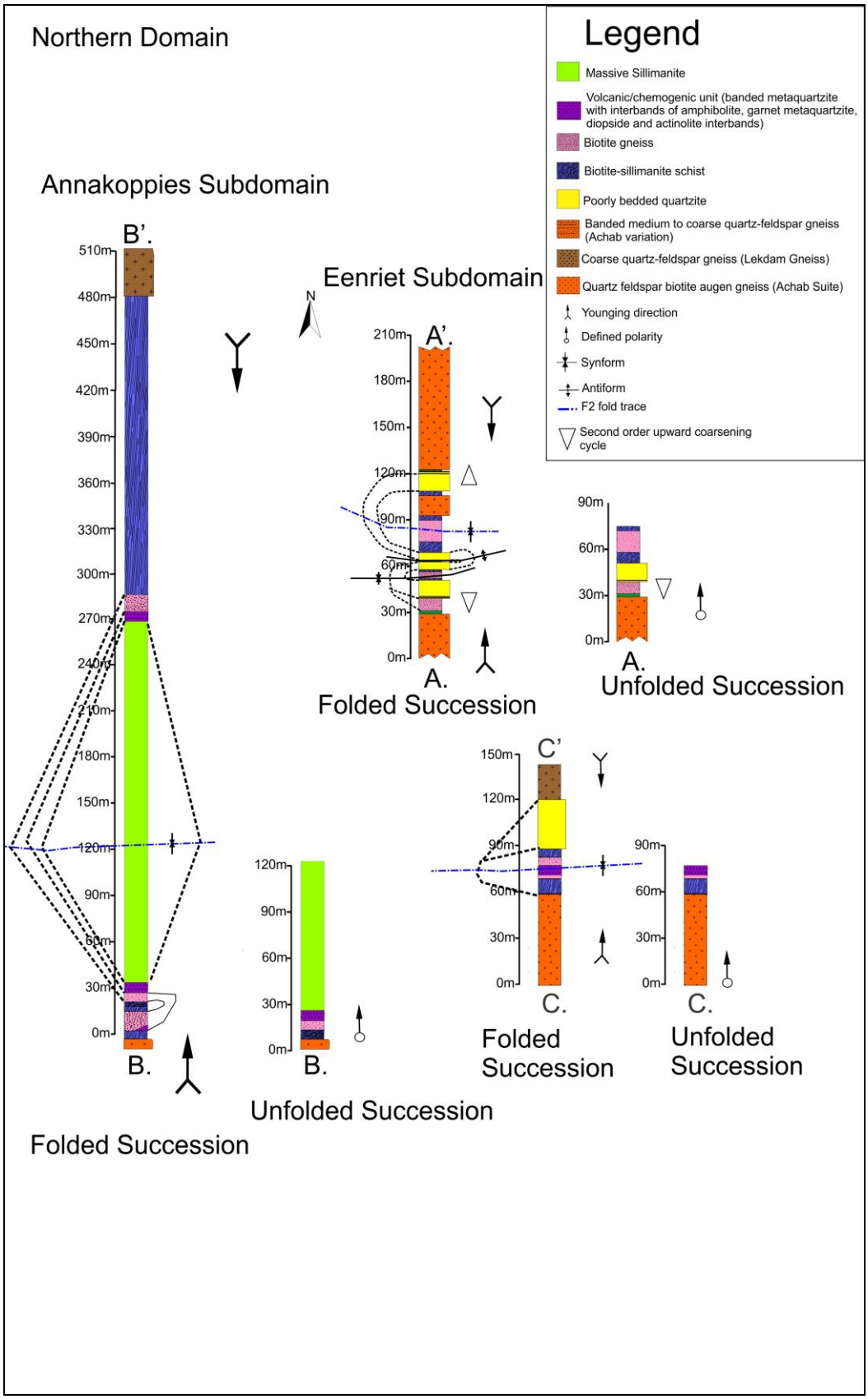

Figure 5.4: Stratigraphic properties associated with the Northern Domain (Profiles A, B and C) of the T-Goob Structure. The folded and restored succession is illustrated for each sub-domain. Profile locations shown in Figure 5.3.

Central Domain

T-Goob se Berg Sub-Domain

The Goob se Berg Sub-domain is represented by Profile D-D' (Figure 5.5), which intersects a part of the T-Goob Structure, in which the stratigraphy is well represented (Figure 5.3). The Achab Suite and Lekdam Gneiss also surround the structure in both the northern and southern limbs. The base of the succession is defined by a well foliated variation of the Achab Suite, and a sharp contact is found with a nodular rhythmic sillimanite-quartz-feldspar gneiss, with interbands of biotite sillimanite schist. A poorly bedded quartzite overlying this unit defines a second order upward coarsening cycle. Overlying the poorly bedded quartzite, a thick succession of biotite-sillimanite schist is found, together with a thick sequence of biotite gneiss. An interbanded volcanoclastic/chemogenic unit is found defined by actinolite, diopside and banded quartzite, which represents the central hinge of the structure. Above the central hinge of the structure a well foliated medium quartz-feldspar gneiss is found, which is not found on the southern limb of the structure. Above this unit, duplicated sets of rhythmic nodular sillimanite-quartz-feldspar gneisses and poorly bedded quartzites are found.

The Lekdam Gneiss overlies the supracrustal rocks on the northern limb of the structure. What is clear within this structure is that the quartzite-nodular units duplicate and are found on the southern and northern limbs of the structure. Profile E-E', which represents an offset profile, depicts the duplications seen on the southern limb regarding the quartzite-nodular rhythmic gneiss units (Figure 5.3 and 5.5). The defined polarity is represented by nodular rhythmic quartz-feldspar gneiss at the base, overlain by a poorly bedded quartzite, above which a biotite-sillimanite schist and biotite gneiss are found. Interbanded within a volcanoclastic/chemogenic unit represented by actinolite, diopside and banded quartzite is found, representing the upper most unit. When compared to the Annakoppies Sub-domain the rocks in the hinge zone are the same. However, duplicated units on the limbs are seen, which are not present within the Annakoppies sub-domain.

Skeur se Berg Sub-Domain

The Skeur se Berg Sub-domain is represented by Profile F-F' (Figure 5.5), and is located 2 kilometres toward the west of the T-Goob Sub-domain (Figure 5.3). The Achab Suite and Lekdam Gneiss also envelope the structure in the northern and southern limbs. The base of the succession is defined by a well foliated variation of the Achab Suite. Above the Achab Suite a poorly bedded quartzite is found defining a prominent upward coarsening cycle. What is apparent is that the nodular rhythmic sillimanite-quartz-feldspar gneiss is not present and has been sheared out. Above the poorly bedded quartzite a biotite sillimanite schist unit is found together with a biotite gneiss unit. Volcanic/chemogenic unit interbanded within the

biotite gneiss on a metre scale is found and defines the central hinge of the structure (Figure 5.5; Profile F-F'). Above the central hinge (biotite schist, biotite gneiss and volcanoclastic/chemogenic unit) a poorly bedded quartzite unit is found, overlain by a nodular rhythmic sillimanite-quartz-feldspar gneiss, and a well foliated medium-quartz-feldspar gneiss. The coarse-grained Lekdam Gneiss overlies the medium-quartz feldspar gneiss. It can be noted that on the limbs of the structure, the quartzite unit folds around the hinge, but is found below the medium quartz-feldspar gneiss and not above it, as seen in Profile F-F'. Units are once again duplicated and cut-out on the northern limb of the structure. The defined polarity is the same as with the T-Goob se Berg Sub-domain, only difference is that the lithological units of the Skeur se Berg Sub-domain is slightly smaller, due to changes in strain, and that the well foliated medium quartz-feldspar gneiss is found above a newly formed poorly bedded quartzite-nodular rhythmic gneiss unit.

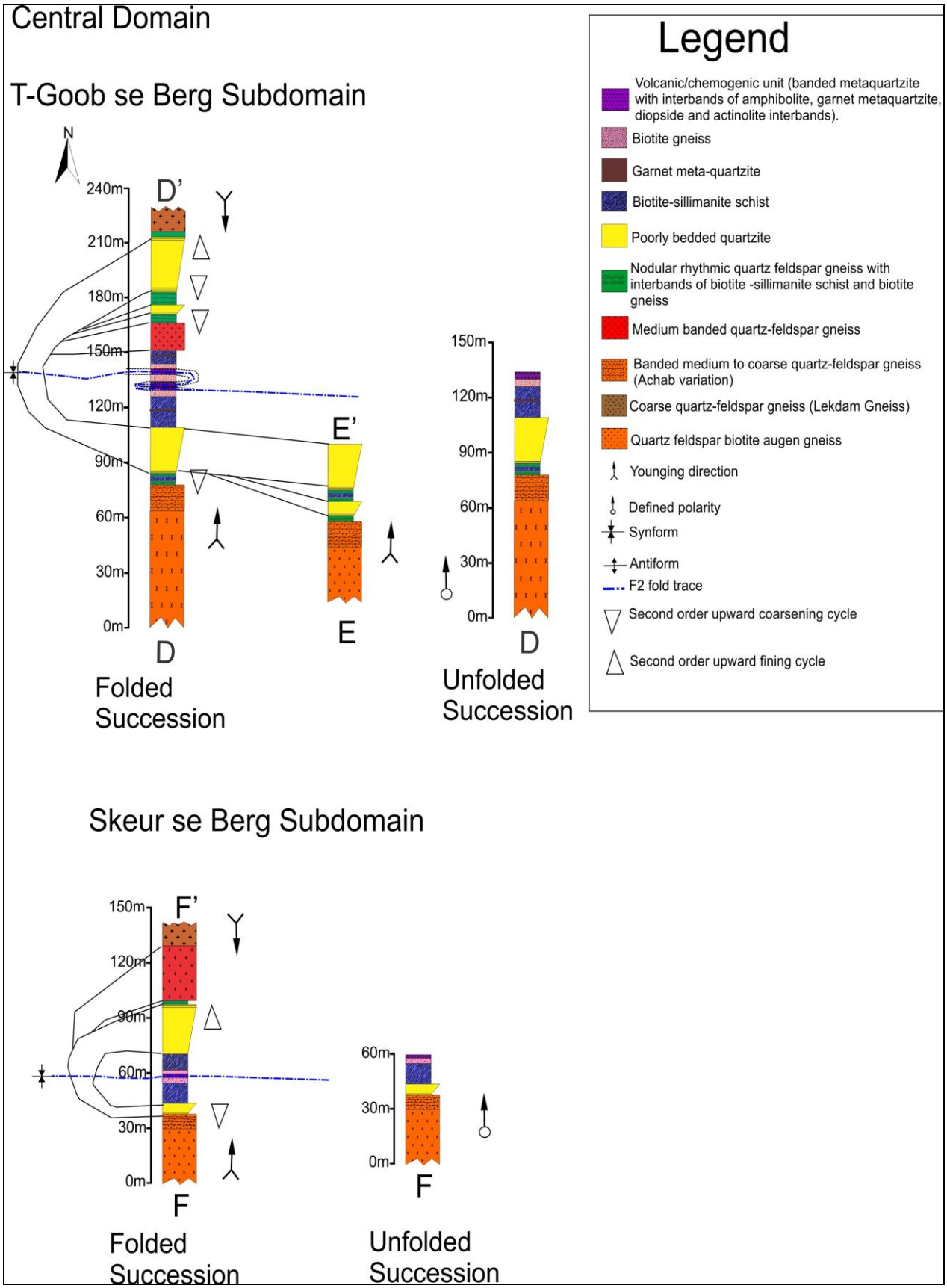

Figure 5.5: Stratigraphic properties associated with the Central Domain of the T-Goob Structure (Profiles D, E and F). The folded and restored successions are illustrated. The profile locations are shown in Figure 5.3.

Southern Domain

Ou-Samoep Sub-Domain

The Ou-Samoep Sub-domain is represented by Profile G-G' (Figure 5.3 and Figure 5.6), which is found in a higher strain zone than the sub-domains seen in the northern and central domains. The base of the succession is defined by well foliated Achab Suite, above which a sharp contact is found with a metre scale unit of biotite gneiss, in contact with a nodular rhythmic sillimanite-quartz-feldspar gneiss (Figure 5.6; Profile G-G'). Towards the west of Profile G-G' the Lekdam Gneiss is 'sandwiched' in between the contact with the Achab Suite and is boudinaged along strike. A poorly bedded quartzite is found above the nodular rhythmic sillimanite quartz-feldspar gneiss, and defines a second order upward coarsening cycle. Overlying the poorly bedded quartzite a thick sequence of biotite-sillimanite schist is found, above which a biotite gneiss is found with an interbedded centimetre scale volcanoclastic/chemogenic unit, which defines the central hinge of the structure (Figure 5.6). The poorly bedded quartzite folds around the hinge of the structure, but is thinned out on the northern limb, while the nodular rhythmic sillimanite-quartz-feldspar gneiss is cut out. Above the upper quartzite on the northern limb the coarse-grained Lekdam Gneiss is found. The defined polarity is represented by biotite gneiss, nodular rhythmic sillimanite-quartz-feldspar gneiss, overlain by a poorly bedded quartzite, above which a biotite-sillimanite schist is found. Above the biotite-sillimanite schist a metre scale biotite gneiss is found, with an interbanded volcanoclastic/chemogenic unit at the top of the succession (Figure 5.6; Profile G-G').

Samoep Sub-Domain

The Samoep Sub-domain is represented by Profile H-H', which represents a section of the southeastern fold closure associated with the T-Goob Structure (Figure 5.3 and Figure 5.6). The Lekdam Gneiss also completely surrounds the lithologies within the Samoep Domain. The base of the succession is defined by a thick sequence of nodular rhythmic sillimanite-quartz-feldspar gneiss, which has a sharp contact with the lower Lekdam Gneiss. Overlying the nodular rhythmic sillimanite-quartz-feldspar gneiss is a poorly bedded quartzite defining a second order upward coarsening cycle (Figure 5.6; Profile H-H'). Biotite-sillimanite schist is interbanded within the poorly bedded quartzite, which defines the central hinge of the structure. What is evident is that the biotite gneiss and volcanoclastic/chemogenic unit are missing within the central hinge zone of the structure. Above the biotite-sillimanite schist unit another poorly bedded quartzite is found, defining the northern limb of the structure. Overlying the poorly bedded quartzite unit is another nodular sillimanite-quartz-feldspar gneiss, found on the northern limb. This results in a well-defined symmetry with regard to the southeastern fold closure. The defined polarity is represented by a nodular rhythmic sillimanite-quartz-

feldspar gneiss at the base, overlain by a poorly bedded quartzite defining a second order upward coarsening cycle. The top unit is defined by a biotite-sillimanite schist, which also represents the hinge zone. What is evident is that the central biotite gneiss and volcanoclastic/chemogenic unit are not present within the hinge zone. The units are also smaller and dramatically thinned out when compared to the northern and central domains (Figure 5.6).

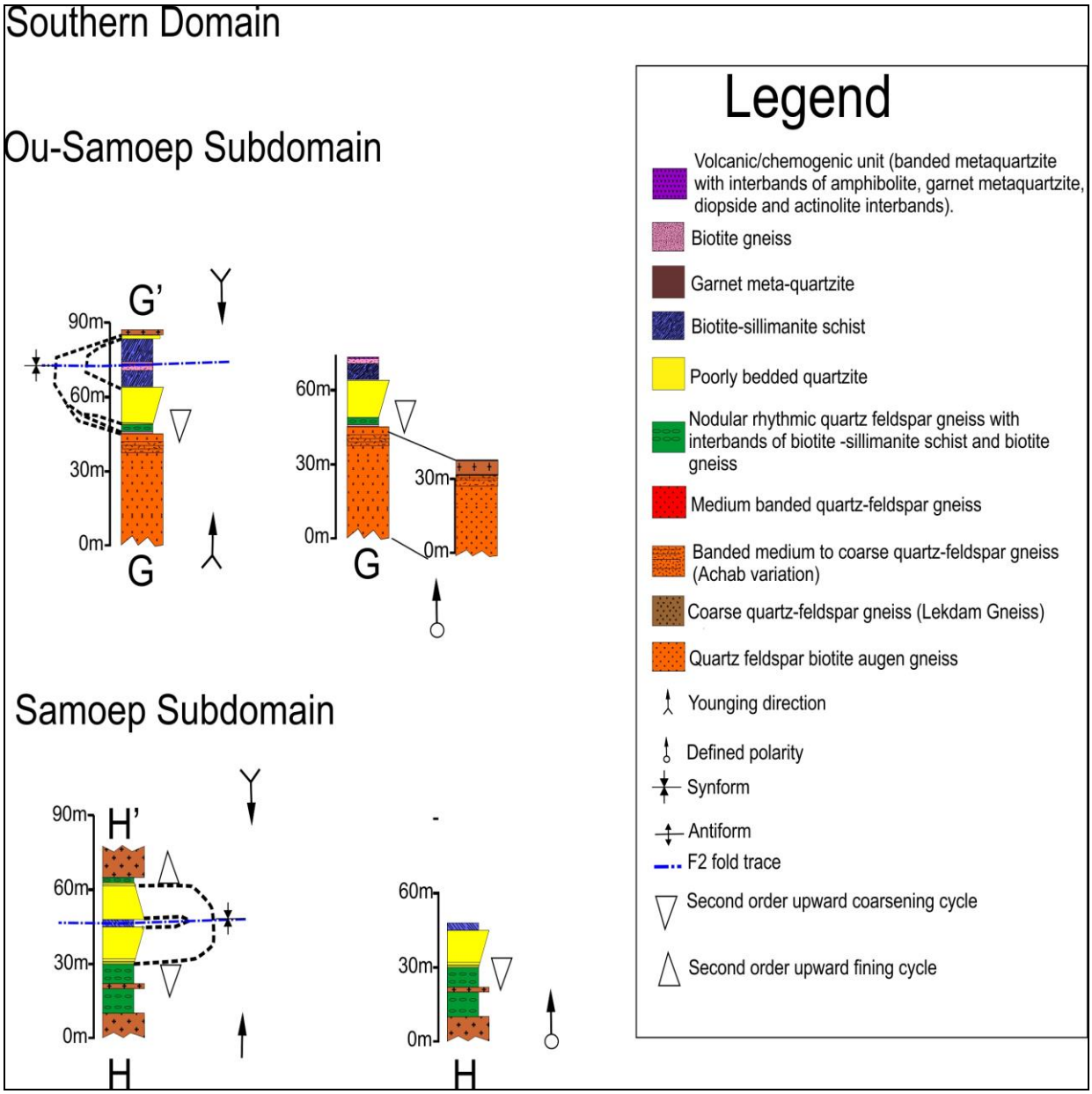

Figure 5.6: The stratigraphic properties associated with the Southern Domain (Profiles G and H). The folded and restored successions are represented. The profile locations can be seen in Figure 5.3.

Stratigraphic Interpretation

When all the profiles associated with each sub-domain are horizontally restored, it is clear that the lithologies within the hinge zone remain consistent throughout the structure from northwest to southeast (Figure 5.7). Throughout the structure the hinge zone is defined by a sillimanite ore body in the centre, surrounded by banded volcanoclastic/chemogenic unit that is defined by banded quartzite, actinolite and diopside (Figure 5.8 A). Surrounding the central volcanoclastic unit, a prominent unit of biotite gneiss is found (Figure 5.8 B), together with biotite sillimanite schist with interbanded lenses of garnet bearing meta-quartzite (Figure 5.8 C and D). The lithologies of the central hinge zone can be found consistently along strike, except for the sillimanite ore body which is only found within the Annakoppies Sub-domain (Figure 5.7). The central hinge zone units also thin out dramatically towards the south of the structure, due to increase in strain (Figure 5.7). The lithologies from northwest to southeast thin out dramatically, due to increase in strain from north to south, with the southern domain representing the zone of highest strain. Lithologies duplicate and cut-out both on the northern and southern limb due to thrusting, this is well expressed in the poorly bedded quartzite units, which often define second order upward coarsening cycles and nodular rhythmic sillimanite-quartz-feldspar gneiss units (Figure 5.8 E and F), and is well expressed in the central domain of the structure (Figure 5.7). The most prominent duplications are seen on the northern limb in the T-Goob Sub-domain. A pronounced well foliated medium-quartz-feldspar gneiss is also found on the northern limb of the structure, and nowhere else throughout the structure (Figure 5.7 and 5.8 G). The symmetry associated with the northwestern and southeastern fold closures is well presented, providing lithological evidence for the presence of fold closures (Figure 5.7). The defined polarity and younging direction coincide throughout the structure, showing 'younging' toward the axial plane of the structure, with cross bedding, identified within the volcanoclastic/chemogenic unit (Figure 5.8 H).

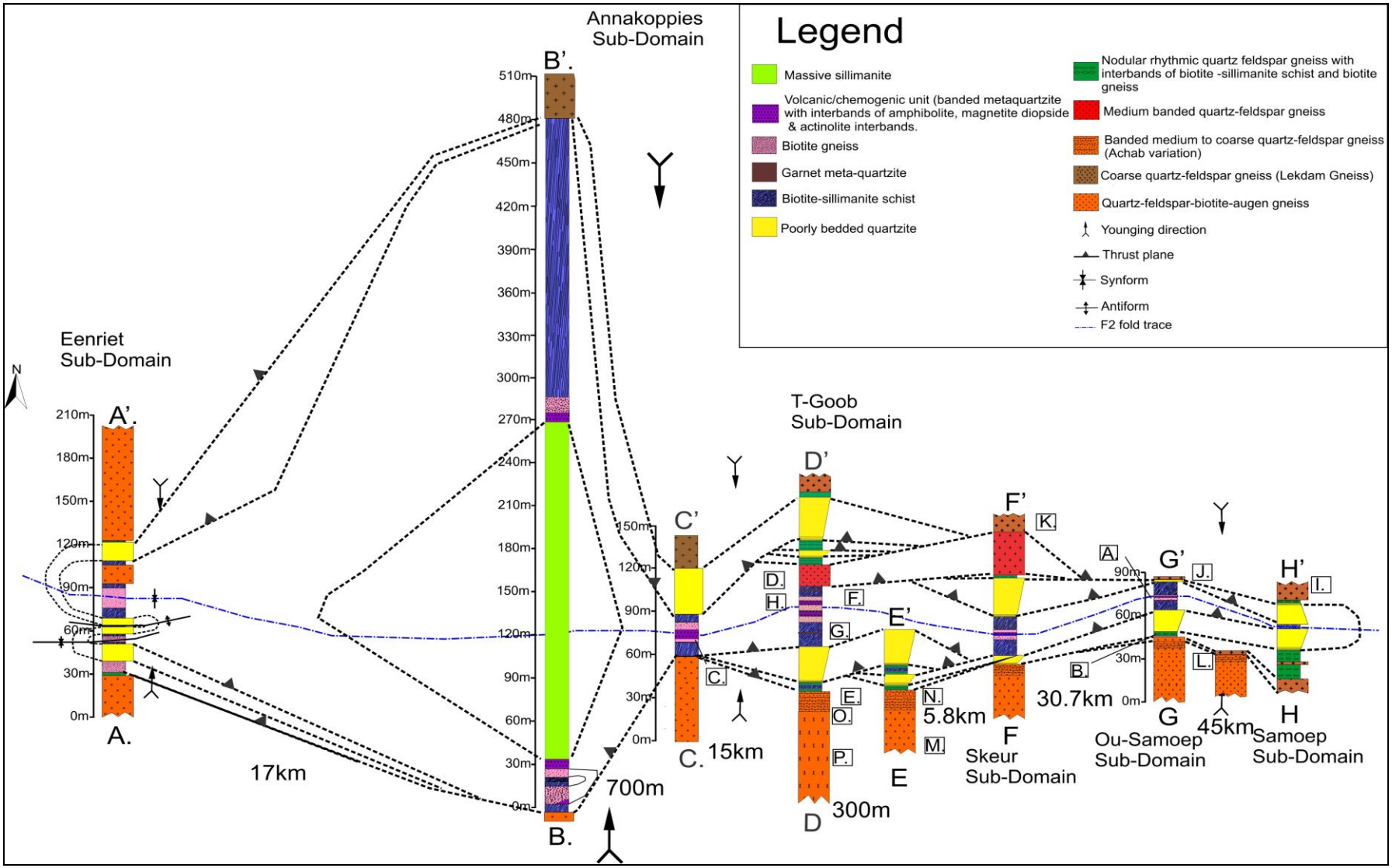

Figure 5.7: Stratigraphic interpretation of the D2 T-Goob Structure. The D3 and D4 phases of deformation have been removed. The profile locations can be seen in Figure 5.3. The small letters are the locations of photographs asspciated with the stratigraphy and intrusives throughout the study area, and can be seen in Figures 5.8 and 5.9.

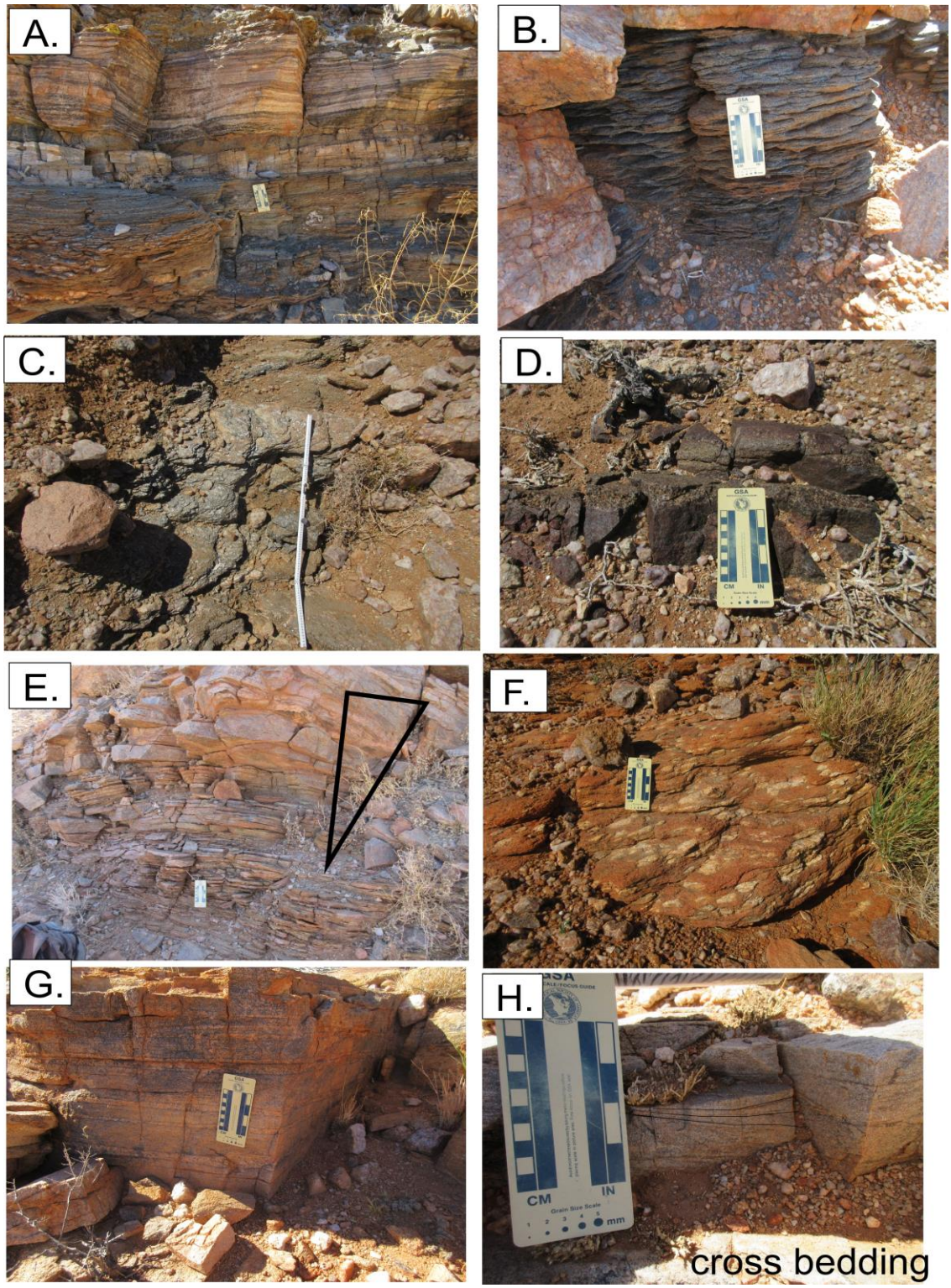

Figure 5.8: Stratigraphic photographs associated with the T-Goob Structure, the locations of the photographs can be seen in Figure 5.7. A: Volcanic/chemogenic unit defined by banded quartzite, diopside and actinolite, found within the central hinge of the structure. B: Well foliated biotite gneiss associated with the central hinge zone of the structure. C: Biotite-sillimanite schist often found in the central hinge of the structure. D: Garnet meta-quartzite interbanded within the biotite-sillimanite schist unit, and found surrounding the central hinge of the structure. E: Contact between the nodular rhythmic sillimanite-quartz-feldspar gneiss and poorly bedded quartzite, defining a second order upward coarsening cycle, on the lower limb of the structure. F: Nodular rhythmic sillimanite-quartz-feldspar gneiss found on the limbs of the structure. Prominent ellipsoidal sillimanite nodules are associated with this unit. G: Well foliated medium quartz-feldspar gneiss found on the northern limb of the structure. H: Cross bedding within the volcanoclastic/chemogenic unit, displayed within a feldspathic quartzite unit.

Intrusive rocks

Across the T-Goob Structure two prominent intrusive units are found, namely the Lekdam Gneiss and Achab Suite (Figure 5.3). Both intrusive units fold around the structure, with the Lekdam Gneiss enclosing the structure in the south and the Achab Suite enveloping the structure in the north (Figure 5.3). The contact represent an intra-terrane thrust boundary that is also folded by the T-Goob Structure. The Lekdam is located on the northern limb of the structure throughout the central and southern domains, and surrounds the southern fold closure of the structure. The Lekdam Gneiss is defined as a poorly foliated coarse-grained quartz-feldspar gneiss ± biotite and muscovite. The gneiss has a massive grey appearance (Figure 5.9 I), and when weathered, has a reddish-pink appearance. The Lekdam Gneiss is also associated with late-syntectonic to post-tectonic growths of garnet. The garnet minerals often give the gneiss a speckled appearance (Figure 5.9 J). The S1 foliation is often associated with biotite and muscovite, is at certain locations not well developed. The Lekdam Gneiss also contains xenoliths of biotite gneiss and rythmic-nodular gneiss associated with the T-Goob Structure (Figure 5.9 K).The Achab Suite is located on the southern limb of the T-Goob Structure (Northern, Central and Southern Domains) and surrounds the northwestern fold closure (Figure 5.3). The Achab Suite has been previously mapped by Watkeys (1986) and Pretorius (1986). Watkeys (1986) mapped the Achab Suite within the central domain and named it the Achab Gneiss. The Achab suite was interpreted to be the basement to a 'pre-Bushmanland' Sequence. However the Achab Suite was only mapped on the southern limb of the structure, and the textural variation across the Aggeneys Terrane was not considered. Pretorius (1986) mapped variations of the Achab Suite along the southern limb of the T-Goob Structure. Pretorius (1986), however, never considered the units on the northern limb of the structure and its extension toward the east, as well as its tectonic significance regionally. The Achab Suite can be classified in general as quartz-feldspar augen gneisses ± biotite and amphibolite (Figure 5.9 L)

The Achab Suite has a hetreogeneous character due to changes in strain, with banded variations, flattened variations seen in high strain zones (Figure 5.9 M & N). This can be noted on the southern limb of the structure, specifiically in the central and southern domains. On microscopic scale, minerals like quartz, plagioclase, k-feldspar, with accessory minerals of biotite and amphibolite, have been identified (Pretorius, 1986). The Achab Suite also contains xenoliths of the various supracrustal rocks it surrounds in the T-Goob Structure. (Figure 5.9 O). The Lekdam Gneiss and Achab Suite have a sharp contact with one another, which is well exposed on the southern limb of the structure, within the southern domain (Figure 5.9 P). However, along strike the Lekdam Gneiss is cut out on the intra-terrane thrust contact, with only slivers being exposed as you move toward the north of the structure. The Achab Suite

and Lekdam Gneiss are interpreted to cut out against the Groothoek Thrust on the northern limb of the T-Goob Structure (Figure 5.3).

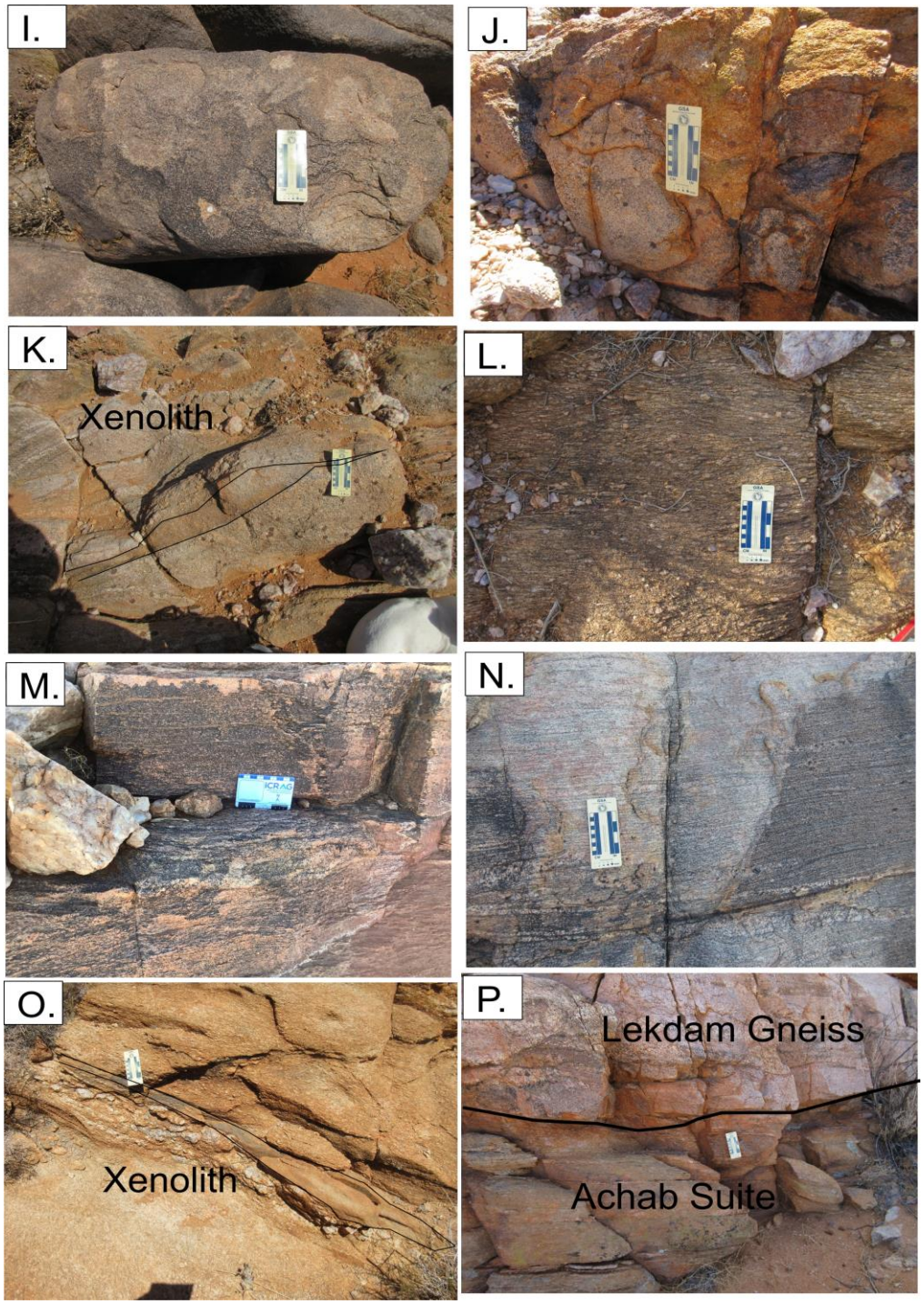

Figure 5.9: Photographs associated with the Lekdam Gneiss and Achab Suite. I: Poorly foliated massive grey appearance synonymous with the Lekdam Gneiss. J: Reddish appearance of the Lekdam Gneiss, with garnet overgrowths associated with the Lekdam Gneiss, giving it a speckled appearance. K: Xenolith of biotite gneiss found within the biotite gneiss on the northern limb of the T-Goob Structure. L: Quartz-feldspar augen gneiss ± biotite associated with the Achab Suite. M: Flattened banded variation of the Achab Suite within high strain zones of the Achab Suite on the southern limb of the structure. N: Well foliated variation of the Achab Gneiss, alsp located within a high strain zone within the southern limb of the T-Goob Structure. O: Xenolith of biotite gneiss found within the Achab Suite on the southern limb of the T-Goob Structure. P: Sharp contact between the Lekdam Gneiss and Achab Suite on the southern limb of the T-Goob Structure within the Samoep Sub-domain.

5.4 Structure

Sequence mapping (see methodology, Chapter 2.2.1) and comprehensive stratigraphy (see Stratigraphy, Figure 5.7), were critical in unravelling the 121 km complexly deformed macroscopic double vergent isoclinal fold structure (Figure 5.10). The exposed structural architecture of the T-Goob fold structure is that of a package of metasediments/metavolcanic lithologies sandwiched between sheets of Achab and Lekdam orthogneiss. The double vergent isocline has closures in the north at the Eenriet Subdomain and in the southeast within the Samoep Sub-domain (Figure 5.10). The change in NW-strike of the axial plane trace is due to the late folding (D4) deforming the axial plane trace into antiforms and synforms with large wavelengths and easterly trending axial traces (Figure 5.10). The new structural sequence description that follows the map of the T-Goob structure is sub-divided into a number of domains/sub-domains namely; the northern domain, central domain and southern domain (Figure 5.2), where the structure, stratigraphy, fabrics and kinematics of each domain is described from northwest to southeast. Geometrically constrained geological sections (cross and long sections) are presented as a series of exploded sections in Figure 5.18 and Appendix 5.1 to show the structural pattern along the strike of the macroscopic isocline. The locations of the structural sections can be viewed in Figure 5.10 and Appendix 5.1. The evolution of the structural features and the controls on the structural development by the lithological framework are described. The Geometric properties are summarised in Table 5.3 and Table 5.4.

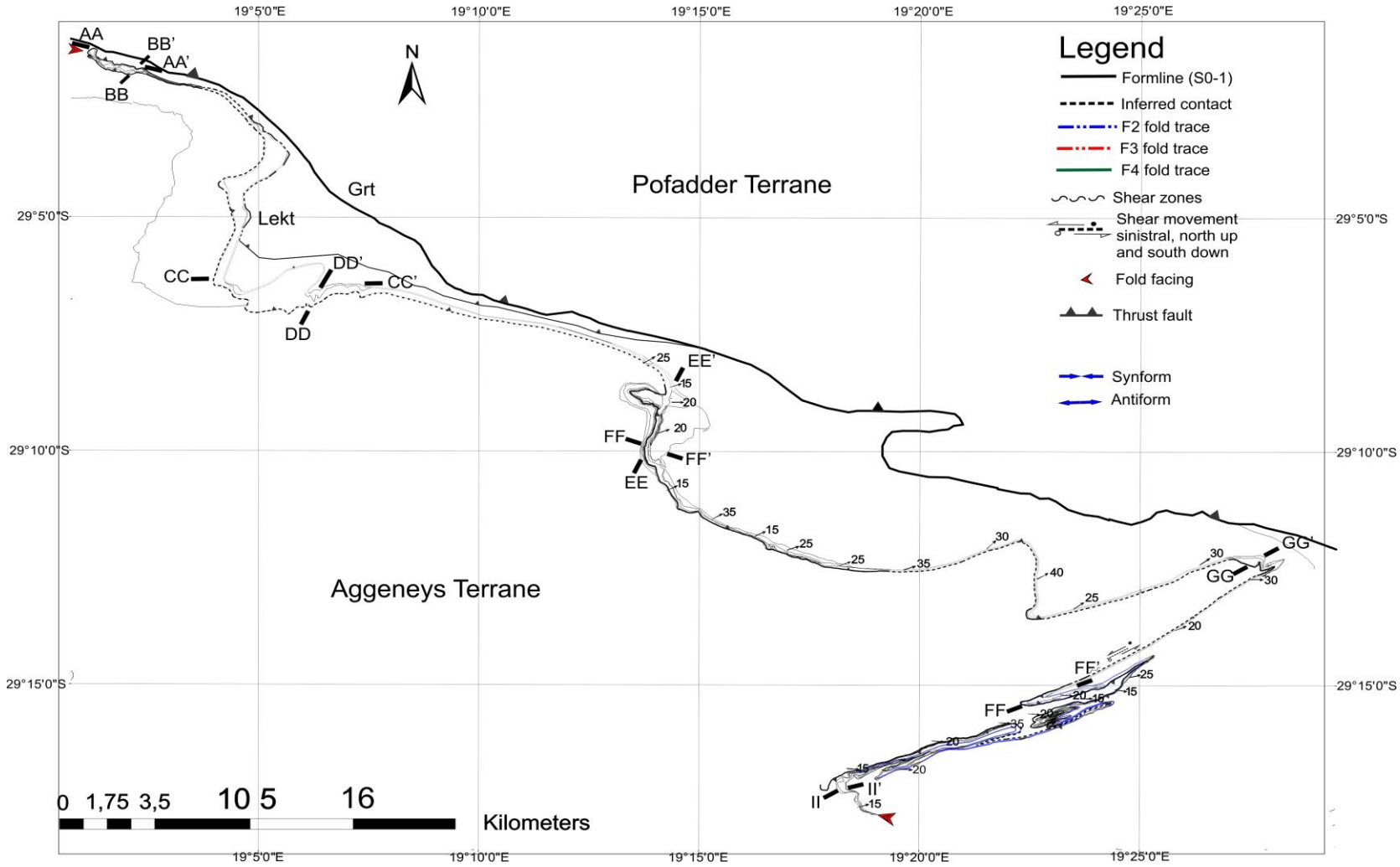

Figure 5.10: Simplified formline map associated with the T-Goob Structure. The fold traces, domains, sub-domains and section locations (AA-II) are illustrated. The section details can be seen in Appendix 5.1 and Figure 5.18.

Table 5.3: Summary of geometric data associated with the northern and central domains. The Annakoppies Sub-domain is the only sub-domain where no geometric data could be collected.

Domain	Regional Foliation	Regional Lineation	F2 folds	F3 folds	F4 folds
Eenriet Sub-domain	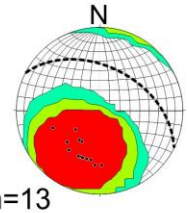 n=13	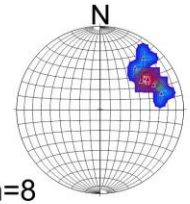 n=8	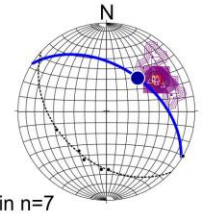 Lin n=7 Stretching Lineation F2 Fold axis Poles to bedding F2 axial Plane Eenriet Fold closure		
T-Goob Sub-domain	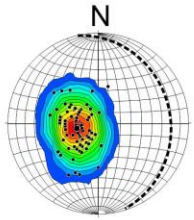 n=80	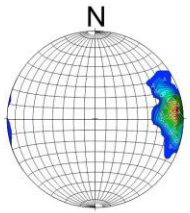 Lin=31			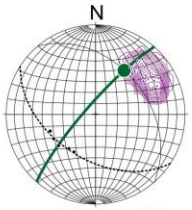 Lin n=26 Stretching Lineation F4 Fold axis Poles to bedding F4 axial Plane
Skeur se Berg Sub-domain	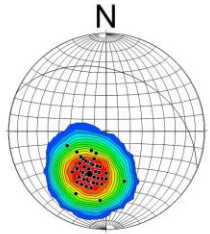 n=77	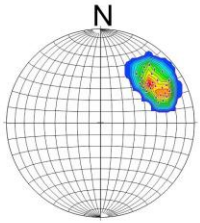 Lin n=26			

Table 5. 4: Summary of the geometric data associated with the southern domains of the T-Goob Structure.

Domain	Regional Foliation	Regional Lineation	F2 folds	F3 folds	F4 folds
Ou-Samoep Sub-domain	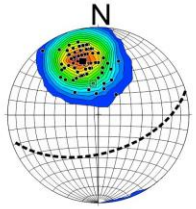 n=106	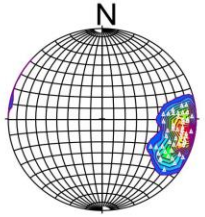 Lin n=61		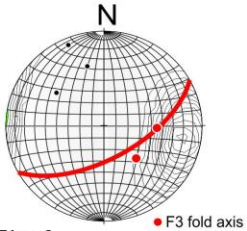 FA n=3 Lin n=66 F3 fold axis F3 axial plane poles to the axial planes	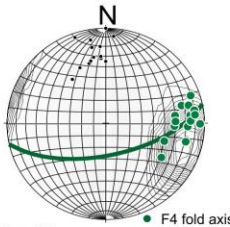 FA n=15 Lin n=98 F4 fold axis F4 axial plane poles to the axial planes
Samoep Sub-domain	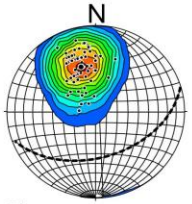 n=54	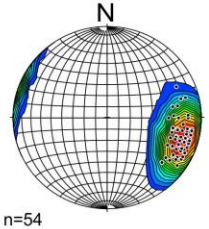 n=54		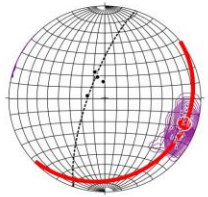 Lin n=21	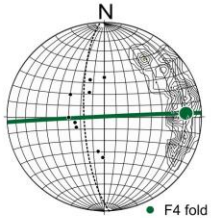 Lin n=23 F4 fold axis F4 axial plane poles to the axial planes
	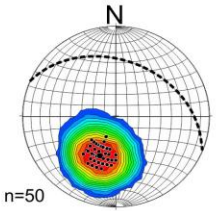 n=50 Lekdam F2 closure	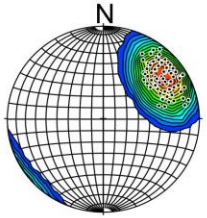 n=66 Lekdam F2 closure	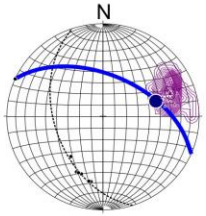 Lin n=15 Lekdam F2 closure		

Northern Domain

Eenriet Sub-domain

The Eenriet Sub-domain represents the far northwestern fold closure of the T-Goob Structure (Figure 5.10, section AA-AA' & BB-BB'; Appendix 5.1). The Eenriet fold closure is defined as a synformal F2 sheath fold closure, that folds an S0//S1 foliation and has a penetrative S2 axial planar foliation (Figure 5.12 A). The S2 axial planar foliation represents the regional S2 foliation seen across the structure. Macroscopic S and Z folds, and mesoscopic model 1 folds (Chapter 3.1.1) are parasitic to the larger F2 fold closure, and fold within the YZ planes of the regional foliation (Figure 5.12 C and D). Model 2 folds are also found within the XZ planes of the regional foliation (Figure 5.12 B). The macroscopic F2 sheath fold axes plunge toward the northeast and are co-linear to the regional L1 stretching lineation, defined by feldspar aggregates, sillimanite needles, nodules and biotite. The F2 axial plane dips moderately toward the northeast, and is sub-parallel to the regional S1//S2 foliation (Table 5.3; Eenriet Sub-domain). In section the hinge zone is well represented, with biotite-sillimanite schist and biotite gneiss found in the centre of the structure (Appendix 5.1, Section AA-AA'; BB-BB'). The poorly bedded quartzites and nodular rhythmic gneiss units which define the limbs of the structure, are folded around the central hinge. The thick biotite gneiss unit on the lower limb can be seen cutting out against the upper quartzite. The central hinge zone starts to thin westward. The Achab Suite envelopes the northwestern fold hinge, defines a sharp contact with the overlying supracrustal rocks (Appendix 5.1, Section AA-AA'). The Lekdam thrust, also folds around the Eenriet fold closure in the northwest (Appendix 5.1, Section AA-AA'; Figure 5.18). The fold facing of the structure which is defined as "the direction perpendicular to the fold axis, within the axial plane, towards the younger rocks" (Shackleton, 1958), faces towards the southeast. The fold facing shows younging towards the axial plane of the synformal F2 sheath fold closure.

Annakoppies Sub-domain

The Annakoppies Sub domain (Figure 5.10 section CC-CC' and BB-BB', Appendix 5.1), represents a section of the structure, where the stratigraphy is thickened, due to boudinage effects across the study area (Appendix 5.1, section CC-CC' and DD-DD'). The central core of the T-Goob structure is exposed in the Annakoppies Sub-domain by a large sillimanite body, which defines the central 'eye'(core) of the structure. The core of the structure reflects an irregular 'omega' structure that closes off on both sides toward the east and west. The central core of the sillimanite body is enveloped by the volcanoclastic/chemogenic unit, biotite gneiss and biotite-sillimanite schist units. On the lower southern limb, the poorly bedded quartzite and nodular rhythmic gneiss unit have been cut out. On the northern limb, thick poorly bedded

quartzites are found with no nodular rhythmic sillimanite-quartz-feldspar gneiss units, and thick poorly bedded quartzites are boudinaged and fragmented, with the nodular rhythmic sillimanite-quartz-feldspar gneiss units being absent. On the southern and northern limb of the structure; parasitic Z folds are found within the lithologies of the central hinge of the structure (Appendix 5.1, Section CC-CC'). The lithologies are symmetrical and fold around the hinge zone of the structure, while lithologies on the northern and southern limbs are cut-out and boudinaged. The Lekdam Thrust is also found on the southern limb of the structure at Annakoppies, representing the intra-terrane thrust contact. In section, the Lekdam Thrust cuts out the Lekdam Gneiss around the D2 hinge zone of the structure (Appendix 5.1 Section DD-DD').

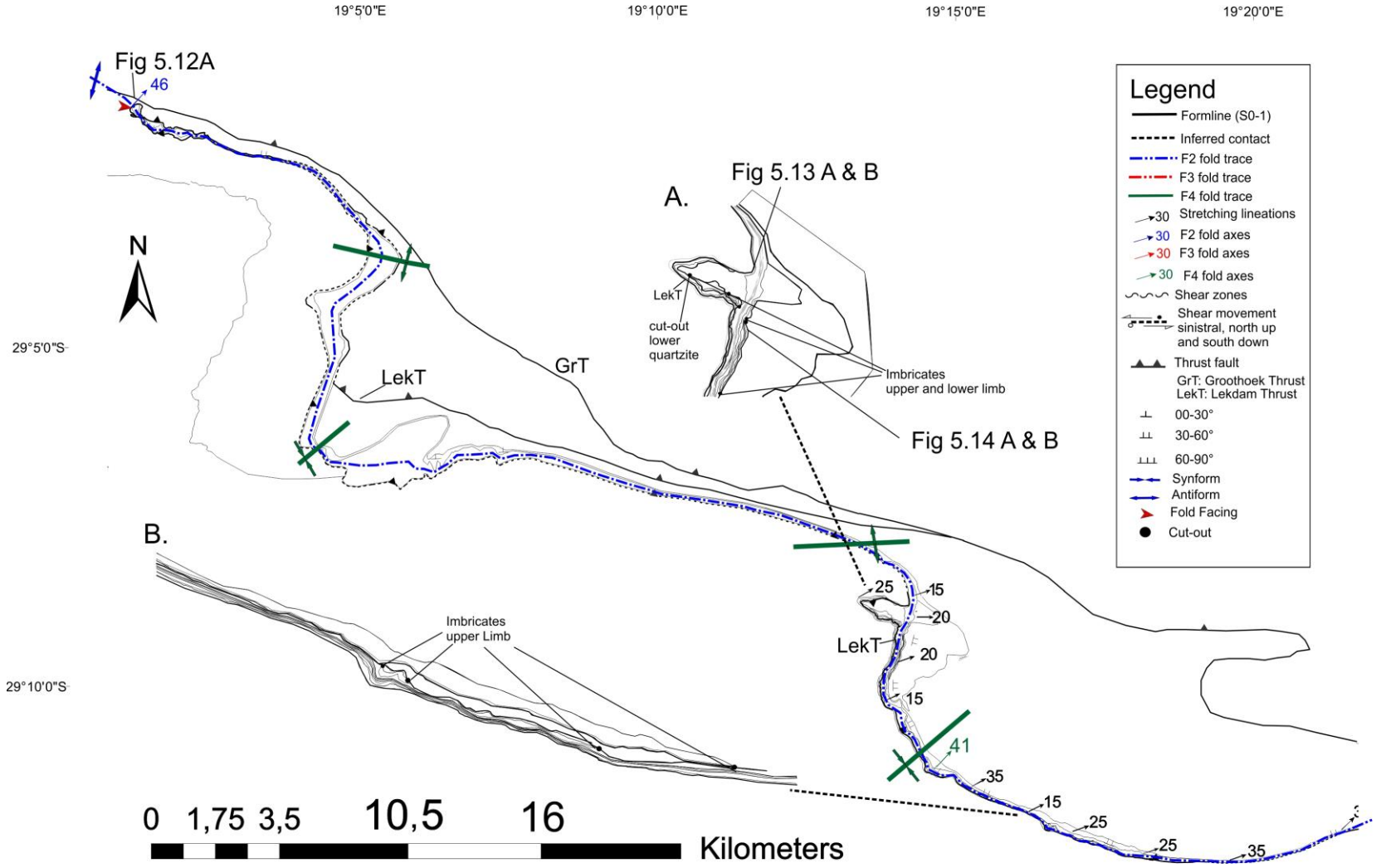

Figure 5. 11: Structural formline associated with the Northern Domain of the T-Goob Structure. The fold axes, fold traces and stretching lineations are illustrated.. Figure A: Blow-up diagram of the northern section of the T-Goob Sub-domain, showing the various imbricate structures found on the upper and lower limb of the structure. Figure B: Imbricate structures found on the upper northern limb associated with the Skeur se Berg Sub-domain. The locations of relevant photographs in Figure 5.12; 5.13 and 5.14 are also represented in the diagram.

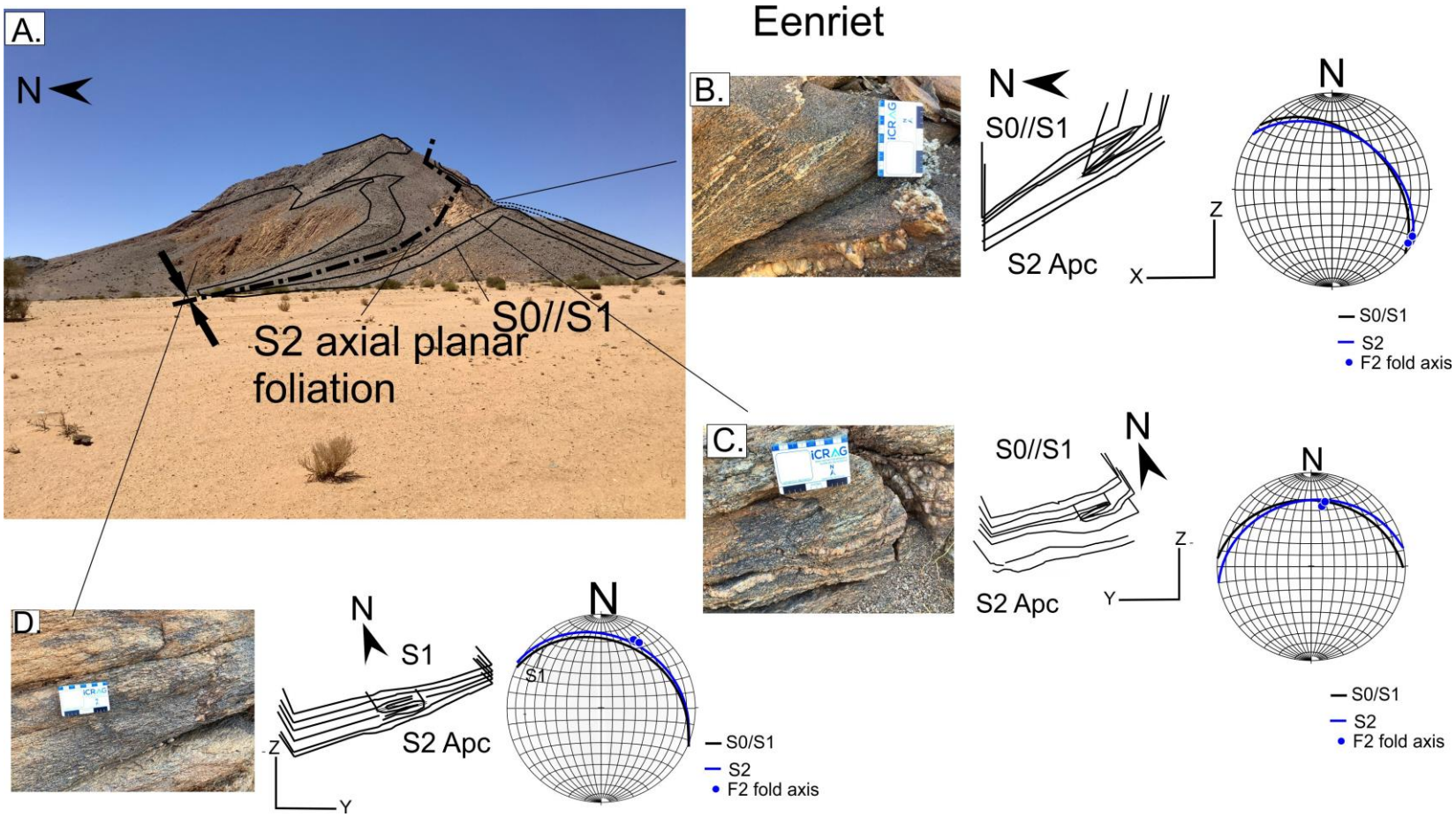

Figure 5.12: Photographs depicting structural characteristics associated with the Eenriet Sub-domain. Figure A: Photograph of the northwestern Eenriet synformal fold closure, looking towards the east. Figure B: Mesoscopic F2 fold, folding within the XZ foliation plane, folding an S0//S1 foliation and defining an S2 axial planar cleavage. The fold axes trend towards the southeast, with the axial planes dipping moderately towards the northeast. Figure C: A F2 mesoscopic Z fold, folding within the YZ foliation planes. The F2 fold, folds a S0//S1 foliation and defines an S2 axial planar cleavage, with the fold axes trending toward the north-northeast and an axial plane dipping moderately towards the north. Figure D: Mesoscopic F2 S fold folding within the YZ foliation planes, folding an S1 foliation and defining an S2 axial planar foliation. The fold axes trend towards the northeast, with the axial plane having a sub-horizontal dip towards the northeast.

Central Domain

T-Goob se Berg Sub-domain

The F2 fold trace extends toward the central domain and is folded by the F4 open folds, resulting in a rotation of foliation planes and lineations toward the east (Figure 5.10; sections EE-EE' and FF-FF'; Appendix 5.1). The F4 folds define a number of Z asymmetry structures within the northern domain of the structure (Figure 5.11). The F4 fold axes trend toward the north-east, co-linear to the regional L1 stretching lineation (Table 5.3, T-Goob se Berg Domain). The regional S2 foliation dips toward the east, and deflects back toward the northeast as the fold trace continues eastwards toward the Skeur se Berg sub-domain (Table 5.3; T-Goob se Berg and Skeur se Berg sub-domains). The L1 mineral stretching lineation defined by sillimanite, actinolite and feldspar aggregates also trends toward the east within the T-Goob se Berg Sub-domain (Table 5.3). The central hinge is thinned out in comparison to the Annakoppies subdomain (Appendix 5.1; sections CC-CC' and DD-DD'). The central sillimanite body is absent in the T-Goob se Berg domain. The lithologies associated with the central hinge zone (volcanoclastic/chemogenic unit, biotite gneiss and biotite-sillimanite schist units), can be traced consistently along strike, toward the Skeur se Berg Sub-domain. However duplications and cut-out structures are seen on the lower and upper limbs of the structure, together with the presence of a well foliated medium-quartz-feldspar gneiss wedged in on the upper limb of the structure (Figure 5.10; sections EE-EE' and FF-FF'; Appendix 5.1).

Duplications in the form of imbricates are seen duplicating the poorly bedded quartzite and nodular-rhythmic sillimanite-quartz-feldspar gneiss units occur on both the upper and lower limbs of the structure, with the upper limb being the most affected (Appendix 5.1; section FF-FF'; Figure 5.13 A&B; Figure 5.14 A&B). Duplications deform the S0-1 foliation on the limb of the structure and represent D1 intra-stratigraphic thrusting (Appendix 5.1, section FF; Figure 5.14 A&B). The Achab Suite is found on the lower western limb of the structure, with the Lekdam Gneiss found on the upper eastern limb of the structure. In section within the XZ plane of the regional foliation, it is interpreted that the intra-terrane Lekdam Thrust contact on the lower limb associated with the Achab Suite cuts out the Lekdam Gneiss around the fold closure in depth (Appendix 5.1, section FF-FF'; Figure 5.18). The associated imbricate structures and the lithologies associated with the hinge zone can also be viewed in Figure 5.13 A & B. Mesoscopic model 1 and 2 F2 folds are found within the XZ and YZ planes, and also fold an S0//S1 foliation and define an S2 axial planar foliation (Figure 5.13 C and D). Mesoscopic sheath fold structures folding within the XZ planes also occur within the structure (Figure 5.13 E). The intra-stratigraphic thrusting that takes place on the upper limb of the structure is also well illustrated in Figure 5.14 A and B. F2 model 1 and 2 folds found in the

YZ and XZ planes are also represented on centimetre and decametre scale. The folds all fold an S0//S1 foliation and define an S2 axial planar foliation (Figure 5.14 C and D). Small sinistral S-C cleavages are also found deforming the S1//S2 foliation. Throughout the structure a dominant sinistral movement was identified, with a vertical north up movement. The F2 folds found within the XZ planes of the regional foliation also show an oblique north up movement (Figure 5.14 E), with folds verging toward the south-west.

Skeur se Berg Sub-Domain

The Skeur se Berg Sub-domain, represents an extension of the stratigraphy associated with T-Goob se Berg toward the east (Figure 5.11). Toward the Skeur se Berg Sub-domain, the overlying lithologies cut-out against the medium-quartz-feldspar gneiss on the northern limb, and shown in section (Appendix 5.1, section FF-FF'). Another quartzite unit duplicates on the lower limb of the structure, beneath the medium-quartz-feldspar gneiss. Duplications also occur on the northern limb due to imbrication between the poorly bedded quartzite unit and nodular-rhythmic sillimanite-quartz-feldspar gneiss (Figure 5.11 B). The hinge zone thins out around the F4 fold closure between the two sub-domains, resulting in minor fragments of the volcamoclastic/chemogenic unit and biotite gneiss units being present. The regional S2 foliation dips toward the northeast, together with the L1 lineation that also trends toward the northeast, corresponding to the south western directed tectonic transport direction (Table 5.3, Skeur se Berg Sub-domain).

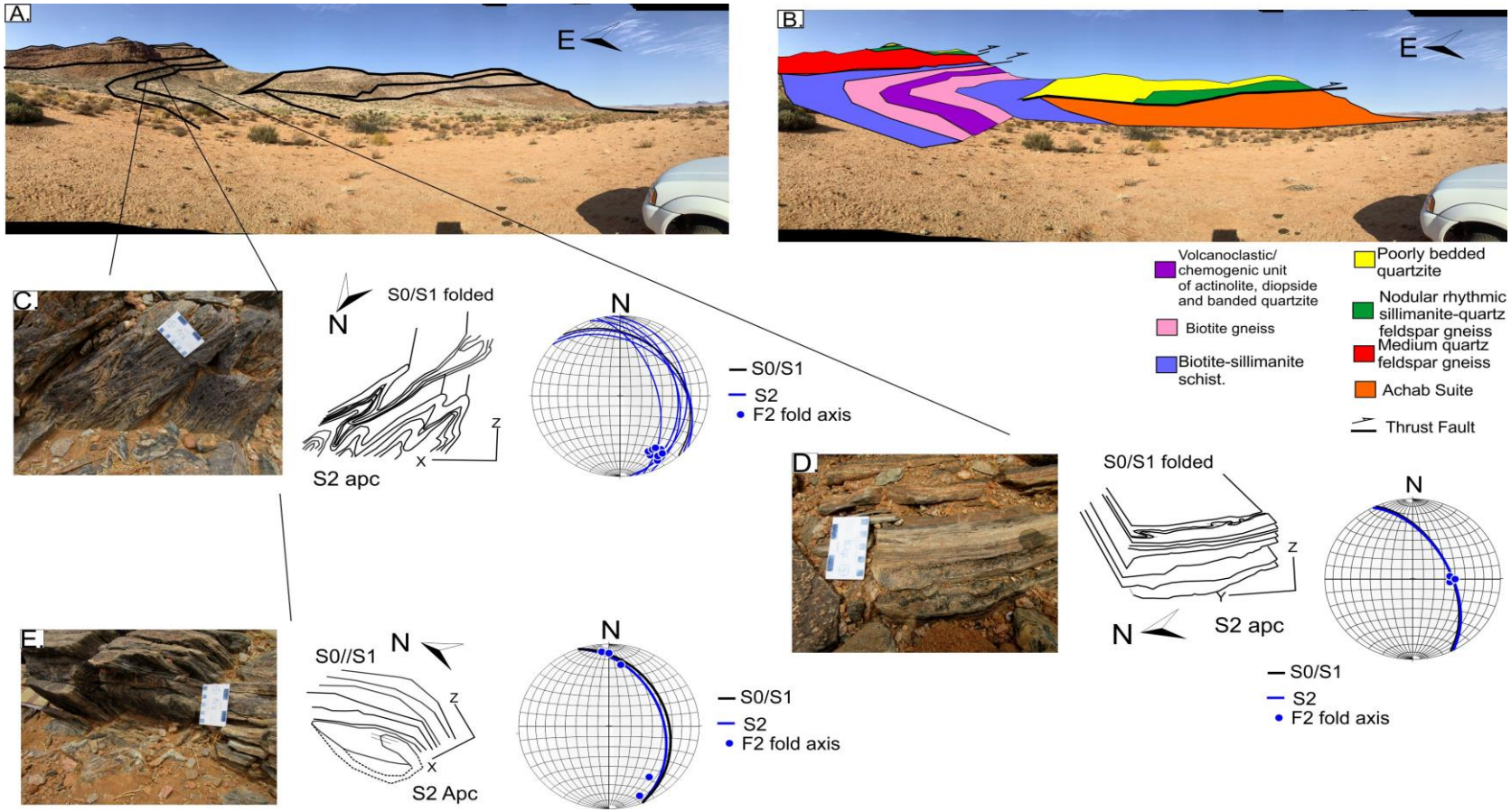

Figure 5.13: Illustrates the structural and kinematic characteristics associated with the Central Domain of the T-Goob Structure. A and B: Diagrams showing the contact relationships associated with the structure looking towards the south; the various lithologies and thrust contacts are depicted on the limbs and central hinge zone of the structure C: A mesoscopic model 2 F2 folds within the XZ plane of the foliation defining Z assymmetries looking toward the south. The F2 folds verge in the direction of overthrusting and fold an S0//S1 foliation, defining an S2 axial planar cleavage.The axial planes are parallel to the bedding and dip moderately towards the east, with the fold axis trending toward the southeast. Figure D: Defines a mesoscopic model 1 F2 fold in YZ plane of the foliation, forming an omega structure. The structure folds an S0//S1 foliation and defines an S2 axial planar foliation. The axial plane dips moderately toward the east-north-east, with the fold axis plunging steeply toward the east. E: Mesoscopic F2 sheath fold, located in XZ planes of the foliation. The structure folds an S0//S1 foliation and has a prominent S2 axial planar foliation. The axial plane dips moderately toward the east, with the fold axes trending toward the north and south-southeast. The fold axes show a curvilinear trend associated with the hinge zone as they rotate around the hinge zone.

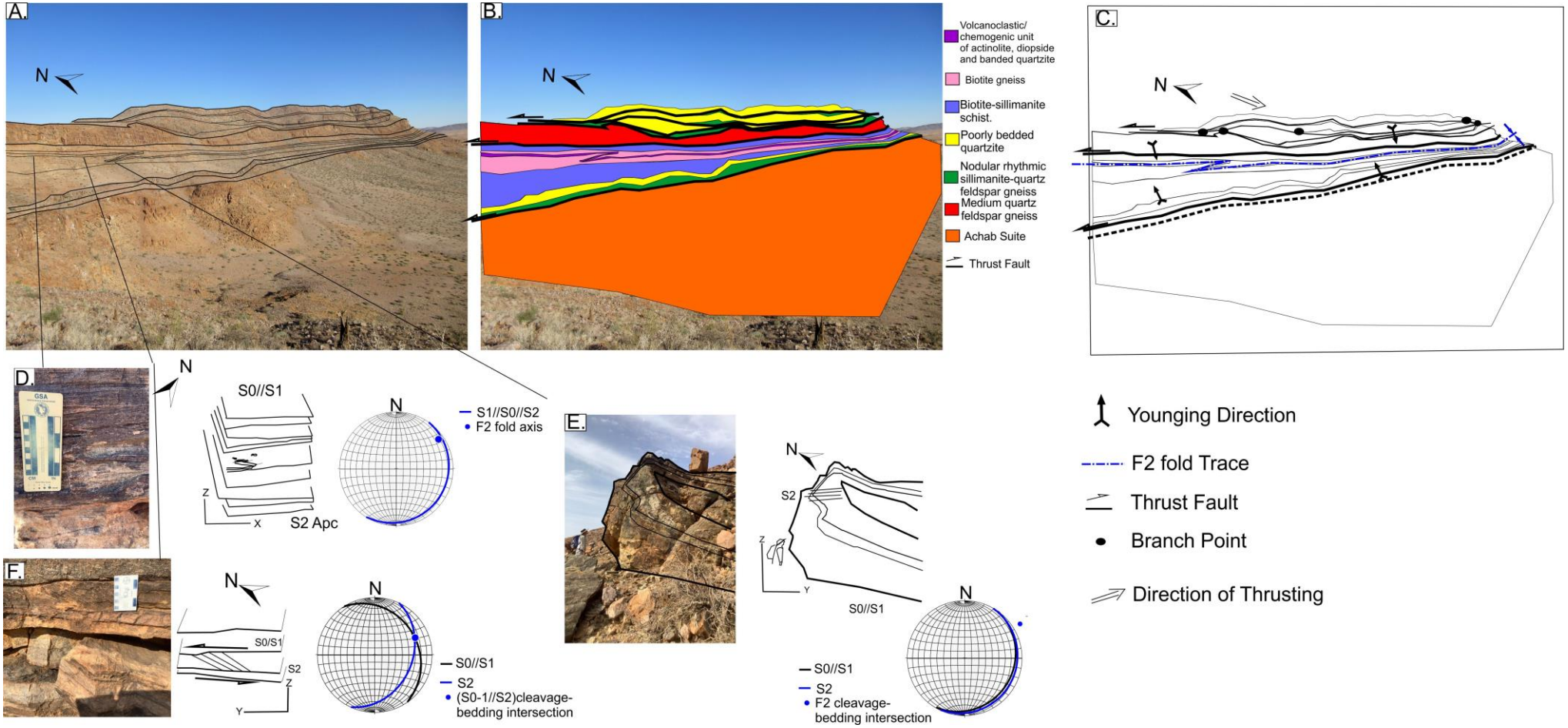

Figure 5.14: Structural and kinematic characteristics associated with the Central Domain. A and B: The lithological contacts and intra-stratigraphic thrusting on the upper limb of the structure. The diagram is taken looking towards the east-southeast. C: Formline interpretation of Diagram B Imbricates on the northern limb, together with branch points, cutting out the different lithologies. D Mesoscopic F2 fold found within the XZ foliation plane. The structure folds an S0//S1 foliation and defines an S2 axial planar foliation, that has a co-planar relationship. The fold axes has a shallow plunge towards the northeast, with the axial plane having a shallow dip towards the east-southeast. E: Decametre scale F2 fold, that is folded within the YZ foliation plane. The structure folds an S0//S1 foliation and defines an S2 axial planar foliation. The fold axis has a shallow plunge toward the east-southeast, with the axial plane having a shallow dip in the same direction. F: Mesoscopic S-C cleavage, showing a sinistral sense of movement, deforming the S0//S1 and S2 foliations. The cleavage-bedding intersection (S1//S2), trends toward the northeast.

Southern Domain

Ou-Samoep Sub-domain

The Ou-Samoep Sub-domain is a major S-fold structure, representing the eastern part of a kilometre scale omega structure having an S and Z fold asymmetry (Figure 5.15). The Ou-Samoep Sub-domain represents an F3 S structure refolding the F2 fold trace. Towards the south the limb of the S-Structure is severely folded and sheared by the D4 and D5 phases of deformation, forming very tight isoclinal folds. The east-west shears are located on the easterly striking limbs of the T-Goob structure, resulting in fold hinges being attenuated, flattened and sheared (Figure 5.15). The southern limb (nodular rhythmic gneiss, poorly bedded quartzite unit) of the T-Goob structure is well exposed, while the northern limb is thinned out and strongly boudinaged due to east-west shearing; this is illustrated in section (Appendix 5.1, Section HH-HH'). The central F2 hinge is poorly exposed, with the central volcanoclastic/chemogenic and biotite gneiss units thinned out to centimetre scale. The Achab Suite is visible on the southern limb, with the Lekdam gneiss still located on the northern limb of the structure. The contact between the Achab Suite and Lekdam Gneiss that defines the Lekdam thrust contact is also seen in the Ou-Samoep Sub-domain, on the southern limb of the structure. Fragments of Lekdam Gneiss occur along the thrust contact and boudinaged along strike (Appendix 5.1, Section HH-HH'). The contact is better defined toward the east, where a sharp contact is found between the Lekdam Gneiss and Achab Suite. The L1 lineations, as well as the F3 and F4 fold axes are rotated toward the south-southeast, due to later D5 deformation (Table 5.4; Ou Samoep Sub-domain). Axial planes of F3 and F4 folds and regional S2 foliations are also rotated towards the south-eastsouth and southeast (Table 5.4, Ou Samoep Sub-domain). Mesoscopic folds are found in both the YZ and XZ planes of the regional foliation within the Ou-Samoep Sub-domain (Figure 5.15 B, C and D). Both model 1 and model 2 folds, fold an S0//S1 foliation and define an S2 axial planar foliation. The S1 fabric associated with the D1 phase of deformation is also well represented within a folded xenolith unit, where the S1 fabric is folded and an S2 axial planar foliation is defined (Figure 5.15 B), the S2 foliation then becomes the regional foliation. Prominent S-C cleavages are also found deforming the S1//S2 foliations (Figure 5.15 E).

Samoep Sub-domain

Within the Samoep Sub-domain the major F2 fold trace is refolded as a Z fold by the D3 phase of folding. It is also folded by the D4 phase of folding, forming a major synclinal F4 fold in the far west of the Samoep Sub-domain (Figure 5.15). The major synformal F4 fold rotates the regional stretching lineations from south-southeast to northeast and the regional foliations from south to north, the axial plane also has a sub-vertical dip toward the north (Table 5.4,

Samoep Sub-domain). The Z fold is also flattened and sheared by the D5 east-west shear zones (Figure 5.15). The regional fabric dips towards the south within the Samoep Sub-domain, the L1 lineations have also rotated towards the south-eastsouth. The F3 fold axes also trend toward south-east, with the axial plane dipping moderately toward the southeast (Table 5.4, Samoep Sub-domain). The far southeastern F2 fold closure within the Samoep Sub-domain (Table 5.4; Figure 5.15) trends toward the north-northeast, with the F2 axial plane dipping moderately toward the northeast (Table 5.4, Samoep Sub-domain). D1 intra-stratigraphic thrusting is found on the northern side of the southern limb of the T-Goob structure, with duplications occurring between the poorly bedded quartzites and nodular rhythmic sillimanite-quartz-feldspar gneiss (Figure 5.15 A). The L1 lineations around the F2 fold closure also have a mean trend toward the north-northeast (Table 5.4, Samoep Sub-domain). In the far southeastern fold closure the Lekdam Gneiss surrounds the fold closure, with the Achab Suite absent (Appendix 5.1, section ii-ii'; Figure 5.18). The volcanoclastic/chemogenic unit is absent in the hinge of the F2 fold closure, together with the biotite gneiss unit, which closes off towards the west of the structure. The hinge here is now defined by biotite-sillimanite schist, with nodular rhythmic sillimanite-quartz-feldspar gneiss and poorly bedded quartzite folding around the hinge (Appendix 5.1, section ii-ii'). Towards the west the northern limb is boudinaged with regard to the poorly bedded quartzite, nodular rhythmic sillimanite-quartz-feldspar gneiss and central hinge lithologies.

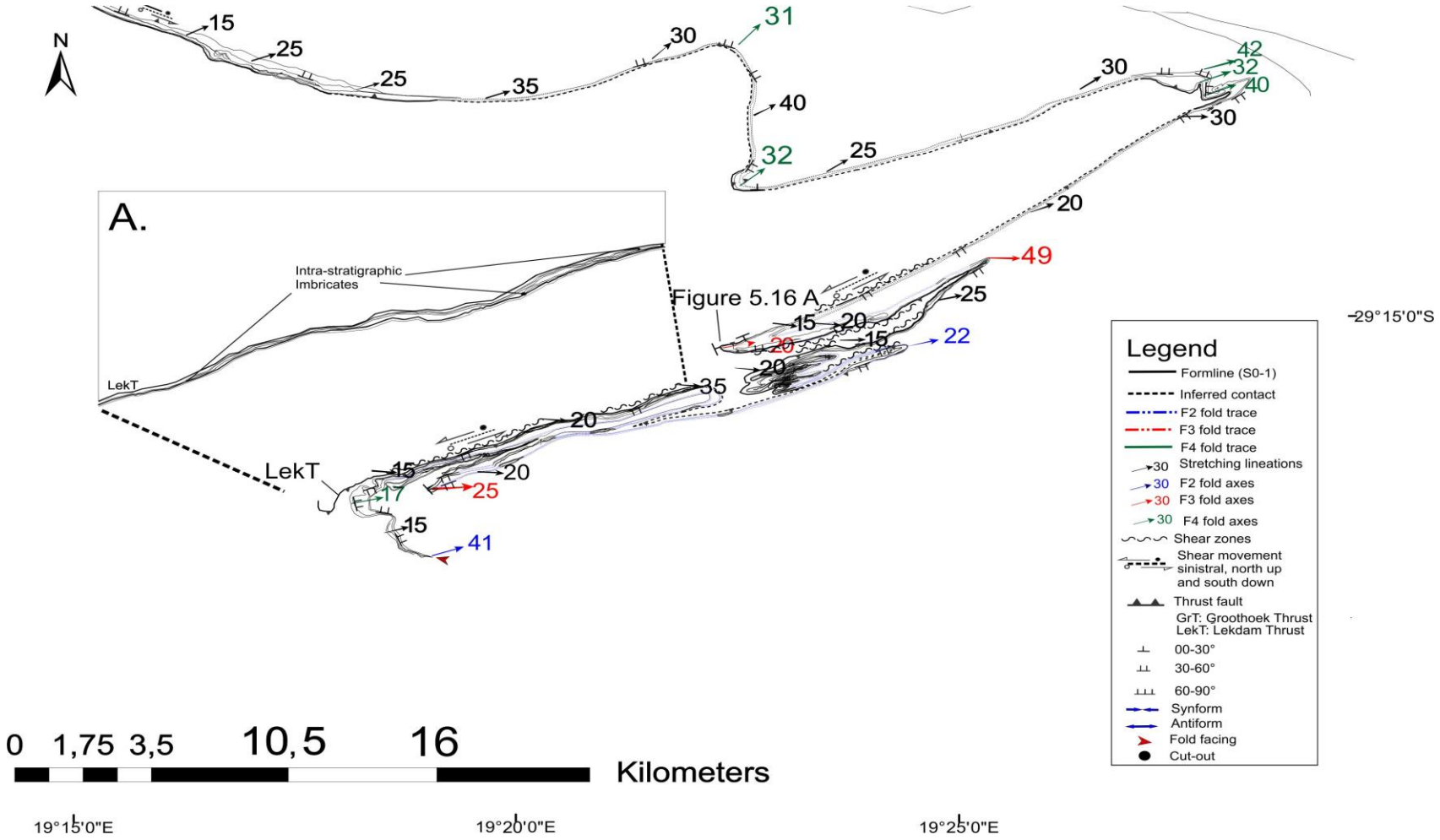

Figure 5.15: Formline map of the Southern Domain. The fold axes, fold traces and lineations are also illustrated. The sections drawn across the Southern Domain are indicated by the letters G to I. Figure A: A simplified diagram of imbricate structures located on the southern limb of the T-Goob structure. The location of relevant photographs taken within the Southern Domain is shown in Figure 5.16 A.

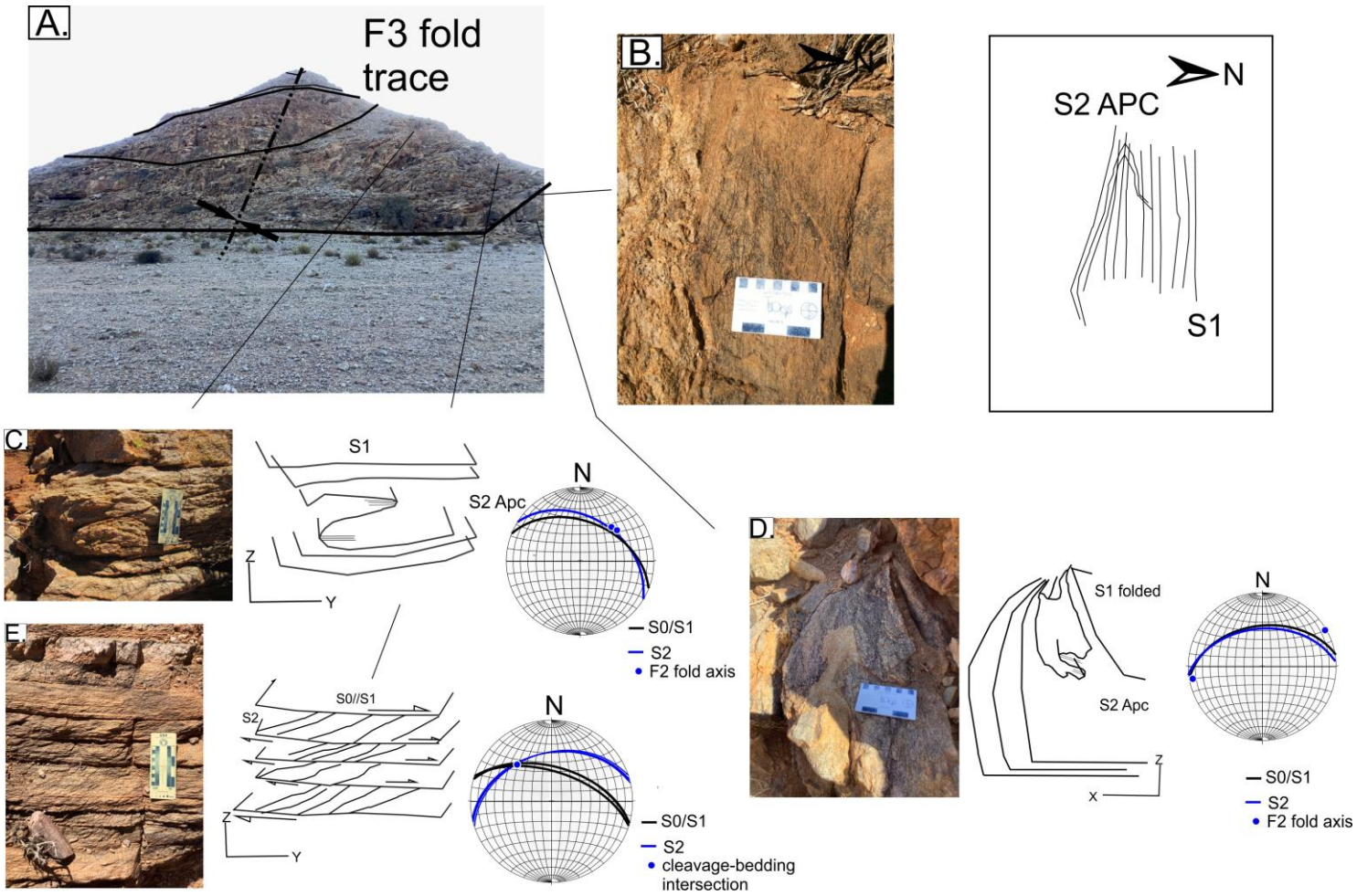

Figure 5.16: Photographs and diagrams associated with the structural and kinematic characteristics associated with the Ou-Samoep Sub-Domain. A: The Ou-Samoep fold closure looking towards the east, with the Achab Suite and supracrustal rocks folding around the hinge. B: Defines a mesoscopic Model 1 F2 fold within the YZ plane of the foliation. The F2 fold is associated with a xenolith located within the Achab Suite. The structure folds an S1 foliation and defines an S2 axial planar foliation. C: A F2 mesocopic fold within the YZ foliation planes and folds an S1 foliation and defines an S2 axial planar foliation. The fold axes trend towards the northeast and the axial plane dips moderately toward the northeast. D: Mesocopic F2 fold that folds within the XZ foliation plane, and folds an S1 foliation and defines an S2 axial planar cleavage. The hinge has a curvilinear characteristics as the fold axes rotate around the hinge and have shallow plunges towards the northeast and southwest. The axial plane dips moderately towards the north. Figure E: Defines dextral S-C clevages, whiich are parasitic to the larger F2 fold closure toward the west. The bedding cleavage intersection trends toward the southwest.

5.5 Discussion

5.5.1 Phases of Deformation

The T-Goob Structure represents a highly refolded isoclinal sheath fold with double vergence geometries that is affected by five phases of deformation as summarised in Table 5.5.

D1 Phase of Deformation

The D1 phase is defined by the S1 foliation associated with the intrusion of the Lekdam Gneiss and Achab Suite. The D1 phase is clearly visible at the Ou-Samoep Domain within the mesoscopic F2 fold, found within the Achab Suite (Figure 5.16 A). Where the S1 foliation is clearly seen folding on the limbs of F2 model 1 fold in the YZ planes of the foliation, with the model 1 F2 fold defining an S2 axial planar foliation, associated with the D2 phase. Macroscopically S1 fabric is sub-parallel to the S0 compositional banding, and is only identified macroscopically within F2 sheath fold hinges. The D1 phase is also associated with intra-terrane thrusting, which defines the contact between the Lekdam Gneiss and Achab Suite (Lekdam Thrust), located on the lower limb of the structure, and folds around the northwestern fold closure of the structure. Intra-stratigraphic thrusting, which involves the duplication of lithologies on the flanks of the T-Goob Structure is also associated with the D1 phase of deformation. Along strike various lithological units are cut out and duplicated, deforming the S1//S0 foliation on the limbs of the T-Goob structure, and are partitioned in zones of low to moderate strain. Lithologies and duplications on the northern and southern limbs are best represented within the central domain within the T-Goob se Berg sub-domain and Skeur se Berg Sub-domain (Figure 5.11 A & B; Figure 5.15 A). Duplications and cut-out structures are however best observed on the northern limb of the structure (Figure 5.11 A; figure 5.14 A & B; Appendix 5.1, section E-E' and F-F').

However, if one considers the total restoration of the T-Goob Structure (Figure 5.17 A), it is interpreted to represent a set of thrusted imbricates (McClay, 1991), folded by the D2 phase of deformation (Figure 5.17 B). Two prominent sets of poorly bedded quartzite, together with nodular rhythmic gneiss units, duplicate and cut-out against one another, closing of both in the northwest and southeast of the structure. Minor subsidiary imbrication is also seen within the quartzite-nodular rhythmic sillimanite-quartz-feldspar gneiss units (Figure 5.17 A & B). A prominent medium-quartz-feldspar gneiss unit is also wedged in between the two quartzite units. The medium quartz-feldspar gneiss is not seen anywhere else in the structure, except on the northern limb. This could be due to the fact that the medium-quartz-feldspar gneiss represents a thrusted sheet of Lekdam Gneiss, which has changed its character due to change in strain. Upon restoration the medium quartz-feldspar gneiss (assumed to be Lekdam Gneiss)

is thrusted over the two quartzite and nodular rhythmic sillimanite-quartz-feldspar gneiss units (Figure 5.17 A). The Lekdam Gneiss lies above the Achab Suite upon restoration, with the central Lekdam Thrust contact being sheared out due to the D5 phase of deformation, and attenuates the thrust contact (Figure 5.17 A). No duplications were observed within the hinge zone of the structure. The D1 thrusting phase also associated with an L1 stretching, which forms within the regional XY foliation plane and represents the X-direction of the regional strain ellipse, is parallel to the southwesterly direction of overthrusting (Colliston et al., 1991). The L1 lineation comprises of sillimanite, biotite, diopside and actinolite minerals, together with feldspar aggregates.

Table 5. 5: The general attributes and characteristics associated with the phases of deformation observed within the T-Goob Structure.

Phase of Deformation	S and L Structures	Attributes	Folds
D1 Phase	Penetrative S1 fabric-formed at upper amphibolite grade conditions. Associated with the D1 phase of thrusting. S1 fabric observed within the Lekdam Gneiss and Achab Suite. The S1 fabrics is parallel to the regional S0 banding. S1//S0 fabric is found on the limbs of the T-Goob Structure. L1 lineations develops within the foliation plane, and is defined by acicular minerals (sillimanite, feldspar amphibole)and long axes of sillimanite clasts.	S1 fabric associated with the emplacement of intrusive sheets, due to D1 intra-terrane thrusting. The S1 fabric is parallel to the bedding (S0). D1 intra-stratigraphic thrusting units occuring on the limbs of the T-Goob Structure, associated mostly with the outer quartzite-nodular rhythmic gneiss units.	No F1 folds were observed in the T-Goob Structure. The S1//S0 fabric is observed however on the limbs of F2 mesoscopic and macroscopic structures.
D2 Phase	Penetrative S2 foliation, formed at amphibolite grade conditions, and identified as an axial planar foliation within the hinge zones of F2 fold structures. The S2 foliation is co-planar to the S0//S1 foliation. The S2 fabric is defined as the regional fabric throughout the structure.	Associated with macroscopic F2 sheath fold development and mesoscopic F2 folds. The F2 sheath fold closures are identified in the NW Eenriet fold closure and SE Lekdam fold closure. F2 Model 1-2 folds are found throughout and located within the XZ and YZ planes of the foliation, and is contained within the XY plane of the regional strain ellipse. F2 model 1 folds within the YZ planes of the foliation are parasitic to the macroscopic F2 sheath fold and forms double vergence geometries. F2 fold closures associated with a S2 axial planar foliation, which is parallel to S0//S1. The F2 Model 1-2 fold axes are co-linear/obliqueto the L1stretching lineation.The F2 sheath fold axes are co-linear to the regional L1 lineation.	Development of macroscopic T-Goob sheath fold. The T-Goob Structure represents a sheath fold with double vergence geometries. The development of mesoscopic F2 folds which fold within the XZ and YZ foliation planes.
D3 Phase	Associated with macroscopic F3 folds which refold the F2 fold trace in the southern domain of the T-Goob Structure. Development of a locally developed S3 Fabric within the F3 hinge zones. The S3 foliation is parallel to the S0//S1//S2 foliations.	The F3 macroscopic folds form prominent S and Z folds in the south of the structure, which define double vergence geometries. The F3 fold axes are rotated toward the east-south east, together with the L1 lineation around D4 hinges.	Define macroscopic S and Z folds, found in the south of the T-Goob Structure.
D4 Phase	Associated with macroscopic F4 open folds that refold the S0//S1//S2 foliation. No S4 foliation was indentified throughout the T-Goob Structure.	Formation of F4 open folds which form due to sinistral wrench shear. The F4 folds refold the F2 sheath fold trace and form a typical Z assymetry. The F4 folds fold the T-Goob Structure across all domains. The F4 fold axes are co-linear to the F2, F3 fold axes and the L1 stretching lineation. The F4 fold axes trend toward the NE in the north of the structure and rotate toward the east-south-east of the structure in the Southern Domain.	Defined by F4 Z-shaped open folds which fold the F2 sheath fold trace.
D5 Phase	Deforms all earlier foliations and is defined by a conspicuous mylonitic foliation.	Defined by prominent east-west shear zones, which is associated with reactivated movements on the intra-terrane thrust contact between Lekdam Gneiss and Achab Suite. The late easterly trending shear zones also tighten up later F2, F3 and F4 fold structures to form isoclinal fold structures, specifically in the south of the T-Goob Structure. Boudinage effects are also seen on the limbs of the T-Goob Structure, and the thickening of the central core of the structure within the Annakoppies Sub-domain. The D5 east-west shears also rotate S and L structures around the D4 hinges.	No F5 oblique folds were formed. Instead the F3 and F4 fold hinges are flattened and boudined by the east-west shears.

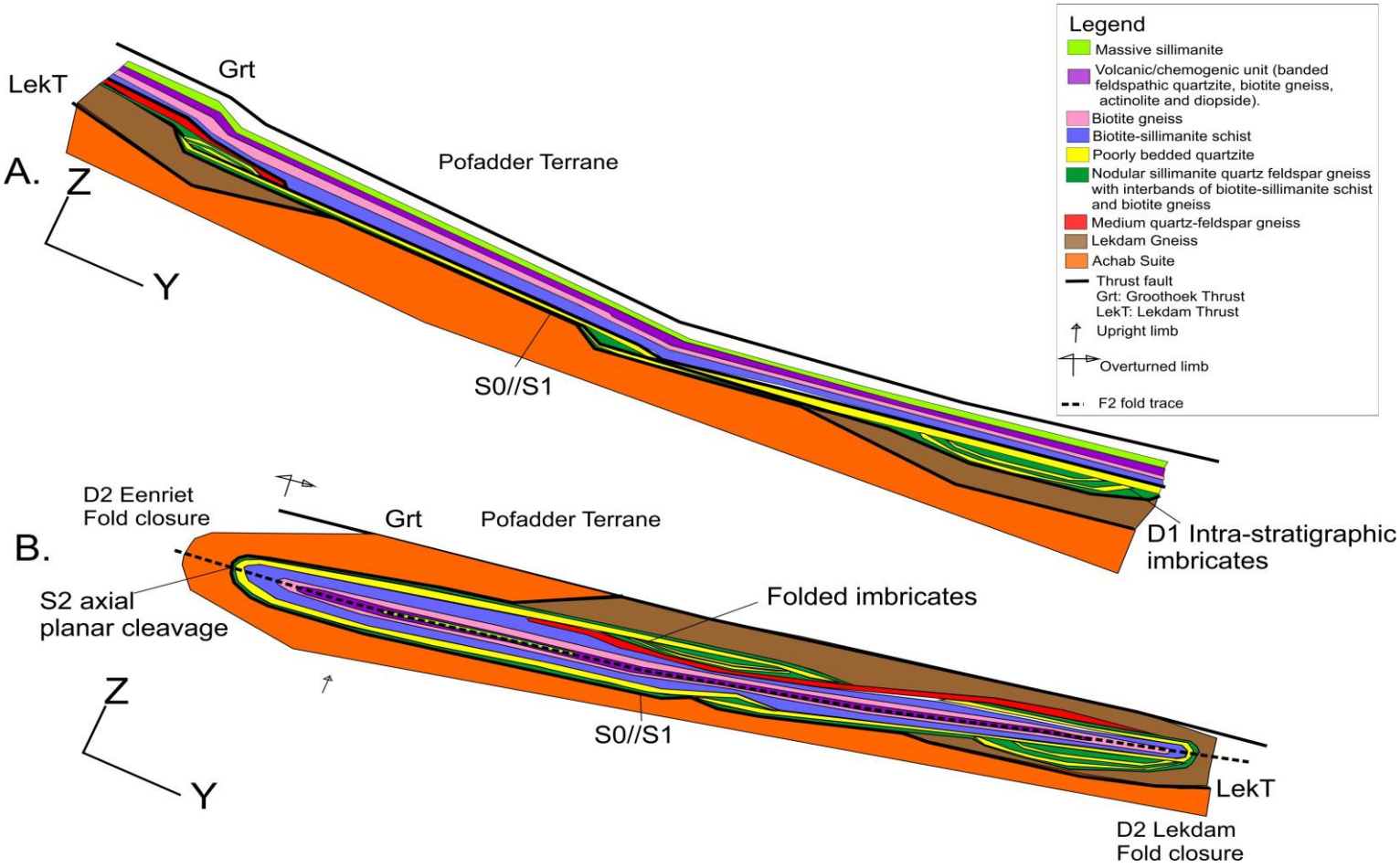

Figure 5.17: Schematic model of the character of D2 imbricates associated with the supracrustal rocks on the limbs of the T-Goob Structure on the Y-Z plane of the foliation. A:A schematic restoration of the T-Goob structure during the D1 phase. Imbrication is clearly noted within the poorly bedded quartzite and nodular rhythmic gneiss units. The well foliated medium quartz-feldspar gneiss is also thrusted in above the upper most poorly bedded quartzite. The medium grained quartz-feldspar gneiss is interpreted to be a possible sheet of Lekdam Gneiss that has been deformed. What is also apparent is that the upper stratigraphic units are not duplicated. The relationship between the Lekdam Gneiss and Achab Suite is also well illustrated, with the central section being highly sheared by the D5 phase of deformation, shearing out the Lekdam Gneiss on the thrust contact. B: Schematic diagram of the D1 imbricates being folded by the D2 phase of deformation. The Lekdam Thrust is also folded by the D2 phase of deformation.

D2 Phase

The D2 phase is defined by F2 model 1-2 fold phase and sheath fold phase. The D2 phase folding folds an SO//S1 foliation and defines an S2 axial planar foliation that is seen on macroscopic and mesoscopic scale. On macroscopic scale the S2 foliation can be seen in the northwestern and southeastern D2 sheath fold closures. Within both fold closures the F2 fold axes are co-linear to the regional L1 stretching lineations, and the F2 axial planes are co-planar to the regional S2 foliation (Table 5.3 and Table 5.4). The younging direction shows toward the axial plane, with the northwestern fold closure facing towards the south east, and the southeastern fold closure facing towards the northwest (Figure 5.20) The D2 phase of deformation also folds the Achab Suite and Lekdam Gneiss around the F2 fold closures, and also folds the D1 Lekdam Thrust contact (Figure 5.17 B). A series of exploded sections, illustrates this fact (Figure 5.18 A-C).In Figure 5.18 A and B, the Lekdam Gneiss and Achab Suite are folded around both the northwestern and southeastern F2 fold closures. In Figure 5.18 C and D, the Lekdam Thrust cuts-out the Lekdam Gneiss around the F2 fold hinges, showing only the Achab Suite on the southern limb of the structure. The D2 phase is also defined by F2 mesoscopic model 1-2 folds, found on the YZ (model 1) and XZ (model 2) planes of the regional foliation. The mesoscopic F2 folds, fold an S0//S1 foliation and also define an S2 axial planar foliation. The F2 mesoscopic model 1 folds found on the YZ planes of the foliation, are parasitic to the larger macroscopic F2 sheath fold, vergence direction toward the south west, seen within the model 2 folds, correspond to the direction of over-thrusting. The F2 fold axes of the macroscopic sheath fold and mesoscopic F2 model 1-2 folds are co-linear to the L1 stretching lineation, and are sub-parallel to the southwestern tectonic transport direction (Colliston et al., 1991).

D3 Phase

The D3 phase of deformation is defined by F3 folds which refold the F2 sheath fold trace. The F3 folds form macroscopic S and Z folds in the YZ plane of the regional foliation and define structures with double vergence geometries, which is common in sheath fold structures (Alsop and Holdsworth, 2004a). The F3 fold axes and axial planes are rotated towards the southeast and east-southeast, together with the L1 stretching lineations (Table 5.4, Ou-Samoep and Samoep Sub-domains). This is seen within the Southern Domain of the T-Goob structure, where the S and L structures are rotated by the D5 phase of deformation around F4 fold hinges. The F3 fold axes and L1 lineations are co-linear and the F3 axial planes are co-planar to the rotated regional S2 foliation (Table 5.4)

.

D4 Phase

The D4 phase of folding is defined by the F4 open folds, which fold the F2 fold trace throughout the entire structure from northwest to southeast. The F4 folds form a prominent Z asymmetry, associated with sinistral wrench shear (Colliston and Schoch, 2013), and refolds the F2 fold trace throughout the structure (Figure 5.10 and Figure 5.11). The fold axes of the F4 folds in the north of the structure trend toward the northeast, and are sub-parallel to the L1 lineation, with the axial planes having sub-vertical attitudes toward the northwest (Table 5.3). Toward the south of the structure, the F4 fold axes and L1 lineations are rotated by the D5 east-west shears and plunge toward the southeast and east-southeast (Table 5.4). The F4 fold axes have a co-linear relationship to the rotated F3 fold axes, and their axial planes are co-planar (Table 5.4). The foliation planes (S0//S1//S2) are folded, and rotated around the F4 fold hinges.

D5 Phase of Deformation

The D5 phase is associated with east-west shear zone development located along the limbs of the T-Goob Structure. The effects are most prominently seen in the southern domain of the structure, where the fold hinges of the F3 and F4 folds are tightened by the D5 phase. All the shear zones show a sinistral shear movement, together with a north-up and south-down sense of vertical movement. The D5 phase also results in the boudinage effects seen in the central hinge of the structure, as well as in the Annakoppies Sub-domain, which results in the thickening of the stratigraphy associated with the core of the structure. The D5 phase also affects the Lekdam Thrust Sheet, which is sheared out on the southern limb of the T-Goob Structure, and northern fold closure. Boudinage effects also occur on the contact between the Lekdam Gneiss and Achab Suite. Southwards lithologies of the central hinge are strongly boudinaged. The D5 east-west shears also rotate all the planar and linear structures in the southern domain of the T-Goob sheath fold. The planar structure (S0-1 and S2 fabrics, fold axial planes) are rotated from north to south (Table 5.3 and 5.4), and the linear structures are rotated from north-northeast/northeast to the southeast (Table 5.3 and 5.4).

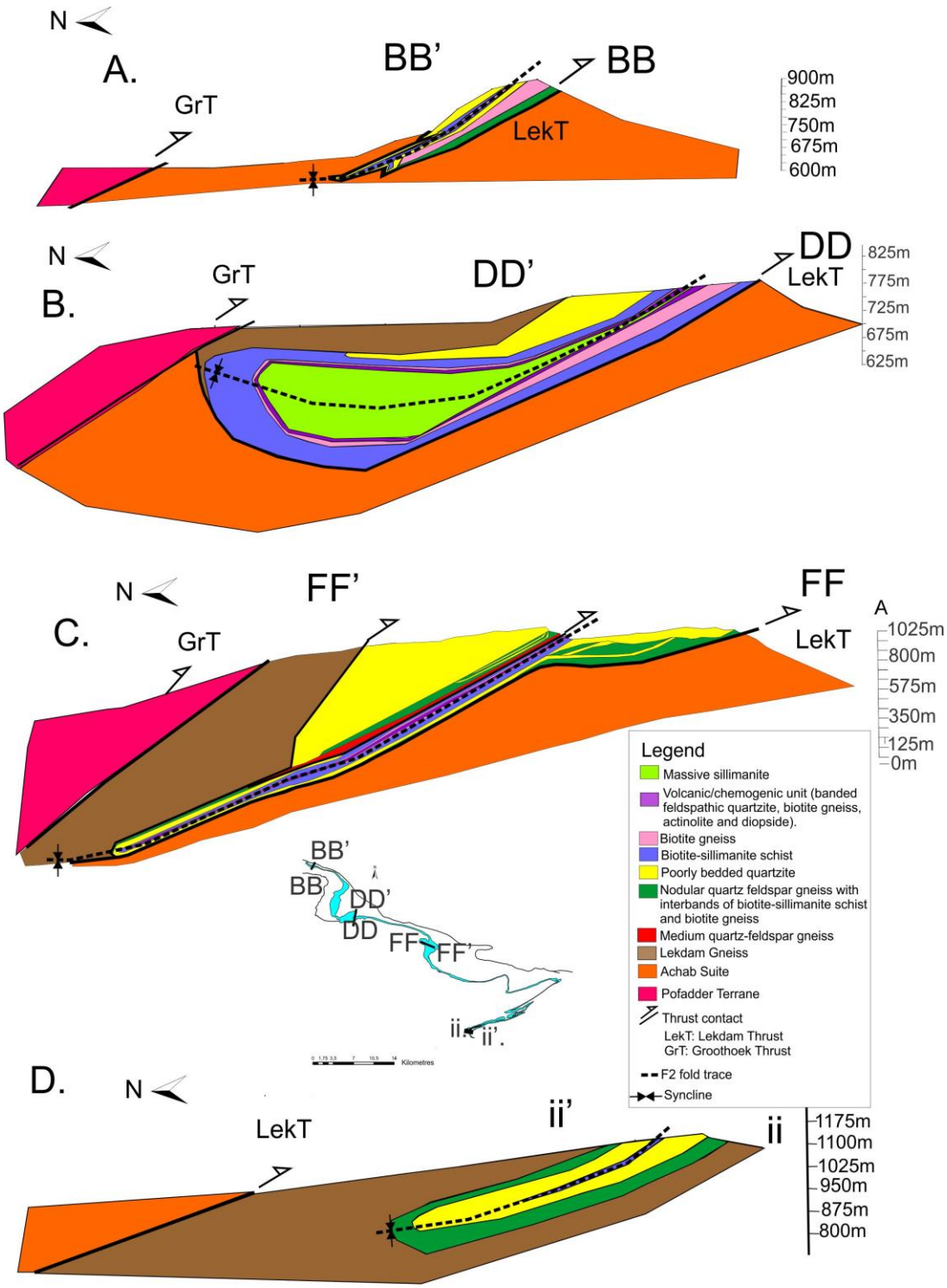

Figure 5.18: A series of restored exploded sections on the XZ plane of the regional foliation. The section locations can be seen in the location map on the diagram, and correspond to the section locations in Figure 5.10. A: Cross section associated with the Eenriet fold closure in the northwest of the structure. The Achab Suite can be seen folding around the fold closure, with the Groothoek Thrust found adjacent to the structure. B: Cross section on the XZ plane of the foliation at Annakoppies. The Achab Suite folds around the fold hinge and cuts out against the Groothoek Thrust. The sillimanite body is seen in the central hinge of the structure. C: Cross section across the T-Goob se Berg Sub-domain. The Lekdam Thrust is found on the southern limb of the structure. The Lekdam Gneiss is cut-off by the Achab Suite around the F2 fold hingeon the XZ plane of the regional foliation. A set of imbricate structures is found on the lower and upper limb of the structure. The D1 imbricates are interpreted to be folded by the D2 phase of deformation. D: The D2 fold closure found in the southeast of the structure. The D2 fold closure is completely enveloped by the Lekdam Gneiss, with the Lekdam Thrust found adjacent to the structure on the northern limb.

5.5.2 Summary and Classification of the T-Goob Sheath Fold

Within the T-Goob Structure, certain structural and stratigraphic characteristics can be used to aid and compare certain attributes to that of sheath fold structures identified globally, and this is summarised in Table 5.6. The stratigraphic and structural attributes are summarised in as follows:

- Regarding the stratigraphy of the T-Goob Structure, the central hinge lithologies are fairly constant, with added complications of thrusting effecting lithologies on the limbs of the T-Goob sheath fold. The massive sillimanite body represents the core of the D2 sheath fold that is surrounded by volcanoclastic/chemogenic (Figure 5.7), biotite gneiss and biotites-sillimanite schist units, that represent a well-defined symmetrical arrangement of lithologies, that show younging toward the inside of the structure. This symmetrical arrangement of lithologies is typical of large scale D2 sheath folds identified globally (Alsop et al., 2007).
- Throughout the T-Goob sheath fold the linear fabrics (L1 stretching lineation, F2, F3 and F4 fold axes) are co-linear to one another and have a constant trend and plunge towards the northeast and east-northeast, and is subparallel to the tectonic transport direction and represents the X direction of the regional strain ellipse (Colliston, 1990). There are complications where the linear fabrics are rotated by the D5 east-west shears. However, there is still a linear relationship (Table 5.3 and 5.4). The rotation of linear elements towards the X direction or direction of shear is also typical of sheath folds (Cobbold and Quinquis, 1980; Fowler and Kalioubi, 2002).
- The planar structures throughout the study area are also co-planar (S0-1 and S2 fabrics, fold axial planes of various phases of folding), and is also typical of sheath folds in high strain zones where the foliation planes rotate into parallelism with one another within the shear planes (Ramsay, 1980). Good examples on macroscopic scale is seen within the western Aggeneys Terrane (Colliston and Schoch, 2002).
- Mesoscopic F2 model 1 folds and macroscopic F3 folds define S and Z asymmetries across the sheath fold, and are located on the YZ planes of the regional foliation. This reversal in asymmetry is also common in sheath folds, both on mesoscopic and macroscopic levels (Alsop and Holdsworth, 2004b).
- Sheath folds that form in zones of high strain, are often accompanied by large displacements or tectonic discontinuities such a thrust faults (Alsop, 1994). This is seen on the southern limb of the T-Goob sheath fold, which is an intra-terrane thrust boundary.

- The T-Goob structure also has a non-continuous axial plane, although it is highly folded by the D2-D3 phase and extends for a distance of 121km. Non-continous axial planes are also typical of sheath fold structures (Fowler and Kalioubi, 2002).

Table 5.6: Comparison table of the structural features of the T-Goob structure, and the sheath fold criteria, necessary for the T-Goob structure to be classified as a sheath fold.

T-Goob Structure	Sheath Fold Criteria
1. Symmetrical arrangement of lithologies is associated with the T-Goob Structure, with the central core of the structure being defined by the massive sillimanite body (Figure 5.7).	Large sheath folds contain smaller sheath folds, and also define a symmetrical arrangement of lithologies, representing different layers of the sheath fold (Alsop et al., 2007).
2. The linear fabrics (L1 stretching lineation, F2 sheath fold axis, and F3 and F4 fold axes) of the T-Goob Structure have a co-linear relationship to one another and rotate toward the X-direction or tectonic transport direction (Table 5.3 and 5.4).	Sheath folds often show elongation toward the X direction, together with stretching lineations, that also rotate toward the X-direction (Ramsay, 1980; Cobbold and Quinquis, 1980).
3. Throughout the T-Goob Structure, the the planar fabrics (S0-1, S2 and fold axial planes of the various phases of folding) have a coplanar relationship to one another, and rotate parallel to one another within the shear plane (Table 5.3 and 5.4) (Ramsay, 1980).	Coplanar fabrics have been typically identified within macroscopic sheath folds within high strain zones seen in the western Aggeneys Terrane (Colliston and Schoch, 2002).
4. Both mesoscopic and macroscopic model 1 folds form double vergence geometries defining S and Z folds, exposed on the YZ planes of the regional foliation.	Reversals in asymmetry across major axial planes, forming S and Z folds, is typical structures associated with sheath folds (Alsop and Holdsworth, 2004b).
5. The D1 Lekdam Thrust located on the lower limb of the T-Goob Structure, together with the D1	In zones of high strain tectonic thrust sequences or tectonic discontinuities often accompany sheath folds (Alsop, 1994).

Groothoek Thrust lying adjacent to the T-Goob Structure.	
6. T-Goob Structure has a non-continuous axial plane.	Non-continuous axial planes are often associated with sheath folds (Fowler and Kalioubi, 2002).

5.5.3 Sheath Fold Classification

Sheath folds are defined as folds with curvilinear hinges and are recognized in high strain zones within orogenic belts (Mathee, 2017; Alsop and Holdsworth, 2004b; Colliston and Schoch, 2002; Minnigh, 1979). Using the stratigraphic and structural characteristics summarised in Table 5.6, the following criteria associated with sheath folds can be applied to the T-Goob Structure in order for it to qualify as a sheath fold.

Criteria

- Symmetrical arrangement of stratigraphy throughout the structure, defining the central core/or hinge zone of the T-Goob Structure, can be used in this classification (Alsop, 1994; Colliston and Schoch, 2002; Alsop et al., 2007). This can be seen within the T-Goob Structure across the study area, with the central core or 'eye' being represented by the massive sillimanite body at Annakoppies (Figure 5.7; Table 5.6).
- The T-Goob Structure although highly refolded, is extending for a distance of 121km. The hinge zone and axial plane is non-continuous, that is typical of sheath folds globally (Fowler and Kalioubi, 2002; Mathee 2017). The T-Goob structure is therefore non-continuous and is exposed on the YZ foliation plane (Table 5.6; Figure 5.19).
- The T-Goob se Berg sheath fold also shows elongation or extension toward the X-direction (tectonic transport direction). The direction of shear is constant, resulting in the L1 lineations and fold axes rotating toward the tectonic transport direction (Table 5.3 and 5.4; Figure 5.19). This is evident throughout the entire T-Goob Structure (Table 5.6) (except for certain sections of the southern domain where the S and L structures are rotated by the D5 east-west shears). The rotation of linear structures toward the X direction is typical of most sheath fold structures observed globally (Cobbold and Quinquis, 1980; Colliston and Schoch, 2002; Fowler and Kalioubi, 2002; Alsop and Holdsworth, 2004b). This is well represented by the two end fold closures (Figure 5.19).
- Parasitic fold (S and Z) structures have reversals in assymetry across the T-Goob structure, forming minor double vergence structures, typically associated with sheath folds (Alsop and Holdsworth, 2004b). The F2 fold exposed on the YZ foliation plane,

and is folded by the F3 phase of folding, forming macroscopic S and Z structures (Table 5.6), this is evident when the T-Goob sheath fold is restored, removing the D4 effects on the structure (Figure 5.19). The model 1 folds also form S and Z assymetries (Figure 5.19).

- The T-Goob sheath fold is also associated with zones of tectonic discontinuities, namely thrust contacts where movement can occur (Alsop, 1994; Alsop and Holdsworth, 1999). The T-Goob Structure is associated with the Lekdam intra-terrane thrust contact and Groothoek inter-terrane thrust contact. The direction of shear associated with overthrusting is sub-parallel to the long axes of the sheath folds. This is evident in the co-linear relationship of the L1 stretching lineations, and is typical in mylonite zones and thrust fronts in zones of high strain (Alsop, 1994; Colliston and Schoch, 2002)
- Reversals in fold obliquity also rotate fold hinges towards the tectonic transport direction (Alsop and Holdsworth, 1999; Alsop and Holdsworth, 2004b). The fold hinges of the model 1 folds rotate towards the tectonic transport direction and is parallel to the tectonic transport direction.

Tectonic Implications

The T-Goob se Berg sheath fold represents one of the most significant sheath fold structures within the Aggeneys Terrane, extending along strike for a distance of a 121 kilometres. The T-Goob Structure represents a kilometre scale sheath fold representing double vergence geometries, typical in sheath fold structures (Alsop and Holdsworth, 1999; Alsop and Holdsworth, 2004b). The T-Goob Structure is not formed due to discrete episodes, but has formed due to progressive deformation, through sub-simple shear conditions, as seen from the co-linear, and co-planar relationship of LS-tectonite fabrics (Table 5.3, 5.4 & 5.6). The T-Goob sheath fold provides information regarding the nature and orientation of the strain ellipse, as co-linear fabrics trend towards the northeast, subparallel to the tectonic transport direction (Colliston et al., 1991), and represents the X direction of the regional strain ellipse, while the co-planar fabrics have a shallow dip towards the northeast, representing the XY plane of the strain ellipse. This is well illustrated in the geometry of the two end closures (Figure 5.19).

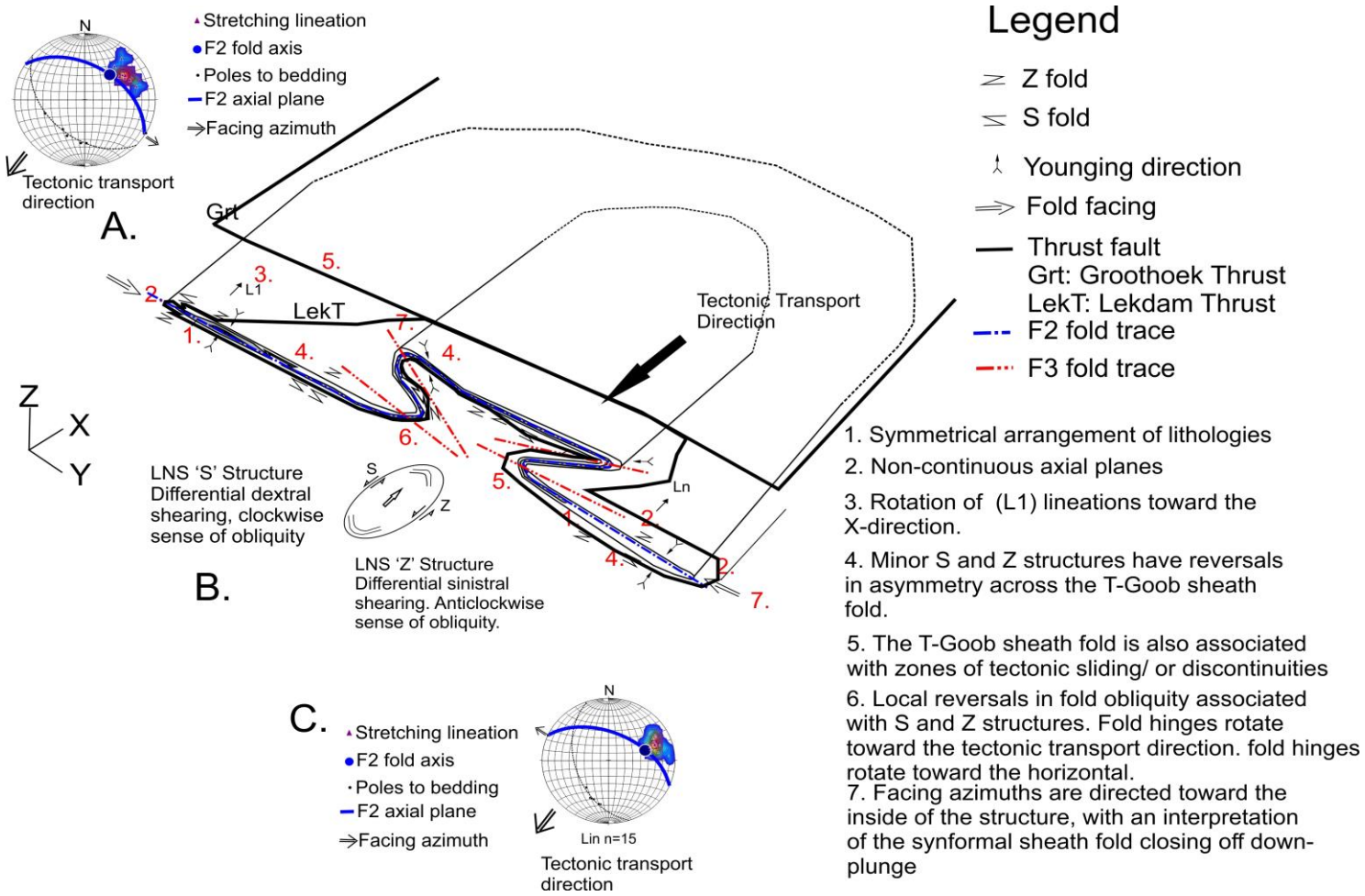

Figure 5.19: Schematic diagram illustrating a restored version of the T-Goob Structure with the removal of the D4 phases of deformation. The restoration is done on the YZ plane of the regional foliation. A: T-Goob Structure represents a sheath fold structure defining macroscopic S and Z structures, if the D4 phase is removed. The criteria needed to define sheath fold structures is defined by numbers 1-7, with the description, found adjacent to the diagram. B: A flow cell model associated with layer normal shearing and the clockwise and anticlockwise rotation of folds to form S and Z structures associated with the macroscopic 'omega' structure. Dextral shearing results in the development of S structures, with sinistral shearing forming Z structures. Localised reversals in fold obliquity are also illustrated, rotating fold hinges toward the horizontal (modified after Alsop and Holdsworth, 2007). C: Stereonets associated with the D2 fold closures drawn at both ends of the T-Goob sheath fold, and are co-linear to the tectonic transport direction. The geometry of these two closure give information regarding the nature and orientation of the regional strain ellipse..

5.5.4 Model 1 and Model 2 folds

Throughout the T-Goob se Berg Structure, two types of F2 folds have been observed on mesoscopic scale and macroscopic scale (Chapter 3.1.1). These type of folds have been identified within the Scottish Highlands (Alsop and Holdsworth, 2007; Alsop and Holdsworth, 2002), and within the eastern and western Namaqua Mobile Belt (Mathee, 2017). The model 1 and model 2 folds are both associated with the D2 phase of deformation and attributes can be seen in Figure 5.20.

Model 1 folds

Model 1 folds form within the layering (S0//S1), and form S and Z structures, which form double vergence geometries ('omega' structures). The model 1 fold axes are co-linear to the regional stretching L1 lineations, and have an S2 axial planar foliation, which is co-planar to the regional S0//S1 foliation. According to the flow model defined by Alsop and Holdsworth (2007), model 1 folds form in the YZ plane of the foliation (where the XY plane of the regional strain ellipse and the S2 foliation plane are assumed to be coincidental) (Figure 5. 20 A), and are associated with lateral ramps. Model 1 folds form due to gradient velocities that form normal to the flow, and form due to normal layer shearing. Model 1 folds form due to retardation in flow, forming strain ellipses which fall within the shortening sector. These strain ellipses rotate clockwise (S-shapes) and anticlockwise (Z-shapes) to form 'omega' folds which define double vergence geometries (Alsop and Holdsworth, 2002; Alsop and Holdsworth, 2007). Model 1 folds are exposed on the YZ foliation plane forming S and Z assymetries acoss the structure (Figure 5.19).

Model 2 Folds

Model 2 folds form oblique and perpendicular to the layering, and form in the XZ planes of the foliation (Figure 5.20 B). Model 2 folds form S and Z folds, with S being the main asymmetry that is representative of the southwest direction of overthrusting. The fold axes are oblique or normal to the L1 lineation. Model 2 folds also folds an S0//S1 foliation and defines an S2 axial planar foliation. According to the flow models defined by Alsop and Holdsworth (2007), model 2 folds show gradient velocities parallel to the flow direction, and are associated with layer parallel shear. Layer parallel shear forms folds at a high angle to the flow direction, and will verge in the direction of flow. This is often seen within the model 2 folds (Alsop and Holdsworth, 2002; Alsop and Holdsworth, 2007).

Application with regard to the T-Goob Structure

Within the T-Goob Structure both model 1 and model 2 folds were identified. The model 1 folds are often parasitic to the larger F2 sheath fold closures, and also form double vergence

geometries with regard to the larger structure (Figure 5.19). The F3 fold phase, that folds the F2 fold trace in the YZ plane of the foliation can be defined as macroscopic Model 1 folds, which produce double vergence geometries (Alsop and Holdsworth, 2002). The F2 model 2 folds have vergence directions corresponding to the direction of overthrusting. Their fold axes vary form oblique, to perpendicular to the regional L1 stretching lineations. The D2 T-Goob se Berg sheath fold is exposed on the surface, perpendicular to its shallow NE plunging fold axis i.e. in the YZ plane of the sheath fold and therefore has double vergence geometries. The structure represents a synformal sheath fold structure, showing younging toward the inside of the structure. The fold-facing shows faces toward the southeast and northwest, toward the inside of the structure. Therefore the structure is interpreted to close-off down-plunge beneath the surface (Figure 5.20 C).

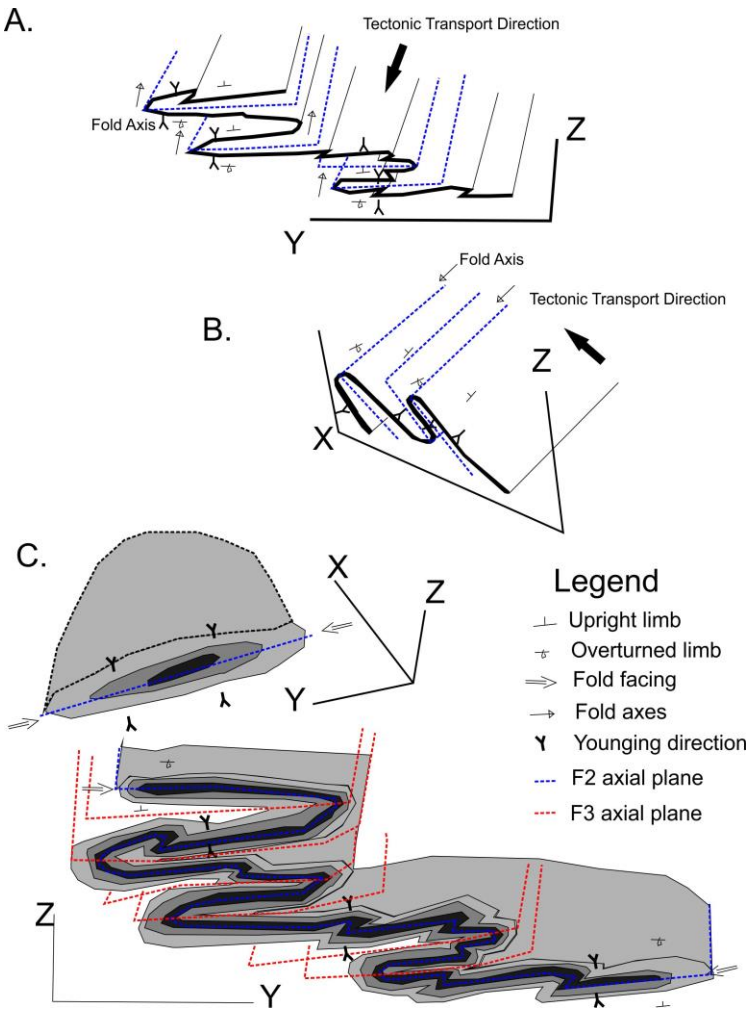

Figure 5.20: Schematic illustration of model 1 and model 2 folds identified within the T-Goob Structure. A: Schematic depiction of a model 1 fold formed through layer normal shearing. Model 1 folds fold the layering, and fold within the YZ plane of the foliation. B: Schematic illustration of Model 2 folds which form due to layer-parallel shear. Model 2 folds, fold within the layering, and therefore folds within the XZ foliation planes. C: A schematic diagram of a model 1 synclinal sheath fold that has been refolded by later phases of folding. The example is synonymous with the attributes associated with the T-Goob sheath fold, with the younging direction directed towards the inside of the structure, and facing azimuths that are directed towards the inside of the structure.

5.5.5 Interpretation Compared to Previous Workers

Two authors, namely Watkeys (1986) and Pretorius (1986) mapped sections of the T-Goob se Berg sheath fold. Watkeys (1986) mapped the Central Domain of the structure, which includes the T-Goob se Berg and Skeur se Berg sub-domains (Figure 5.2), while Pretorius (1986) mapped the Northern and Central Domain of the structure, which includes the Eenriet, Annakoppies and T-Goob se Berg sub-domains (Figure 5.2). The comparison of interpretations and mapping results of both Pretorius (1986), Watkeys (1986) and the author are represented in Figure 5.21 and Figure 5.22.

Watkeys (1986)

Watkeys (1986) interpreted the supracrustal rocks overlying the Achab Suite to be replicated, with the base of each replication being represented by a melange zone (zone of high strain), defined, by well laminated quartzo-feldspathic gneiss and a quartzite unit (Figure 5.21 B). The melange zone is interpreted to be a tectonic-melange, separating the supracrustal rocks from the Achab Suite at the base. This led to the interpretation of the Achab Suite to intrude a 'pre-Bushmanland' sequence, and represents the 'floor' to the overlying supracrustal rocks (Watkeys, 1986). Although this interpretation is based on a thrust model, and also interpretations made at prominent locations (e.g. The Skeur se Berg and T-Goob se Berg), the fact that the stratigraphy is poorly represented, resulted in this interpretation to be incorrect. If the mapped area of Watkeys (1986) is compared to that of the author (Figure 5.21), significant differences are noted. Watkeys mapped the medium grained quartz-feldspar gneiss correctly on the northern limb, and interpreted it to be located on the southern limb. The medium quartz-feldspar gneiss inferred to be on the southern limb, is in fact a nodular-rhythmic nodular sillimanite-quartz-feldspar gneiss with interbands of biotite-sillimanite schist (Figure 5.21 A & B'). Therefore the duplication of units is a misinterpretation by Watkeys (1986).

The duplications and cut-out of stratigraphic units on the northern and southern limbs of the structure were also not considered (Figure 5.21 A). The central hinge was also poorly defined by Watkeys (op.cit), as it was represented to be a massive amphibolite unit, interbanded within a biotite schist unit (Figure 5.21 A & B). This is however not correct, as it is defined by biotite-sillimanite schist, biotite gneiss and a volcanoclastic/chemogenic unit defined by actinolite, diopside and banded quartzite. The central hinge was also insufficiently mapped toward the southeast on the Skeur se Berg Sub-domain of the structure. The lower southern quartzite unit was also inferred to be duplicated toward the south, which is not the case. Toward the Skeur se Berg, duplications and cut-out structures are observed on the northern limb and not on the southern limb. The central hinge zone was not recognised toward the east, together

with the segments above and below it on the limbs of the Skeur se Berg (Figure 5.22 A and B). Although the Achab Suite was located on the southern limb of the structure, no intrusive rocks or units were mapped to the north of the structure (Figure 5.21 B). This also makes Watkeys (1986) interpretation problematic, as the Lekdam Gneiss is found on the northern limb of the structure, which is different to the Achab Suite (Figure 5.21 A). The major difference between both structures, is that the stratigraphy defined by Watkeys (1986) is too simplistic, and not a true reflection of the T-Goob Structure, as large sequences are not duplicated as one would expect in thrust sequences, but that duplications are only present on the limbs of the T-Goob Strucrure, with the structure representing a folded sheath fold structure, that folds a set of earlier D1 imbricates. This interpretation can however only be made if lithological units are mapped and traced along strike for kilometres and the fold hinges at the extremeties are identified. This study disagrees with the Watkeys (op.cit) thrust fault model for the T-Goob-Skeur se Berg sections of the T-Goob sheath fold.

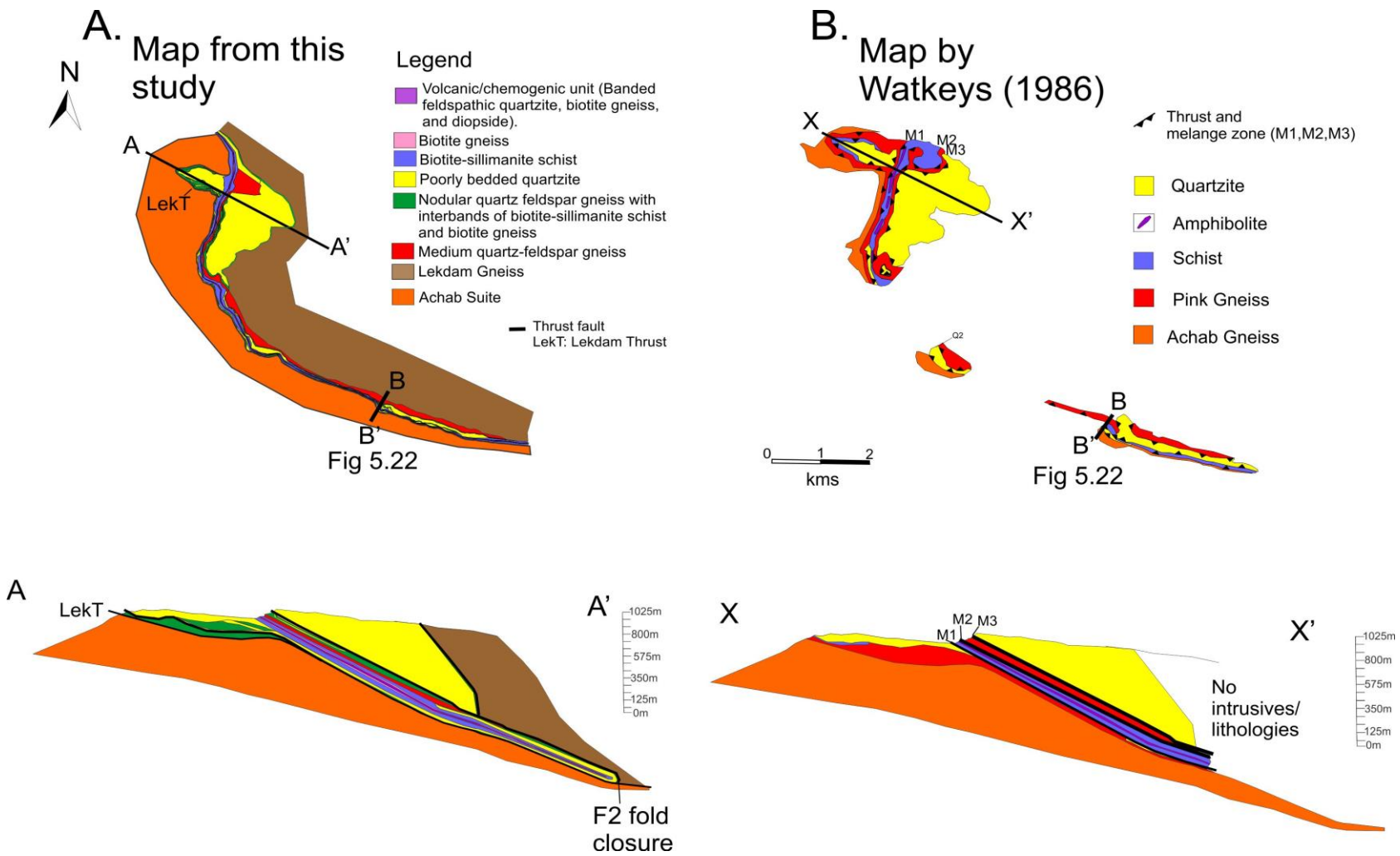

Figure 5.21: Comparitive diagram illustrating the mapping differences between this study and Watkeys (1986). Figure A: A simplified geological map of the T-Goob sub-domain mapped by the author. Section A-A' represents a section across the XZ foliation plane illustrating the Lekdam Thrust contact and folded imbricates seen within the T-Goob Sub-domain. Figure B: A simplified geological map of Watkeys (1986) of the T-Goob Sub-domain. Section A-A' represents a section across the XZ foliation plane illustrating the stratigraphy mapped by Watkeys (1986) and the melange zones (M1, M2 and M3) interpreted by Watkeys (1986). Modified after Watkeys (1986).

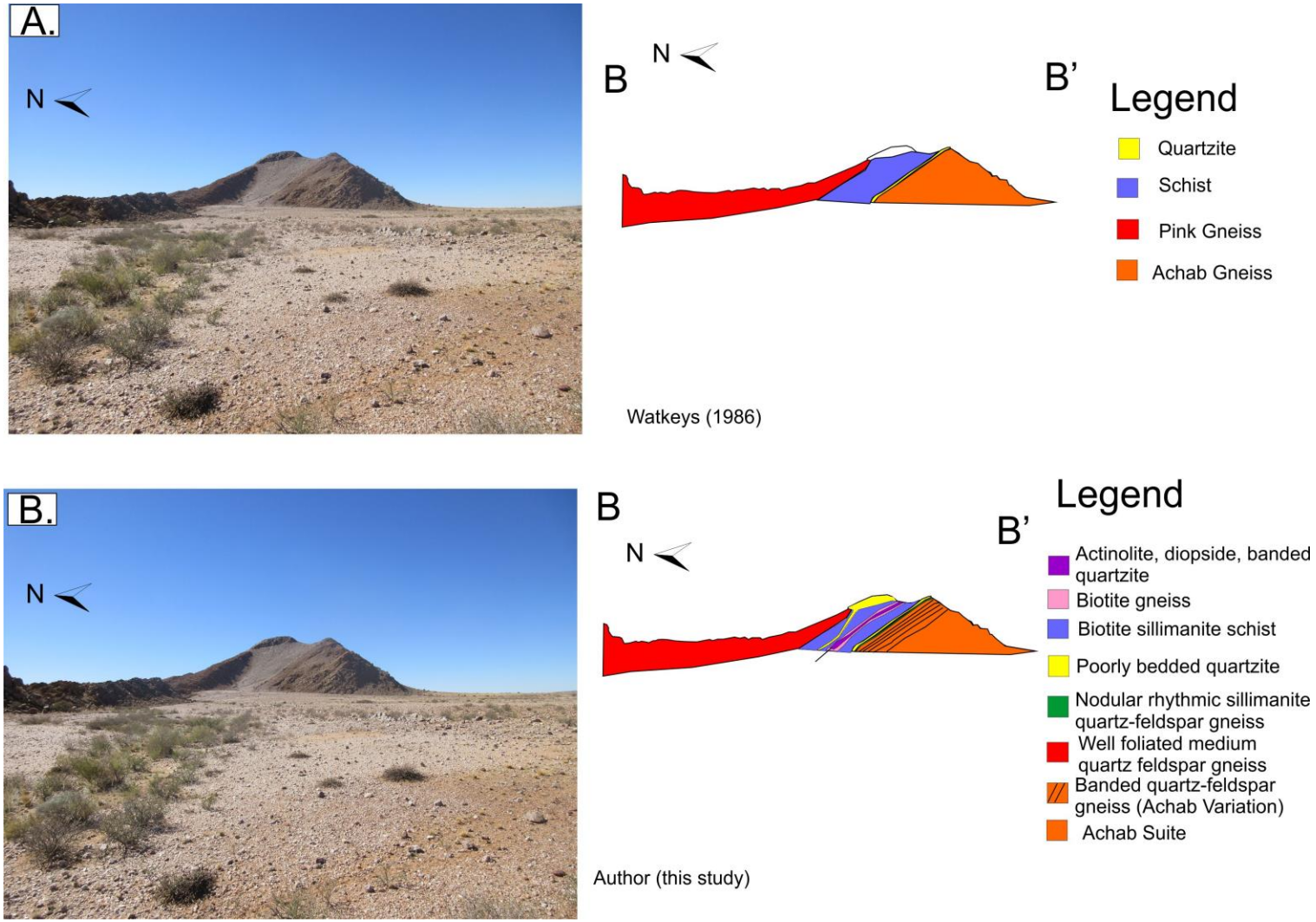

Figure 5.22: Photographic differences illustrate in section on XZ planes to the foliation at the Skeur se Berg looking toward the east (location can be seen in Figure 5.21; section B-B'), depicting the differences in mapping between the author and Watkeys (1986). A; Photo of a section across the structure, with an interpretation of the stratigraphic units as identified by Watkeys (1986). B: Same photo of a section across the structure, with a different interpretation of the stratigraphic units as identified by the author across the structure.

Pretoruis (1986)

Pretorius (1986) mapped a section of the Central Domain at T-Goob se Berg, and the entire Northern Domain of the structure (Figure 5.23 A). He sub-divided the stratigraphy into the Annakoppies Formation and T-Goob Formations, but never correlated the two formations even though the stratigraphy were similar. The stratigraphy at the Eenriet sub-domain was also never correlated. Pretorius (1986) interpreted the T-Goob Structure to be represented by an imbricated tectonic unit, which is thrusted out toward the northwest. Although the variations of the Achab Suite were well mapped on the lower limb of the structure, no intrusive units were accurately mapped on the upper limb of the structure (Figure 5.23 A and B). The stratigraphy in the hinge zone of the structure was also misinterpreted, between the biotite-schist and biotite gneiss units. The central volcanic/chemogenic units was also mapped as a massive amphibolite unit, which is not correct. The extrapolation of this unit toward the Annakoppies Sub-domain and Eenriet Sub-domain was also done rather haphazardly. Another major concern is that Pretorius (1986) never mapped the central core/hinge of the structure, which is defined by the sillimanite ore body (Figure 5.23 A and B).

Summary

With regard to both interpretations, the major issues are associated with the intrusive units (Lekdam Gneiss and Achab Suite) and their contact relationships that were not mapped on the upper limb of the T-Goob sheath fold. For both interpretations, only local structural and stratigraphic attributes were considered. The extrapolation and interpretation of attributes towards the southeast and northwest were not considered, making their tectonic models and interpretations to be vague, and unfounded for the T-Goob se Berg structure which is a D2 macroscopic sheath fold. What is also apparent is that there are large discrepancies when the stratigraphy is considered and that not enough of the structure and stratigraphy was investigated and physically mapped by the two researchers.

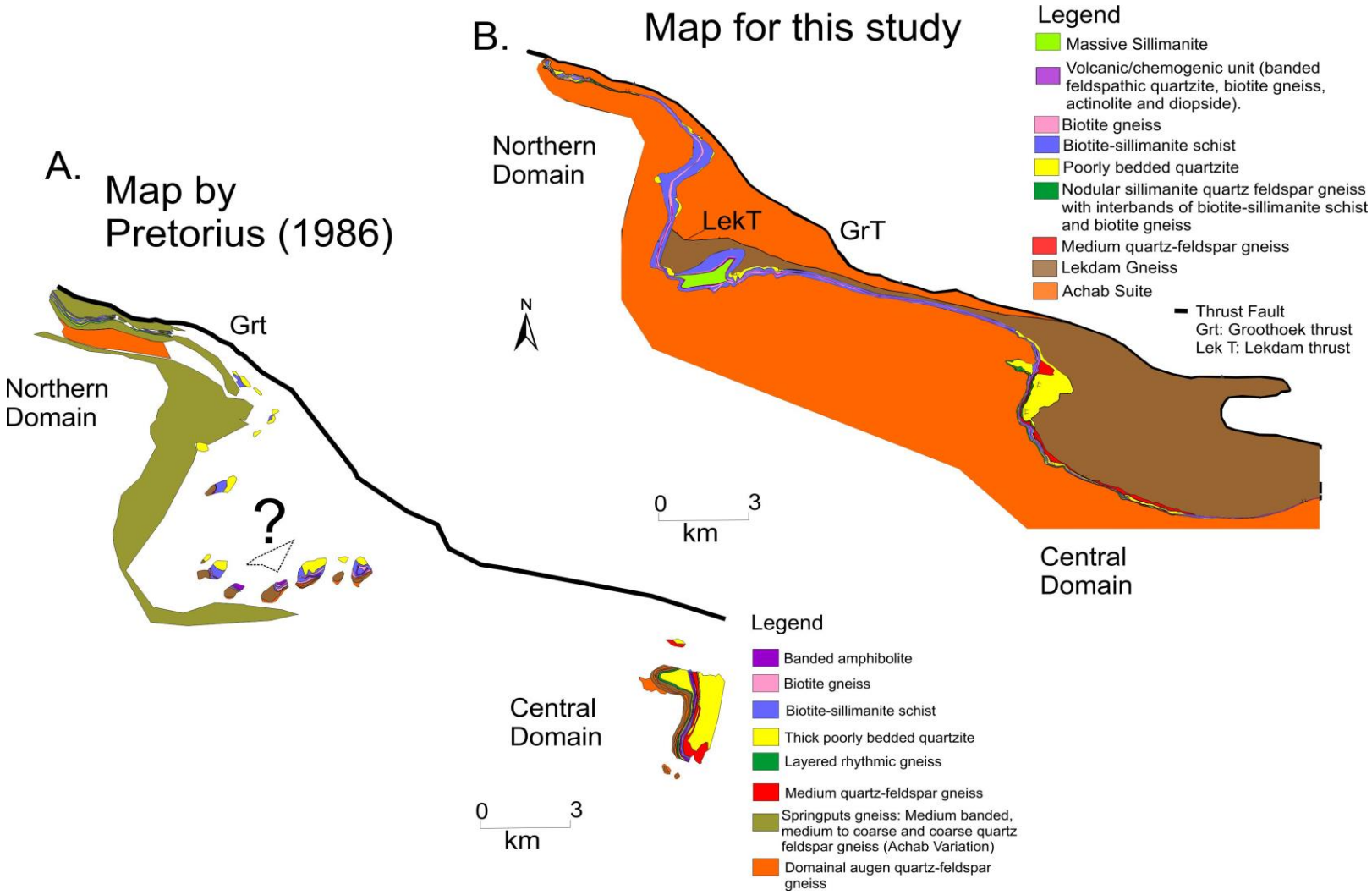

Figure 5.23: Comparative diagram of the geology associated with the Northern Domain between the author and Pretorius (1986). A: The geological map modified after Pretorius (1986). The map is insufficiently compiled, with fragmented stratigraphic units. The sillimanite ore body associated with the core of the structure is missing at the large question mark sign. The variations in the Achab Suite is well represented in the southwestern portion of the structure. The northern Lekdam Gneiss in the north of the structure is not mapped at all. B: Represents a simplified geological map by the author of the Northern Domain, illustrating the relationship between the supracrustal and the intrusive rocks.

5.6 Summary

- The T-Goob Structure represents a highly folded kilometre scale sheath fold structure that has been affected by five phases of deformation.
- The D1 phase is defined by an S1 foliation associated with the intrusion of the Lekdam Gneiss and Achab Suite. The S1 foliation is co-planar to the S0-fabric (bedding). The D1 phase is also defined by the D1 intra-terrane thrusts (Lekdam Gneiss), and by intra-stratigraphic thrusting, that involves the duplication and cutting out of stratigraphic units on the limbs of the T-Goob Structure. The L1 stretching lineation, developed during the D1 thrusting, trends toward the northeast, and coincides with the regional tectonic transport direction (Colliston et al., 1991)
- The D2 phase is defined by macroscopic sheath fold development, which folds an S0-1 and defines an S2 axial planar foliation. The D2 phase also folds the Lekdam Thrust contact and associated intrusive units (Achab Suite and Lekdam Gneiss). The D2 phase is also defined by model 1 and model 2 folds, that fold an S0//S1 foliation and define an S2 axial planar foliation. The F2 fold axes and F2 sheath fold axes are co-linear to the L1 regional stretching lienation, and this corresponds to the southwesterly directed tectonic transport direction (Colliston et al., 1991).
- The D3 phase is defined by macroscopic double vergent folds which form S and Z asymmetries and refolded the F2 fold trace.
- The D4 phase is defined by F4 open folds which form Z asymmetries, due to sinistral wrench shear (Colliston and Schoch, 2013), and refolds the F2 fold trace, both in the southern and northern domain. The F4 fold axes are co-linear to the F2 fold axes and L1 stretching lineations.
- The D5 phase is defined by east-west shears located on the limbs of the T-goob sheath fold. D5 results in the intense isoclinal folding of D3 and D4 structures, and also result in boudinage effects seen across the structure, affecting the limbs and central hinge of the structure. The D5 phase also rotates S and L structures in the Southern Domain of the T-Goob sheath fold.
- The D2 T-Goob sheath fold can also be defined as a synformal kilometre scale sheath fold in the elliptical end closures with facing azimuths directed toward one another.
- The D2 T-Goob sheath fold has not been formed through discrete deformational episodes, but through a single long-lived progressive ductile shear process (Colliston et al., 1991), with the various planar fabrics (S1-2 fabric, F2 sheath fold axes) being co-planar and linear fabrics (fold axes of sheath folds and L1 stretching lineations) being co-linear plunging in an east-northeasterly to northeasterly direction, coinciding with the regional tectonic transport direction (Colliston et al., 1991; Colliston and

Schoch, 2013; Mathee, 2017). The co-linear and co-planar elements are indicative of a sub-simple shear environment under deep crustal levels (Colliston et al., 1991; Colliston and Schoch, 2002).

CHAPTER 6

Summary and Conclusions

6.1 Summary and Conclusions

- The stratigraphic successions and style of deformation differ from west to east across the Aggeneys Terrane. One notable characteristic is the fragmented nature of the stratigraphy found in the eastern Aggeneys Terrane in the form of double vergence isoclinal structures, elliptical structures, and refolded isoclinal structures, all classified as sheath folds. Nowhere in the study area are the stratigraphic sequences in contact with one another, which is representative of a higher strain zone. It is similar to the high strain zone in the western Aggeneys Terrane containing the Broken Hill, Swartberg, Aggeneys and Gamsberg structures (Colliston et al., 1991; Colliston et al., 2012).
- The area investigated consists of four well defined structural domains, with all domains being interpreted as kilometre scale intra-terrane thrust sheets. Each thrust sheet contains fragmented tectonic sequences that define sheath folds. The fragmented stratigraphic sequences can be divided into four well-defined structural domains: Structural Domain 1 (Witkoppies Structural Domain), Structural Domain 2 (Samoep Structural Domain), Structural Domain 3 (Lekdam Structural Domain), and Structural Domain 4 (Houmoed Structural Domain).
- When vertically restored, the upper structural sequences namely: Structural Domain 1 (Witkoppies Structural Domain) and Structural Domain 2 (Samoep Structural Domain) represent new stratigraphy, not previously identified toward the west, and differ from traditional Wortel Formation supracrustal rocks (Praekelt and Schoch, 1997). The lower structural sequences associated with Structural Domain 3 (Lekdam Structural Domain) and Structural Domain 4 (Houmoed Structural Domain) can be correlated with the top portion of the Wortel Formation in the Haramoep Mountains in the west (Praekelt, 1994).
- The pressure-temperature conditions for the Aggeneys Terrane reflect upper amphibolite facies conditions (van Zyl, 1986; Pretorius, 1986), with the development of prominent L-S fabrics seen across the study area. All the phases of deformation occurred progressively (D1-D6) within the study area, similar to what has been identified in other parts of the Namaqua Mobile Belt (Colliston and Schoch, 2013).
- The D1 thrusting phase represents the 1st phase of deformation defined by terrane accretion, together with the emplacement of the large intra-terrane syntectonic thrust sheets. The D1 phase defines prominent S1 foliation formed during upper amphibolite conditions (Pretorius, 1986; van Zyl, 1986), and are seen across all structural domains. The S1 foliation is co-planar to the S0 compositional banding. All the phases of deformation are associated with the Namaqua Orogeny (1.2-1.4Ga), with the D1 phase

interpreted to take place at 1.3 GA, associated with the emplacement of syntectonic sheet intrusives (Figure 6.1). The first metamorphic event associated with the S1 fabric (amphibolite grade conditions, is also interpreted to occur at 1.3 GA (Figure 6.1).

- The D2 phase is defined by the formation of macroscopic sheath fold structures, which is seen across the study area in all domains, and represents all fragmented structural sequences. The sheath fold structures define an axial planar S2 foliation which is co-planar to S0//S1 foliation, that folds around the F2 fold hinges and are interpreted to form under upper amphibolite conditions (van Zyl, 1986). The S2 axial planar foliation also defines the regional penetrative S2 foliation, seen across the entire study area. The D2 sheath fold phase also folds both intrusives and supracrustal sequences and are interpreted to form at 1.2 Ga (Figure 6.1).
- The development of L1 stretching lineations lie within the XY foliation plane and represent the X-direction of the regional strain ellipse. The L1 stretching lineations have moderate to shallow plunges and trend east-northeasterly, sub-parallel to the tectonic transport direction (Colliston et al., 1991). The L1 lineations are co-linear concerning the F2, F3 and F4 fold axes identified regionally.
- The D3 phase of deformation is defined by the refolding of D2 sheath fold structures, which forms a localised S3 foliation within some F3 fold hinges. The S3 foliation is parallel to S0//S1 and S2 foliations. The F3 fold axes also have a co-linear relationship with regard to the F2 fold axes and L1 stretching lineations. The D3 phase of deformation is interpreted to have taken place at 1.1 Ga (Figure 6.1).
- The post accretion D4 phase of folding associated with wrench shearing (Colliston and Schoch, 2013) consists of macroscopic F4 open folds with Z asymmetries. The D4 phase of folding folds earlier structures and affects all structural domains. Essentially the entire study area is dominated by this, and can be defined as a macroscopic D4 structure. The D4 phase is interpreted to form at 1, 05 Ga (Figure 6.1), and is associated with the intrusion of the Koperberg Suite into F4 folds within the Okiep Terrane (Colliston and Schoch, 2013, Clifford et al., 2004; Joubert, 1986).
- The D5 east-west shear zone events deformed all earlier foliations, and also caused the D4 open folds to tighten and become isoclinal, with increasing shear strain, which also resulted in the boudinage effect seen in the hinge zones and limbs of the D2-D3 sheath fold structures. The D5 phase deforms a mylonitic foliation and often occurs on the limbs of the megascopic sheath fold structures and causes reactivated movements seen on intra-terrane thrust boundaries. The D5 east-west shears result in the rotation of S and L structures in the northern limb of the major D4 structure. The D5 phase of deformation has been interpreted to form at 1 Ga (Figure 6.1).

- The D6 phase of deformation associated with the northwest- southeast trending shears is well exposed on the eastern part of the study area, close to the Groothoek Thrust contact and in the eastern part of the Witkoppies Structural Domain. The D6 phase is associated with Tantalite Valley deformation, and has a dextral sense of shear, and is associated with mylonitic fabrics (Colliston, 1990). The D6 phase is also interpreted to occur just after the D5 phase at 1 Ga.
- The different sheath fold structures were classified using listed criteria published by various authors globally.
- The dominant deformation process gave rise to structures and fabrics that is of general shear. Evidence for the latter is a well-developed regional foliation, with grain size reduction features and a consistent preferred orientation of minerals, the co-planar relationship of planar structures (fabrics and axial planes of earlier folds) and the co-linear relationship of linear elements (mineral stretching lineations, fold axes of sheath folds and late folds). The linear fabric defines the X-direction of shear which trends northeasterly to east-northeasterly (Colliston, 1990; Colliston et al., 1991; Colliston and Schoch, 2013).
- The XY planes of the regional strain ellipse (represented by the regional S2 foliation), dip shallowly north-northeasterly and the X-direction of the ellipse trends east-northeasterly, parallel to the tectonic transport direction. However, the strain ellipse is calculated to not only be dominated by a simple shear process, as the cores of the sheath folds, when used for the purpose of calculating strain (Alsop and Holdsworth, 2006), and show a component of oblate flattening giving rise to a process of sub-simple/general shear.
- A punctuated progressive ductile shear model is therefore proposed under general shear conditions for the eastern sector of the Aggeneys Terrane, coinciding with results obtained in the western and eastern Namaqua Mobile Belt (Colliston et al., 1991; Colliston and Schoch, 2013; Mathee, 2017), with the earlier phases of deformation being similar to the phases identified in the west (Colliston and Schoch, 2002).

Table 6. 1: Correlation of age dates associated with the Pofadder and Aggeneys Terranes, and their association with the structural domains found within the eastern Aggeneys Terrane.

Age Ga	Pofadder Terrane	Integrated Sequence of Magamatic and Structural Events Eastern Aggeneys Terrane (Study Region)				Event	Orogeny
			Houmoed Structural Domain	Lekdam Structural Domain	Witkoppies Structural Domain		
2.0	Orange River Volcanism					Pre-Vioolsdrif deformation	Orange River
1.9	Vioolsdrif Suite						
1.73							
2.0		Aggeneys Subgroub Wortel (base) Formation (qtz, sch, iron fm, amph/calcsilicate unit).	Rest of Subgroub absent eastwards		Volcanic Unit (Witkoppies Sequence)		
1.8							
1.7 (4)							
1.6 (2)		Koeris Formation (top)			Nouzees Mafic Intrusives		
1.4 (4)							
1.3		Syntectonic Sheet Intrusives	D1 M1 Mi1 Achab Suite	D1 M1 Mi1 Lekdam Gneiss	D1 M1 Mi1 Vaalputs Suite	Penetrative amphibolite grade regional fabric associated with augen gneisses, thrusting and macro sheath folds.	Namaqua
1.2			D2 Mi2	D2 Mi2	D2 Mi2		
1.1			D3	D3	D3	Isoclinal refolding of sheath folds.	
1.05 (1)	Koperberg Suite		D4	D4	D4	East-west open folds.	
			D5	D5	D5	Dextral shearing along regional easterly fabric.	
1.0 (3)	Pegmatites		D6	D6	D6	NW-SE dextral shearing.	

(1) Joubert (1986)
(2) Colliston and Schoch (2000)
(3) Cornell et al. (2006)
(4) Joubert (1986)

modified after Colliston and Schoch (2000)

M: Metamorphism
Mi: Migmatites

CHAPTER 7

Acknowledgements

7.1 Acknowledgements

I would firstly like to thank my creator, the Lord God Almighty, as it was through His grace only that this M.Sc. could be completed. It is only in Him and through Him that I could accomplish this study.

To my promoter and mentor Prof Wayne P. Colliston I would also like to thank for his criticism and guidance through the years. A special thanks also to two previous colleagues of mine Marthinus Mathee and Photos Kalpakiotis, for their insights into melts and sheath folds that contributed greatly to this study, especially in the early years.

I would also like to thank my loving wife Carika for all her emotional support and understanding! Your love and patience helped me tremendously through the years!

Special thanks to my parents (Errol and Ansie), who supported me from day one! Your sacrifices and love will never be forgotten. A word of thanks I would also like to extend to my grandparents and parents-in-law, who also supported me through the years.

Special thanks also to the farmers' association in Pofadder, who assisted me in the start of this study, and to the many farmers in the Bushmanland District, your hospitality and friendships, will never be forgotten. Special thanks also goes to Wilhelm and Alida van Niekerk (Poortjies), Abrie van Niekerk (Poortjies), Gerrard and Liesel Visser (Skietpoort), Wimpie and Esna Visser (Namies South), Thys and Dirna Steenkamp (Nouzees), Gert and Marie van Zyl (Nouzees), Jannie and Alta Kruger (Samoep), Nikkie Steenkamp (Gannapoort Berg), Piet van Niekerk (De Neus), Japie and Susan Kruger (Boomrivier) and Piet Truter (Witkoppies and Vaalputs). A word of thanks also to Dominee Alwyn Roux, your sermons on Sundays, special visits in my caravan and friendship will never be forgotten.

A very special thanks goes to Anna and Gert Kruger (De-Rust). Baie dankie vir julle vriendskap en opofferings, veral in die begin van my studie. Dankie dat julle my gehuisves het, en gehulp het al was dit droog! Ek sal julle ondersteuning en vriendskap nooit vergeet nie. De Rust sal altyd a plek in my hart he, en mag die Here julle Seen!

A very very special thanks also goes to Sunette van Zyl (Houmoed). Baie baie dankie tannie vir jou opoffering en hulp tydens hierdie studie en dat ek Houmoed kon gebruik as n navorsings tuiste. Jou Godsdiens, vriendskap en raad tydens die moeilike tye sal ek nooit vergeet nie. Mag die Here jou Seen! En mag die reen altyd kom wanneer dit nodig is!

Thank you also goes to the REI grant and national research fund.

Word of thanks also to the Geology Department at the University of the Free State.

CHAPTER 8

References

8.1 References

Agenbacht, A.L.D. and Praekelt, H.E., 2007. The Pofadder sheet 2918, Geological Series 1:250,000. *Council for Geoscience*, Pretoria, South Africa.

Agenbacht, A.L.D., 1992. 'n Geologiese ondersoek van die T'oubep Suite, suidwes van Kakamas, Noordwes-Kaap. pp. 115, 58.

Agenbacht, A.L.D., 2007. The geology of the Pofadder area; Explanation sheet 2918; Scale: 1:250,000. Pretoria: *Council for Geoscience*, South Africa.

Albat, H.M., 1984. The Proterozoic graulite facies terrane around Kliprand, Namaqualand Metamorphic Complex. *Bulletin Precambrian Research Unit*, University of Cape Town, Volume 33, pp. 382.

Allmendinger, R., Cardozo, N. & Fisher, D., 2013. Structural Geology Algorithms: Vectors & Tensors. Cambridge, England: Cambridge University Press, pp. 289.

Alsop, G.I., 1994. Relationships between distributed and localised shear in the tectonic evolution of a Caledonian fold and thrust zone, northwest Ireland. *Geological Magazine*, Volume 131, pp. 353-362.

Alsop, G.I. and Holdsworth, R.E., 1999. Vergence and facing patterns in large-scale sheath folds. *Journal of Structural Geology*, Volume 21, pp. 1335-1349.

Alsop, G.I. and Holdsworth, R.E., 2002. The geometry and kinematics of flow perturbation folds. *Tectonophysics*, Volume 350, pp. 99-125.

Alsop, G.I. and Holdsworth, R.E., 2004a. Shear zone folds: records of flow pertubation or structural inheritance? In: Alsop, G.I., Holdsworth, R.E., McCaffrey, KJW., Hand, M. (Eds.), Flow processes in faults and shear zones. Special Publication 224. *Geological Society, London*, pp. 177-199.

Alsop, G.I. and Holdsworth, R.E., 2004b. The geometry and topology of natural sheath folds: a new tool for structural analysis. *Journal of Structural Geology*. Volume 26, pp. 1561-1589.

Alsop, G.I. and Holdsworth, R.E., 2006. Sheath folds as discriminators of bulk strain type. *Journal of Structural Geology*, Volume 28, pp. 1588-1606.

Alsop, G.I. and Holdsworth, R.E., 2007. Flow pertubation folding in shear zones. In: Deformation of the Continental Crust: The legacy of Mike Coward. *Special Publications London: Geological Society*, Volume 272, pp. 77-103.

Alsop, G.I., Holdsworth, R.E. and McCaffrey, K.J.W., 2007. Scale Invariant sheath folds in salt, sediments and shear zones. *Journal of Structural Geology*, Volume 29, pp. 1585-1604.

Alsop, G.I. and Holdsworth, R.E., 2012. The three dimensional shape and localisation of deformation within multilayer sheath folds. *Journal of Structural Geology,* Volume 44, pp. 110-128.

Barton, E.S., 1983. Reconnaissance isotopic investigations in the Namaqua Mobile Belt and implications for Proterozoic crustal evolution Namaqualand Geotraverse, pp. 45-66. In: B. Botha, ed. Namaqualand Metamorphic Complex, *Special Publication Geological Society of South Africa*., Volume 10, pp.198.

Blignault, H.J., 1980. Orange River Group, pp. 282-288. *In*: SACS (Compiler, L.E. Kent). *Stratigraphy of South Africa*, Part1. Handboek. geol. Surv. South Africa, 8, pp. 690.

Blignault, H.J., van Aswegen, G., van der Merwe, S.W. and Colliston, W.P., 1983. The Namaqualand Geotraverse and environs: part of the Proterozoic Namaqua Mobile Belt. *In*: B. Botha, ed. Namaqualand Metamorphic Complex. *Special Publication Geological Society of South Africa*, Volume 10, pp. 198.

Busk, H.G., 1929. Earth Flexures. Cambridge University Press.

Clifford, T.N., Barton, E.S., Stern, R.A. and Duchesne, J.-C., 2004. U-Pb calender for Namaquan (Grenville) crustal events in the granulite-facies terrane of the O'okiep Copper District of South Africa. *Journal of Petrology,* Volume 45, pp. 669-691.

Cobbald, P.R. and Quinquis, H., 1980. Development of sheath folds in shear regimes. *Journal of Structural Geology*, Volume 2, pp. 119-126.

Coetzee, C.B., 1941. Sillimanite-corundumn rock: A metamorphosed bauxite in Namaqualand. Geological Society of South Africa, Volume 28, pp. 199-205.

Coetzee, C.B., 1958. Manganiferous iron ore, haematite, barite and sillimanite on Gams (Portion1), Namaqualand. *Bulletin Geological Survey of South Africa*, Volume 28, p. 29.

Colliston, W.P., 1990. A stratigraphic and structural investigation of part of the Namaqua Mobile Belt between Dabenoris and Steyerkraal, South Africa. Ph.D. thesis (unpublished), *University of the Orange Free State*, Bloemfontein, pp. 259.

Colliston, W.P. (Editor), Praekelt, H.E., Strydom, D., Pretorius, JJ. and Schoch, A.E. (Coordinator), 1986. Stratigraphic map of Central Bushmanland (1:100,000 geological map). Department of Geology, University of the Orange Free State, Bloemfontein, South Africa, (One sheet).

Colliston, W.P. and Schoch, A.E., 2000. Mid-Proterozoic tectonic evolution along the Orange River on the border between South African and Namibia. *Communs Geological Survey of Namibia*, Volume 12, pp. 53-62.

Colliston, W.P. and Schoch, A.E., 2002. The structural development of the Aggeneys Hills, Namaqua Metamorphic Complex. *South African Journal of Geology*, Volume 105, pp. 301-324.

Colliston, W.P. and Schoch, A.E., 2006. The distribution and diagnostic features of deformed plutonic rocks in two terranes of the Namaqua Mobile Belt along the Orange (Gariep) River, South Africa. *South African Journal of Geology*, Volume 105, pp. 369-392.

Colliston, W.P. and Schoch, A.E., 2013. Wrench-shearing during the Namaqua Orogenesis – Mesoproterozoic late stage deformation effects during Rodinia assembly. *Precambrian Research*, Volume 223, pp. 44-58.

Colliston, W.P., Cornell, D., Schoch, A.E. and Praekelt, H.E., 2015. Geochronological constraints on the Hartbees River Thrust and Augrabies Nappe: New insights into the assembly of the Mesoproterozoic Namaqua-Natal Province of Southern Africa. *Precambrian Research*, Volume 265, pp. 150-165.

Colliston, W.P., Praekelt, H.E. and Schoch, A.E., 1989. A broad perspective (Haramoep) of geological relations established by sequence mapping in the Proterozoic Aggeneys Terrane, Bushmanland. *South African Journal of Geology*, Volume 92(1), pp. 42-48.

Colliston, W.P., Praekelt, H.E. and Schoch, A.E., 1991. A progressive ductile shear model for the Proterozoic Aggeneys Terrane. *Precambrian Research*, Volume 49, pp. 205-215.

Colliston, W.P., Praekelt, H.E., Strydom, D. and Loock, J.C., 1986. Aspects of the stratigraphy and depositional environment of part of the Bushmanland Group in the Aggeneys Terrane, Namaqua Mobile Belt. Abstr. *Geocongress*, Johannesburg, pp. 773-776.

Colliston, W.P., Schoch, A.E. and Praekelt, H.E., 2012. Stratigraphy of the Mesoproterozoic Aggeneys Terrane, Western Namaqua Mobile Belt, South Africa. *South African Journal of Geology*, Volume 115(4), pp. 449-464.

Coney, P., Jones, D. and Monger, J., 1980. Cordilleran suspect terranes. *Nature*, Volume 288, pp. 329-333.

Cornell, D.H., Thomas, R.J., Moen, H.F.G., Reid, D.L., Moore, J.M., Gibson, R.L, 2006. Namaqua-Natal Province. *In*: Johnson, M.R., Anhaeusser, C.R., Thomas, R.J. (Eds.),

Geology of South Africa. *Geological Society of South Africa and Council for Geoscience*, Pretoria. pp. 325-379.

De Jager, D.H. and Von Backstronm, J.W., 1961. The sillimanite deposits in Namaqualand near Pofadder. *Bulletin Geological Survey of South Africa*, Volume 33, pp. 49.

Diener, J., 2014. Low-P-high-T metamorphism of the Aggeneys Terrane, Namaqua Metamorphic Complex, South Africa. *South African Journal of Geology*, Volume 117(1), pp. 31-44.

Fleuty, M., 1964. The description of folds. London: *Proceedings of the Geologists' Association*, Volume 75, pp. 461-492.

Flinn, D., 1962. On folding during three-dimensional progressive deformation. Quarterly *Journal of the Geological Society.* London 118, pp. 385-433.

Fossen, H. and Rykkelid, E., 1990. Shearzone structures in the Øxygarden area, West Norway. *Tectonophysics,* Volume 174, pp. 385-397.

Fossen, H., Carolina, G., Cavalcanteb, G., Vizeu, R. L. and Carlos, P., 2019. Deformation-progressive or multiphase. *Journal of Structural Geology*, Volume 125, pp. 82-99.

Fowler, A.R. and Kalioub, B.E., 2002. The Migif-Hafafit gneissic Complex of the Egyptian Eastern Desert: fold interference patterns involving mutiply deformed sheath folds. *Tectonophysics*, Volume 346, pp. 247-275.

Frick, C. and Coetzee, C.B., 1974. The mineralogy and the petrology of the sillimanite deposits west of Pofadder, Namaqualand. Transactions of the *Geological Society of South Africa*, Volume 77(2), pp. 169-183.

Gevers, T.W., 1936. Phase of Mineralisation in Namaqualand Pegmatites. *Transactions of Geological Society of South Africa,* Volume 39, pp. 331-377.

Ghosh, S.K. and Segupta, S., 1999. Planar, non-planar and refolded sheath folds in the Phulad Shear Zone, Rajasthan, India. *Journal of Structural Geology*, Volume 21, pp. 1715-1729.

Hartnady, C., Joubert, P. and Stowe, C., 1985. Proterozoic crustal evolution in south-western Africa. *Episodes,* Volume 8(4), pp. 236-244.

Henderson, J.R., 1981. Structural analysis of sheath folds with horizontal X-axes, northeast Canada. *Journal of Structural Geology*, Volume 3, pp. 203-210.

Hobbs, B.E, Means W.D. and Williams, P.F., 1976. *An Outline of Structural Geology.* New York: John Wiley and Sons.

Huddelston, P.J., 1992. A comparison between glacial movement and thrust sheet or nappe emplacement and associated structures. In: Mitra, S., Fischer, G.W. (Eds), Structural Geology of Fold and Thrust Belts. Baltimore: *Johns Hopkins University Press*, pp. 81-91.

Joubert, P., 1971. The regional tectonism of the gneisses of part of Namaqualand*. Bulletin Precambrian Research Unit*, University of Cape Town.10, pp. 220.

Joubert, P., 1973a. Geological map of the Aggeneys area, Scale: 1:100,000. *Precambrian Research Unit,* University of Cape Town, 1 sheet.

Joubert, P., 1973b. Geological map, of the Pofadder area, Scale: 1:100,000. *Precambrian Research Unit,* University of Cape Town, 1 sheet.

Joubert, P., 1974. The gneisses of Namaqualand and their deformation. *Transactions of Geological Society of South Africa*, Volume 77, pp. 339-345.

Joubert, J., 1975. Geological maps of the Aggeneys and Pofadder areas (1:100,000). *Precambrain Research Unit*, University of Cape Town. Two sheets.

Joubert, P., 1986. The Namaqualand Complex - a model of Proterozoic accretion? *Transactions of the Geological Society of South Africa,* Volume 89, pp. 79-96.

Lipson, R., 1978. Some aspects of the geology of part of the Aggeneysberge and surrounding gneisses, Namaqualand. Johannesburg: University of the Witwatersrand South Africa, pp. 100.

Maclaren, A.H., 1988. The geology of the area east of Pofadder with emphasis on shearing associated with the Pofadder Lineament, North West Cape. Unpublished M.Sc thesis. *University of Cape Town*, South Africa pp. 123.

Mathee, H.L.M., 2017. Structural-stratigraphic investigation of an area near Kakamas and environs, Namaqua Mobile Belt, South Africa. Unpublished MSc thesis. University of the Free State, South Africa pp. 162

McClay, K., 1991. Glossary of thrust tectonic terms. In: McClay, K.R. (Ed), Thrust tectonics. London: *Chapman & Hall*, pp. 419-433.

McClung, C.R., 2006. Basin analysis of the Bushmanland Basin, Namaqualand Metamorphic Complex, Northern Cape Province, South Africa. Ph.D. thesis (unpublished), *University of Johannesburg*, South Africa, pp. 320.

McCourt, S., Armstrong, R.A., Grantham, G.H and Thomas, R.J., 2006. Geology and evolution of the Natal Belt, South Africa. *Journal of African Earth Sciences*, Volume 46, pp. 71-92.

Minigh, L.D., 1979. Structural analysis of sheath folds in a meta-chert from the western Italian Alps. *Journal of Structural Geology*, Volume 1, pp. 275-282.

Moore, J., 1977. The geology of the Namiesberg, Northern Cape. Bulletin, *Precambrian Research Unit, University of Cape Town*, South Africa, 20, pp 69.

Odling, N.E., 1987. The structure of Gamsberg, Namaqualand, NE Cape. Annual Report. Precambrian Research Unit, University of Cape Town, pp. 76-104.

Paizes, P.E., 1975. The geology of an area between Vaalkop and Aggeneys in the vicinity of Pofadder, north-western Cape Province. M.Sc. thesis (unpublished), *University of Witwatersrand*, Johannesburg, pp. 220.

Praekelt, H.E., 1994. Die metasedementere gesteentes van die Aggeneys Terrein in die Haramoep-Omgewing. Ph.D. thesis (unpublished), *University of the Orange Free State*, South Africa, pp 373.

Praekelt, H.E. and Schoch, A.E., 1997. Stratigraphical synthesis of the metasediments of the Aggeneys Terrane in the Namaqua Mobile Belt. *South African Journal of Geology*, Volume 100, pp. 85-100.

Pretorius, J., 1986. Die kontakverwantskappe van die graniete, gneise, metavulkaniese gesteentes en metasedimente van die Pella-Pofadderomgeweing. M.Sc. thesis (unpublished), *University of the Free State*, South Africa pp 280.

Quinquis, H., Audren, C., Brun, J.P and Cobbold, P., 1978. Intensive progressive shear in Ile de Groix blueschists and compatibility with subduction or obduction. *Nature,* Volume 274, pp. 43-45.

Ramsay, J., 1967. Folding and fracturing of rocks. New York: McGraw-Hill. 568pp.

Ramsay, J.G., 1980. Shear zone geometry: a review. *Journal of Structural Geology*, Volume 2, pp. 83-99.

Ramsay, J.G. and Huber, M., 1987. The Techniques of Modern Structural Geology. Volume 2: Folds and Fractures. Londen: *Academic Press*.

Reid, D.L. and Barton, E., 1983. Geochemical characterization of granitoids in the Namaqualand geotreverse. *Special Publications Geological Society of South Africa*., Volume 10, pp. 67-82.

Reid, D.L., Welke, H.J., Erlank, A.J. and Betton, P.J., 1987. Composition, age and tectonic setting of amphibolites in the Central Bushmanland Group, Western Namaqua Province, South Africa. *Precambrian Research,* Volume 36, pp. 99-126.

Roberts, A., 1989. Fold and thrust structures in the Kintradwell "Boulder beds", Moray Firth. *Scottish Journal of Geology*, Volume 25, pp. 173-186.

Rozendaal, A., 1975. The geology of Gamsberg, Namaqualand, South Africa. M.Sc. Thesis (unpublished), *University of Stellenbosch*.

Rozendaal, A., 1978. The Gamsberg zinc deposit, Namaqualand, South Africa.235-265. In:W.J. Verwoerd,Ed., Mineralization in metamorphic terranes. *Geol.Soc. S.Afr.Spes.Publ*, Volume 4, pp. 552.

Rozendaal, A., 1982. The petrology of the Gamsberg zinc deposit and the Bushmanland iron-formations, with special reference to their relationship and genesis. Ph.D thesis (unpublished), *University of Stellenbosch*, South Africa pp. 349.

Sawyer, E.W., 2008. Atlas of migmatites, The Canadian Mineralogist, *Special Publication 9. Ontario: Natural Resources Canada*.

Schoch, A.E., Colliston, W.P. and Praekelt, H.E., 1987. The Bushmanland Project, Final Report. Department Geology, *University of the Orange Free State*, Bloemfontein, pp. 110.

Shackleton, R.M., 1958. Downward facing structures of the Highland Border. Quarterly *Journal of the Geological Society of London*, Volume 113, pp. 361-392.

Skjernaa, L., 1989. Tubular folds and sheath folds: definitions and conceptual models for their development with examples from the Grapesvare area, northern Sweden. *Journal of Structural Geology*, Volume 11, pp. 689-703.

Stedman, D.P., 1980. The structural geology and metamorphic petrology of Black Mountain, Namaqualand. M.Sc Thesis (unpublished) *University of the Witwatersrand*, South Africa, pp 169.

Stockwell, C.H., 1960. The use of plunge in the construction of cross sections of folds. *Proc. Geological Association of Canada*, Volume 3, pp. 97-121.

Stowe, C.W., Hartnady, C.J.H. and Joubert, P., 1984. Proterozoic tectonic provinces of Southern Africa. *Precambrian Research*, Volume 25, pp. 229-231.

Strydom, D., 1982. Geselskapbank-Areb region, 1:100,000 geological map. *Department of Geology,University of the Orange Free State, Bloemfontein, South Africa (one sheet)..*

Strydom, D. and Visser, J.N.J., 1986. Nappe structures in the highly deformed Proterozoic metasedimentary, Aggeneys-type sequence of western Bushmanland, South Africa. *Precambrian Research*, Volume 33, pp. 171-187.

Strydom, D., 1985. ‘n Struktureel-stratigrafiese studie van die metasedimente en ander metamorfiete van Noordwestelike Boesmanland. Ph.D. (unpublished), *University of the Orange Free State*, South Africa, pp. 159.

Talbot, C.J., 1979. Fold trains in a glacier of salt in southern Iran. *Journal of Structural Geology*, Volume 1, pp. 5-18.

Tankard, A.J., Jackson, M.P.A., Eriksson, K.A., Hobday, D.K., Hunter, D.R. and Minter, W.E.L., 1982. Crustal evolution of southern Africa - 3.8 billion years of earth history. *Springer Verlag*, pp. 523.

Thomas, R.J., Cornell, D., Moore, J.M. and Jacobs, J., 1994. Crustal evolution of the Namaqua-Natal Metamorphic Province, Southern Africa. *South African Journal of Geology*, Volume 97(1), pp. 8-14.

Toogood, D.J., 1974. Prelimnary Report on the geology of the Onseepkans area, south-eastern South West Africa. Annual Report, *Precambrian Research Unit, University of Cape Town*, pp. 10-11, 31-37.

Toogood, D.J., 1976. Structural and metamorphic evolution of a gneiss terrain in the Namaqua belt, near Onseepkans, South West Africa. *Bulletin Precambrian Research Unit, University of Cape Town*, pp. 189.

van Aswegen, G., Strydom, D., Colliston, W.P., Praekelt, H.E., Schoch, A.E., Blignault, H.J., Botha, B.J.V. and van der Merwe, S.W., 1986. The structural-stratigraphic development of the Namaqua Metamorphic Complex-an example of major thrust tectonics. In: A. Kroner, ed. *Proterozoic Lithosphere Evolution,* Volume 17*, Special Publ. Am. Geophys Unit (Geodyn.Ser).*, pp. 207-216.

van Aswegen, G., 1983. The Gladkop Suite - the grey and pink gneisses of Steinkopf. *Special Publication*, *Geological Society of South Africa*, Volume 10, pp. 31-44.

van Aswegen, G., 1988. The evolution of the proterozoic gneisses and other metamorphites between Springbok and Vioolsdrif, South Africa. Ph.D. thesis (unpublished), *University of the Orange Free State*, South Africa, 293pp.

van der Merwe, S.W., 1986. The structural development of part of the Namaqua mobile belt in an area between Springbok and Vioolsdrif. Ph.D. thesis (unpublished), *University of the Orange Free State*, Bloemfontein, pp. 373.

van der Merwe, S.W. and Botha, B.J.V., 1989. The Groothoek Thrust Belt in Western Namaqualand; an example of a mid-crustal structure. *South African Journal of Geology,* 92(2), pp. 155-166.

van Zyl, V.C., 1986. Metamorphic studies in the Protorozoic rocks of part of northern Bushmanland. M.Sc. thesis (unpublished), *University of the Orange Free State*, Bloemfontein, South Africa, pp. 401.

Velaj, T., Davison, I., Serjani, A., Alsop, G.I., 1999. Thrust tectonics and the role of evaporites in the Ionian Zone of the Albanides. *American Association of Petroleum Geologists and Bulletin*, Volume 83, pp. 1408-1425.

Watkeys, M.K., Moore, J.M. and Duncan, A.R., 1988. The pink gneiss of Bushmanland: Mid-Proterozoic felsic pyroclastic. Abstract. *Geocongress*, Durban, pp. 717-720.

Watkeys, M.K., 1986. The Achab Gneiss: A "floor" in Bushmanland or a flaw in Namaqualand?. *Transaction of the Geological Society of South Africa*, Volume 89, pp. 103-116.

Williams, P.F. and Zwart, H.J., 1977. A model for development of the Seve-Koli Caledonian Nappe Complex, pp. 169-187.In: Saxena, S.K., Bhattacharji, S.(Eds.),. Energetics of Geological Processes. Springer-Verlang, New York.

Willner A., Schreyer, W and J.M. Moore, 1990. Peraluminous metamorphic rocks from the Namaqualand Metamorphic Complex (South Africa): Geochemical evidence for an exhalation-related, sedimentary origin in a Mid-Proterozoic rift system. *Chemical Geology*, Volume 81, pp. 221-240.

A STRATIGRAPHIC-STRUCTURAL INVESTIGATION OF AN AREA SOUTH OF POFADDER, NAMAQUA MOBILE BELT, SOUTH AFRICA.

Appendices

Wayne Justin Nel

Submitted in fulfilment of the requirements for the degree of Magister Scientiae

In the

Faculty of Science

Geology Department

University of the Free State, Bloemfontein

Supervisor: Prof W.P. Colliston

December 2021

Table of Contents

Appendices Chapter 1

Appendix 1.1: Literature Review 1

Appendices Chapter 2: Stratigraphy Photos

2.1 Witkoppies Sequence: Inner Witkoppies member (see Figure 2.28) 4

2.2 Outer Witkoppies Member (see Figure 2.29) 5

2.3 The Gannapoort Berg Sequence (see Figure 2.32) 6

2.4 Samoep se Berg Sequence (see Figure 2.33) 7

2.5 Middle Samoep Sequence (see Figure 2.35) 8

2.6 The S-Berg Sequence (see Figure 2.37) 9

2.7 The Klein Pofadder Sequence (see Figure 2.41) 10

2.8 Inner Koppies Member (see Figure 2.44) 11

2.9 Outer Koppies Member (see Figure 2.45) 12

2.10 Poort se Berg Sequence (see Figure 2.48) 13

2.11 T-Goob Sequence (see Figure 2.49) 14

2.12 Outer Lekdam Sequence (see Figure 2.50) 15

2.13 Skewe Berg Sequence (see Figure 2.53) 16

2.14 Xenolith Sequence (see Figure 2.54) 17

2.15 Draai-Berg Sequence (see Figure 2.55) 18

2.16 Platberg Sequence (see Figure 2.56) 18

2.17 Sy-Berg Sequence (see Figure 2.57) 19

2.18 Achab Sequence (see Figure 2.61) 20

2.19 De Rust Sequence (see Figure 2.63) 21

2.20 Inner Dwarsberg Member (see Figure 2.65) 22

2.21 Outer Dwarsberg Member (see Figure 2.66) 22

2.22 The Hom Formation (see Figure 2.69) 23

2.23 The Van Tittensville Formation (see Figure 2.71) 24

2. 24. Geological Map of an area south of Pofadder 25

Appendices Chapter 3

3.1. Structural formline map 26

3.1 A: Lineation map..... 27
3.1 B: Detailed map of the far western fold hinge of the D4 macroscopic structure.. 28
3.1 C: Detailed map of the central section of the macroscopic D4 structure 29
3.1 D: Detailed map of the northern limb of the macroscopic D4 structure..... 30
3.1 E: Detailed map of the southern limb of the macroscopic D4 structure 31
3.2: Geometric properties of eight structures across the study area 32
3.3.1: Structural long section across the study area..... 33
3.3.2: Structural cross section across the study area..... 34
3.4.1: The D1 phase of deformation 35
3.4.2: The D2 phase of deformation 36
3.4.3: The D3 phase of deformation 37
3.4.4: The D4 phase of deformation 38
3.4.5: The D5 and D6 phase of deformation 39
3.5 Domain 1E Witkoppies ‘Eye’ Structure 40
3.6 Domain 3A; Gannapoort Berg ‘Eye’ Structure..... 41

Appendices Chapter 4

4.1 The Samoep Succession..... 42
4.2 The Koppies and Klein Pofadder Sequence 43
4.3 The T-Goob Succession..... 44
4.4 The Inner Lekdam Succession 45
4.5 The De-Rust Succession..... 46
4.6 Sheath Fold Classification Diagram..... 47

Appendices Chapter 5

5.1 Sections of the T-Goob Sheath Fold..... 48

List of Appendices

Appendix 1.1: Reference map showing previous research conducted regionally adjacent to the study area. 3

Appendix 2.1: Witkoppies Sequence: The Inner Witkoppies Member. Figure A: Actinolite lenses found at the base of the succession and gives a light greyish colour in the field. Figure B: Sillimanite nodules associated with the actinolite lenses .Figure C: Feldspar bands are often associated with the black-banded calc-silicate rocks found throughout the stratigraphic succession.Figure D: Banded variation associated with the calc-silicate rocks. Banded variations are often associated with feldspar leucosome melts, which are parallel to the foliation planes. Figure E: Light coloured calc-silicate rocks, crystals of magnetite are often associated with these type of rocks. Figure F: Represents the massive amphibolite units found throughout the succession. 4

Appendix 2.2: Photographs of lithologies related to the Outer Witkoppies Member. Figure A: Shows the biotite gneiss unit which makes up the bulk of the Outer Sheath Member. Figure B: Quartz clasts (lapilli) are associated with volcanic bombs, and occur sporadically throughout the stratigraphic succession. Figure C: Poorly foliated light calc-silicate rock showing prominent growth of epidote minerals. Figure D: Prominent feldspar leucobands associated with light banded calc-silicate rock. Figure E: Feldspar bands associated with dark calc-silicate rocks found throughout the succession. Figure F: Coarse-grained feldspar leucosomes associated with metatexite melts which occur throughout the stratigraphic succession. 5

Appendix 2.3: Lithological features associated with the Gannapoort Berg Sequence. Figure A: Thick biotite gneiss unit found at the base of the Gannapoort Berg Member. Figure B: Sharp contacts associated with the upper quartzite, lower biotite-sillimanite schist, and biotite gneiss units in the northern limb of the structure. Figure C: Upper quartzite showing a prominent 2nd order upward coarsening cycle, indicating the younging direction. The quartzite also has a mylonitic texture due to late shearing. Figure D: Biotite-sillimanite schist with prominent sillimanite nodules found on top of the stratigraphic succession. Figure E: Amphibolite associated with the intercalated volcanic unit found within the upper biotite-sillimanite schist unit. Figure F: Intercalated units of calc-silicate rock associated with the volcanic unit found on top of the stratigraphic succession. 6

Appendix 2.4: Lithological features of the Samoep se Berg Sequence. Figure A: Thick unit of biotite gneiss found at the base. Figure B: Interbanded units of black calc-silicate rocks within the lower biotite gneiss unit. Figure C: Biotiet- sillimanite schist found close to the contact with the upper quartzite. Figure D: Dark-blue garnet quartzite unit found on the contact with the

upper quartzite. Figure E: Upper poorly bedded quartzite, often associated with a 2nd order upward coarsening cycle. Figure F: Primary bedding in the form of cross-bedding associated with the upper quartzite. 7

Appendix 2.5: Lithological features of the Middle Samoep Sequence. Figure A: Feldspathic quartzite with inter-banded units of biotite gneiss. Figure B: Represents a 3rd order upward fining cycles associated with the feldspathic quartzite unit. Prominent laminations of biotite and feldspar define the 3rd order fining cycles. Figure C: Cross-bedding associated with the feldspathic quartzite unit and shows younging direction toward the top of the succession. Figure D: Illustrates biotite sillimanite schist with interbanded units of dark-blue garnet-bearing quartzite. Figure E: Garnet overgrowths on the dark-blue quartzite unit within the XY foliation plane, which are interpreted to be late to syntectonic growths. Figure F: Bedded quartzite associated with the upper succession. At certain locations defines a prominent second-order upward coarsening cycle. 8

Appendix 2.6: Lithological features of the S-Berg Sequence. Figure A: Thick units of biotite gneiss found at the base of the succession. Figure B: Ferruginous magnetite quartzite units interlayered within the lower biotite gneiss unit. Figure C: Inter-banded calc-silicate units found within the biotite gneiss unit. Figure D: Biotite bands associated with the upper quartzite, further toward the east. Figure E: Poorly bedded quartzite displaying a prominent 2nd order upward coarsening cycle. Figure F: Biotite-sillimanite schist unit found at the top of the stratigraphic succession. 9

Appendix 2.7: Lithological features of the Klein Pofadder Sequence. Figure A: Thick biotite-sillimanite schist associated with the lower succession. Figure B: Massive poorly bedded quartzite defining a prominent second-order upward coarsening cycle. Figure C: Dark-blue poorly bedded quartzites associated with the upper succession. Figure D: Late to syntectonic garnets associated with the upper dark-blue quartzite unit. 10

Appendix 2.8: Lithological features of the Inner Koppies Member. Figure A: Biotite-sillimanite schist associated with the lower succession. Figure B: Interbande ferruginous garnet meta-quartzite found in the lower portion of the stratigraphic succession. Figure C: Poorly bedded upper quartzite found in the upper succession defining prominent second-order upward coarsening cycle. Figure D: Nodular sillimanite-quartz-feldspar rhythmic gneiss found in the upper part of the succession. Prominent nodules of sillimanite can be observed on the YZ foliation plane. 11

Appendix 2.9: Photos associated with the stratigraphy related to the Outer Koppies Member. Figure A: Intercalated units of ferruginous garnet quartzite associated within the biotite-sillimanite schist unit. Figure B: Dark-blue character often associated with the upper quartzite.

Figure C: Nodular rhythmic gneiss associated with the top portion of the outer sheath member. 12

Appendix 2.10: Lithological features associated with the Poort se Berh Sequence (upper (Figures A-E) and lower Poort se Berg Member (Figures F-H)). Figure A: Massive biotite sillimanite schist unit, with intrusive units of Lekdam Gneiss found within. Figure B: Depicts the feldspathic quartzite unit associated with the volcanic/chemogenic unit found at the base of the Poort Member. Primary bedding in the form of flame structures, can be observed within the feldspathic quartzite. Figure C: The ferruginous garnet quartzite unit intercalated within the large biotite-sillimanite schist unit associated with upper Poort se Berg Member.Figure.D: Upper poorly bedded quartzite displaying a prominent second-order upward coarsening cycle. Figure E: Nodular rhythmic sillimanite- quartz-feldspar gneiss found toward the top of the upper Poort se Berg Member. Prominent sillimanite nodules can be seen in the diagram. Figure F: Thick well laminated feldspathic quartzite unit associated with the lower Poort se Berg Member. Figure G: Centimetre to metre scale biotite gneiss found at the base of the lower Poort se Berg Member. Figure H: Nodular rhythmic sillimanite-quartz-feldspar gneiss showing prominent sillimanite nodules found in the upper section of the lower Poort se Berg Member. 13

Appendix 2.11: Lithological features of the T-Goob se Berg Sequence. Figure A: Contact between the upper quartzite and lower nodular sillimanite-quartz-feldspar rhythmic gneiss defining a second-order upward coarsening cycle. Figure B: Volcanic unit defined by blue-white quartzites with interlayered units of diopside, actinolite, and biotite gneiss. Figure C: Volcanic/chemogenic unit depicting interbanded quartzite and diopside units. Figure D: Interlayered sequences of actinolite associated with the central volcanic unit found within the biotite-sillimanite schist unit. Figure E: Biotite gneiss associated with the central portion of the stratigraphic succession. Figure F: Biotite gneiss with overgrowths of garnet seen on the XZ foliation plane. Figure G: Well laminated medium quartz-feldspar gneiss found on the top portion of the stratigraphic succession. Figure H: Nodular sillimanite-quartz-feldspar rhythmic gneiss associated with the upper succession of the T- Goob Sequence. 14

Appendix 2.12: Lithological features associated with the Outer Lekdam Sequence. Figure A: Feldspathic quartzite with interbanded units of biotite gneiss. Figure B: Feldspathic quartzite units intercalated within the biotite-sillimanite schist units. Figure C: Biotite-sillimanite schist associated with the lower succession of the Outer Lekdam Sequence. Figure D: Poorly to well-bedded upper quartzite displaying prominent biotite bands. Figure E: Well bedded character depicted within certain portions of the Outer Ledkam Sequence, displaying prominent second-order upward coarsening cycles. Figure F: Nodular sillimanite-quartz-feldspar rhythmic gneiss

associated with the top part of the stratigraphic succession. Sillimanite nodules can be seen on the YZ and XY foliation planes. 15

Appendix 2.13: Lithological features of the Skewe Berg Sequence: Figure A: Garnet meta-quartzite units interbanded within the lower biotite-sillimanite schist unit. Figure. B: Biotite gneiss interbanded within the biotite-sillimanite schist unit. Figure C: Thick sequence of biotite-sillimanite schist associated with the middle and lower portion of the stratigraphic succession. Figure D: Nodular sillimanite-quartz-feldspar rhythmic gneiss associated with the upper portion of the stratigraphy, often associated with prominent sillimanite nodules. 16

Appendix 2.14: Lithostratigraphic features associated with the Xenolith Sequence. Figure A: Garnet bearing meta-quartzite; and showing chocolate tablet boudinage. Garnets are aligned parallel to the foliation planes. Figure B: Depicts the feldspathic quartzites associated with the Xenolith Member. Figure C: Biotite-sillimanite schist unit associated with the upper stratigraphic succession. Figure D: Biotite-sillimanite schist unit. Small sillimanite nodules can be seen on the YZ foliation plane at centimetre scale. 17

Appendix 2.15: Lithostratigraphic features of the Draai-Berg Sequence. Figure A: Feldspathic quartzite unit found within the lower succession. Figure B: Garnet-bearing meta-quartzite units interbanded within the lower biotite-sillimanite schist unit. Figure C: Dark calc-silicate rocks with prominent feldspar bands found at the base of the succession. Figure D: Poorly bedded quartzite defining a second-order upward coarsening cycle, associated with the upper echelon of the sequence. 18

Appendix 2.16: Lithostratigraphic features associated with the Platberg Sequence: Figure A: Biotite sillimanite schist unit in contact with a poorly bedded quartzite, displaying a second-order upward coarsening cycle.Figure B: Prominent garnet-bearing quartzite unit (BIF), which folds around the Platberg structure and is found at the bottom of the stratigraphic succession. 18

Appendix 2.17: Photos of the stratigraphy related to the Sy-Berg Sequence. Figure A: Small feldspathic quartzite unit found at the base of the succession. Figure B: Poorly to well-bedded quartzite, showing a second-order upward fining cycle. Figure C: Dark-blue quartzite unit interlayered within the central biotite-sillimanite schist unit. 19

Appendix 2.18: Lithological features of the Achab Sequence. Figure A: Medium quartz-feldspar Namies Gneiss found at the base of the succession. Figure B: Massive units of biotite-sillimanite schist found at the base of the Achab Sequence just above the Namies Gneiss. Figure C: Interbanded units of amphibolite associated with the stratigraphic succession. Figure D; Interbanded units of calc-silicate rock which occur sporadically throughout. Figure E:

Banded units of ferruginous garnet meta-quartzites, interbanded within the lower biotite-sillimanite schist units. Figure F: Massive poorly bedded quartzites which show second-order upward coarsening cycles. 20

Appendix 2.19: Lithostratigraphic features of the De Rust Sequence. Figure A: Nodular sillimanite-quartz-feldspar rhythmic gneiss, found at the base of the succession. Prominent sillimanite nodules can be viewed on the YZ foliation surface. Figure B: Thick unit of biotite-sillimanite schist unit, found toward the top of the succession. Figure C: Upper poorly bedded quartzite, showing a second-order upward coarsening cycle. Figure D: Well to poorly foliated medium quartz-feldspar Namies Gneiss found at the top of the stratigraphic succession. .. 21

Appendix 2.20: Lithostratigraphic features associated with the Inner Dwarsberg Member. Figure A: Biotite-sillimanite schist associated with the lower and upper portions of the Inner Dwarsberg Member. Figure B: Black calc-silicate rock unit found at the base of the stratigraphic succession, found within the biotite-sillimanite schist unit. Figure C: Large amphibolite interbanded within the lower biotite-sillimanite schist unit. Figure D: Second-order upward coarsening cycle associated with the upper quartzite. 22

Appendix 2.21: Lithostratigraphic features associated with the Outer Dwarsberg Member: Figure A: Biotite-sillimanite schist unit associated with the Outer Dwarsberg Member. Figure B: Second-order upward coarsening cycle associated with the upper quartzite unit. 22

Appendix 2.22: Lithostratigraphic features associated with the Hom Formation. Figure A: Swartmodder Gneiss which intrudes within the entire succession. Figure B: Leucobands associated with a higher strain variation of the Swartmodder Gneiss. Figure C: Leucocratic finely laminated felsic gneiss found throughout the succession. Figure D: Poryphyritic volcanic bombs, showing a porphyritic appearance of mafic and feldspar clasts. Figure E: Volcanoclastic bombs, which at certain locations have leucocratic appearance due to an increase in feldspar clasts. Figure F: Quartz eyes found in the interbanded amphibolite units. The quartz eyes are often associated with most of the hornblende gneisses, biotite gneiss, and calc-silicate rocks. 23

Appendix 2.23: Lithostratigraphic features associated with the Van Tittensville Formation. Figure A: Lower biotite gneiss unit found at the base of the succession. Figure B: Calc-silicate units interbanded within the Van Tittensville Formation, often associated with the lower biotite gneiss unit. Figure C: Biotite-muscovite-sillimanite schist associated with the upper part of the stratigraphic succession. Figure D: Prominent magnetite bands associated with the upper quartzite, displaying a third-order upward fining cycle. 24

Appendiix 2.24: Geologiical map of an area south of Pofadder. 25

Appendix 3.1: Detailed structural formline map across the study area. The location map of the different domains can be viewed to the left of the diagram. 26

Appendix 3.1 A: Lineation pattern across all domains. 27

Appendix 3.1 B: Detailed structural formline map of the far western fold closure associated with the major D4 synformal structure. A: Location of the detailed map within the study area (in purple). 28

Appendix 3.1 C: Detailed structural formline map of the central section of the major D4 synformal structure. A: Location of the detailed map within the study area (in purple). 29

Appendix 3.1 D: Detailed structural formline map of the northeastern limb of the major D4 synformal structure. A: Location of the detailed map within the study area (in purple). 30

Appendix 3.1 E: Detailed structural formline map of the southeastern limb of the major D4 synformal structure. A: Location of the detailed map within the study area (in purple). 31

Appendix 3.2: Geometric properties associated with eight prominent structural domians, together with a description of the general characteristics associated with each structure. The geometric properties have the same general characteristics as all 22 structures encountered within the study area. A: Diagram showing a fold illustrating the rotation foliations from north to south around the D4 hinges.This rotational effect can be seen in Domains 1 E, 3D, 3I and 3J; and is represented by the inverted stereonets. B: Regional location map, showing the distribution of all structures across the domains and sub-domains. 32

Appendix 3.3.1: Structural long section across the study area. Section was constructed using a combination of the Busk Method (Busk, 1929) and the projection technique by Stockwell (1960). Figure A: Composite long section across the study area drawn perpendicular to the transport direction. D2 and D3 fold structures, are located on both the northwestern and southeastern limbs of a major synformal D4 structure. Intra-terrane thrust contacts are also seen folding around the D4 hinge in the center of the structure. Figure B: Simplified geological map, showing the positions (A-C) where the long section was constructed. Figure C and D: Stereonets showing the average trend of the regional L1 stretching lineation, with average trends toward the north-east with mean plunge of 30°..... 33

Appendix 3.3.2: Structural cross section across the study area. Section was constructed using a combination of the Busk Method (Busk, 1929) and the projection technique of Stockwell (1960). Figure A: Composite cross section drawn oblique to the tectonic transport direction. Shows the folding of D2 structures by D4 phase of folding and the location of D3 and D2 structures on the southeastern limb of the major D4 structure. The tightening of D2,

D3 and D4 hinges can be seen on the southeastern limb, caused by the D5 east-west shear effects. Towards the far east, the fold traces are drawn parallel due to the D6 phase of deformation (D2-D3). Thrust contacts can also be seen folding around the D4 hinges. Figure B: Shows a simplified geological map, which shows the positions (A-F) where the sections were constructed. Figure C: Stereonet diagram depicting the average regional stretching lineation trend (L1). The L1 lineations have an average plunge of 30° in a northeasterly direction. 34

Appendix 3.4.1: Simplified structural form line map depicting the best locations associated with the D1 phase of deformation throughout the study area. The red star symbols (★) represent locations where the D1 fabric (S1) can be seen. The purple star symbol (★) shows the location where the D1 phase of intra-stratigraphic thrusting can be seen, where imbrication and cut-out structures can be seen duplicating the S1//S0 fabric. 35

Appendix 3.4.2: Simplified structural form line map depicting the F2 fold traces throughout the study area. The star symbols (★) represent locations where the D2 phase (macroscopic F2 folds closures) is visible on macroscopic scale. 36

Appendix 3.4.3: Simplified structural formline map depicting the F3 fold traces throughout the study area. The pentagon symbols (⬟) represent locations where the D3 phase (F3 fold closures) is visible on macroscopic scale. 37

Appendix 3.4.4: Simplified structural form line map depicting the F4 fold traces throughout the study area. The pentagon symbols (⬟) represent locations where the D4 phase (F4 fold closures) are visible on macroscopic scale. 38

Appendix 3.4.5: Simplified structural formline map depicting the D5 and D6 phase of deformation throughout the study area. The D5 east-west shear zones are located on intra-terrane thrust contacts and on the limbs of D2, D3 and D4 structures. The D6 NW-SE shear zones are found in the far eastern sector of the study area. The F5 oblique open folds are also seen across the study area. 39

Appendix 3.5: Structural formline map of the Witkoppies 'Eye' Structure. Figure A: Simplified locality map of the structure within the study area. The map is divided into a western and eastern sector representing a lower strain zone and the latter a higher strain zone. The various fold phases with their respective fold traces, branch points, foliations and lineations are represented. 40

Appendix 3.6: Structural formline map associated with the Gannapoort Berg "Eye' structure that is defined by two isoclinal fold structures refolding adjacent to one another. Figure A:

Locality map of the Gannapoort Berg 'Eye' Structure within the study area. Figure B: Simplified geological map showing the major lithologies and intrusives associated with the Gannapoort Berg Structure. It can be noted how the two isoclinal fold structures are refolded adjacent to one another. Figure C: Simplified formline map depicting the location of the mesoscopic Model 1 folds. 41

Appendix 4.1: The comparison between the Samoep Succession and the Wortel Formation supracrustal succession toward the west. Figure A: Shows the similarities and dissimilarities between the Samoep Succession and Wortel Formation in the Haramoep Mountains. Figure B: The location of the Stratigraphic profiles associated with the Samoep Succession and Wortel Formation toward the west. Figure C: An enlarged location diagram depicting the profile positions of the Samoep Succession. The Wortel Formation profiles were modified after Praekelt (1994). For the construction of all stratigraphic profiles, the upright limbs of structures are used for interpretation. 42

Appendix 4.2: The comparison between the Koppies Sequence, Klein Pofadder Sequence and the Wortel Formation supracrustal succession toward the west. Figure A: The similarities and dissimilarities associated with the Koppies-Klein Pofadder Sequences and the Wortel Formation in the west. Figure B: The location of the stratigraphic profiles associated with the Koppies, Klein Pofadder Sequence and the Wortel Formation rocks in the Haramoep Mountains. Figure C: Offset diagrams showing the profile locations of the Koppies and Klein Pofadder Sequences. The stratigraphic profiles of the Wortel Formation towards the west is modified after Praekelt (1994). For the construction of all stratigraphic profiles, the upright limbs of structures are used in the interpretation. 43

Appendix 4.3: The comparison between the T-Goob Succession and the Wortel Formation rocks found toward the west. Figure A: The similarities and dissimilarities in stratigraphy between the T-Goob Succession and Wortel Formation. Figure B: The location of the stratigraphic profiles of the Wortel Formation found in the Haramoep Mountains. Figure C: An offset diagram showing the location of the stratigraphic profiles associated with T-Goob Succession. The Wortel Formation profiles are modified after Praekelt (1994). For the construction of all stratigraphic profiles, the upright limbs of structures are used in the interpretation. 44

Appendix 4.4: The comparison between the Inner Lekdam Sequence and the Wortel Formation supracrustal succession toward the west. Figure A: The similarities and dissimilarities in stratigraphy between the Inner Lekdam Succession and Wortel Formation. Figure B: The location of the stratigraphic profiles associated with the Wortel Formation in the west. Figure C: An offset diagram showing the location of the Inner Lekdam Succession

throughout the study area. For the construction of all stratigraphic profiles, the upright limbs of structures are used in the interpretation. 45

Appendix 4.5: The comparison between the De Rust Succession and the Wortel Formation toward the west. Figure A: The similarities and dissimilarities in the stratigraphy between the De-Rust Succession and Wortel Formation in the west. Figure B: The location of the stratigraphic profiles associated with the Wortel Formation in the west. Figure C: An offset diagram showing the location of the stratigraphic profiles associated with the De Rust Succession. Stratigraphic profiles associated with the Wortel Formation toward the west is modified after Praekelt (1994). For the construction of all stratigraphic profiles the upright limbs of structures are used in the interpretation. 46

Appendix 4.6: Examples of two prominent sheath fold structures within the study area, namely; the Samoep se Berg Sheath Fold (A) and Dwarsberg Sheath Fold (B). For each structure a set of criteria (1-10) is applied, proving that the structures are indeed sheath fold structures as discussed in chapter 4.2. Figure A: The Samoep se Berg Sheath fold in its deformed state and in its undeformed state where the later phases of deformation is removed. Stereonet depicting the F2 folds and regional stretching lineations is also shown. Figure B: The Dwarsberg Sheath fold in its deformed state and undeformed state, where the D3 phase of folding is removed, the geometric properties in the form of F2-F3 fold axes and regional L1 stretching lineation is also presented. 47

Appendix 5.1: Sections (AA-ii) constructed parallel and oblique to the regional stretching lineation, together with the 2D cutaway diagrams, that show the structural and stratigraphic variation across the T-Goob Sheath fold. Figure A: Location map of the section locations. Figure B: Stereonet showing the restored lineation trend across the study area. 48

Appendices Chapter 1

Appendix 1.1: Literature Review

The Pofadder and Aggeneys regions have been the center of attention over the past few decades with detailed studies being undertaken both toward the north and west of the study area, together with mapping projects eastwards (Appendix 1.1). The earliest studies in the study area were undertaken by Gevers (1936) which described the mineralisation seen in the rocks regionally. Studies were also undertaken by Coetzee (1941, 1958) who described the sillimanite-cordierite rocks in the vicinity of Pella. Studies were also done by De Jager and Von Backstroom (1961) looking at the magnetite BIFs, barite, and sillimanite deposits associated with the Gamsberg structure.

The most quoted regional study was done by Joubert (1971, 1974, 1975, 1986), in which the regional tectonics and lithologies were discussed, and where he proved that the rocks of the Richtersveld are indeed different from the rocks found in the Bushmanland Sub-province (Joubert, 1986). This study paved the way for future research, in which more detailed mapping projects and stratigraphic studies were done. To the west of the current study area, Pretorius (1986) mapped the northern and part of the southern section at Pella, in which complexities and differences associated with the granitoids in Bushmanland were mapped, as well as chemical attributes and metamorphic studies were conducted. Watkeys (1986) mapped a portion of the Aggeneys hills, the gneisses situated on the northern side of Achab se berg and the major thrust zone seen at T-Goob se Berg and Skeur se Berg. In his results, he concluded that the Achab Gneiss is the 'basement' of Bushmanland and is separated by the Aggeneys metasediments through major thrust sheets. This argument was disproved, as xenoliths within the Achab gneiss were encountered (Colliston et al., 2012).

Further toward the west more complete studies associated with the Bushmanland Sub-province were done by the University of the Free State which formed part of the Bushmanland Project in partnership with Goldfields Ltd, which extended for a period of 6 years (Colliston et al., 1986), in which the stratigraphy associated with the Aggeneys meta-sediments and the mineralisation associated with the massive sulphide deposits were investigated (Schoch et al., 1987). Strydom (1982, 1985) did a structural and stratigraphic investigation in the Geselskapbank region, in which major thrust faults and recumbent fold axes were identified. A klippe associated with the Grunau Terrane was also identified (Colliston and Schoch, 2013). Praekelt (1994) mapped the Haramoep Mountains looking at the stratigraphy of the Aggeneys meta-sediments, providing sedimentological models associated with the various formations. van der Merwe (1986) mapped the meta-volcanics and granitoids associated with the

Springbok and Vioolsdrif area, various major inter-terrain thrusts like the Groothoek and Skelmfontein Thrust Zones were identified and studied (van der Merwe and Botha, 1989). The metamorphites and granitoids associated with the Springbok-Vioolsdrif area was studied by van Aswegen (1988) in which field relationships, chemistries and mapping out of various granitoids were investigated, specifically the granitoids associated with the Gladkop Suite, which encompasses the rocks of the Steinkopf Terrane and is thought to reflect a lower lithospheric origin (van Aswegen, 1983). Further studies looking at the chemistry associated with the metamorphics and mineralisation seen in the ore bodies (associated with the Aggeneys Hills and Gamsberg Structure), chemistry of the metasediments, and variations seen in the granites were studied by Rozendaal (1975); Lipson (1978); Moore (1977) and Stedman (1980).

Further toward the east of the study area Paizies (1975) mapped a part of the Houmoed Mountains, as well as the area associated with the Putsberg ore deposit. Part of the Gamsberg structure was also mapped and interpreted. These studies were largely pioneer studies and a broad exploration perspective is given in terms of the stratigraphy and mineralisation. Maclaren (1988) also mapped toward the east and south-east of the current study area, encompassing the Houmoed Mountains and the Nouzess intrusives. However, the mapping done was incomplete, the stratigraphy interpreted incorrectly, not providing an insightful geological perspective of the eastern portion of the Bushmanland Sub-province.

Towards the north of the study area Colliston (1990) did a detailed stratigraphic and structural study associated with rocks mostly associated with the Pofadder Terrane, together with the associated terrane boundaries. The theories associated with suspect terranes and progressive deformation were applied during this specific study, as well as detailed stratigraphic and structural study associated with the Tantalite Valley Shear Zone. Toogood (1974, 1976) mapped the continuation of the Pofadder Terrane rocks toward Namibia, and the deformation associated with the Tantalite Valley Shear Zone was also interpreted.

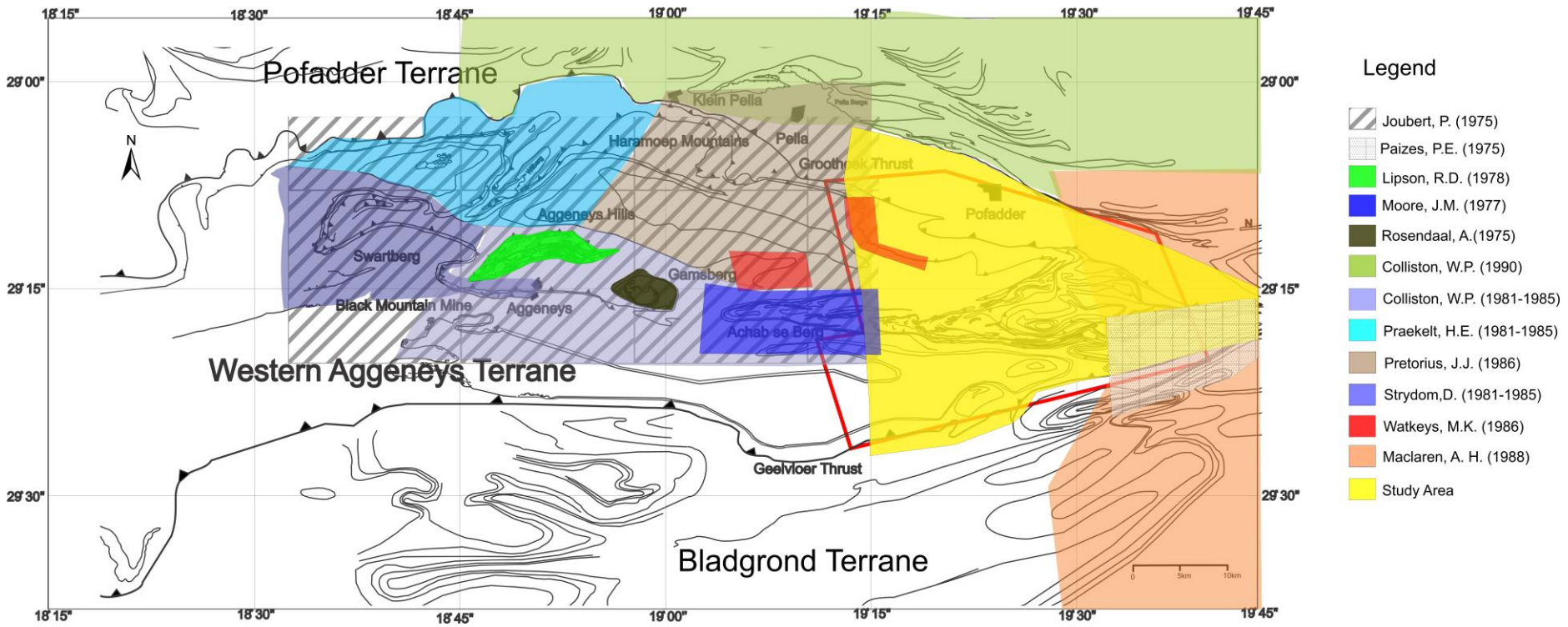

Appendix 1.1: Reference map showing previous research conducted regionally adjacent to the study area.

Appendices Chapter 2: Stratigraphy Photos

2.1 Witkoppies Sequence: Inner Witkoppies Member (see Figure 2.28)

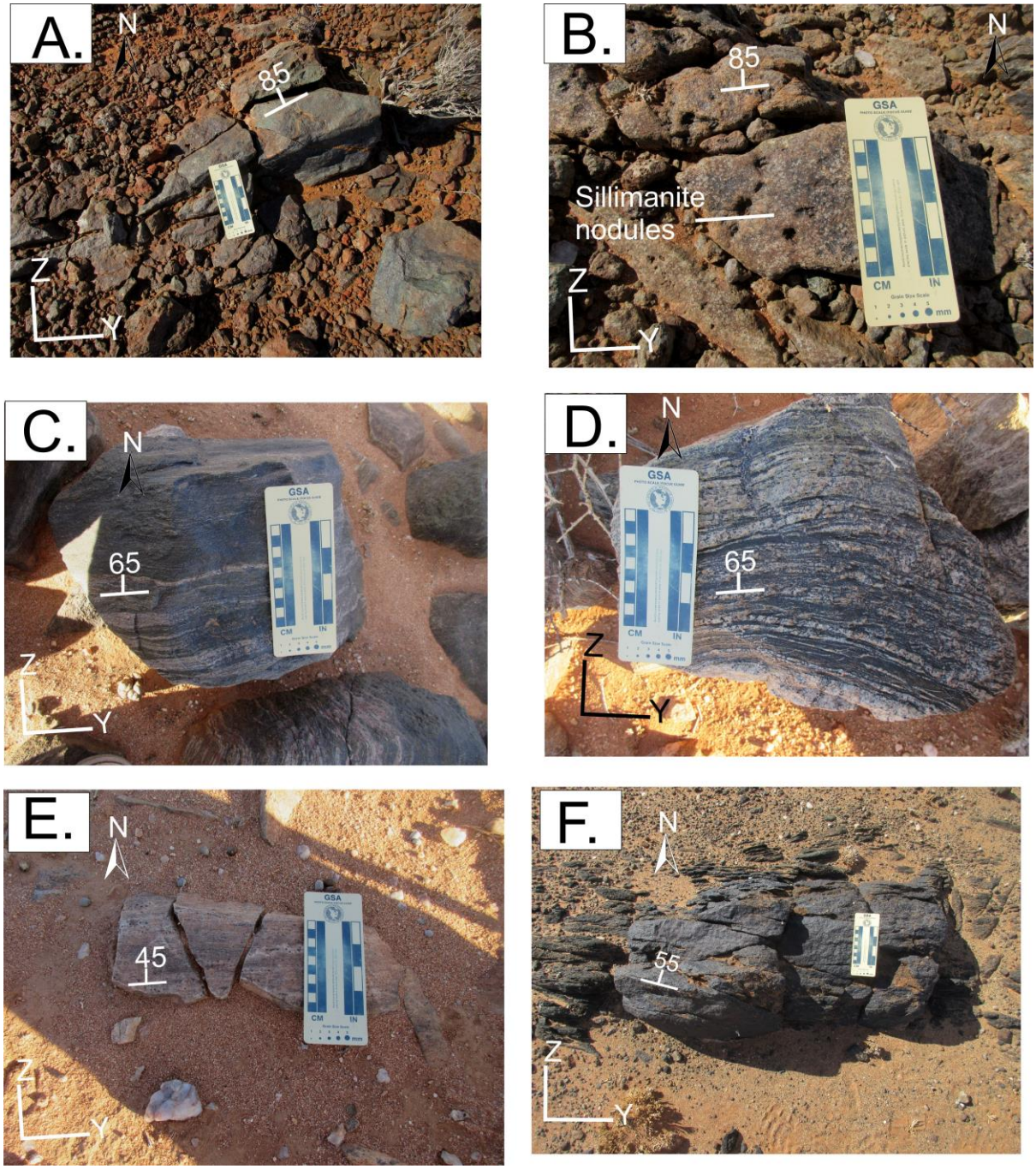

Appendix 2.1: Witkoppies Sequence: The Inner Witkoppies Member. Figure A: Actinolite lenses found at the base of the succession and gives a light greyish colour in the field. Figure B: Sillimanite nodules associated with the actinolite lenses. Figure C: Feldspar bands are often associated with the black-banded calc-silicate rocks found throughout the stratigraphic succession. Figure D: Banded variation associated with the calc-silicate rocks. Banded variations are often associated with feldspar leucosome melts, which are parallel to the foliation planes. Figure E: Light coloured calc-silicate rocks, crystals of magnetite are often associated with these type of rocks. Figure F: Represents the massive amphibolite units found throughout the succession.

2.2 Outer Witkoppies Member (see Figure 2.29)

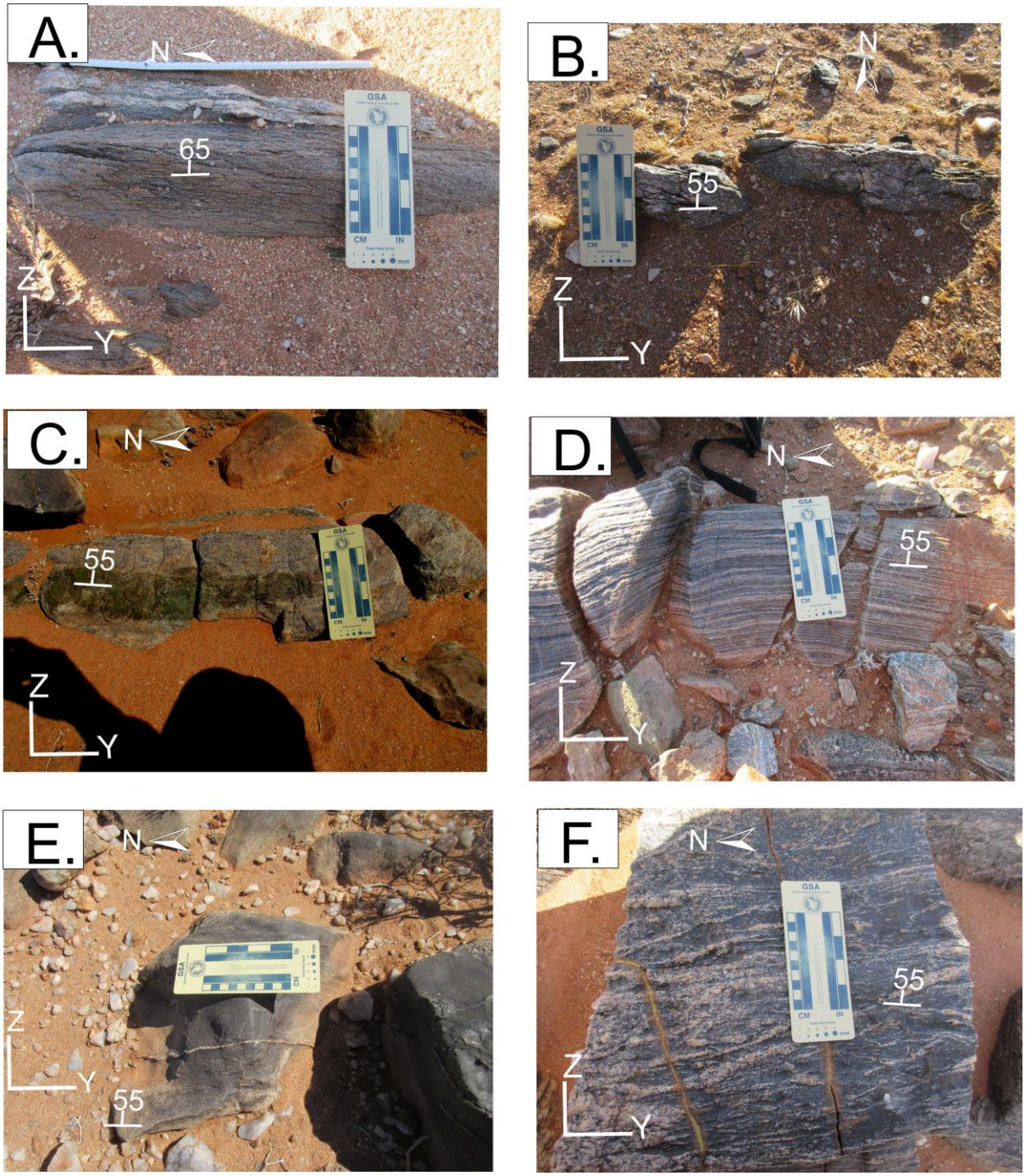

Appendix 2.2: Photographs of lithologies related to the Outer Witkoppies Member. Figure A: Shows the biotite gneiss unit which makes up the bulk of the Outer Sheath Member. Figure B: Quartz clasts (lapilli) are associated with volcanic bombs, and occur sporadically throughout the stratigraphic succession. Figure C: Poorly foliated light calc-silicate rock showing prominent growth of epidote minerals. Figure D: Prominent feldspar leucobands associated with light banded calc-silicate rock. Figure E: Feldspar bands associated with dark calc-silicate rocks found throughout the succession. Figure F: Coarse-grained feldspar leucosomes associated with metatexite melts which occur throughout the stratigraphic succession.

2.3 The Gannapoort Berg Sequence (see Figure 2.32)

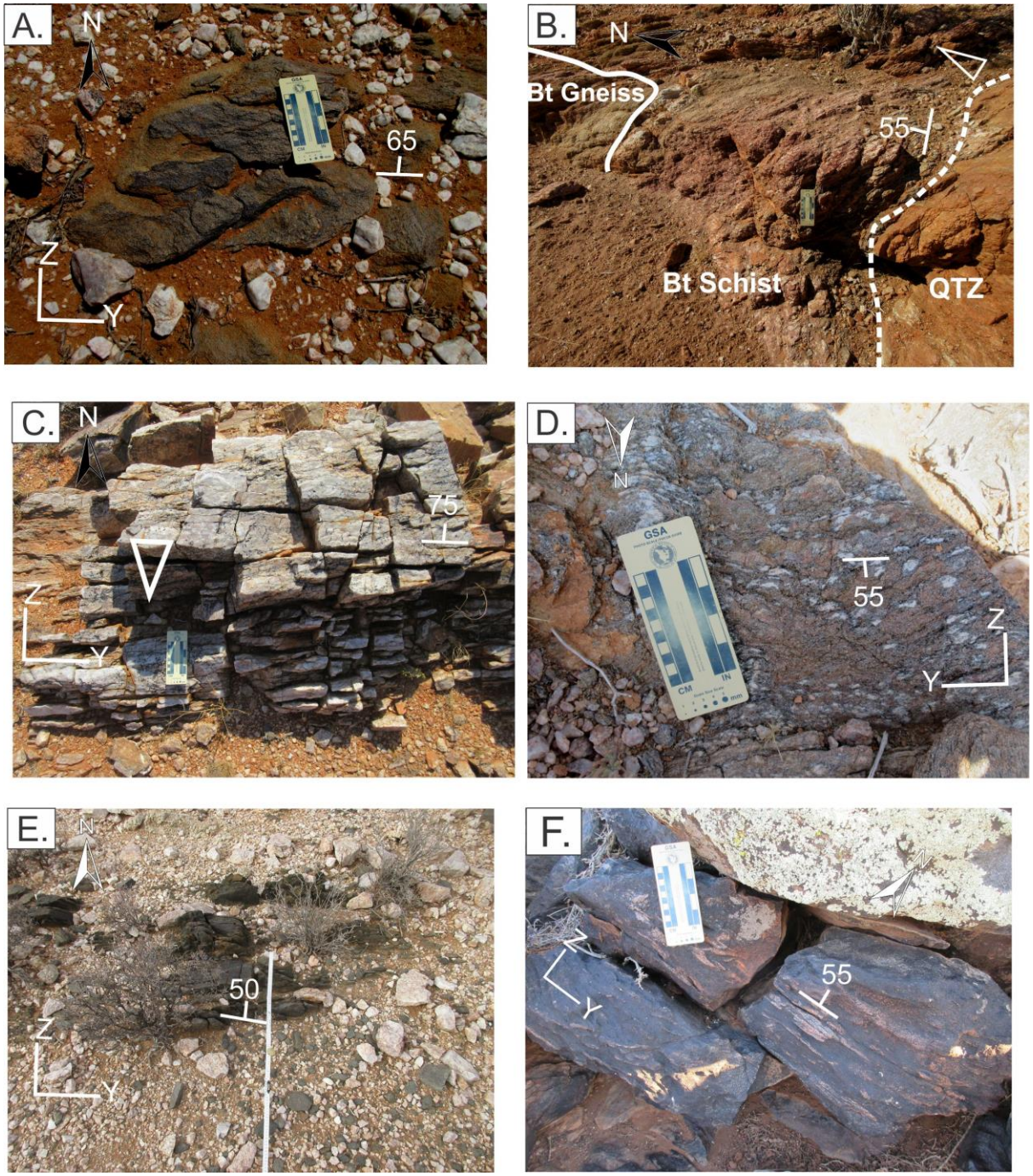

Appendix 2.3: Lithological features associated with the Gannapoort Berg Sequence. Figure A: Thick biotite gneiss unit found at the base of the Gannapoort Berg Member. Figure B: Sharp contacts associated with the upper quartzite, lower biotite-sillimanite schist, and biotite gneiss units in the northern limb of the structure. Figure C: Upper quartzite showing a prominent 2nd order upward coarsening cycle, indicating the younging direction. The quartzite also has a mylonitic texture due to late shearing. Figure D: Biotite-sillimanite schist with prominent sillimanite nodules found on top of the stratigraphic succession. Figure E: Amphibolite associated with the intercalated volcanic unit found within the upper biotite-sillimanite schist unit. Figure F: Intercalated units of calc-silicate rock associated with the volcanic unit found on top of the stratigraphic succession.

2.4 Samoep se Berg Sequence (see Figure 2.33)

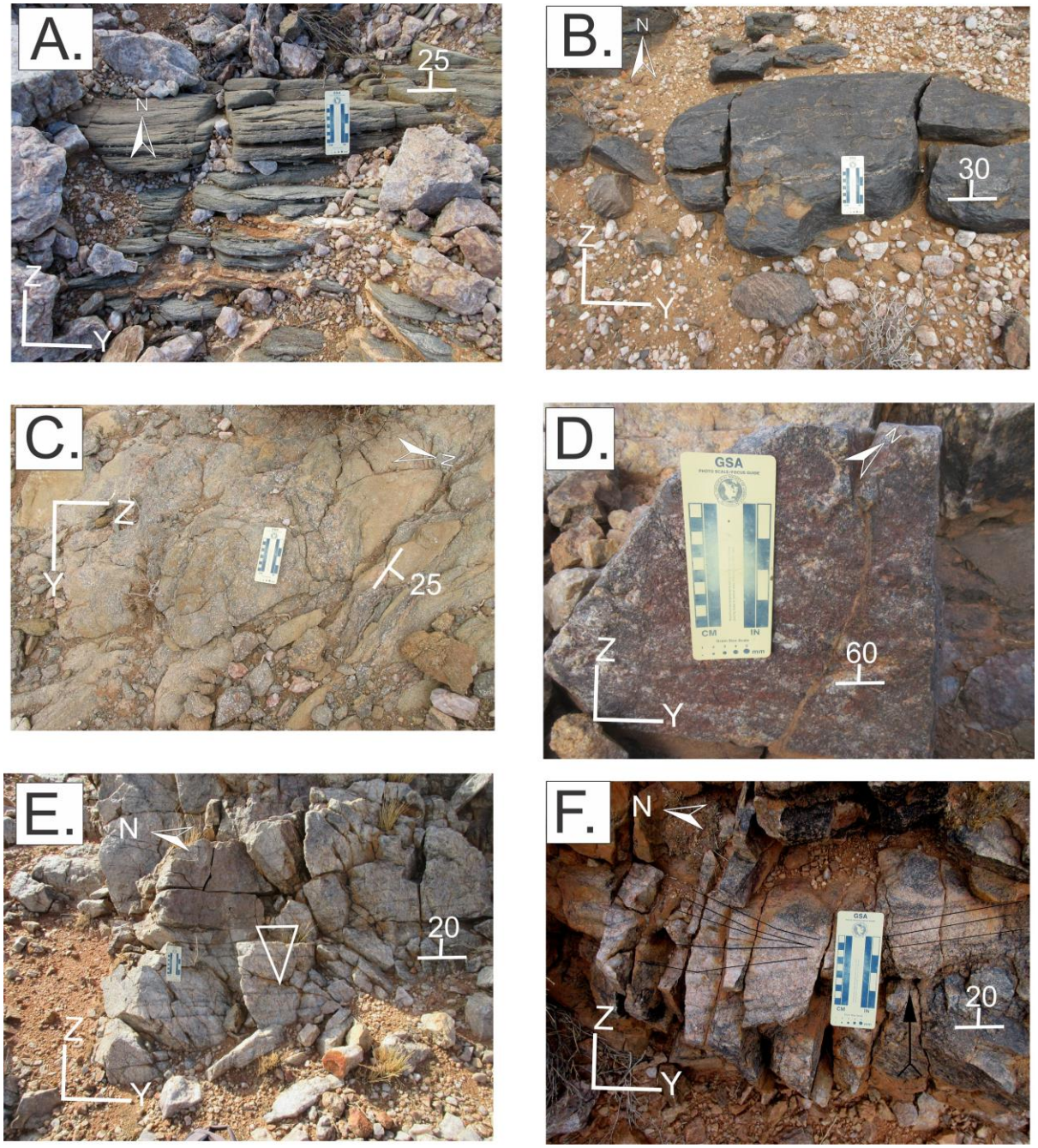

Appendix 2.4: Lithological features of the Samoep se Berg Sequence. Figure A: Thick unit of biotite gneiss found at the base. Figure B: Interbanded units of black calc-silicate rocks within the lower biotite gneiss unit. Figure C: Biotiet- sillimanite schist found close to the contact with the upper quartzite. Figure D: Dark-blue garnet quartzite unit found on the contact with the upper quartzite. Figure E: Upper poorly bedded quartzite, often associated with a 2nd order upward coarsening cycle. Figure F: Primary bedding in the form of cross-bedding associated with the upper quartzite.

2.5 Middle Samoep Sequence (see Figure 2.35)

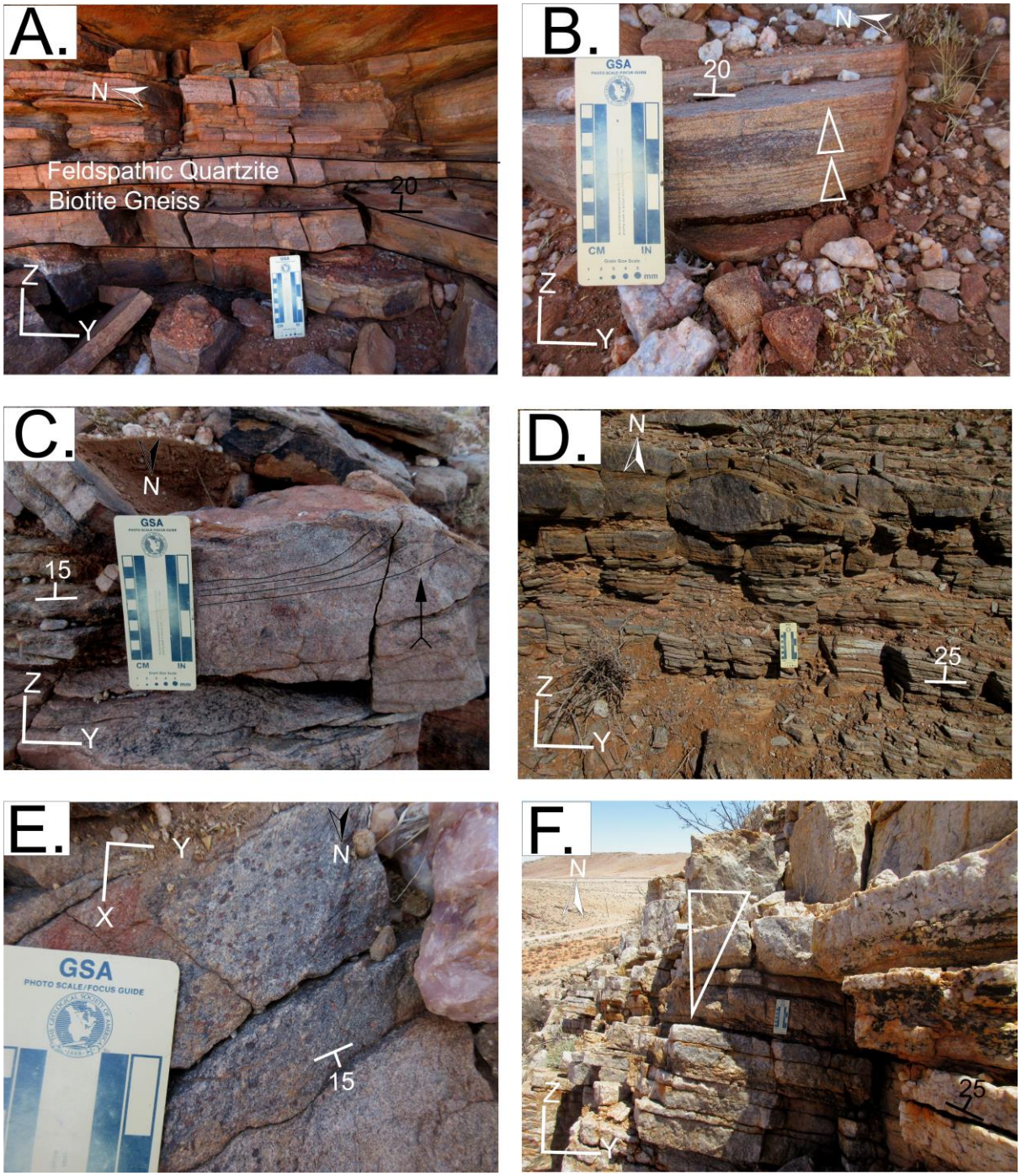

Appendix 2.5: Lithological features of the Middle Samoep Sequence. Figure A: Feldspathic quartzite with inter-banded units of biotite gneiss. Figure B: Represents a 3rd order upward fining cycles associated with the feldspathic quartzite unit. Prominent laminations of biotite and feldspar define the 3rd order fining cycles. Figure C: Cross-bedding associated with the feldspathic quartzite unit and shows younging direction toward the top of the succession. Figure D: Illustrates biotite sillimanite schist with interbanded units of dark-blue garnet-bearing quartzite. Figure E: Garnet overgrowths on the dark-blue quartzite unit within the XY foliation plane, which are interpreted to be late to syntectonic growths. Figure F: Bedded quartzite associated with the upper succession. At certain locations defines a prominent second-order upward coarsening cycle.

2.6 The S-Berg Sequence (see Figure 2.37)

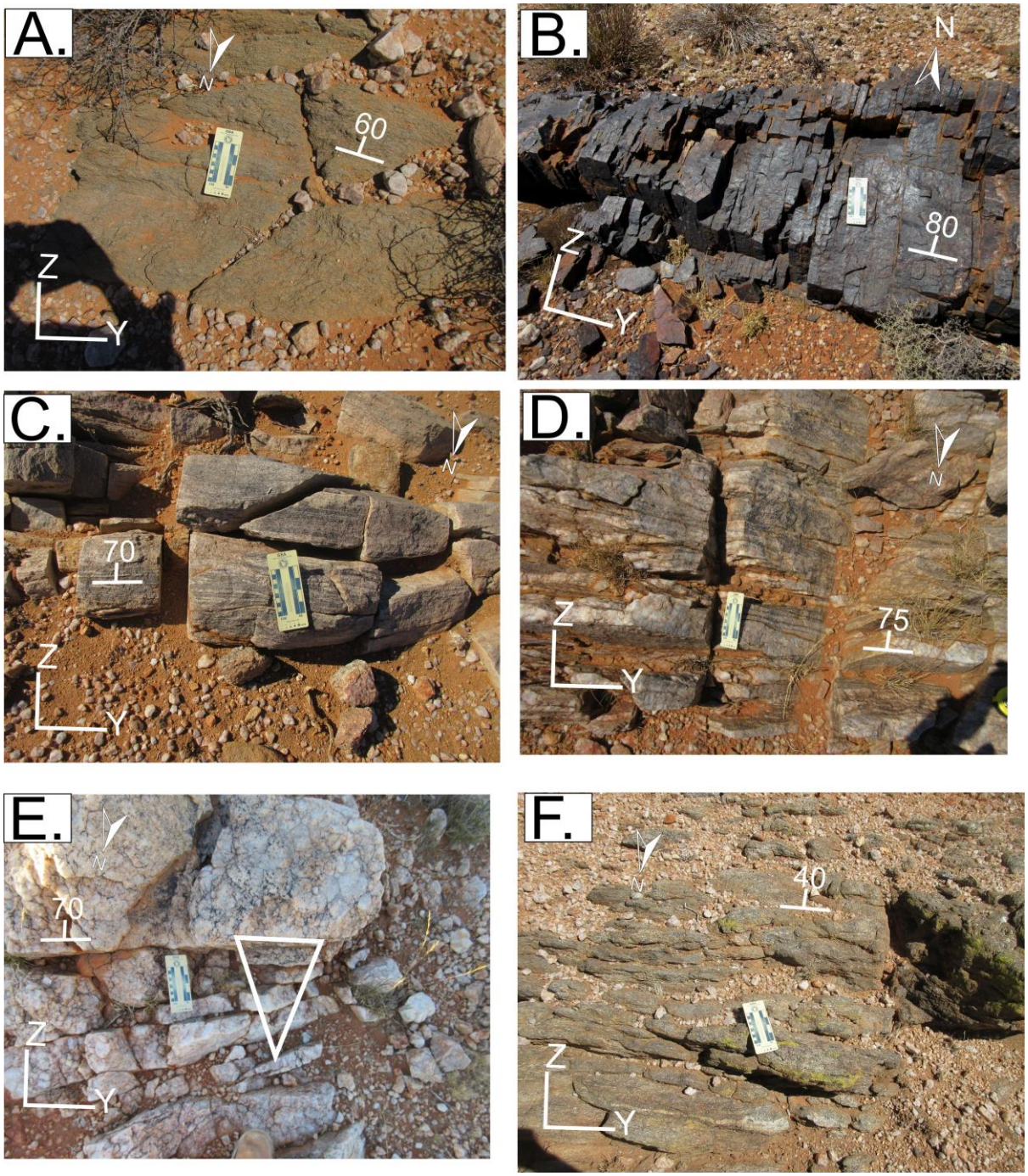

Appendix 2.6: Lithological features of the S-Berg Sequence. Figure A: Thick units of biotite gneiss found at the base of the succession. Figure B: Ferruginous magnetite quartzite units interlayered within the lower biotite gneiss unit. Figure C: Inter-banded calc-silicate units found within the biotite gneiss unit. Figure D: Biotite bands associated with the upper quartzite, further toward the east. Figure E: Poorly bedded quartzite displaying a prominent 2nd order upward coarsening cycle. Figure F: Biotite-sillimanite schist unit found at the top of the stratigraphic succession.

2.7 The Klein Pofadder Sequence (see Figure 2.41)

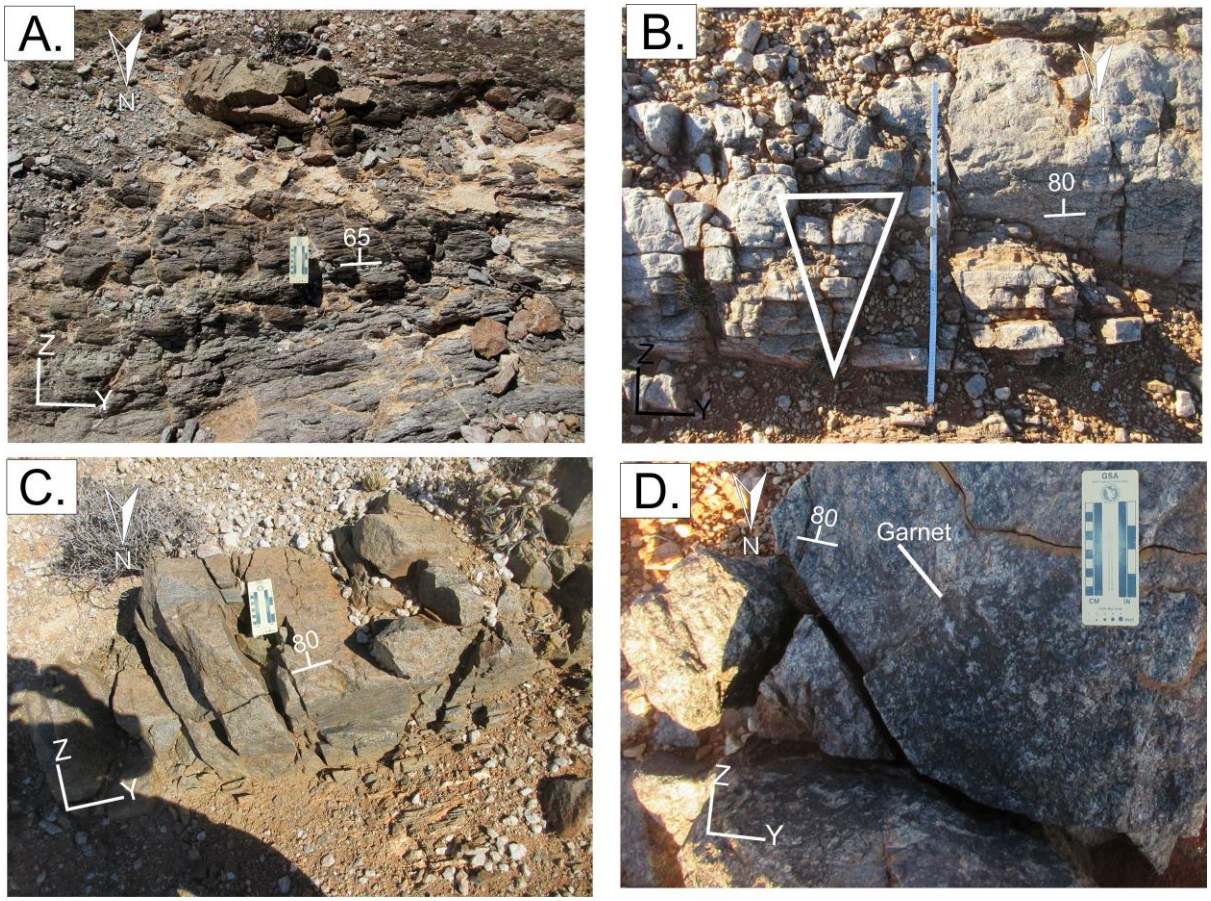

Appendix 2.7: Lithological features of the Klein Pofadder Sequence. Figure A: Thick biotite-sillimanite schist associated with the lower succession. Figure B: Massive poorly bedded quartzite defining a prominent second-order upward coarsening cycle. Figure C: Dark-blue poorly bedded quartzites associated with the upper succession. Figure D: Late to syntectonic garnets associated with the upper dark-blue quartzite unit.

2.8 Inner Koppies Member (see Figure 2.44)

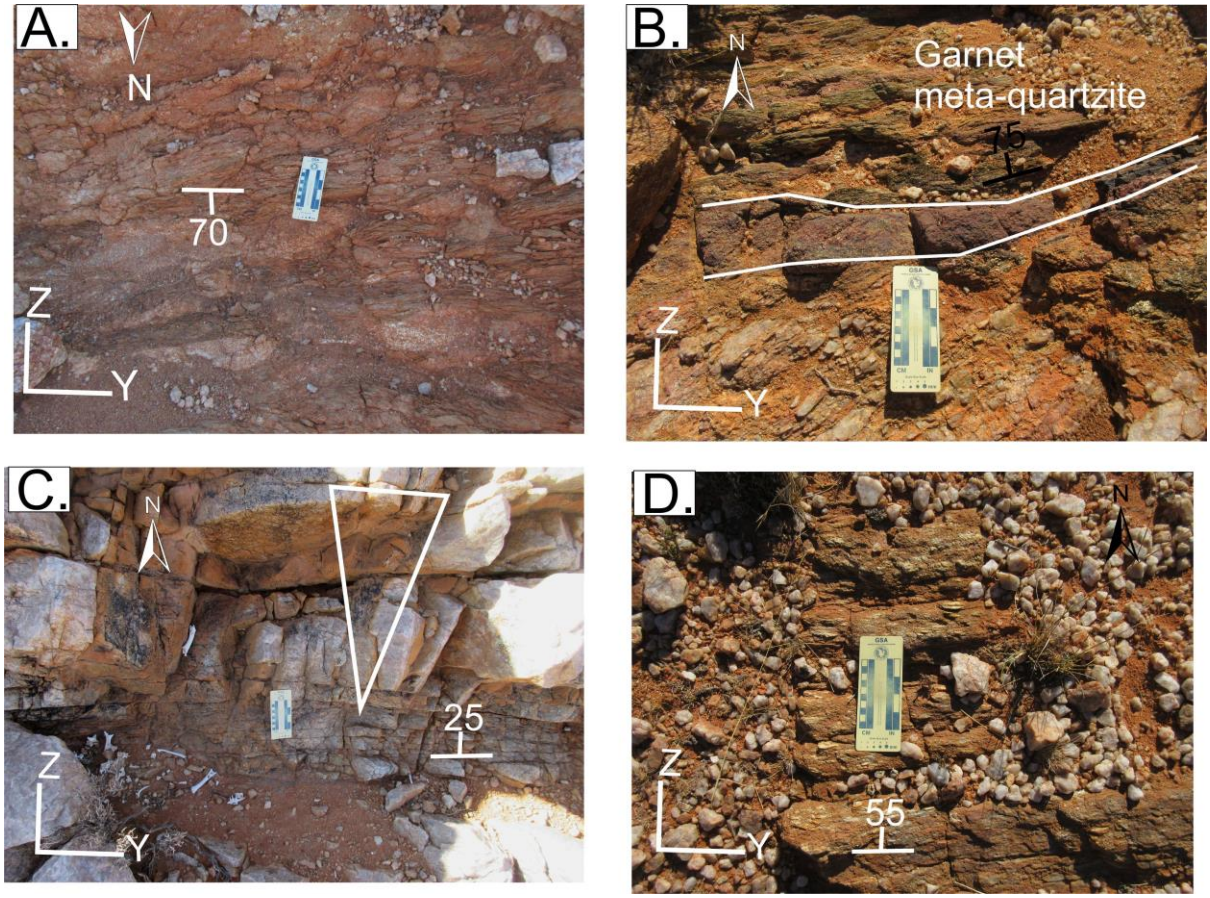

Appendix 2.8: Lithological features of the Inner Koppies Member. Figure A: Biotite-sillimanite schist associated with the lower succession. Figure B: Interbande ferruginous garnet meta-quartzite found in the lower portion of the stratigraphic succession. Figure C: Poorly bedded upper quartzite found in the upper succession defining prominent second-order upward coarsening cycle. Figure D: Nodular sillimanite-quartz-feldspar rhythmic gneiss found in the upper part of the succession. Prominent nodules of sillimanite can be observed on the YZ foliation plane.

2.9 Outer Koppies Member (see Figure 2.45)

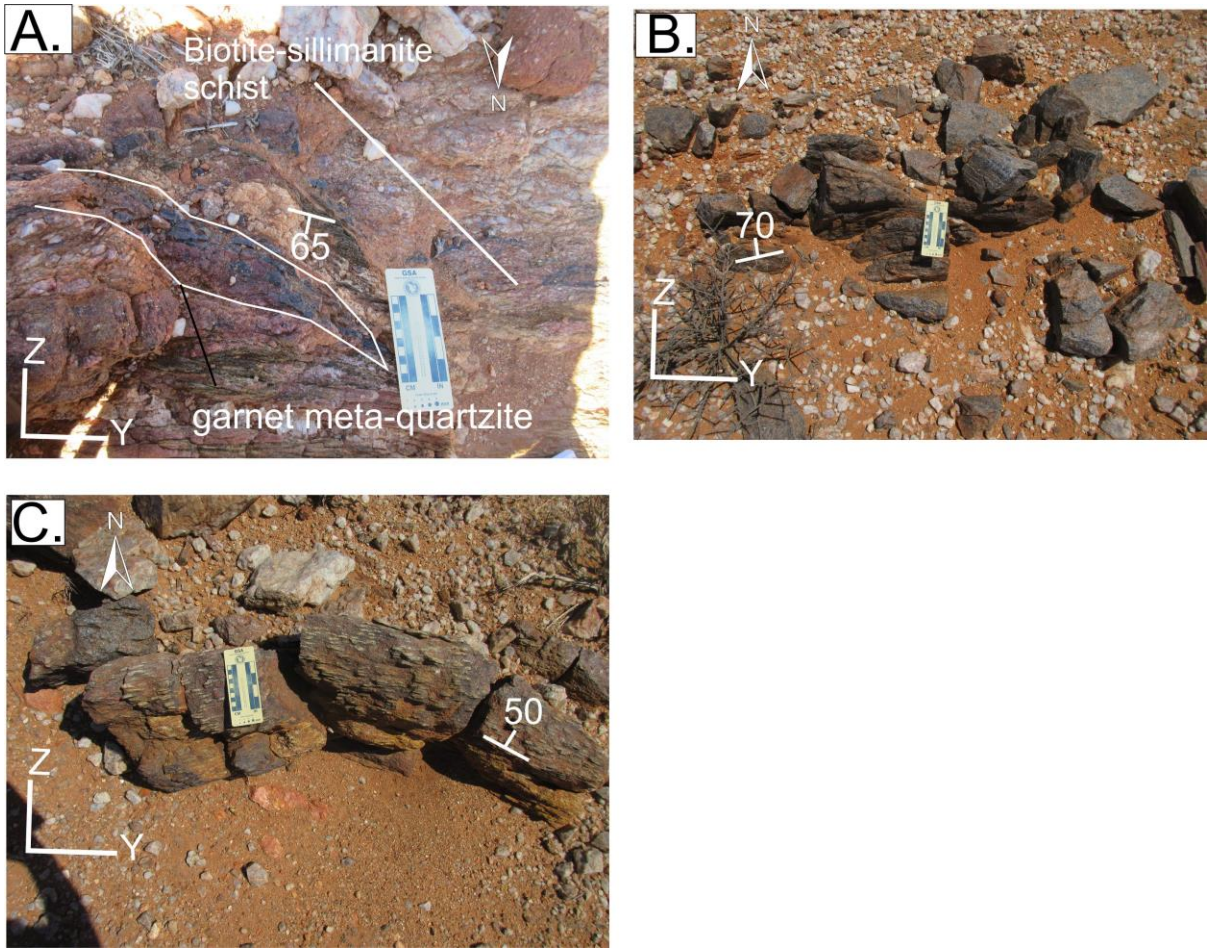

Appendix 2.9: Photos associated with the stratigraphy related to the Outer Koppies Member. Figure A: Intercalated units of ferruginous garnet quartzite associated within the biotite-sillimanite schist unit. Figure B: Dark-blue character often associated with the upper quartzite. Figure C: Nodular rhythmic gneiss associated with the top portion of the outer sheath member.

2.10 Poort se Berg Sequence (see Figure 2.48)

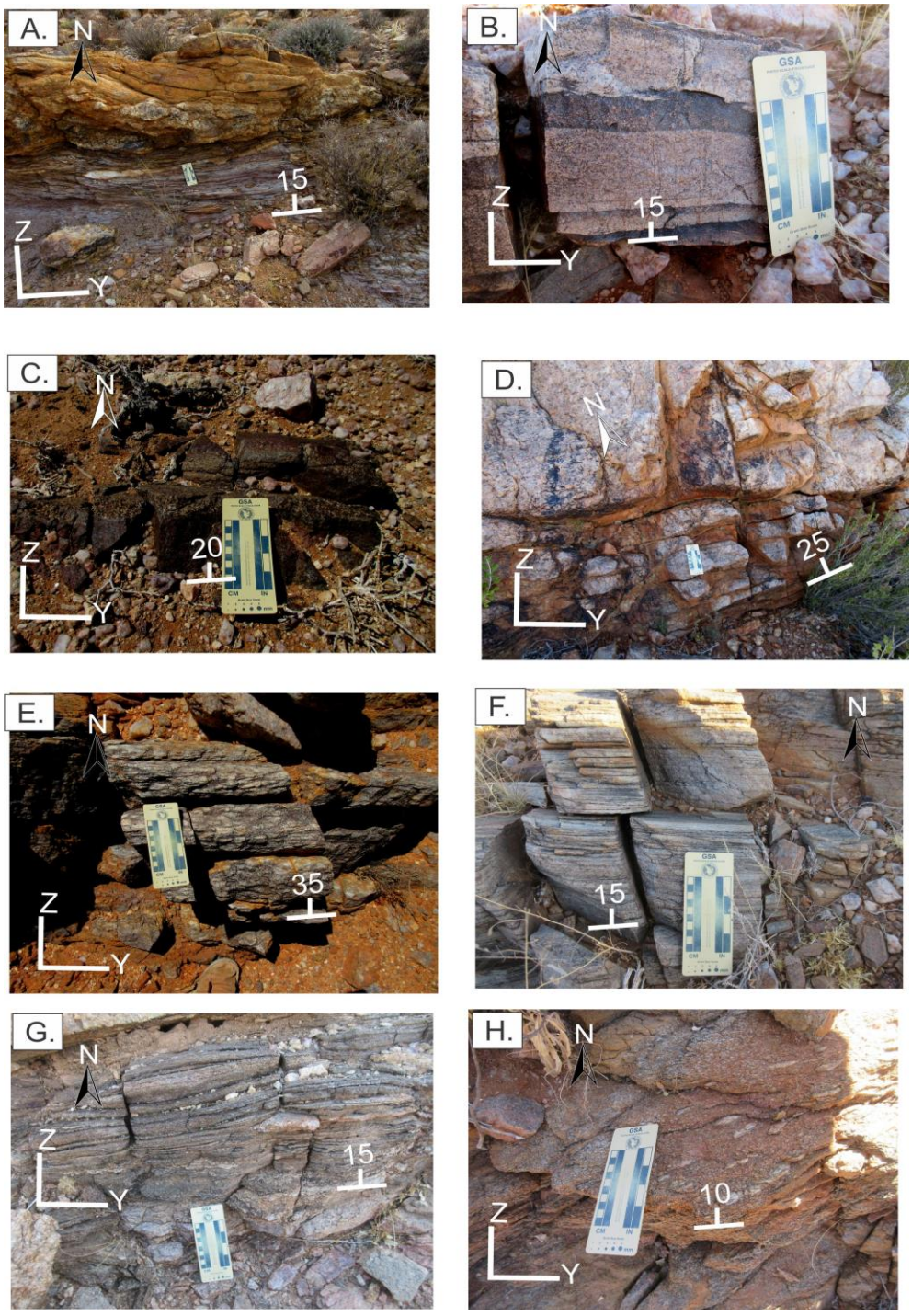

Appendix 2.10: Lithological features associated with the Poort se Berh Sequence (upper (Figures A-E) and lower Poort se Berg Member (Figures F-H)). Figure A: Massive biotite sillimanite schist unit, with intrusive units of Lekdam Gneiss found within. Figure B: Depicts the feldspathic quartzite unit associated with the volcanic/chemogenic unit found at the base of the Poort Member. Primary bedding in the form of flame structures, can be observed within the feldspathic quartzite. Figure C: The ferruginous garnet quartzite unit intercalated within the large biotite-sillimanite schist unit associated with upper Poort se Berg Member.Figure.D: Upper poorly bedded quartzite displaying a prominent second-order upward coarsening cycle. Figure E: Nodular rhythmic sillimanite- quartz-feldspar gneiss found toward the top of the upper Poort se Berg Member. Prominent sillimanite nodules can be seen in the diagram. Figure F: Thick well laminated feldspathic quartzite unit associated with the lower Poort se Berg Member. Figure G: Centimetre to metre scale biotite gneiss found at the base of the lower Poort se Berg Member. Figure H: Nodular rhythmic sillimanite-quartz-feldspar gneiss showing prominent sillimanite nodules found in the upper section of the lower Poort se Berg Member.

2.11 T-Goob Sequence (see Figure 2.49)

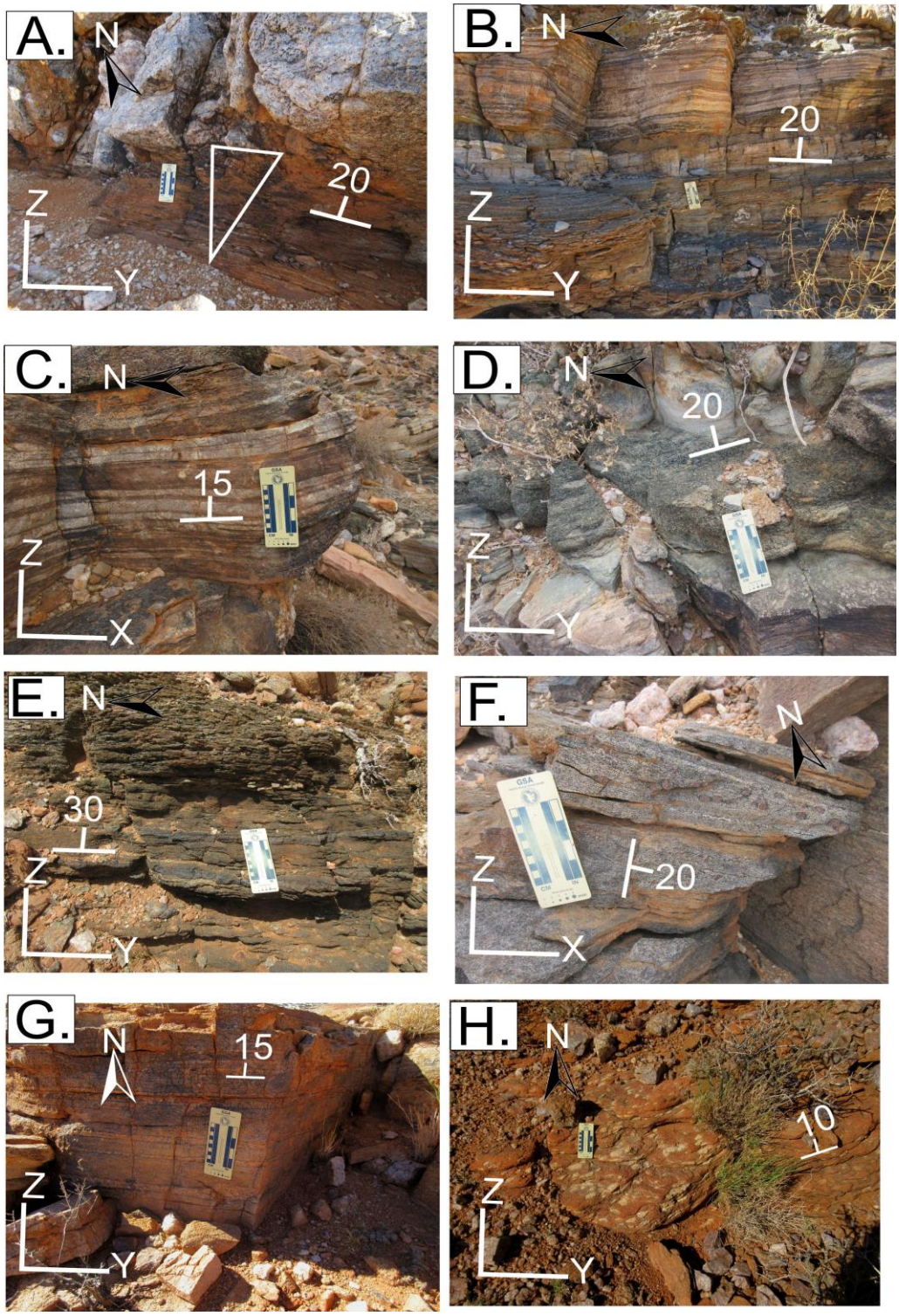

Appendix 2.11: Lithological features of the T-Goob se Berg Sequence. Figure A: Contact between the upper quartzite and lower nodular sillimanite-quartz-feldspar rhythmic gneiss defining a second-order upward coarsening cycle. Figure B: Volcanic unit defined by blue-white quartzites with interlayered units of diopside, actinolite, and biotite gneiss. Figure C: Volcanic/chemogenic unit depicting interbanded quartzite and diopside units. Figure D: Interlayered sequences of actinolite associated with the central volcanic unit found within the biotite-sillimanite schist unit. Figure E: Biotite gneiss associated with the central portion of the stratigraphic succession. Figure F: Biotite gneiss with overgrowths of garnet seen on the XZ foliation plane. Figure G: Well laminated medium quartz-feldspar gneiss found on the top portion of the stratigraphic succession. Figure H: Nodular sillimanite-quartz-feldspar rhythmic gneiss associated with the upper succession of the T- Goob Sequence.

2.12 Outer Lekdam Sequence (see Figure 2.50)

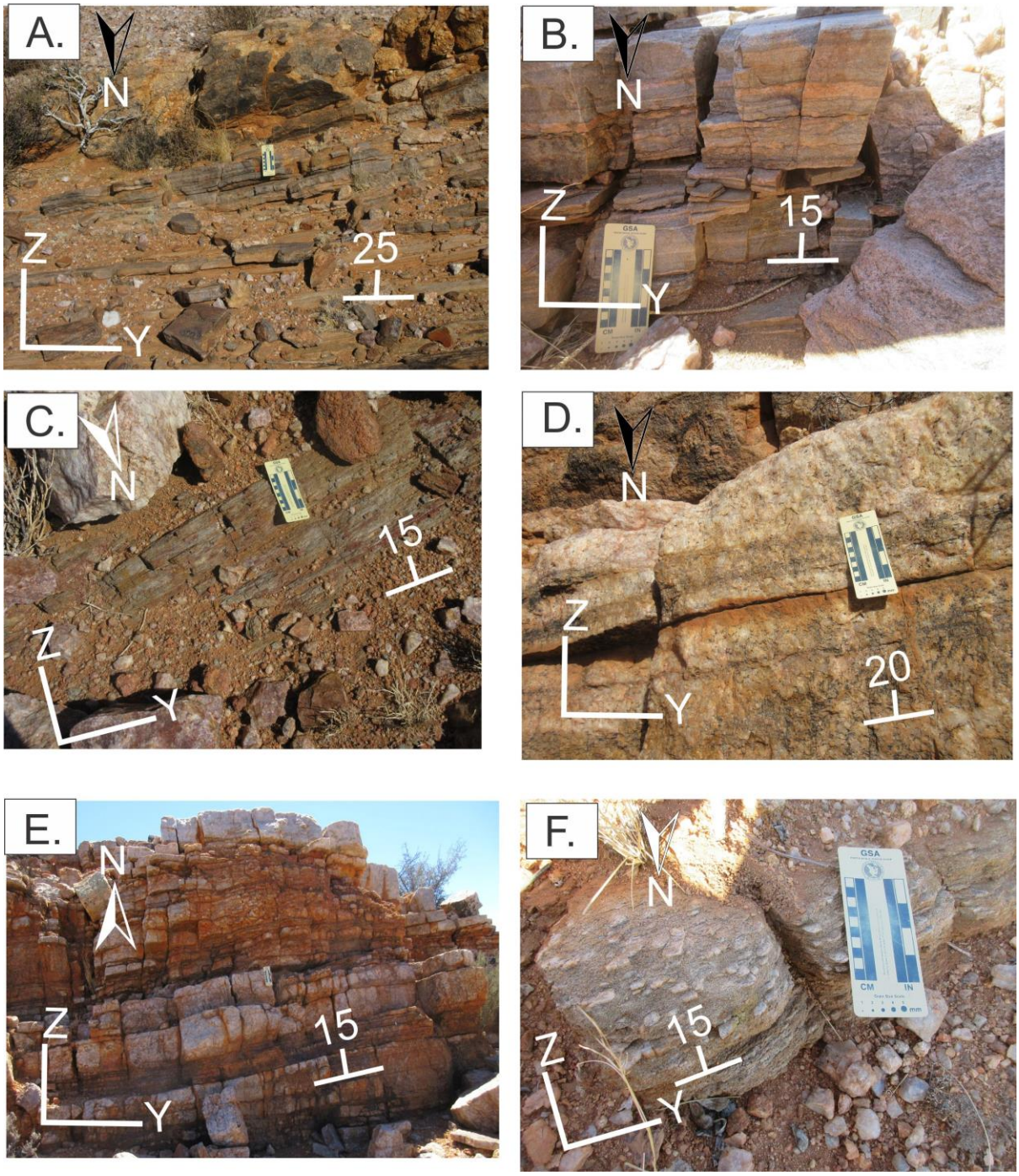

Appendix 2.12: Lithological features associated with the Outer Lekdam Sequence. Figure A: Feldspathic quartzite with interbanded units of biotite gneiss. Figure B: Feldspathic quartzite units intercalated within the biotite-sillimanite schist units. Figure C: Biotite-sillimanite schist associated with the lower succession of the Outer Lekdam Sequence. Figure D: Poorly to well-bedded upper quartzite displaying prominent biotite bands. Figure E: Well bedded character depicted within certain portions of the Outer Ledkam Sequence, displaying prominent second-order upward coarsening cycles. Figure F: Nodular sillimanite-quartz-feldspar rhythmic gneiss associated with the top part of the stratigraphic succession. Sillimanite nodules can be seen on the YZ and XY foliation planes.

2.13 Skewe Berg Sequence (see Figure 2.53)

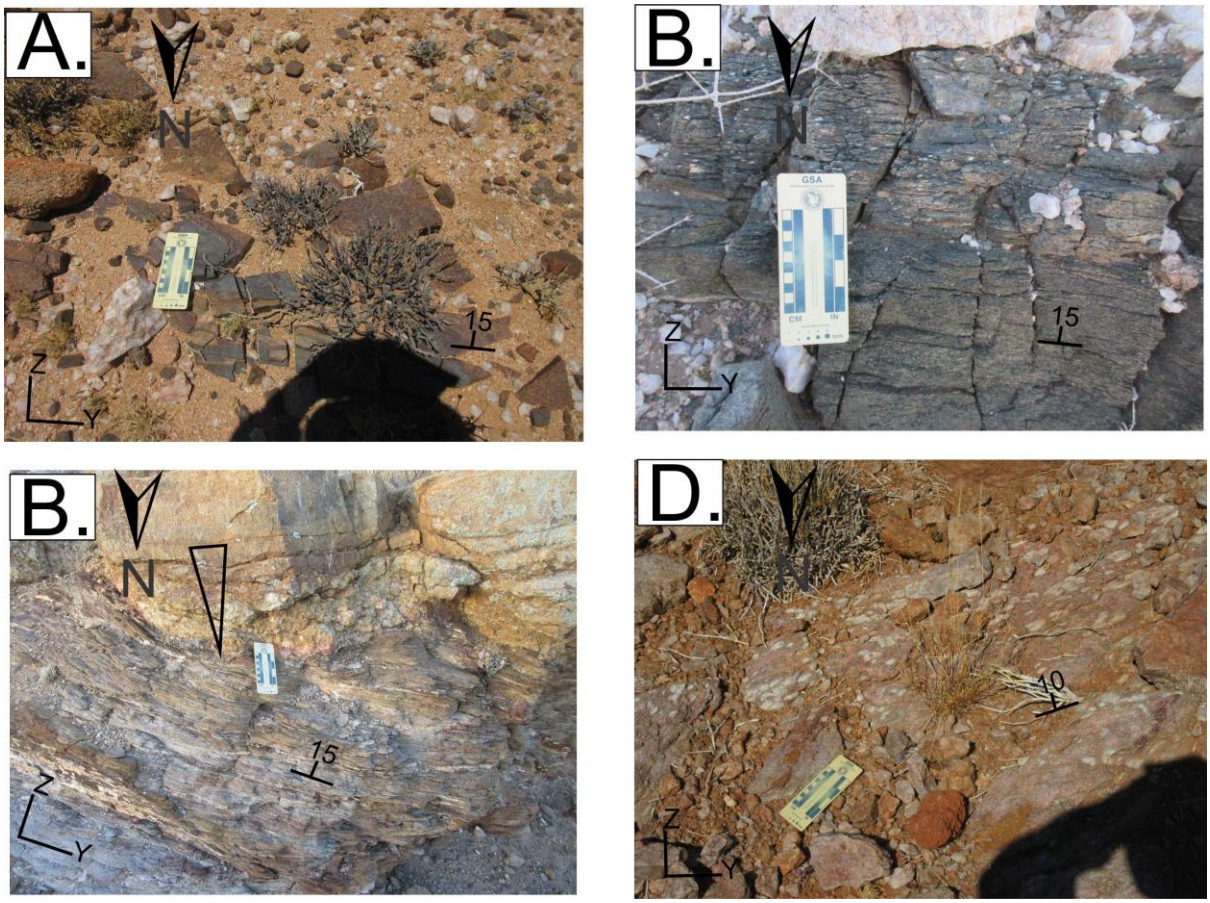

Appendix 2.13: Lithological features of the Skewe Berg Sequence: Figure A: Garnet meta-quartzite units interbanded within the lower biotite-sillimanite schist unit. Figure. B: Biotite gneiss interbanded within the biotite-sillimanite schist unit. Figure C: Thick sequence of biotite-sillimanite schist associated with the middle and lower portion of the stratigraphic succession. Figure D: Nodular sillimanite-quartz-feldspar rhythmic gneiss associated with the upper portion of the stratigraphy, often associated with prominent sillimanite nodules.

2.14 Xenolith Sequence (see Figure 2.54)

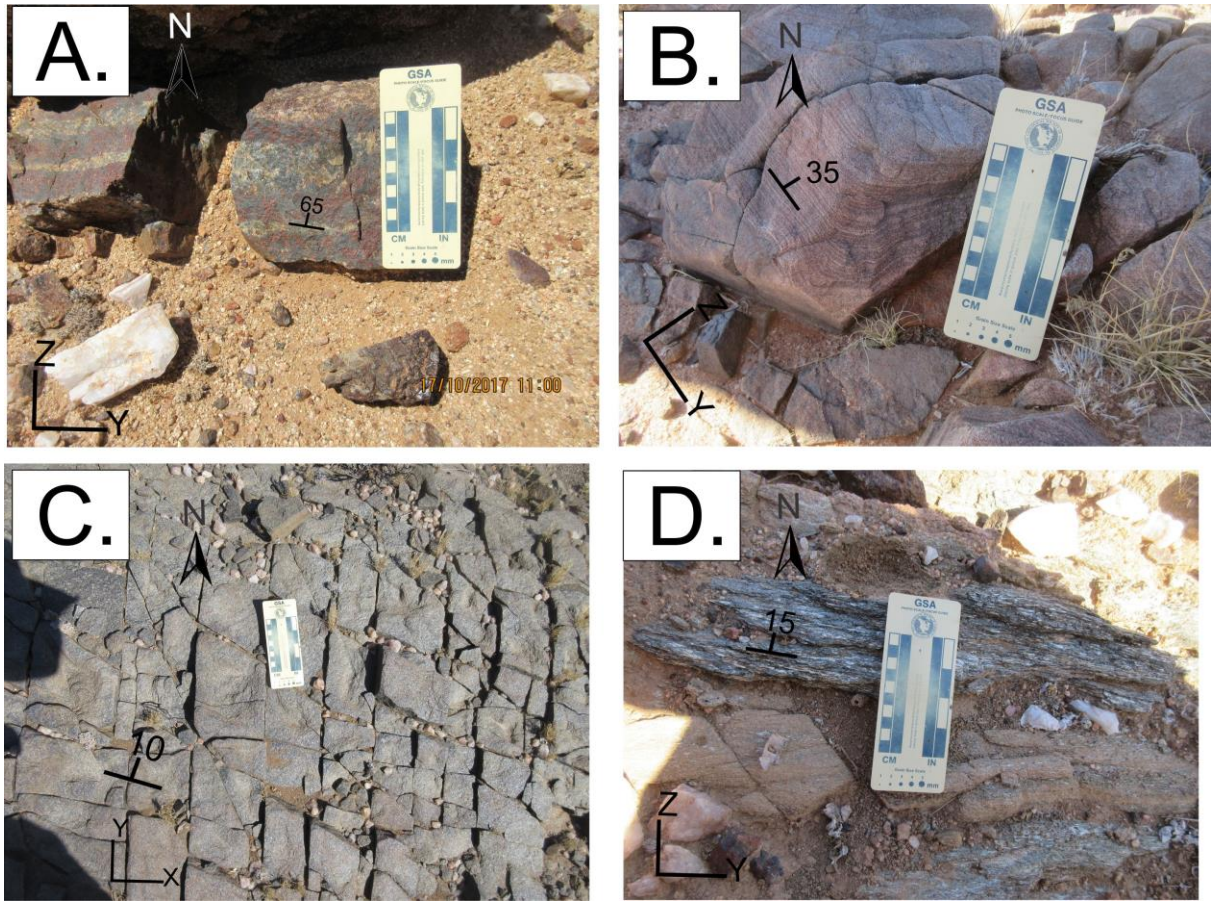

Appendix 2.14: Lithostratigraphic features associated with the Xenolith Sequence. Figure A: Garnet bearing meta-quartzite; and showing chocolate tablet boudinage. Garnets are aligned parallel to the foliation planes. Figure B: Depicts the feldspathic quartzites associated with the Xenolith Member. Figure C: Biotite-sillimanite schist unit associated with the upper stratigraphic succession. Figure D: Biotite-sillimanite schist unit. Small sillimanite nodules can be seen on the YZ foliation plane at centimetre scale.

2.15 Draai-Berg Sequence (see Figure 2.55)

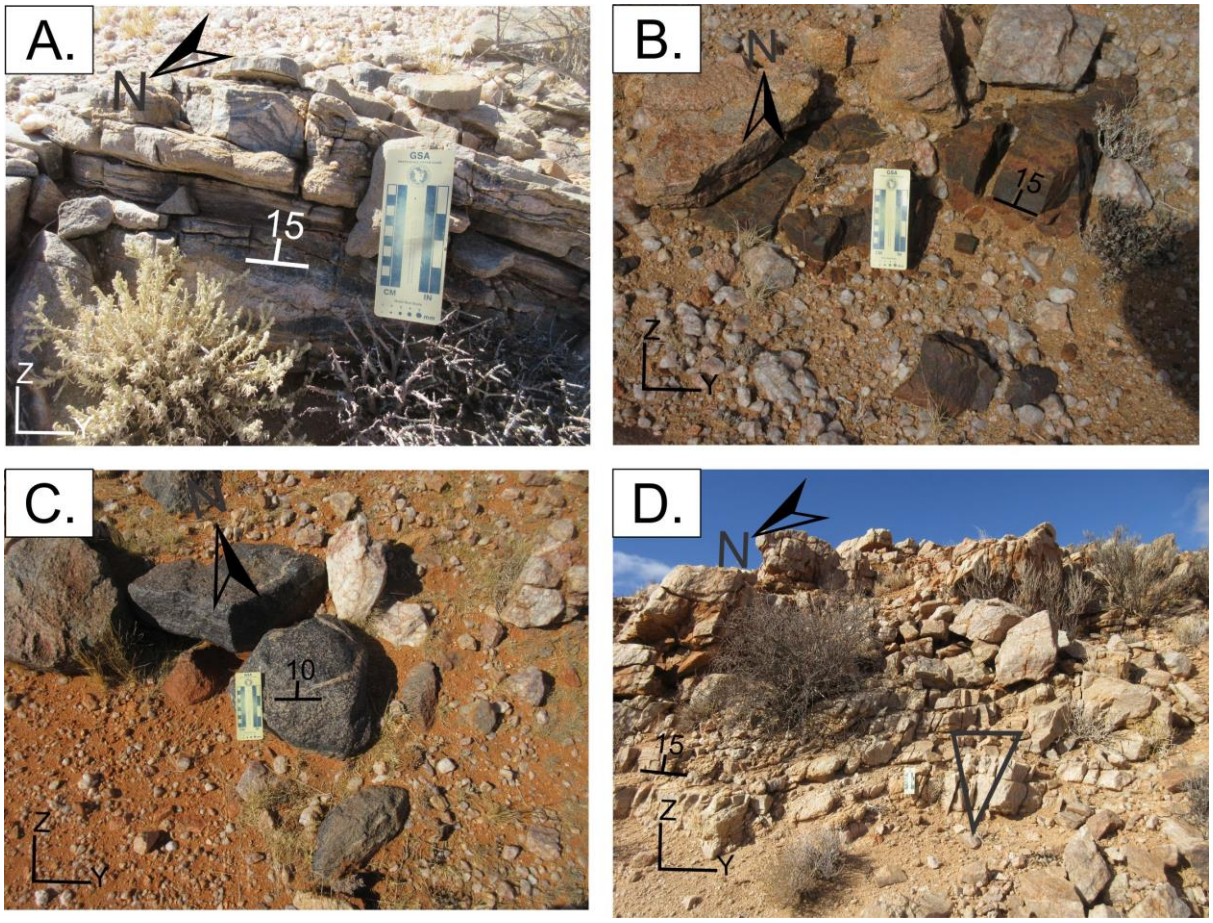

Appendix 2.15: Lithostratigraphic features of the Draai-Berg Sequence. Figure A: Feldspathic quartzite unit found within the lower succession. Figure B: Garnet-bearing meta-quartzite units interbanded within the lower biotite-sillimanite schist unit. Figure C: Dark calc-silicate rocks with prominent feldspar bands found at the base of the succession. Figure D: Poorly bedded quartzite defining a second-order upward coarsening cycle, associated with the upper echelon of the sequence.

2.16 Platberg Sequence (see Figure 2.56)

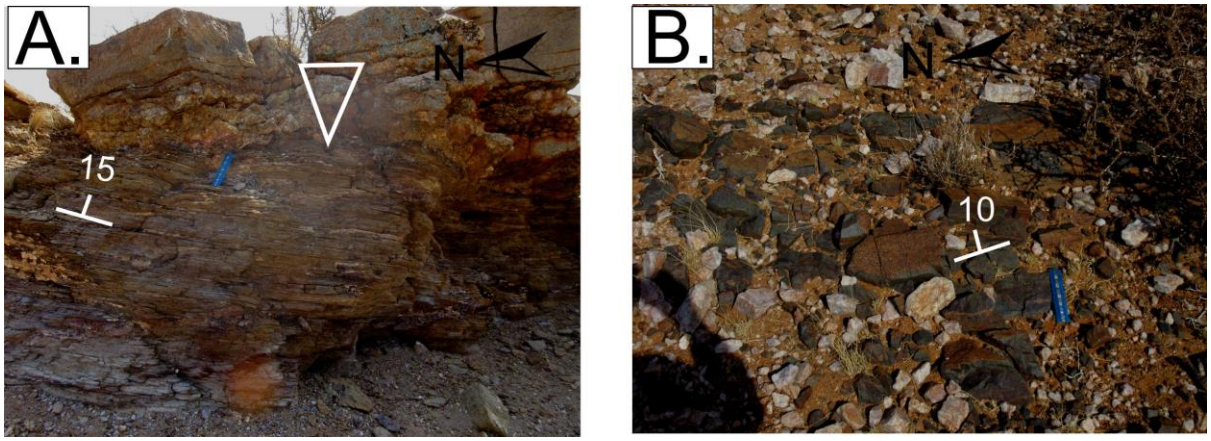

Appendix 2.16: Lithostratigraphic features associated with the Platberg Sequence: Figure A: Biotite sillimanite schist unit in contact with a poorly bedded quartzite, displaying a second-order upward coarsening cycle.Figure B: Prominent garnet-bearing quartzite unit (BIF), which folds around the Platberg structure and is found at the bottom of the stratigraphic succession.

2.17 Sy-Berg Sequence (see Figure 2.57)

Appendix 2.17: Photos of the stratigraphy related to the Sy-Berg Sequence. Figure A: Small feldspathic quartzite unit found at the base of the succession. Figure B: Poorly to well-bedded quartzite, showing a second-order upward fining cycle. Figure C: Dark-blue quartzite unit interlayered within the central biotite-sillimanite schist unit.

2.18 Achab Sequence (see Figure 2.61)

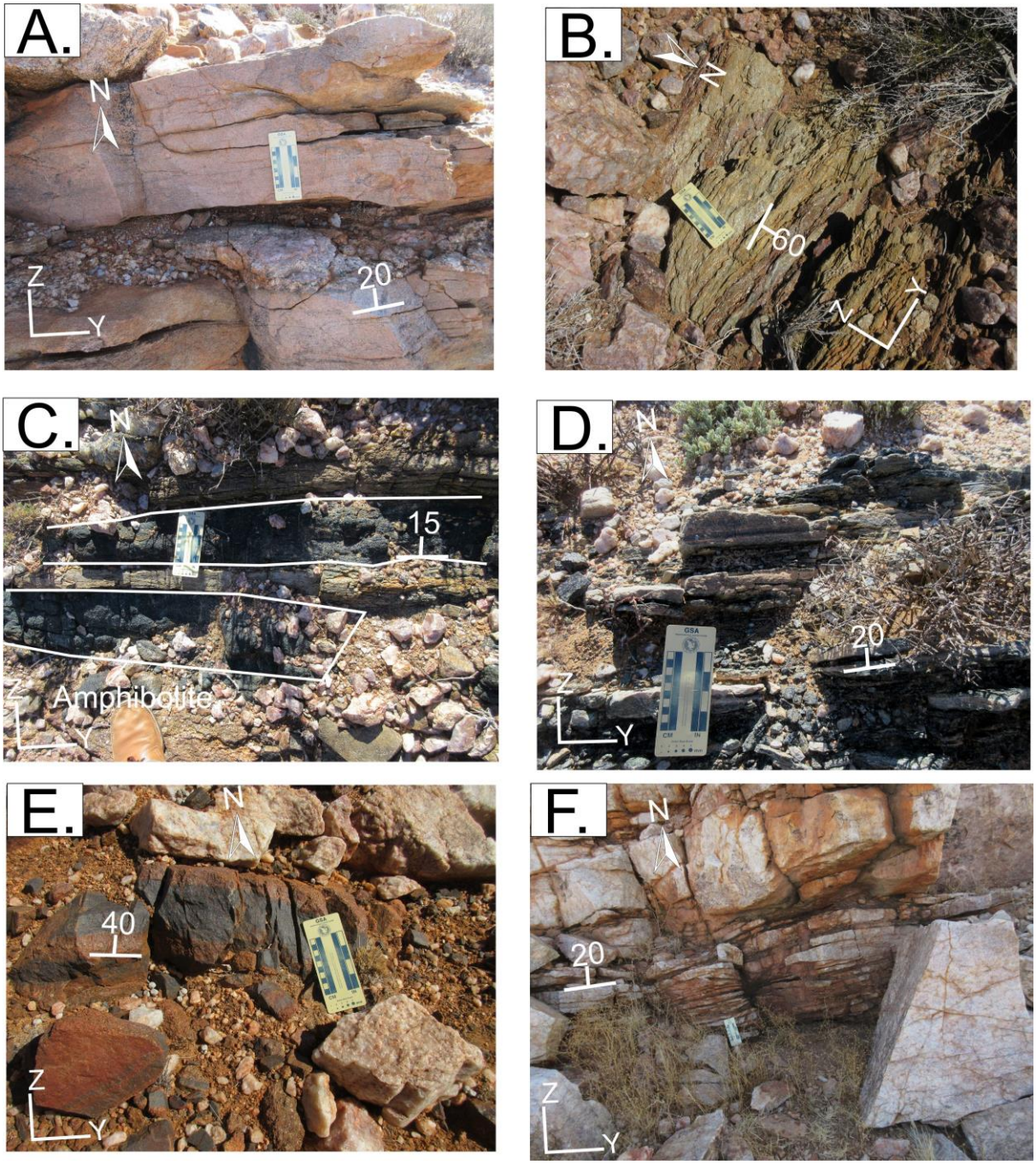

Appendix 2.18: Lithological features of the Achab Sequence. Figure A: Medium quartz-feldspar Namies Gneiss found at the base of the succession. Figure B: Massive units of biotite-sillimanite schist found at the base of the Achab Sequence just above the Namies Gneiss. Figure C: Interbanded units of amphibolite associated with the stratigraphic succession. Figure D; Interbanded units of calc-silicate rock which occur sporadically throughout. Figure E: Banded units of ferruginous garnet meta-quartzites, interbanded within the lower biotite-sillimanite schist units. Figure F: Massive poorly bedded quartzites which show second-order upward coarsening cycles.

2.19 De Rust Sequence (see Figure 2.63)

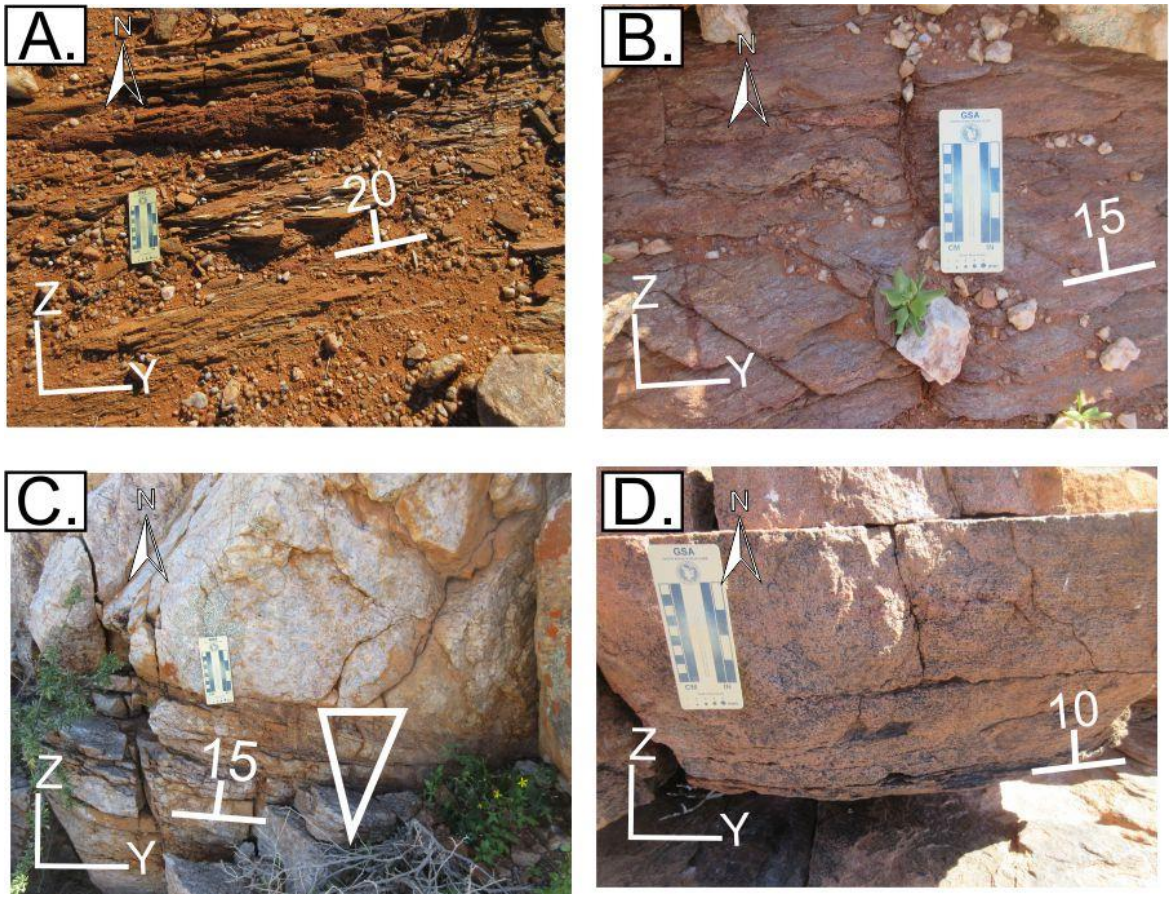

Appendix 2.19: Lithostratigraphic features of the De Rust Sequence. Figure A: Nodular sillimanite-quartz-feldspar rhythmic gneiss, found at the base of the succession. Prominent sillimanite nodules can be viewed on the YZ foliation surface. Figure B: Thick unit of biotite-sillimanite schist unit, found toward the top of the succession. Figure C: Upper poorly bedded quartzite, showing a second-order upward coarsening cycle. Figure D: Well to poorly foliated medium quartz-feldspar Namies Gneiss found at the top of the stratigraphic succession.

2.20 Inner Dwarsberg Member (see Figure 2.65)

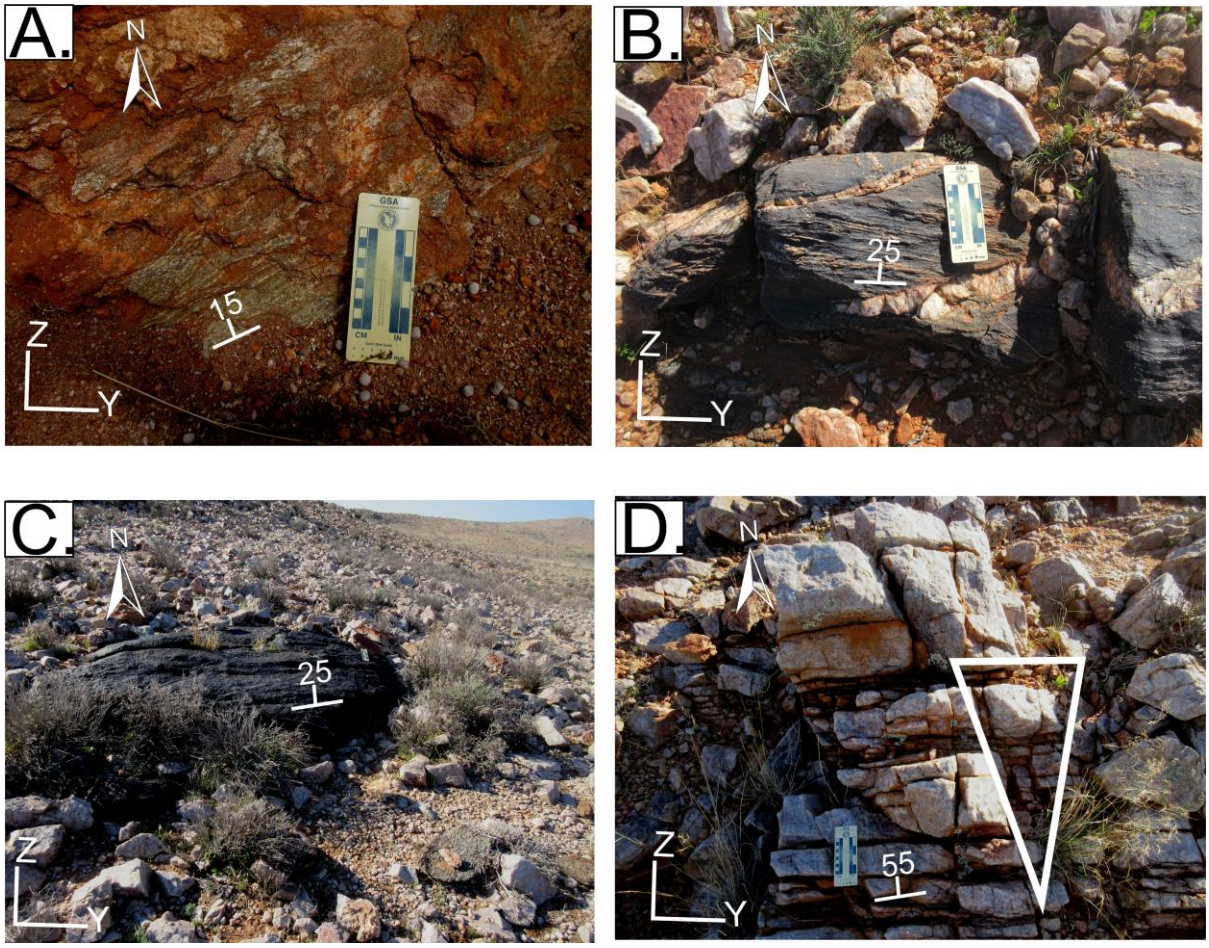

Appendix 2.20: Lithostratigraphic features associated with the Inner Dwarsberg Member. Figure A: Biotite-sillimanite schist associated with the lower and upper portions of the Inner Dwarsberg Member. Figure B: Black calc-silicate rock unit found at the base of the stratigraphic succession, found within the biotite-sillimanite schist unit. Figure C: Large amphibolite interbanded within the lower biotite-sillimanite schist unit. Figure D: Second-order upward coarsening cycle associated with the upper quartzite.

2.21 Outer Dwarsberg Member (see Figure 2.66)

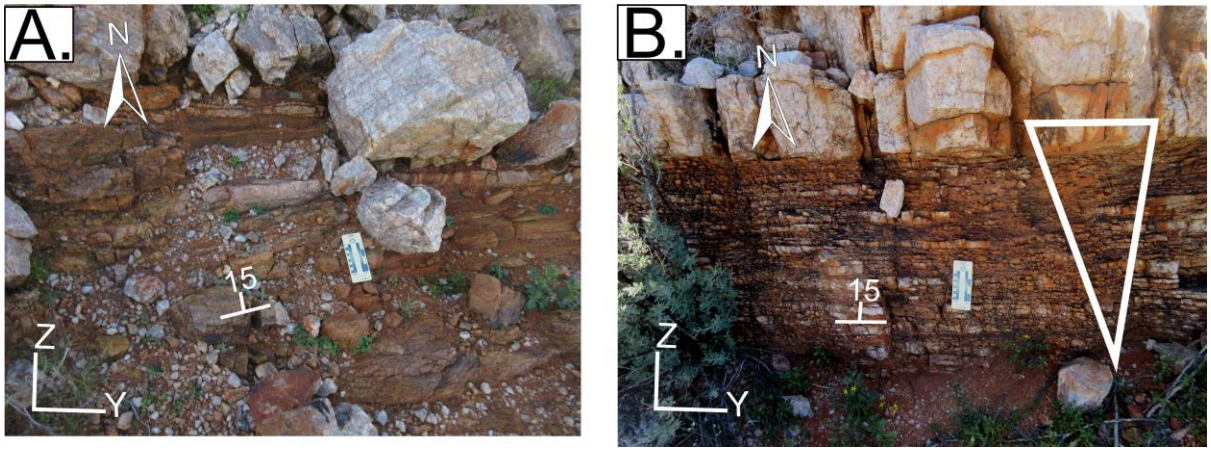

Appendix 2.21: Lithostratigraphic features associated with the Outer Dwarsberg Member: Figure A: Biotite-sillimanite schist unit associated with the Outer Dwarsberg Member. Figure B: Second-order upward coarsening cycle associated with the upper quartzite unit.

2.22 The Hom Formation (see Figure 2.69)

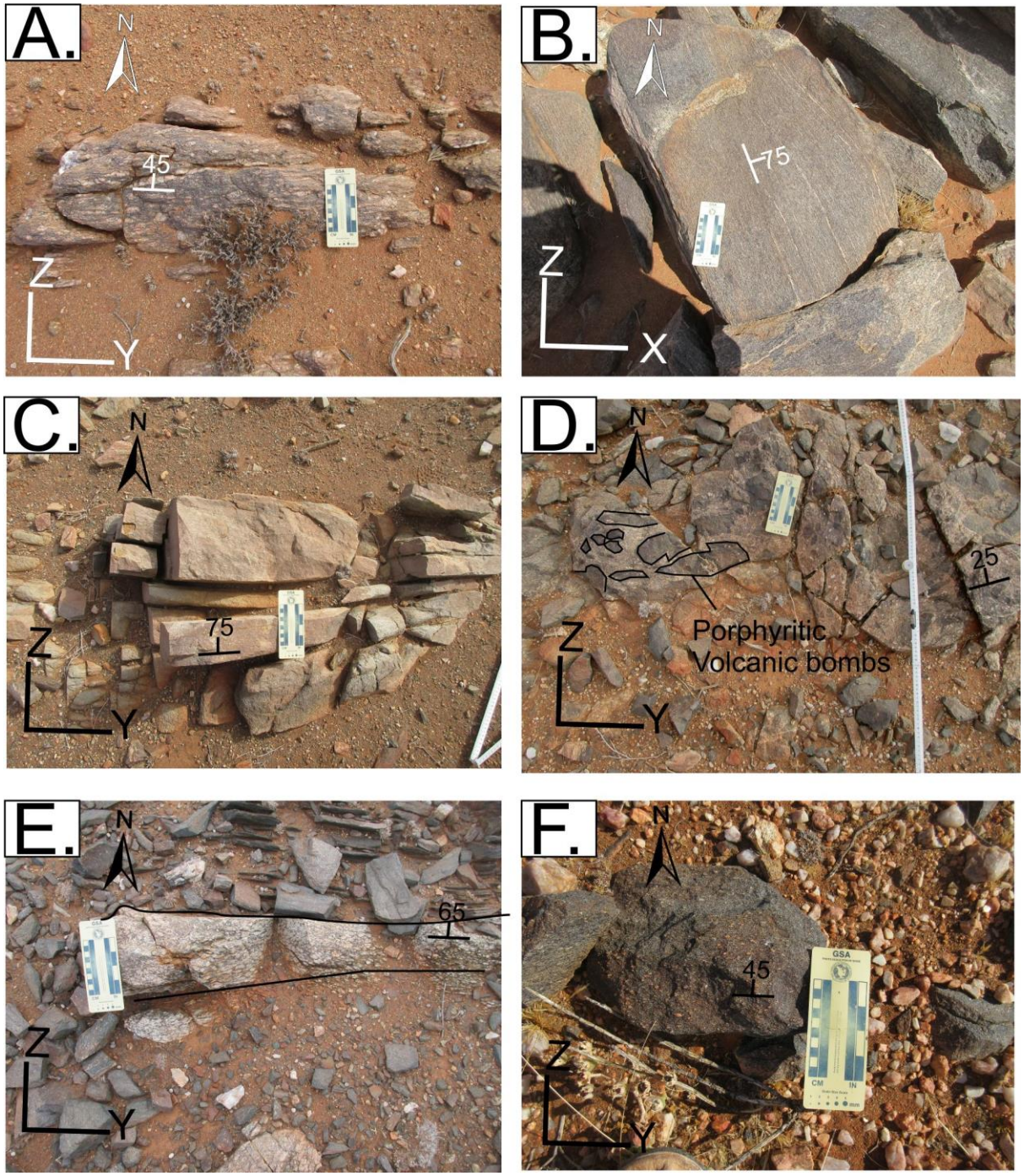

Appendix 2.22: Lithostratigraphic features associated with the Hom Formation. Figure A: Swartmodder Gneiss which intrudes within the entire succession. Figure B: Leucobands associated with a higher strain variation of the Swartmodder Gneiss. Figure C: Leucocratic finely laminated felsic gneiss found throughout the succession. Figure D: Poryphyritic volcanic bombs, showing a porphyritic appearance of mafic and feldspar clasts. Figure E: Volcanoclastic bombs, which at certain locations have leucocratic appearance due to an increase in feldspar clasts. Figure F: Quartz eyes found in the interbanded amphibolite units. The quartz eyes are often associated with most of the hornblende gneisses, biotite gneiss, and calc-silicate rocks.

2.23 The Van Tittensville Formation (see Figure 2.71)

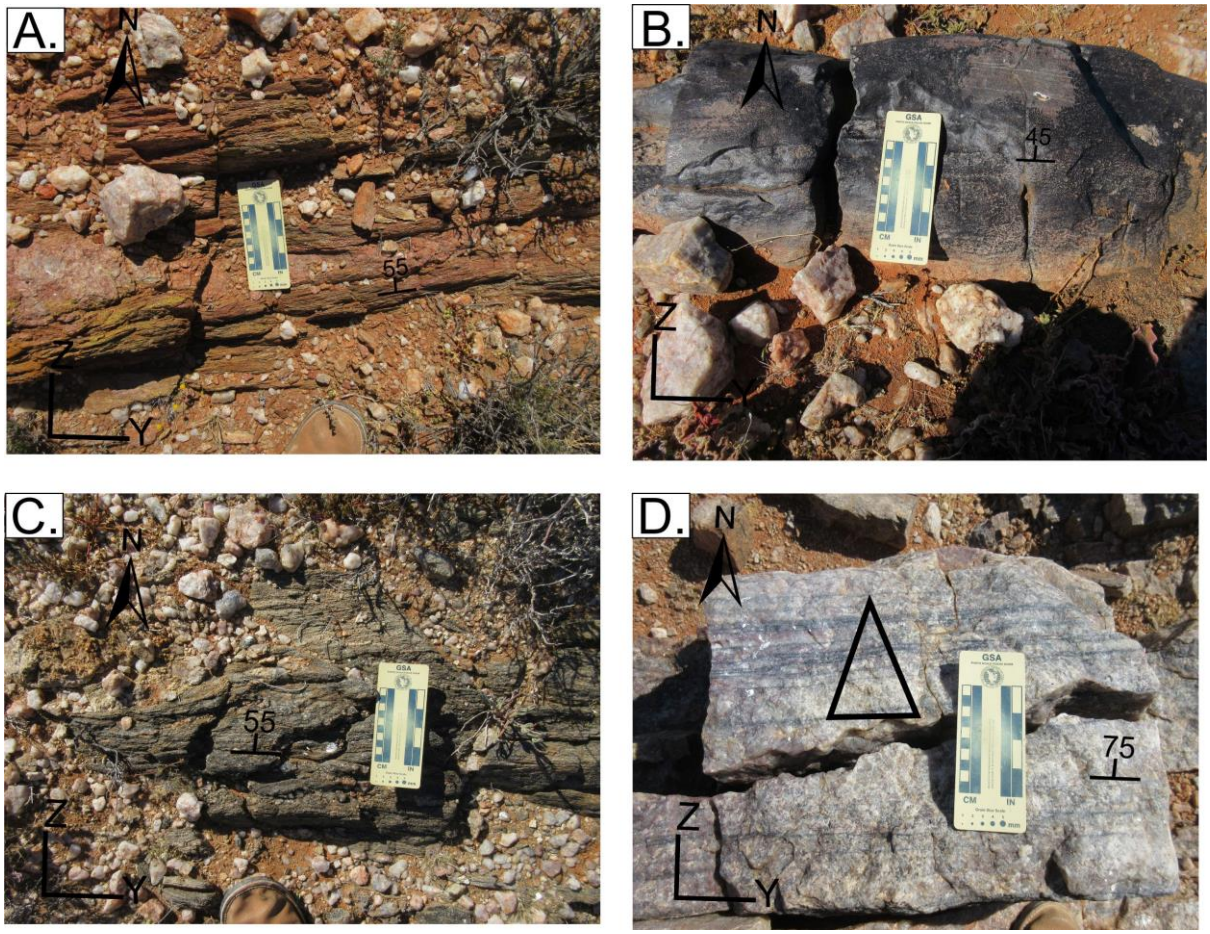

Appendix 2.23: Lithostratigraphic features associated with the Van Tittensville Formation. Figure A: Lower biotite gneiss unit found at the base of the succession. Figure B: Calc-silicate units interbanded within the Van Tittensville Formation, often associated with the lower biotite gneiss unit. Figure C: Biotite-muscovite-sillimanite schist associated with the upper part of the stratigraphic succession. Figure D: Prominent magnetite bands associated with the upper quartzite, displaying a third-order upward fining cycle.

Appendix 2.24 Geological Map of An Area South of Pofadder

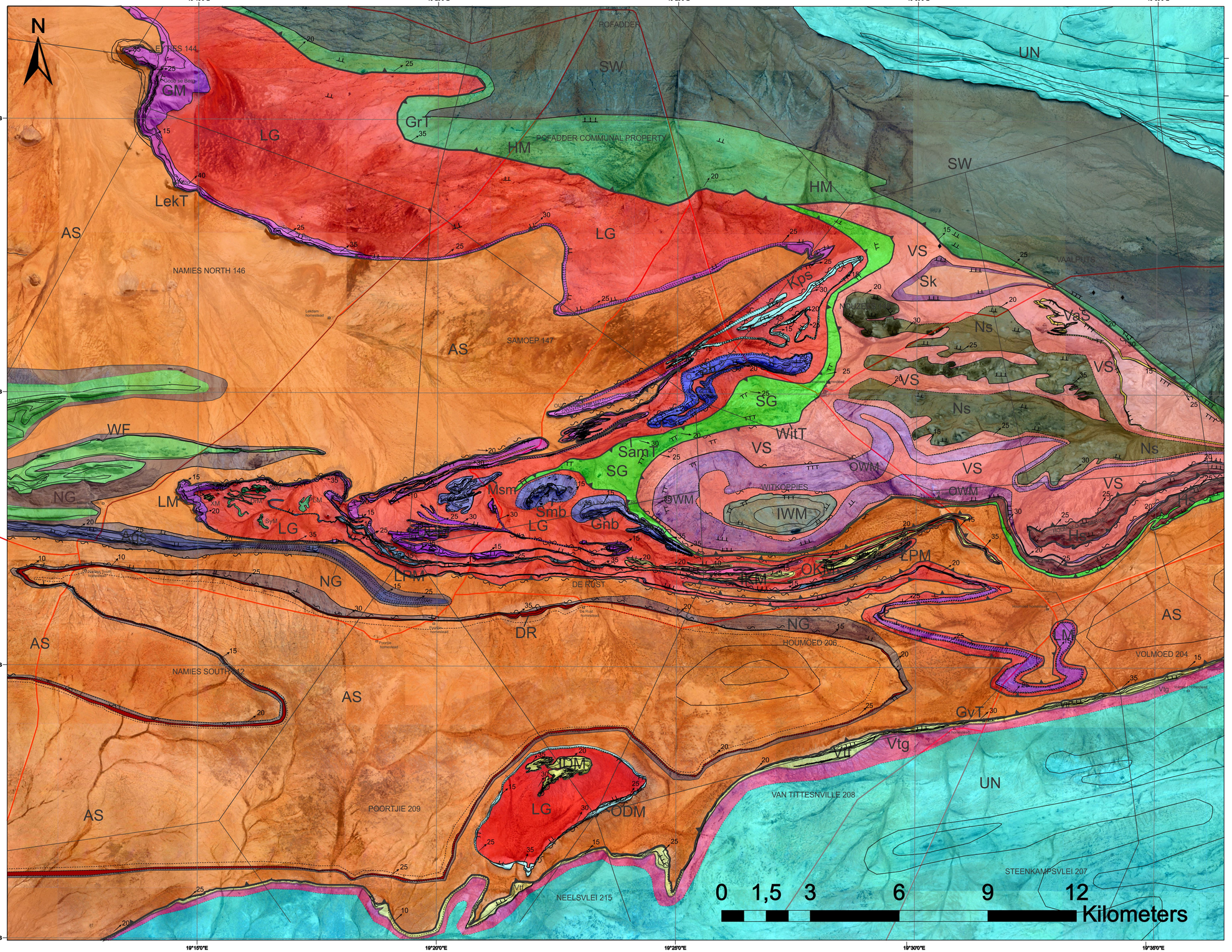

Geological Legend

Supracrustals

Aggeneys Terrane

UN	Undifferentiated Pofadder and Bladgrond Terrane.		
Sk	Thick succession of biotite gneiss, calc-silicate rock, amphibolite rock and poorly bedded quartzite.	Swartkop Sequence	Witkoppies Sequence; Witkoppies Thrust Sheet (Domain 1)
VaS	Thick succession of poorly bedded quartzite, feldspathic quartzite, magnetite quartzite, amphibolite and thick succession of biotite gneiss.	Vaalputs Sequence	
Ns	Thick succession of biotite gneiss, amphibolite, poorly-well bedded feldspathic quartzite and gabbro-norite intrusives.	Nouzees Sequence	
Hs	Thick succession of biotite-sillimanite schist, actinolite, dark-blue quartzite and poorly bedded quartzite.	Houmoed Sequence	
IWM	Thick succession of biotite gneiss, black banded marble bearing calc-silicate rock, white banded diopside-magnetite calc-silicate rock and actinolite lenses.	Inner Witkoppies Member	Witkoppies Sequence; Samoep Thrust Sheet (Domain 2
OWM	Thick succession of biotite gneiss, black banded marble bearing calc-silicate rock, white banded diopside-magnetite calc-silicate rock and amphibolite.	Outer Witkoppies Member	
SG	Well foliated medium quartz-feldspar gneisss biotite.		
Gnb	Thick sequence of biotite gneiss, poorly bedded quartzite, dark-blue quartzite, amphibolite calc-silicate rock.	Gannapoort Berg Sequence	Samoep Succession; Lekdam Thrust Sheet (Domain 3)
Smb	Thick sequence of biotite. gneiss, black calc-silicate rock, biotite-sillimanite schist, dark blue garnet bearing quartzite, poorly bedded quartzite.	Samoep se Berg Sequence	
Msn	Thin sequence of biotite gneiss, feldspathic quartzite, biotite-sillimanite schist, dark-blue garnet bearing quartzite, poorly bedded quartzite.	Middle Samoep Sequence	
Sb	Thick sequence of biotite gneiss, feldspathic quartzite, biotite-sillimanite schist, dark quartzite, Thick succession poorly bedded quartzite.	S-Berg Sequence	
Kps	Thick sequence of biotite-sillimanite schist, dark blue garnet bearing quartzite, poorly bedded quartzite.	Klein Pofadder Sequence	
IKM	Thick to thin sequence of biotite-sillimanite, nodular rhythmic gneiss, garnet bearing meta-quartzite, poorly bedded blue/white quartzite	Inner Koppies Member	Koppies Sequence; Poort se Berg Sequence; T-Goob Succession
OKM	Thick to thin sequence of biotite-sillimanite, nodular rhythmic gneiss, garnet bearing meta-quartzite, poorly bedded blue/white quartzite	Outer Koppies Member	
UPM	Thick sequence of biotite sillimanite schist, garnet meta-quartzite, feldspathic quartzite, interbanded units of diopside and actinolite calc-silicate rock, amphibolite, poorly bedded quartzite and thick sequence of nodular rhythmic gneiss.	Upper Poort se Berg Member	
LPM	Thick sequence of biotite sillimanite schist, garnet metaquartzite, feldspathic quartzite, poorly bedded quartzite, nodular rhythmic gneiss.	Lower Poort se Berg Member	
GM	Nodular rhythmic gneiss, poorly bedded quartzite, thick successions of biotite sillimanite schist, biotite gneiss, banded blue white quartzite, actinolite, diopside and garnet bearing quartzite	T-Goob Sequence	
LM	Feldspathic quartzite, biotite gneiss, thick sequences of biotite sillimanite schist, garnet bearing quartzite, poorly bedded quartzite and nodular rhythmic gneiss.	Outer Lekdam Sequence	
SkM	Thick sequence of biotite sillimanite schist, garnet metaquartzite, biotite gneiss, amphibolite, poorly bedded quartzite, nodular rhythmic gneiss.	Skewe Berg Sequence	Inner Lekdam Succession
XM	Thin to thick sequence of garnet bearing meta-quartzite, feldspathic quartzite and biotite-sillimanite schist.	Xenolith Sequence	
DrM	Thin sequence of biotite-sillimanite schist, feldspathic quartzite, calc-silicate rock, poorly bedded quartzite.	Draai Berg Sequence	
PLM	Thick sequence of biotite-sillimanite schist, intercalated garnet bearing meta-quartzite and thick sequence of poorly bedded quartzite.	Platberg Sequence	
SyM	Thin sequence of biotite-sillimanite schist feldspathic quartzite, dark-blue quartzite and poorly bedded quartzite.	Sy-Berg Sequence	
WF	Thick quartz-biotite-sillimanite schist with interbanded units:Lenticular white metaquartzite, biotite gneiss, amphibolite, calc-silicate rock and magnetite metaquartzite.	Well defined Wortel Formation	Houmoed Thrust Sheet (Domain 4)
Ags	Thick succession of biotite-sillimanite schist, poorly bedded quartzite, medium-quartz-feldspar gneiss, amphibolite and calc-silicate rock.	Achab Sequence	
DR	Thick succession of biotite-sillimanite schist, nodular rhythmic gneiss, amphibolite, calc-silicate rock and poorly bedded quartzite.	De Rust Sequence	Dwarsberg Sequence
IDM	Thick to thin succession of biotite-sillimanite schist, rhythmic gneiss, amphibolite, calc-silicate rock and poorly bedded quartzite.	Inner Dwarsberg Member	
ODM	Thick to thin succession of biotite-sillimanite schist, rhythmic gneiss, and poorly bedded quartzite.	Outer Dwarsberg Member	
HM	Felsic gneiss with thin layered mafic zones and interbanded cordierite-antophyllite rock, biotite-saphirine rock, calc-silicate rock, schist and metaquartzite.	Hom Formation	Pofadder Terrane
Vtf	Thick succession of biotite gneiss, thick sequence of poorly bedded quartzite, amphibolite and calc-silicate rock.	Van-tittensville Formation	Bladgrond Terrane

Plutonic Rocks

VS	Quartz-feldspar-plagioclase augen gneiss ± biotite.	Vaalpits Suite	Witkoppies Thrust Sheet (Structural Domain1)
SG	Well foliated medium quartz-feldspar gneisss biotite.	Samoep Gneiss	Samoep Thrust Sheet (Structural Domain 2)
LG	Coarse quartz-feldspar gneiss ± biotite, muscovite and garnet.	Lekdam Gneiss	Lekdam Thrust Sheet (Structural Domain 3)
NG	Well foliated medium quartz-feldspar gneiss ± biotite.	Medium quartz-feldspar Namies Gneiss	Houmoed Thrust Sheet (Structural Domain 4)
AS	Domainal medium to coarse quartz-feldspar-gneisss Biotite.	Achab Suite	
SW	Well foliated medium to coarse grained quartz-feldspar-biotite-hornblende augen gneiss.	Swartmodder Gneiss	
Vtg	Leucocratic quartz-feldspar augen gneisss. biotite and amphibole.	Van-Tittensville Gneiss	

Structural Symbols

- 00-30°
- 30-60°
- 60-90°
- 90°

Strike & Dip of Foliation

20 Mineral stretching lineation

Strike line of layering/foliation

Geological contact: definite, approximate

Kimberlite Pipe

Thrust Fault

SamT: Samoep Thrust
LekT: Lekdam Thrust
WitT: Witkoppies Thrust
GrT: Groothoek Thrust
GvT: Geelvloer Thrust

Shearzone

Geographic Symbols

Farm Boundary

Road

Farm house/ Town

Appendix 3.1: Structural formline map

Aggeneys Terrane

1 Structural Domain 1 (Witkoppies Thrust Sheet)

- 1A Swartkop Sheath Fold
- 1B Vaalputs Sheath Fold
- 1C Nouzees Sheath Fold
- 1D Houmoed Sheath Fold
- 1E Witkoppies Sheath Fold

Structural Domain 2 (Samoep Thrust Sheet)

- 2 Samoep Sheet

3 Structural Domain 3 (Lekdam Thrust Sheet)

- 3A Gannapoort Berg Sheath Fold
- 3B Samoep se Berg Sheath Fold
- 3C Middle Samoep Sheath Fold
- 3D S-Berg Sheath Fold
- 3E Koppies Sheath Fold
- 3F Klein Pofadder Sheath Fold
- 3G Upper Poort se Berg Sheath Fold
- 3H Lower Poort se Berg Sheath Fold
- 3I T-Goob Sheath Fold
- 3J Outer Lekdam Sheath Fold
- 3K Xenolith Structure
- 3L Skewe Berg Sheath Fold
- 3M Draai Berg Sheath Fold
- 3N Platberg Sheath Fold
- 3O Sy-Berg Sheath Fold

4 Structural Domain 4 (Houmoed Thrust Sheet)

- 4A Achab Sheath Fold
- 4B De Rust Sheath Fold
- 4C Dwarsberg Sheath Fold

Pofadder Terrane

- 5 Groothoek Thrust Zone

Bladgrond Terrane

- 6 Geelvloer Thrust Zone

Domain Sub-divisions

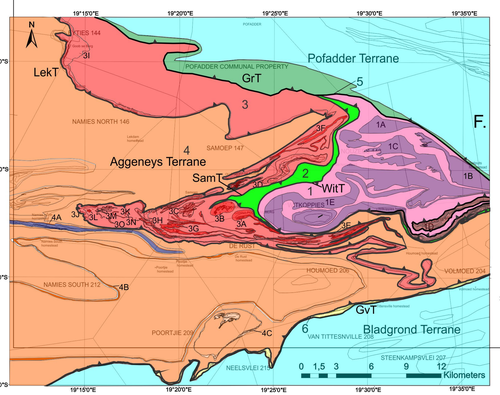

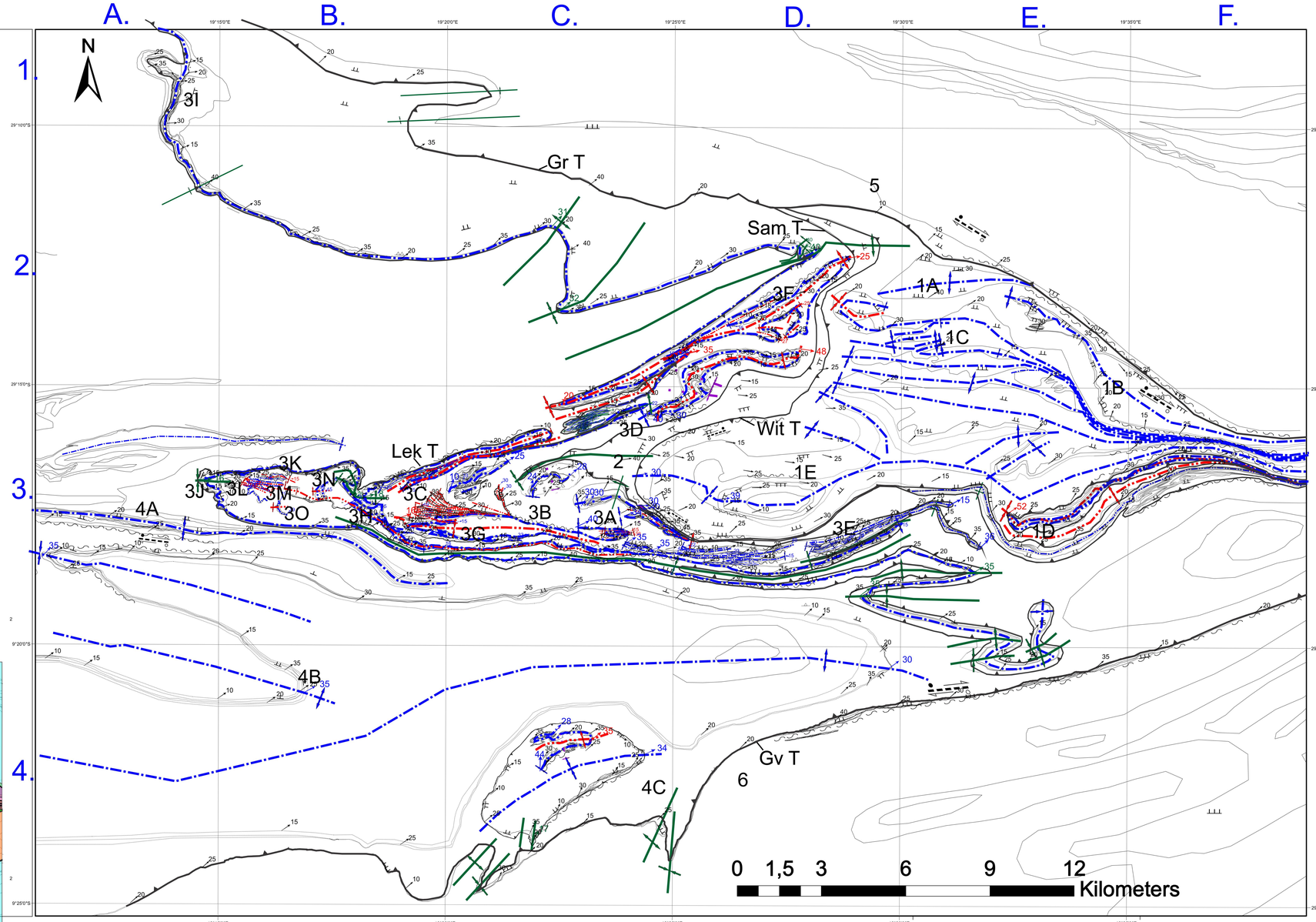

Legend

- Formline (S0-1)
- Inferred Contact
- F2 fold trace
- F3 fold trace
- F4 fold trace
- F5 fold trace
- Thrust
- GrT: Groothoek thrust
- GvT: Geelvloer thrust
- WitT: Witkoppies thrust
- SamT: Samoep thrust
- LekT: Lekdam thrust
- A-F : Designated zone
- 30 Stretching lineations
- 30 F2 Fold Axes
- 30 F3 Fold Axes
- 30 F4 Fold Axes
- Shear zones
- Shear Movements (Down / Up)
- Synform
- Antiform
- 00-30°
- 30-60°
- 60-90°

Appendix 3.1: Detailed structural formline map across the study area. The location map of the different domains can be viewed to the left of the diagram.

Appendix 3.1 A: Lineation map

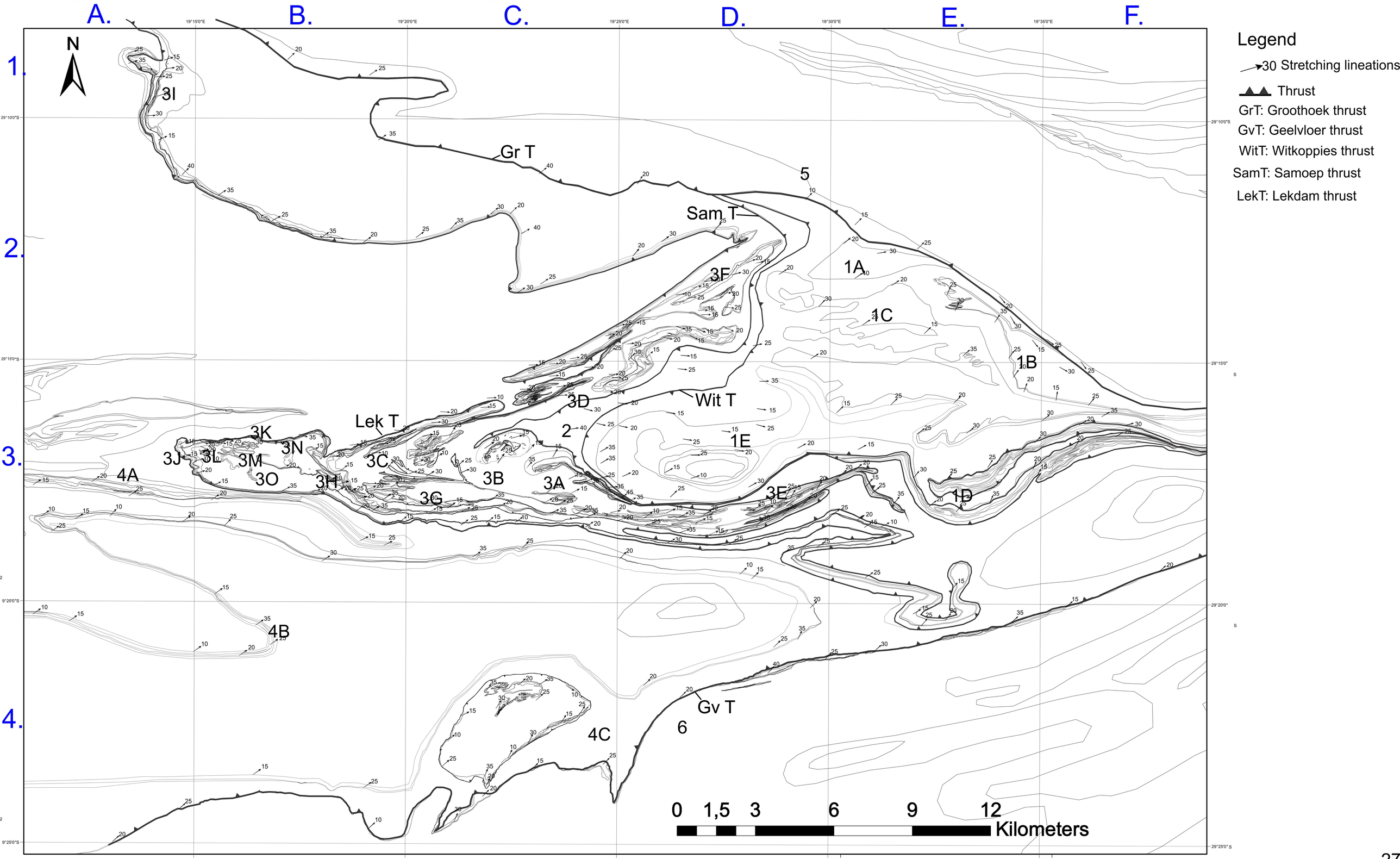

Appendix 3. 1 A: Lineation pattern across all domains.

Appendix 3.1 B: Detailed Map of The Far Western Fold Hinge of the D4 Macroscopic Structure

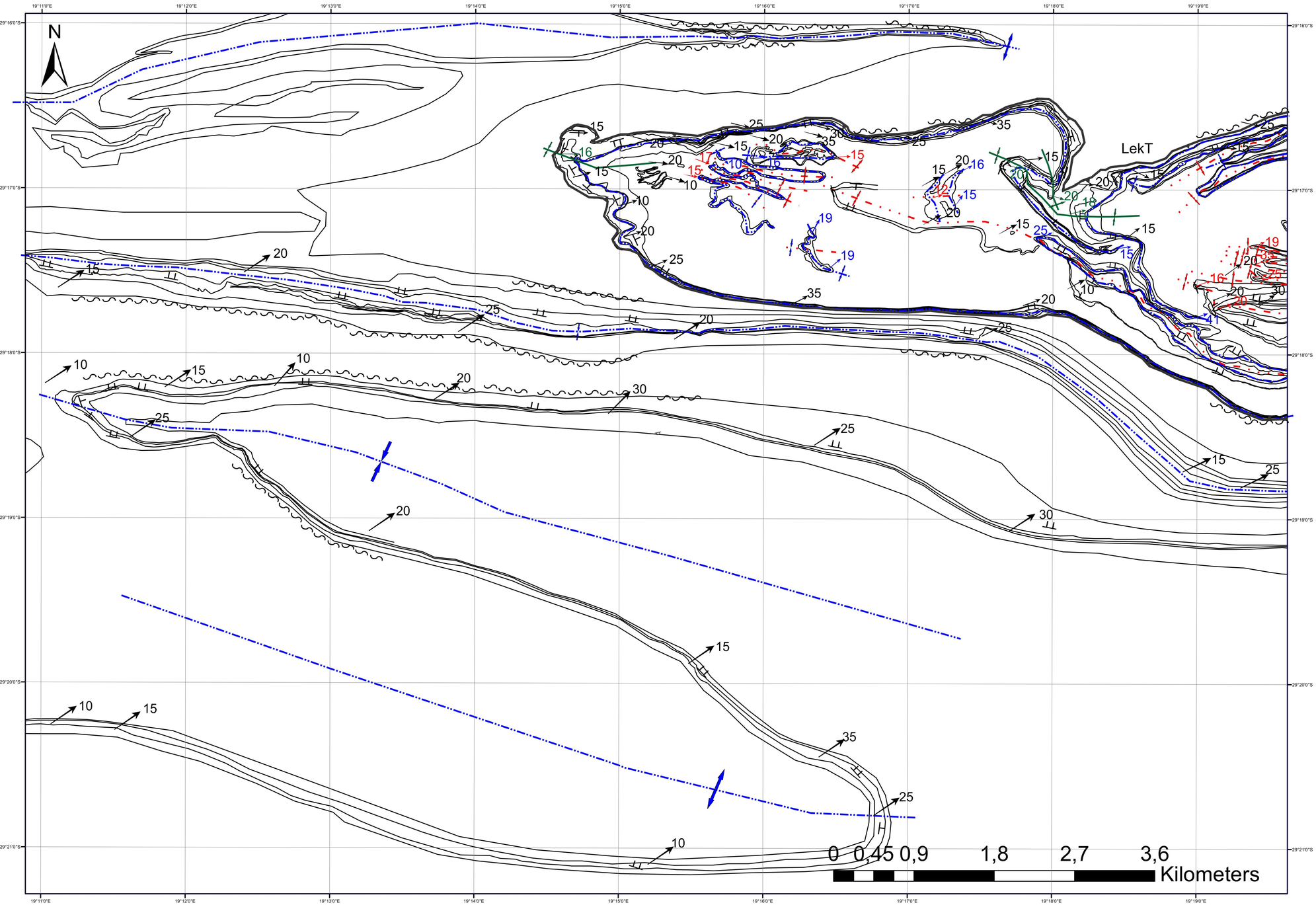

Legend

- Formline (S0//S1)
- F2 fold trace
- F3 fold trace
- F4 fold trace
- F5 fold trace
- Thrust Fault
- GrT: Groothoek thrust
- GvT: Geelvloer thrust
- WitT: Witkoppies thrust
- SamT: Samoep thrust
- LekT: Lekdam thrust
- A-F : Designated zone
- 30 Stretching lineations
- 30 F2 Fold Axes
- 30 F3 Fold Axes
- 30 F4 Fold Axes
- Shear zones
- Shear Movements (Down / Up)
- Synform
- Antiform
- 00-30°
- 30-60°
- 60-90°

A: Location Map

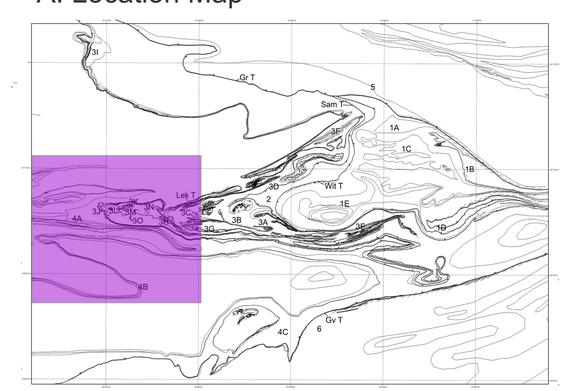

Appendix 3.1 B: Detailed structural formline map of the far western fold closure of the major D4 synformal structure. A: Location of the detailed map within the study area (in purple).

Appendix 3.1 C: Detailed Map of the Central Section of the Macroscopic D4 Structure

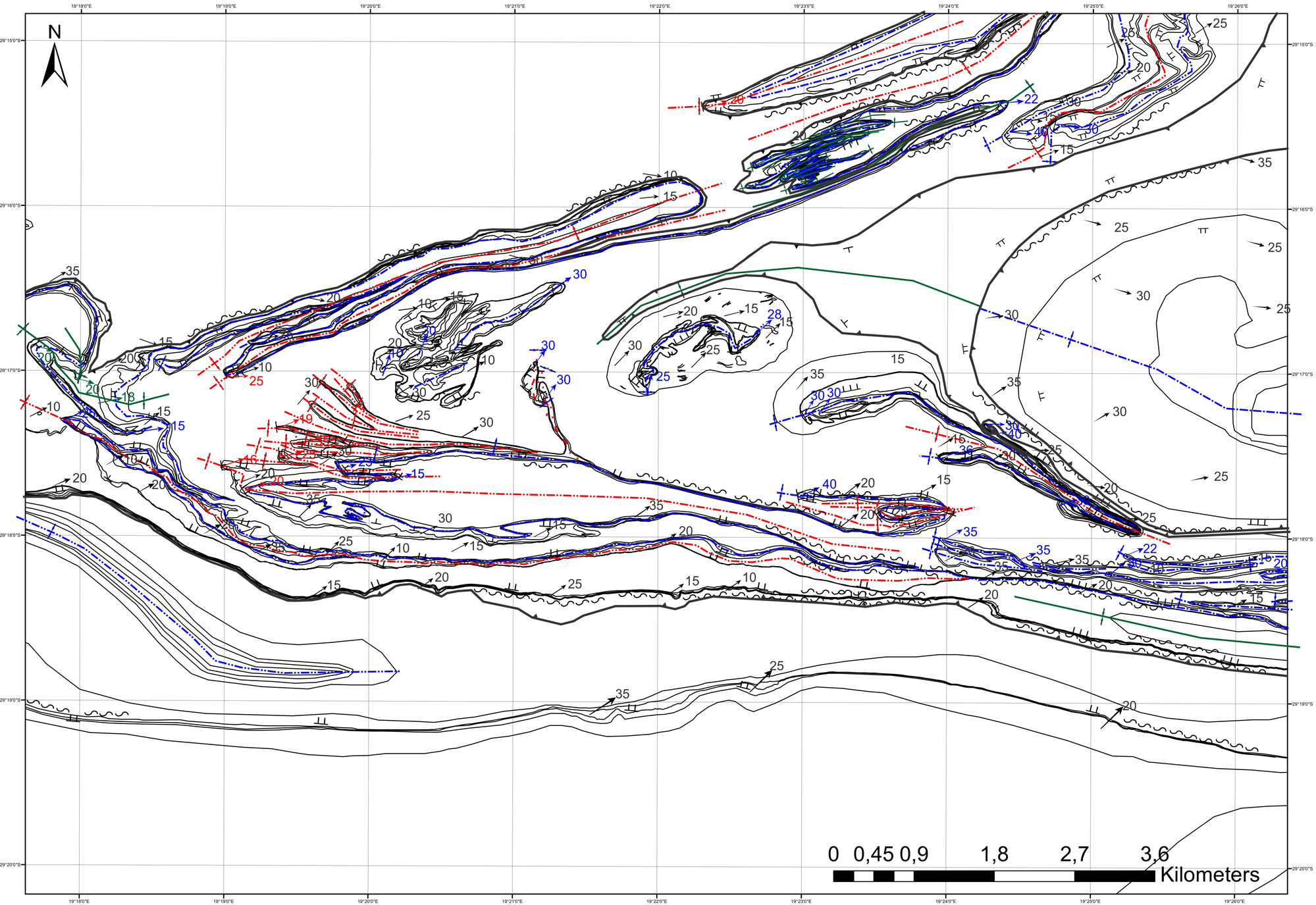

Legend

- Formline (S0//S1)
- F2 fold trace
- F3 fold trace
- F4 fold trace
- F5 fold trace
- Thrust Fault
- GrT: Groothoek thrust
- GvT: Geelvloer thrust
- WitT: Witkoppies thrust
- SamT: Samoep thrust
- LekT: Lekdam thrust
- A-F : Designated zone
- 30 Stretching lineations
- 30 F2 Fold Axes
- 30 F3 Fold Axes
- 30 F4 Fold Axes
- Shear zones
- Shear Movements (Down / Up)
- Synform
- Antiform
- 00-30°
- 30-60°
- 60-90°

A: Location Map

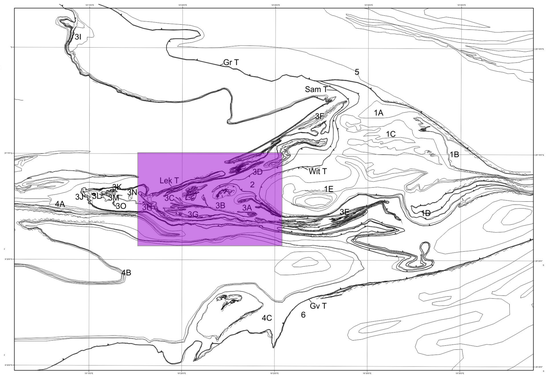

Appendix 3.1 C: Detailed structural formline map of the central section of the major D4 synformal structure. A: Location of the detailed map within the study area (in purple).

Appendix 3.1 D: Detailed Map of the Northern Limb of the Macroscopic D4 Structure

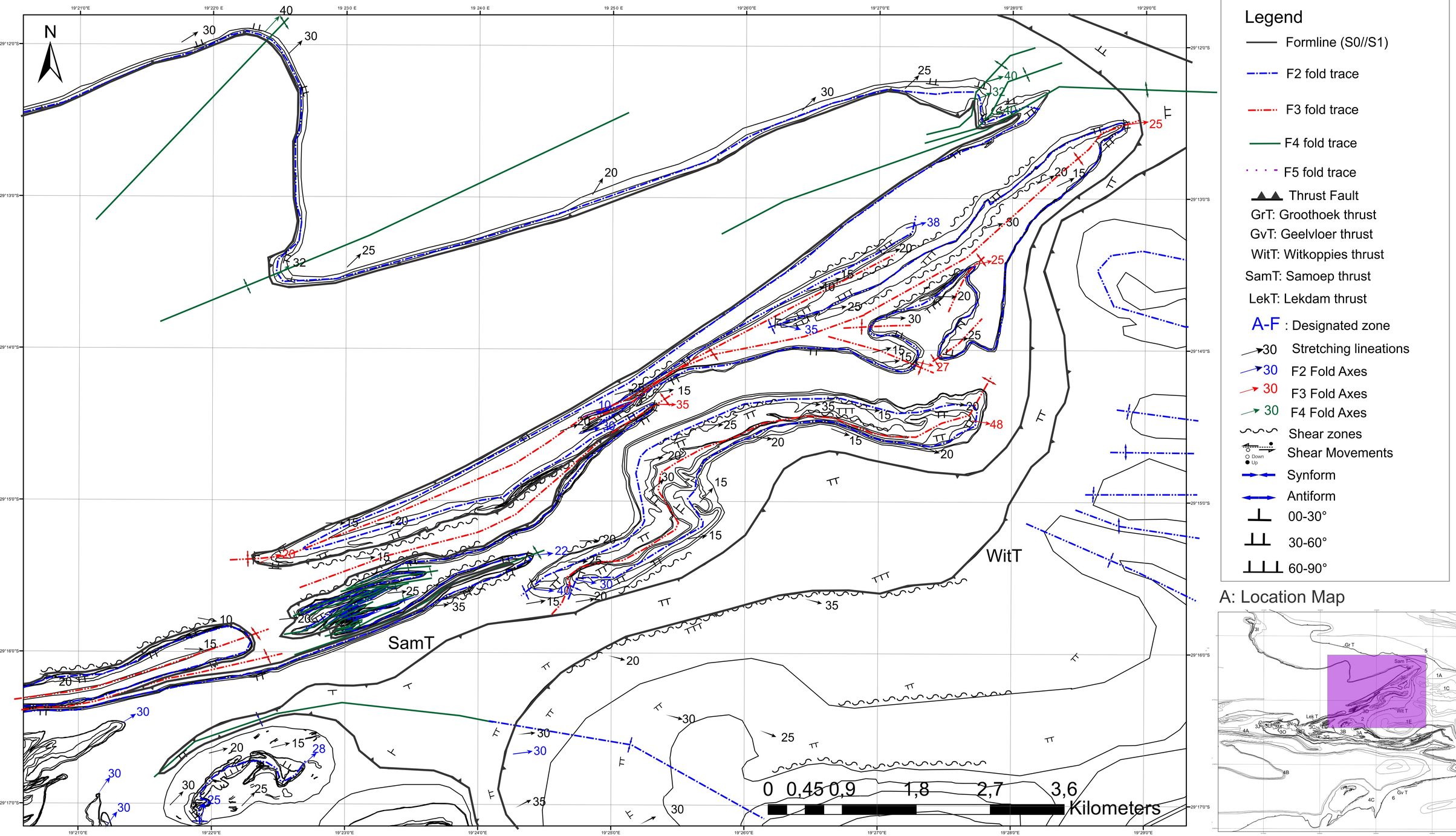

Appendix 3.1 D: Detailed structural formline map of the northeastern limb of the major D4 synformal structure. A: Location of the detailed map within the study area (in purple).

Appendix 3.1 E: Detailed map of the Southern Limb of the Macroscopic D4 Structure

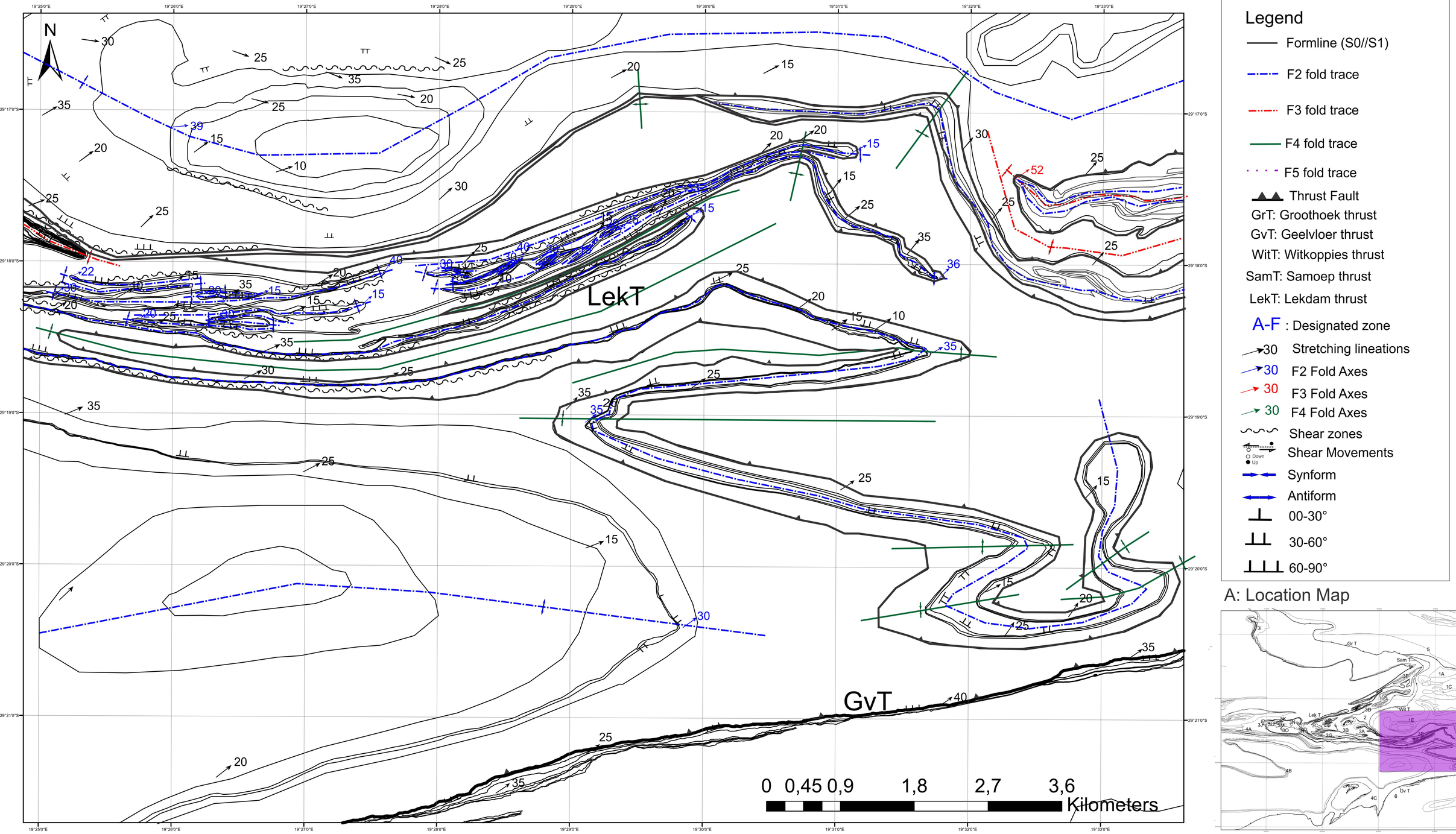

Appendix 3.1 E: Detailed structural formline map of the southeastern limb of the major D4 synformal structure. A: Location of the detailed map within the study area (in purple).

Appendix 3.2: Geometric properties of eight structures across the study area.

Domain	Regional Foliation	Regional Lineation	Regional Foliation Intrusives	Regional Lineation Intrusives	Fold Geometry: F2 folds	Fold Geometry: F3 folds	F4 open folds	Mesoscopic Structures	Type of Structure	Fold Facing and Defined Polarity
Witkoppies 'Eye' Structure Domain 1E	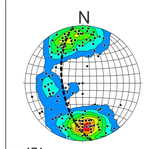 n=171	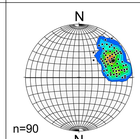 n=90 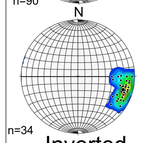 n=34 Inverted	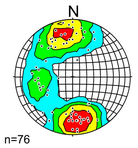 n=76	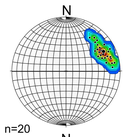 n=20 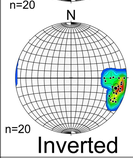 n=20 Inverted	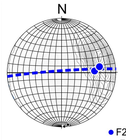 F2 fold axis; F2 axial plane; poles to the axial planes; FA n=2; Lin n= 191	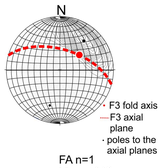 F3 fold axis; F3 axial plane; poles to the axial planes; FA n=1; Lin n= 140		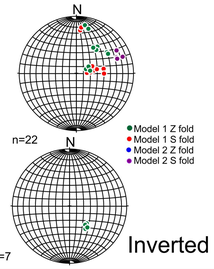 n=22 n=7 Inverted; Model 1 Z fold; Model 1 S fold; Model 2 Z fold; Model 2 S fold	Structure defined by a elliptical ring structure or 'Eye' in the center of the structurewith double vergence geometries.	Northern Limb: overturned Southern Limb: upright Younging not confirmed defined polarity shows 'younging' toward the inside of the structure.
Gannapoort Berg 'Eye' Structure Domain 3A	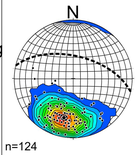 n=124	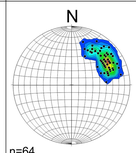 n=64	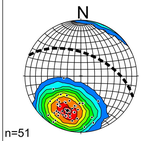 n=51	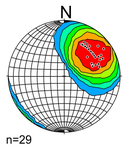 n=29	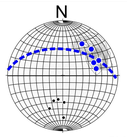 FA n=4; Lin n= 64; F2 fold axis; F2 axial plane; poles to the axial planes	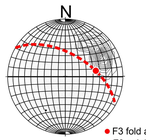 FA n=1; Lin n= 64; F3 fold axis; F3 axial plane; poles to the axial planes		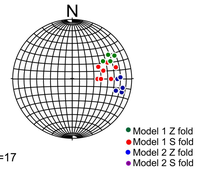 n=17; Model 1 Z fold; Model 1 S fold; Model 2 Z fold; Model 2 S fold	Refolded elliptical isoclinal fold structure.D2 isoclinal fold is refolded by D3 phase of folding.	Northern Limb: Overturned Southern Limb: upright Younging not confirmed defined polarity shows 'younging' toward the inside of the structure.
Samoep se Berg Structure Domain 3B	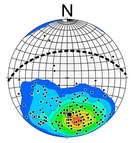 n=169	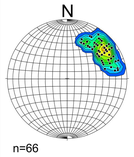 n=66	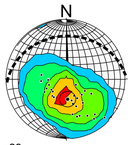 n=29	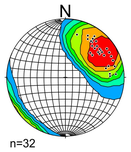 n=32	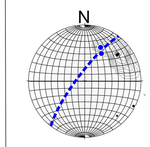 FA n=2; Lin n= 66; F2 fold axis; F2 axial plane; poles to the axial planes			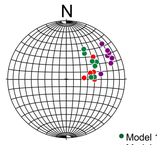 n=22; Model 1 Z fold; Model 1 S fold; Model 2 Z fold; Model 2 S fold	Flattened D2 synclinal fold structure with double vergence geometries.	Overturned Limb: Northern limb Upright Limb: Southern Limb Younging direction: confirmed Western F2 closure: Fold facing toward NE Eastern F2 closure: Fold facing toward SW
S-Berg Structure Domain 3D	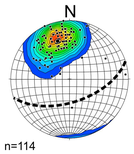 n=114 Inverted	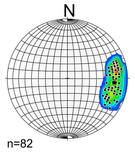 n=82 Inverted	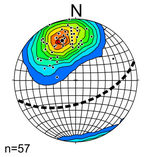 n=57 Inverted	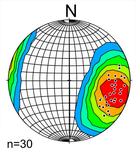 n=30 Inverted	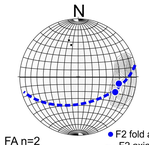 FA n=2; Lin n= 88; F2 fold axis; F2 axial plane; poles to the axial planes Inverted	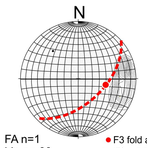 FA n=1; Lin n= 88; F3 fold axis; F3 axial plane; poles to the axial planes Inverted		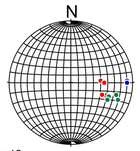 n=12 Inverted; Model 1 Z fold; Model 1 S fold; Model 2 Z fold; Model 2 S fold	Refolded flattened synclinal fold structure with double vergence geometries. D2 fold, refolded by the D3 phase of folding	Northern Limb: Overturned Southern Limb: upright Younging not confirmed defined polarity shows 'younging' toward the inside of the structure.
T-Goob se Berg Structure Domain 3I	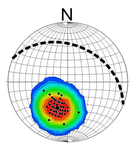 n=77 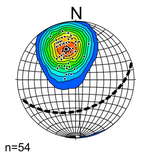 n=54 Inverted	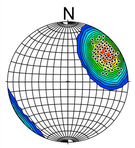 n=66 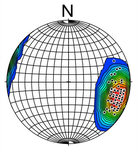 n=98 Inverted	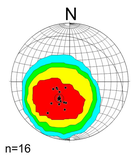 n=16 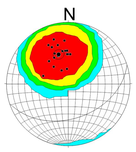 n=22 Inverted	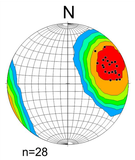 n=28 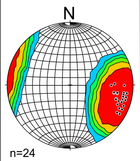 n=24 Inverted	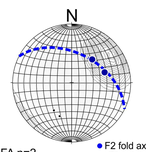 FA n=2; Lin n=93; F2 fold axis; F2 axial plane; poles to the axial planes	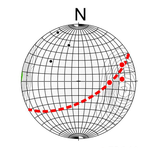 FA n=3; Lin n=66; F3 fold axis; F3 axial plane; poles to the axial planes	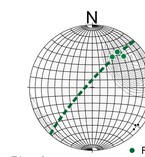 FA n=3; Lin n=93; F4 fold axis; F4 axial plane; poles to the axial planes 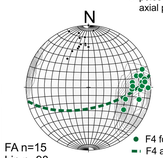 FA n=15; Lin n=98; F4 fold axis; F4 axial plane; poles to the axial planes Inverted	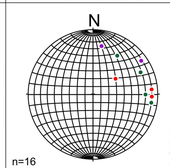 n=16 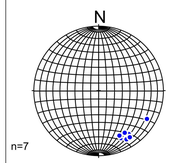 n=7 Inverted; Model 1 Z fold; Model 1 S fold; Model 2 Z fold; Model 2 S fold	Refolded isoclinal fold structure with double vergence geometries. D2 fold structure refolded by the D3 and D4 phase of folding.	Overturned Limb: Northern limb Upright Limb: Southern Limb. Younging direction: confirmed Northern F2 closure: Fold facing toward SE Southern F2 closure: Fold facing toward NW
Outer Lekdam Structure Domain 3J	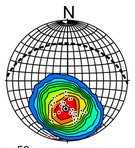 n=50 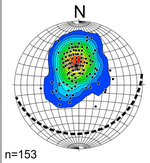 n=153 Inverted	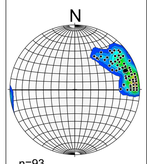 n=93 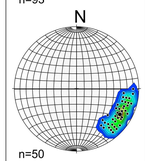 n=50 Inverted	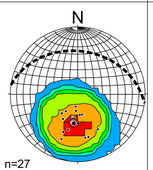 n=27 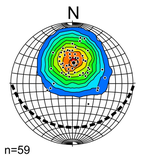 n=59 Inverted	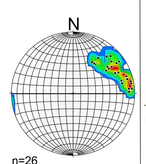 n=26 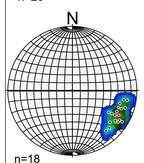 n=18 Inverted	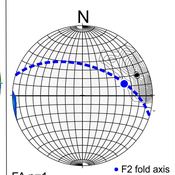 FA n=1; Lin n=93; F2 fold axis; F2 axial plane; poles to the axial planes		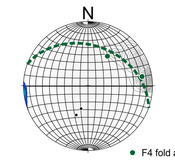 FA n=2; Lin n=93; F4 fold axis; F4 axial plane; poles to the axial planes 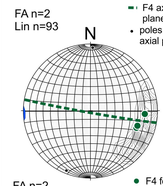 FA n=2; Lin n=67; F4 fold axis; F4 axial plane; poles to the axial planes Inverted	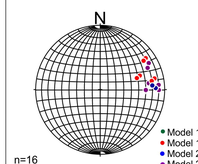 n=16 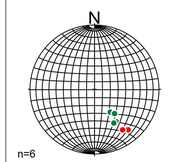 n=6 Inverted; Model 1 Z fold; Model 1 S fold; Model 2 Z fold; Model 2 S fold	Refolded D2 isoclinal fold structure, folded by the D4 phase of folding.	Northern Limb: Overturned Southern Limb: upright Younging not confirmed defined polarity shows 'younging' toward the inside of the structure.
Dwarsberg Structure Domain 4C	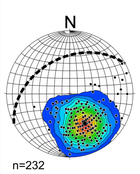 n=232	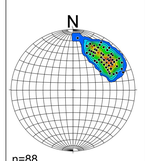 n=88	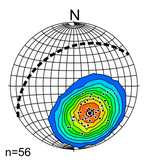 n=56	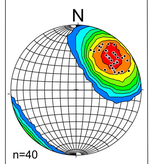 n=40	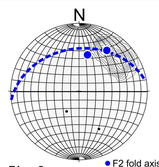 FA n=2; Lin n=85; F2 fold axis; F2 axial plane; poles to the axial planes		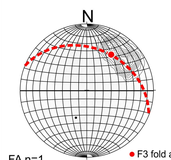 FA n=1; Lin n=85; F3 fold axis; F3 axial plane; poles to the axial planes	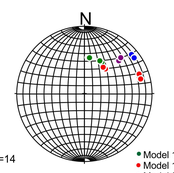 n=14; Model 1 Z fold; Model 1 S fold; Model 2 Z fold; Model 2 S fold	Refolded D2 fold structure with double vergence geometries. D2 fold structure is refolded by the D3 phase of folding.	Northern Limb: Overturned Southern Limb: upright Younging not confirmed defined polarity shows 'younging' toward the inside of the structure.

A.

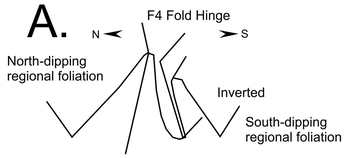

Aggeneys Terrane

1 Structural Domain 1 (Witkoppies Thrust Sheet)

1A Swartkop Sheath Fold
1B Vaalputs Sheath Fold
1C Nouzees Sheath Fold
1D Houmoed Sheath Fold
1E Witkoppies Sheath Fold

Structural Domain 2 (Samoep Thrust Sheet)

2 Samoep Sheet

3 Structural Domain 3 (Lekdam Thrust Sheet)

3A Gannapoort Berg Sheath Fold
3B Samoep se Berg Sheath Fold
3C Middle Samoep Sheath Fold
3D S-Berg Sheath Fold
3E Koppies Sheath Fold
3F Klein Pofadder Sheath Fold
3G Upper Poort se Berg Sheath Fold
3H Lower Poort se Berg Sheath Fold
3I T-Goob Sheath Fold
3J Outer Lekdam Sheath Fold
3K Xenolith Structure
3L Skewe Berg Sheath Fold
3M Draai Berg Sheath Fold
3N Platberg Sheath Fold
3O Sy-Berg Sheath Fold

4 Structural Domain 4 (Houmoed Thrust Sheet)

4A Achab Sheath Fold
4B De-Rust Sheath Fold
4C Dwarsberg Sheath Fold

Pofadder Terrane

5 Groothoek Thrust Zone

Bladgrond Terrane

6 Geelvloer Thrust Zone

B.

Domain Sub-divisions

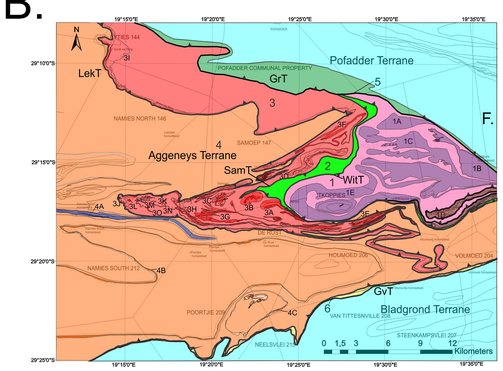

Appendix 3.2: Geometric properties associated with eight prominent structural domians, together with a description of the general characteristics associated with each structure. The geometric properties have the same general characteristics as all 22 structures encountered within the study area. A: Diagram showing a fold illustrating the rotation foliations from north to south around the D4 hinges.This rotational effect can be seen in Domains 1 E,3D, 3I and 3J; and is represented by the inverted stereonets. B: Regional location map, showing the distribution of all structures across the domains and sub-domains.

Appendix 3.3.1: Structural long section across the study area

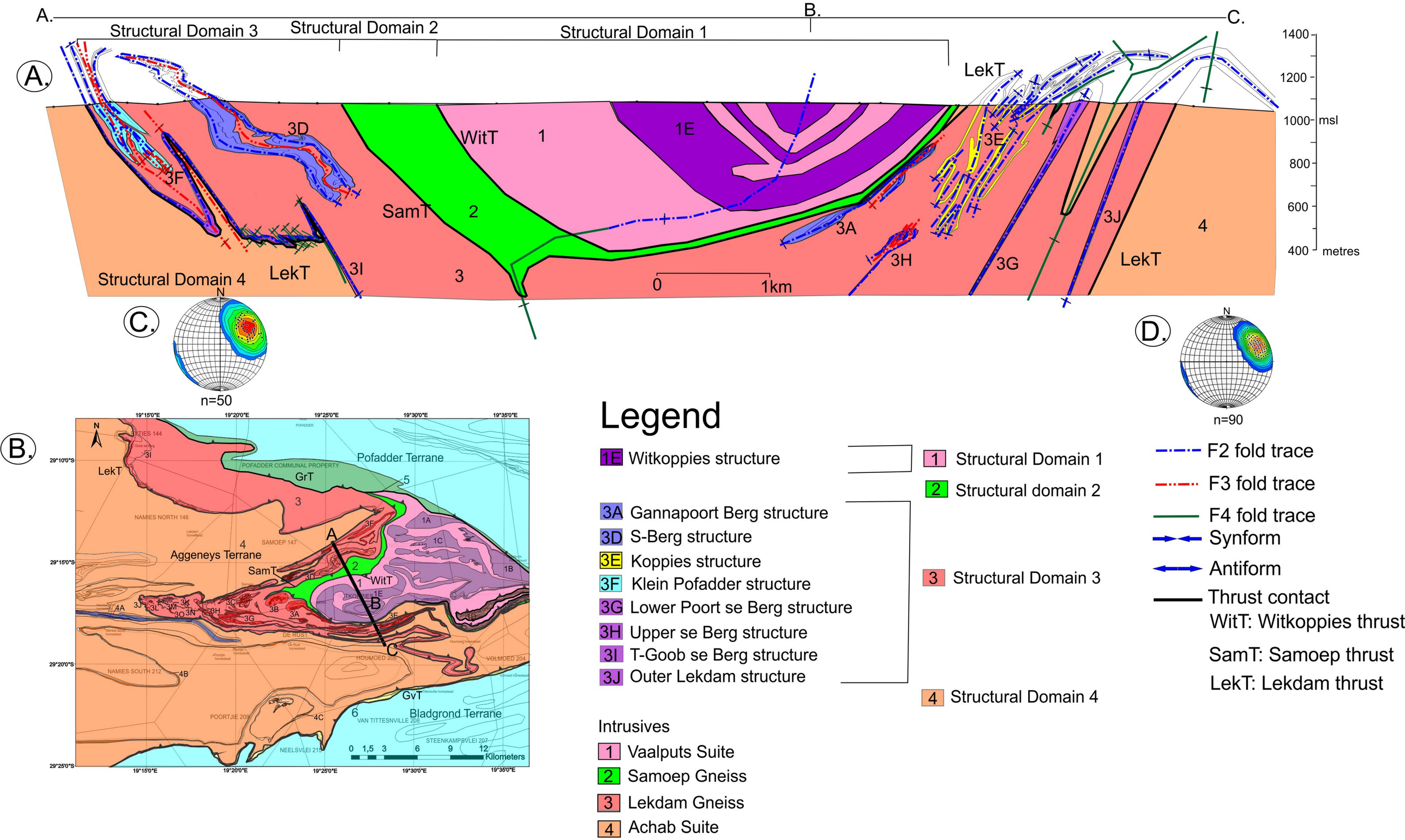

Appendix 3.3.1: Structural long section across the study area. Section was constructed using a combination of the Busk Method (Busk,1929) and the projection technique by Stockwell (1960). Figure A: Composite long section across the study area drawn perpendicular to the transport direction. D2 and D3 fold structures, are located on both the northwestern and southeastern limbs of a major synformal D4 structure. Intra-terrane thrust contacts are also seen folding around the D4 hinge in the center of the structure. Figure B: Simplified geological map, showing the positions (A-C) where the long section was constructed. Figure C and D: Stereonets showing the average trend of the regional L1 stretching lineation, with average trends toward the north-east with mean plunge of 30°.

Appendix 3.3.2: Structural cross section across the study area

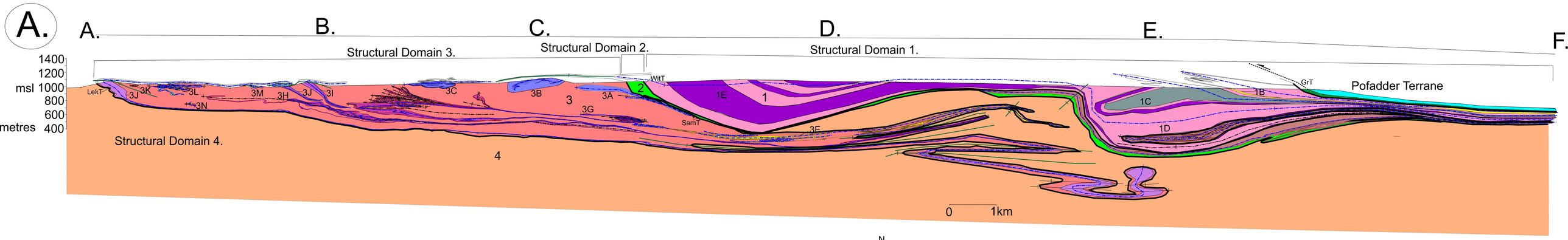

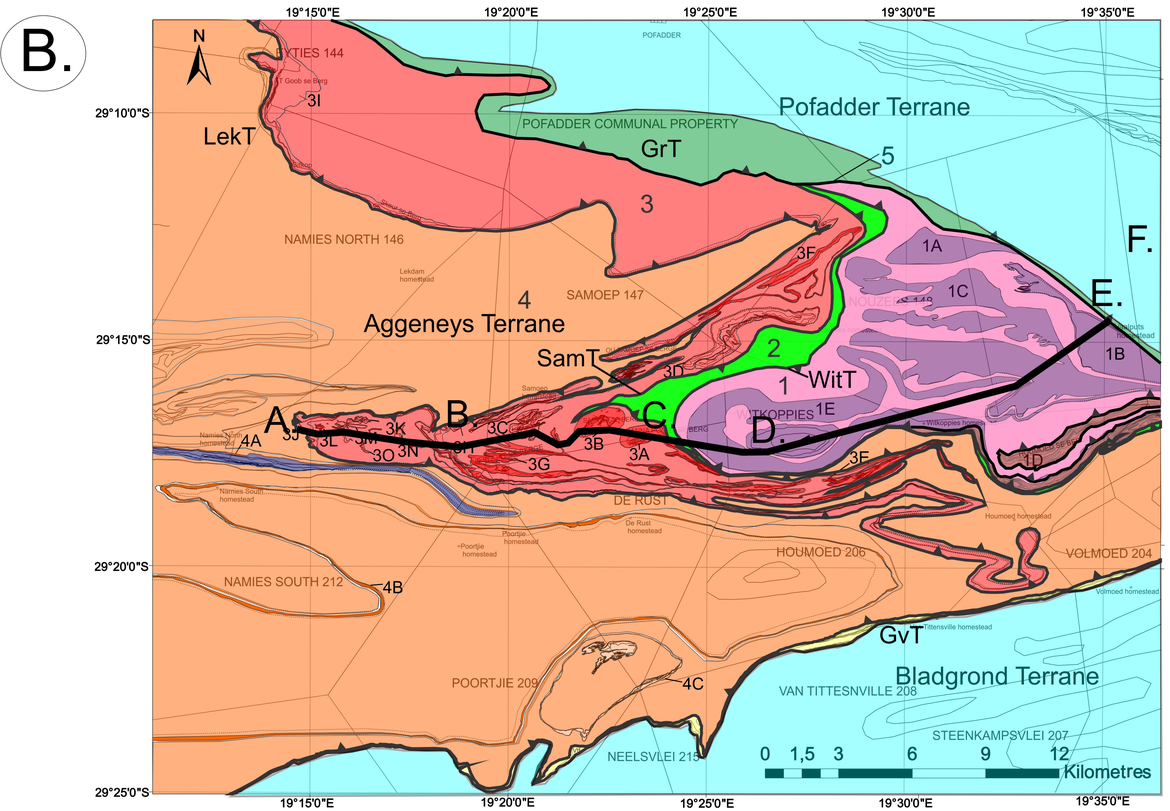

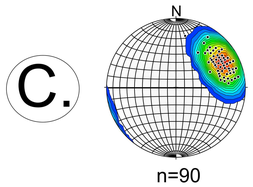

Legend

- 1B Vaalputs structure
- 1C Nouzees structure
- 1D Houmoed structure
- 1E Witkoppies structure

1 Structural Domain 1

- 3A Gannapoort Berg structure
- 3B Samoep se Berg structure
- 3C Middle Samoep structure
- 3E Koppies structure
- 3G Upper Poort se Berg structure
- 3H Lower Poort se Berg structure
- 3I T-Goob se Berg structure
- 3J Outer Lekdam structure
- 3L Xenolith structure
- 3M Draaiberg structure
- 3N Platberg structure
- 3O Sy-Berg structure

2 Structural domain 2

3 Structural Domain 3

4 Structural Domain 4

5 Hom Formation

Intrusive Rocks

- 1 Vaalputs Suite
- 2 Samoep Gneiss
- 3 Lekdam Gneiss
- 4 Achab Suite

- F2 fold trace
- F3 fold trace
- F4 fold trace
- Synform
- Antiform
- Thrust fault contact
- GrT: Groothoek thrust
- WitT: Witkoppies thrust
- SamT: Samoep thrust
- LekT: Lekdam thrust

Appendix 3.3.2 :Structural cross section across the study area. Section was constructed using a combination of the Busk Method (Busk,1929) and the projection technique of Stockwell (1960). Figure A: Composite cross section drawn oblique to the tectonic transport direction. Shows the folding of D2 structures by D4 phase of folding and the location of D3 and D2 structures on the southeastern limb of the major D4 structure. The tightening of D2, D3 and D4 hinges can be seen on the southeastern limb, caused by the D5 east-west shear effects. Towards the far east, the fold traces are drawn parallel due to the D6 phase of deformation (D2-D3). Thrust contacts can also be seen folding around the D4 hinges. Figure B: Shows a simplified geological map, which shows the positions (A-F) where the sections were constructed. Figure C: Stereonet diagram depicting the average regional stretching lineation trend (L1). The L1 lineations have an average plunge of 30° in a northeasterly direction.

Appendix 3.4.1: The D1 Phase of Deformation

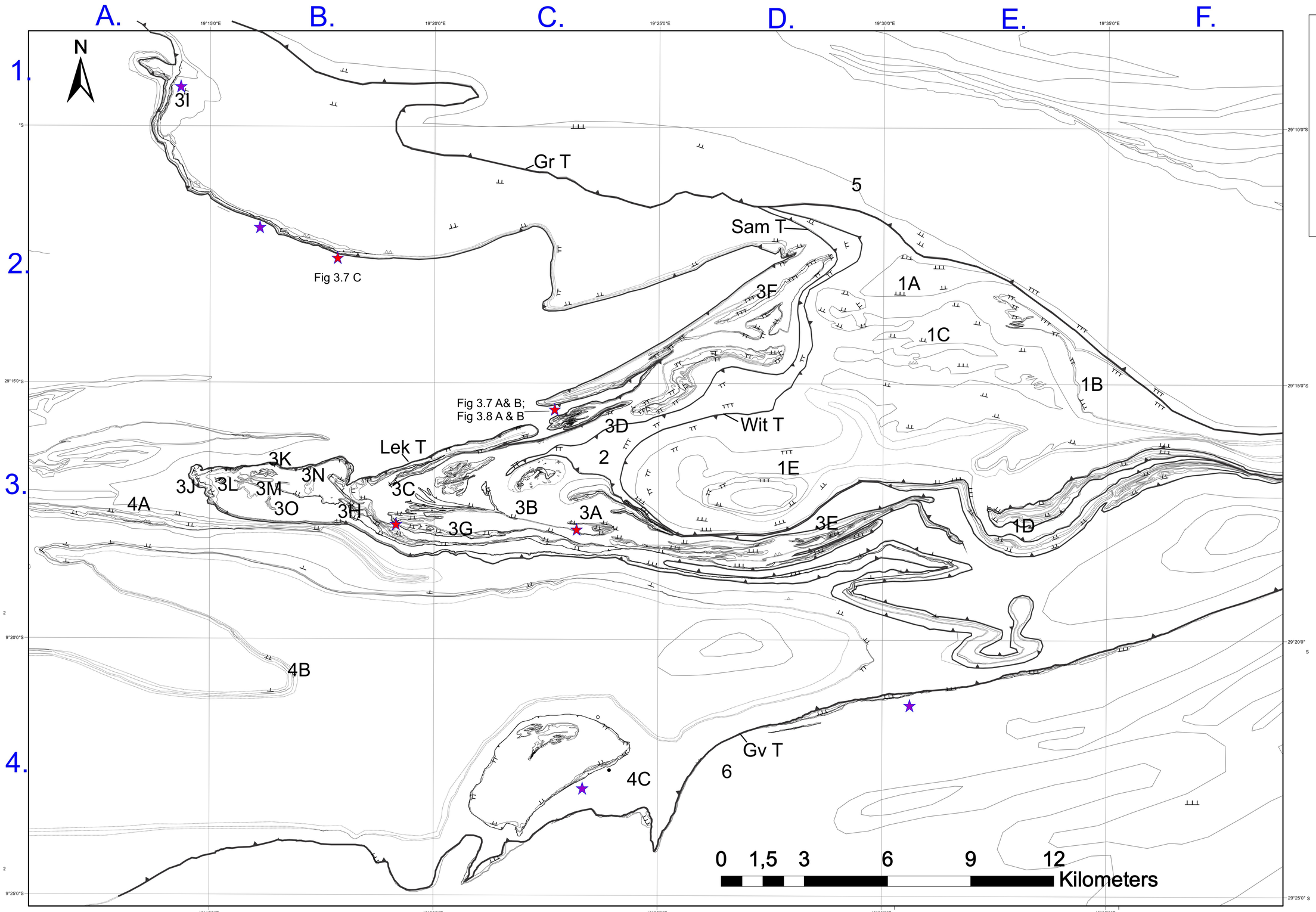

Appendix 3.4.1: Simplified structural form line map depicting the best locations associated with the D1 phase of deformation throughout the study area. The red star symbols (★) represent locations where the D1 fabric (S1) can be seen. The purple star symbol (★) shows the location where the D1 phase of intra-stratigraphic thrusting can be seen, where imbrication and cut-out structures can be seen duplicating the S1//S0 fabric.

Appendix 3.4.2: D2 Phase of Deformation

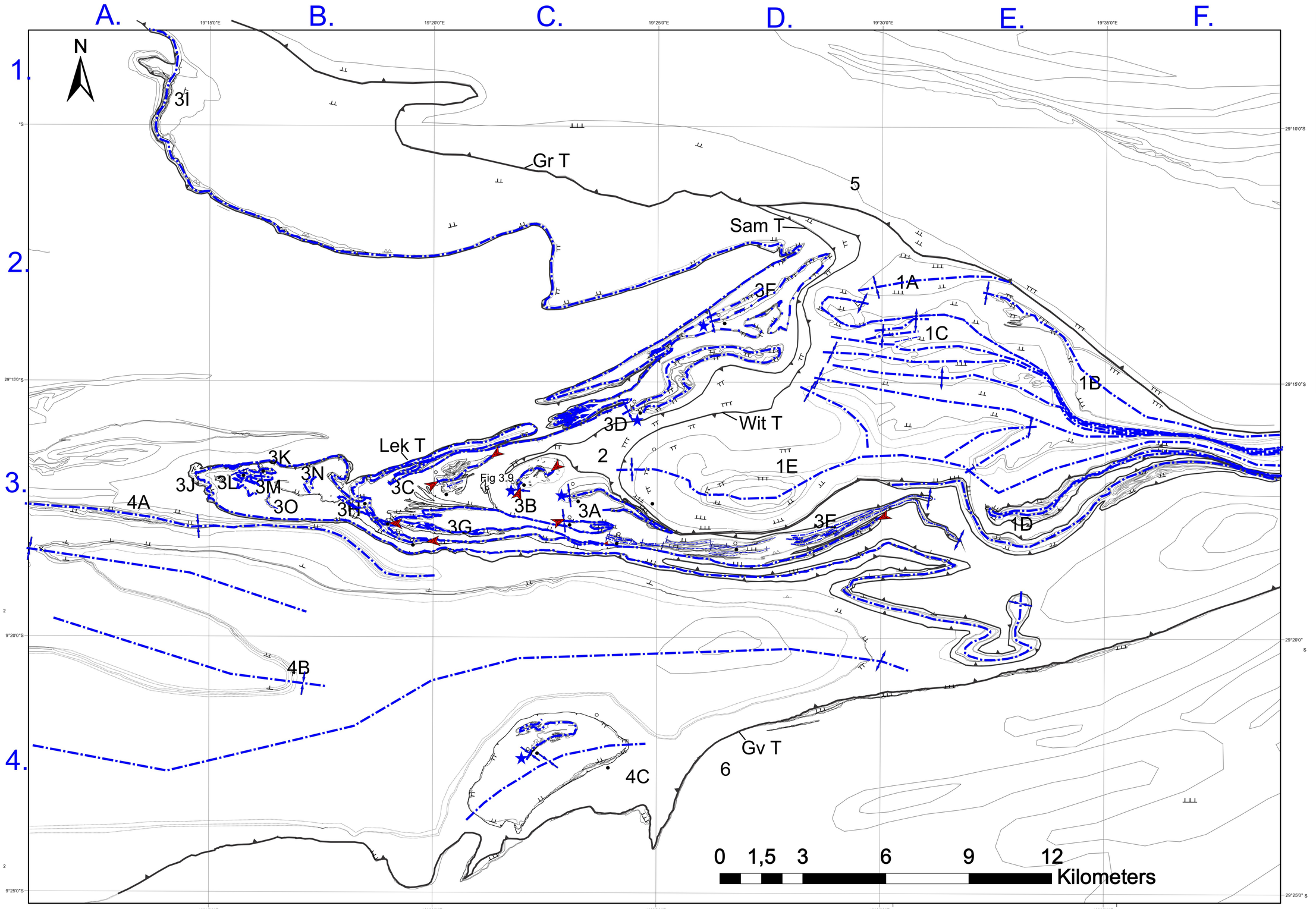

Appendix 3.4.2: Simplified structural form line map depicting the F2 fold traces throughout the study area. The star symbols (★) represent locations where the D2 phase (macroscopic F2 folds closures) is visible on macroscopic scale.

Appendix 3.4.3: The D3 Phase of Deformation

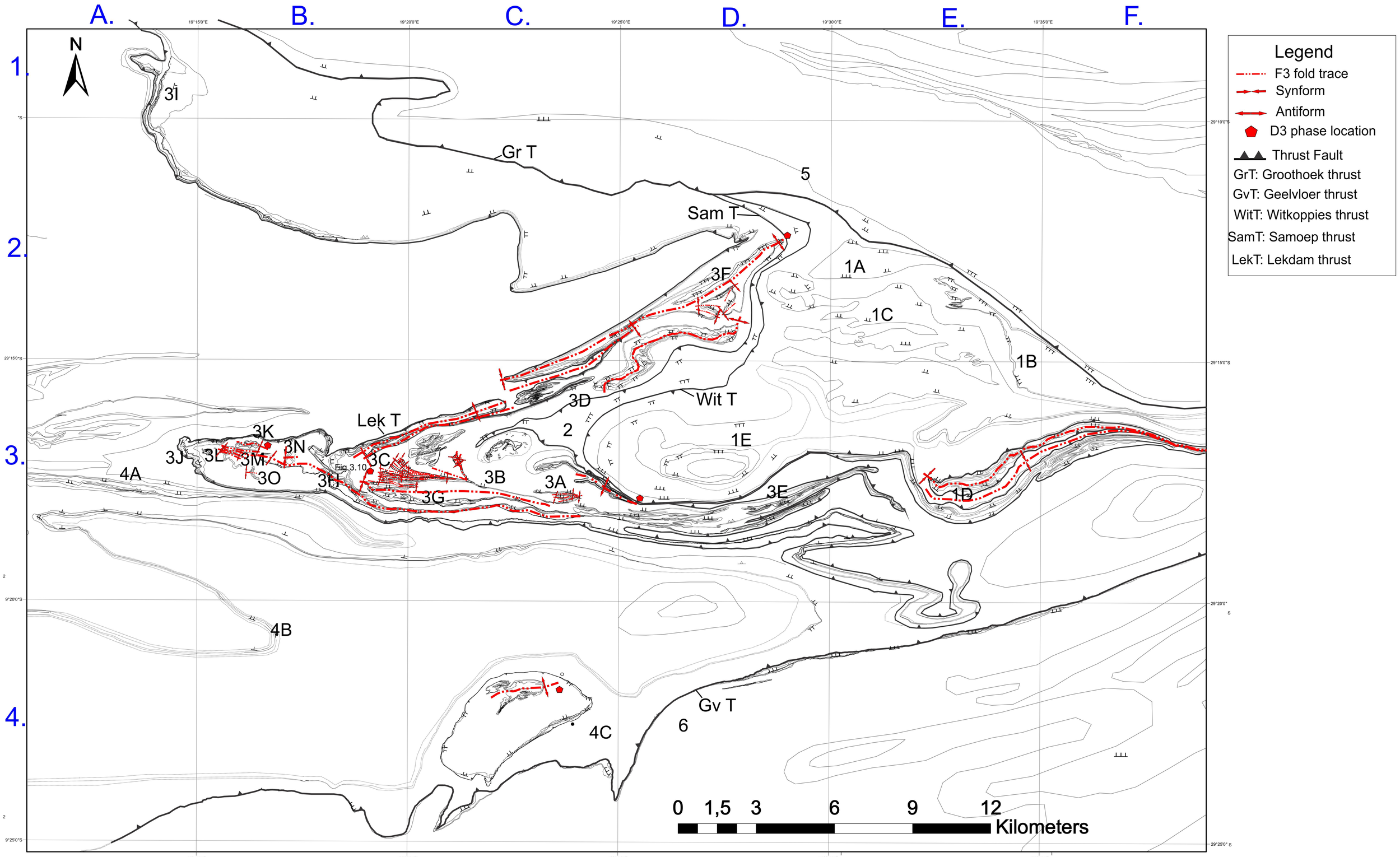

Appendix 3.4.3: Simplified structural formline map depicting the F3 fold traces throughout the study area. The pentagon symbols (⬟) represent locations where the D3 phase (F3 fold closures) is visible on macroscopic scale.

Appendix 3.4.4: The D4 phase of deformation

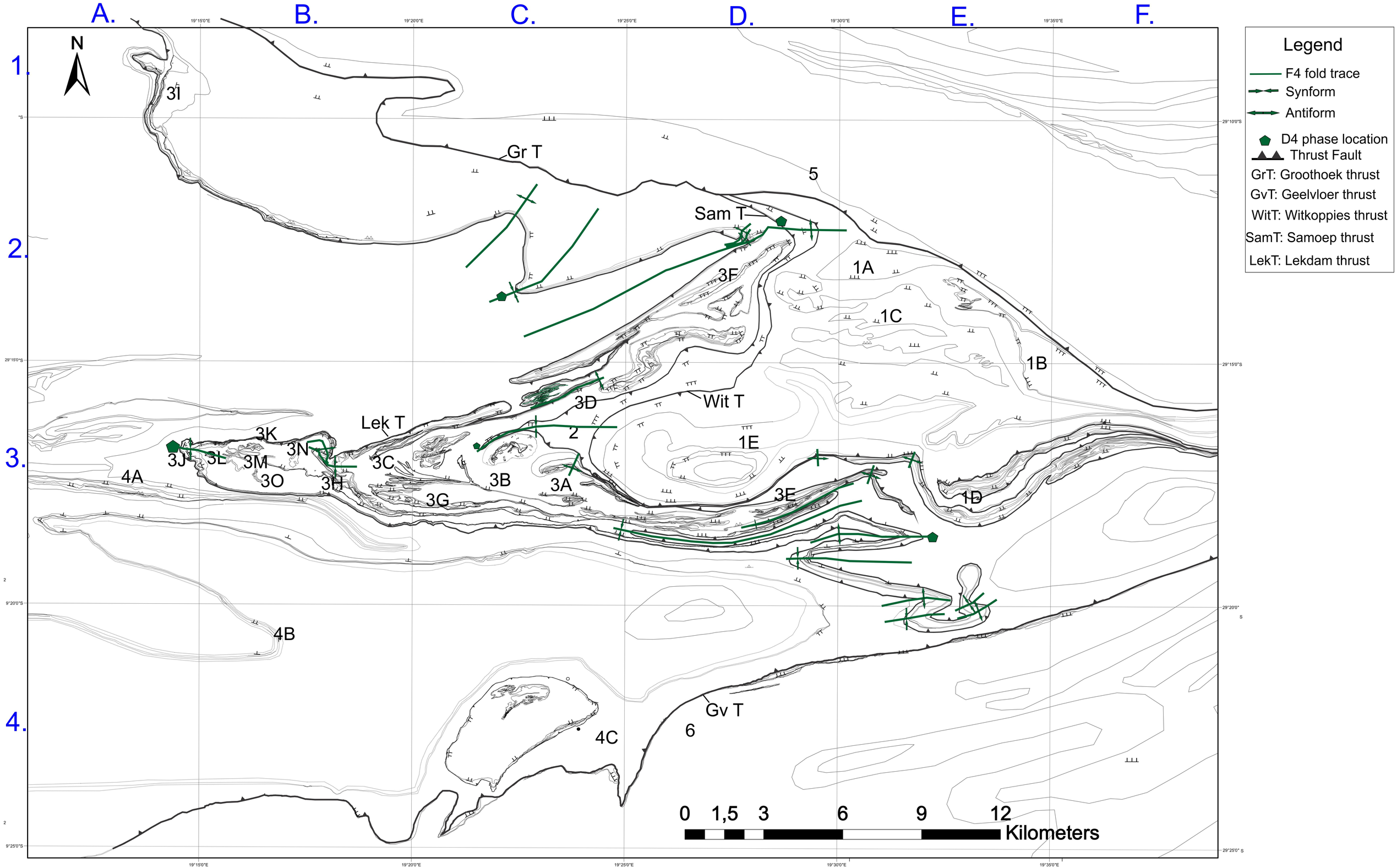

Appendix 3.4.4: Simplified structural form line map depicting the F4 fold traces throughout the study area. The pentagon symbols (⬟) represent locations where the D4 phase (F4 fold closures) are visible on macroscopic scale.

Appendix 3.4.5: D5 and D6 Phase of Deformation

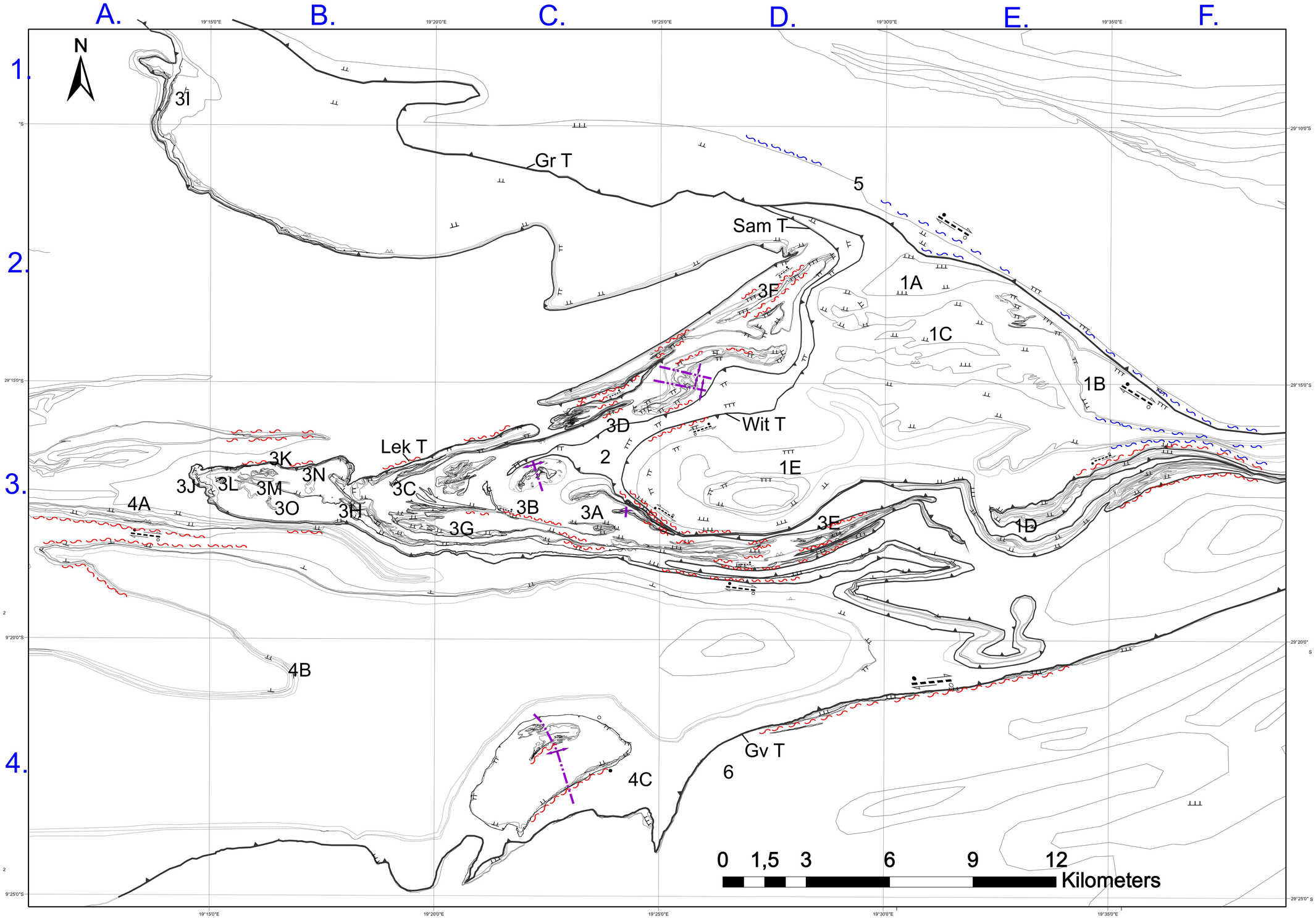

Appendix 3.4.5: Simplified structural formline map depicting the D5 and D6 phase of deformation throughout the study area. The D5 east-west shear zones are located on intra-terrane thrust contacts and on the limbs of D2, D3 and D4 structures. The D6 NW-SE shear zones are found in the far eastern sector of the study area. The F5 oblique open folds are also seen across the study area.

Appendix 3.5 Domain 1E
Witkoppies 'Eye' Structure

Appendix 3.5: Structural formline map of the Witkoppies 'Eye' Structure. Figure A: Simplified locality map of the structurewithin the study area. The map is divided into a western and eastern sector representing a lower strain zone and the latter a higher strain zone. The various fold phases with their respective fold traces, branch points, foliations and lineations are represented..

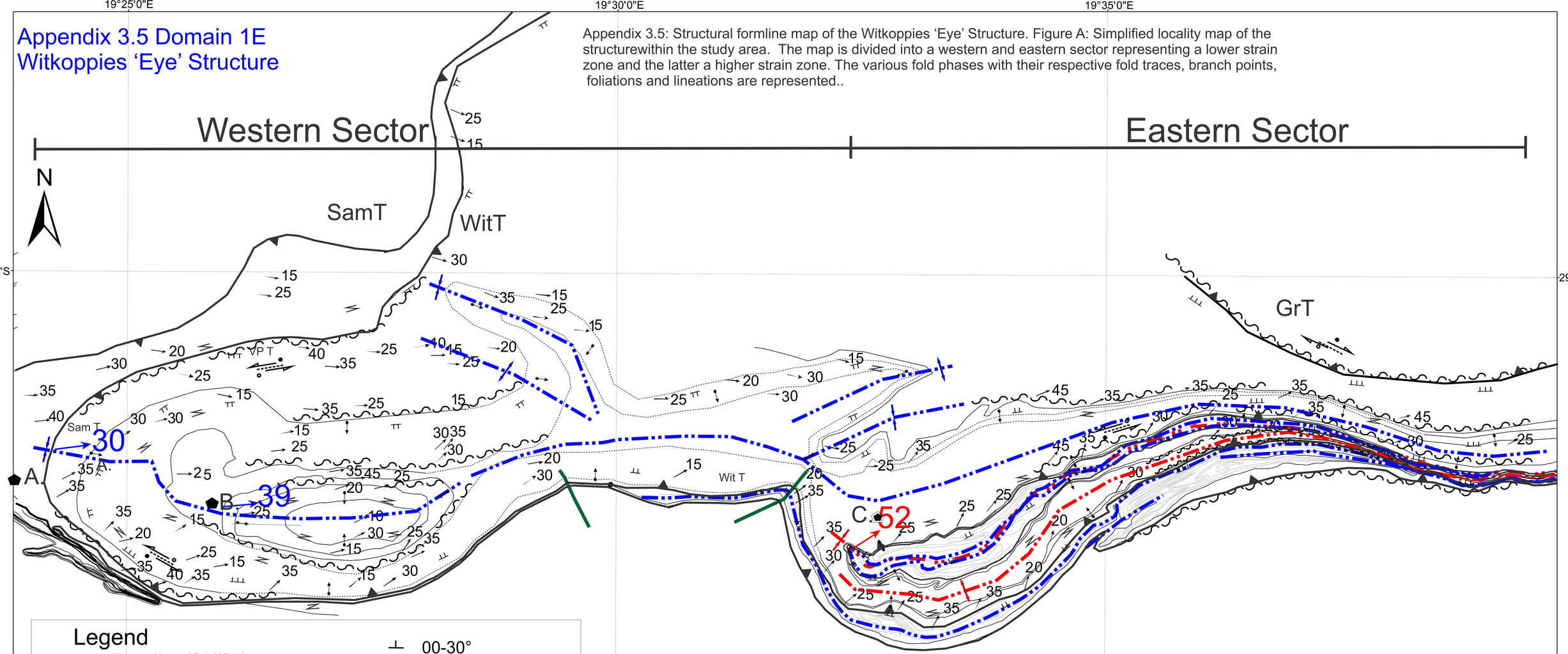

Legend

- Form line (S0//S1)
- Inferred contact
- F2 fold trace
- F3 fold trace
- F4 fold trace
- Defined Polarity
- Branch Point
- Thrust
  - Sam T: Samoep Thrust contact
  - Wit T: Witkoppies Thrust contact
  - GrT: Groothoek Thrust
- 30 Stretching lineations
- 30 F2 Fold Axes
- 30 F3 Fold Axes
- Shear zones
- Shear Movements (Down / Up)
- Synform
- Antiform
- 00-30°
- 30-60°
- 60-90°
- Folding S0//S1
- Folding S0//S1//S2
- A-C Fold closures
- Mesoscopic Model 1 Z fold.
- Mesoscopic Model 1 S fold.

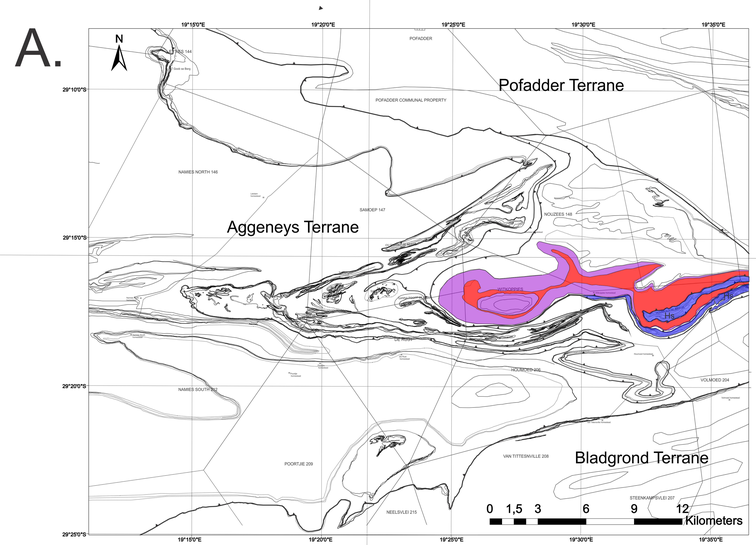

0 0,751,5 3 4,5 6 Kilometers

Samoep Structural Domain

Appendix 3.6
Domain 3A: Gannapoort Berg
'Eye' Structure

N

Sam T

Wit T

I.

A.

B.

C.

D.

E.

F.

G.

H.

Legend

- Form line (S0//S1)
- Inferred contact
- F2 fold trace
- F3 fold trace
- F4 fold trace
- F5 fold trace
- 30 Stretching lineations
- 30 F2 Fold Axes
- 30 F3 Fold Axes
- 30 F4 Fold Axes
- 30 F5 Fold Axes
- Thrust
- Branch Point
- Shear zones
- Shear zone movement (Down, Up)
- Defined Polarity
- 00-30°
- 30-60°
- 60-90°
- Synform
- Antiform
- Sam T: Samoep Thrust
- Wit T: Samoep Thrust
- Folding S0//S1
- Folding S0//S1//S2
- A-H Fold Closures

B.

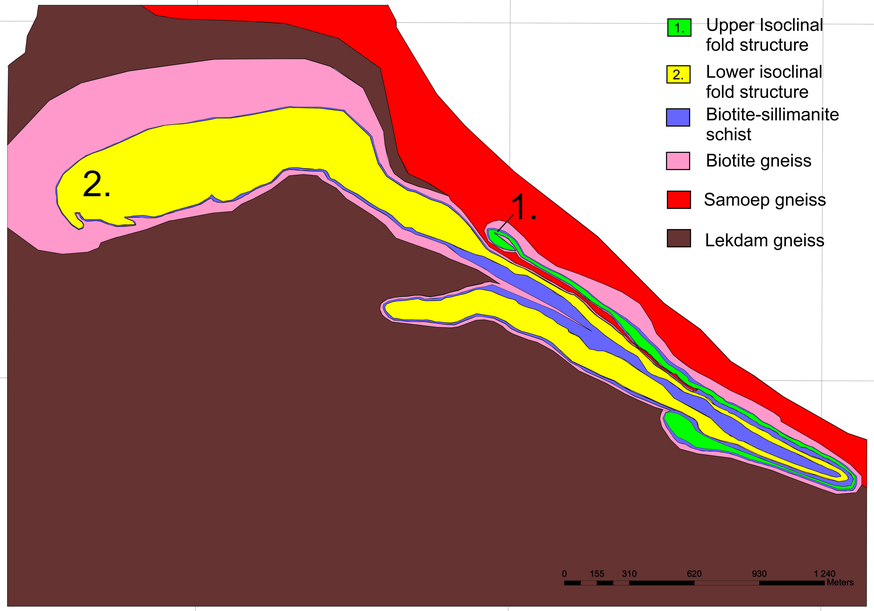

1. Upper Isoclinal fold structure
2. Lower isoclinal fold structure
- Biotite-sillimanite schist
- Biotite gneiss
- Samoep gneiss
- Lekdam gneiss

Witkoppies Structural Domain

Lekdam Structural Domain

A.

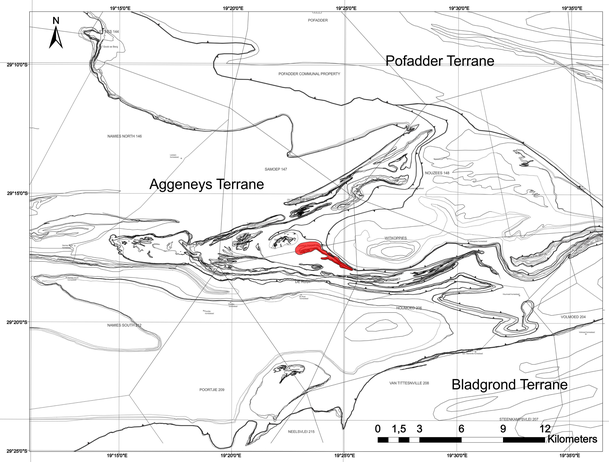

Gannapoort Berg 'Eye' Structure (3A)

C.

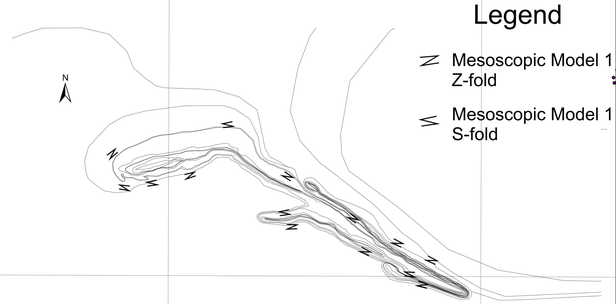

Legend

- Mesoscopic Model 1 Z-fold
- Mesoscopic Model 1 S-fold

0 0,22 0,45 0,9 1,35 1,8 Kilometers

Appendix 3.6: Structural formline map associated with the Gannapoort Berg "Eye' structure that is defined by two isoclinal fold structures refolding adjacent to one another.Figure A: Locality map of the Gannapoort Berg 'Eye' Structure within the study area. Figure B: Simplified geological map showing the major lithologies and intrusives associated with the Gannapoort Berg Structure. It can be noted how the two isoclinal fold structures are refolded adjacent to one another. Figure C: Simplified formline map depicting the location of the mesoscopic Model 1 folds.

0 0,25 0,45 0,9 1,35 1,8 Kilometers

Appendix 4.1: The Samoep Succession

1. Samoep Succession

2. Stratigraphic profiles of the Wortel Formation in the west

A.

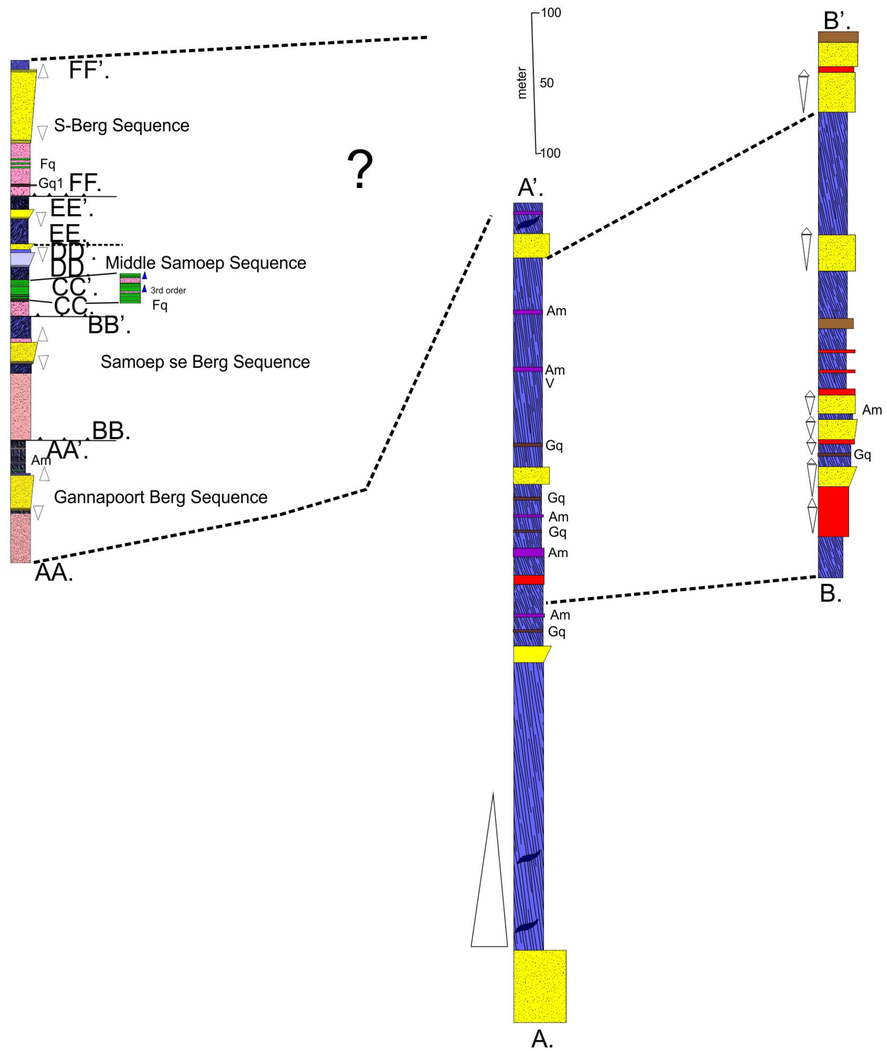

B.

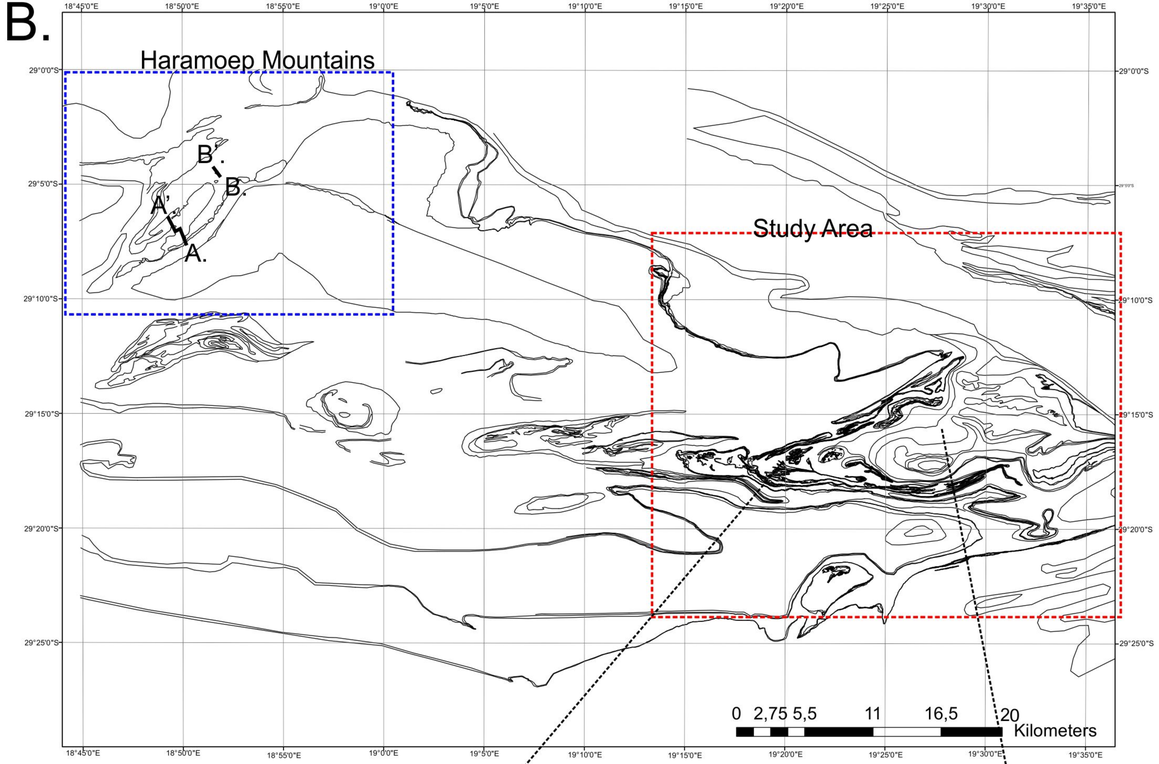

C.

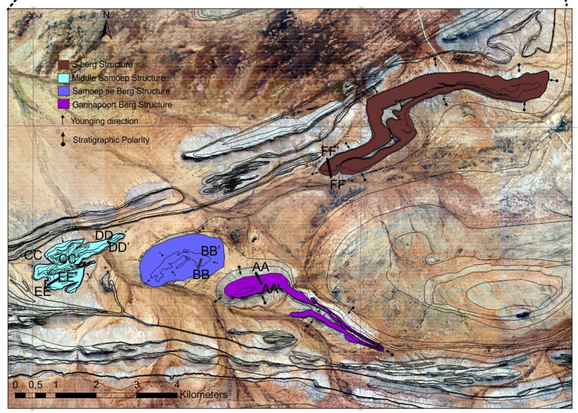

Legend

- Poorly bedded white quartzite
- Biotite-sillimanite schist
- Poorly bedded light-blue quartzite
- Biotite gneiss
- Light banded feldspathic quartzite with interbands of biotite gneiss.
- Medium quartz-feldspar-gneiss (Namies Gneiss)
- Koeipoort Gneiss
- V — Volcanic/chemogenic unit, with interbands of actinolite, diopside banded quartzite.
- Am — Amphibolite/calc-silicate rock
- Gq — Garnet bearing magnetite quartzite (BIF)
- Gq1 — Magnetite quartzite (BIF) without garnet
- Fq — Centimeter scale Feldspathic quartzite
- Massive sillimanite ore body
- 2nd order upward coarsening cycle
- 2nd order upward fining cycle
- 3rd order upward fining cycle
- Thrusting

Appendix 4.1: The comparison between the Samoep Succession and the Wortel Formation supracrustal succession toward the west. Figure A: The similarities and dissimilarities between the Samoep Succession and Wortel Formation in the Haramoep Mountains. Figure B: The location of the Stratigraphic profiles associated with the Samoep Succession and Wortel Formation towards the west. Figure C: An enlarged location diagram depicting the profile positions of the Samoep Succession. The Wortel Formation profiles were modified after Praekelt (1994). For the construction of all stratigraphic profiles, the upright limbs of structures are used for interpretation.

Appendix 4.2: The Koppies and Klein Pofadder Sequences

A.

1. Klein Pofadder Sequence and Koppies Sequence

2. Stratigraphic profiles of the Wortel Formation toward the west

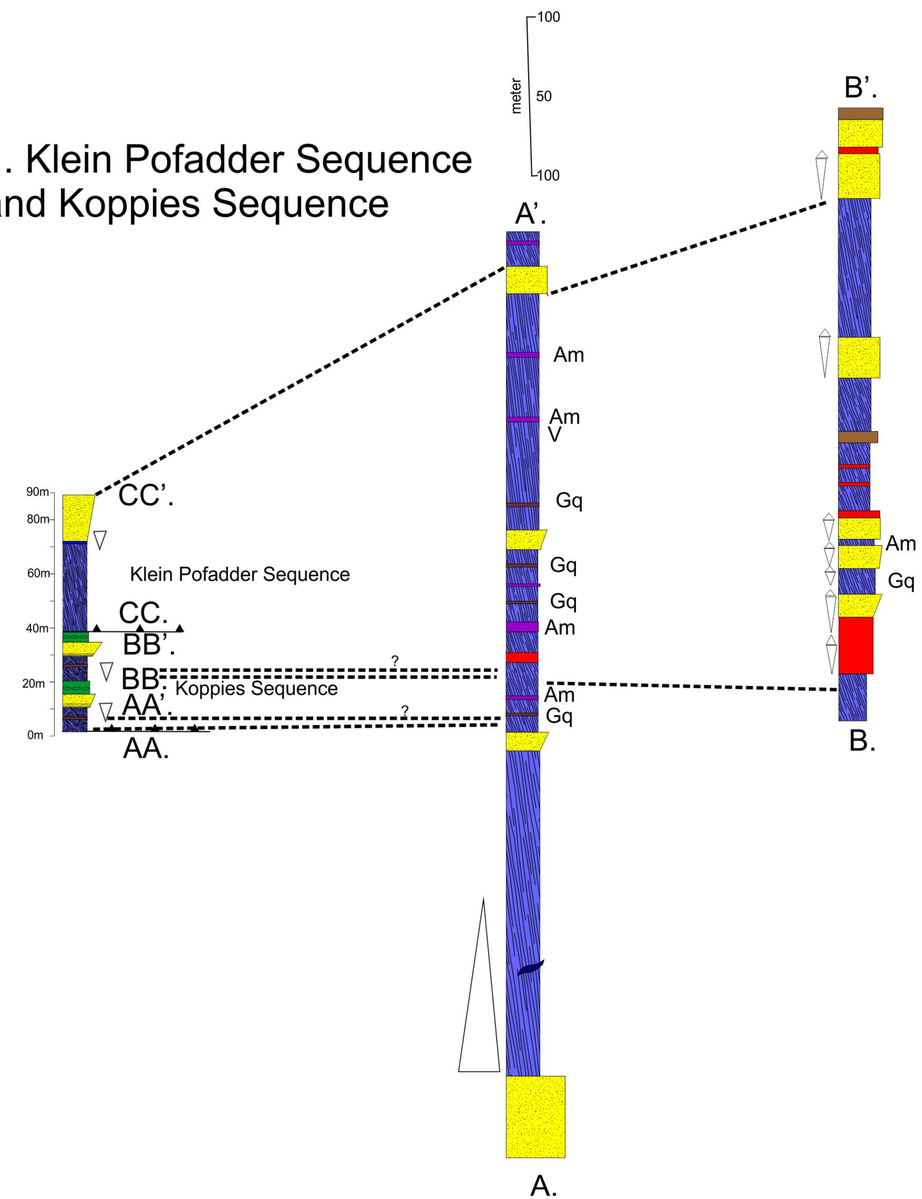

B.

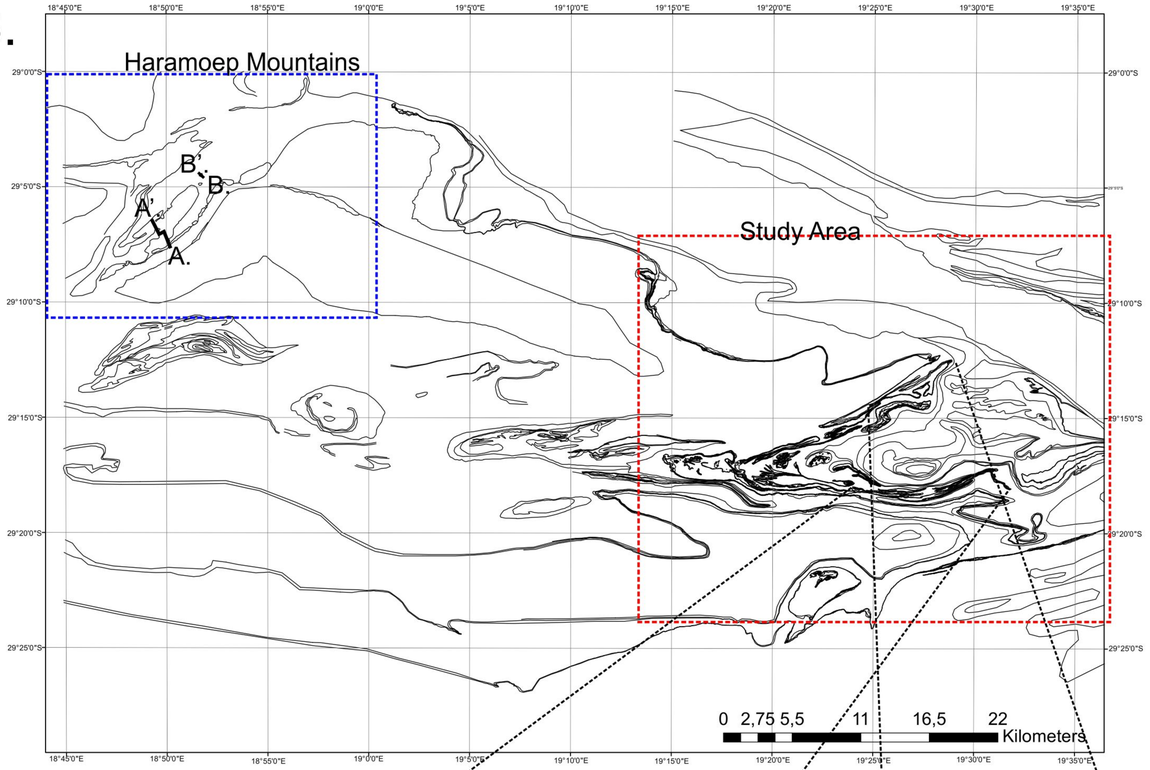

C.

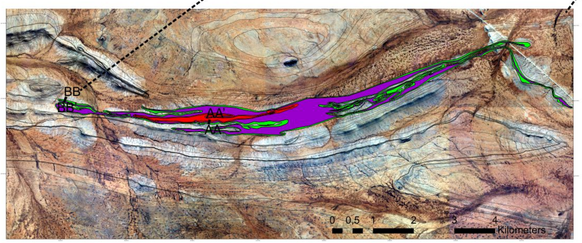

D.

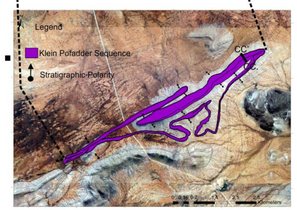

Legend

- Poorly bedded white quartzite
- Biotite-sillimanite schist
- Nodular rhythmic gneiss
- Biotite gneiss
- Medium quartz-feldspar-gneiss
- Koeipoort Gneiss
- V — Volcanic/chemogenic unit, with interbands of actinolite, diopside banded quartzite.
- Am — Centimeter scale Amphibolite/calc-silicate rock
- Gq — Garnet bearing magnetite quartzite (BIF)
- Fq — Feldspathic quartzite
- 2nd order upward coarsening cycle
- 2nd order upward fining cycle
- Sillimanite lenses
- Thrusting

Appendix 4.2: The comparison between the Koppies Sequence, Klein Pofadder Sequence and the Wortel Formation supracrustal succession toward the west. Figure A: The similarities and dissimilarities associated with the Koppies-Klein Pofadder Sequences and the Wortel Formation in the west. Figure B: The location of the stratigraphic profiles associated with the Koppies, Klein Pofadder Sequence and the Wortel Formation rocks in the Haramoep Mountains. Figure C: Offset diagrams showing the profile locations of the Koppies and Klein Pofadder Sequences. The stratigraphic profiles of the Wortel Formation towards the west is modified after Praekelt (1994). For the construction of all stratigraphic profiles, the upright limbs of structures are used in the interpretation.

Appendix 4.3: The T-Goob Succession

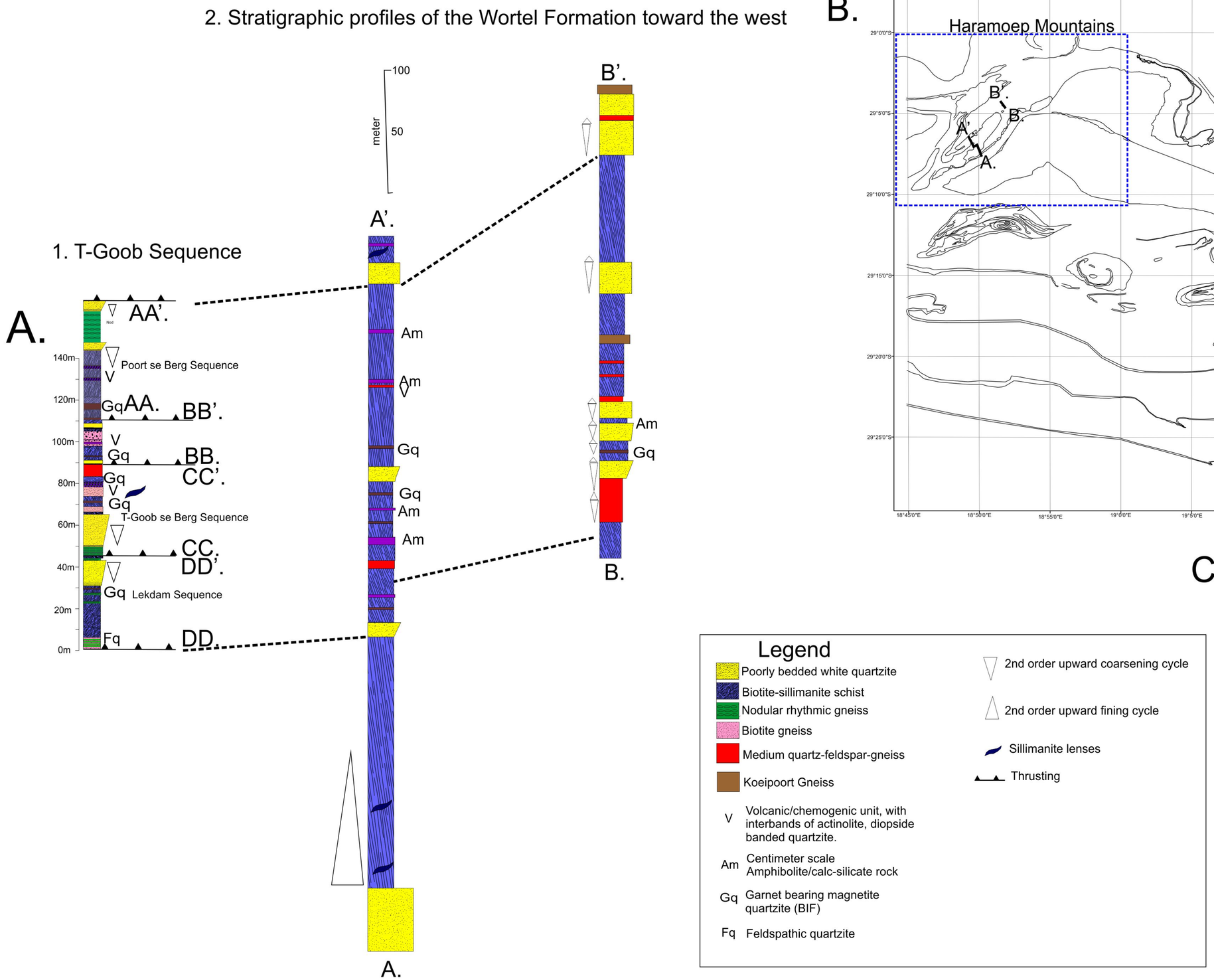

Appendix 4.3: The comparison between the T-Goob Succession and the Wortel Formation rocks found toward the west. Figure A: The similarities and dissimilarities in stratigraphy between the T-Goob Succession and Wortel Formation. Figure B: The location of the stratigraphic profiles of the Wortel Formation found in the Haramoep Mountains. Figure C: An offset diagram showing the location of the stratigraphic profiles associated with T-Goob Succession. The Wortel Formation profiles are modified after Praekelt (1994). For the construction of all stratigraphic profiles, the upright limbs of structures are used in the interpretation.

Appendix 4.4: The Inner Lekdam Succession

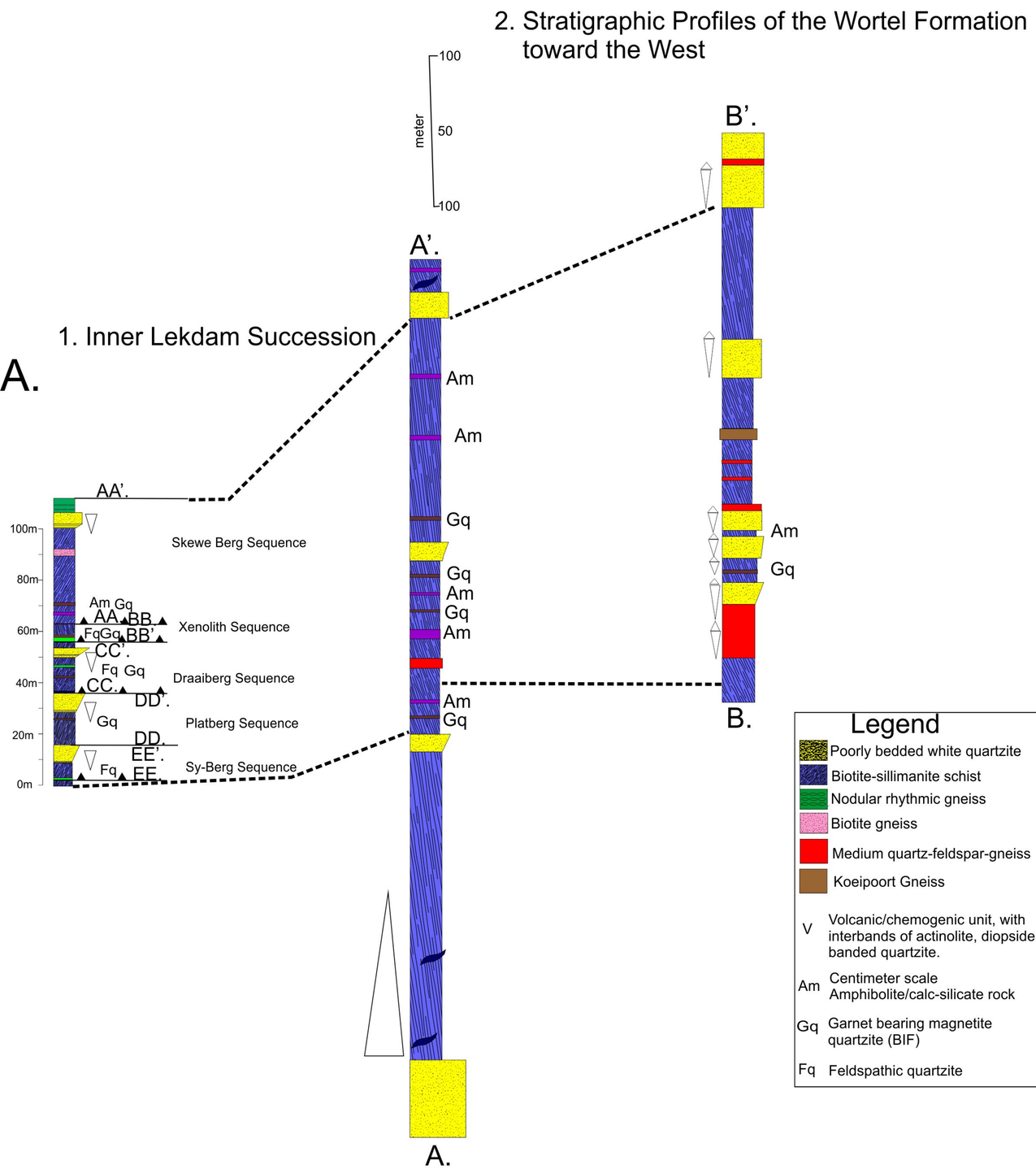

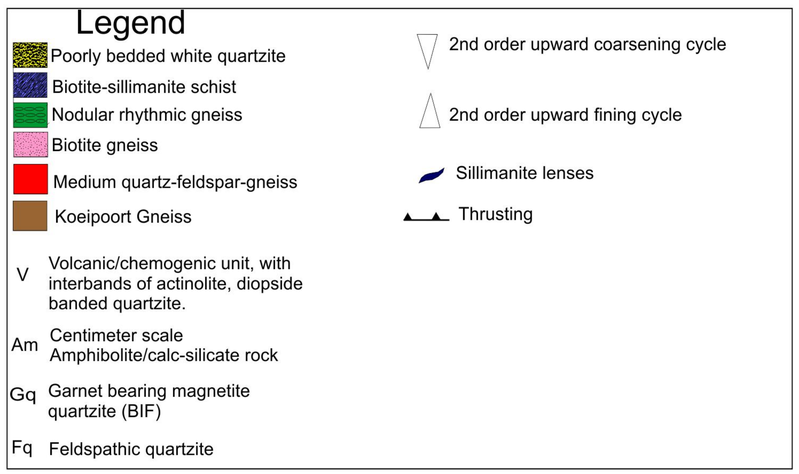

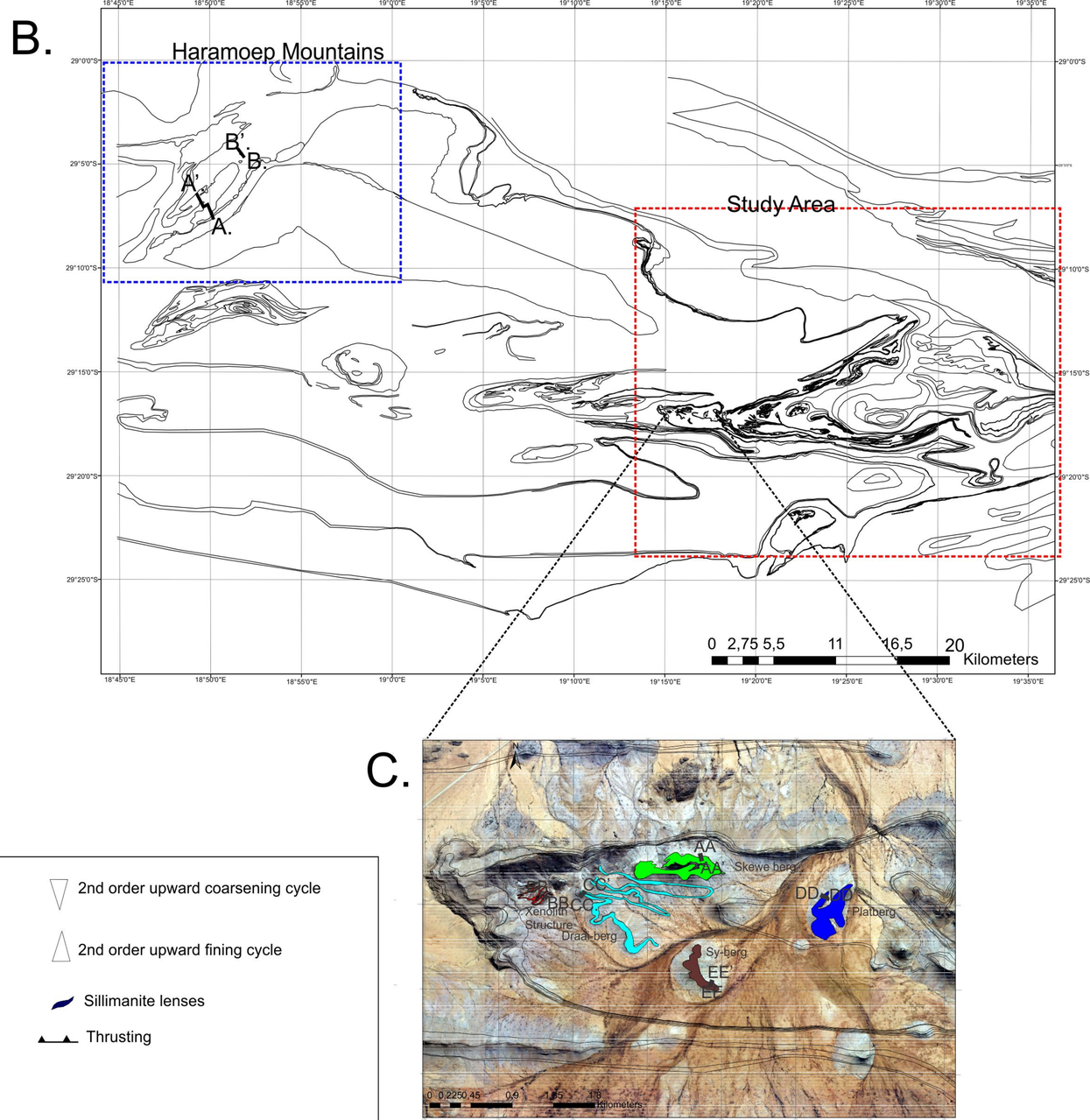

Appendix 4.4: The comparison between the Inner Lekdam Sequence and the Wortel Formation supracrustal succession toward the west. Figure A: The similarities and dissimilarities in stratigraphy between the Inner Lekdam Succession and Wortel Formation. Figure B: The location of the stratigraphic profiles associated with the Wortel Formation in the west. Figure C: An offset diagram showing the location of the Inner Lekdam Succession throughout the study area. For the construction of all stratigraphic profiles, the upright limbs of structures are used in the interpretation.

Appendix 4.5: The De Rust Succession

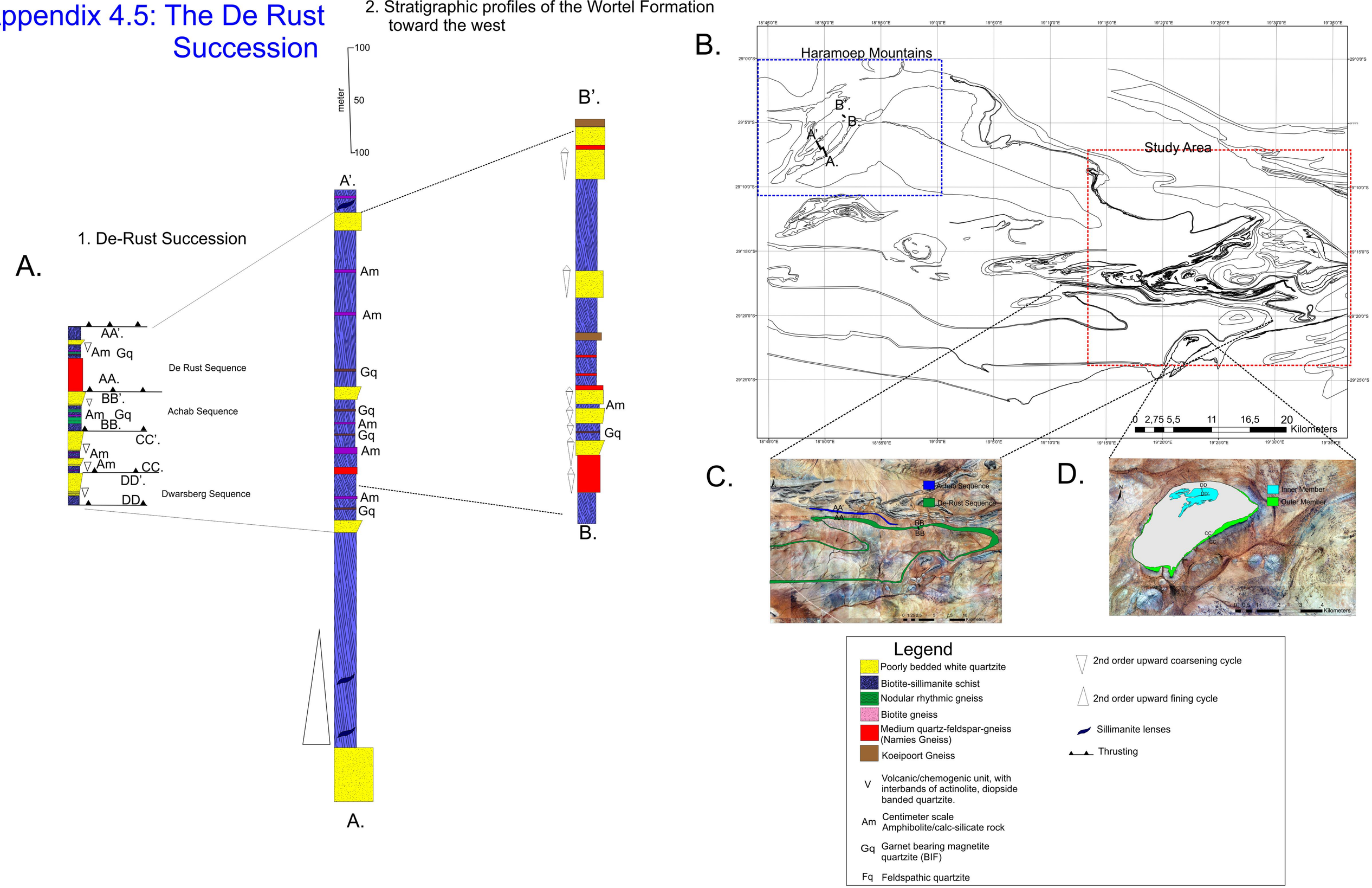

Appendix 4.5: The comparison between the De Rust Succession and the Wortel Formation toward the west. Figure A: The similarities and dissimilarities in the stratigraphy between the De-Rust Succession and Wortel Formation in the west. Figure B: The location of the stratigraphic profiles associated with the Wortel Formation in the west. Figure C: An offset diagram showing the location of the stratigraphic profiles associated with the De Rust Succession. Stratigraphic profiles associated with the Wortel Formation toward the west is modified after Praekelt (1994). For the construction of all stratigraphic profiles the upright limbs of structures are used in the interpretation.

Appendix 4.6: Sheath Fold Classification

Samoep se Berg Sheath Fold

A.

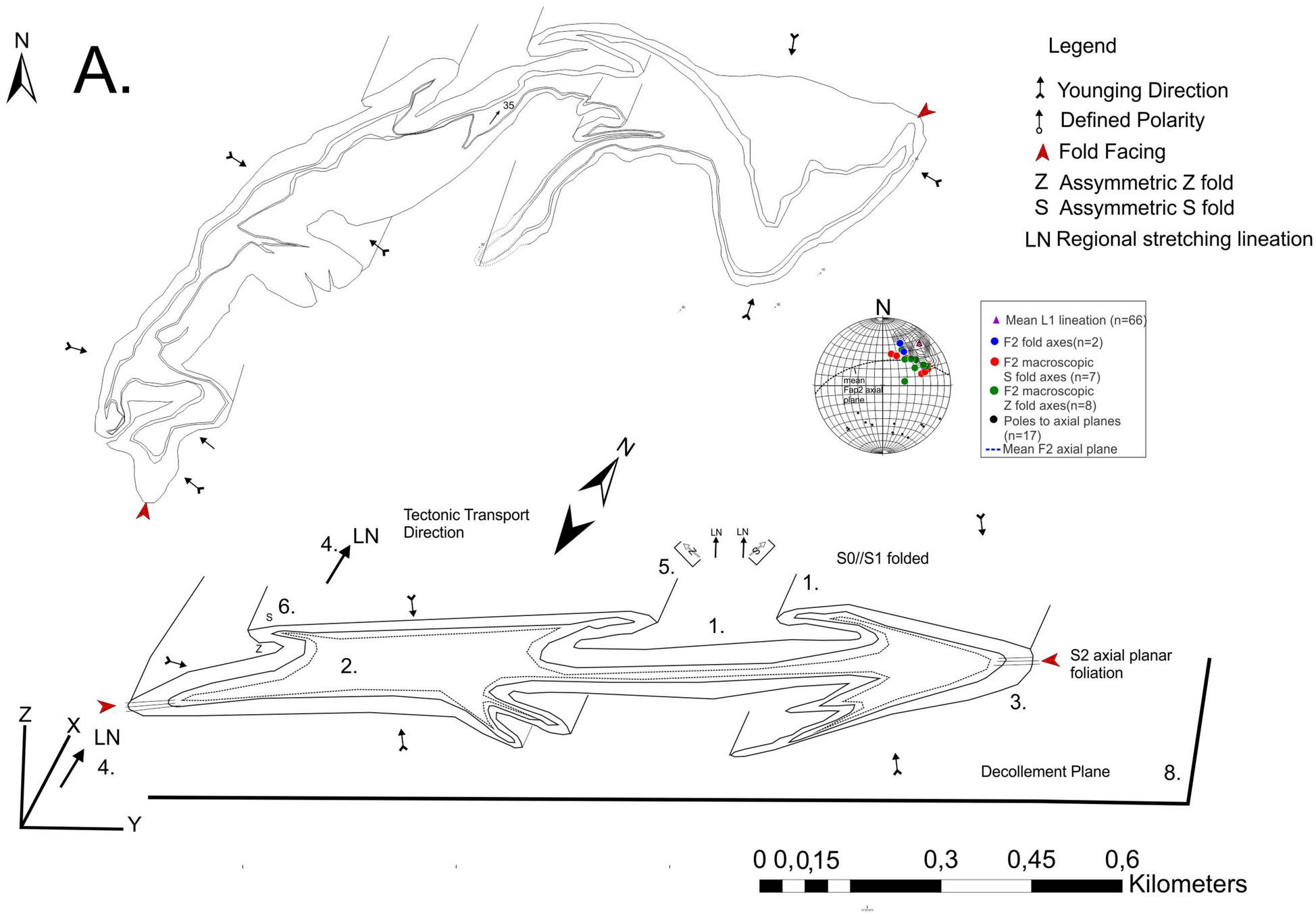

1. Double vergeance structures with S and Z assymetries
2. Symmetrical arrangement of lithologies within the sheath fold structure defining the hinge zone.
3. Sheath folds which have non-continues hinge zones and axial planes
4. Sheath folds show elongation toward the X direction, fold hinges rotate toward the x-direction, parallel to the regional stretching lineation
5. Reversals in obliquity, rotate fold hinges toward the tectonic transport direction with an increase in shear strain (fold obliquity decreases).
6. Minor S and Z folds have reversals in assymetry across the strike of major fold axial traces.
7. Refolding of D2 sheath folds by later D3 folds. The D2 and D3 fold axes are co-linear to one another, together with the L1 stretching lineation.
8. Tectonic displacement and sliding along discontinuous tectonic boundaries such as thrust sheet boundaries and decollement planes.

Dwarsberg Sheath Fold

B.

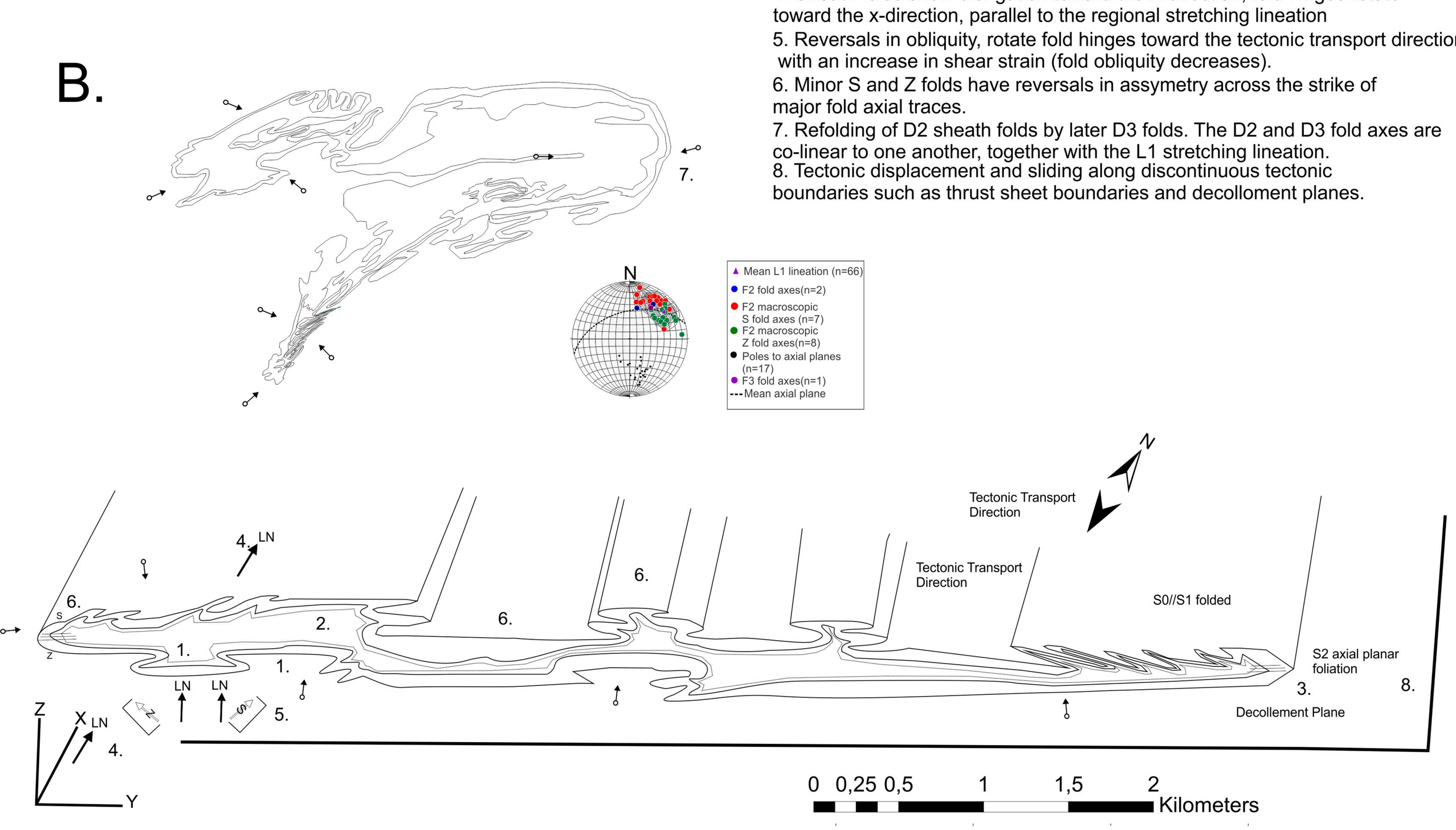

Appendix 4.6: Examples of two prominent sheath fold structures within the study area namely: The Samoep se Berg Sheath Fold (A) and Dwarsberg Sheath Fold (B). For each structure a set of criteria (1-10) is applied, proving that the structures are indeed sheath folds as discussed in chapter 4.2. Figure A: Depicts the Samoep se Berg Sheath fold in its deformed state and in its undeformed state where the later phases of deformation is removed. Stereonet depicting the F2 folds and regional stretching lineations is also shown. Figure B: Shows the Dwarsberg Sheath fold in its deformed state and undeformed state, where the D3 phase of folding is removed, the geometric properties in the form of F2-F3 fold axes and regional L1 stretching lineation is also presented.

Appendix 5.1: Sections of the T-Goob Sheath fold

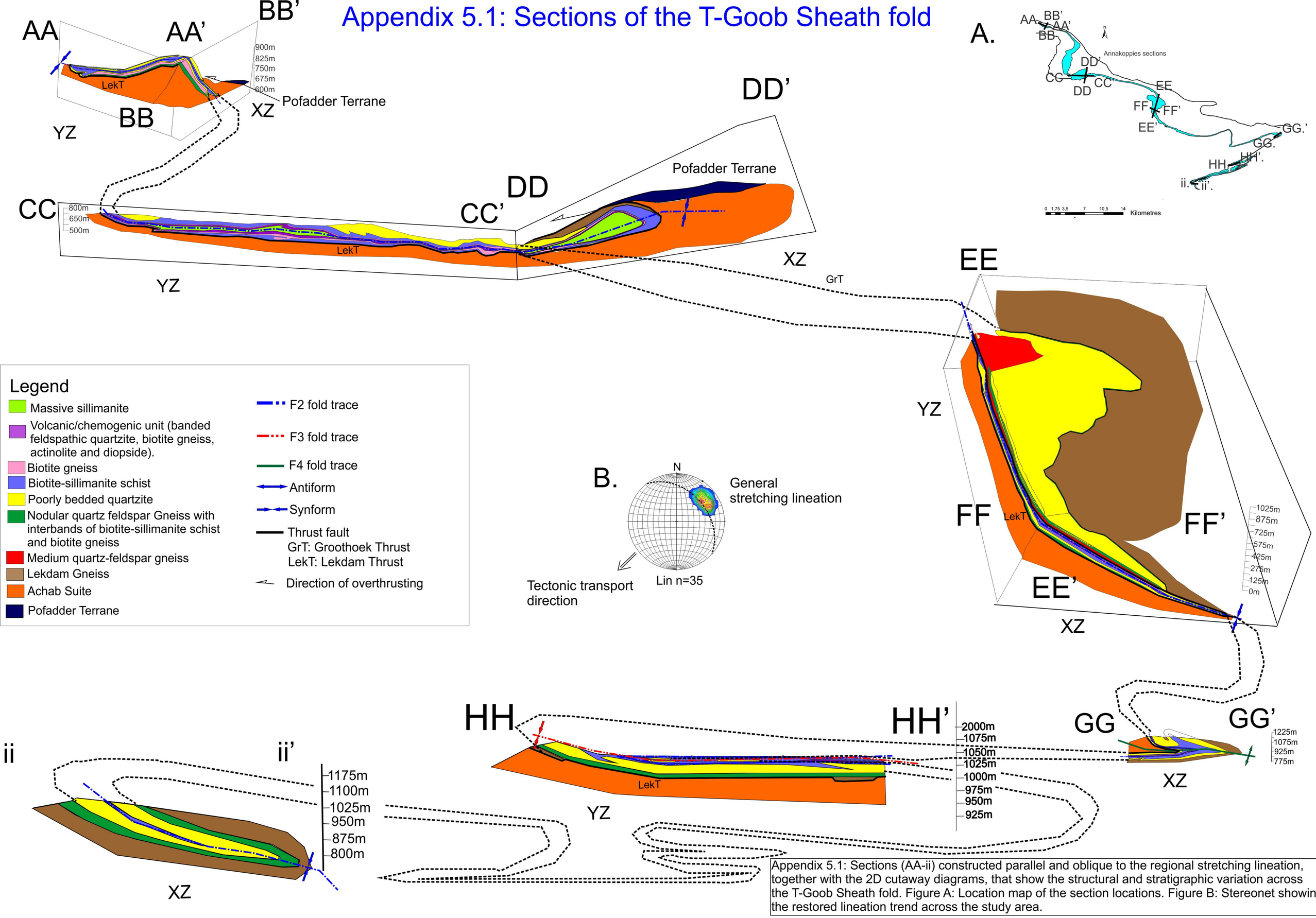

Appendix 5.1: Sections (AA-ii) constructed parallel and oblique to the regional stretching lineation, together with the 2D cutaway diagrams, that show the structural and stratigraphic variation across the T-Goob Sheath fold. Figure A: Location map of the section locations. Figure B: Stereonet showing the restored lineation trend across the study area.